CENTRO INTERNACIONAL DE ESTUDOS
DE DOUTORAMENTO E AVANZADOS
DA USC (CIEDUS)

Tese de Doutoramento

THEORETICAL STUDY OF FULLERENE ENCAPSULATION BY CYCLOPARAPHENYLENE-BASED CARBON NANORINGS

Iván González Veloso

ESCOLA DE DOUTORAMENTO INTERNACIONAL

PROGRAMA DE DOUTORAMENTO EN CIENCIA E TECNOLOXÍA QUÍMICA

Santiago de Compostela

2019

USC
UNIVERSIDADE
DE SANTIAGO
DE COMPOSTELA

DECLARACIÓN DO AUTOR/A DA TESE

THEORETICAL STUDY OF FULLERENE ENCAPSULATION BY CYCLOPARAPHENYLENE-BASED CARBON NANORINGS

D./Dna. Iván González Veloso

Presento a miña tese, seguindo o procedemento axeitado ao Regulamento, e declaro que:

1. A tese abarca os resultados da elaboración do meu traballo.
2. De selo caso, na tese faise referencia ás colaboracións que tivo este traballo.
3. A tese é a versión definitiva presentada para a súa defensa e coincide coa versión enviada en formato electrónico.
4. Confirmo que a tese non incorre en ningún tipo de plaxio doutros autores nin de traballos presentados por min para a obtención doutros títulos.

En Santiago de Compostela, 16 de Maio de 2019

Asdo. .....

USC
UNIVERSIDADE
DE SANTIAGO
DE COMPOSTELA

AUTORIZACIÓN DO DIRECTOR / TITOR DA TESE

THEORETICAL STUDY OF FULLERENE ENCAPSULATION BY CYCLOPARAPHENYLENE-BASED CARBON NANORINGS

D./Dna. Jesús Rodríguez Otero

D./Dna. Enrique Manuel Cabaleiro Lago

INFORMA/N

Que a presente tese, correspóndese co traballo realizado por D/Dna. Iván González Veloso, baixo a miña dirección, e autorizo a súa presentación, considerando que reúne os requisitos esixidos no Regulamento de Estudos de Doutoramento da USC, e que como director desta non incorre nas causas de abstención establecidas na Lei 40/2015.

En Santiago de Compostela, 25 de Marzo de 2019

Asdo. .....
Jesús Rodríguez Otero

Asdo. .....
Enrique Manuel Cabaleiro Lago

USC
UNIVERSIDADE
DE SANTIAGO
DE COMPOSTELA

Agradecimientos

Primero me gustaría agradecer el esfuerzo, la ayuda y el apoyo que me brindaron mis directores de tesis, Jesús y Enrique, durante mis años de investigación y escritura de la tesis. Pero no solo durante estos años, si no también durante el máster y el último año de carrera, en el cual decidí optar por la rama teórica y computacional.

También me gustaría expresar mi agradecimiento a mi familia, en especial a mis padres, por todo el apoyo que me brindaron durante estos años. A mi hermano, porque siempre pude contar con él en los momentos complicados. A mis abuelos por guiarme durante la niñez y la adolescencia, sin vuestra guía no estaría donde estoy.

A mis amigos del colegio que siempre estuvieron ahí apoyándome cuando las cosas se torcieron y sacandome de fiesta en los momentos bajos para despejar la mente. De igual manera me gustaría agradecer a la gente con la que compartí mis años de carrera en Santiago que hicieron que esos años pasados en Condesa fueron algo inolvidable lleno de grandes experiencias, en especial las comidas que hacíamos todos juntos y que se podían alargar por horas.

A mis compañeros de despacho David, Martín y Luis que empezaron solo siendo compañeros pero al final se conviertieron en verdaderos amigos con lo que discutir de química o salir a tomar una cañas.

Por último y no menos importante a todos los profesores de teórica, por los sabios consejos, la ayuda durante los años de tesis y las cenas de grupo que ayudaron a descrubir nuevos sitios de Santiago.

USC
UNIVERSIDADE
DE SANTIAGO
DE COMPOSTELA

Contents

Resumen **vii**

1 Introduction **1**
1.1 Intermolecular interactions . . . 1
1.1.1 Long-range interactions . . . 1
1.1.2 Short-range interactions . . . 3
1.2 Supramolecular chemistry . . . 4
1.3 Interactions between aromatic systems . . . 5
1.3.1 X-H$\cdots\pi$ interactions . . . 6
1.3.2 Ion$\cdots\pi$ interactions . . . 6
1.3.3 $\pi\cdots\pi$ interactions . . . 8
1.3.3.1 Concave–convex $\pi\cdots\pi$ interactions . . . 10
1.4 Curved $\pi\cdots\pi$ systems . . . 11
1.4.1 Fullerenes . . . 11
1.4.1.1 Organic photovoltaic cell . . . 14
1.4.1.2 Endohedral fullerenes . . . 15
1.4.2 Curved fullerene receptors . . . 16
1.4.2.1 Buckybowls . . . 17
1.4.2.2 Carbon nanotubes . . . 18
1.4.2.3 Carbon nanorings . . . 21
References . . . 25

2 Objectives **37**

3 Methodology **41**
3.1 Interaction energy . . . 41
3.1.1 Perturbation method . . . 41
3.1.2 Supermolecule method . . . 42
3.1.3 Basis set superposition error (BSSE) . . . 42
3.1.3.1 Counterpoise correction . . . 43
3.1.3.2 Complexation energy . . . 43
3.2 Density functional theory (DFT) . . . 44
3.2.1 Kohn-Sham theory . . . 45
3.2.2 Classification of exchange-correlation functionals . . . 47
3.2.2.1 Local Density Approximation (LDA) . . . 47
3.2.2.2 Generalized Gradient Approximation (GGA) . . . 47
3.2.2.3 Meta-GGA . . . 48

3.2.2.4 Hybrid . . . 48
3.2.2.5 Long-range corrected functionals . . . 48
3.2.3 Time-dependent DFT . . . 49
3.2.3.1 Visualization of charge transfer excitations . . . 50
3.2.4 Problematic cases for using in DFT . . . 52
3.2.5 Dispersion correction . . . 53
3.2.5.1 Grimme's dispersion corrections . . . 53
3.2.5.2 Other corrections . . . 56
3.2.6 Basis sets . . . 57
3.2.6.1 Contracted basis set . . . 58
3.2.6.2 Effective core potentials . . . 60
3.3 Reducing computational cost . . . 61
3.3.1 Resolution of identity (RI) . . . 61
3.3.2 Chain-of-spheres . . . 62
3.3.3 Density-functional tight-binding (DFTB) . . . 62
3.3.3.1 DFTB3 . . . 63
3.3.3.2 Dispersion . . . 65
3.3.3.3 Parameterization . . . 66
3.3.3.4 Limitations . . . 66
3.4 Properties and analysis . . . 67
3.4.1 Non-Covalent Interaction Index (NCI) . . . 67
3.4.2 Molecular electrostatic potential (MEP) . . . 69
3.4.3 SAPT . . . 70
3.4.4 Local energy decomposition (LED) . . . 72
3.4.4.1 DLPNO-CCSD(T) . . . 72
3.5 Euler angles . . . 75
References . . . 76

4 Carbon-nanorings ([10]CPP and [6]CPPA) as fullerene (C_{60} and C_{70}) receptors: a comprehensive dispersion-corrected DFT study 85
4.1 Introduction . . . 85
4.2 Computational details . . . 87
4.3 Results and discussion . . . 88
4.3.1 C_{60}@[10]CPP complex . . . 88
4.3.2 C_{60}@[6]CPPA complex . . . 91
4.3.3 C_{70}@[10]CPP complex . . . 92
4.3.4 C_{70}@[6]CPPA complex . . . 94
4.3.5 Comparison between complexes . . . 95
4.3.6 Comparison between DFT functionals . . . 98
4.4 Conclusions . . . 99
References . . . 100

5 Size and shape effects on complexes of fullerenes with carbon nanorings: C_{50} and C_{76} as [10]CPP and [6]CPPA guest 103
5.1 Introduction . . . 103
5.2 Computational details . . . 105
5.3 Results and discussion . . . 107

5.3.1 Calculation of complexation energies . . . 107
5.3.2 Comparation between complexes . . . 109
5.4 Conclusions . . . 114
References . . . 114

6 Assessment of electronic transitions involving intermolecular charge transfer in complexes formed by fullerenes and donor–acceptor nanohoops 119
6.1 Introduction . . . 119
6.2 Computational details . . . 122
6.3 Results and discussion . . . 123
6.3.1 Structure and stability . . . 123
6.3.2 Density analysis of the complexes . . . 130
6.3.3 Electronic transitions . . . 131
6.3.4 Optimising nanohoop size . . . 135
6.4 Conclusions . . . 136
References . . . 137

7 Fullerene Size Controls the Selective Complexation of [11]CPP with Pristine and Endohedral Fullerenes 143
7.1 Introduction . . . 143
7.2 Computational details . . . 145
7.3 Results and discussion . . . 147
7.3.1 Fullerenes . . . 147
7.3.2 [11]CPP complexes with pristine Fullerenes. C_{60}, C_{70}, C_{76}, C_{78} . . . 149
7.3.3 [11]CPP complexes with $Sc_3N@C_{80}$, $Y@C_{82}$, $Tm@C_{82}$, $Y_2@C_{82}$, $Lu_2@C_{82}$ . . . 153
7.3.4 Global trends in stability and charge transfer between fullerene and nanoring . . . 155
7.4 Conclusions . . . 157
References . . . 157

8 Endohedral alkali cations promote charge transfer transitions in complexes of C_{60} with [10]cycloparaphenylenes 163
8.1 Introduction . . . 163
8.2 Computational details . . . 164
8.3 Results and discussion . . . 166
8.3.1 $M^+@C_{60}$ endofullerenes . . . 166
8.3.2 $M^+@C_{60}\cdots$[10]CPP complexes . . . 169
8.3.2.1 Structure and stability . . . 169
8.3.2.2 Electronic transitions and charge transfer . . . 172
8.4 Conclusions . . . 176
References . . . 177

9 Conclusions 183

A Supplementary information Chapter 4 **187**
A.1 Rotation throught Euler angles . . . 187
A.2 Vertical departure of the C_{60} . . . 188
A.3 Searching minima of complex C_{60}@[10]CPP with a systematic scanning procedure. . . . 189
A.4 Searching minima of complex C_{60}@[6]CPPA with a systematic scanning procedure. . . . 193
A.5 Searching minima of complex C_{70}@[10]CPP with a systematic scanning procedure. . . . 195
A.6 Searching minima of complex C_{70}@[6]CPPA with a systematic scanning procedure. . . . 198
A.7 Interaction between [10]CPP and fullerenes . . . 201
A.8 Distance between centres of the six-membered ring . . . 202
A.9 Dispersion breakdown . . . 203
A.10 Complexation energy . . . 204

B Supplementary information Chapter 5 **207**
B.1 Rotation throught Euler angles . . . 207
B.2 Details of the search for the best orientation of C_{50}@[10]CPP, C_{50}@[6]CPPA and C_{76}@[10]CPP complexes . . . 208
B.3 Searching minima of complex C_{76}@[6]CPPA with a systematic scanning procedure . . . 215
B.4 Vertical departure of the C_{60} . . . 218
B.5 Complexation energy versus dispersion and N_{contacts} . . . 219
B.6 Fitting into an ellipse . . . 220

C Supplementary information Chapter 6 **221**
C.1 Fitting nanohoops and most stable complexes . . . 221
C.2 HOMO-LUMO Orbitals . . . 222
C.3 Centre of mass and centre of the ring in the nanohoops . . . 224
C.4 Energetic profile for X axis displacement . . . 225
C.5 Energetic profile at the centre of the nanohoops . . . 226
C.6 Energetic profile for the departure of the fullerene . . . 227
C.7 NCIPLOT images for the departure of C_{70} . . . 229
C.8 Bond critical points in complexes . . . 230
C.9 Absorption spectra . . . 232
C.10 Charge transfer in monomers . . . 233
C.11 HOMO-LUMO orbitals for complexes . . . 235
C.12 Position of the barycentres . . . 236
C.13 Charge transfer in different nanohoops . . . 237
C.14 Complexation energies at B3LYP-D3(BJ)/def2-TZVP level . . . 239
C.15 [10]CPA molecules . . . 240
C.16 [10]CPA complexation energy . . . 241
C.17 [10]CPA MEP . . . 242
C.18 [10]CPA charge transfer . . . 243
C.19 Anthracene-substituted [8]CPP complexes . . . 245
C.20 Structures for C_{100} with the nanohoops . . . 247

D Supplementary information Chapter 7 **249**
D.1 Fitting to an ellipse . . . 249
D.2 NBO second order perturbation analysis . . . 250
D.3 HOMO-LUMO . . . 251
D.4 Euler angle . . . 252
D.5 Energy profile in Euler rotations . . . 253
D.6 Energy profile C_{60} . . . 254
D.7 Interaction energy in corannulene dimer . . . 255
D.8 Energy profile C_{70} . . . 256
D.9 Energy profile C_{80}@Sc_3N . . . 257
D.10 Additional structures for C_{60} and C_{76} . . . 258
D.11 2D-NCIPLOT for endohedral fullerene . . . 259
D.12 Correlation between dispersion energy and complexation energy . . . 260

E Supplementary information Chapter 8 **261**
E.1 Energetic and geometric results for M^+@C_{60} complexes . . . 261
E.2 Molecular electrostatic potential . . . 262
E.3 HOMO-LUMO monomers . . . 263
E.4 Searching of the most stable structure of M^+@$C_{60}\cdots$[10]CPP complexes . 264
E.5 Structures of the most favourable complexes . . . 279
E.6 Comparison of interaction energy in corannulene dimer for different methodologies . . . 283
E.7 Local Energy Decomposition based on DLPNO-CCSD(T) . . . 284
E.8 Absorption spectra for the monomers . . . 285
E.9 Absorption spectra for the complexes . . . 286
E.10 Position of the barycentres . . . 287
E.11 Charge transfer in different complexes with TPSS-D3(BJ) geometry . . . 289
E.12 Absorption spectra with TPSS-D3(BJ) geometry . . . 290

USC
UNIVERSIDADE
DE SANTIAGO
DE COMPOSTELA

Resumen

En 1985 la tercera forma alotrópica del carbono fue descubierta por Richard Smalley, Robert Curl y Harold Kroto, recibiendo el nombre de fulereno. Este tipo de compuestos curvados de carbono recibieron una gran atención durante los últimos años debido a la gran variedad de estructuras que presentan ya que, aunque el C_{60} es el más común seguido del C_{70}, existen otros fulerenos más pequeños, como el C_{32}, o mucho más grandes, llegando a estar formados por más de 500 átomos de carbono. Además de estas variaciones en el número de carbonos y el tamaño, la mayor parte de los fulerenos también presentan numerosos isómeros que normalmente cumplen la regla de que no puede haber dos pentágonos adyacentes en la estructura. Así, por ejemplo, el C_{78} presenta cinco estructuras estables que cumplen con la regla de los pentágonos aislados. Esta gran variedad estructural junto con sus interesantes propiedades electrónicas, y más concretamente su uso en células fotovoltaicas orgánicas, los hacen fascinantes, llegando a ser el centro de distintos estudios en diversos campos como por ejemplo en química, en física o en ciencia de materiales.

El desarrollo de células fotovoltaicas orgánicas ha experimentado un gran avance en los últimos años debido a las ventajas que presentan con respecto a las tradicionales de silicio, tales como su bajo peso, su bajo coste o la posibilidad de hacer dispositivos fotovoltaicos flexibles. Últimamente, estos dispositivos suelen estar basados en películas de polímeros dopados con fulerenos. Por las propiedades del fulereno (alta afinidad electrónica), éste actúa como aceptor de electrones, mientras que el polímero actúa como dador de electrones cuando absorbe radiación. Sin embargo, para obtener un buen rendimiento en estos dispositivos, se requiere de unas estructuras ordenadas a nivel microscópico que garanticen el contacto íntimo entre dador y aceptor. En este caso, el uso de receptores de fulerenos puede ser de gran ayuda para obtener estas estructuras.

Se pueden utilizar numerosos tipos de receptores para atrapar fulerenos, estando los siguientes entre los más comunes: receptores planos como las porfirinas que a pesar de la falta de complementariedad con la superficie convexa de los fulerenos son capaces de formar complejos estables, huéspedes macrocíclicos clásicos como las ciclodextrinas que presentan una estructura con forma de anillo donde atrapar al fulereno y compuestos aromáticos que presentan superficies cóncavas que “encajan” con la convexidad de los fulerenos. Entre estos últimos receptores destacan los buckybowls, compuestos aromáticos con forma de cuenco, como por ejemplo el coranuleno o el sumaneno, capaces de interaccionar con los fulerenos. Otro tipo de receptores cóncavos, los cuales constituyen el objetivo principal de esta tesis, son especies como los cicloparafenilenos, formados por la concatenación de anillos aromáticos dando lugar a una estructura cerrada en forma de anillo con una cavidad apropiada para la inserción de fulerenos.

El uso de compuestos aromáticos cóncavos está experimentando un gran desarrollo durante los últimos años, sobre todo después de que en el año 2007 se publicara un trabajo

en el cual se sintetizaba una pinza formada por dos unidades de coranuleno unidas por medio de ciclooctatretraeno, que permitía capturar de forma efectiva el fulereno C_{60}, demostrando además la fortaleza de las interacciones $\pi\cdots\pi$, que podían ser empleadas como parámetro de diseño de nuevos receptores. (A. Sygula, F. R. Fronczek, R. Sygula, P. W. Rabideau y M. M. Olmstead, *Journal of the American Chemical Society*, 2007, **129**, 3842-3843).

Por otra parte, el desarrollo de nuevas rutas sintéticas para obtener nanoanillos de carbono está permitiendo la obtención de una gran variedad de los mismos, desde los que se corresponden con las unidades fundamentales de los nanotubos de carbono como es el caso de los cicloparafenilenos, hasta otras variedades que presentan sustituyentes en el anillo, como grupos atractores de carga o grupos etinil. Todos estos avances permiten adaptar el anillo con el propósito de capturar un determinado fulereno en su interior mediante el uso exclusivo de fuerzas intermoleculares. De hecho, se ha verificado experimentalmente la formación de complejos de inclusión de fulerenos y nanoanillos de carbono, e incluso se ha podido determinar su estructura en algunos casos.

Aun así, el estudio de este tipo de compuestos aún se encuentra en sus primeras etapas, ya que buena parte de ellos solo han sido obtenidos muy recientemente (en los últimos 10 años). Además, el gran tamaño de estos compuestos, así como la complejidad de la disposición del fulereno dentro del anillo, hace que su estudio sea bastante complejo desde el punto de vista teórico/computacional. En todo caso, un estudio teórico en profundidad de este tipo de sistemas puede ser de gran ayuda para establecer las características de estos complejos y conocer los factores que controlan su estabilidad y propiedades fotofísicas, especialmente su tendencia a formar pares dador/aceptor para su posible uso en células fotovoltaicas orgánicas.

Esta tesis se puede resumir en dos propósitos no totalmente separables: en un primer bloque se estudia principalmente la interacción entre los nanoanillos de carbono y fulerenos de distinto tipo y tamaño. Para llevar a cabo estos estudios se han utilizado distintos tipos de fulerenos, incluyendo los fulerenos más abundantes C_{60} y C_{70}, así como otros fulerenos menos abundantes como C_{50}, C_{76} o C_{78}. Además, se han considerado representantes de los conocidos como endofulerenos, fulerenos que contienen alguna especie en su interior. Estas especies fueron detectadas poco después de la identificación del fulereno C_{60}, y desde entonces su número no ha dejado de crecer, conteniendo una o varias especies metálicas o incluso un pequeño agregado atómico como en el caso del $Sc_3N@C_{80}$, el tercer fulereno más abundante tras C_{60} y C_{70}. Los complejos de estos fulerenos con diversos nanoanillos de carbono han sido estudiados, fundamentalmente considerando [n]cicloparafenilenos de distinto tamaño ([n]CPP), que forman la unidad básica que se repite en algunos nanotubos. Además, se han considerado otros nanoanillos como el [6]CPPA, que fue el primer nanoanillo de carbono sintetizado y alterna grupos parafenileno y etinil, así como modificaciones de los CPPs que incluyen unidades de antraceno. Con el conjunto de estudios de este bloque, dedicado al estudio de la interacción, se pretende poder predecir la estabilidad de los complejos y obtener información acerca que cuáles son las claves que controlan la estabilidad en este tipo de sistemas.

El segundo propósito en esta tesis es obtener información acerca de la posibilidad de emplear estos complejos entre nanoanillos y fulerenos como pares dador/aceptor que tengan uso potencial en células orgánicas fotovoltaicas. Para ello, empleando combinaciones apropiadas de nanoanillos sustituidos y/o endofulerenos catiónicos se estudia el espectro

de absorción de los complejos para así determinar si hay bandas de absorción intensas asociadas al proceso de transferencia de carga intermolecular entre el anillo y el fulereno y averiguar qué factores controlan este proceso.

En todo caso, como se comenta más arriba, estos dos propósitos globales no son totalmente separables, de modo que también se podría estructurar la tesis en dos bloques: uno dedicado a sistemas conteniendo fulerenos formados únicamente por carbono y un segundo en el que se han utilizado endofulerenos, siendo precisamente ésta la estructura usada durante la escritura de esta tesis.

El estudio de los complejos formados por nanoanillos y fulerenos se ha llevado a cabo mediante el uso de diversas técnicas computacionales. La mayoría de los cálculos de la tesis se realizaron aplicando la Teoría del Funcional de la Densidad (DFT) la cual, en los últimos años, y gracias a la aplicación de correcciones empíricas para describir apropiadamente la dispersión, así como a técnicas de reducción del coste computacional (entre las que destaca la resolución de identidad, "Resolution of Identity"), produce unos resultados adecuados a la vez que permite tratar sistemas grandes, de más de 150 átomos, en los cuales la dispersión es importante. Sin embargo, también han sido utilizados otros métodos además de DFT, como es el caso del método de perturbación adaptado en simetría (SAPT) o la descomposición de energía local basada en CCSD(T) local ("LED DLPNO-CCSD(T)"). Este tipo de técnicas han sido utilizadas para obtener una idea más clara de la naturaleza de la interacción que se establece entre los monómeros y las distintas contribuciones físicas a la energía de coordinación.

Por otra parte, para describir las transiciones electrónicas en los sistemas estudiados, se ha hecho uso de la DFT dependiente del tiempo (TD-DFT), que permite una descripción razonable del espectro de absorción de estos complejos. Por último, el uso de técnicas de tipo semiempírico como tight-binding DFT (DFTB) permite estudiar con un coste computacional reducido la multitud de orientaciones relativas que los fulerenos pueden adoptar dentro de los anillos. De este modo, se puede hacer un cribado estructural previo antes de la aplicación de métodos más costosos. Todos los métodos empleados en la tesis se encuentran detallados en el **capítulo 3** dedicado a metodología.

La sección de resultados de esta tesis se inicia con el **capítulo 4**, en el que se detalla el estudio inicial que se llevó a cabo con el fin de estudiar en detalle las características de los complejos formados por los fulerenos más típicos, C_{60} y C_{70}, y dos anillos de diferente naturaleza, [10]CPP y [6]CPPA. Al tratarse del estudio inicial, se ha centrado más en aspectos de tipo metodológico, con el fin de poder definir un protocolo computacional a seguir para determinar las estructuras más estables de los complejos y sus estabilidades.

Un primer problema al que hay que enfrentarse al estudiar los complejos formados por nanoanillos y fulerenos es el elevado número de estructuras que presentan una estabilidad similar. Las superficies de energía potencial de los complejos son poco variables ante rotaciones del fulereno dentro del anillo, generando multitud de mínimos locales. Para poder obtener la estructura más favorable de cada complejo, se han probado dos protocolos con diferente coste computacional.

El primer método consiste en emplear las dos orientaciones más relevantes de los fulerenos estudiados (C_{60} orientado según un eje pasando entre anillos pentagonales o hexagonales opuestos y para el C_{70}, con forma de pelota de rugby, orientaciones siguiendo los ejes mayor y menor) y situarlos en el centro del anillo. Una vez en el interior del anillo se realiza una rotación y se obtiene la estructura rotada más favorable; finalmente, se

desplaza el fulereno verticalmente fuera del anillo para determinar si es energéticamente más favorable que el centro del fulereno esté en el plano del anillo o desplazado hacia el exterior. El segundo método, más seguro pero mucho más costoso, debido a la cantidad de cálculos que requiere, consiste en obtener una superficie energética rotando el fulereno siguiendo tres ángulos (ángulos de Euler) para muestrear todas las posibles disposiciones dentro del anillo, y también aplicar desplazamientos verticales desde el centro del anillo. Con este último método se obtiene una mayor certeza de cuál es la disposición óptima del fulereno dentro del anillo, pero también requiere mucho más tiempo. Se ha comprobado que el método más simple permite obtener la estructura más estable de los complejos, por lo que en estudios posteriores se evitara aplicar la exploración más costosa.

Para determinar la estabilidad de estos complejos se calculó la energía de coordinación de las estructuras más estables mediante el nivel B97-D2/def2-TZVP, obteniéndose que la mayor contribución a la estabilización del sistema es la dispersión. Por otro lado, en cuanto a la disposición del fulereno dentro del anillo, cuando el C_{60} está en el interior del [10]CPP, se obtiene una ligera preferencia por las estructuras con los anillos pentagonales en la parte superior e inferior del fulereno (comparado con la orientación a través de anillos hexagonales). Los resultados muestran que esta preferencia se debe a la gran superficie de contacto que se produce por la disposición paralela de los anillos bencénicos del fulereno y del nanoanillo. Este mismo motivo es encontrado entre el C_{70} y el [10]CPP cuando el fulereno está en una disposición vertical (a lo largo del eje mayor), que es la más favorable debido al tamaño del [10]CPP.

El otro nanoanillo estudiado es el [6]CPPA, formado por unidades fenileno y etinil alternadas en el ciclo. La estructura más estable localizada para el complejo con C_{60} presenta una disposición diferente a la encontrada con el [10]CPP, y muestra los anillos hexagonales del fulereno perpendicularmente al nanoanillo. En el caso del complejo con C_{70}, el fulereno sigue presentando la disposición vertical con el eje mayor perpendicular al plano del nanoanillo. El [6]CPPA es demasiado pequeño para contener adecuadamente al C_{70} con su eje mayor dentro del anillo; de hecho, debido al menor tamaño del [6]CPPA se produce un ligero desplazamiento vertical del C_{70} fuera del anillo, así como una rotación de su eje para aumentar la superficie de contacto y, por lo tanto, las interacciones favorables entre los monómeros.

Considerando los complejos estudiados, se observa que los formados con [10]CPP son más estables que los formados con [6]CPPA. El motivo de esta estabilidad extra se debe a que en los complejos con [10]CPP hay más anillos aromáticos próximos a la superficie del fulereno, contribuyendo a la estabilidad del complejo mediante dispersión; los grupos etinil del [6]CPPA tienen menos átomos próximos al fulereno y por lo tanto su contribución es menor. Los resultados sugieren que la estabilidad dependerá de un ajuste entre los tamaños de la cavidad del anillo y el fulereno, así como del número de átomos próximos que contribuyen a la estabilidad (superficie de contacto).

Como ya se ha comentado, en este trabajo inicial se han considerado otros aspectos metodológicos. Así, se han probado diversos funcionales con dispersión empírica como el TPSS-D3, B3LYP-D3, BLYP-D2 o PBE0-D3, así como funcionales de uso general como M06-2X. Con todos los funcionales utilizados se obtienen tendencias similares para las estabilidades de los complejos, aunque en el caso del M06-2X se observa una clara subestimación de la estabilidad, por lo que no se recomienda su uso en este tipo de sistemas.

El **capítulo 5** es una extensión del capítulo anterior. Con el propósito de ampliar

el conocimiento acerca de los efectos del tamaño y disposición de los fulerenos en los complejos con [10]CPP y [6]CPPA se consideran dos nuevos fulerenos de tamaños menor (C_{50}) y mayor (C_{76}) que los estudiados en el capítulo anterior. En este caso tras el estudio inicial de la disposición del fulereno dentro del anillo se encuentra que el C_{50} se sitúa en el centro de los anillos a pesar de que su tamaño es relativamente pequeño comparado con el de las cavidades de los anillos. Si bien se forman complejos estables con el C_{50}, su estabilidad es significativamente inferior a la obtenida con C_{60} o C_{70}. Esto es evidentemente una consecuencia del menor tamaño del C_{50} que impide contactar de forma efectiva con la pared interior del nanoanillo. El C_{76} es un fulereno ligeramente grande para estos anillos; se obtiene una mayor estabilidad que con el C_{70}, pero el cambio es pequeño, mostrando que el aumento del tamaño del fulereno, una vez que éste presenta cierto tamaño y es capaz de llenar la cavidad del nanoanillo, casi no afecta a la estabilidad. Igualmente, estos resultados muestran que los anillos tienen cierta capacidad para deformarse y adaptarse a la forma de los fulerenos que se encuentran en su interior. Teniendo en cuenta estos resultados y los obtenidos en el capítulo anterior, se puede determinar que [10]CPP es capaz de encapsular adecuadamente a C_{60} y C_{70} a lo largo de su eje mayor, mientras que [6]CPPA es capaz de incluir al C_{60} de forma efectiva. De hecho, debido al tamaño ligeramente menor del [6]CPPA, el C_{76} se encuentra desplazado verticalmente a una distancia bastante considerable para así disminuir su sección y encajar en el interior del [6]CPPA, lo cual remarca el inadecuado tamaño de este fulereno para este anillo.

En el **capítulo 6** se estudian los complejos formados con unos anillos derivados del [10]CPP recientemente sintetizados por Kuwabara (T. Kuwabara, J. Orii, Y. Segawa y K. Itami, *Angewandte Chemie - International Edition*, 2015, **54**, 9646-9649). Estos nanoanillos modificados han sido sintetizados de modo que se incluye una unidad de antraceno en su estructura, convenientemente sustituida de modo que se corresponde a una antraquinona ([10]CPAq) o a una tetracianoantraquinona ([10]CPTcaq). El propósito de estas modificaciones es conseguir un nanoanillo en el que se encuentren simultáneamente dos bloques que actúen como dador y aceptor de electrones. Mediante absorción de radiación, los anillos parafenileno actúan como dadores mientras el grupo antraquinona o tetracianoantraquinona actúa como aceptor. Con el propósito de comprobar si estos anillos forman complejos estables con fulerenos y si puede darse transferencia de carga intermolecular entre nanoanillo y fulereno, se han estudiado los complejos de estos anillos sustituidos con los fulerenos más comunes C_{60} y C_{70}. Como sistema de referencia se utiliza el [12]CPP, que presenta un tamaño de cavidad similar.

Estos nanoanillos presentan una cavidad demasiado grande para los fulerenos considerados, por lo que, en las estructuras más estables, éstos se encuentran desplazados acercándose hacia los grupos fenileno, y en la mayoría de los casos alejándose del grupo antraceno. Como los fulerenos no son capaces de establecer interacciones favorables con todas las unidades del anillo, la estabilidad de los complejos es significativa pero inferior a las observadas con [10]CPP. A pesar de que la contribución principal a la estabilidad de los complejos sigue siendo la dispersión, se observa que la estabilidad relativa de las estructuras obtenidas viene determinada por el coste de la deformación del anillo para adaptarse a la forma del fulereno en su interior. La estabilidad de los complejos con C_{70} es mayor que con C_{60} debido a que en este caso el C_{70} puede situarse con su eje mayor en el interior del anillo, dando lugar a una mayor superficie de contacto.

El estudio de las transiciones electrónicas de los complejos se ha llevado a cabo em-

pleando el funcional CAM-B3LYP. Se observa que en los complejos formados con los nanoanillos sustituidos hay una mayor tendencia a que aparezcan transiciones intensas asociadas a transferencia de carga intermolecular desde el anillo hacia el fulereno. A pesar de que el grupo antraceno no participa directamente en estas transiciones, su presencia parece fundamental para que ocurran, ya que no se observan para el anillo de referencia [12]CPP.

Precisamente, se ha comprobado que un anillo conteniendo el grupo antraceno, pero sin los grupos ciano o quinona, forma complejos similares a los ya observados, si bien en este caso, el fulereno se desplaza hacia el grupo antraceno. La estabilidad de los complejos es similar a los ya observados, al igual que sus transiciones electrónicas, que también son parecidas a las observadas con [10]CPAq o [10]CPTcaq.

Aunque estos complejos presentan un comportamiento dador/aceptor adecuado, su estabilidad no es la óptima, por lo que se ha reducido el tamaño de los anillos, utilizando las variantes [8]CPAq y [8]CPTcaq, que tienen un diámetro similar al [10]CPP. Se ha comprobado que los complejos de C_{60} y C_{70} con estos anillos cumplen con el doble propósito de obtener estabilidades más altas, similares a las obtenidas para los complejos con [10]CPP, a la vez que mantienen las características electrónicas de los anillos más grandes; es decir, se observan transiciones asociadas a la transferencia de carga intermolecular entre anillo y fulereno.

El **capítulo 7** se dedica al estudio de complejos formados por fulerenos de diverso tamaño y naturaleza, atrapados en el interior del [11]CPP. El estudio se centra en la posible coordinación selectiva del [11]CPP, que permitiría separar determinados fulerenos de una mezcla, y por tanto ser empleado para purificar la misma. Para ello, nos hemos basado en el estudio experimental de Nakanishi (Y. Nakanishi, H. Omachi, S. Matsuura, Y. Miyata, R. Kitaura, Y. Segawa, K. Itami y H. Shinohara, *Angewandte Chemie - International Edition*, 2014, **53**, 3102-3106), en el que indica que el [11]CPP es capaz de extraer selectivamente C_{82}.

En este estudio se han utilizado fulerenos de distinto tamaño formados únicamente por carbono, C_{60}, C_{70}, C_{76} y C_{78}, así como diversos endofulerenos conteniendo un átomo metálico en su interior ($Y@C_{82}$ o $Tm@C_{82}$), dos átomos metálicos ($Y_2@C_{82}$ o $Lu_2@C_{82}$) o un pequeño agregado atómico ($Sc_3N@C_{80}$). Este conjunto de fulerenos presenta diversos tamaños y formas, así como distinta naturaleza debido a las especies endohédricas. Además, $Y@C_{82}$ o $Tm@C_{82}$ son especies de capa abierta mientras que el resto tienen todos sus electrones apareados.

Inicialmente se consideran los fulerenos formados por carbono, y se buscan los complejos más estables. Salvo el C_{60}, estos fulerenos no presentan estructuras esféricas, sino que corresponden a distintos elipsoides con variedad de tamaños según el eje considerado. Esta menor simetría de los fulerenos junto con la propia flexibilidad del [11]CPP hacen que existan una gran variedad de posibilidades para orientar al fulereno dentro del anillo. Una vez encontrada la estructura óptima para cada complejo, se obtiene su estabilidad, lo que permite concluir que el [11]CPP podría discriminar entre los fulerenos de menor tamaño, que no pueden interaccionar favorablemente con todas las regiones del nanoanillo, y fulerenos de más de 70 átomos, que pueden llenar la cavidad del anillo de forma efectiva. Al aumentar el tamaño del fulereno el número de contactos interatómicos también aumenta incrementando así la dispersión, y como ésta constituye la mayor contribución a la interacción entre el fulereno y el nanoanillo, esto conduce a una mayor estabilización

del complejo.

Con los endofulerenos se sigue un procedimiento similar, obteniéndose que en todos los casos las estabilidades son similares. Esto ocurre independientemente de las distintas formas de los endofulerenos, y tampoco se observa un efecto significativo de la naturaleza de la especie endohédrica. Incluso en los sistemas de capa abierta la estabilidad es similar a la de los otros endofulerenos. Estos resultados indican claramente que el factor controlante de la interacción son los contactos favorables entre la caja de átomos de carbono del fulereno y el anillo. A partir de un determinado tamaño, todos los fulerenos son capaces de establecer contactos favorables con todos los grupos fenileno del anillo, dando lugar a estabilidades similares. El apantallamiento producido por la caja carbonada del fulereno es tan efectivo que no se registra ningún efecto de la especie endohédrica en la interacción.

El análisis de los resultados de forma conjunta permite establecer que el [11]CPP sería capaz de separar selectivamente fulerenos mayores que C_{76} de una mezcla que también contenga fulerenos de menor tamaño. Sin embargo, no podría diferenciar entre los fulerenos C_{78}, $Sc_3N@C_{80}$ y las diferentes variantes de endofulerenos C_{82}.

En el **capítulo 8** se estudian los complejos formados por [10]CPP y endofulerenos que contienen un catión alcalino. El punto de partida de este capítulo es la observación experimental del endofulereno catiónico $Li^+@C_{60}$ y su complejo con [10]CPP. El $Li^+@C_{60}$ es un mejor aceptor de electrones que el C_{60}, y por tanto su uso podría se ventajoso en sistemas dador/aceptor. Por lo tanto, se consideran los complejos de [10]CPP con los endofulerenos $Li^+@C_{60}$, $Na^+@C_{60}$ y $K^+@C_{60}$ para determinar sus características y su capacidad para exhibir transferencia de carga intermolecular. Tras un estudio previo de la posición que ocupa el catión dentro del C_{60} y de cómo afecta a sus propiedades, se procede a determinar las estructuras más favorables de los complejos con [10]CPP. Para ello, se ha seguido un cribado previo de las diferentes estructuras aplicando el método DFTB3, reduciendo así muy significativamente el coste computacional. Tras este cribado previo, se han obtenido dos orientaciones claramente diferenciadas para cada uno de los fulerenos: orientado con dos anillos pentagonales o hexagonales perpendiculares al plano del anillo.

Las estabilidades de los diferentes complejos con $M^+@C_{60}$ son muy parecidas. Si bien la caja carbonada del fulereno apantalla los cationes de forma muy efectiva, se aprecia una mejora significativa en la estabilidad de los complejos comparados con el complejo formado con C_{60}. Esta mejora se debe a un incremento de las contribuciones electrostática e inductiva, a pesar de que la mayor contribución a la estabilización del complejo se debe a la dispersión, la cual no experimenta ningún cambio significativo asociado a la presencia de cationes en el interior del fulereno.

Sin embargo, la presencia de los cationes en el interior del C_{60} produce importantes cambios en el espectro de absorción de los complejos, de modo que aparecen nuevas bandas de absorción en torno a 700 nm que se corresponden a transiciones de transferencia de carga intermolecular entre el nanoanillo y el endofulereno. Estas nuevas bandas presentan una gran dependencia de la orientación del fulereno dentro del anillo, de modo que no aparecen si el fulereno está orientado con los anillos pentagonales perpendiculares al nanoanillo. En todo caso, el comportamiento observado parece indicar que este tipo de complejos podrían ser empleados de manera eficaz en dispositivos fotovoltaicos.

USC
UNIVERSIDADE
DE SANTIAGO
DE COMPOSTELA

Chapter 1

Introduction

1.1 Intermolecular interactions

One of the cornerstones of chemistry is the realization that molecules consist of a series of atoms which are held among each other by means of chemical bonds. The chemical bonds are normally strong enough to keep a fixed topological arrangement within a molecule that only changes when a chemical reaction takes place.

However, a different behaviour is observed when considering more than one molecule; while the molecules keep their identity, there are some physical phenomena producing the attraction and/or repulsion between a given molecule and the others surrounding it. This is clearly reflected in the macroscopic properties; for instance, in water, when the molecules become close to each other the interactions among them produce the formation of a condensed phase that allows to contain the molecules in a recipient; however, it is impossible to easily compress water more than a certain quantity because the repulsive forces among molecules would not allow it. This general behaviour indicates the presence of interactions among molecules that, even though they have a similar origin as chemical bonds, are typically weaker by several orders of magnitude and therefore lead to more subtle consequences. The most common form of the interaction energy can be expressed as a function of the distance between molecules (see Figure 1.1), showing an attractive region which becomes repulsive as the molecules come closer.

There are different classifications for the intermolecular interactions, for instance based on the repulsive or attractive character of the interaction. However, it is more common to classify an interaction according to the distance range where it acts effectively. Thus, in "long-range" interactions the energy depends of some inverse power of the distance between the molecules (R^{-n}) and reaches larger separations from the molecules, while in "short-range" interactions the energy decreases exponentially with the distance ($e^{-\alpha R}$), being effective only when the molecules are close by.[1–4]

1.1.1 Long-range interactions

Long-range effects can be divided into five contributions:[2,4]

1. **Electrostatic:** This effect comes from the classical coulombic interaction between the charge distributions of the molecules. The electrostatic interaction is strictly

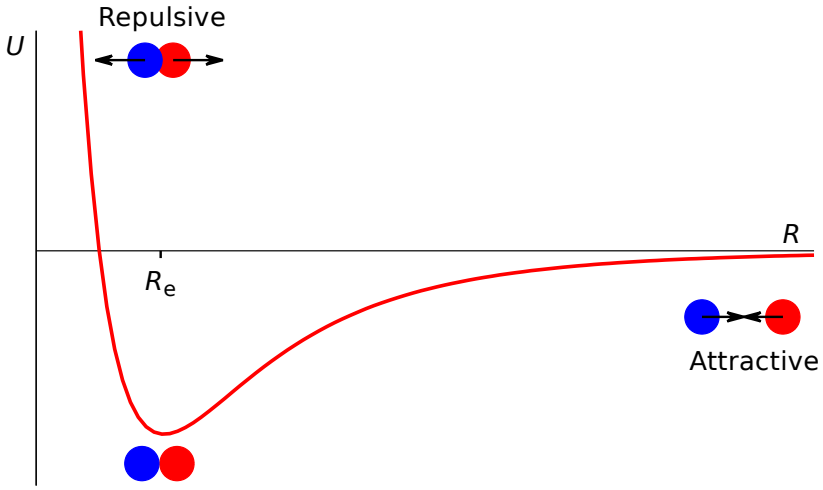

Figure 1.1: Typical intermolecular potential energy curve. This graph shows the variation of the energy with the distance between molecules (R), being R_e the equilibrium distance.

pairwise additive and can be attractive or repulsive depending on the orientation between the molecules. In order to represent the continuous charge distribution of the molecule, it is common to use a multipolar expansion approach. Thus, the charge distribution of the molecules is represented by a series of multipoles (charge, dipole, quadrupole, octupole, etc.) and the interaction is obtained as a series of charge–charge, charge–dipole, dipole–dipole, dipole–quadrupole, ... contributions. Depending on the nature of the interacting system more or less components are included. The distance dependency is particular for each of these terms, but in all cases it can be expressed as a R^{-n} decay and thus of long-range character. This description is only valid for large distances, because when the overlap between the charge distributions is important the multipolar approach breaks down.

2. **Induction:** Inductive forces appear when the charge distribution of a molecule is affected by an external field, the one generated by charged molecules or molecules with permanet multipoles. A polar molecule produces a distortion in the charge distribution of another neighbouring molecule, resulting in an induced dipole that always generates an attractive force between both species. This induction interaction is strongly nonadditive because it depends of all surrounding molecules that contribute to the electric field, and that can reinforce each other or cancel out. This interaction shows a $1/R^{-6}$ dependency with the distance for a dipole-induced dipole interaction; however, for the ion-induced dipole interaction the distance dependency is longer-ranged (decays more slowly with distance, $1/R^{-4}$). Due to this dependency with the distance, the inductive forces are considered as a long-range interaction.

3. **Dispersion:** Dispersion is a non-classical phenomenon, making its comprehension somewhat more difficult. Nevertheless, this interaction is found among all molecules and it is a fundamental aspect to understand their behaviour. It is specially important between molecules without charge or permanent multipoles.

   The first simple model to explain dispersion was developed in 1930 by London[5] as

a result from second order perturbation theory. The classical way to describe this effect is by considering that electrons are continuously moving through the molecule, originating instantaneous asymmetries in the charge distribution that lead to instantaneous dipole moments, giving rise to an attractive interaction. In fact, dispersion interactions favour the lower–energy configuration because the movements of the electrons between the two molecules are correlated. This intermolecular correlation depends on the distance between the molecules and for this reason the closer the molecules the larger the effect. The magnitude of dispersion can be correlated with the polarizability, the size and the shape of the molecules; when size and polarizability increase the dispersion raises too.

4. **Resonance:** The resonance interaction occurs in two possible situations: when one of the molecules is in a degenerate state, commonly an excited state, or when the molecules are identical but at least one is in an excited state. This type of interaction it not common because it does not occur in closed-shell molecules in their ground state.

5. **Magnetic:** The magnetic interaction is a tiny contribution, normally several orders of magnitude smaller than the previous ones. For this reason, it is the one that contributes less to the long-range interactions. It can be divided into two types, one that involves electrons and occurs when both molecules have unpaired spin, and another that involves the non-zero spin nuclei, more common but usually negligible.

1.1.2 Short-range interactions

These interactions are relevant when the distance between molecules is short, allowing a significant overlap between charge distributions. The presence of significant overlap and exchange effects makes more difficult a proper identification and description of the different interactions, though the most commonly considered ones are the following:[2,4]

1. **Exchange:** The exchange energy usually groups two factors. The first one is an attractive term caused by the looser movement of the electrons around the entire molecule. This leads to an increase in the uncertainty in the position of the electrons and to a decrease in the energy of the molecule. On the other hand, a repulsive term is due to the electrons trying to occupy the same region in space. However, when the electrons have the same spin this movement is forbidden by the Pauli exclusion principle, creating a low-density region. Due to the depletion in density, the nuclei are partially unshielded so they repel each other introducing a repulsion effect.

2. **Charge transfer:** Mulliken in 1952 introduced the term charge transfer for molecular complexes.[6] These molecular complexes have an electron acceptor with a high electron affinity (poor-electron species) and an electron donor with a low ionization potential (electron-rich component). Upon the formation of the complex, electrons are transferred from the donor to the acceptor. This is a controversial term, since in many of the theoretical formulations of intermolecular interactions is not defined explicitly but it is a part of the induction contributions. It is also a term largely

affected by basis set incompleteness that can produce large unphysical values. Nowadays it is still a discussing matter, and its role usually depends on the theoretical framework employed.[7–10]

3. **Charge penetration:** This effect occurs at short distance when the charge clouds overlap significantly and penetrate each other. In this situation, part of the electron cloud of a molecule is close to the nuclei of another one, experiencing an electrostatic attraction. This is the part of the electrostatic interaction that cannot be represented by means of multipolar expansions.

1.2 Supramolecular chemistry

Most of the chemistry traditionally deals with the formation and breaking of chemical bonds, while non-covalent interactions have played a minor role and have been scarcely employed as a design parameter or controlling motif of the processes.

Despite existing studies about molecular complexes dating from 1967 in which the discover of crown ethers opened the doors of the host-guest chemistry,[11] it was in 1978 when Jean-Marie Lehn put forward the possibility of chemistry based on non-covalent interactions: "Just as there is a field of molecular chemistry based on the covalent bond, there is a field of supramolecular chemistry, the chemistry of molecular assemblies and of the intermolecular bond".[12]

This opened the field of supramolecular chemistry, which employs non-covalent interactions as controlling motif in order to organize and modify molecular systems. The final boost for supramolecular chemistry was given in 1987 when Donald J. Cram, Jean Marie Lehn and Charles J. Pedersen won the Nobel Prize "for their development and use of molecules with structure-specific interactions of high selectivity". Nowadays, supramolecular chemistry not only covers the formation of complexes of two components interacting by means of non-covalent bonds; besides these it includes many fields such as biological processes, catalysis, developing of new materials and medicinal chemistry. This large interdisciplinary nature allows the participation of many scientific disciplines like physicists, biologists, theoretical modellers or synthetic organic chemists.[13]

Within the supramolecular chemistry, one of the most active fields is the design of receptors that can interact with a given species or family of species (see Figure 1.2). To design proper receptors there is a need of a profound knowledge of the nature and characteristics of the non-covalent interactions governing the process. Instead of describing the interactions in terms of long-range and short-range contributions as commented above, it is much more common to rationalize the interactions considering typical interacting motifs that correspond to the presence of a functional group or group of atoms. In such a way, there is a list of different non-covalent interactions that can be employed and considered for explaining a given process or for designing a suitable receptor.[14–17] All these interaction types correspond in the last term to the contributions described above: electrostatic, induction, dispersion, repulsion, etc. A short description of the most typical ones follows.

- Ion pairs: the strong interaction between charged species can be a powerful controlling motif. Ion pairs are usually very strong, though their effect is much diminished in the presence of polar solvents.

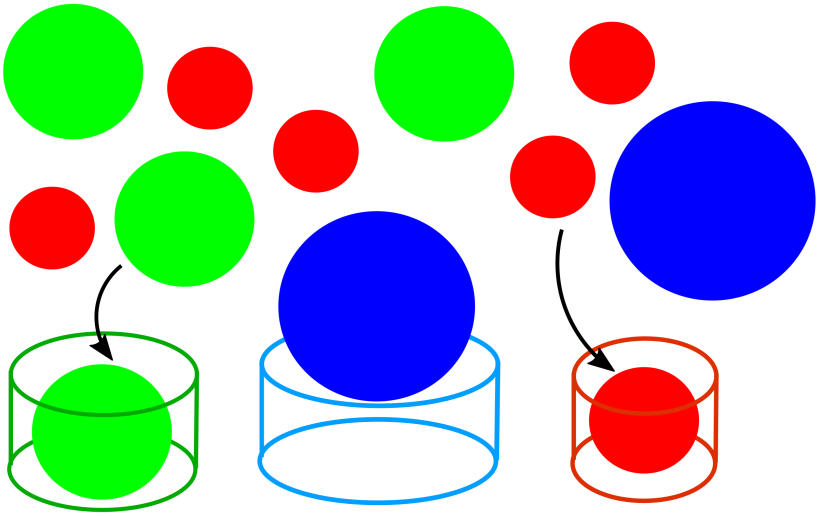

Figure 1.2: Schematic diagram for the host-guest interaction.

- Hydrogen bond: probably the most widespread intermolecular interaction, with multiple applications. It is a moderately strong interaction present in a multitude of systems. Its marked directionality makes hydrogen bond a good option for directing different species to be located at proper relative orientations.

- Sigma-hole interaction: quite recently a series of new interaction types sharing common features has emerged, all displaying a so-called sigma-hole, corresponding to a positive region on the region opposite to a bonded atom, making them suitable for interacting with electron-rich regions. The first interaction of this kind was the so-called halogen bond, quickly followed by other similar contacts such as the chalcogen bond or the pnictogen bond. These interactions show also great directionality and can complement the role of hydrogen bonds.

- Aromatic interactions: aromatic species interact in a specific way that can be exploited for controlling the behaviour of the systems. There are different ways that an aromatic moiety can interact with another molecule, but the most relevant are the $\pi\cdots\pi$ interaction, the X-H$\cdots\pi$ interaction and the ion$\cdots\pi$ interaction. Since aromatic interactions are the main subject in this thesis, they will be described in greater detail.

1.3 Interactions between aromatic systems

Non-covalent interactions comprise a wide range of interactions that depend on the nature and the characteristics of the interacting species. The interactions involving aromatic species are common in many systems, and crucial for understanding the structure of, for instance, DNA or proteins, as well as for designing new drug receptors and pharmaceuticals.[18–21] The presence of the aromatic species introduces specific characteristics to the interactions not observed when aliphatic units are involved.[3,22–30]

1.3.1 X-H$\cdots\pi$ interactions

The hydrogen bonding between a X-H system, usually C-H, N-H and O-H, and a π cloud has been extensively studied because it is present in a large number of situations like the structure of biological molecules, the control of biochemical processes or the arrangement of crystal structures.[31] Usually the distance between the hydrogen atom and the π cloud is between 2.4 and 3.2 Å, a larger distance than the typical hydrogen bond as in O-H$\cdots$O or N-H$\cdots$N.

The first report that mentioned the presence of a X-H$\cdots\pi$ interaction was in 1952,[32] when Tamres noted the presence of an attractive interaction between a C-H group and a π-system. He found that the presence of this kind of interaction is the reason why chloroform can dissolve in benzene. In recent years experimental evidence of this kind of interaction was found, usually using spectroscopic methods; the most common are the nuclear magnetic resonance (NMR) and infrared (IR) spectroscopy.[33–35] Despite of the relatively weak X-H$\cdots\pi$ hydrogen bonds (about 2$-$4 kcal mol^{-1} for O-H$\cdots\pi$ and N-H$\cdots\pi$ and even weaker for C-H$\cdots\pi$, 0.5$-$2 kcal mol^{-1}) they are still important for the supramolecular geometry due to the additive effect, since many weak interactions can produce a huge effect.[24]

The X-H$\cdots\pi$ interaction has a different nature than conventional hydrogen bonds. After many works[31,36–39] it has been found that the main contribution to the interaction is usually dispersion, in contrast with the behaviour found in conventional hydrogen bond, usually dominated by electrostatics. However, this typical behaviour may have exceptions, as in the presence of highly acidic C-H bonds, in which the electrostatic component predominates.[23] When the carbon atom is exchanged for nitrogen or oxygen (N-H$\cdots\pi$ and O-H$\cdots\pi$) the electrostatic component also dominates the interaction energy and the interaction is more susceptible to the electronic nature of the substituents of the arene. Finally it is worth mentioning the directionally of the bond; conventional hydrogen bonds are strongly directional because the main component is the electrostatic, usually giving place to a linear bond; opposite to this and due to the more dispersive nature of the C-H$\cdots\pi$ interactions, it is possible to find some bonds with an angle up to 30° with a minimum loss in the interaction energy.[17,23,31,40]

1.3.2 Ion$\cdots\pi$ interactions

Another different interaction with a π cloud is established between a charged species and a π-system. In 1981 Kebarle *et al.*[41] performed the first experimental evidence of the cation$\cdots\pi$ interaction in gas phase between a K^+ cation and benzene.[26] This cation is more strongly stabilised in benzene than in water, showing a preference for the molecule with the π cloud despite of the lone pairs and the large dipole moment of water.

The cation$\cdots\pi$ interactions have some important applications in different fields. One of them is in biological systems, in which the preferent selection of the K^+ cation in potassium channels is due to the cation$\cdots\pi$ interaction.[42] Another important application is their role in the protein structure since several works show the importance of these interactions for the higher-order structure of the proteins.[26,43] Moreover, the presence of the cation$\cdots\pi$ interaction between enzyme and substrate can stabilise the transition state and reaction intermediates giving rise to a decrease of the reaction barrier.[26] Finally, the cation$\cdots\pi$ interaction is fundamental in some biological receptors, for example, the

preference of the nicotine for the brain receptors is due to the formation of these kind of interactions.[44]

The most important contribution to the interaction energy in this kind of interaction is the electrostatic component. When the interaction between alkali cations and benzene are analysed in gas phase a clear electrostatic trend is showed: the most stable complex is formed with the lithium cation and the less stable one with the rubidium cation, following a classical electrostatic sequence. If dispersion were the main contribution then the higher size of the rubidium would lead to a better interaction, but this is not the case.[45] A simple way to obtain a qualitative idea of the bond strength is to use the molecular electrostatic potential. Through this methodology it is possible to obtain an approximate idea of the electronic character of the π cloud and the more negative the potential the stronger the cation$\cdots\pi$ interaction.[46]

However, despite of the importance of the electrostatic component of this interaction, there are other factors such as charge transfer and polarization that also contribute to the interaction. Actually the fraction of the electrostatic component that contributes to the interaction energy varies according to the specific aromatic system. For example, the contribution of the electrostatic is *ca.* 60% in Na$\cdots$benzene but it is practically null for the Na$\cdots$1,3,5-trifluorobenzene,[47] so usually the nonelectrostatic component of these interactions is mostly related to the polarizability of the aromatic ring. Therefore, if a molecule with a dipole moment is near to a cation and this is placed in the right way, at the end of the dipole, both molecules experiment a favourable interaction. Nevertheless, in the case of benzene there is not a dipole but a quadrupole that produces a nonspherical charge distribution around the molecule that shows favourable positions for the interactions between the cation and benzene. Thus, the electronic distribution around the molecule due to the quadrupole is usually employed as a guide to distinguish the most favourable locations to place the cation and to show the effects of the different substituents. In general, the electron donating substituents increase the strength of the interaction, while the withdrawing substituents decreases it.[48]

Of course, this is a simplified description of the cation$\cdots\pi$ interaction. Induction contribution can be significant, as already shown in different works.[49–54] In fact, induction can be the responsible of the stability of the complex in cases where the electrostatic term is repulsive.[49] Carrazana-García *et al.* showed that the induction component for the cation$\cdots\pi$ interaction in curved aromatic systems is an important contribution, though when the cation increases its size dispersion can be the dominating factor.[49,50]

All the previous trends are in the gas phase, but the environment can have a deep impact on the characteristics of the cation$\cdots\pi$ interaction. The presence of the solvent changes the order of stability of the complexes between alkali metals and benzene, so it becomes $K^+ > Rb^+ \gg Na^+ > Li^+$ in water. The explanation comes from the fact that there is a competition between the solvation effects of water and the cation$\cdots\pi$ interactions. The K^+ cation is less strongly solvated than Li^+, so it requires less desolvation energy to be free and bind to benzene. On the other hand the desolvation energy for the Li^+ is too high to bind with the aromatic system.[42] In the case of aromatic solvents there is a dependence on the dielectric constant, so when the dielectric constant increases the strength of the cation$\cdots\pi$ interaction slightly decreases.[55]

Different studies on the microhydration of cation$\cdots\pi$ systems showed a complex arrangement of water molecules and aromatic species around the cation. As the size of

the cation increases, the hydrogen bonds with water molecules become more competitive and not all water molecules are coordinated to the cation, which eventually can be surrounded only by water molecules breaking the cation$\cdots\pi$ contact.[56–59] Also, the presence of other aromatic species interacting with the cation and the counteranion can modify the intensity of the cation$\cdots\pi$ interaction.[60]

On the other hand, anion$\cdots\pi$ interactions describe the interaction between a negatively-charged species and a π cloud of an electron-deficient arene. Contrary to what was expected (a repulsion between the cloud and the anion) there are experimental and theoretical evidences of the formation of these non-covalent interactions.[61–64] The main mechanism for the formation of these interactions is the ability to modulate the electron donor capacity of the aromatic ring through withdrawing substituents, so, converting the aromatic ring in an electron-deficient ring allowing an attractive interaction. These anion$\cdots\pi$ interactions are usually dominated by electrostatic and induction components. The electrostatic component can be explained through the quadrupole of the aromatic ring. So, when this quadrupole moment shows a positive value perpendicular to the ring plane then a favourable interaction is established. For the benzene molecule this quadrupole is negative in this direction, but when some withdrawing substituents are attached to the ring this quadrupole can be turned into positive. Another possibility to obtain a positive quadrupole moment is through the use of heteroaromatics rings, in special those with nitrogens. As in the case of cation$\cdots\pi$ interactions the substituent effects usually follow the trend based on the electrostatic character. On the other hand, the polarization contribution to the interaction energy is due to the interaction between the ion and the generated induced dipole. Small anions induce greater polarization what translates into a strengthening of the interaction. Finally, it should be kept in mind that anion$\cdots\pi$ interactions are dominated by electrostatic contributions when the quadrupoles are very positive, whereas in the case of small quadrupoles the polarization dominates the interaction.[23,24] Also, the presence of the counterion has a significant effect modulating the strength of the anion$\cdots\pi$ interaction.[65–68]

Several studies between substituted buckybowls (bowl-shaped polycyclic aromatic compounds) and anions showed that these interactions are dominated by the electrostatic contribution followed by dispersion. Moreover, the less negative charge of the concave face in these bowls leads to a preferential interaction of the anion with this face.[66–69] The presence of the counterion modulates the anion$\cdots\pi$ interaction. Finally, and with the purpose to analysing the behaviour of a mixture of these interactions, a complex formed by a cation, an anion and a π-system was studied. So, when the anion interacts with the cation$\cdots\pi$ system the main contribution to this interaction is the polarization, whereas the interaction between the cation and the π-system is dominated by the electrostatic contributions.[65]

1.3.3 $\pi\cdots\pi$ interactions

The non-covalent interactions between neutral aromatic systems are denoted as $\pi\cdots\pi$ interactions. The description of this kind of interaction began to be extensively studied after 1990, when Hunter and Sanders proposed a simple model to explain the different geometries observed between interacting aromatic systems.[70] The proposed model is based in two steps, firstly the electrostatic effects, which determine the geometry of the inter-

acting system due to the repulsive and attractive forces; and secondly the van der Waals interactions that indicate how strong is the interaction.

The $\pi\cdots\pi$ stacking interactions for the well-studied benzene dimer lead to three different geometries: parallel stacked (PS), parallel displaced (PD) and "T"-shaped which corresponds to a X-H$\cdots\pi$ interaction (see Figure 1.3). The "T"-shaped and PD geometries have a similar stability while the PS geometry is significantly less stable. The quadrupoles of the different orientations as shown in Figure 1.3 reveal that the most stable geometries, "T"-shaped and PD, reflect interactions between positive and negative regions while the PS geometry shows an interaction between negative regions producing an electrostatically repulsive interaction.

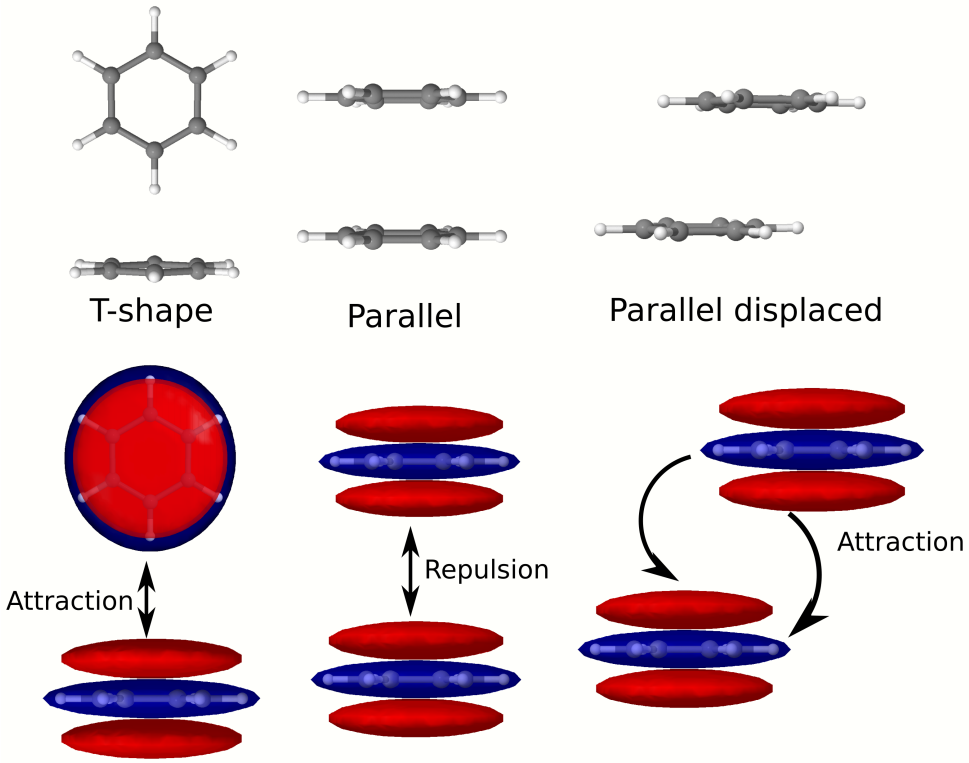

Figure 1.3: Different benzene dimer structures accompanied by a schematic representation of the quadrupole. The blue surface represent a region with a positive potential while the red surface is a negative potential region.

Nowadays, after several *ab initio* works it is considered that the dispersion is the main component in the $\pi\cdots\pi$ interaction; however, a large amount of this energy is cancelled by the exchange repulsion.[71–73] On the other hand, the electrostatic contribution is useful when the interaction strength is compared across several substituted homologues because it gives an idea of which establishes the strongest interaction.[36,74–79]

According to the π-polarization model developed by Hunter and Sanders,[70] the insertion of an electron-withdrawing substituent in the aromatic ring decreases the repulsion between the π clouds because it removes a portion of the electron density of the π-system through resonance. On the other hand the introduction of an electron donating group should destabilise the complex due to a weaker interaction between the π-systems. Nevertheless, in recent years this model has been a source of controversy because many

ab initio studies suggest that the presence of electron-donating or electron-withdrawing substituents always increase the strength of the $\pi\cdots\pi$ interaction compared with the interaction in the benzene dimer.[23,80] A new model developed by Wheeler and Houk[81] suggested that the π-system of a substituted benzene is not involved in the interaction in the benzene dimer with the PS configuration. The increase of the stability in these complexes arise from the direct electrostatic interaction between the substituent and the other ring. Moreover, the dispersion interaction between the substituents and the other ring improves the stability in most cases. Some years later the validity of this model was confirmed by a theoretical work of Sherrill.[82] However, most of the works have been performed with a phenyl ring and Cabaleiro-Lago and Rodríguez-Otero showed that the model of Wheeler and Houk fails when trying to estimate the substituent effect in extended aromatic systems because the model predicts a fast change of the molecular electrostatic potential that does not actually happens.[83] In fact, Sherrill indicates that both mechanism (Hunter-Sanders and Wheeler-Houk) are present though the Wheeler-Houk one dominates. Finally, it is worth noting that the increment of the size of the aromatic ring (naphthalene, anthracene, tetracene and so on) leads to an increase of the interaction energy between the monomers due to the decrease of the negative charge of the π cloud placed in a PS geometry.[84] Nevertheless, Cabaleiro-Lago and Rodríguez-Otero found that the increase of the size of these molecules leads to an increase in dispersion, being this contribution the main reason for the enhancement of the interaction energy and not the decrease of the negative charge as other authors postulate.[74]

1.3.3.1 Concave–convex $\pi\cdots\pi$ interactions

During the last years, the large development of fullerene chemistry led to a side effect, a new group of $\pi\cdots\pi$ interactions established between curved systems. This interaction called curved $\pi\cdots\pi$ interaction or concave–convex $\pi\cdots\pi$ interaction should be different to the interaction established between flat π systems. The main difference is a result of the polarization of the concave and convex sides of the curved π-systems such as fullerenes or corannulenes.[85]

The knowledge of concave–convex $\pi\cdots\pi$ interaction seems essential for many fields like supramolecular chemistry between fullerenes and belt-shaped molecules or the crystal structure of corannulene or fullerenes. Therefore, a big effort has been spent for a better comprehension of this kind of interaction. In 2009 Sygula and Saebø studied the concave–convex $\pi\cdots\pi$ interactions between corannulenes exploring the curvature effects leading to some important conclusions:[86]

1. While the planar system prefers a staggered conformation, the corannulenes establish better interactions when the monomers are in an eclipsed conformation.

2. In curved systems a significant part of the interaction energy comes from the electrostatic dipole-dipole attraction, which is absent in planar dimers, although dispersion in curved systems still remains the main component of the interaction energy. Despite of the electrostatic contribution in curved systems, the interaction energy for both types, planar and curved, has a comparable magnitude.

Some years later, Kennedy *et al.*[87] carried out a study that shows the importance of curvature. Corannulenes lead to a different behaviour of all the main components of the in-

teraction energy according to the SAPT methodology (dispersion, electrostatic, exchange and polarization). The difference is due to a decrease of the average interatomic distance between monomers affecting mostly to dispersion and exchange components. Finally they show a correlation between the curvature of the molecule and the interaction energy; if the curvature increase then the interatomic distance decreases and the interaction energy increases. However, later studies do not find any evidence of this trend.[88,89]

Josa *et al.* focused a considerable effort in the study of $\pi\cdots\pi$ interaction and specifically among curved systems. They found that the main contribution for the $\pi\cdots\pi$ interactions in these systems is the dispersion energy but some part of the interaction energy came from the electrostatics. Moreover the presence of $CH\cdots\pi$ interactions in curved systems can lead to an improvement of the interaction energy due to an increase in the dispersion contribution.[88,90–92] Some years later, Cabaleiro-Lago *et al.* studied the concave–convex $\pi\cdots\pi$ interaction using Symmetry Adapted Perturbation Theory (SAPT) and obtaining that the main contribution of these kind of interactions is the dispersion, followed by electrostatics, what agrees with the results obtained by Josa. Furthermore, in these curved systems the presence of substituents produces a change in the same amount of both contributions, dispersion and electrostatics.[93] Lastly, it should be noted that the stability in curved systems is defined by the amount of surface in contact between molecules, even though other effects like $CH\cdots\pi$ interactions can modify this behaviour.

1.4 Curved $\pi\cdots\pi$ systems

1.4.1 Fullerenes

One obvious candidate for using curved $\pi\cdots\pi$ interactions as a tool for recognition are the convex surfaces of fullerenes. Fullerenes were discovered in 1985 by Richard Smalley, Robert Curl, and Harold Kroto,[94] who in 1996 were awarded with the Nobel prize in chemistry for their discovery.

Although their discovery was in 1985 it was five years later that their synthesis in gram scale was possible, allowing for these species to be widely used.[95] Pristine fullerenes are the third carbon allotrope, comprising a series of closed carbon nets of diferent composition. The most common fullerene is the buckminsterfullerene, C_{60}, a spherical structure formed by sixty carbon atoms associated in twelve pentagonal and twenty hexagonal faces (see Figure 1.4). Its name was chosen in honour to the american architect Richard Buckminster Fuller, due to the geodesic domes of his constructions.

The second most abundant fullerene is C_{70}, a structure with the shape of a rugby ball formed by seventy carbon atoms. During the past few decades more fullerenes were characterized and isolated. Several theoretical investigations were performed to find the stability of small fullerenes, discovering that the C_{26} or C_{28} structures are stable.[96] However, the smallest fullerene found in experimental abundance is C_{32} and in the case of C_{30} only weak signals are found.[97] On the opposite side the biggest fullerene would contain more than 400 atoms of carbons, giving rise to large structures.[98]

A further complication when dealing with fullerenes is that for each composition there could be a large number of different isomers showing different carbon cages.[99,100] As a simple rule for explaining the stability of some isomers over others, Kroto proposed the so-called Isolated Pentagon Rule (IPR),[101] according to which each pentagonal ring in

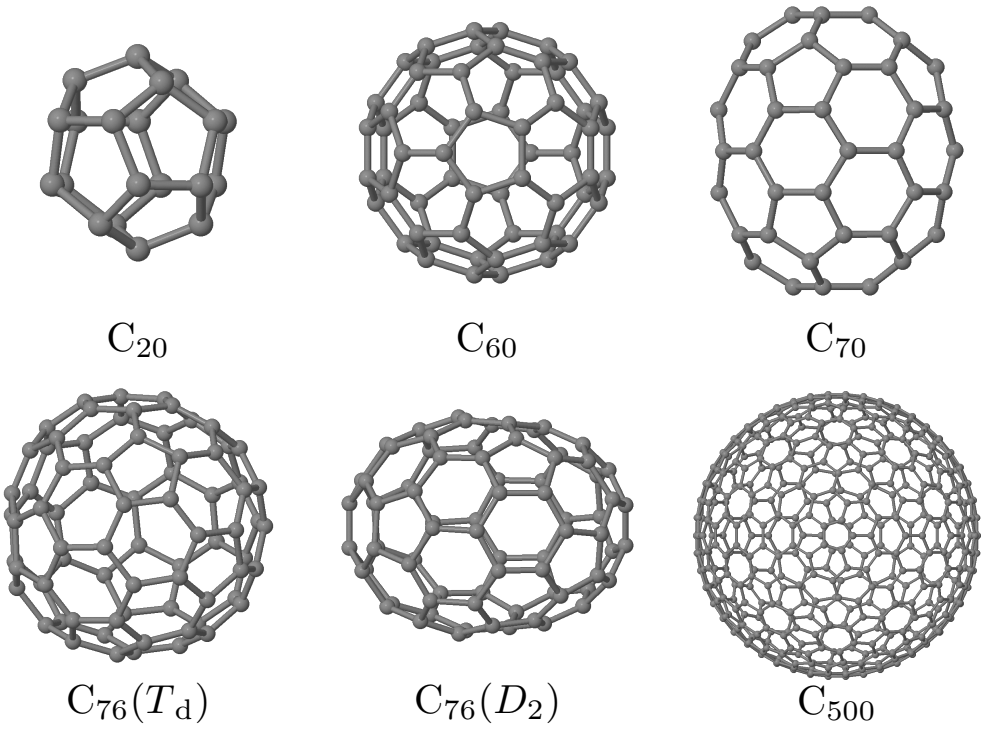

Figure 1.4: Structures of differents fullerenes and isomers.

a stable fullerene must be surrounded by five hexagonal rings. Thus, even when many possible isomers are possible, only those complaining with the IPR will be stable. Of course, for a given fullerene there could be more than one isomer fulfilling the IPR, as it is the case for example of C_{76}, with two IPR isomers with different symmetry (see Figure 1.4).

The smallest fullerene that is theoretically possible to create is C_{20}; however, there is little experimental evidence of its formation because the structure is only formed by pentagonal carbon structures, that entails a strongly unstable structure. The presence of two pentagon structures sharing an edge breaks the IPR and leads to a structure with low stability. However, it is possible to find a similar carbon structure with hydrogen substituted in all the carbon atoms ($C_{20}H_{20}$). Moreover, some synthetic routes starting with this substituted fullerene showed promising results to synthesize C_{20}.[102,103]

Fullerenes have a higher heat of formation than graphite or diamond. This means that fullerenes are thermodynamically less stable; nevertheless, it is expected that the difference in energy decreases when the size of the fullerene increases. Measurements of the electron affinity (E_A) show that the increase of the size of the fullerene entails an increase of the E_A. Most of the properties are referred to C_{60} and C_{70} due to their higher abundance; therefore, most of the works are focused on these fullerenes. The electronic absorption spectra of these fullerenes shows stronger absorption in regions between 190 and 410 nm, but the transitions that correspond to the visible region (400−700 nm) are weaker as a result of orbital forbidden singlet–singlet transitions.[100]

Fullerenes are often obtained by means of an arc discharge, producing a soot with a mixture of different fullerenes. Thus, the purification step is extremely relevant to

separate among different fullerenes. The first technique to purify a mixture of fullerene was through simple sublimation with a Bunsen burner;[104,105] however, the most popular technique used through the years is extraction.[100] The C_{60} and C_{70} fullerenes are easily dissolved in hexane but bigger fullerenes are not extracted with this solvent. However, if a solvent with higher boiling point is used then the higher fullerenes are extracted with the mixture of C_{60} and C_{70}. Another technique widely investigated is the liquid chromatography using reverse phase due to the poor retention times in the normal phase. A better performance is obtained using aromatic eluents and a better selectivity is found at low temperatures using liquid chromatography. Another alternative is the use of supercritical fluids, but the fullerenes are not soluble in CO_2, so it is necessary a mixture with toluene for a more effective extraction; nevertheless only the surface of the soot is extracted with this procedure, but it allows a selective extraction of fullerenes changing the temperature, the pressure and the toluene/CO_2 ratio. The use of activated charcoal has been employed, too; the most commonly used is Norit A, in which the mixture with a determined amount of silica gel is extremely important to avoid the irreversible adsorption of the fullerenes in the charcoal; nevertheless a portion of the fullerenes are stuck in the charcoal. Finally, crystallization is used to increase the purity of C_{60} until 99.5% though a previous chromatography process is necessary.[106]

The knowledge of fullerene solubility seems crucial for the purification of these molecules. The most common solvents for C_{60} and C_{70} fullerenes are aromatic solvents or carbon disulfide, being insoluble in water or polar organic solvents. Thus, the insolubility in water is one of the big problems to use fullerenes in biological processes. However, when the fullerene is functionalized, adding hydrofilic compounds, it is possible to increase its solubility in water.[107] The behaviour of solubility can be extended to larger fullerenes with higher band-gaps, such as C_{76}, C_{78}, C_{84} and so on, but smaller fullerenes or C_{74} with a small band-gap do not follow this behaviour, since these last compounds are insoluble in organic solvents.

Overall, the main method to purify the mixture is through chromatography[108] due to the large range of solubility of fullerenes in different solvents. However, in the last decades the use of supramolecular compounds to purify a mixture of fullerenes has been considered. These supramolecular receptors can be very selective, but their synthesis entails some difficulties due to the large size of the hosts.[109]

In the last years a large number of investigations focused their attention at donor/acceptor systems and in particular using C_{60} as acceptor due to its high electron affinity and small reorganization energy. The reorganization energy is one of the variables that controls the rate of electron transfer and the lower its value, the higher the rate. Another important characteristic of fullerenes is that the electrons are delocalized over the whole fullerene, therefore the radicals formed are very stable. Moreover, other feature that enhances the use of C_{60} in photochemistry is that the crystal structure exhibits a n-type semiconductor behaviour with a band gap of 1.5 eV that is the optimal value for photovoltaic devices of single junction type.[108]

The chemistry of fullerenes is complex and in the case of higher fullerenes it is still in its first steps due to the difficulty to obtain a large quantity of isomerically pure compounds. However, the properties of these higher fullerenes are similar to C_{60} and it would be expected that the chemistry of these molecules would also be similar to the one observed for C_{60}. There are two main chemistries regarding fullerenes: endohedral and exohedral.

The endohedral chemistry is more difficult to explore due to the challenging process to obtain an experimental suitable model, which helps to understand the chemical behaviour of the inner side of fullerenes, for this reason there are less variety for endohedral than exhohedral compounds. The most known compounds are metallofullerenes or noble gas guest which are useless to study covalent bond formation inside the fullerenes; these compounds are described in more detail below. On the other hand the exohedral chemistry has been widely explored during these last years obtaining a large number of different reactions classified in two main types: reductions and additions. Within the addition group is possible to distinguish among the nucleophilic or electrophilic reactions, cycloadditions and reactions with free radicals or transition metal complexes. A large number of these addition reactions are exothermic because they reduce the strain energy of the C_{60}.[100]

As a result of these properties and the vast number of chemical reactions, fullerenes exhibit a large number of applications in many different fields, from material science to pharmacology. They can be used in drug delivery, because they have been shown to be relatively non-toxic compounds in some studies in vitro or in vivo. Moreover, another possibility is funcionalising their surface, leading to changes in properties like solubility or the ability to cross the cell membrane.[110] Furthermore, their antioxidant character allows them to be used in cosmetics, like sun protection cream.[111] Finally, some studies show their antiviral or antibacterial activity and they can be used to fight against some infections.[108,111,112]

However, one of the most important applications in the last years is their use in organic solar cells due to some inherent properties of fullerenes.

1.4.1.1 Organic photovoltaic cell

The organic photovoltaic cell (OPVC) is a photovoltaic cell that uses organic semiconductors for light absorption and charge transport. Using different fullerene derivatives has allowed an improvement in the power conversion efficiency from 1% to 12% in recent years.[113]

The widespread use of fullerenes and their derivates as acceptors in OPVC is because they have a higher electron affinity than polymers or small molecules in this kind of devices, although alternatives to fullerenes have been proposed recently.[114,115] The OPVCs are characterized by the presence of a donor and an acceptor material which generate the photocurrent. In particular these OPVCs belong to the excitation cell group because after the light radiation affects the material an electron-hole pair strongly bound is generated. The general mechanism in OPVs is shown in the Figure 1.5.

When the donor material is irradiated with light, one electron in the donor is excited from the HOMO to the LUMO. However, it is necessary the presence of an acceptor with the purpose to create an intrinsic internal field that allows to release the exciton and move through the interface. In a second step, the exciton must diffuse some distance called diffusion distance (L_D) toward the interface to avoid the recombination to the fundamental state. In the third step the exciton suffers a charge transfer (CT) process with the purpose to form a CT exciton. The hole formed by this transference is found in the donor while the electron moves to the acceptor. Even though the distance between the electron and the hole increases, their are still bounded through coulombic forces. The last step is the transportation of the hole and the electron through their respectively phases to the anode and the cathode.

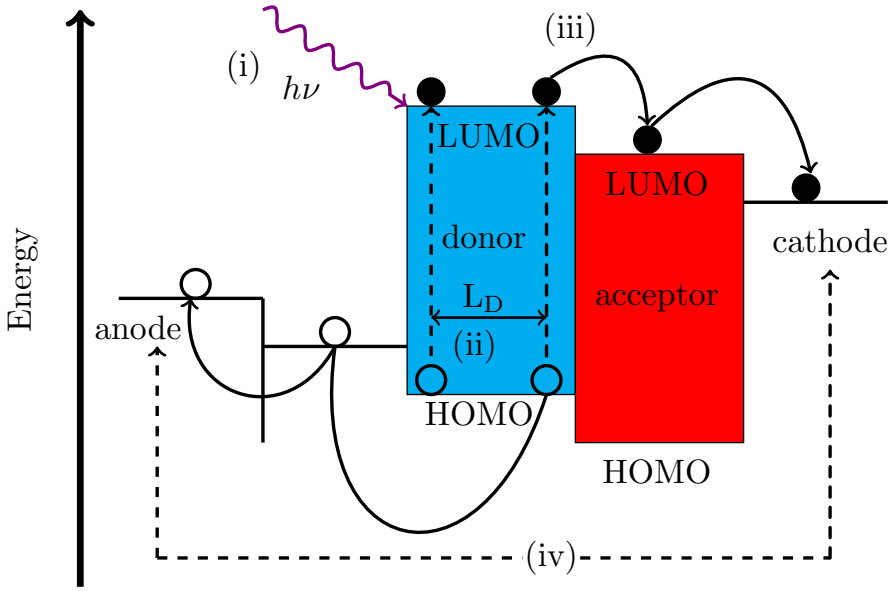

Figure 1.5: Scheme of an organic photovoltaic cell.

The use of OPVC has several advantages over inorganic solar cells, like a decrease on the manufacturing cost, an easy manufacturing of the device, and they are harder materials and they reduce the contamination during the synthesis. However, there are not only advantages, in OPVC the correct choice for the active space between the donor and the acceptor and its morphology are extremely important to generate an effective current in the cell. For these reason, there could be an advantageous idea to exploit intermolecular interactions to develop a favourable interaction and orientation between fullerene and acceptor.

1.4.1.2 Endohedral fullerenes

In any case, despite of the interesting properties of the pristine fullerenes, one of the most fascinating properties is the possibility of fullerenes of containig other species into their cage. The cage formed by carbon atoms and the atoms or complexes inside are known as "endohedral fullerenes", though the IUPAC recommended the term "incar fullerene".[116,117] The first evidence of endohedral fullerenes dates from 1985[118] in which a lanthanum atom was detected inside a C_{82} carbon cage, but it was not until 1990 that this endohedral fullerene was isolated. During the 1990's many other metal atoms were put into the fullerene but the yield of the synthesis of all these molecules were very low (about 1%).

With the development of a deeper knowledge of these molecules the synthesis of the endohedral fullerenes has been improved and the yields rose. It is worth noting the family of metal-nitride clusterfullerenes, obtained when discharging the arch in the presence of nitrogen. In fact the $Sc_3N@C_{80}$ clusterfullerene is the third most abundant fullerene after C_{60} and C_{70}. After a couple of years of the metal-nitride clusterfullerenes synthesis, the first carbide clusterfullerene, $Sc_2C_2@C_{84}$, was synthesized[119] and in further years the improvement on separation techniques and synthesis dramatically increased the number of endohedral fullerenes available.[116,117,120]

However, not only metallic atoms are found inside the fullerenes. So, it is possible to incarcerate nitrogen, hydrogen or noble gases. These endofullerenes had been prepared heating C_{60} and applying high pressure in the presence of the gases. The main difference with the metallic endofullerenes is the possibility to release the gases incarcerate inside the fullerene increasing the temperature.

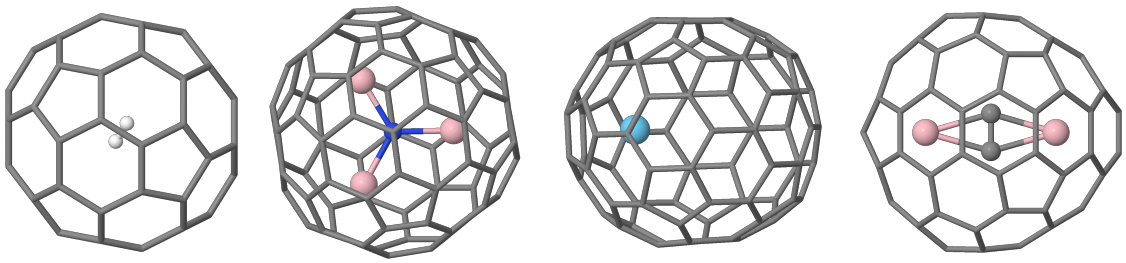

Figure 1.6: Different endohedral fullerene structures.

The study of these new fullerenes resulted in different structures, electronic and chemical properties than the pristine fullerene. In fact, it is most common that the strong interactions between the endohedral species and the carbon cage produces endofullerenes with a different carbon cage that the one obtained for the pristine fullerene. For instance the presence of a metal or a complex inside the fullerene can stabilise pentagons that share the same edge, leading to a invalidation of the well-know IPR.[121–123]

The most common applications of the endohedral fullerenes are in the biomedical field with a wide range of applications like in magnetic resonance imaging (MRI) or X-Ray as contrast agents, or in pharmaceuticals due to their resistance in metabolism and kinetic stability or their antitumour activity. Another use of these endohedral fullerenes is in organic photovoltaic cells like pristine fullerenes.[117]

1.4.2 Curved fullerene receptors

One of the most interesting fields in fullerene chemistry is the search for molecules that can act as a host for fullerenes. Many different molecules were tested with the purpose to obtain an excelent "catcher" for fullerenes. The first example was an azacrown ether in which the fullerene is incorporated into the cavity.[124] Following this approach other molecules with a cavity were tested, such as cucurbit[7]uril or γ-cyclodextrin being reasonably good hosts for fullerenes. In particular, the complexes formed between γ-cyclodextrin and fullerenes were extensively studied due to the biological application because they form water soluble compounds.

Other important complexes were formed by the combination between fullerenes and traditional hosts like calix[n]arene, oxacarix[3]arene, and cyclotriveratrylene. The crystal structure of these complexes shows that the host has a bowl shape and the fullerene is put inside this socket. These traditional hosts can be modified to obtain a stronger interaction with the fullerene; the better alteration is the introduction of strong donating groups, which increases the affinity for the fullerenes. Porphyrins have been also extensively studied as hosts for fullerenes due to their strong interaction, but also to a proper

donor/acceptor match suitable for OPVs.[73,125,126] Finally, subphthalocyanines can be used as host too, and different experimental and theoretical studies show the existence of an excellent interaction between C_{60} and C_{70} and subphthalocyanines.[73,127–129]

Significantly, some of the most interesting fullerene receptors are based on concave–convex π interactions. Therefore, the use of buckybowls, carbon nanotubes or nanoring with the same purpose that all the molecules previously mentioned is a reliable idea. In the next sections a deeper description of these molecules is developed.

1.4.2.1 Buckybowls

Buckybowls are bowl-shaped polycyclic aromatic compounds.[130] The first synthesis of these compounds dates from 1966 when Lawton and Barth after a long synthetic route finally obtained corannulene.[131] This 17-steps synthesis was the biggest problem in the study of corannulene; however, over the years more optimised routes were developed and a better comprehension of corannulene was obtained.[132,133]

Corannulene owes its curved shape to its proper structure formed by a pentagonal central ring surrounded by five benzene rings (see Figure 1.7). The 5-membered ring propitiates the curvature of the molecule because it is impossible to construct a planar structure formed by pentagons and hexagons. This curvature origins a structure with a bowl-shape with two different faces, concave and convex, which can display dissimilar properties. In particular, the molecular electrostatic potential of the convex face is more negative than the concave face.[134]

It was not until 2003 that sumanene was synthesized.[135] Its structure has a hexagonal ring at the centre and surrounded it an alternating succession of hexagons and pentagons. This bowl is deeper and it has an inversion barrier higher than corannulene.[136–139]

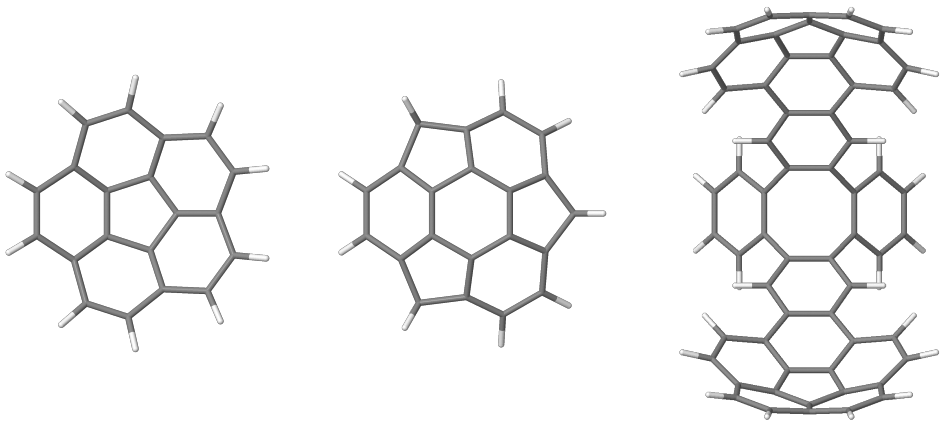

Corannulene Sumanene Sygula's tweezer

Figure 1.7: Different buckybowls.

One of the main points that researchers focus their attention is the possibility to form supramolecular complexes between buckybowls and fullerenes. The first experimental evidence of these complexes was in 1993, when Becker *et al.* found some proof of the formation of a supramolecular complex between C_{60} and cationic corannulene in gas

phase.[140] However, further studies in solution reported the formation of these kind of complexes but without any confirmation of the strong $\pi\cdots\pi$ interaction established between the fullerene and the buckybowl.[141] A couple of years later Sygula synthesized a tweezer composed by two corannulene pincers that allows to catch a fullerene among them; this showed that the interaction between these molecules is a pure $\pi\cdots\pi$ interaction.[142] More recently, Josa *et al.* showed that the inclusion of flexible flaps at the rim of the bowls enhances the capability to catch fullerenes due the increase of dispersion and a better embrace of fullerene. Moreover, they found that the presence of $CH\cdots\pi$ interactions between the buckybowl and the fullerene also leads to a more stable complex due to the increment of the dispersion energy.[88,92,143]

Fortunately, during the last two decades, buckybowls experienced a great impulse with the synthesis of new molecules such as pentaindenocorannulene[144] or Sygula's tweezers,[142] which can be used as host for fullerenes.[145,146] These new buckybowls and their behaviour as host resulted in an increasing number of theoretical works to study the properties of these supramolecular complexes and to find better fullerene hosts.[49,50,66,67,73,88,90–92,143]

1.4.2.2 Carbon nanotubes

Carbon Nanotubes (CNTs), also called buckytubes, are members of the fullerene family; they are allotropes of carbon with a cylindrical nanostructure and they typically end in a hemisphere of a buckyball. These molecules have unique properties that make them useful in many fields like optics, material applications and nanoelectronics.[147–149] Its name comes from the diameter of these molecules, of the order of a few nanometers. CNTs are classified in two types (see Figure 1.8):

- Single-walled carbon nanotubes (SWCNTs), formed by a single layer of carbon atoms. Hard to synthesize in large quantities but easy to characterize.
- Multiple-walled carbon nanotubes (MWCNTs), consisting on several layer of concentric carbon layers. Easy to synthesize but difficult to characterize structurally.

SWCNTs in turn are classified according to their chirality. There are three types of CNTs that depend on how the graphene sheet is wrapped: chiral, zigzag and armchair, as shown in Figure 1.9. The properties of these carbon nanotubes depend on their chirality,

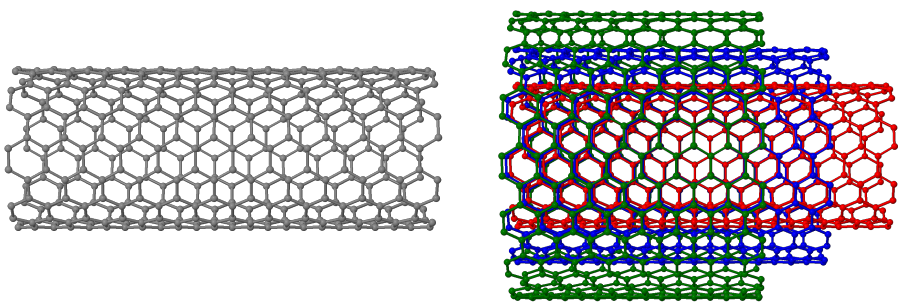

Figure 1.8: Classification of carbon nanotubes.

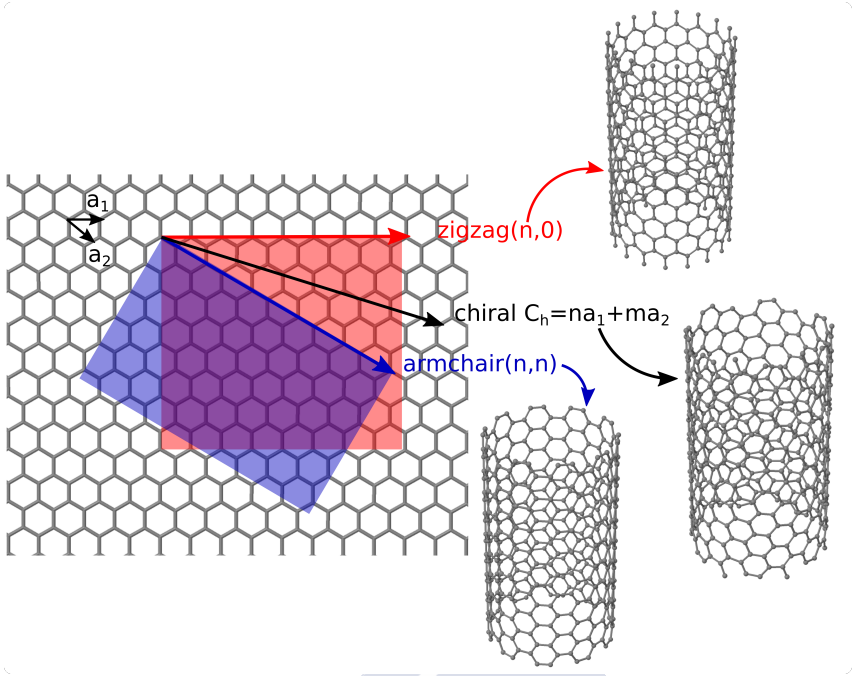

Figure 1.9: Types of nanotubes according to the chirality.

so a change in chirality is associated to a change in their properties. This allows to tune the CNT with the purpose to obtain the desired properties.

The first evidence of CNTs was in 1952 by Radushkevich and Lukyanovich.[150] They reported a structure with the shape like a worm made only by carbons atoms. However this discovery passed almost unnoticed until several years later. In 1991 Iijima[151] synthesized a multi-walled carbon nanotube using a simple arc-evaporation method. A couple of years later Iijima[152] and Bethune *et al.*[153] reported the synthesis of SWCNTs. The problem with SWCNTs is that except in some cases, the SWCNTs materials are formed by a mixture of several types of nanotubes; nevertheless, the use of carbon nanorings could solve this problem because it is possible to employ them to obtain pure SWCNTs with the desired structure through their vertical growth. Another problem with CNTs is the agglomeration between tubes that hamper their solubility. One way to solve this problem is to funcionalize the tube, allowing a better dispersion in polymeric materials and solvents.

One of the most interesting characteristic of CNTs are their electronic properties that allow their use in transistors or other switching applications.[147] The CNTs can behave as conductors or semi-conductors depending on the chirality of the molecule. However, their behaviour is affected by other different factors like the presence of defects, different diameters or the degree of crystallinity.

CNTs have many applications like their use as fillers, in which the CNTs are incorporated to polymers or other materials with the purpose to improve the properties of these materials. Another application is their use in electronic devices because the curvature of the nanotube allows the emission of electrons easily. CNTs can be used merged with lithium to enhance the storage properties and lifetimes of the battery, too. The performance at a low capacitance level was excellent; however, their manipulation is difficult.[147]

1.4.2.2.1 Peapods

Peapods are complexes formed by fullerenes encapsulated inside a carbon nanotube. In 1998 Smith *et al.* reported a well identified peadpod structure.[154] However, the existence of this kind of structure was speculated previously because the synthetic process of the fullerenes and nanotubes is very similar and the van der Waals diameter of C_{60} is 0.7 nm which could be optimally accommodated inside a CNT with a diameter about 1.4 nm (see Figure 1.10).

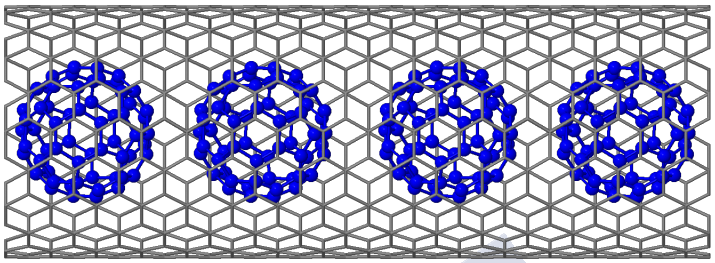

Figure 1.10: Peapod structure of C_{60} inside a CNT.

Since there are many different combinations between fullerenes and CNTs, peapods can be classified in three ways:

1. by fullerene type: pristine, endohedral, functionalized, heterofullerene...
2. by nanotube type: SWCNTs, MWCNTs.
3. by the arrangement of the fullerene inside the tube: linear, silo...

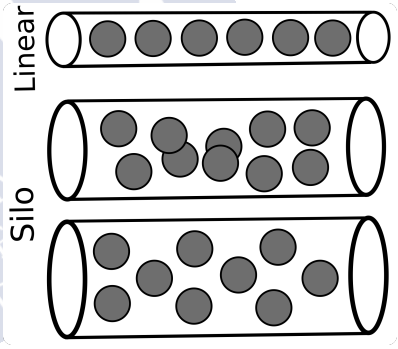

Figure 1.11: Differents arrangements in peapods.

The linear structure of the peapod was recognized in the first work of peapods[154] and further X-Ray diffraction (XRD) shows the same evidence.[155] The fullerenes adopted a linear chain with approximate 1 nm of separation between the centres of the fullerene for C_{60}.[156] The simulation of this peapod shows that there is no evidence of correlation between fullerene chains in neighboring tubes because the nanotube shields this effects.[157] This chain of C_{60}s does not contribute to the conductivity of the nanotube because the Fermi energy of the SWCNTs lies between the HOMO and LUMO level of the fullerene chains as the experimental and theoretical work indicates.[158] The silo configuration is common in large diameter nanotubes that can allow the inclusion of several piled units of fullerene inside their walls.

These peapods have different applications as in transistors because the SWCNTs have a high current-carrying capability, though nanotubes have a large gap that difficults their use. In spite of this, when some endofullerenes are inserted inside the nanotube the gap is reduced to 0.1 eV, allowing an increase in speed and reduced dissipation. In the last decade the development of new renewable energies centres the attention of much research, and the observation that these peapods can act as active electron-hole centres has raised

interest. This means that if the peapods have the active medium and the electrode integrated in their structure they could act alone as a solar cell.[157]

Also, they can be used as drug deliverers due to the biocompability of the carbonaceous material or the possibility to attach active molecules to the nanotube.[159] Other interesting applications are not confirmed yet but they are under investigation. One of these applications is their use like a "nanogun" in which an oscillation of the C_{60} is produced inside the tube when it has a negative charge, but when it is positively charged the C_{60} is displaced with speed about 1 km s^{-1} in one direction like a gun. Another possible application is to use like "Shuttle" memory; the fullerene can move relatively easy inside the nanotube among different minimum-energy structures allowing its use as an information carrier.[157]

1.4.2.3 Carbon nanorings

Since the discovery of CNTs the problem of obtaining a pure structure keeps the researchers busy. One approach to solve this problem is to start the synthesis of the CNT from the fundamental unit. The ring-shaped structures that are obtained when the CNT are separated in pieces perpendicular to the main axis are called carbon nanorings (CNRs) and they are hoop-shaped π conjugated hydrocarbons with a nanosize cavity. For example, cycloparaphenylenes (CPPs) and cyclacenes (CC) are the fundamental part of the armchair and zigzag nanotube (see Figure 1.12) and they are considered the ideal templates to build an uniform CNT.

On the other hand the first nanoring synthesized did not correspond with one of these fundamental units. In 1996 Kawase *et al.* synthesized the first carbon nanorings, 6-cycloparaphenilacetylene ([6]CPPA) and 8-cycloparaphenilacetylene ([8]CPPA).[160] These CNRs possess an alternating structure between 1,4-phenylene and ethynylene units that adopted a belt-shape with a cavity size according to the number of these alternating units. It took more than a decade to achieve the synthesis of a cycloparaphenylene, the fundamental unit of the armchair nanotubes, formed only by 1,4-phenylene units.[161]

As the first CNR synthesized, [n]CPPAs were extensively studied and several nanorings with different sizes were obtained ([5]-[9]CPPA).[85,162–167] CPPAs adopt a rigid and belt shaped structure with the benzene rings parallel to the main axis of the ring. Predictably, when the size of the ring grows the strain energy decreases because the angles become closer to linearity. The absorption spectra show small changes in the maximum absorption wavelength when the size of the nanoring increases, being located between 349−355 nm; however, the emission spectra shows a bathochromic shift when the size of the ring decreases.[85]

The synthesis of [n]CPPs was extensively studied during many years, the first attempt to obtain these nanorings dates from the beginning of the 90s; however, it was not until 2008, barely ten years ago, that the first synthesis of CPPs was a success. This synthetic route was developed by Jasti *et al.* obtaining three different nanorings, [9]CPP, [12]CPP and [18]CPP.[161] Some time later an updating of the methodology previously used allowed to get a selective synthesis of [5]-[12]CPP, and during the application of a similar methodology the [8]CPP and [10]CPP were obtained in a gram-scale.[168–170] However, not only the group of Jasti investigates the synthesis of CPPs; Itami *et al.* reported a selective synthesis of [12]CPP using a slightly different strategy.[171] Moreover, using the same strategy as in [12]CPP but modifying the precursors it is possible to obtain bigger nanorings

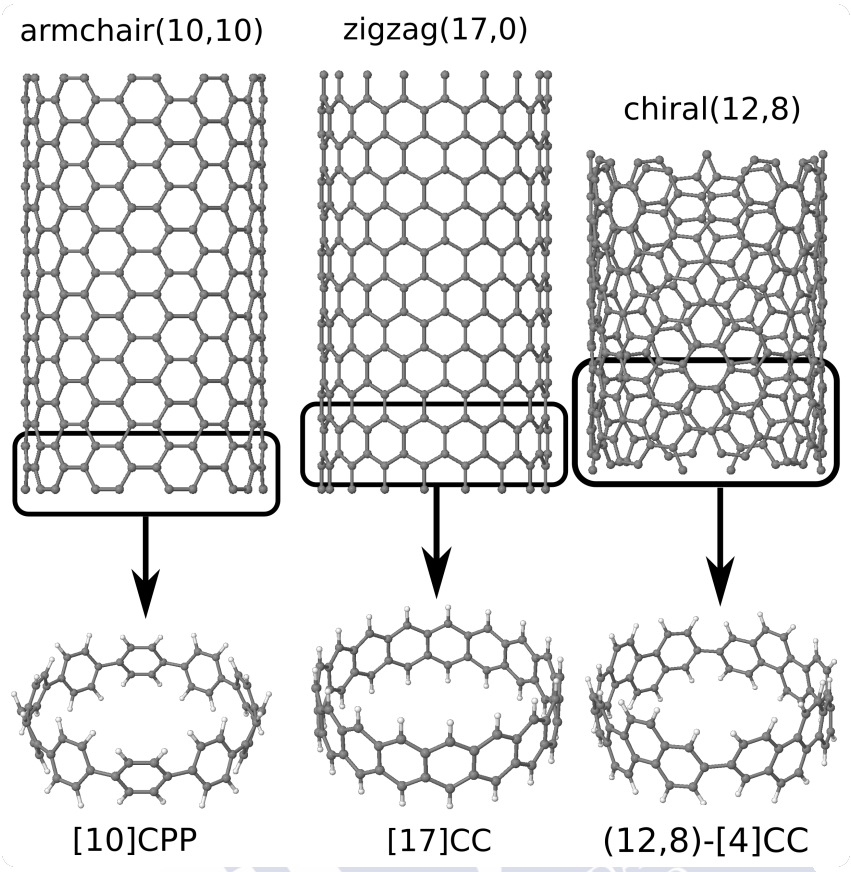

Figure 1.12: Types of nanotubes according to the chirality. [10]cycloparaphenylene ([10]CPP), [17]cyclacene ([17]CC) and [4]cyclo-2,8-chrysenylene ((12,8)-[4]CC).

like [14]CPP, [15]CPP and [16]CPP or smaller ones such as [7]-[11]CPP.[172,173] Finally, another different synthetic route was discovered by Yamago *et al.* using in this case a tetraplatinum precursor which eliminates the strain energy of the molecule.[174] Following this synthetic route the [20]CPP and [21]CPP were obtained for the first time.[175] These synthetic methods are explained in more detail in several reviews published through the years.[85,165,176]

Since the synthesis of CPP nanorings, these molecules have been extensively studied. In the case of [n]CPP, with n as an even-number of phenylene units, benzene rings are in an alternating disposition avoiding steric repulsions between ring edges, while if [n] is odd, the nanorings have one 3-helical moiety in the minimum structure (see Figure 1.13). The dihedral angle between two neighbouring 1,4-phenylene units decreases as the diameter of the ring increases. Furthermore, the benzene rings in [n]CPP can rotate rather freely at room temperature, due to the small barriers for this process.[166] [5]CPP and [7-12]CPP adopt some sort of herringbone packing in the solid state but the [5]CPP structure is much denser than the other structures. On the other hand, [6]CPP adopts a different solid state, stacking in columns.[177]

According to the structure of the CPP it is possible to establish a trend for the strain energy and, unsurprisingly, when the size of the CPP increases, the strain energy decreases reaching to a plateau at large nanoring diameter of about 25 Å.[166] The most strained nanoring is the [5]CPP with a strain energy about 117 kcal mol^{-1}; in the opposite case,

alternating moiety 3-helical moiety

Figure 1.13: Different arrangements of 1,4-phenylene. The red color means that the carbon atom is oriented to the cavity and the blue color is oriented in the opposite direction.

the low strain energy is found in the plateau starting with the [18]CPP and with an energy approximately of 30 kcal mol^{-1},[178] which is similar to the strain energy in cyclopropane (27.5 kcal mol^{-1}).[14] Furthermore, there is a small odd-even effect in the strain energy due to the different structures of the nanoring, and as a rule the odd nanorings have a slightly higher strain than even nanorings.[166] In the case of the HOMO-LUMO levels another trend is found: when the size of the nanoring increases, in other words, when more paraphenylene units are added to the nanoring, the HOMO energy decreases while the LUMO energy increases. This trend produces an increase of the HOMO-LUMO gap until a plateau is reached with 13 paraphenylene units.[146]

Spectroscopic properties of CPPs are also worth noticing. Absorption spectra have a maximum at 340 nm and they are quite independent of the ring size. On the contrary, linear aromatic compounds such as naphthalene, anthracene and so on, show a bathochromic shift of the absorption bands when more rings are added. The fluorescence in CPP nanorings depends on the size of the ring: if $n > 8$ then [n]CPP shows fluorescence, if $n = 7$ the nanoring shows a low fluorescence behaviour and finally for the cases with $n = 6$ or $n = 5$ the nanorings are non-fluorescent.[165] Some phosphorescence measurements were carried out for [8]-[12]CPP and an increasing maximum in wavelength was found when the size of the nanoring is increased; this behaviour is the opposite than the linear oligophenylenes.[179] Moreover, there are some differences in the structure between the excited state and the ground state. The excited state geometry has a local planarization of 5 benzene rings in the [n]CPP when $n > 8$, but when $n < 8$ all the 1,4-phenylene units are planar *i.e.* the benzene ring loses their alternating arrangement.[180]

In addition, Yamago *et al.* carried out several electrochemical studies in small CPPs. The size of the nanorings strongly affects the oxidation potential, showing lower oxidation potential at small sizes.[181–183] The oxidation wave was observed for [5]CPP and [8]–[13]CPP using cyclic voltammetry, but the reduction wave was only observed for the smallest synthesized nanoring ([5]CPP). This cyclic voltammetry shows a clear reversibility for the oxidized species, indicating that these intermediates are stable at room temperature and the experimental evidence was found by the same group, who reported the selectively preparation of the [8]CPP dication.[146]

During the last years all the effort focused on CNRs allowed to obtain new derivatives of these molecules. It has to be emphasized the synthesis of cyclo[10]paraphenylene-9,10-anthraquinon-2,6-ylene ([10]CPAq) as well as cyclo[10]paraphenylene-2,6-tetracyanoanthraquino-dimethanylene ([10]CPTcaq) in which an attractor group is introduced in the nanoring with the purpose to obtain a donor/acceptor molecule.[184] Another new nanoring was obtained by the inclusion of azobencene in order to change between the "cis" and "trans" configuration and facilitate the release of the molecule in the cavity.[185] Following

this strategy, the CPPs can be doped with other heteroatoms with the purpose to modify their properties. Specifically, it is worth noting the synthesis of CNRs based on thiophenes, which exhibit modified absorption spectra, showing an increase on the maximum wavelength as the size of the ring increases (contrary to the behaviour observed in CPPs that show the same wavelength). Moreover, it is possible to exchange a benzene unit for a bigger aromatic group like chrysene or pyrene, or adding phenyl groups to the [n]CPP to increase the vertical size of the nanoring; that is, the surface of the nanoring is increased making it to look like a CNT.[176] Finally some three-dimensional cages have been designed and synthesized.[186]

As in CPPs, several derivates from CPPAs have been obtained. The most common one consists on the inclusion of two naphthalene units in exchange of a benzene unit, but depending on the substituted position, different types of nanoring were obtained.[85,187,188] More recently, another substitution was proposed in which the benzene rings are exchanged by anthracene units.[189] Finally Ohkita and Tsuji synthesized a butadiyne-bridged [4_6]paracyclophyne derivative which has two adjacent acetylene units, but these kind of molecules have a large strain energy due to the bent conformation of the adjacent acetylene units.[85]

Regarding cyclacene, the fundamental part of the zigzag nanotube, it has not been synthesized yet despite considerable efforts, though many theoretical works have been performed with the purpose of studying the stability of these molecules and reasoning why they are not obtained yet.[190–193]

All these nanorings have several potential applications, such as purifying fullerene mixtures, as seeds for growing nanotubes, in asymmetric catalysis or for their use in OPVs.[165]

Beside all these different applications of CNRs they can also be employed in supramolecular chemistry. Specially, their concave cavity is a potential host to "catch" some molecules with a convex surface such as fullerenes. The first complexes were obtained with CPPAs, which were synthesized earlier. $C_{60}\cdots$[6]CPPA and $C_{60}\cdots$[8]CPPA were obtained by Kawase in 2003 and these complexes show a stable behaviour in solution and in solid state.[188]

On the other hand, the first host-guest interaction between CPP and fullerenes was found by Yamago in 2011.[181] In this work they mixed C_{60} and several CPPs of different sizes obtaining through NMR that the fullerene is only encapsulated inside [10]CPP. A couple of years later the same group achieved the encapsulation of C_{70} inside [10]CPP and [11]CPP.[194] In this case the oval shape of the fullerene allows the inclusion in these two nanorings of different size. With [10]CPP, C_{70} is found in a vertical disposition while for [11]CPP is lying along its long axis inside the ring (see Figure 1.14). However this kind of host-guest complexes was a challenge for theoretical chemists and many effort was spent in research the geometry and binding energy of these complexes due to the difficulty to find the best optimised structure and a predictive model of the properties in these complexes.[195,196]

CPPs not only "catch" pristine fullerenes, they also have the ability to form complexes with endofullerenes. Iwamoto *et al.* studied the complex formed between the metallofullerene La@C_{82} and the nanoring [11]CPP, showing that the arrangement of the metallofullerene inside the nanoring is different than the disposition found inside an armchair nanotube, because fullerenes interact among each other within the nanotube. This

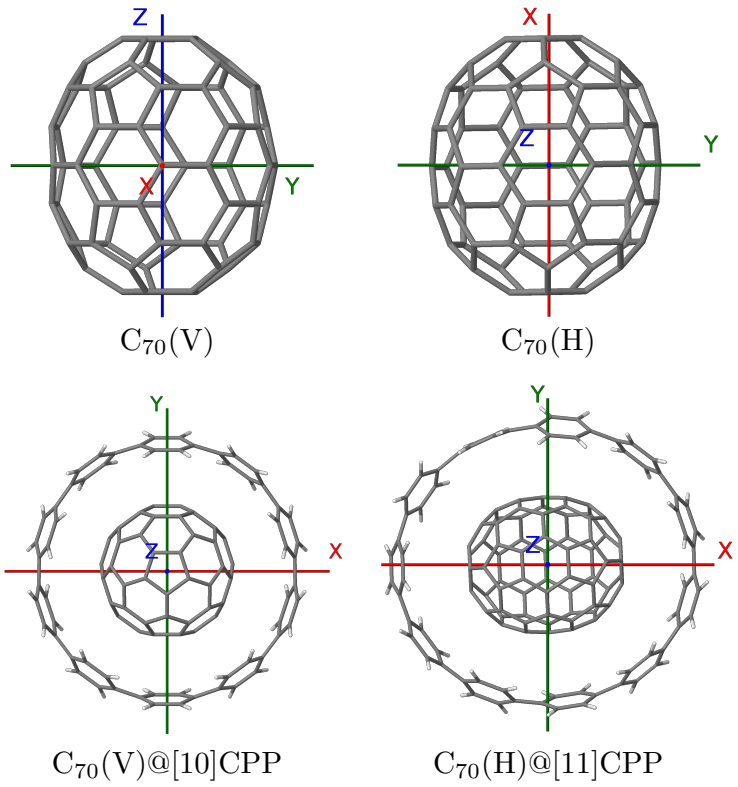

Figure 1.14: Different dispositions for C_{70} inside [10]CPP or [11]CPP.

highlights the role of the interactions between fullerenes inside the nanotube.[197] Also, Nakanishi *et al.* employed [11]CPP to discriminate between a mixture of several pristine fullerenes and endohedral metallofullerenes showing that all the fullerenes except the C_{60} can be "catched" inside the nanoring. However, in this mixture, $M_x@C_{82}$ fullerenes were selectively complexed and extracted.[198] On the other hand Itami *et al.* were able to characterize the crystal structure of $Li^+@C_{60}\cdots$[10]CPP complex investigating also the optoelectronic properties and charge transfer in these complexes.[199] This new kind of supramolecular complexes opens the possibility to form new fullerenes with an encapsulated alkaline ion and interesting optical properties.

Aside from CPPs, other carbon nanorings have been employed for fullerene encapsulation. Firstly a couple of theoretical works showed the stability and geometry of C_{60} encapsulated by cyclacenes, and nanorings of increasing size were tested to obtain an optimal complex.[200,201] Isobe *et al.* studied the host-guest interaction between [4]cyclochrysenylene and C_{60} or some of the fullerene derivates that allowed the formation of a low friction system even in solid state.[202,203] The same group tested another similar nanoring ([4]cyclo-2,8-anthanthrenylene) with a higher interaction surface, but in this case they employed two fullerenes, C_{60} and C_{70}, showing an enthalpy-driven association.[204] Lastly, Du *et al.* studied the complexes formed by a cyclic tetramer of a tetramesityl hexa-perihexabenzocoronene ([4]CHBC) and C_{70} in a 1:1 ratio. They also tried to form the complex between [4]CHBC and C_{60}; however, they did not find any experimental evidence of this complex, maybe because the size of both monomers are incompatible.[205]

References

(1) H. Margenau and N. R. Kestner, *Theory of Intermolecular Forces*, Pergamon Press, Oxford; New York, 1969.

(2) I. G. Kaplan, *Intermolecular interactions : physical picture, computational methods and model potentials*, Wiley, Chichester, UK, 2006.

(3) P. Hobza and K. Muller-Dethlefs, *Non-Covalent Interactions: Theory and Experiment*, Royal Society of Chemistry, Cambridge, UK, 2009.

(4) A. Stone, *The Theory of Intermolecular Forces*, Oxford University Press, Oxford, UK, 2013.

(5) F. London, *Zeitschrift für Physik*, 1930, **63**, 245–279.

(6) R. S. Mulliken, *Journal of Physical Chemistry*, 1952, **56**, 801–822.

(7) A. J. Misquitta, *Journal of Chemical Theory and Computation*, 2013, **9**, 5313–5326.

(8) A. J. Stone, *Journal of Physical Chemistry A*, 2017, **121**, 1531–1534.

(9) F. Weinhold and E. D. Glendening, *Journal of Physical Chemistry A*, 2018, **122**, 724–732.

(10) A. J. Stone and K. Szalewicz, *Journal of Physical Chemistry A*, 2018, **122**, 733–736.

(11) C. J. Pedersen, *Journal of the American Chemical Society*, 1967, **89**, 7017–7036.

(12) J. M. Lehn, *Pure and Applied Chemistry*, 1978, **50**, 871–892.

(13) J. W. Steed and J. L. Atwood, *Supramolecular Chemistry*, Wiley, Chichester, UK, 2009.

(14) E. V. Anslyn and D. A. Dougherty, *Modern Physical Organic Chemistry*, University Science Books, Sausalito, California, 2006.

(15) A. M. Maharramov, K. T. Mahmudov, M. N. Kopylovich and A. J. Pombeiro, *Non-covalent Interactions in the Synthesis and Design of New Compounds*, John Wiley & Sons, Inc, Hoboken, NJ, 2016.

(16) P. Metrangolo and G. Resnati, *Halogen Bonding I: Impact on Materials Chemistry and Life Sciences*, Springer International Publishing, Gewerbestrasse, Switzerland, 2015.

(17) S. J. Grabowski, *Hydrogen bonding - New insights*, ed. S. J. Grabowski, Springer Netherlands, 2006.

(18) K. E. Riley and P. Hobza, *Accounts of Chemical Research*, 2013, **46**, 927–936.

(19) X. Lucas, A. Bauzá, A. Frontera and D. Quiñonero, *Chemical Science*, 2016, **7**, 1038–1050.

(20) B. Safa, C. Lee and D. S. Riddick, *Toxicology Letters*, 1997, **90**, 163–175.

(21) R. Anjana, M. K. Vaishnavi, D. Sherlin, S. P. Kumar, K. Naveen, P. S. Kanth and K. Sekar, *Bioinformation*, 2012, **8**, 1220–1224.

(22) D. W. Johnson and F. Hof, *Aromatic interactions : frontiers in knowledge and application*, Royal Society of Chemistry, Croydon, UK, 2016.

(23) A. J. Neel, M. J. Hilton, M. S. Sigman and F. D. Toste, *Nature*, 2017, **543**, 637–646.

(24) S. Scheiner, *Noncovalent forces*, Springer International Publishing, Switzerland, 2015.

(25) T. Akasaka, A. Osuka, S. Fukuzumi, H. Kandori and Y. Aso, *Chemical Science of π-Electron Systems*, Springer Japan, Tokyo, 2015.

(26) A. S. Mahadevi and G. N. Sastry, *Chemical Reviews*, 2013, **113**, 2100–2138.

(27) S. Tsuzuki and T. Uchimaru, *Current Organic Chemistry*, 2006, **10**, 745–762.

(28) L. M. Salonen, M. Ellermann and F. Diederich, *Angewandte Chemie - International Edition*, 2011, **50**, 4808–4842.

(29) M. L. Waters, *Biopolymers - Peptide Science Section*, 2004, **76**, 435–445.

(30) E. A. Meyer, R. K. Castellano and F. Diederich, *Angewandte Chemie - International Edition*, 2003, **42**, 1210–1250.

(31) S. Tsuzuki and A. Fujii, *Physical Chemistry Chemical Physics*, 2008, **10**, 2584–2594.

(32) M. Tamres, *Journal of the American Chemical Society*, 1952, **74**, 3375–3378.

(33) A. Fujii, S. I. Morita, M. Miyazaki, T. Ebata and N. Mikami, *Journal of Physical Chemistry A*, 2004, **108**, 2652–2658.

(34) A. Fujii, H. Hayashi and S. Tsuzuki, *Chemical Physics Letters*, 2012, **537**, 11–15.

(35) M. J. Plevin, D. L. Bryce and J. Boisbouvier, *Nature Chemistry*, 2010, **2**, 466–471.

(36) S. Tsuzuki, K. Honda, T. Uchimaru, M. Mikami and K. Tanabe, *Journal of the American Chemical Society*, 2000, **122**, 3746–3753.

(37) J. W. G. Bloom, R. K. Raju and S. E. Wheeler, *Journal of Chemical Theory and Computation*, 2012, **8**, 3167–3174.

(38) B. K. Mishra, S. Karthikeyan and V. Ramanathan, *Journal of Chemical Theory and Computation*, 2012, **8**, 1935–1942.

(39) O. Takahashi, Y. Kohno and M. Nishio, *Chemical Reviews*, 2010, **110**, 6049–6076.

(40) M. Nishio, *Physical Chemistry Chemical Physics*, 2011, **13**, 13873–13900.

(41) J. Sunner, K. Nishizawa and P. Kebarle, *Journal of Physical Chemistry*, 1981, **85**, 1814–1820.

(42) R. A. Kumpf and D. A. Dougherty, *Science*, 1993, **261**, 1708–1710.

(43) J. P. Gallivan and D. A. Dougherty, *Proceedings of the National Academy of Sciences of the United States of America*, 1999, **96**, 9459–9464.

(44) X. Xiu, N. L. Puskar, J. A. P. Shanata, H. A. Lester and D. A. Dougherty, *Nature*, 2009, **458**, 534–537.

(45) D. A. Dougherty, *Accounts of Chemical Research*, 2013, **46**, 885–893.

(46) S. Mecozzi, A. P. West, D. A. Dougherty, M. Beckman and H Grubbs, *Proceedings of the National Academy of Sciences*, 1996, **93**, 10566–10571.

(47) S. Mecozzi, A. P. West and D. A. Dougherty, *Journal of the American Chemical Society*, 1996, **118**, 2307–2308.

(48) J. C. Ma and D. A. Dougherty, *Chemical Reviews*, 1997, **97**, 1303–1324.

(49) J. A. Carrazana-García, J. Rodríguez-Otero and E. M. Cabaleiro-Lago, *Journal of Physical Chemistry B*, 2011, **115**, 2774–2782.

(50) J. A. Carrazana-García, E. M. Cabaleiro-Lago and J. Rodríguez-Otero, *Physical Chemistry Chemical Physics*, 2017, **19**, 10543–10553.

(51) N. J. Singh, S. K. Min, D. Y. Kim and K. S. Kim, *Journal of Chemical Theory and Computation*, 2009, **5**, 515–529.

(52) I. Soteras, M. Orozco and F. J. Luque, *Physical Chemistry Chemical Physics*, 2008, **10**, 2616–2624.

(53) A. A. Rodríguez-Sanz, E. M. Cabaleiro-Lago and J. Rodríguez-Otero, *Physical Chemistry Chemical Physics*, 2014, **16**, 22499–22512.

(54) A. A. Rodríguez-Sanz, E. M. Cabaleiro-Lago and J. Rodríguez-Otero, *Organic & Biomolecular Chemistry*, 2015, **13**, 7961–7972.

(55) J. P. Gallivan and D. A. Dougherty, *Journal of the American Chemical Society*, 2000, **122**, 870–874.

(56) A. Campo-Cacharrón, E. M. Cabaleiro-Lago and J. Rodríguez-Otero, *Theoretical Chemistry Accounts*, 2012, **131**, 1–13.

(57) A. A. Rodríguez-Sanz, E. M. Cabaleiro-Lago and J. Rodríguez-Otero, *Journal of Molecular Modeling*, 2014, **20**, 2209.

(58) E. M. Cabaleiro-Lago, J. Rodríguez-Otero and Á. Peña-Gallego, *Journal of Chemical Physics*, 2011, **135**, 214301.

(59) A. A. Rodríguez-Sanz, J. A. Carrazana-García, E. M. Cabaleiro-Lago and J. Rodríguez-Otero, *Journal of Molecular Modeling*, 2013, **19**, 1985–1994.

(60) A. Campo-Cacharrón, E. M. Cabaleiro-Lago, J. A. Carrazana-García and J. Rodríguez-Otero, *Journal of Computational Chemistry*, 2014, **35**, 1290–1301.

(61) D. Quiñonero, C. Garau, C. Rotger, A. Frontera, P. Ballester, A. Costa and P. M. Dey, *Angewandte Chemie - International Edition*, 2002, **41**, 3389–3392.

(62) R. J. Götz, A. Robertazzi, I. Mutikainen, U. Turpeinen, P. Gamez and J. Reedijk, *Chemical Communications*, 2008, **0**, 3384–3386.

(63) A. Frontera, P. Gamez, M. Mascal, T. J. Mooibroek and J. Reedijk, *Angewandte Chemie - International Edition*, 2011, **50**, 9564–9583.

(64) M. Mascal, I. Yakovlev, E. B. Nikitin and J. C. Fettinger, *Angewandte Chemie - International Edition*, 2007, **46**, 8782–8784.

(65) J. A. Carrazana-García, J. Rodríguez-Otero and E. M. Cabaleiro-Lago, *Journal of Physical Chemistry B*, 2012, **116**, 5860–5871.

(66) A. Campo-Cacharrón, E. M. Cabaleiro-Lago, I. González-Veloso and J. Rodríguez-Otero, *Journal of Physical Chemistry A*, 2014, **118**, 6112–6124.

(67) A. Campo-Cacharrón, E. M. Cabaleiro-Lago and J. Rodríguez-Otero, *Journal of Computational Chemistry*, 2014, **35**, 1533–1544.

(68) P. García-Novo, A. Campo-Cacharrón, E. M. Cabaleiro-Lago and J. Rodríguez-Otero, *Physical Chemistry Chemical Physics*, 2012, **14**, 104–112.

(69) A. Campo-Cacharrón, E. M. Cabaleiro-Lago and J. Rodríguez-Otero, *ChemPhysChem*, 2012, **13**, 570–577.

(70) C. A. Hunter and J. K. M. Sanders, *Journal of the American Chemical Society*, 1990, **112**, 5525–5534.

(71) J. P. Wagner and P. R. Schreiner, *Angewandte Chemie - International Edition*, 2015, **54**, 12274–12296.

(72) R. K. Raju, J. W. Bloom, Y. An and S. E. Wheeler, *ChemPhysChem*, 2011, **12**, 3116–3130.

(73) E. M. Cabaleiro-Lago, J. Rodríguez-Otero and J. A. Carrazana-García, *Physical Chemistry Chemical Physics*, 2017, **19**, 26787–26798.

(74) E. M. Cabaleiro-Lago and J. Rodríguez-Otero, *ACS Omega*, 2018, **3**, 9348–9359.

(75) M. O. Sinnokrot and C. D. Sherrill, *Journal of Physical Chemistry A*, 2006, **110**, 10656–10668.

(76) S. Tsuzuki, K. Honda, T. Uchimaru, M. Mikami and K. Tanabe, *Journal of the American Chemical Society*, 2002, **124**, 104–112.

(77) M. Pitoňák, P. Neogrády, J. Řezáč, P. Jurečka, M. Urban and P. Hobza, *Journal of Chemical Theory and Computation*, 2008, **4**, 1829–1834.

(78) M. O. Sinnokrot, E. F. Valeev and C. D. Sherrill, *Journal of the American Chemical Society*, 2002, **124**, 10887–10893.

(79) C. R. Martinez and B. L. Iverson, *Chemical Science*, 2012, **3**, 2191–2201.

(80) M. O. Sinnokrot and C. D. Sherrill, *Journal of the American Chemical Society*, 2004, 7690–7697.

(81) S. E. Wheeler and K. N. Houk, *Journal of the American Chemical Society*, 2008, **130**, 10854–10855.

(82) R. M. Parrish and C. D. Sherrill, *Journal of the American Chemical Society*, 2014, **136**, 17386–17389.

(83) E. M. Cabaleiro-Lago and J. Rodríguez-Otero, *Physical Chemistry Chemical Physics*, 2016, **18**, 13750–13753.

(84) N. J. Silva, F. B. Machado, H. Lischka and A. J. Aquino, *Physical Chemistry Chemical Physics*, 2016, **18**, 22300–22310.

(85) T. Kawase and H. Kurata, *Chemical Reviews*, 2006, **106**, 5250–5273.

(86) A. Sygula and S. Saebø, *International Journal of Quantum Chemistry*, 2009, **109**, 65–72.

(87) M. R. Kennedy, L. A. Burns and C. D. Sherrill, *The Journal of Physical Chemistry A*, 2012, **116**, 11920–11926.

(88) D. Josa, I. González-Veloso, J. Rodríguez-Otero and E. M. Cabaleiro-Lago, *Physical Chemistry Chemical Physics*, 2015, **17**, 6233–6241.

(89) D. Josa, J. Rodríguez-Otero, E. M. Cabaleiro-Lago and M. Rellán-Piñeiro, *Chemical Physics Letters*, 2013, **557**, 170–175.

(90) D. Josa, J. Rodríguez-Otero and E. M. Cabaleiro-Lago, *Physical Chemistry Chemical Physics*, 2011, **13**, 21139–21145.

(91) D. Josa, J. Rodríguez-Otero, E. M. Cabaleiro-Lago, L. A. Santos and T. C. Ramalho, *Journal of Physical Chemistry A*, 2014, **118**, 9521–9528.

(92) D. Josa, L. Azevedo dos Santos, I. González-Veloso, J. Rodríguez-Otero, E. M. Cabaleiro-Lago and T. de Castro Ramalho, *RSC Advances*, 2014, **4**, 29826–29833.

(93) E. M. Cabaleiro-Lago, B. Fernández and J. Rodríguez-Otero, *Journal of Computational Chemistry*, 2018, **39**, 93–104.

(94) H. W. Kroto, J. R. Heath, S. C. O'Brien, R. F. Curl and R. E. Smalley, *Nature*, 1985, **318**, 162–163.

(95) W. Krätschmer, L. D. Lamb, K. Fostiropoulos and D. R. Huffman, *Nature*, 1990, **347**, 354–358.

(96) P. R. C. Kent, M. D. Towler, R. J. Needs and G. Rajagopal, *Physical Review B - Condensed Matter and Materials Physics*, 2000, **62**, 15394–15397.

(97) H. Kietzmann, R. Rochow, G. Ganteför, W. Eberhardt, K. Vietze, G. Seifert and P. W. Fowler, *Physical Review Letters*, 1998, **81**, 5378–5381.

(98) F. Beer, A. Gügel, K. Martin, J. Räder and K. Müllen, *Journal of Materials Chemistry*, 1997, **7**, 1327–1330.

(99) N. Shao, Y. Gao and X. C. Zeng, *Journal of Physical Chemistry C*, 2007, **111**, 17671–17677.

(100) A. Hirsch and M. Brettreich, *Fullerenes: Chemistry and Reactions*, Wiley-VCH, Weiheim, Germany, 2005.

(101) H. W. Kroto, *Nature*, 1987, **329**, 529–531.

(102) F. Wahl, J. Wiirth and H. Prinzbach, *Angewandte Chemie - International Edition*, 1993, **32**, 1722–1726.

(103) H. Prinzbach, A. Weller, P. Landenberger, F. Wahl, J. Wörth, L. T. Scott, M. Gelmont, D. Olevano and B. V. Issendorff, *Nature*, 2000, **407**, 60–63.

(104) K. Fostiropoulos, dissertation, University of Heidelberg, 1991.

(105) C. Yeretzian, J. B. Wiley, K. Holczer, T. Su, S. Nguyen, R. B. Kaner and R. L. Whetten, *Journal of Physical Chemistry*, 1993, **97**, 10097–10101.

(106) J. Théobald, M. Perrut, J. V. Weber, E. Millon and J. F. Muller, *Separation Science and Technology*, 1995, **30**, 2783–2819.

(107) I. Rašović, *Materials Science and Technology*, 2017, **33**, 777–794.

(108) F. Langa and J.-F. Nierengarten, *Fullerenes: Principles and Applications*, Royal Society of Chemistry Publishing, Cambridge CB4 0WF, UK, 2012.

(109) C. García-Simón, M. Garcia-Borràs, L. Gómez, T. Parella, S. Osuna, J. Juanhuix, I. Imaz, D. Maspoch, M. Costas and X. Ribas, *Nature Communications*, 2014, **5**, 5557.

(110) R. D. Bolskar, in *Encyclopedia of Nanotechnology*, ed. B. Bhushan, Springer Netherlands, Dordrecht, 2016, pp. 1267–1281.

(111) R. Bakry, R. M. Vallant, M. Najam-ul Haq, M. Rainer, Z. Szabo, C. W. Huck and G. K. Bonn, *International Journal of Nanomedicine*, 2007, **2**, 639–649.

(112) S. Dostalova, A. Moulick, V. Milosavljevic, R. Guran, M. Kominkova, K. Cihalova, Z. Heger, L. Blazkova, P. Kopel, D. Hynek, M. Vaculovicova, V. Adam and R. Kizek, *Monatshefte fur Chemie*, 2016, **147**, 905–918.

(113) R. Ganesamoorthy, G. Sathiyan and P. Sakthivel, *Solar Energy Materials and Solar Cells*, 2017, **161**, 102–148.

(114) D. Sun, D. Meng, Y. Cai, B. Fan, Y. Li, W. Jiang, L. Huo, Y. Sun and Z. Wang, *Journal of the American Chemical Society*, 2015, **137**, 11156–11162.

(115) S. Chen, S. M. Lee, J. Xu, J. Lee, K. C. Lee, T. Hou, Y. Yang, M. Jeong, B. Lee, Y. Cho, S. Jung, J. Oh, Z.-G. Zhang, C. Zhang, M. Xiao, Y. Li and C. Yang, *Energy and Environmental Science*, 2018, **11**, 2569–2580.

(116) X. Lu, L. Echegoyen, A. L. Balch, S. Nagase and T. Akasaka, *Endohedral Metallofullerenes: Basics and Applications*, CRC Press Taylor & Francis Group, Boca Raton, FL, USA, 2015.

(117) A. A. Popov, S. Yang and L. Dunsch, *Chemical Reviews*, 2013, **113**, 5989–6113.

(118) J. R. Heath, S. C. O'Brien, Q. Zhang, Y. Liu, R. F. Curl, F. K. Tittel and R. E. Smalley, *Journal of the American Chemical Society*, 1985, **107**, 7779–7780.

(119) C. R. Wang, T. Kai, T. Tomiyama, T. Yoshida, Y. Kobayashi, E. Nishibori, M. Takata, M. Sakata and H. Shinohara, *Angewandte Chemie - International Edition*, 2001, **40**, 397–399.

(120) X. Lu, L. Bao, T. Akasaka and S. Nagase, *Chemical Communications*, 2014, **50**, 14701–14715.

(121) P. W. Fowler, T. Glass, J. C. Duchamp, T. Heine, R. Bible, K. Harich, G. Rice, S. Stevenson, H. C. Dorn and E. Hajdu, *Nature*, 2002, **408**, 427–428.

(122) T. Yang, X. Zhao, S. T. Li and S. Nagase, *Inorganic Chemistry*, 2012, **51**, 11223–11225.

(123) A. A. Popov and L. Dunsch, *Journal of the American Chemical Society*, 2007, **129**, 11835–11849.

(124) J. Effing, U. Jonas, L. Jullien, T. Plesnivy, H. Ringsdorf, F. Diederich, C. Thilgen and D. Weinstein, *Angewandte Chemie - International Edition*, 1992, **31**, 1599–1602.

(125) C. L. Wang, W. B. Zhang, R. M. Van Horn, Y. Tu, X. Gong, S. Z. D. Cheng, Y. Sun, M. Tong, J. Seo, B. B. Y. Hsu and A. J. Heeger, *Advanced Materials*, 2011, **23**, 2951–2956.

(126) P. A. Denis and M. Yanney, *RSC Advances*, 2016, **6**, 50978–50984.

(127) I. Sánchez-Molina, B. Grimm, R. M. Krick Calderon, C. G. Claessens, D. M. Guldi and T. Torres, *Journal of the American Chemical Society*, 2013, **135**, 10503–10511.

(128) P. A. Denis, *Chemical Physics Letters*, 2014, **591**, 323–327.

(129) D. V. Konarev, S. I. Troyanov and R. N. Lyubovskaya, *CrystEngComm*, 2015, **17**, 3923–3926.

(130) M. A. Petrukhina and L. T. Scott, *Fragments of Fullerenes and Carbon Nanotubes*, John Wiley & Sons, Hoboken, New Jersey, 2012.

(131) W. E. Barth and R. G. Lawton, *Journal of the American Chemical Society*, 1966, **88**, 380–381.

(132) A. Borchardt, A. Fuchicello, K. V. Kilway, J. S. Siegel and K. K. Baldridge, *Journal of the American Chemical Society*, 1992, **114**, 1921–1923.

(133) A. Sygula, *European Journal of Organic Chemistry*, 2011, **2011**, 1611–1625.

(134) F. Klärner, J. Panitzky, D. Preda and L. Scott, *Jounal Molecular Modeling*, 2000, **6**, 318–327.

(135) H. Sakurai, T. Daiko and T. Hirao, *Science*, 2003, **301**, 1878.

(136) H. Sakurai, T. Daiko, H. Sakane, T. Amaya and T. Hirao, *Journal of the American Chemical Society*, 2005, **127**, 11580–11581.

(137) T. Amaya, H. Sakane, T. Nakata and T. Hirao, *Pure and Applied Chemistry*, 2010, **82**, 969–978.

(138) J. C. Hanson and C. E. Nordman, *Acta Crystallographica Section B: Structural Science, Crystal Engineering and Materials*, 1976, **32**, 1147–1153.

(139) T. J. Seiders, K. K. Baldridge, G. H. Grube and J. S. Siegel, *Journal of the American Chemical Society*, 2001, **123**, 517–525.

(140) H. Becker, G. Javahery, S. Petrie, P. C. Cheng, H. Schwarz, L. T. Scott and D. K. Bohme, *Journal of the American Chemical Society*, 1993, **115**, 11636–11637.

(141) S. Mizyed, P. E. Georghiou, M. Bancu, B. Cuadra, A. K. Rai, P. Cheng and L. T. Scott, *Journal of the American Chemical Society*, 2001, **123**, 12770–12774.

(142) A. Sygula, F. R. Fronczek, R. Sygula, P. W. Rabideau and M. M. Olmstead, *Journal of the American Chemical Society*, 2007, **129**, 3842–3843.

(143) D. Josa, J. Rodríguez-Otero and E. M. Cabaleiro-Lago, *Physical Chemistry Chemical Physics*, 2015, **17**, 13206–13214.

(144) E. A. Jackson, B. D. Steinberg, M. Bancu, A. Wakamiya and L. T. Scott, *Journal of the American Chemical Society*, 2007, **129**, 484–485.

(145) X. Li, F. Kang and M. Inagaki, *Small*, 2016, **12**, 3206–3223.

(146) Q. Miao, *Polycyclic Arenes and Heteroarenes: Synthesis, Properties, and Applications*, Wiley-VCH Verlag GmbH & Co. KGaA, Weinheim, Germany, 2015, pp. 143–162.

(147) K. S. Ibrahim, *Carbon letters*, 2013, **14**, 131–144.

(148) M. O'Connell, *Carbon nanotubes: Properties and Applications*, CRC Press Taylor & Francis Group, Boca Raton, FL, USA, 2006.

(149) S. Reich, C. Thomsen and J. Maultzsch, *Carbon Nanotubes: Basic Concepts and Physical Properties*, Wiley-VCH Verlag GmbH & Co. KGaA, Weinheim, Germany, 2004.

(150) L. Radushkevich and V. Lukyanovich, *Zhurnal Fizicheskoi Khimii*, 1952, **26**, 88–95.

(151) S. Iijima, *Nature*, 1991, **354**, 56–58.

(152) S. Iijima and T. Ichihashi, *Nature*, 1993, **363**, 603–605.

(153) D. S. Bethune, C. H. Klang, M. S. De Vries, G. Gorman, R. Savoy, J. Vazquez and R. Beyers, *Nature*, 1993, **363**, 605–607.

(154) B. W. Smith, M. Monthioux and D. E. Luzzi, *Nature*, 1998, **396**, 323–324.

(155) H. Kataura, Y. Maniwa, M. Abe, A. Fujiwara, T. Kodama, K. Kikuchi, H. Imahori, Y. Misaki, S. Suzuki and Y. Achiba, *Applied Physics A*, 2002, **74**, 349–354.

(156) H. Chadli, A. Rahmani, K. Sbai, P. Hermet, S. Rols and J. L. Sauvajol, *Physical Review B - Condensed Matter and Materials Physics*, 2006, **74**, 1–8.

(157) F. Simon and M. Monthioux, in *Carbon Meta-Nanotubes: Synthesis, Properties and Applications*, ed. M. Monthioux, John Wiley & Sons, Ltd, Chichester, UK, 2011, pp. 273–321.

(158) Y. G. Yoon, M. S. Mazzoni and S. G. Louie, *Applied Physics Letters*, 2003, **83**, 5217–5219.

(159) A. Bianco, K. Kostarelos and M. Prato, *Current Opinion in Chemical Biology*, 2005, **9**, 674–679.

(160) T. Kawase, H. R. Darabi and M. Oda, *Angewandte Chemie - International Edition*, 1996, **35**, 2664–2666.

(161) R. Jasti, J. Bhattacharjee, J. B. Neaton and C. R. Bertozzi, *Journal of the American Chemical Society*, 2008, **130**, 17646–17647.

(162) T. Kawase, N. Ueda, K. Tanaka, Y. Seirai and M. Oda, *Tetrahedron Letters*, 2001, **42**, 5509–5511.

(163) T. Kawase, K. Tanaka, Y. Seirai, N. Shiono and M. Oda, *Angewandte Chemie - International Edition*, 2003, **42**, 5597–5600.

(164) T. Kawase, Y. Nishiyama, T. Nakamura, T. Ebi, K. Matsumoto, H. Kurata and M. Oda, *Angewandte Chemie - International Edition*, 2007, **46**, 1086–1088.

(165) S. E. Lewis, *Chemical Society Reviews*, 2015, **44**, 2221–2304.

(166) Y. Segawa, H. Omachi and K. Itami, *Organic Letters*, 2010, **12**, 2262–2265.

(167) T. Kawase and M. Oda, *Pure and Applied Chemistry*, 2006, **78**, 831–839.

(168) J. Xia, J. W. Bacon and R. Jasti, *Chemical Science*, 2012, **3**, 3018–3021.

(169) P. J. Evans, E. R. Darzi and R. Jasti, *Nature Chemistry*, 2014, **6**, 404–408.

(170) E. R. Darzi, T. J. Sisto and R. Jasti, *The Journal of Organic Chemistry*, 2012, **77**, 6624–6628.

(171) H. Takaba, H. Omachi, Y. Yamamoto, J. Bouffard and K. Itami, *Angewandte Chemie International Edition*, 2009, **48**, 6112–6116.

(172) Y. Ishii, Y. Nakanishi, H. Omachi, S. Matsuura, K. Matsui, H. Shinohara, Y. Segawa and K. Itami, *Chemical Science*, 2012, **3**, 2340–2345.

(173) F. Sibbel, K. Matsui, Y. Segawa, A. Studer and K. Itami, *Chemical Communications*, 2014, **50**, 954–956.

(174) S. Yamago, Y. Watanabe and T. Iwamoto, *Angewandte Chemie - International Edition*, 2010, **49**, 757–759.

(175) E. Kayahara, Y. Cheng and S. Yamago, *Chemistry Letters*, 2018, **47**, 1108–1111.

(176) D. Wu, W. Cheng, X. Ban and J. Xia, *Asian Journal of Organic Chemistry*, 2018, **7**, 2161–2181.

(177) E. R. Darzi and R. Jasti, *Chemical Society Reviews*, 2015, **44**, 6401–6410.

(178) S. M. Bachrach and D. Stück, *Journal of Organic Chemistry*, 2010, **75**, 6595–6604.

(179) M. Fujitsuka, C. Lu, T. Iwamoto, E. Kayahara, S. Yamago and T. Majima, *Journal of Physical Chemistry A*, 2014, **118**, 4527–4532.

(180) L. Adamska, I. Nayyar, H. Chen, A. K. Swan, N. Oldani, S. Fernandez-Alberti, M. R. Golder, R. Jasti, S. K. Doorn and S. Tretiak, *Nano Letters*, 2014, **14**, 6539–6546.

(181) T. Iwamoto, Y. Watanabe, T. Sadahiro, T. Haino and S. Yamago, *Angewandte Chemie - International Edition*, 2011, **50**, 8342–8344.

(182) E. Kayahara, T. Iwamoto, T. Suzuki and S. Yamago, *Chemistry Letters*, 2013, **42**, 621–623.

(183) E. Kayahara, V. K. Patel and S. Yamago, *Journal of the American Chemical Society*, 2014, **136**, 2284–2287.

(184) T. Kuwabara, J. Orii, Y. Segawa and K. Itami, *Angewandte Chemie - International Edition*, 2015, **54**, 9646–9649.

(185) K. Yuan, Y.-J. Guo, T. Yang, J.-S. Dang, P. Zhao, Q.-Z. Li and X. Zhao, *Journal of Physical Organic Chemistry*, 2014, **27**, 772–782.

(186) K. Matsui, Y. Segawa, T. Namikawa, K. Kamada and K. Itami, *Chemical Science*, 2013, **4**, 84–88.

(187) K. Tanaka, N. Ueda, T. Kawase, M. Oda and Y. Seirai, *Tetrahedron Letters*, 2001, **42**, 5509–5511.

(188) T. Kawase, K. Tanaka, N. Fujiwara, H. R. Darabi and M. Oda, *Angewandte Chemie - International Edition*, 2003, **42**, 1624–1628.

(189) K. Miki, T. Matsushita, Y. Inoue, Y. Senda, T. Kowada and K. Ohe, *Chemical Communications*, 2013, **49**, 9092–9094.

(190) D. Sadowsky, K. McNeill and C. J. Cramer, *Faraday Discuss.*, 2010, **145**, 507–521.

(191) G. Povie, Y. Segawa, T. Nishihara, Y. Miyauchi and K. Itami, *Science*, 2017, **356**, 172–175.

(192) S. Battaglia, H. A. Le, G. L. Bendazzoli, N. Faginas-Lago, T. Leininger and S. Evangelisti, *International Journal of Quantum Chemistry*, 2018, **118**, e25569.

(193) C.-S. Wu, P.-Y. Lee and J.-D. Chai, *Scientific Report*, 2016, **6**, 1–9.

(194) T. Iwamoto, Y. Watanabe, H. Takaya, T. Haino, N. Yasuda and S. Yamago, *Chemistry - A European Journal*, 2013, **19**, 14061–14068.

(195) K. Yuan, Y.-J. Guo and X. Zhao, *The Journal of Physical Chemistry C*, 2015, **119**, 5168–5179.

(196) K. Yuan, C.-H. Zhou, Y.-C. Zhu and X. Zhao, *Physical Chemistry Chemical Physics*, 2015, **17**, 18802–18812.

(197) T. Iwamoto, Z. Slanina, N. Mizorogi, J. Guo, T. Akasaka, S. Nagase, H. Takaya, N. Yasuda, T. Kato and S. Yamago, *Chemistry - A European Journal*, 2014, **20**, 14403–14409.

(198) Y. Nakanishi, H. Omachi, S. Matsuura, Y. Miyata, R. Kitaura, Y. Segawa, K. Itami and H. Shinohara, *Angewandte Chemie - International Edition*, 2014, **53**, 3102–3106.

(199) H. Ueno, T. Nishihara, Y. Segawa and K. Itami, *Angewandte Chemie - International Edition*, 2015, **54**, 3707–3711.

(200) S. Kigure and S. Okada, *Journal of the Physical Society of Japan*, 2013, **82**, 094717.

(201) S. Kigure and S. Okada, *Journal of the Physical Society of Japan*, 2014, **53**, 06JD06.

(202) H. Isobe, S. Hitosugi, T. Yamasaki and R. Iizuka, *Chemical Science*, 2013, **4**, 1293–1287.

(203) H. Isobe, K. Nakamura, S. Hitosugi, S. Sato, H. Tokoyama, H. Yamakado, K. Ohno and H. Kono, *Chemical Science*, 2015, **6**, 2746–2753.

(204) T. Matsuno, S. Sato, R. Iizuka and H. Isobe, *Chemical Science*, 2015, **6**, 909–916.

(205) D. Lu, G. Zhuang, H. Wu, S. Wang, S. Yang and P. Du, *Angewandte Chemie - International Edition*, 2017, **56**, 158–162.

USC
UNIVERSIDADE
DE SANTIAGO
DE COMPOSTELA

Chapter 2

Objectives

This thesis is focused on studying the interactions established between fullerenes and ring-shaped molecules with nanosized inner cavity, commonly known as nanorings, nanohoops or nanobelts.

Since the discovery of fullerenes in 1985 many efforts have been spent in the study of their properties and, particularly in recent years, the possibility of their encapsulation with diverse species. Different molecules can form stable complexes with fullerenes such as porphyrins, subphthalocyanines or buckybowls. Many of these species exploit the size and shape complementarity between the convex surface of fullerenes and the concave surface of the host molecules, relying on the so-called concave–convex $\pi\cdots\pi$ interactions in most cases. Among the different kind of molecules capable of encapsulating fullerenes, the nanorings, and more specifically cycloparaphenylenes, have recently attracted much attention. These hoop-shaped species, synthesized barely a decade ago, are built with conjugated hydrocarbon units forming a concave cavity that can host molecules with convex surfaces as fullerenes. The possibility of tuning the cavity size and its properties makes these carbon nanorings a very interesting option for fullerene encapsulation. Due to their relative novelty, studies dealing with the characteristics of these species and their complexes are scarce. Therefore, a better comprehension of the interaction between fullerenes and nanorings seems mandatory to gain a deeper understanding of its characteristics in order to propose and design new complexes with specific properties.

The use of quantum chemistry calculations has amply demonstrated its potential and usefulness when it comes to making a rigorous and detailed interpretation of the characteristics of the systems studied. The application of computational methods allows an intimate knowledge, at a microscopic level, of the causes responsible of the behaviour of the chemical systems, allowing to rationalize the design of new complex systems such as those considered in this thesis. However, aromatic nanosystems show subtle dependencies between their structure, dynamics and photophysical properties that make them a challenge for modelling. The recent advances in computational chemistry, specifically the development of new functionals able to treat intermolecular interactions in a fairly precise way, together with the progress of cost-reducing methodologies, allow to treat these large systems. This opens a path for a better understanding of the interactions between host and guest in these complexes, as well as for proposing new host species with the proper electronic behaviour for the different fullerenes.

The study of the characteristics of complexes formed by fullerenes and nanorings is

a too wide field. Considering the relative novelty of these systems, this thesis will be focused on a better understanding on the fundamental level of the interaction between a variety of fullerenes and different nanorings. This thesis covers different aspects of nanoring-fullerene complexes, though it can be roughly divided on studies dealing with pristine fullerenes (Chapters 4–6) and studies considering endofullerenes (Chapters 7 and 8). Also, while Chapters 4, 5 and 7 deal with the fundamental questions of structure and stability of these complexes, in Chapters 6 and 8 the potential of nanoring-fullerene complexes as donor/acceptor pairs for photovoltaic devices is evaluated. A more detailed description of the objectives of each chapter is given in the following.

Chapters 4 and 5 are devoted to the interactions between pristine fullerenes (C_{50}, C_{60}, C_{70} and C_{76}) and nanorings ([10]CPP and [6]CPPA). In these chapters a thorough systematic search for the best arrangement of fullerenes inside the nanorings is performed. To this end, two different approaches are tested. The first one is to choose a subset of the most representative orientations of the fullerene inside the nanoring and optimise them, while the second strategy consists on a systematic search of all possible arrangements of the fullerenes inside the nanoring. The second approach is more computationally expensive by far and hardly applicable routinely for the rest of the systems under study. Thus, it is especially important to check whether the simplified search can guarantee a proper exploration of the configurational space of the complexes. On the other hand, the study of the interactions in these systems can help to understand which is the optimum size of the fullerene for each nanoring as well as the factors that control the interaction. The information gathered from these chapters would facilitate the study of more complex systems undergone in the rest of the thesis.

In Chapter 6, complexes formed by the most common fullerenes (C_{60} and C_{70}) and the nanohoops recently proposed by Kuwabara are considered. Kuwabara's nanohoops have been built with the purpose to act simultaneously as donor and acceptor moieties, with phenylene units acting as electron donors to an anthracene unit embedded in the nanoring. The presence of a complexed fullerene could lead to intermolecular charge transfer to the fullerene as in typical organic photovoltaic devices. A first goal of this chapter is to determine whether a stable complex is formed with the fullerene inside the cavity of the nanohoops (the cavity of these nanohoops is in fact too large for the fullerenes studied so encapsulation could be non-effective). The second goal is to study the electronic spectra of the complexes to check the characteristics of the transitions and the possibility of intermolecular charge transfer from the nanohoop to the fullerene.

Chapter 7 is devoted to study complexes formed by [11]CPP and a series of pristine and endohedral fullerenes, as the experimental study performed by Nakanishi proposing that mixtures of fullerenes could be purified by selective extraction with [11]CPP. In this chapter, pristine fullerenes of different size and shape (C_{60}, C_{70}, C_{76} and C_{78}) as well as endohedral fullerenes of diverse nature such as the clusterfullerene $Sc_3N@C_{80}$, the monometallic endofullerenes $Y@C_{82}$ and $Tm@C_{82}$, and the dimetallic endofullerenes $Y_2@C_{82}$ and $Lu_2@C_{82}$ have been employed to study the characteristics of their interaction with [11]CPP. The different sizes of the fullerenes employed would allow to obtain a deep knowledge of the relation between the fullerene/nanoring size matching and the complex stability. Moreover, the involvement of endofullerenes allows to check possible differences between the behaviour of pristine and endohedral fullerenes due to the presence of the endohedral units. Also, the results would give information about the origin of the

selectivity observed in the experiment.

Chapter 8 continues with the study of endohedral fullerenes but in this case considering endofullerenes containing a single alkali cation. The complexes formed by [10]CPP and several cationic endofullerenes were studied in order to obtain a better comprehension of the interaction between the nanoring and an endofullerene bearing a positive charge. The goal of this chapter is three-fold. First, a study has to be performed to determine the position of the cations inside the fullerene and how the presence of the cation modifies its electrostatic properties. Second, the characteristics of the interaction of the cationic endofullerenes and [10]CPP have to be determined, especially whether the presence of the cation modifies the strength of the interaction and the disposition of the fullerene inside the nanoring. Third, the study of the absorption spectra could be interesting, with the purpose to understand how the cationic endofullerene shifts the bands compared with pristine fullerenes. Also, it will be checked if enhancement of charge transfer transitions is observed and in such a case what is the origin of this behaviour.

USC
UNIVERSIDADE
DE SANTIAGO
DE COMPOSTELA

Chapter 3

Methodology

3.1 Interaction energy

The interaction energy accounts for the strength of the interaction that allows two molecules stay together (or not). This interaction energy is usually smaller than the bond energy, but it is essential in many systems like DNA or proteins to show a certain structure. When a system of several molecules is treated by a quantum chemistry method, an energy for the whole complex is obtained. The difference between this energy and the energy of the fragments that make up the complex is the interaction energy. For a complex formed by two fragments the energy would be given by:

$$E_{\mathrm{AB}} = E_{\mathrm{A}} + E_{\mathrm{B}} + \Delta E_{\mathrm{int}} \tag{3.1}$$

There are two different methodologies to calculate the interaction energy between two or more molecules, atoms, ions and so on. In the supermolecule method[1,2] the interaction energy is simply given as the difference between the energy of the complex and the energy of the monomers. Alternatively, the perturbation method[2–6] treats the interaction between the monomers as a perturbation and the interaction energy is obtained directly as a result.

3.1.1 Perturbation method

The basic theory of non-covalent interactions and the different contributions to the interaction as commented in the introduction has its origins in the application of the Perturbation Theory to a system formed by two molecules.[2]

By applying the perturbation method, different contributions to the interaction can be obtained that in many cases can be related with physically sound phenomena. The sum of these contributions is the total interaction energy. For a complex of two molecules the Hamiltonian of the system can be written as:

$$\hat{H} = \hat{H}_1 + \hat{H}_2 + \hat{V} \tag{3.2}$$

where $\hat{H}_1$ and $\hat{H}_2$ correspond to the Hamiltonian of molecules 1 and 2 and $\hat{V}$ is the intermolecular operator:

$$\hat{V} = \sum_{A1}\sum_{B2}\frac{Z_A Z_B}{r_{AB}} - \sum_{A1}\sum_{b2}\frac{Z_A}{r_{Ab}} - \sum_{a1}\sum_{B2}\frac{Z_B}{r_{aB}} + \sum_{a1}\sum_{b2}\frac{1}{r_{ab}} \tag{3.3}$$

where a and b are the electrons of molecules 1 and 2 and the uppercase corresponds to the nuclei.

With this selection of Hamiltonian that takes as reference system the two isolated molecules, perturbation theory is applied considering that the molecules are far apart, excluding intermolecular exchange effects. As a result, the following terms are obtained to second order, corresponding to electrostatic, polarization and dispersion contributions:

$$E_{es} = \langle \psi_{1,0}\psi_{2,0}|V|\psi_{1,0}\psi_{2,0}\rangle \tag{3.4}$$

$$E_{pol} = \sum_{i>0} \frac{|\langle \psi_{1,0}\psi_{2,0}|V|\psi_{1,i}\psi_{2,0}\rangle|^2}{\varepsilon_{1,0} - \varepsilon_{1,i}} + \sum_{j>0} \frac{|\langle \psi_{1,0}\psi_{2,0}|V|\psi_{1,0}\psi_{2,j}\rangle|^2}{\varepsilon_{2,0} - \varepsilon_{2,j}} \tag{3.5}$$

$$E_{disp} = \sum_{i>0}\sum_{j>0} \frac{|\langle \psi_{1,0}\psi_{2,0}|V|\psi_{1,i}\psi_{2,j}\rangle|^2}{\varepsilon_{1,0} + \varepsilon_{2,0} - \varepsilon_{1,i} - \varepsilon_{2,j}} \tag{3.6}$$

considering that the ground-state wavefunctions are $\psi_{1,0}$ and $\psi_{2,0}$, the excited-state wavefunctions are $\psi_{1,i}$ and $\psi_{2,j}$ and the corresponding eigenvalues are $\varepsilon_{1,0}$, $\varepsilon_{2,0}$, $\varepsilon_{1,i}$ and $\varepsilon_{2,j}$.

Of course, the neglect of exchange effects invalidates this approach at short distances, so more involved approaches have been developed such as symmetry adapted perturbation theory (SAPT)[5] or intermolecular perturbation theory (IMPT)[7] in which the exchange effects are included.

3.1.2 Supermolecule method

In the supermolecule method the interaction energy is simply obtained as the difference between the energy of the complex and the energies of its constituent fragments.[2] The interaction energy can be obtained as:

$$\Delta E_{\text{int}} = E_{\text{AB}}^{\text{AB}}(\text{AB}) - E_{\text{A}}^{\text{AB}}(\text{A}) - E_{\text{B}}^{\text{AB}}(\text{B}) \tag{3.7}$$

where the subscript refers to the energy of the dimer (AB) or the monomer (A,B), the superscript indicates the geometry of the species, and the term in parentheses refers to the basis set employed.

The interaction energy is usually a small quantity that is obtained as a difference between two much larger quantities. Therefore, the consistency of the values obtained for the complex and the fragments has to be ensured to get proper values. This is in fact the origin of the most famous error associated to the computation of interaction energies, the basis set superposition error (BSSE).

3.1.3 Basis set superposition error (BSSE)

The supermolecule method has a major drawback: in the study of the interaction energy an artificial shortening of the distance and a strengthening of the interaction between the monomers are usually found. The origin of these artifacts is the use of a finite basis set. Due to the physical impossibility to use a complete basis set, the complex is described with a finite basis set, in which the monomer A is artificially stabilised as it is approximated to monomer B. The reason of this extra stabilisation with respect to the isolated monomers

is that the monomer A uses the basis set of the monomer B and vice versa. That is to say, the energy of the different monomers are obtained through their respective basis set, while the energy of the complex is obtained through a combination of the basis sets of the monomers. The unphysical extra stabilisation due to the combined basis set is known as basis set extension effect.[8] This error, due to the unbalanced basis set used in the description of the different parts of the systems is known as basis set superposition error (BSSE) and it was reported by Kestner in 1968,[9] though the term BSSE was introduced 5 years later.[10]

The BSSE does not have a physical reason because it is caused by a mathematical artifact. This error depends on several factors like the size of the basis set, the level of calculation or the system treated. For example, if the basis set is near to the complete basis set then the BSSE is practically null; also, when post-HF methods are used usually the error is bigger than in HF methods. However, this error does not affect only the complexes, in a single molecule one part of the system can be stabilised by a basis set of another part of the molecule leading to an error in the final energy.[11,12] In conclusion, the BSSE depends on several factor but the most important one is the method and extension of the basis set used.[13]

3.1.3.1 Counterpoise correction

There are several methods to correct the BSSE, but one of the most widely used is the counterpoise correction (CP) developed by Boys and Bernardi.[14] In the CP, the energy of the monomers is obtained with the same basis set as the complex, *i.e.*, all the energies are evaluated with the same basis set. Therefore the interaction energy is the difference between the energy of the dimer and the monomers as following:

$$\Delta E_{\text{int}}^{CP} = E_{\text{AB}}^{\text{AB}}(\text{AB}) - E_{\text{A}}^{\text{AB}}(\text{AB}) - E_{\text{B}}^{\text{AB}}(\text{AB}) \tag{3.8}$$

The BSSE based on equation 3.7 and 3.8 could be defined as:

$$BSSE = E_{\text{A}}^{\text{AB}}(\text{A}) - E_{\text{A}}^{\text{AB}}(\text{AB}) + E_{\text{B}}^{\text{AB}}(\text{B}) - E_{\text{B}}^{\text{AB}}(\text{AB}) \tag{3.9}$$

The use of the CP correction removes the BSSE for the basis set, but if the election of the level of calculation is wrong the resulting interaction energy, even using the CP, is wrong and it may be far from the experimental value. For this reason a careful choice of the basis set seems mandatory for a proper interaction energy. Another problem with the CP correction is an overcorrection when a small basis set is used, but it is easily solved increasing the size of the basis set.

3.1.3.2 Complexation energy

A slight variation of the interaction energy is the complexation energy that it is crutial to study the complex formation.[15,16] The complexation energy is the interaction energy plus a new term called deformation energy. The new term is the energy cost involved in changing the geometry of the monomer from its optimised structure to the geometry in the complex. In literature the deformation energy is also denoted as preparation energy (the energy associated to prepare the monomers to form the complex)[17] or relaxation

energy (is the term opposite to the deformation energy, the geometry of the monomer in the complex needs to relax in order to assume the geometry when it is isolated).[18]

$$\Delta E_{\text{compl}} = \Delta E_{\text{int}} + \Delta E_{\text{def}} \tag{3.10}$$

$$E_{\text{def}} = E_{\text{A}}^{\text{AB}}(\text{A}) - E_{\text{A}}^{\text{A}}(\text{A}) + E_{\text{B}}^{\text{AB}}(\text{B}) - E_{\text{B}}^{\text{B}}(\text{B}) \tag{3.11}$$

To sum up, the BSSE is originated by the use of an incomplete basis set to describe the system and the counterpoise correction is one of the solutions to solve the BSSE. However, during the last decades the BSSE and CP have been broadly studied,[19–22] but they are still controversial. On the other hand the use of the complexation energy is important to obtain a proper interpretation of the system, especially when large geometry changes occur in monomers to form the final complex.

3.2 Density functional theory (DFT)

Nowadays, DFT is one of the most used methods to obtain different properties of the molecules, due to the good results obtained with smaller computational cost compared to the post-Hartree-Fock (post-HF) methods that also include the electronic correlation.[23,24] The main premise of this theory is that the information can be obtained through the electron density unlike the HF or post-HF methods that are based in the wavefunction. In wavefunction methods, the wavefunction includes four variables, three spacial and one spin coordinate for each electron, whereas DFT only includes the three spacial coordinates, decreasing the computational cost and being independent of the number of electrons of the system.

The first approximations to DFT was developed by Thomas and Fermi in 1927.[25–27] However, the high inaccuracy of their development made this method useless for years. It had to wait until 1964 when Hohenberg and Kohn[28–30] formulated two theorems that are essential to establishing DFT as a new methodology:

Theorem 1 (Hohenberg-Kohn Existance Theorem)**.** *Any observable of a stationary non-degenerate ground state can be calculated, exactly in theory, from the electron density of the ground state. In other words, any observable can be written as a functional of the electron density of the ground state.*

This first theorem is only valid when the electron density ($\rho(\boldsymbol{r})$) is N-representable and v-representable. The density is N-representable when there is a function defined in the entire space for $\rho(\boldsymbol{r})$ that must be positive, and the value of its integral must match with the number of electrons:

$$\rho(\boldsymbol{r}) \geq 0 \qquad \text{and} \qquad \int \rho(\boldsymbol{r}) d\boldsymbol{r} = N \tag{3.12}$$

The density is v-representable if there is an external potential from which it is possible to derive the density $\rho(\boldsymbol{r})$. When these two premises are fulfilled and the ground state is non-degenerate the energy of the system is:

$$E[\rho] = T[\rho] + V_{Ne}[\rho] + V_{ee}[\rho]\ (+V_{NN}[\rho]) \tag{3.13}$$

where $T[\rho]$ is the kinetic energy, $V_{Ne}[\rho]$ is the nuclear-electron attraction, $V_{ee}[\rho]$ is the electron-electron repulsion and $V_{NN}[\rho]$ is the nucleus-nucleus potential (when the Born-Oppenheimer approximation[31] is applied this term is constant).

According to the previous equation and for a specific external potential the energy has the form:

$$E_v[\rho] = T[\rho] + \int \rho(\boldsymbol{r}) v_n(\boldsymbol{r}) d\boldsymbol{r} + V_{ee}[\rho] \tag{3.14}$$

Theorem 2 (Hohenberg-Kohn Variational Theorem)**.** *The electron density of a non-degenerate ground state can be calculated, exactly in theory, determining the density that minimizes the energy of the ground state.*

Therefore if a trial density is $\widetilde{\rho}(\boldsymbol{r})$, then the exact energy, E_0 is:

$$E_0 \leq E_v[\widetilde{\rho}(\boldsymbol{r})] \tag{3.15}$$

So, according to equation 3.15 the variational principle for the energy is fulfilled, so it is possible to try to find the density that minimizes the energy, thus obtaining the exact energy for the ground state.

$$\left[\frac{\partial E_v[\rho]}{\partial \rho}\right] = 0 \tag{3.16}$$

3.2.1 Kohn-Sham theory

In spite of the great relevance of the Hohemberg-Kohn theorems they only say that it is possible to obtain the energy of a system using the density, but not the way to find it. It had to wait only one year until Kohn and Sham proposed a method that consists in introducing orbitals to calculate the energy from the density.[23,32] The starting point consists on the use of a system in which the electrons do not interact among themselves and move under a external potential. In this system the Hamiltonian and the exact wavefunction are:

$$\hat{H}_s = -\frac{1}{2}\sum_{i=1}^{N} \nabla^2(i) + \sum_{i=1}^{N} \hat{v}_s(i) \tag{3.17}$$

$$\phi_s = \frac{1}{\sqrt{N!}} \left|\chi_1(1) \cdots \chi_N(N)\right| \tag{3.18}$$

When the external potential is applied to the system it provides a wavefunction with the same density as the real system and after applying the fundamental equation of DFT the following equation is obtained:

$$\frac{\partial E_v[\rho]}{\partial \rho(\boldsymbol{r})} = \frac{\partial T_s[\rho]}{\partial \rho(\boldsymbol{r})} + v_s(\boldsymbol{r}) = \mu \tag{3.19}$$

with

$$E_v[\rho] = T_s[\rho] + \int \rho(\boldsymbol{r}) v_s(\boldsymbol{r}) d\boldsymbol{r} \tag{3.20}$$

where the subscript s refers to the single-electron term.

The equations 3.14 and 3.20 show the energy for the real system and the non-interacting system, respectively. The equation 3.20 omits the term for the electron repulsion because in the reference system it is considered that the electrons do no interact among themselves. Finally, it should be kept in mind that the kinetic energy for the real system, $T[\rho]$, and for the reference system $T_s[\rho]$ are different and they are only the same when the HF solution is exact.

Considering that $J[\rho]$ is the Coulomb repulsion energy, the equation 3.14 can be reorganised in the following way:

$$\begin{aligned} E_v[\rho] &= T[\rho] + \int \rho(\boldsymbol{r}) v_n(\boldsymbol{r}) d\boldsymbol{r} + V_{ee}[\rho] - J[\rho] + J[\rho] - T_s[\rho] + T_s[\rho] \\ &= T_s[\rho] + \int \rho(\boldsymbol{r}) v_n(\boldsymbol{r}) d\boldsymbol{r} + J[\rho] + (T[\rho] - T_s[\rho]) + (V_{ee}[\rho] - J[\rho]) \end{aligned} \tag{3.21}$$

In the above equation it is possible to extract the exchange-correlation energy, obtaining the following form:

$$E_{XC}[\rho] = (T[\rho] - T_s[\rho]) + (V_{ee}[\rho] - J[\rho]) \tag{3.22}$$

$(T[\rho] - T_s[\rho])$ is the correlation kinetic energy and $(V_{ee}[\rho] - J[\rho])$ is the exchange-correlation energy. This equation gives the different contributions to the energy that are impossible to express as a function of the electron density. Particularly this expression includes the exchange and correlation energy, and two corrections, one for the kinetic energy of the reference system and another for the self interaction energy through the term $J[\rho]$.

As in the reference system after applying the fundamental equation of DFT we obtain the same equation but changing $v_s(\boldsymbol{r})$ for $v_{eff}(\boldsymbol{r})$:

$$v_{eff}(\boldsymbol{r}) = v_n(\boldsymbol{r}) + \int \frac{\rho(\boldsymbol{r}_2)}{|\boldsymbol{r}_1 - \boldsymbol{r}_2|} d\boldsymbol{r} + v_{XC}(\boldsymbol{r}) \tag{3.23}$$

where the subscript n refers to a system with n interacting electrons. Therefore the next equations are obtained:

$$\hat{h}_{KS}\chi_i = \varepsilon_i \chi_i \tag{3.24}$$

$$\hat{H}_{KS} = -\frac{1}{2}\nabla^2 + \sum_{i=1}^{N} \hat{v}_s(i); \qquad \langle \chi_i | \chi_j \rangle = \delta_{ij} \tag{3.25}$$

The previous equations are similar to the Hartree-Fock equations, but the orbitals are the Kohn-Sham orbitals from which the electron density is calculated. The resolution of the equation starts with a set of trial molecular orbitals, $\{\chi_i(\boldsymbol{r})\}$, from which the density is obtained and they are used to calculate $v_{eff}(\boldsymbol{r})$ and to obtain the values and the eigenfunctions through the equation 3.24. Like Hartree-Fock, this process must be repeated until the convergence of values.

Keep in mind that ψ^{KS} is only an approximation, and even if the $v_{XC}(\boldsymbol{r})$ are exact, ψ^{KS} is not the exact wavefunction, thus it is preferable to avoid its use to calculate observable values. However, some works show that the use of the eigenvalues of the Kohn-Sham equations have a good agreement with the experimetal values or the wavefuncion methods like HF to calculate the affinity or the ionization energy. Moreover, the shape and the symmetry show a suitable agreement too.[33,34]

Finally, all the terms in equation 3.24 are known except the exchange-correlation energy, thus the density of the system and the energy approximate to their exact values as $v_{XC}(\boldsymbol{r})$ approximates to the exact exchange-correlation potential. For this reason a proper development of the $v_{XC}(\boldsymbol{r})$ seems mandatory to obtain accurate results.[30]

3.2.2 Classification of exchange-correlation functionals

The exchange-correlation functional (v_{XC}) is essential to obtain good results in DFT, so the choice of this functional is extremely important. There are two main approaches to obtain the parameters during the development of these functionals. The first one is to fit some parameters to experimental data, while the other approach is to fulfil some properties that the exact functional should have; nevertheless, the combination of the two previous methods is used too.[35,36]

The exchange-correlation energy (E_{XC}) should be separated in two parts due to different scaling properties, a pure exchange part E_X and a pure correlation part E_C. However, only the combination of the two parts has a physical meaning.

In wavefunction methods the quality of the method can be categorized through the way in which the correlation energy is obtained. On the other hand, the different approximations for the exchange-correlation functional makes more difficult a similar classification in DFT. In 2001 Perdew suggested the "Jacob's ladder" approach,[37,38] where each step of the ladder assumed comes with a improvement in the accuracy of the method. Consequently the first steps of the ladder are:

3.2.2.1 Local Density Approximation (LDA)

In this approximation the exchange-correlation energy is treated as an uniform electron gas, in which the value of the exchange-correlation functional on a given point depends only on the density at that point. LDA assumes that the density for α and β are equal, but in open-shell systems this is not true. Therefore, this approximation must be replaced by the "Local Spin Density Approximation" (LSDA). Usually in LSDA the exchange and the correlation part are different functionals and the final energy is the sum of these contributions. Unfortunately, this approximation gives energies about 10% less than the exact energy in molecular systems, nevertheless it is widely used in metallic systems in which the electron density varies slowly. The most common functional is VWN.[39]

3.2.2.2 Generalized Gradient Approximation (GGA)

The next step is the GGA which is an improvement of LSDA. In this case the exchange-correlation energy does not only depends on the density, but also includes a dependency on the gradient of the density. However, the straightforward inclusion of this term destroys some important properties, and for that reason it is necessary to add some modification to fulfil the properties that the exact functional must satisfy. Like the LDA functionals the GGA functionals are usually divided into the exchange and the correlation contribution and generally each of those contributions has a different functional.

One of the most common functionals for the exchange part was developed by Becke (B or B88)[40,41] while for the correlation part the most common functional was developed by Lee, Yang and Parr (LYP).[42] The combination of the exchange and correlation parts give

the functional BLYP. However, other researchers prefer to develop the exchange and the correlation part at the same time being possible its division in these different contributions, like Perdew-Wang (PW91)[43] or Perdew-Burke-Ernzerhof (PBE).[44] On the other hand, the functional B97-D developed by Grimme[45] has the correlation and exchange part mixed, that is to say, it is impossible to obtain the exchange part separately from the correlation.

3.2.2.3 Meta-GGA

The Meta-GGA functionals consist in the inclusion of the second derivative of the density, being the Laplacian ($\Delta^2\rho$) the second-order term. However, like an alternative to the Laplacian, it is possible to use the orbital kinetic energy density (τ) because it provides the same information and it is numerically more stable. The meta-GGA has a small increase in the computational cost with respect to the GGA, but in general they produce higher accuracy in their results than the previous steps. Some functionals of this type are B95[46] and TPSS.[47]

3.2.2.4 Hybrid

The hybrid functionals include part of the exact Hartree-Fock exchange energy in the exchange-correlation functional, *i.e.*, the exchange energy for the hybrid functional is the combination of three terms: the exact exchange energy or at least a part of it, the LSDA energy and the gradient correction term. On the other hand, the correlation energy only includes two terms, the LSDA energy and the gradient correction.

The most common hybrid functional is B3LYP.[48] This functional includes three parameters that are fitted to experimental data with the purpose to obtain the value of each term. Other functionals are PBE0,[49] in which the starting point is the functional PBE and the exact exchange part is added, or TPSSh[47] that includes about 10% of the exact exchange energy. Usually these hybrid functionals improve the results of the previous steps because the inclusion of the exact exchange part reduces the self-interaction error.

3.2.2.5 Long-range corrected functionals

The long-range corrected functionals were proposed by Savin[50] to solve some of the problems of the exchange-correlation functional like the wrong excitation energies for charge-transfer states or the underestimation of Rydberg states. Following the equation proposed by Tsunada[51] the two electron operator can be divided into two parts:

$$\frac{1}{r_{12}} = \frac{1-\mathrm{erf}(\mu r_{12})}{r_{12}} + \frac{\mathrm{erf}(\mu r_{12})}{r_{12}} \tag{3.26}$$

In this correction there are a first part for the short-range interaction which uses the DFT exchange functional, and a second part for the long-range interactions in which the HF exchange integrals are employed to describe the long-range orbital-orbital exchange interaction.

CAM-B3LYP[52] is the long-range correction of the functional B3LYP. B3LYP functional is one of the most used functional; nevertheless it has some problems in the description of excitations in Rydberg or charge transfer states. These problems at long-range distance can be understood due to a wrong behaviour of the exchange potential, B3LYP

behaves as $-0.2r^{-1}$ instead of $-r^{-1}$ which is the correct potential shape. Using the equation 3.26 and adding two extra parameters (α and β) it is possible to correct this behaviour. The best parameters for these variables are $\alpha = 0.19$ and $\alpha + \beta = 0.65$, while $\mu = 0.33$ which is the mixing parameter between the B88 exchange functional and HF exchange, for correlation the Becke's VWN5/LYP functional is employed. However, this is not the only long-range functional, other functionals are ωB97XD[53] or LC-ωPBE.[54]

3.2.3 Time-dependent DFT

Time-dependent density functional theory (TD-DFT) was developed with the purpose to describe systems that are not stationary, that is to say, a system that is found in the ground state initially and exposed to a time-dependent perturbation that produces a modification in the external potential. TD-DFT allows to calculate the structure in the excited states besides other properties like emission wavelength, dipole moment or to resolve the optical spectra.[55,56]

TD-DFT started in 1984 when Runge and Gross demonstrated a theorem that proves that the dependence between the time-dependent one-body density $\rho(\boldsymbol{r}, t)$ and the time-dependent potential $v(\boldsymbol{r}, t)$ is unique.[57] In 1995 Casida developed a formalism, called Casida's equations, which allows a fast and effectively solution of the TD-DFT equations.[58] The method used to solve the TD-DFT is similar to the Kohn-Sham for DFT leading to the time-dependent Kohn-Sham equation:

$$i\frac{\partial}{\partial t}\psi_i(\boldsymbol{r}, t) = \left[-\frac{\nabla^2}{2} + v_{eff}(\boldsymbol{r}, t)\right]\psi_i(\boldsymbol{r}, t) \tag{3.27}$$

where the orbitals used are the time-dependent Kohn-Sham orbitals.

As in the case of the time-independent solution, it is necessary to use an auxiliary system of non-interacting electrons, but at the end the same density as the real system is obtained. Following a similar procedure than the time-independent version an almost identical equation is obtained:

$$v_{eff}(\boldsymbol{r}) = v_{ext}(\boldsymbol{r}, t) + \int \frac{\rho(\boldsymbol{r}_2, t)}{|\boldsymbol{r}_1 - \boldsymbol{r}_2|} d\boldsymbol{r} + v_{XC}(\boldsymbol{r}, t) \tag{3.28}$$

If the equation 3.23 is compared to equation 3.28 the main difference is that $v_n(\boldsymbol{r})$ in the time-independent case is changed for $v_{ext}(\boldsymbol{r}, t)$. This term includes the interaction between electrons and nuclei, whose position change with the time, and other potential which involves the dependency with time. The other difference is the use of a time-dependent exchange-correlation functional. The most common solution to avoid using time-dependent exchange-correlation functionals is to use the same functionals than DFT but using an electron density that changes with time. The electron density is obtained at different times and employed to solve the time-dependent problem. This is possible because most of the functionals use the adiabatic approximation that allows the use of the time-independent solution.

There are two ways to solve a TD-DFT problem, the first one is the linear-response theory which is possible to apply when the time-dependent potential is weak, and the second one is the full solution of the Kohn-Sham equations that is mandatory when the time-dependent potential is strong.

In the case of the linear-response theory, all the excitation energies present a pole in the response function, thus it is possible to calculate the excitation energies through the poles. The linear response depends linearly on the external potential and the density-density response function (χ), but while χ is difficult to calculate, the density-density response function for a non-interacting system (χ_s) is more affordable and it allows to obtain $\delta\rho(\boldsymbol{r},\omega)$.

$$\delta\rho(\boldsymbol{r},\omega) = \int d\boldsymbol{r}'\chi_s(\boldsymbol{r},\boldsymbol{r}',\omega)\delta v_{eff}(\boldsymbol{r}',\omega) \tag{3.29}$$

After some transformations it is possible to obtain an eigenvalue problem, so its solution gives the true excitation energies (Ω):

$$\sum_{q'}(M_{qq'}(\Omega) + \omega_q\delta_{qq'})\beta_{q'} = \Omega\beta_q \tag{3.30}$$

where q is a pair of Kohn-Sham orbitals, ω_q is the difference in orbital energy for the Kohn-Sham orbitals and $M_{qq'}$ are the elements of the coupling matrix.

With the purpose to solve this equation some truncations can be applied; the most common used is the Single-Pole Approximation with a remarkable concordance with experimental results.

On the other hand a full TD-DFT solution must be applied to obtain a proper value for non-linear optical properties or for a large number of photochemical reactions due to the strong dependency of the time-dependant potential. To solve equation 3.27 an initial state is considered at ($t = 0$) and the electron density is obtained through the Kohn-Sham orbitals. After that, this state is propagated according the Kohn-Sham orbitals until a final time. However, due to the large interval of time it is usually divided into smaller intervals to increase the accuracy.

Another fundamental part for the full solution is the nuclei motion that can be obtained by the Verlet algorithm.[59] Solving both equations, the TD-DFT and the motion of the nuclei, it is possible to study many photochemical reactions.

Finally, it is important to notice that TD-DFT has several problems like an incorrect description of conical intersections, the prohibitive cost in large system and the wrong description of charge transfer. This last error and in particular the transfer of an electron of one molecule to another was extensively studied in literature.[60–62] The GGA functionals underestimate the excitation energy by several eV, but its value it is partially fixed using hybrid functionals. One step forward is the use of long-range functionals like CAM-B3LYP which improves results in charge transfer process.[63]

3.2.3.1 Visualization of charge transfer excitations

Organic photovoltaic devices (OPVs) usually work by means of an electron transfer associated to a transition due to the absorption of light. Thus, the core of a OPV is a couple formed by a pair of species acting as electron acceptor and electron donor, respectively. As commented in the introduction, most OPVs employ fullerenes as electron acceptors, while a large variety of species can be employed as donors. Upon excitation, an electron of the electron donor ends at the electron acceptor creating the electric current. Therefore, to test the capability of a given donor/acceptor pair, some way of estimating its tendency to electron transfer must be employed. This implies some problems, because common

functionals do not describe charge transfer transitions properly, though long range corrected variants such as CAM-B3LYP or ωB97XD are capable to improve the predictions. Even though some transitions can be associated to charge transfer, the transfer rarely moves one electron from the donor to the acceptor because in many cases, the electron is delocalized in the intermolecular regions.

In this context, it would be very interesting to have a tool that allows to quantify whether a transition corresponds to a charge-transfer one, and whether this transition is associated to the donation of an electron from the donor to the receptor species. Le Bahers *et al.*[64] developed some indexes with the goal of allowing a better comprehension of the charge transfer phenomena using the electronic densities of the ground ($\rho_{\mathrm{GT}}(r)$) and the excited states ($\rho_{\mathrm{EX}}(r)$).

The density change associated to a specific electronic transition is given by:

$$\Delta\rho(r) = \rho_{\mathrm{EX}}(r) - \rho_{\mathrm{GS}}(r) \tag{3.31}$$

Now, two new functions are defined to take into account the increment or depletion of the density during the absorption:

$$\rho_+(r) = \begin{cases} \Delta\rho(r) & \text{if } \Delta\rho(r) > 0 \\ 0 & \text{if } \Delta\rho(r) < 0 \end{cases} \tag{3.32}$$

$$\rho_-(r) = \begin{cases} \Delta\rho(r) & \text{if } \Delta\rho(r) < 0 \\ 0 & \text{if } \Delta\rho(r) > 0 \end{cases} \tag{3.33}$$

The barycentre associated to the spatial region of the incremented and depleted density, $\rho_+(r)$ and $\rho_-(r)$ respectively, can be defined as:

$$R_+ = \frac{\int r\rho_+(r)dr}{\int \rho_+(r)dr} = (x_+, y_+, z_+) \tag{3.34}$$

$$R_- = \frac{\int r\rho_-(r)dr}{\int \rho_-(r)dr} = (x_-, y_-, z_-) \tag{3.35}$$

Finally, the distance between the positive and negative barycentre can be used to measure the CT excitation length (D_{CT}).

$$D_{\mathrm{CT}} = |R_+ - R_-| \tag{3.36}$$

While the amount of charge transfer between the donor and the acceptor (q_{CT}) can be defined as:

$$q_{\mathrm{CT}} = \int \rho_+(r)dr = -\int \rho_-(r)dr \tag{3.37}$$

Figure 3.1 shows an example of this procedure for a given transition in a fullerene-nanoring complex. The regions where electron density is depleted are shown in red and the regions where the density increases in blue. The figure helps to understand how the charge moves upon excitation, which regions of the system are involved, and whether there is an intermolecular charge transfer from donor to acceptor. The position of the

barycentres of charge shown in Figure 3.1b helps to visualize the extent of the electron transfer.

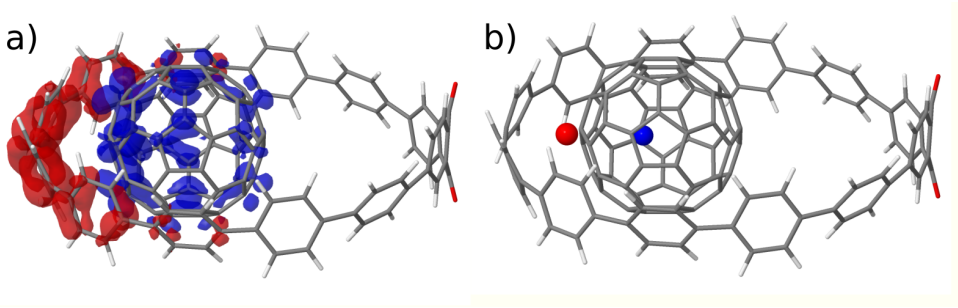

Figure 3.1: a) Difference density between the ground state and the excited state, b) Position of the barycentre of charge. The blue sphere correspond to the positive barycentre (R_+) and the blue sphere is the negative barycentre (R_-).

3.2.4 Problematic cases for using in DFT

Undoubtedly, DFT is a very promising method with many achievements in different fields. Nevertheless, it has some weak points due to the form to obtain the exchange-correlation functional.[35] Some of the cases were DFT has shown problems are:

1. **Transition states or breaking bonds:** The systems which dissociate in two parts with odd-electrons have a poor description of the dissociation energy with DFT. This dissociation shows an artificial barrier in some situations. Also, the transition states are predicted to be more stable than they really are, because the barriers are underestimated. A solution to this problem is the inclusion of the exact exchange energy, thus the use of hybrid functional usually gives reasonable barriers.

2. **Weak interactions:** Weak interactions between nonpolar molecules are usually dispersive in nature. No common functional is capable of reproducing the R^{-6} dependence at long distances. Therefore, the description of dispersion interactions is wrong with most functionals. In fact, most functional even display a repulsive interaction between nonpolar systems such as graphene sheets or dimers of noble gases. One easy way to solve this problem is the use of empirical dispersion corrections.

3. **Self-interaction error (SIE):** In wavefunction methods the Coulomb interaction just includes interactions for two particles. However in DFT, the energy is a functional of the single-particle density. For that reason, it is very difficult to distinguish between the interactions that happen between two bodies or the interaction of a particle with itself, that means that the Coulomb energy includes the interaction of a particle with its own density. The way to decrease the effect of the SIE is through a optimum exchange-correlation functional, or using hybrid functionals.[65]

4. **Charge transfer excitations:** When one electron is transferred over a long distance the exchange-correlation functional produces an error of several eV in the excitation energy. This problem is due to a poor description of the Coulombic

attraction between the excited electron and the hole formed by its excitation, produced by a wrong long-range behaviour of the exchange-correlation functionals.[60,66] For this reason the long-range correction was developed.

5. **States with different spin density are not proper described:** The energy difference between a singlet state and a triple state depends on the exchange-correlation functional. Pure DFT functionals have some errors in the description of this different spin density. Nevertheless, the hybrid methods produce better results because they include part of the exact exchange energy.

3.2.5 Dispersion correction

As mentioned above, one of the problems with DFT is the incorrect description of long-range dispersion. The semi-local nature of common DFT functionals leads to an incorrect description of the asymptotic decay of the electron density and in consequence cannot reproduce the R^{-6} behaviour of dispersion at long distances. This error was firstly found in the description of rare gases, but it was quickly realized that it was a more general problem, affecting the values obtained for interacting systems ranging from nitrogen dimer to graphite sheets. Thus, while functionals such as PW91 are capable to provide a qualitatively correct interaction potential (they predict a potential energy well), others (among them the very popular B3LYP) produce a pure repulsive interaction potential, in clear disagreement with observation.

For this reason, different corrections have been developed during the last years to correct common DFT functionals and make them suitable for the description of dispersion. These dispersion corrections are based in different approaches; for instance, Grimme's group developed some corrections that only requires the geometry to obtain the dispersion energy, but the parameters used to obtain the dispersion coefficients are computed by time-dependent DFT in their models.[45,67–69] Other approaches depend on the electron density (Tkatchenko and Scheffler),[70] exchange dipole moment (Becke and Johnson),[71] or they are based on a local-response dispersion model (Sato and Nakai).[72,73]

3.2.5.1 Grimme's dispersion corrections

During the last decade the most used approximations have been the empirical corrections proposed by Grimme, which give quite good results at a negligible computational cost. The procedure followed by Grimme simply consists on adding an empirical term describing the part of the dispersion interaction that cannot be recovered by the functional, thus improving the global performance of the functional when dispersion contributions to the energy are important.[74]

$$E_{\text{DFT-D}} = E_{\text{DFT}} + E_{\text{disp}} \tag{3.38}$$

Grimme has proposed different dispersion models of increasing complexity and accuracy in order to make these terms more universal while keeping the simplicity of the original formulation. Following there is a more detailed description of these terms as employed in this thesis.

3.2.5.1.1 DFT-D2

The first empirical correction for dispersion proposed by Grimme was developed for a restricted set of atoms and functionals,[67] and a couple of years later was improved to give rise to the so-called DFT-D2 method.[45] The new dispersion correction corrected some of the deficiencies observed in the first model, such as an overestimation of the contribution of the light atoms due to the combination rules applied for obtaining the dispersion coefficients. Also, the model was extended to a larger set of atoms and functionals. The empirical dispersion term in this method is obtained as:

$$E_{\text{disp}} = -S_6 \sum_{i=1}^{N_{at}-1} \sum_{j=i+1}^{N_{at}} \frac{C_6^{ij}}{R_{ij}^6} f_{dmp}(R_{ij}) \tag{3.39}$$

where N_{at} is the number of the atoms in the system, C_6^{ij} is the dispersion coefficient for a given atom pair ij, S_6 is a scaling factor that depends on the functional used (1.25 in B97-D2), R_{ij} is the interatomic distance and f_{dmp} is a damping function to avoid collapse of the dispersion contribution at short distances. The S_6 parameters are obtained through a fitting of the complexation energy and intermolecular distance for typical molecules of a data set. On the other hand, the dispersion coefficients for a given atom pair are obtained from atomic values by applying a suitable combination rule, in this case a geometric mean:

$$C_6^{ij} = \sqrt{C_6^i C_6^j} \tag{3.40}$$

with the atomic coefficients for a given atom obtained as:

$$C_6^a = 0.05 N I_p^a \alpha^a \tag{3.41}$$

where I_p^a is the ionization potential and α^a is the static dipole polarizability. The damping function has the form:

$$f_{\text{dmp}}(R_{ij}) = \frac{1}{1 + e^{-d(R_{ij}/R_r - 1)}} \tag{3.42}$$

where R_r is the sum of the van der Waals radii of atoms i and j, and d is a constant with value 20. The value of the damping function only depends on atomic parameters obtained for free atoms, and on the specific geometry considered.

The inclusion of this quite simple empirical function greatly improves the results obtained from common functionals for non-covalent complexes, as it greatly improves the description of concave–convex interactions, π stacking, and other interactions with significant role of dispersion.[45,69,75,76]

3.2.5.1.2 DFT-D3

Some years later a new version of DFT-D, so-called DFT-D3, was released by Grimme.[68] This new dispersion-corrected method is less empirical that the previous one. Among the changes made in this version are the inclusion of an asymptotically correction for all the functionals, both for finite systems and nonmetallic infinite systems and the explicit calculation of atom pair-specific dispersion coefficients and cutoff radii. Nevertheless, the most important new feature is the inclusion of environment-dependent coefficients, that allows to assign different dispersion coefficients for a given atom in different molecular environments.

To reduce the degree of empiricism of the method, a new way to obtain the atomic contributions is considered; the atomic coefficients (C_6^{AB}) are calculated now at time-dependent DFT (TD-DFT) level, while the higher-multipole terms are obtained by recursion relations (C_8^{AB} or C_{10}^{AB}). Only the C_8^{AB} is included on this method because the other higher order terms leads to an unstable situation when rare molecules are considered, moreover these terms do not improve the results for the most common cases. The well known Casimir-Polder formula is the starting point in this method:

$$C_6^{AB} = \frac{3}{\pi}\int_0^\infty \alpha^A(i\omega)\alpha^B(i\omega)d\omega \tag{3.43}$$

where $\alpha^A(i\omega)$ is the averaged dipole polarizability at imaginary frequency ω.

The recursion relation for C_8^{AB} is:

$$C_8^{AB} = 3C_6^{AB}\sqrt{Q^A Q^B} \tag{3.44}$$

where

$$Q^A = s_{42}\sqrt{Z^A}\frac{\langle r^4\rangle^A}{\langle r^2\rangle^A} \tag{3.45}$$

where $\langle r^4\rangle$ and $\langle r^2\rangle$ are simple multipole-type expectation values derived from atomic densities.

The problem in equation 3.43 is that the polarizability found in free atoms is very different from that found in molecules due to the quenching produced by electron transfer or bond formation. For this reason, it is better to obtain the C_6 coefficients based on separate computations for simple hydrides like A_mH_n and B_kH_l and remove the contribution of the hydrogens:

$$C_6^{AB} = \frac{3}{\pi}\int_0^\infty d\omega \frac{1}{m}\left[\alpha^{A_mH_n}(i\omega) - \frac{n}{2}\alpha^{H_2}(i\omega)\right] \times \frac{1}{k}\left[\alpha^{B_kH_l}(i\omega) - \frac{l}{2}\alpha^{H_2}(i\omega)\right] \tag{3.46}$$

where α^{H_2} is the corresponding value for the dihydrogen molecule, $\alpha^{A_mH_n}$ corresponds to the reference molecule A_mH_n and m, n, k, l are stoichiometric factors. With this scheme, the effect of the environment is included by means of C_6 coefficients obtained by interpolation between several hydrides. For a given bond situation, the bond order is simply estimated considering the close-up atoms, which modifies the atomic coefficient of a pair of atoms obtained by interpolation between the values of different hydrides.

The original damping function for the DFT-D3 correction is the variant proposed by Chai and Head-Gordon,[53] so when the distance tends to zero the value of the function approximates zero too. However, a later study allowed a better comprehension of this damping function and its importance in the interaction, leading to a new proposal for the damping function.[69] From then on the Becke and Johnson function is employed, so the function goes to a constant value as the distance between the atoms tends to zero.[71] With this new empirical correction and using the Becke and Johnson function, the pair-specific cut-off radii is not needed as also happens with the artificial repulsion at short interatomic distances.

To sum up, the main advantage of this new dispersion model is a more consistent treatment of dispersion coefficients, that extends its use to a larger number of atom

types, and the possibility to tune the coefficients depending on the environment. It must be taken into account, though, that the improvement over DFT-D2 occurs mainly for the "heavier" systems, metallic and bulk, while in "light" systems the results are very similar to the previous model. Also, the more complex dependence on the environment can lead to somewhat strange behaviours, as already observed in the case of complexes with alkaline cations.[77]

These dispersion corrections have been extensively tested in a variety of situations, ranging from non-covalent interactions to thermochemistry, showing a systematic improvement over their non-corrected versions, leading in many cases to the DFT methods that are the best possible choice. The process of optimisation of the empirical term continues, and recently Grimme has proposed the D4 version,[77] with improvements for the description of polar, organometallic, and ionic systems though it has not been employed in this thesis. A note of caution: literature is quite confusing about which of the different dispersion-corrected models is employed in each case, since in many cases any of the models described above is simply denoted as DFT-D, and sometimes there is no clear reference about whether the D2 or D3 version is employed or which damping function is used in the D3 correction.

3.2.5.2 Other corrections

On the other hand, some specific functionals are developed with the purpose to take into account the role of dispersion. Truhlar *et al.* have proposed some functionals that capture medium-range electron correlation like M05-2X[78] and M06-2X[79] that are commonly used. The way to include part of the dispersion is through a fitting of parameters using a set that includes non-covalent interactions, and doubling the exact exchange part of the analogous M05[80] and M06[79] (that is the meaning of "2X"). These medium-range corrected functionals give reasonable results for geometries and thermochemistry in complexes with a separation of ∼5 Å between their molecules but, when the distance increases worse results are obtained. During the past years Truhlar developed new functionals like M08-SO (with 44 parameters), M11 (a range-separated version of M08-SO with 40 parameters), MN12-SX (with 58 parameters) and MN15 (with 59 parameters), in which a trend with an increasing number of parameters is following. These new functionals, obtained with a higher and more complete data set, were developed with the purpose to solve some of the problems found in the predecessor; so, they lead to a better description of a higher number of molecules. Nevertheless they are less used than M05-2X or M06-2X functionals.[81]

However, these are not the unique functionals developed with the purpose to take into account the non-covalent interactions. B97-D[45] is a reparameterized version of B97 to consider the van der Waals interactions through the fitting of different data and including the Grimme empirical dispersion model (the D2 one). Another functional is ωB97X-D[53] developed by Chai and Head-Gordon. It is a long-range functional in which the long-range interactions are treated by the full HF exchange and the short-range interactions are treated as a hybrid functional, but the long and the short range include an empirical dispersion model. Some other functionals were developed with the purpose to include the van der Waals forces such as vdW-DF,[82] in which a more realistic description of benzene systems is obtained. Its second version vdW-DF2[83] improves the results for the equilibrium distance and binding energy. Voorhis *et al.* developed a new functional for weakly-bound systems so-called VV10,[84] this functional uses the PBE functional for the

semilocal correlation, a refitted PW86 for the exchange and the authors add a Non-Local contribution to correlation with the purpose to improve the treatment of non-covalent interactions. Finally XYG3 is a double hybrid functional based on B3LYP that was developed with the purpose to increase the accuracy in non-bonded systems, thermochemistry and reaction barrier heights.[85]

3.2.6 Basis sets

Most wavefunction and DFT methods construct the wavefunction as a combination of molecular orbitals constructed as linear combinations of one electron functions. In single-determinant methods, the molecular orbitals are employed to construct a Slater determinant which is the representation of the wavefunction of the system. In multi-determinant methods, different N-electron determinants are combined to represent the wavefunction of the system.[35,86]

If the set of one electron functions employed is complete, and the functional is exact the result obtained would be exact, but this is not possible in practical calculations due to the higher computational cost and the unknown functional, (in post-HF methods the one electron basis set should be complete and all N-electron determinants should be included for the exact solution). A proper selection of the basis set is essential to obtain good results, and generally, the larger the basis set the better the results. Nevertheless, the type of the functions used in the basis set affects the accuracy of the results obtained.

The Slater Type Orbitals (STO)[87] and Gaussian Type Orbitals (GTO)[88] are two of the most used functions in electronic calculations. The STOs have the functional form:

$$\chi_{\zeta,n,l,m}(r,\theta,\varphi) = NY_{l,m}(\theta,\varphi)r^{n-1}e^{\zeta r} \tag{3.47}$$

where N is the normalization constant and $Y_{l,m}$ are spherical harmonic functions.

The exponential dependence of the STO produces a fast convergence with an increasing number of functions; nevertheless, the calculation of the three- and four-centres two electron integrals cannot be solved analytically. For that reason, the STOs are used in semi-empirical methods where these kind of integrals are neglected or in density functional methods that do not include the exact exchange and an auxiliary basis set is used to obtain the Coulomb energy. Nevertheless, in recent years some improvements in DFT allows the development of quantum packages that employ STO with hybrid functionals like ADF.[89]

On the other hand, the GTOs can be written in two forms, one that uses the cartesian coordinates and the other with polar coordinates.

$$\begin{aligned} \chi_{\zeta,l_x,l_y,l_z}(x,y,z) =& Nx^{l_x}x^{l_y}x^{l_z}e^{\zeta r^2} \\ \chi_{\zeta,n,l,m}(r,\theta,\varphi) =& NY_{l,m}(\theta,\varphi)r^{2n-2-l}e^{\zeta r^2} \end{aligned} \tag{3.48}$$

These functions depend on r^2, generating two problems. The first is the description of the "cusp"; the STO has a cusp at the nucleus, but the GTO has a softened region with a zero slope so the behaviour at the nucleus is not described properly with the gaussian functions (see Figure 3.2). The second problem is that the GTO falls off rapidly when it moves away from the nucleus, while the STO has a better representation of the

"tail". With the purpose of solving these problems more GTOs are used to achieve a certain accuracy. Figure 3.2 shows that the use of three GTOs (STO-3G) produces a similar behaviour than the STO, but when only one GTO (STO-1G) is used a worse representation of the function is obtained. This increase on the number of GTOs is compensated by the simpler way in which their integrals are calculated. As a result, the GTOs are the most used one-electron functions in electronic structure calculations.

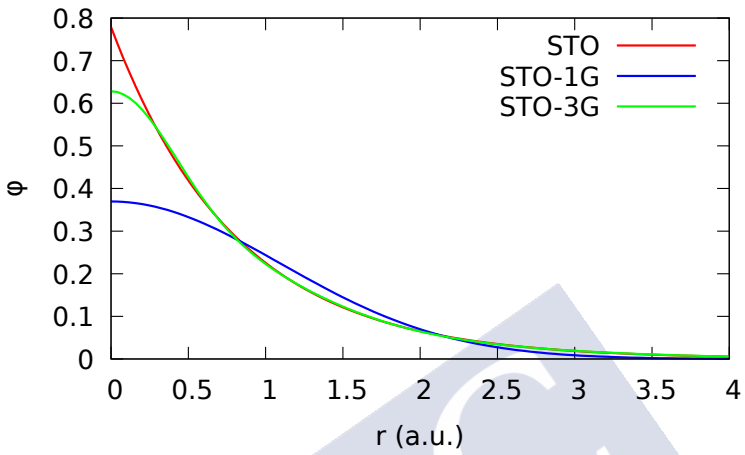

Figure 3.2: Comparison between STO, STO-1G and STO-3G functions for the hydrogen.

3.2.6.1 Contracted basis set

The core electrons of an atom have a huge importance in the total energy of the atom and for this reason a large number of functions are used to describe this part due to the erroneous description of the "cusp" region. However, the most interesting part in chemistry is related to the valence electrons and a smaller number of functions describe this part. It should be kept in mind that even when the core electrons have a large contribution to the energy, the optimisation of its exponents does not vary a lot, because they have a small dependence with the bonding situation. Thus, the bigger computational effort is spent describing the core electrons that do not change a lot and they are not chemical interesting.

One way to improve this is through a linear combination of the primitive GTO (PGTO), this combination gives place to the contracted GTO (CGTO):

$$\chi(\text{CGTO}) = \sum_{i}^{k} a_i \chi_i(\text{PGTO}) \tag{3.49}$$

The number of functions in CGTO that will be handled by the variational principle has been reduced when it compares with the PGTO. For example, the PGTO (6s3p) after the contraction is changed into the CGTO [2s1p]. Thus, this contraction always increases the energy of the system because it reduces the flexibility of the basis set, but the computational cost is reduced too.[35]

The minimum basis set has the smallest number of functions to contain all the electrons of the system; in other words, a single basis function is used for each orbital. An example of this basis set is the STO-3G developed by Pople,[90] in which 3 PGTO are used to

describe the STO. With the purpose to improve this basis, the Double Zeta (DZ) variety was developed. In this case the number of basis functions used is the double than the minimal basis set. The higher number of functions used in DZ allows a better description of the behaviour of electrons. However, in many situations it is better to only double the valence basis set, because the core electrons hardly change with the environment. In this case the number of valence basis is doubled to produce a split valence basis, in which the same name is used. The Triple Zeta (TZ) and Quadruple Zeta (QZ) variants work in the same way except that they use three and four times more functions than the minimum basis set. The same names are used if the split valence basis sets are considered.

3.2.6.1.1 Polarization and diffuse functions

The polarization functions are functions with a higher angular momentum than the functions included in the minimal basis set. For example, in the case of the hydrogen atom a p-orbital is added, or a d-orbital is added to polarize the elements of the first row. These polarization functions are important for an accurate description of bonding between atoms, in intermolecular interactions or when the electron correlation is important.

It is possible to add only polarization functions to the non-hydrogen atoms. This fact decreases the computational cost as it reduces the basis set in three basis functions per hydrogen atom. Nevertheless, if the hydrogens play an important role in the description of the system, it is better to also include the polarization functions in the hydrogen. Before adding the polarization functions we make sure that a large enough number of functions are present on the basis set. Usually it is applied the rule of thumb which says that the number of functions with a higher angular momentum has to be less than the number with the previous angular momentum, that is to say, a 3s2p1d basis set is balanced but a 2s2p2d basis set is too heavily polarized and the optimisation of the basis set uses higher angular momentum function that can produce artifacts.

The diffuse functions are functions with small exponents, thus they are used to fit the tail of the function. For this reason they are important when loosely bonds are present, like anions or excited states, or when we try to measure some property that depends on the tails of the function.

3.2.6.1.2 Basis set types

There are many basis sets developed during the last decades and built in quantum programs to perform a calculation. In most of the cases the user only needs to select a basis set according to their system and perform the calculation, but a smart selection of the basis set can lead to an accurate energy and a reduction of the computational cost.

One of the first frequently used GTOs were developed by Pople *et al.* and it is the minimum basis set STO-nG. In this basis set several gaussian functions (n) are used to adopt the form of the STO; nevertheless, there is a small improvement on the results when more than 3 PGTO are used. After this minimum basis set, they developed a split valence type. The notation for this basis set is k-nlmG, k representing the number of PGTO that are used to form a contracted function that represents the core orbitals, nl indicates that it is a split valence, the n value indicates that the inner part of the valence orbitals is the contraction of n PGTO, while the l shows the number of PGTO used for the outer part. The m value indicates a triple split valence, in other words, the valence orbitals are splitted into three functions, such as 6-311G basis set.[91]

In addition to that it is possible to add polarization and/or diffuse functions. The diffuse functions are denoted by + and are constructed adding one set of diffuse functions. On the other hand, there are two ways to denote the polarization functions. The first way is to add (d,p) after the G in which the polarization functions are added to the hydrogen and heavy atoms or the other possibility is adding two * symbols. If we are interested in polarize only the heavy atoms only the letter d or one * is necessary.

Another basis set family is the XVZ basis set developed by the group of Ahlrichs.[92–94] This basis set family has been frequently used during the development of this thesis. The simplest basis set is the Split Valence (SV) in which occurs a (7s4p) → [3s2p] contraction for the carbon atom. The following basis sets are the Triple Zeta Valence (TZV) and Quadruple Zeta Valence (QZV), in which more contracted *s*-functions are employed than their names indicate. Some years later these basis sets were redefined with the purpose to improve the results and the prefix "def2" is added to these basis set to be able to distinguish them from the previous ones.[95] In these basis sets it is possible to add some polarization functions denoted with the letter "P". For example, def2-TZVP adds the polarization on non-hydrogen atoms, while def2-TZVPP adds the polarization to all atoms for a TZV basis set after the redefinition. The exponents and the contraction coefficients for the polarization functions are taken from the correlation consistent basis sets developed by Dunning.[96]

3.2.6.2 Effective core potentials

Molecules with atoms from the lower part of the periodic table have a large number of electrons that increase the computational cost. However, the electrons corresponding to the core of the element do not have an important chemical role in most cases. Nevertheless, it is necessary to include these core electrons in order to obtain a suitable description of the valence orbitals, *i.e.*, the core electrons cannot be deleted from the basis set without including them in another way. Furthermore, the elements of the lower part of the periodic table have relativistic effects that complicate the calculation even more. A way to overcome these problems is to use a function for modelling all these core electrons while treating the valence electrons explicitly. The modelling function allows to avoid the inclusion of the basis set for the core electrons but including their behaviour during the calculation.

The function that models the core electrons is called effective core potential (ECP). When the gaussian functions are used to describe the valence orbitals, normally the same type of functions are used in the ECP. The number of electrons which is included in the ECP determines its quality. For example, the "full-core" type includes all the electrons of the core, but a "small-core" version only includes a part of the core electrons. For instance, in the case of iodine the electrons replaced by the ECP are:

- Full-core: $(1s)^2(2s)^2(2p)^6(3s)^2(3p)^6(3d)^{10}(4s)^2(4p)^6(4d)^{10}$
- Small-core: $(1s)^2(2s)^2(2p)^6(3s)^2(3p)^6(3d)^{10}$

In the first case 46 electrons are included in the ECP, thus only 7 electrons are treated explicitly, those corresponding to $(5s)^2(5p)^5$. For the small-core ECP, 28 electrons are included in the ECP and the other are treated explicitly. Therefore, the use of the full-core allows a higher decrease of the computational cost for these elements and normally

they give reasonable geometries, although the energetic values in some cases are not always acceptable. On the other hand, the small-core ECPs do not reduce to the same extent the cost but better results are obtained.

3.3 Reducing computational cost

3.3.1 Resolution of identity (RI)

The bottleneck in DFT is the time needed to calculate the four-index two-electron integrals required in the evaluation of the Coulomb part. It would be desirable to apply approaches leading to significant reductions of time in the calculation of the Coulomb part, thus increasing the size of the systems that can be treated within reasonable computational cost. One of these approaches is the so-called density fitting approach, also known as resolution of identity (RI).[97–99] Density fitting reduces the computational cost by transforming the four-index two-electron integrals into three-index integrals through the use of an auxiliary basis set.[100]

Starting with the usual two-electron integral:

$$(pq|rs) = \int d\mathbf{r}_1 \int d\mathbf{r}_2 \phi_p(\mathbf{r}_1)\phi_q(\mathbf{r}_1)\frac{1}{r_{12}}\phi_r(\mathbf{r}_2)\phi_s(\mathbf{r}_2) \tag{3.50}$$

Considering $\phi_p(\mathbf{r}_1)\phi_q(\mathbf{r}_1) = \rho_{pq}(\mathbf{r})$; these densities can be approximated by the use of an auxiliary basis set.

$$\rho_{pq}(\mathbf{r}) \approx \tilde{\rho}_{pq}(\mathbf{r}) = \sum_{P}^{N_{fit}} d_P^{pq}\chi_P(\mathbf{r}) \tag{3.51}$$

There are several methods for obtaining the fitting coefficients. Following the procedure proposed by Dunlap *et al.*[101,102] the coefficients are obtained as:

$$d_Q^{pq} = \sum_P (pq|P)[J^{-1}]_{PQ} \tag{3.52}$$

where the components of the previous equation have the following expressions:

$$(pq|P) = \int d\mathbf{r}_1 \int d\mathbf{r}_2 \phi_p(\mathbf{r}_1)\phi_q(\mathbf{r}_1)\frac{1}{r_{12}}\chi_P(\mathbf{r}_2) \tag{3.53}$$

$$J_{PQ} = \int d\mathbf{r}_1 \int d\mathbf{r}_2 \chi_P(\mathbf{r}_1)\frac{1}{r_{12}}\chi_Q(\mathbf{r}_2) \tag{3.54}$$

When the equations 3.53 and 3.54 are replaced in the usual four-index, two-electron integral the following expression is obtained:

$$\begin{gathered}(pq|rs) = \int d\mathbf{r}_1 \int d\mathbf{r}_2 \sum_Q d_Q^{PQ}\chi_P(\mathbf{r}_1)\frac{1}{r_{12}}\phi_r(\mathbf{r}_2)\phi_s(\mathbf{r}_2) = \\ \sum_Q d_Q^{PQ}(Q|rs) = \sum_{PQ}(pq|Q)[J^{-1}]_{PQ}(Q|rs)\end{gathered} \tag{3.55}$$

This approach leads to a 10−100 fold reduction in computational cost, because the three-index two-electron integrals are more easily evaluated and require less space to

storage. This approach can be also employed for speeding up the calculation of the correlation energy in MP2. Its application within DFT is restricted to pure functionals; hybrid functionals include at least part of exact exchange from HF, and the procedure described above is not effective for reducing the cost needed for the exchange integrals.

Weigend *et al.*[103] developed a new version of the resolution of identity for the exchange part (RI-JK), though it required newly optimised auxiliary basis sets (the requirements for the auxiliary basis sets for exchange are more demanding than for the Coulomb part).[104] With these basis sets, the RI-JK approach can be effectively used in HF calculations and with hybrid functionals.

Another approach proposed for reducing the cost of the exchange integrals is the so-called chain-of-spheres (COSX) for exchange approach.[105]

3.3.2 Chain-of-spheres

The chain-of-spheres is a method that employs a seminumerical approximation to solve the electron repulsion integrals.[105–108] COSX performs the exchange integrals over a numerical grid ($\boldsymbol{r}_g$) and it is only employed for the exchange integrals because its use for the coulomb integrals shows an increase of computational cost when compared to the RI approximation. In this approximation the exchange matrix elements have the following expression:

$$K_{\mu\nu} \simeq \sum_{\mathrm{g}} X_{\mu\mathrm{g}} \sum_{\sigma} A_{\nu\sigma}(\boldsymbol{r}_{\mathrm{g}}) \sum P^{\lambda\sigma} X_{\lambda\mathrm{g}} \tag{3.56}$$

where $X_{\mu\mathrm{g}} = \sqrt{w_{\mathrm{g}}}\phi_\lambda(\boldsymbol{r}_{\mathrm{g}})$ in which w_{g} is the grid weight, $A_{\nu\sigma} = \int \phi_\nu \phi_\sigma |r - r_{\mathrm{g}}|^{-1} d\boldsymbol{r}$ and $P^{\lambda\sigma}$ is the density matrix.

The numerical error of COSX due to the numerical integration can be reduced by different fitting schemes, nevertheless the use of this numerical integration allows to reduce the scaling for the exchange integral from $O(N^4)$ to $O(N^2M)$ where N is the number of basis functions and M is the number of grid points used for the evaluation. Usually the number of grid points is larger than the number of basis functions, $M > N$, reaching to a limit of efficiency when $M \simeq N^2$. For this reason an increase of the grid is related with an increase of accuracy until the limit of efficiency is reached. However, generally the number of points is smaller than N^2 reducing the computational cost. Finally, it is important to mention that this method does not require to storage the four and three-index integrals reducing the amount of memory needed and the time for writing and reading data.

Both approximations, RI-JK and COSX, present their best results with big basis sets, obtaining significant reductions on computational cost, though not as large as the ones obtained for the Coulomb part. Of course, these approximations decrease the accuracy, but the errors are systematically small, especially for relative energies.

3.3.3 Density-functional tight-binding (DFTB)

Even when the use of approaches like density fitting enables to increase the size of the systems that can be treated with a reasonable computational cost, large systems can still be very demanding, specially if a large conformational flexibility is possible. In such cases, the use of regular DFT methods is too demanding to allow a proper exploration of the potential energy surface. Thus, cheaper methods are needed, allowing a faster primary

exploration of the systems considered while keeping an accurate-enough description. One of the possibilities is the use of the density-functional tight-binding (DFTB).[109–113]

DFTB is a computational model derived from DFT around the reference density (ρ_0) of the molecular system. There are different models of DFTB, which can be obtained expanding the exchange-correlation energy functional around the density in different orders through a Taylor expansion. The first order one is called DFTB1[114,115] and it can be used in systems in which the charge transfer is not important or where a complete charge transfer between atoms occurs, like in NaCl. This first implementation is about 5 to 10 times faster than the second and third order ones. However, the second order (DFTB2[116] or SCC-DFTB) is essential for molecules with partial charge transfer where the first order approach fails. Finally the third order (DFTB3[117,118]) is also useful for charged molecules but it enhances the charge dependence solving some problematic approximations within DFTB2.

3.3.3.1 DFTB3

The starting point for the DFTB model is the reference density (ρ_0) of the molecular system, that can be approximately obtained as a superposition of the neutral densities (ρ_0^a) of the atoms which constitute the molecule.

$$\rho_0 = \sum_A \rho_0^a \tag{3.57}$$

where the superscript a correspond to the different atoms.

The ground state density can be written in terms of the ρ_0 and the density fluctuation ($\delta\rho$) as:

$$\rho = \rho_0 + \delta\rho \tag{3.58}$$

Finally the DFTB3 total energy can be obtained starting with the energy expression of the Kohn-Sham density functional theory but using a reference density (ρ_0) perturbed by some density fluctuation. Using a Taylor series, the exchange-correlation energy functional is expanded until the third order terms, so the expression for the total energy of the system remains as:

$$E[\rho] = E^0[\rho_0] + E^1[\rho_0, \delta\rho] + E^2\left[\rho_0, (\delta\rho)^2\right] + E^3\left[\rho_0, (\delta\rho)^3\right] \tag{3.59}$$

According to equation 3.59 the different terms are:

- $\boldsymbol{E^0[\rho_0]}$: This term is part of the DFTB1 model and it depends only on the reference density and therefore it does not depend on the chemical environment of the molecule. For this reason it is possible to obtain an appropriate "referenced system" and then use it in other molecules. According to this, the transferability of the derived parameters is possible.

  This term defines the repulsion energy E_{rep} of the system and it only considers the interactions between two centres, ignoring the three-body contributions. The solution of this term is approximated by a sum of pair interactions which is parametrized by DFT calculations or fitted to empirical data.

$$E_{req} = \frac{1}{2}\sum_{ab} V_{ab}^{rep} \tag{3.60}$$

- $\boldsymbol{E^1\left[\rho_0, \delta\rho\right]}$: This term, as the previous one, is included in DFTB1 and corresponds to the Hamiltonian matrix elements:

$$E^1\left[\rho_0, \delta\rho\right] = \sum_i n_i \left\langle \psi_i \middle| \hat{H}\left[\rho^0\right] \middle| \psi_i \right\rangle \tag{3.61}$$

where $\hat{H}$ is the Kohn-Sham Hamiltonian using the density of the reference system and ψ_i are the Kohn-Sham orbitals.

This approximation uses a minimal basis set in the Kohn-Sham orbitals, $\psi_i = \sum_\mu c_{\mu i}\phi_\mu$; particularly it uses a single zeta basis with the purpose to reduce the size of the eigenvalue problem. This minimal basis set reproduces quite well the bonding properties, but it has some problems to describe the low density parts, which are important for non-covalent interactions. The diagonal elements of the Hamiltonian are DFT eigenvalues evaluated with the exchange-correlation functional developed by Perdew Burke Ernzerhoff (PBE)[44] and they are calculated with a two-centre approximation. Since the Hamiltonian only has contributions for one- and two-centres, it is possible to calculate and tabulate these contributions previously, reducing the computational cost.

- $\boldsymbol{E^2\left[\rho_0, (\delta\rho)^2\right]}$: This term is included in the second order expansion (DFTB2) in which the electron density fluctuation $\delta\rho$ is expanded with a multipole expansion:

$$E^2\left[\rho_0, (\delta\rho)^2\right] = \frac{1}{2}\int\left(\frac{1}{|\boldsymbol{r}-\boldsymbol{r'}|} + \frac{\delta^2 E_{XC}[\rho]}{\delta\rho(\boldsymbol{r})\delta\rho(\boldsymbol{r'})}\Big|_{\rho^0}\right)\delta\rho(\boldsymbol{r})\delta\rho(\boldsymbol{r'})d\boldsymbol{r}d\boldsymbol{r'} \tag{3.62}$$

It is possible to describe this term analytically if some approximations are used. $\delta\rho$ can be written as a sum of the atomic contributions and using a Slater function centred on the nuclei the spherical atomic contributions can be approximated as:

$$\delta\rho = \sum_a \delta\rho_a \approx \Delta q_a \frac{\tau_a^3}{8\pi} e^{-\tau_a|\boldsymbol{r}-\boldsymbol{R}_a|} \tag{3.63}$$

where Δq_a is the difference between the Mulliken charge of the atom a and the number of valence electrons for this atom in its neutral charge centred on the nuclei at $\boldsymbol{R}_a$. τ_a is chosen to describe appropriately the atomic chemical hardness.

Using the previous approximation and neglecting the term $\frac{\delta^2 E_{XC}[\rho]}{\delta\rho(\boldsymbol{r})\delta\rho(\boldsymbol{r'})}$, the Hartree integrals in equation 3.62 can be evaluated analytically leading to the analytical function γ_{ab}. This function has an inverse relation to the chemical hardness, that it is a measure of the resistance of an atom or a chemical specie to change its electronic configuration.

Finally the second-order term can be written as:

$$E^2\left[\rho_0, (\delta\rho)^2\right] = \sum_{ab} \Delta q_a q_b \gamma_{ab} \tag{3.64}$$

- $\boldsymbol{E^3\left[\rho_0,(\delta\rho)^3\right]}$: This term includes the diagonal and off-diagonal contributions for the DFTB3 model through the equation:

$$E^3\left[\rho_0,(\delta\rho)^3\right]=\frac{1}{6}\int\int\ +\frac{\delta^3E_{XC}[\rho]}{\delta\rho(\boldsymbol{r})\delta\rho(\boldsymbol{r}')\delta\rho(\boldsymbol{r}'')}\bigg|_{\rho^0}\delta\rho(\boldsymbol{r})\delta\rho(\boldsymbol{r}')\delta\rho(\boldsymbol{r}'')d\boldsymbol{r}d\boldsymbol{r}'d\boldsymbol{r}'' \quad (3.65)$$

In $E^3\left[\rho_0,(\delta\rho)^3\right]$ a similar procedure than $E^2\left[\rho_0,(\delta\rho)^2\right]$ is followed with the insertion of a new parameter, U^d, which is the derivation of the chemical hardness that can be obtained through DFT calculations or an optimisation to improve the model. This new parameter is included through the Γ-function, which is the derivative of γ_{ab} with respect to the atomic charge leading to the following expression:

$$E^3\left[\rho_0,(\delta\rho)^3\right]=\sum_{ab}\Delta(q_a)^2q_b\Gamma_{ab} \quad (3.66)$$

This third-order term does not greatly improve the accuracy of the results, but it introduces a charge dependence that compensates the deficiencies originated in the second-order terms like the fixed shape of the original density or an excessive simple scheme for the fluctuation density.

After the approximation of the different terms the final DFTB3 energy can be obtained as:

$$E^{DFTB3}=\frac{1}{2}\sum_{ab}V_{ab}^{rep}+\sum_{iab}\sum_{\mu\in a}\sum_{\upsilon\in b}n_ic_{\mu i}c_{\upsilon i}H_\mu^0+\frac{1}{2}\sum_{ab}\Delta q_aq_b\gamma_{ab}+\frac{1}{3}\sum_{ab}\Delta(q_a)^2q_b\Gamma_{ab} \quad (3.67)$$

3.3.3.2 Dispersion

Due to the important role of dispersion in non-covalent interactions, DFTB2 was modified to include an empirical term with the purpose to improve the description of the systems with this kind of interactions.[119] The first way to include the dispersion is through a modified Lennard-Jones potential in which the normal Lennard-Jones potential is used at long-range distance and a polynomial form is used at distances smaller than the node found at $R_{ij}/\sqrt[6]{2}$ with the purpose to avoid repulsion at short distances.

$$U_{ij}(R)=\begin{cases} d_{ij}\left[-2\left(\frac{R_{ij}}{R}\right)^6+\left(\frac{R_{ij}}{R}\right)^{12}\right] & \text{if } R\geq R_{ij}/\sqrt[6]{2} \\ U_0-U_1R^n-U_2R^{2n} & \text{if } R<R_{ij}/\sqrt[6]{2}\end{cases} \quad (3.68)$$

d_{ij} is the well depth, R_{ij} the van der Waals distances and U_0, U_1 and U_2 are three parameters that are obtained under the condition that the derivates at R_0 match with the Lennard-Jones potential.

However, the DFTB2 model uses a minimal basis set that leads to an underestimation of the distance in the van der Waals interactions and hydrogens bonds, because the electron density is not well described for long-term interactions. The new parametrization, 3OB,[120] developed for the DFTB3 model solves this problem because it uses a more

extended basis set. As mentioned in section 3.2.5.1.2, Grimme *et al.* developed a new empirical model, called D3,[68] which is parametrized for different functionals and DFTB3. This D3 model can be added to the results of DFTB3 improving the results for long-range interactions obtained by the modified Lenard-Jones potential.

3.3.3.3 Parameterization

DFTB is a model that includes some parameters for the terms needed to obtain the final energy. For this reason a proper description of these parameters seems mandatory. Usually, the first step is to obtain the parameters for E^1, which involves the atomic orbitals basis set (ϕ_μ) and the neutral density for each atom (ρ_a^0), with the purpose to solve one- and two-electron integrals and tabulate the results. These parameters are the wavefunction confinement radius that is usually twice the covalent radius and the density confinement radius that is obtained in a somewhat empirical form. An adequate choice of these parameters can lead to an improvement of energies.

The second step is to determine three parameters used in E^2 and E^3. The first parameter is the atomic partial charge, which is usually obtained through a Mulliken partition scheme.[121] The second parameter is the Hubbard parameter or chemical hardness (U_a), which is computed from DFT results and is necessary to obtain $\gamma_{ab}(U_a, R_{ab})$. Due to the relation of γ_{ab} with the size of the atom, the value should be changed between the different rows of the periodic table. For example, in the case of the hydrogen atom a modified γ_{ab} function is employed with the purpose to fix the underestimation on the hydrogen bond energies. The final parameter is the charge derivative of U_a (U_a^d) that is necessary to calculate $\Gamma_{ab}(U_a, U_a^d, R_{ab})$. As a first approach to obtain Γ_{ab} only the diagonal elements are considered. This approach works well for the first row, but in some cases like the deprotonation of nitrogen or phosphorus it implies some error because the off-diagonal terms are important. With the purpose to solve this problem all the elements are taking into account, that it to say, the diagonal and the off-diagonal elements of Γ_{ab} are calculated. However, the full third order only can be solved if U_a^d is treated as an adjustable parameter.

The final step is to obtain the parameters for E^0, but in the last decade some automated techniques were developed with the purpose of simplifying this process.[122] The parametrization of E^0 only depends on the ρ_0 and for this reason once the parameters are obtained they can be used in all the DFTB models. However, the parameters are normally fitted for each model to obtain a fine tune of the results. For example, DFTB2 uses the "mio" parameters which in turn can be used in DFTB3, but for this last method a new parametrization has been obtained called "3OB" which only differs in the electronic parameters and gives better results when DFTB3 model is used.

3.3.3.4 Limitations

DFTB3 gives good results for biomolecules or organic compounds, but even when the development of DFTB3 resolves some errors and problems that are present in the previous models, DFTB3 has other limitations:[123]

1. DFTB underestimates the rotational barrier of different conformers. This fact difficults the comparison with experimental results or the study of conformational dynamics of proteins.

2. DFTB is parametrized with DFT-GGA so it inherits the problems associated with this method such as the self-interaction error,[65] problems with charge-transfer excited states, missing of the dispersion interaction and the tendency to overpolarize extended π-conjugate systems.[124]

3. The use of a minimal basis set tends to cause problems during the calculation of the IR or Raman spectra due to the absence of polarization functions. For example, when the nitrogen is bonded to four atoms there are some problems to obtain a good description using this model. However, the development of new parameters for these elements can solve this problem.

4. It has problems for the description of the hydrogen bond breaking. DFTB needs another parametrization when this process occurs.

5. The use of the monopole approximation does not allow to obtain a good quality in the description of molecules in different environments like bulk or the interface between water and air.

3.4 Properties and analysis

3.4.1 Non-Covalent Interaction Index (NCI)

The study of non-covalent interactions is essential in many fields like biology, supramolecular chemistry and materials science. As mentioned previously, these non-covalent interactions span a wide range of different interactions and, though the physical phenomena behind all the interactions are the same (electrostatic origin) it is usual to classify the interactions according to more chemically intuitive types like hydrogen bonding, dipole-dipole interactions, steric repulsion and so on. With the purpose to find a method to visualize these non-covalent interactions Johnson and Contreras-García developed a new index that allows their visualization.[125,126] This, Non-Covalent Interaction Index (NCI) uses the electron density (ρ) and the reduced density gradient (RGD, s) to provide information about the non-covalent regions.

$$s = \frac{1}{2(3\pi)^{1/3}} \frac{|\nabla\rho|}{\rho^{4/3}} \tag{3.69}$$

In the case that ρ and s have low values a non-covalent interaction is found. However, the only presence of these two values is not enough to distinguish whether the interactions to be attractive or repulsive; the Laplacian of the density is employed with this purpose. The Laplacian through its eigenvalues can be decomposed along the three principal axes: $\nabla^2\rho = \lambda_1 + \lambda_2 + \lambda_3$. The interatomic regions between two bonded atoms are characterized by a negative value of the Laplacian with $\lambda_1 < 0$; $\lambda_2 < 0$ and $\lambda_3 > 0$. On the other hand, the interatomic region that corresponds to the non-covalent interactions, is characterized by a positive value of the Laplacian. In this interatomic region the sign of the λ_2 allows to distinguish between bonding interaction like the hydrongen bond ($\lambda_2 < 0$) in which the electron density is accumulated perpendicular to the bond, from nonbonding interaction like steric repulsion ($\lambda_2 > 0$) where density is depleted; van der Waals interactions show a small value of λ_2 close to zero.

The different interactions can be observed in Figure 3.3; the 2D-NCI plot allows to differentiate the peaks for the hydrogen bond with a blue color, van der Waals interaction with a small density and green color and finally, the steric repulsion with red color it is found in the positive region of the graph. A 3D visualization of the interactions can be obtained by using an isosurface of RDG color-mapped depending on the value of the density times the sign of the second eigenvalue of the Hessian, as shown on the bottom of Figure 3.3.

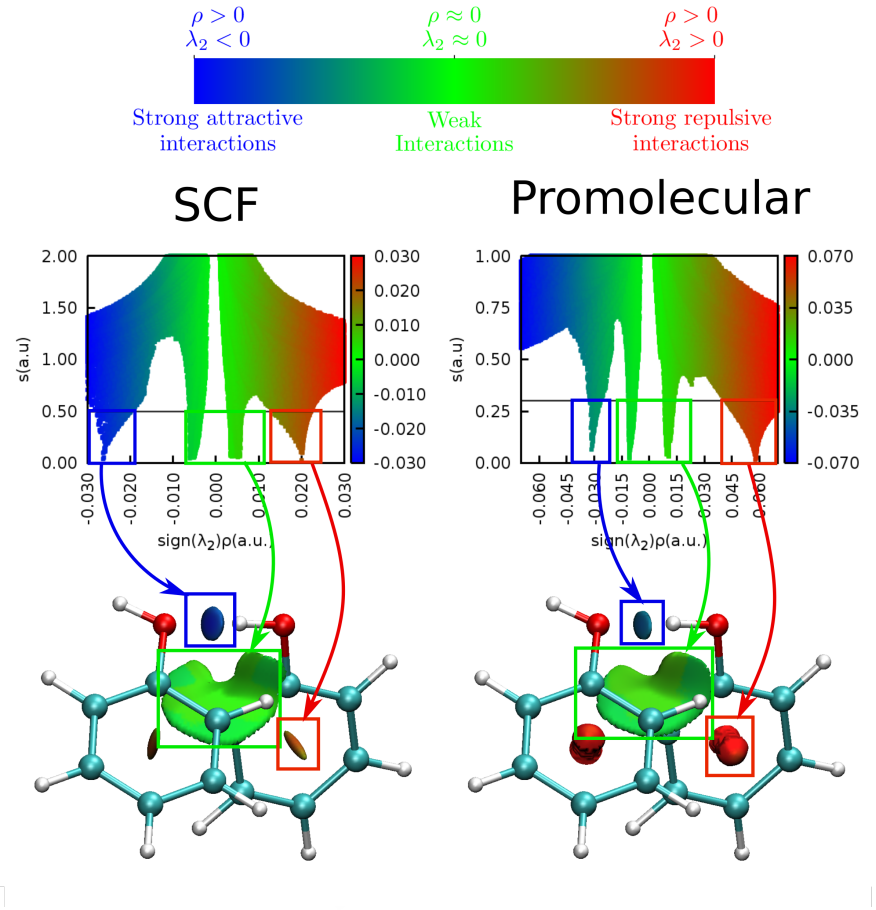

Figure 3.3: Different types of calculation in NCI for the phenol dimer. The SCF calculation uses an isosurface of 0.5 a.u. for the reduced density gradient and a color scale going from −0.030 a.u. (blue) to 0.030 (red) a.u. The promolecular calculation uses an isosurface of 0.3 a.u. for the reduced density gradient and a color scale going from −0.070 a.u. (blue) to 0.070 (red) a.u.

The density of the molecular system can be obtained from a quantum-mechanical calculation, but it can also be estimated by means of the combination of promolecular densities. The promolecular approach is obtained when the molecular density (ρ^{pro}) is computed by the sum of the atomic contributions, only needing the cartesian coordinates of the molecule and avoiding the full calculation of the molecular density.

$$\rho^{pro} = \sum_i \rho_i^{at} \tag{3.70}$$

The atomic densities used in equation 3.70 are written as a simple sum of exponential

functions, thus the NCI surface can be calculated analytically in an easy way when the LSDA free-atomic densities are stored for neutral atoms.

On the other hand, SCF densities are obtained by the wavefunction calculated at a given theoretical level. The use of SCF densities produces better results, but it is more time consuming and for this reason the use of promolecular densities in large systems can be very useful.

Figure 3.3 shows the two different methods for obtaining the NCI surfaces for the phenol dimer. Both methods show a hydrogen bond between the hydroxyl groups of both molecules, a van der Waals interaction between closer parts of the phenyl ring and a steric repulsion in the ring. However, the promolecular calculation gives a little stronger H-bond, bigger value of the density, and a stronger repulsion in the ring, but the same surfaces are plotted and the same interactions are represented in both methodologies. Therefore, the use of promolecular densities gives the same qualitative picture of the interactions than the more costly fully-calculated densities.

3.4.2 Molecular electrostatic potential (MEP)

One way to understand the different interactions between the molecules is through the 3D-NCI plots because they show the surface of interaction and the difference between a bonding or nonbonding interaction. However, this is not the only way to do this and the use of molecular electrostatic potential (MEP) can help to understand the interaction between molecules and to find the best location within a molecule to carry out a specific reaction.[127]

The electrons and nuclei in a molecule produce a distribution of electric charge that creates an electric potential $V(\vec{r})$ in the surrounding space. If the electronic density function (ρ) for a molecule is obtained, then the electrostatic potential at a given position $\vec{r}$ can be exactly calculated as:

$$V(\vec{r}) = \sum_A \frac{Z_A}{\left|\vec{R}_A - \vec{r}\right|} - \int \frac{\rho(\vec{r}\,')d\vec{r}\,'}{|\vec{r}\,' - \vec{r}\,|} \tag{3.71}$$

where Z_a is the charge in the nucleus A at the position $\vec{R}_A$.

The first term of the equation 3.71 is positive and it is related to the contributions of the nuclei. On the other hand, the second term is negative due to the contribution of the electrons. Usually the result of this equation is written in atomic units.[128]

This equation gives the result for the exact electrostatic potential. However, $\rho(\vec{r})$ is obtained from an *ab initio* or semiempirical wavefunction, and for this reason the electrostatic potential is an approximation, but even when a computational level as Hartree-Fock is employed the results for $V(\vec{r})$ are reasonable good.[129]

The MEP allows a visualization in three dimensions of the charge distribution in a molecule. Nevertheless, this surface just provides a qualitative information of the charge. Another important feature of this surface is that it is an observable that can be measured experimentally by diffraction methods and the results can be compared with the theoretical ones.[128]

Figure 3.4 shows the molecular electrostatic potential of a molecule mapped onto an isofurface of constant electron density. The red section of the surface corresponds to the negative potential, which is usually related to an electron-rich region of the molecule. This

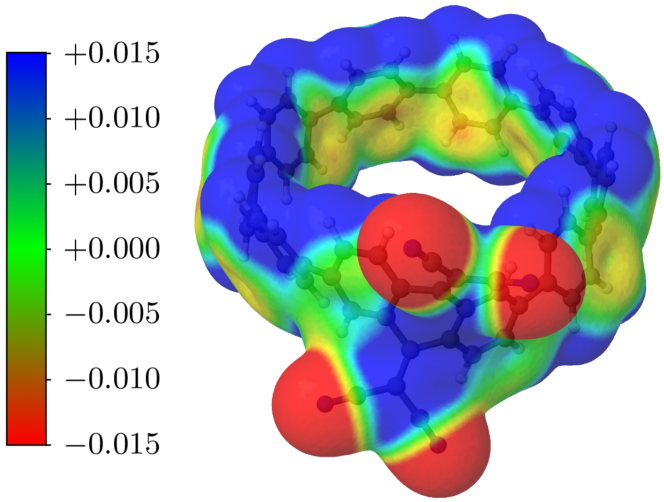

Figure 3.4: Molecular electrostatic potential for the cyclo[10]paraphenylene-2,6-tetracyanoanthraquino-dimethanylene mapped on a 0.001 a.u. electron density isosurface.

part is mostly localized over the cyano-substituents, with a smaller negative contribution in the centre of the phenyl rings. The blue part corresponds to the positive potential of the molecule, which is a poor electron region and it is located over the hydrogens and the anthracene ring. Finally, the green regions indicate regions with neutral electrostatic potential.

The MEP is an useful tool to predict some properties of the molecule, though it has some limitations in its use. $V(\vec{r})$ is defined for a given isolated molecule, and for this reason it does not change when a molecule approaches to another species. Another limitation is that a positive region in the potential does not always associate with a favourable tendency to react with nucleophiles, a chemical species that donates electrons. The positive charge of the nuclei could create a positive potential that exceeds the negative contribution of the electrons, but this positive surface does not mean a greater affinity for the nucleophiles.

3.4.3 SAPT

As mentioned previously there are two ways to calculate the non-covalent interaction energy: the supramolecular approach and the perturbative method. The perturbative approaches calculate the interaction energy as a perturbation of the Hamiltonian of the individual monomers. The most common of these approaches is the Symmetry-Adapted Perturbation Theory (SAPT),[5] that gives the interaction energy plus its physical components: electrostatic, repulsion, induction, and dispersion. This allows a better understanding of the type of intereaction established between monomers and how to enhance it.

It is possible to write the SAPT interaction energy as a perturbation series that can be truncated according to the level of accuracy that the system needs.[130,131] The fundamental SAPT interaction energy (IE) is the zeroth order one and it can be written as follows:

$$E_{\mathrm{IE}}^{\mathrm{SAPT0}} = E_{\mathrm{IE}}^{\mathrm{HF}} + \left[E_{\mathrm{disp}}^{(20)} + E_{\mathrm{exch\text{-}disp}}^{(20)}\right]_{\mathrm{disp}} = \left[E_{\mathrm{elst}}^{(10)}\right]_{\mathrm{elst}} + \left[E_{\mathrm{exch}}^{(10)}\right]_{\mathrm{exch}} + \left[E_{\mathrm{ind,r}}^{(20)} + E_{\mathrm{exch\text{-}ind,r}}^{(20)} + \delta E_{\mathrm{HF}}^{(2)}\right]_{\mathrm{ind}} + \left[E_{\mathrm{disp}}^{(20)} + E_{\mathrm{exch\text{-}disp}}^{(20)}\right]_{\mathrm{disp}} \tag{3.72}$$

where $E_{\mathrm{IE}}^{\mathrm{HF}}$ is the Hartree-Fock interaction energy obtained with the supermolecular method. For the other terms the first number of the superscript is the intermolecular order and the second number is the intramolecular order. The subscript "disp" is the contribution to the dispersion energy, "ind" is the contribution to the induction energy, "exch" is the contribution to the exchange (repulsion) energy and "elst" is the electrostatic contribution. When a "r" appears in the subscript the term includes the relaxation effect of the orbitals.

This method includes the Hartree-Fock energy for the monomers and several terms of the second-order perturbation theory to treat the electrostatic, induction and exchange. This equation also includes a correction term ($\delta E_{\mathrm{HF}}^{(2)}$) for contributions of the polarization beyond the second-order that are important in polar systems.

If a better accuracy is needed a higher order of SAPT seems mandatory. SAPT2 adds terms for the exchange, induction and electrostatic up to second-order for the intramolecular level:

$$E_{\mathrm{IE}}^{\mathrm{SAPT2}} = E_{\mathrm{IE}}^{\mathrm{SAPT0}} \left[E_{\mathrm{elst,r}}^{(12)}\right]_{\mathrm{elst}} + \left[E_{\mathrm{exch}}^{(11)} + E_{\mathrm{exch}}^{(12)}\right]_{\mathrm{exch}} + \left[{}^{t}E_{\mathrm{ind}}^{(22)} + {}^{t}E_{\mathrm{exch\text{-}ind}}^{(22)}\right]_{\mathrm{ind}} \tag{3.73}$$

Higher orders contributions can be included, SAPT2+, SAPT2+(3) or SAPT2+3, but a higher computational demand follows this increasing accuracy. Nowadays, the resolution of identity can be applied to SAPT, decreasing the time consuming and allowing the use of higher order of SAPT increasing the accuracy and the size of the problem that can be treated.[130,131]

The wavefunction used in SAPT is obtained through a Hartree-Fock method; however it is possible to use a DFT wavefunction like in the methods DFT-SAPT or SAPT(DFT).[132,133] The first attempt to use DFT consists in changing the HF orbitals for the KS orbitals and to apply a perturbation that only includes the intermolecular interaction because the intramolecular correlation is contained in DFT.[134] However, this exchange of orbitals produces poor results due to inaccuracies on the asymptotic behaviour of the exchange-correlation functional. With the purpose to correct this behaviour an adiabatic correction using the Tozer-Handy splicing scheme together with the Fermi-Amaldi asymptotic potential was developed.[135] This adiabatic correction rectifies the value for v_{XC} by a factor of $IP + \varepsilon_{\mathrm{HOMO}}$ at larger distance. IP is the lowest ionization potential that can be obtained through experimental or theoretical values and $\varepsilon_{\mathrm{HOMO}}$ is the energy of the highest occupied molecular orbital obtained with the exchange-correlation potential.[136] The equation for the SAPT(DFT) is the same than the equation 3.72. However, this is not the unique method thus developed; Grüning *et al.* proposed an alternative method in conjunction with the van Leeuwen-Baerends asymptotic potential to solve the same problem.[137,138] This gradient-regulated asymptotic correction (GRAC) corrects some problems of the previous correction such as the indirect relation with the electronic density and the possible existance of rough regions in both ends of the switch regions.[139]

One of the advantages of this method is the reduction of the computational cost because it takes into account the intramolecular correlation without expensive intermolecular higher order terms. Another advange is the posiblity to use the resolution of identity which reduces the computational cost even more. SAPT(DFT) has been known to produce results in agreement with CCSD(T) benchmarks at a reduced cost.[131,140,141]

3.4.4 Local energy decomposition (LED)

The supermolecule method gives as result the interaction energy of a given complex as a single number, thus providing little information about the underlying physics governing the interaction. Thus, a variety of schemes partitioning the interaction energy into contributions related with known physical effects have been developed (as those already provided by SAPT). These procedures,[17] usually known as Energy Decomposition Analysis (EDA) are applied a posteriori after performing a supermolecule calculation. One of the first ones is the Kitaura-Morokuma partition,[142] that divides the interaction energy into exchange, electrostatic, polarization and charge transfer contributions. These terms are the most common contributions to the interaction energy, like in other methods as the reduced variational space scheme[143] or Absolutely Localized Molecular Orbital (ALMO) EDA.[144] In contrast, SAPT methods based on perturbation theory provide directly the different contributions to the interaction.

In any case, most of EDA methods separate the interaction energy in different contributions, but mostly lack of a consistent description of dispersion effects. The problem of the dispersion is found in DFT EDA because many of the functionals were developed without the dispersion contribution; for this reason, the contribution from dispersion is often estimated using one of the empirical model described previously.

A different partitioning scheme that includes correlation and dispersion consistently into the partition has been recently proposed by Schneider *et al.*,[145] using the inherent locality of the recently developed Local Pair Natural Methods, and more specifically DLPNO-CCSD(T).[146–149]

3.4.4.1 DLPNO-CCSD(T)

The LED scheme developed by Schneider with the purpose to obtain the physical contributions to the energy is based in the domain-based local pair natural orbital coupled cluster single and doubles with perturbative triples correction (DLPNO-CCSD(T)) method. DLPNO-CCSD(T) was developed with the purpose to reduce the computational cost of the post-Hartree-Fock methods. The first method developed was the domain-based local pair natural orbital couple cluster singles and doubles (DLPNO-CCSD)[146–148] and later it was improved with the inclusion of the triples correction (DLPNO-CCSD(T)).[149] This method allows a linear scaling with the system size, reducing the computational cost of big systems making it look like the cost of DFT.[150]

The first step in DLPNO calculations is to locate the internal orbital space by means of an orbital location procedure, usually Foster-Boys[151] criterion or Pipek-Mezey[152] localization. After localization, domains are constructed for each orbital, including the virtual orbitals that fullfill a certain cutoff (see Figure 3.5). To construct these domains, the cutoff T_{CutMKN} is used with the purpose to determine the size of the initial domain in which

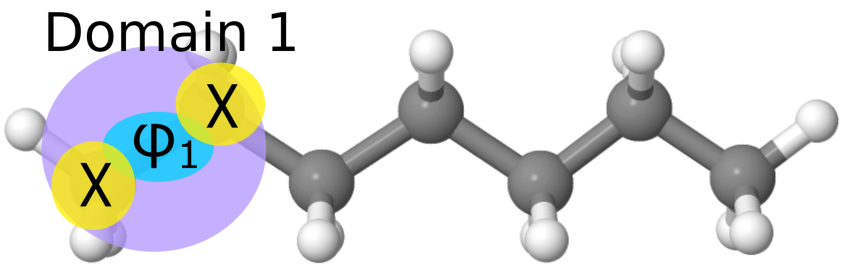

Figure 3.5: Domains for the heptane molecule.

the pair natural orbitals (PNOs) are expanded. The atoms with a Mulliken population higher than T_{CutMKN} for a localized molecular orbital ϕ_1 are contained in the domain.

The next step is to classify the electron pairs in different categories that will be treated with different computational approaches (see Figure 3.6). With the purpose to obtain this classification, a first prescreening based on a multipole estimation of the pair correlation energy is performed. The "Multipole pairs", those who do not fulfill multipole prescreening, are excluded from the following steps due to the minor contribution to the energy; however, their energy obtained with the multipole estimation is added to the final correlation energy. For the pairs that pass the first step the semicanonical local MP2 (SC-LMP2) pair correlation energy is computed. The pairs with an energy above a threshold T_{CutPairs} are included in the CCSD(T) treatment, "Strong pairs", and the contribution from pairs not included in CCSD(T) are computed at the MP2 level (in Figure 3.6 they are referred as "Weak pairs").

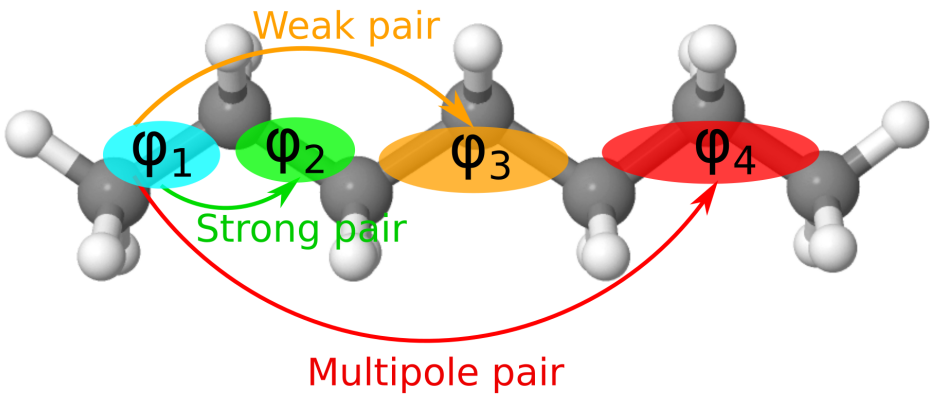

Figure 3.6: Different interactions between electrons pair in heptane molecule.

After that, using the SC-LMP2 pair densities, the PNOs are constructed and expanded in terms of projected atomic orbitals (PAO), that are the localized virtual orbitals. Another threshold, T_{CutPNO}, is used to define the size of this orbital space for each electron pair. All the orbitals in which the occupation number exceeds the threshold are used in the coupled cluster treatment, that is to say, all electron pairs have their own virtual space for the excitations.

As mentioned above the complexation energy can be split into two terms, the pure interaction energy (ΔE_{int}) and the deformation energy (ΔE_{def}), that it is the energy cost

for the geometric preparation of the monomer to adopt the geometry they have in the complex.

Also, for a post-HF method, the interaction energy can be further divided into two contributions, corresponding to the HF interaction energy ($\Delta E^{HF}_{\text{int}}$) and to the correlation contribution to the interaction energy ($\Delta E^{C}_{\text{int}}$):

$$\Delta E_{\text{int}} = \Delta E^{HF}_{\text{int}} + \Delta E^{C}_{\text{int}} \tag{3.74}$$

Now, according to the LED partitioning scheme, the interaction energy at the HF level is divided into three contributions. The electronic preparation ($E^{\text{HF}}_{el-prep}$), is the energy that the separated monomers need to adopt the electronic structure optimal for interacting in the complex and according to this scheme this energy is always positive and, therefore, repulsive. The second contribution is the electrostatic interaction (E^{HF}_{elec}) between the fragments; this energy is different from that used in SAPT[153,154] and in most EDAs that use the unperturbed electron density while DLPNO-CCSD(T) takes into account the distorted electron density distribution between the different fragments. Finally, the exchange interaction term (E^{HF}_{exch}) is always negative because it reduces the repulsion between electrons with the same spin.

$$\Delta E^{HF}_{\text{int}} = \Delta E^{HF}_{el-prep} + E^{HF}_{elec} + E^{HF}_{exch} \tag{3.75}$$

On the other hand, the correlation energy could be divided in four contributions. The electronic preparation ($\Delta E^{C}_{el-prep}$) for the correlation part of the energy energy is, similarly to the $\Delta E^{HF}_{el-prep}$ case, the energy cost required by the electronic reorganization by the weak and strong pairs. The charge transfer energy (E_{CT}) is the sum of the charge transfer energies between the first monomer (A) and the second monomer (B) and in opposite direction (see Figure 3.7). The dispersion energy (E_{disp}), which can be divided in turn into two other contributions, the London dispersion for the strong pairs and the weak pair contribution that is basically dipersive in nature. Finally, the last contribution is the triples correction between the fragments in CCSD(T) ($E_{(T)}$).

$$\Delta E^{C}_{\text{int}} = \Delta E^{C}_{el-prep} + E^{C}_{disp} + E^{C}_{CT} + E^{C}_{(T)} \tag{3.76}$$

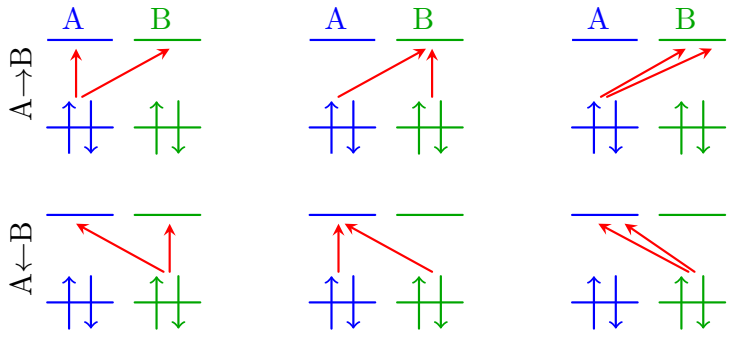

Figure 3.7: Scheme for the charge transfer between the fragment A and the fragment B.

Lastly, it is good to note that the weak pair contributions of the dispersion energy are the "weak pairs" that are excluded from the CCSD treatment (according to a cutoff) and treated at second order perturbation theory. The reason to exclude this "weak pairs"

from the CCSD treatment is that their contribution to the pair correlation energy is much smaller, usually giving rise to a negligible contribution that does not justify its computation with the expensive CCSD method. On the contrary, the rest of the electron pairs are included in the CCSD and so-called "strong pairs".

3.5 Euler angles

According to Euler's rotation theorem[155,156] using three angles, α, β and γ any rotation could be defined and, therefore, the orientation of a body can be described using these three angles with respect to a fixed coordinate system.

There are twelve possibilities to do the rotation which, in turn, are divided in two groups. If the Euler's rotation uses two different axes during the rotation, in other words, the first rotation is around an axis, the second uses a different axis and the last one uses the first axis again, there are six possibilities: Z-X-Z, Z-Y-Z, Y-X-Y, Y-Z-Y, X-Y-X and X-Z-X. On the other hand, the Tait-Bryan formalism uses three different axes in the rotation and it is usually employed in aerospace applications. In this case there are six possibilities as the Euler's rotation, the possibilities are X-Y-Z, Y-Z-X, Z-X-Y, X-Z-Y, Z-Y-X and Y-X-Z.

Also, there are two possible choices depending on the reference frame used for defining the axis:

1. **Intrinsic rotations**: The axes of the rotation are associated to the body that rotates; for this reason, after the first rotation, the axes also rotates and the next rotation uses these new axes.

2. **Extrinsic rotations**: The axes of the rotation are fixed in an external (lab) reference frame, that is to say, all the rotations use the same axes.

For example, the intrinsic rotation matrix with the Z-X-Z sequence through the angles α, β and γ, where c is cosine and s is sine, can be defined as:

$$R_{ZXZ} = R_Z(\gamma)R_Y(\beta)R_Z(\alpha) \tag{3.77}$$

In which the rotation matrix for each axis is:

$$R_Z(\alpha) = \begin{bmatrix} c(\alpha) & s(\alpha) & 0 \\ -s(\alpha) & c(\alpha) & 0 \\ 0 & 0 & 1 \end{bmatrix} \tag{3.78}$$

$$R_X(\beta) = \begin{bmatrix} 1 & 0 & 0 \\ 0 & c(\beta) & s(\beta) \\ 0 & -s(\beta) & c(\beta) \end{bmatrix} \tag{3.79}$$

$$R_Z(\gamma) = \begin{bmatrix} c(\gamma) & s(\gamma) & 0 \\ -s(\gamma) & c(\gamma) & 0 \\ 0 & 0 & 1 \end{bmatrix} \tag{3.80}$$

And the final rotation matrix is:

$$R_{ZXZ} = \begin{bmatrix} c(\alpha)c(\gamma) - c(\beta)s(\alpha)s(\gamma) & c(\alpha)c(\beta)s(\gamma) + c(\gamma)s(\alpha) & s(\beta)s(\gamma) \\ -c(\alpha)s(\gamma) - c(\beta)c(\gamma)s(\alpha) & c(\alpha)c(\beta)c(\gamma) - s(\alpha)s(\gamma) & c(\gamma)s(\beta) \\ s(\alpha)s(\beta) & -c(\alpha)s(\beta) & c(\beta) \end{bmatrix} \tag{3.81}$$

According to equation 3.81 the range for the angle α and γ are 2π, thus a valid range could be $[-\pi, \pi)$. On the other hand, β covers the range π and its valid range could be $[0, \pi)$ or $[-\pi/2, \pi/2)$.

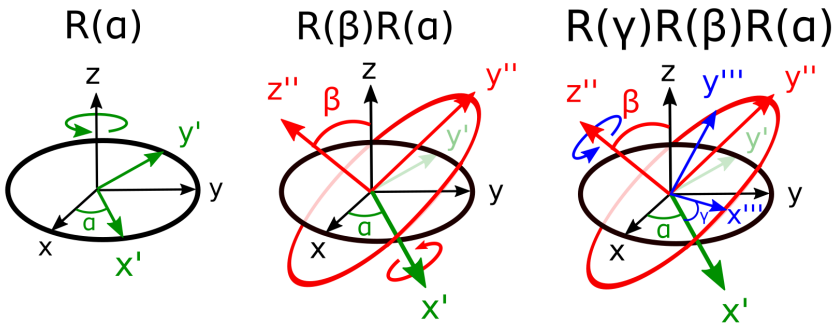

Figure 3.8: Schematic Z-X-Z rotation.

Figure 3.8 shows the ZXZ intrinsic rotation. In this figure the first rotation is through the z axis that produces the change of the x and y axes obtaining x′ and y′ (in green color). The second rotation is through the x′ axis and z″ and y″ axes is obtained (in red color). Finally the last rotation is through the z″ axis obtaining the last position x‴ and y‴ (in blue color).

References

(1) K. E. Riley, M. Pitončák, P. Jurečcka and P. Hobza, *Chemical Reviews*, 2010, **110**, 5023–5063.

(2) A. Stone, *The Theory of Intermolecular Forces*, Oxford University Press, Oxford, UK, 2013.

(3) S. Rybak, K. Szalewicz and B. Jeziorski, *Journal of Chemical Physics*, 1989, **91**, 4779–4784.

(4) K. Szalewicz, K. Patkowski and B. Jeziorski, in *Intermolecular Forces and Clusters II*, ed. D. Wales, Springer-Verlag, Berlin/Heidelberg, 2005, pp. 43–117.

(5) B. Jeziorski, R. Moszynski and K. Szalewicz, *Chemical Reviews*, 1994, **94**, 1887–1930.

(6) E. G. Hohenstein and C. D. Sherrill, *Wiley Interdisciplinary Reviews: Computational Molecular Science*, 2012, **2**, 304–326.

(7) I. C. Hayes and A. J. Stone, *Molecular Physics*, 1984, **53**, 83–105.

(8) G. Chalasinski and M. Gutowski, *Chemical Reviews*, 1988, **88**, 943–962.

(9) N. R. Kestner, *Journal of Chemical Physics*, 1968, **48**, 252–257.

(10) B. Liu and A. D. McLean, *Journal of Chemical Physics*, 1973, **59**, 4557–4558.

(11) D. Asturiol, M. Duran and P. Salvador, *Journal of Chemical Theory and Computation*, 2009, **5**, 2574–2581.

(12) R. M. Balabin, *Journal of Chemical Physics*, 2010, **132**, 231101.

(13) H. Valdés, V. Klusák, M. Pitoňák, O. Exner, I. Starý, P. Hobza and L. Rulíšek, *Journal of Computational Chemistry*, 2008, **29**, 861–870.

(14) S. F. Boys and F. Bernardi, *Molecular Physics*, 1970, **19**, 553–566.

(15) S. S. Xantheas, *Journal of Chemical Physics*, 1996, **104**, 8821–8824.

(16) K. Szalewicz and B. Jeziorski, *Journal of Chemical Physics*, 1998, **109**, 1198–1200.

(17) M. von Hopffgarten and G. Frenking, *Wiley Interdisciplinary Reviews: Computational Molecular Science*, 2012, **2**, 43–62.

(18) G. Chałasiński and M. M. Szczęśniak, *Chemical Reviews*, 2000, **100**, 4227–4252.

(19) M. Mentel and E. J. Baerends, *Journal of Chemical Theory and Computation*, 2014, **10**, 252–267.

(20) F. B. Van Duijneveldt, J. G. C. M. Van Duijneveldt-Van De Rijdt and J. H. Van Lenthe, *Chemical Reviews*, 1994, **94**, 1873–1874.

(21) X. W. Sheng, L. Mentel, O. V. Gritsenko and E. J. Baerends, *Journal of Computational Chemistry*, 2011, **32**, 2896–2901.

(22) K. B. Lipkowitz and D. B. Boyd, *Reviews in computational chemistry. Volume 13*, Wiley-VCH, Toronto, Canada, 1999.

(23) W. Koch and M. C. Holthausen, *A Chemist's Guide to Density Functional Theory*, Wiley-VCH Verlag GmbH, Weinheim, Germany, 2001.

(24) A. D. Becke, *Journal of Chemical Physics*, 2014, **140**, 18A301.

(25) L. H. Thomas, *Mathematical Proceedings of the Cambridge Philosophical Society*, 1927, **23**, 542.

(26) E. Fermi, *Accademia Nazionale dei Lincei*, 1927, **6**, 602–607.

(27) H. O. Rocco, F. Lanzini and J. C. Aguiar, *European Journal of Physics*, 2016, **37**, 065402.

(28) P. Hohenberg and W. Kohn, *Physical Review*, 1964, **136**, B864–B871.

(29) V. Sahni, in *Quantal Density Functional Theory*, ed. V. Sahni, Springer Berlin Heidelberg, Berlin, Heidelberg, 2004, pp. 99–123.

(30) J. Andrés and J. Bertran, *Theoretical and Computational Chemistry: Foundations, Methods and Technique*, Publicacions de la Universitat Jaume I, 2007.

(31) M. Born and R. Oppenheimer, *Annalen der Physik*, 1927, **389**, 457–484.

(32) W. Kohn and L. J. Sham, *Physical Review*, 1965, **140**, A1133–A1138.

(33) R. Stowasser and R. Hoffmann, *Journal of the American Chemical Society*, 1999, **121**, 3414–3420.

(34) K. Capelle, *Brazilian Journal of Physics*, 2006, **36**, 1318–1343.

(35) F Jensen, *Introduction to Computational Chemistry*, Wiley, Chichester, England, 2007.

(36) T. Tsuneda, *Density functional theory in quantum chemistry*, Springer Japan, Tokyo, 2014, vol. 9784431548.

(37) J. P. Perdew and K. Schmidt, in *Density Functional Theory and Its Application to Materials*, ed. V. Doren, C. V. Alsenoy and P. Geerlings, AIP, Melville, NY, 2001.

(38) J. P. Perdew, A. Ruzsinszky, J. Tao, V. N. Staroverov, G. E. Scuseria and G. I. Csonka, *Journal of Chemical Physics*, 2005, **123**, 062201.

(39) S. H. Vosko, L. Wilk and M. Nusair, *Canadian Journal of Physics*, 1980, **58**, 1200–1211.

(40) A. D. Becke, *Physical Review A*, 1988, **38**, 3098–3100.

(41) B. Miehlich, A. Savin, H. Stoll and H. Preuss, *Chemical Physics Letters*, 1989, **157**, 200–206.

(42) C. Lee, W. Yang and R. G. Parr, *Physical Review B*, 1988, **37**, 785–789.

(43) J. P. Perdew, J. A. Chevary, S. H. Vosko, K. A. Jackson, M. R. Pederson, D. J. Singh and C. Fiolhais, *Physical Review B*, 1992, **46**, 6671–6687.

(44) J. P. Perdew, K. Burke and M. Ernzerhof, *Physical Review Letters*, 1996, **77**, 3865–3868.

(45) S. Grimme, *Journal of Computational Chemistry*, 2006, **27**, 1787–1799.

(46) A. D. Becke, *Journal of Chemical Physics*, 1996, **104**, 1040–1046.

(47) J. Tao, J. P. Perdew, V. N. Staroverov and G. E. Scuseria, *Physical Review Letters*, 2003, **91**, 146401.

(48) A. D. Becke, *Journal of Chemical Physics*, 1993, **98**, 5648–5652.

(49) C. Adamo and V. Barone, *Journal of Chemical Physics*, 1999, **110**, 6158–6170.

(50) A. Savin, in *Recent Developments and Applications of Modern Density Functional Theory*, ed. J. Seminario, Elsevier, 1996, pp. 327–357.

(51) T. Tsuneda and K. Hirao, *Wiley Interdisciplinary Reviews: Computational Molecular Science*, 2014, **4**, 375–390.

(52) T. Yanai, D. P. Tew and N. C. Handy, *Chemical Physics Letters*, 2004, **393**, 51–57.

(53) J.-D. Chai and M. Head-Gordon, *Physical Chemistry Chemical Physics*, 2008, **10**, 6615–6620.

(54) T. M. Henderson, A. F. Izmaylov, G. Scalmani and G. E. Scuseria, *Journal of Chemical Physics*, 2009, **131**, 044108.

(55) C. Ullrich, *Time-dependent density-functional theory : concepts and applications*, Oxford; New York, 2011.

(56) M. A. Marques, N. T. Maitra, F. M. Nogueira, E. Gross and A. Rubio, *Fundamentals of Time-Dependent Density Functional Theory*, Springer, Berlin, Heidelberg, 2012.

(57) E. Runge and E. K. U. Gross, *Physical Review Letters*, 1984, **52**, 997–1000.

(58) M. Casida, in *Recent Advances in Density Functional Methods, Part I*, ed. D. Chong, Singapore, 1995, vol. 136.

(59) L. Verlet, *Physical Review*, 1967, **159**, 98–103.

(60) A. Dreuw, J. L. Weisman and M. Head-Gordon, *Journal of Chemical Physics*, 2003, **119**, 2943–2946.

(61) A. Dreuw and M. Head-Gordon, *J. Am. Chem. Soc*, 2004, **126**, 4007–4016.

(62) O. Gritsenko and E. J. Baerends, *Journal of Chemical Physics*, 2004, **121**, 655–660.

(63) M. J. G. Peach, P. Benfield, T. Helgaker and D. J. Tozer, *The Journal of Chemical Physics*, 2008, **128**, 044118.

(64) T. Le Bahers, C. Adamo and I. Ciofini, *Journal of Chemical Theory and Computation*, 2011, **7**, 2498–2506.

(65) J. L. Bao, L. Gagliardi and D. G. Truhlar, *Journal of Physical Chemistry Letters*, 2018, **9**, 2353–2358.

(66) C. M. Isborn, B. D. Mar, B. F. E. Curchod, I. Tavernelli and T. J. Martínez, *Journal of Physical Chemistry B*, 2013, **117**, 12189–12201.

(67) S. Grimme, *Journal of Computational Chemistry*, 2004, **25**, 1463–1473.

(68) S. Grimme, J. Antony, S. Ehrlich and H. Krieg, *Journal of Chemical Physics*, 2010, **132**, 154104.

(69) S. Grimme, *Wiley Interdisciplinary Reviews: Computational Molecular Science*, 2011, **1**, 211–228.

(70) A. Tkatchenko and M. Scheffler, *Physical Review Letters*, 2009, **102**, 073005.

(71) A. D. Becke and E. R. Johnson, *Journal of Chemical Physics*, 2005, **122**, 154104.

(72) T. Sato and H. Nakai, *Journal of Chemical Physics*, 2009, **131**, 224104.

(73) T. Sato and H. Nakai, *Journal of Chemical Physics*, 2010, **133**, 194101.

(74) A. Otero de la Roza and G. A. DiLabio, *Non-covalent interactions in quantum chemistry and physics : theory and applications*, Elsevier Science, Oxford, UK, 2017.

(75) D. Josa, J. Rodríguez-Otero, E. M. Cabaleiro-Lago and M. Rellán-Piñeiro, *Chemical Physics Letters*, 2013, **557**, 170–175.

(76) E. M. Cabaleiro-Lago, B. Fernández and J. Rodríguez-Otero, *Journal of Computational Chemistry*, 2018, **39**, 93–104.

(77) E. Caldeweyher, C. Bannwarth and S. Grimme, *Journal of Chemical Physics*, 2017, **147**, 034112.

(78) Y. Zhao, N. E. Schultz and D. G. Truhlar, *Journal of Chemical Theory and Computation*, 2006, **2**, 364–382.

(79) Y. Zhao and D. G. Truhlar, *Theoretical Chemistry Accounts*, 2008, **120**, 215–241.

(80) Y. Zhao, N. E. Schultz and D. G. Truhlar, *Journal of Chemical Physics*, 2005, **123**, 161103.

(81) N. Mardirossian and M. Head-Gordon, *Journal of Chemical Theory and Computation*, 2016, **12**, 4303–4325.

(82) M Dion, H Rydberg, E Schrö, D. C. Langreth and B. I. Lundqvist, *Physical Review Letters*, 2004, **92**, 246401.

(83) K. Lee, É. D. Murray, L. Kong, B. I. Lundqvist and D. C. Langreth, *Physical Review B - Condensed Matter and Materials Physics*, 2010, **82**, 081101.

(84) O. A. Vydrov and T. Van Voorhis, *Journal of Chemical Physics*, 2010, **133**, 244103.

(85) L. A. Burns, Á. Vázquez-Mayagoitia, B. G. Sumpter and C. D. Sherrill, *Journal of Chemical Physics*, 2011, **134**, 84107.

(86) B. Nagy and F. Jensen, in *Reviews in Computational Chemistry, Volume 30*, ed. A. L. Parrill and K. B. Lipkowitz, John Wiley & Sons, Inc, Hoboken, New Jersey, 2017, pp. 93–149.

(87) J. C. Slater, *Physical Review*, 1930, **36**, 57–64.

(88) S. F. Boys, *Proceedings of the Royal Society A: Mathematical, Physical and Engineering Sciences*, 1950, **200**, 542–554.

(89) G. te Velde, F. M. Bickelhaupt, E. J. Baerends, C. Fonseca Guerra, S. J. van Gisbergen, J. G. Snijders and T. Ziegler, *Journal of Computational Chemistry*, 2001, **22**, 931–967.

(90) W. J. Hehre, R. F. Stewart and J. A. Pople, *Journal of Chemical Physics*, 1969, **51**, 2657–2664.

(91) R. Krishnan, J. S. Binkley, R. Seeger and J. A. Pople, *Journal of Chemical Physics*, 1980, **72**, 650–654.

(92) A. Schäfer, H. Horn and R. Ahlrichs, *Journal of Chemical Physics*, 1992, **97**, 2571–2577.

(93) A. Schäfer, C. Huber and R. Ahlrichs, *Journal of Chemical Physics*, 1994, **100**, 5829–5835.

(94) F. Weigend, F. Furche and R. Ahlrichs, *Journal of Chemical Physics*, 2003, **119**, 12753–12762.

(95) F. Weigend and R. Ahlrichs, *Physical Chemistry Chemical Physics*, 2005, **7**, 3297–3305.

(96) T. H. Dunning, *Journal of Chemical Physics*, 1989, **90**, 1007–1023.

(97) H. J. Werner, F. R. Manby and P. J. Knowles, *Journal of Chemical Physics*, 2003, **118**, 8149–8160.

(98) C. Van Alsenoy, *Journal of Computational Chemistry*, 1988, **9**, 620–626.

(99) M. Feyereisen, G. Fitzgerald and A. Komornicki, *Chemical Physics Letters*, 1993, **208**, 359–363.

(100) K. Eichkorn, O. Treutler, H. Öhm, M. Häser and R. Ahlrichs, *Chemical Physics Letters*, 1995, **240**, 283–289.

(101) B. I. Dunlap, J. W. D. Connolly and J. R. Sabin, *International Journal of Quantum Chemistry*, 1977, **12**, 81–87.

(102) B. I. Dunlap, J. W. Connolly and J. R. Sabin, *Journal of Chemical Physics*, 1979, **71**, 3396–3402.

(103) F. Weigend, *Physical Chemistry Chemical Physics*, 2002, **4**, 4285–4291.

(104) F. Weigend, *Journal of Computational Chemistry*, 2008, **29**, 167–175.

(105) R. Izsák, F. Neese and W. Klopper, *Journal of Chemical Physics*, 2013, **139**, 094111.

(106) F. Neese, F. Wennmohs, A. Hansen and U. Becker, *Chemical Physics*, 2009, **356**, 98–109.

(107) E. Rebolini, R. Izsák, S. S. Reine, T. Helgaker and T. B. Pedersen, *Journal of Chemical Theory and Computation*, 2016, **12**, 3514–3522.

(108) R. Izsák and F. Neese, *Journal of Chemical Physics*, 2011, **135**, 144105.

(109) G. Seifert, *Journal of Physical Chemistry A*, 2007, **111**, 5609–5613.

(110) A. F. Oliveira, G. Seifert, T. Heine and H. A. Duarte, *Journal of the Brazilian Chemical Society*, 2009, **20**, 1193–1205.

(111) P. Koskinen and V. Mäkinen, *Computational Materials Science*, 2009, **47**, 237–253.

(112) M. Elstner and G. Seifert, *Philosophical Transactions of the Royal Society A*, 2014, **372**, 20120483.

(113) G. Seifert and J. O. Joswig, *Wiley Interdisciplinary Reviews: Computational Molecular Science*, 2012, **2**, 456–465.

(114) D. Porezag, T. Frauenheim, T. Köhler, G. Seifert and R. Kaschner, *Physical Review B*, 1995, **51**, 12947–12957.

(115) G. Seifert, D. Porezag and T. Frauenheim, *International Journal of Quantum Chemistry*, 1996, **58**, 185–192.

(116) M. Elstner, D. Porezag, G. Jungnickel, J. Elsner, M. Haugk and T. Frauenheim, *Physical Review B - Condensed Matter and Materials Physics*, 1998, **58**, 7260–7268.

(117) M. Gaus, Q. Cui and M. Elstner, *J. Chem. Theory Comput.*, 2011, **7**, 931–948.

(118) Y. Yang, H. Yu, D. York, Q. Cui and M. Elstner, *Journal of Physical Chemistry A*, 2007, **111**, 10861–10873.

(119) M. Elstner, P. Hobza, T. Frauenheim, S. Suhai and E. Kaxiras, *Journal of Chemical Physics*, 2001, **114**, 5149–5155.

(120) M. Gaus, A. Goez and M. Elstner, *Journal of Chemical Theory and Computation*, 2013, **9**, 338–354.

(121) R. S. Mulliken, *Journal of Chemical Physics*, 1955, **23**, 1833–1840.

(122) Z. Bodrog, B. Aradi and T. Frauenheim, *Journal of Chemical Theory and Computation*, 2011, **7**, 2654–2664.

(123) M. Gaus, Q. Cui and M. Elstner, *Wiley Interdisciplinary Reviews: Computational Molecular Science*, 2014, **4**, 49–61.

(124) M. Wanko, M. Hoffmann, T. Frauenheim and M. Elstner, *Journal of Computer-Aided Molecular Design*, 2006, **20**, 511–518.

(125) E. R. Johnson, S. Keinan, P. Mori-Sánchez, J. Contreras-García, A. J. Cohen and W. Yang, *Journal of the American Chemical Society*, 2010, **132**, 6498–6506.

(126) J. Contreras-García, E. R. Johnson, S. Keinan, R. Chaudret, J. P. Piquemal, D. N. Beratan and W. Yang, *Journal of Chemical Theory and Computation*, 2011, **7**, 625–632.

(127) P. Politzer, P. R. Laurence and K. Jayasuriya, *Environmental Health Perspectives*, 1985, **61**, 191–202.

(128) P. Politzer and D. G. Truhlar, *Chemical Applications of Atomic and Molecular Electrostatic Potentials*, Springer US, Boston, MA, 1981.

(129) M Cohen and A Dalgarno, *Proceedings of the Physical Society*, 1961, **77**, 748–750.

(130) E. G. Hohenstein, R. M. Parrish, C. D. Sherrill, J. M. Turney and H. F. Schaefer III, *Journal of Chemical Physics*, 2011, **135**, 174107.

(131) T. M. Parker, L. A. Burns, R. M. Parrish, A. G. Ryno and C. D. Sherrill, *Journal of Chemical Physics*, 2014, **140**, 094106.

(132) K. Szalewicz, *Wiley Interdisciplinary Reviews: Computational Molecular Science*, 2012, **2**, 254–272.

(133) G. Jansen, *Wiley Interdisciplinary Reviews: Computational Molecular Science*, 2014, **4**, 127–144.

(134) H. L. Williams and C. F. Chabalowski, *Journal of Physical Chemistry A*, 2001, **105**, 646–659.

(135) D. J. Tozer and N. C. Handy, *Journal of Chemical Physics*, 1998, **109**, 10180–10189.

(136) K. U. Lao and J. M. Herbert, *Journal of Chemical Physics*, 2014, **140**, 044108.

(137) R. Van Leeuwen and E. J. Baerends, *Physical Review A*, 1994, **49**, 2421–2431.

(138) M. Grüning, O. V. Gritsenko, S. J. A. Van Gisbergen and E. J. Baerends, *Journal of Chemical Physics*, 2001, **114**, 652–660.

(139) W. Cencek and K. Szalewicz, *Journal of Chemical Physics*, 2013, **139**, 024104.

(140) A. Tekin and G. Jansen, *Physical Chemistry Chemical Physics*, 2007, **9**, 1680–1687.

(141) M. Pitoňák, K. E. Riley, P. Neogrády and P. Hobza, *ChemPhysChem*, 2008, **9**, 1636–1644.

(142) K. Kitaura and K. Morokuma, *International Journal of Quantum Chemistry*, 1976, **10**, 325–340.

(143) W. Chen and M. S. Gordon, *Journal of Physical Chemistry*, 1996, **100**, 14316–14328.

(144) R. Z. Khaliullin, E. A. Cobar, R. C. Lochan, A. T. Bell and M. Head-Gordon, *Journal of Physical Chemistry A*, 2007, **111**, 8753–8765.

(145) W. B. Schneider, G. Bistoni, M. Sparta, M. Saitow, C. Riplinger, A. A. Auer and F. Neese, *Journal of Chemical Theory and Computation*, 2016, **12**, 4778–4792.

(146) C. Riplinger and F. Neese, *Journal of Chemical Physics*, 2013, **138**, 034106.

(147) D. G. Liakos, M. Sparta, M. K. Kesharwani, J. M. Martin and F. Neese, *Journal of Chemical Theory and Computation*, 2015, **11**, 1525–1539.

(148) C. Riplinger, P. Pinski, U. Becker, E. F. Valeev and F. Neese, *Journal of Chemical Physics*, 2016, **144**, 024109.

(149) C. Riplinger, B. Sandhoefer, A. Hansen and F. Neese, *Journal of Chemical Physics*, 2013, **139**, 134101.

(150) D. G. Liakos and F. Neese, *Journal of Chemical Theory and Computation*, 2015, **11**, 4054–4063.

(151) S. F. Boys, *Reviews of Modern Physics*, 1960, **32**, 296–299.

(152) J. Pipek and P. G. Mezey, *Journal of Chemical Physics*, 1989, **90**, 4916–4926.

(153) A. Heßelmann, *Journal of Chemical Physics*, 2005, **122**, 244108.

(154) R. J. Azar and M. Head-Gordon, *Journal of Chemical Physics*, 2012, **136**, 024103.

(155) L. Euler, *Novi commentarii Academiae Scientiarum Imperialis Petropolitanae*, 1776, **20**, 189–207, translated by Johan Sten in http://www.17centurymaths.com/contents/euler/e478tr.pdf.

(156) H. Goldstein, *Classical mechanics*, Addison-Wesley Pub. Co, Boston, MA, 1980.

USC UNIVERSIDADE DE SANTIAGO DE COMPOSTELA

USC
UNIVERSIDADE
DE SANTIAGO
DE COMPOSTELA

Chapter 4

Carbon-nanorings ([10]CPP and [6]CPPA) as fullerene (C_{60} and C_{70}) receptors: a comprehensive dispersion-corrected DFT study

4.1 Introduction

At the present time, one of the most active fields in fullerene chemistry is the design of suitable fullerene receptors, in order to give rise to stable complexes useful for developing new materials for solar energy conversion, optoelectronics, catalysis and switching.[1–3] Dispersion forces are essential for the stabilisation of fullerene complexes. The use of concave–convex complementarity can be an excellent strategy to maximize these forces in order to design new molecular receptors. However, the concave fullerene receptors are relatively scarce given that curved molecules are not always an easy synthetic target due to their tensioned structures.[4] Anyway, in recent years the interest in concave–convex $\pi\cdots\pi$ interactions has greatly increased, and a significant number of works has been published.[5–18] Among the different kinds of fullerene receptors, ones that have recently drawn attention are the so-called carbon-nanorings, CNRs. These hoop-shaped π-conjugated hydrocarbon molecules possess nanosized concave cavities that can act as hosts for π-conjugated molecules with convex surfaces, such as fullerenes. Two different types of CNRs are cycloparaphenylenes ([n]CPP) and cycloparaphenyleneacetylenes ([n]CPPA). [n]CPPs contain a series of 1,4-phenylene units, whereas [n]CPPAs possess alternating 1,4-phenylene and ethynylene units, both adopting rigid and belt-shaped structures with well-defined cavities.

In this work we will focus on two of these CNRs (see Figure 4.1), which are those that have generated more interest from both experimental and theoretical points of views: [10]CPP and [6]CPPA.[19–27] This is because these two CNRs have the appropriate diameter (about 13–14 Å) to "catch" the most common fullerenes, C_{60} and C_{70}.

Cycloparaphenylenes (CPPs) were synthesized in 2008[28] ([10]CPP, at the gram-scale, in 2012[20]) and represent the simplest structural unit of armchair carbon nanotubes, CNTs. On the other hand, [6]CPPA had already been synthesized in 1996 by Kawase *et al.*[29] The same authors proved the formation of stable complexes between this CNR and fullerenes

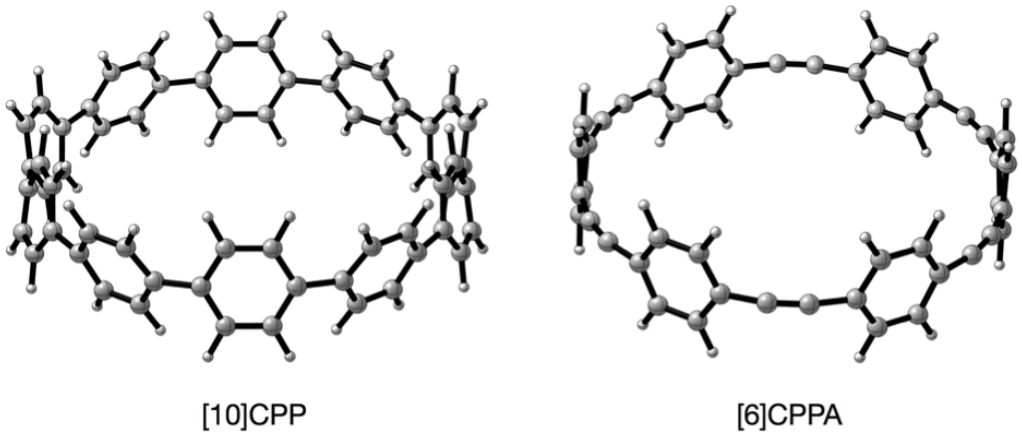

Figure 4.1: The two CNRs studied: [10]CPP and [6]CPPA.

C_{60} and C_{70}, attributing the driving force for forming [*n*]CPPA supramolecular complexes to concave–convex $\pi\cdots\pi$ interactions.[19,30] According to the association constants found in benzene, complexation with C_{70} is slightly better than with C_{60}. Later, Iwamoto *et al.* found that [10]CPP in toluene was a much better receptor of C_{60} than [6]CPPA, obtaining an association constant that is 100 times larger.[22] Finally, the same authors achieved the encapsulation of C_{70} by [10]CPP in toluene and 1,2-dichlorobenzene.[21] In this last solvent (which is better for C_{70} than toluene), the association constant with [10]CPP is somewhat larger for C_{70} than for C_{60} (8.5×10^3 *vs.* 6.0×10^3 mol L^{-1}).

From the theoretical point of view some studies were carried out regarding the stability of the complexes formed by the CNRs [10]CPP and [6]CPPA, and the fullerenes C_{60} and C_{70}.[21,23–25,27] Although these studies provide results of great interest, there are several weaknesses that prevent performing a thorough and systematic analysis of all possible complexes that can be formed between the CNR and fullerene, as well as a complete interpretation of all the interactions. First, in all cases the M06-2X functional was the only one used. Besides the limitation of using just a single level of calculation, previous studies showed that this functional gives rise to an important underestimation of the complexation energy for concave–convex $\pi\cdots\pi$ interactions.[12,17] Moreover, in the different works different basis sets were used (MIDI!, 6-31G*, 6-31G**, 6-31+G**, 6-311+G**), which prevents a correct comparison of the stability of the complexes. In some cases the basis set superposition error, BSSE, was taken into account but not in others. Finally, it is worth mentioning that, in general, it seems that the search for the best arrangement of the complexes has not been carried out in a systematic way. So, maybe the most stable structures have not been located. Therefore, we believe it is advisable to carry out a systematic study of all the complexes that can be established between a CNR ([10]CPP and [6]CPPA) and a fullerene (C_{60} and C_{70}). A systematic and thorough search of all spatial arrangements of the complexes will be performed, the interaction energy corresponding to all minima will be evaluated, and the ability of the CNRs as hosts for fullerenes will be analysed and interpreted.

4.2 Computational details

Since dispersion effects are crucial to study $\pi\cdots\pi$ interactions, dispersion-corrected DFT methods seem mandatory. Among them, Grimme's empirical dispersion correction is one of the most popular procedures. The original version (DFT-D)[31] was modified in 2006 (DFT-D2)[32] and further corrected in 2010 (DFT-D3)[33] and 2011 (DFT-D3(BJ)).[34]

Recently, for the corannulene dimer, Kennedy *et al.*[6] showed that the best results (compared with the benchmark performed at the QCISD(T)/aug-cc-pVTZ level[12]) correspond to B3LYP-D3(BJ), but with a very small advantage over B3LYP-D2, M06-2X and B97-D2. Of these DFT methods, B97-D2 is the best to take advantage of the noticeable reduction of computational cost that allows the resolution of identity approximation (RI) implemented in Turbomole program suite,[35] since for non-hybrid functionals the RI procedure speeds up calculations by a factor 10 at least (as compared to conventional treatments) without sacrificing accuracy. In addition, calculations using B97-D2 method also provide very good results as can be observed in several previous works.[10,17,18,36] Taking into account the above comments, the size of the studied systems and the software used, the choice of the B97-D2/def2-TZVP level of calculation and the RI approximation seems appropriate (with the def2-TZVPP auxiliary basis set). All the complexes are fully optimised at this level. Moreover, several calculations are carried out at the BLYP-D2/def2-TZVP, B3LYP-D3(BJ)/def2-TZVP, TPSS-D3(BJ)/def2-TZVP, PBE0-D3(BJ)/def2-TZVP and M06-2X/6-311+G** levels (M06-2X calculations are performed with the Gaussian package[37]).

Counterpoise corrections, CP, are applied to all reported interaction energies to avoid basis set superposition error, BSSE.[38] According to this method, the interaction energy of a system A$\cdots$B is calculated according to:

$$\Delta E_{\text{int}} = E_{\text{AB}}^{\text{AB}}(\text{AB}) - \left(E_{\text{A}}^{\text{AB}}(\text{AB}) + E_{\text{B}}^{\text{AB}}(\text{AB})\right) \tag{4.1}$$

where superscript refers to the geometry (that of the system AB) and the term within the parentheses indicates the basis set used (the full basis set of the system A$\cdots$B). If, in addition, the energy cost involved in the deformation of each monomer to adopt the geometry of the dimer is considered:

$$\Delta E_{\text{def}} = \left(E_{\text{A}}^{\text{AB}}(\text{A}) - E_{\text{A}}^{\text{A}}(\text{A})\right) + \left(E_{\text{B}}^{\text{AB}}(\text{B}) - E_{\text{B}}^{\text{B}}(\text{B})\right) \tag{4.2}$$

then, the full complexation energy is obtained as follows:

$$\Delta E_{\text{complex}} = \Delta E_{\text{int}} + \Delta E_{\text{def}} \tag{4.3}$$

The visualization of non-covalent interactions regions is conducted using the NCIPLOT-3.0 program.[39,40] Then, graphic displays of concave–convex $\pi\cdots\pi$ interactions are obtained using the VMD 1.9.1 software.[41] NCI enables identification of non-covalent interactions based on the peaks that appear in the reduced density gradient (RDG) at low densities. Plotting a RDG isosurface for a low value of RDG, the non-covalent regions clearly appear in the supramolecular complex. These interactions correspond to both favourable and unfavourable interactions. In order to differentiate between them, the sign of the second eigenvalue of the density Hessian times the density is colour-mapped onto the isosurface: blue, green and red indicate strongly attractive interactions, weak

vdW interactions, and strongly repulsive interactions, respectively. To save computation time, promolecular densities have been used, as previously done with good results in similar systems.[16]

When the complex CNR$\cdots$fullerene is formed, the spatial disposition of the fullerene inside the belt may lead to a large number of different energy minima. Thus, the search for the absolute minimum is not a very easy task. In the present work, in order to explore the potential energy surface (PES), two different procedures were carried out.

The first method is to place the fullerene inside the CNR and then studying the energetic profile that emerges from the fullerene rotation around an axis perpendicular to the belt. To make this rotation a couple of different spatial dispositions of the fullerene are chosen. Obviously, the choice of these dispositions, although it is made with certain criteria, is somewhat arbitrary. Once found the most favourable minima of those profiles is found, the energetic change that arises from the vertical departure of the fullerene is also studied. By "vertical departure", we mean the displacement of the fullerene along the vertical Z-axis, *i.e.* the distance between the centroid of the fullerene and that of the CNR being 0.0 Å, when the fullerene is fully hosted in the CNR. Finally, the minima found are optimised without any geometrical restrictions, and for the minimized complexes the complexation energy is calculated.

With this first procedure it is feasible that some of the relevant minima are not found. For that reason, another safer procedure (although even it does not provide total certainty) is performed: the fullerene is placed at the centre of the CNR and then it is allowed to rotate in all the directions through a scanning of the three Euler angles (α, β, γ), using steps of 6 degrees (see Figure a.1, in Appendix A). This procedure leads to the computation of a huge number of single point calculations for searching all the space (4464 with C_{60}, and many more with C_{70}). For that reason, these single point calculations are performed using the same functional (B97-D2) but with a smaller basis set, namely the def2-SVP (with the corresponding def2-SVP auxiliary basis set for the RI approximation). Once more stable minima are found, they are optimised without any geometrical restrictions using the chosen level (B97-D2/def2-TZVP), and subsequently the complexation energies are calculated at this level.

4.3 Results and discussion

4.3.1 C_{60}@[10]CPP complex

To study the interaction between buckminsterfullerene C_{60} and [10]CPP, two different spatial dispositions of the fullerene are chosen. In the first one ($C_{60}(5)$), the axis that goes through the centre of the 5-membered top and bottom rings of C_{60} is placed perpendicularly to the CNR and in the centre of the ring. In the second one ($C_{60}(6)$), the axis goes through the centre of the 6-membered top and bottom rings of C_{60}. Figure 4.2a shows the energetic profile that arises from the rotation around those two axes. Two kinds of minima appear for $C_{60}(5)$: I, the most stable one, and II, which is a very irrelevant minimum located on the plateau of the maximum. Minimum I shows a structure where each of the ten rings of [10]CPP is directly faced to a six-membered ring of C_{60}. That is to say, the best overlap between the hexagonal rings of C_{60} and [10]CPP takes place. This happens every 72 degrees, since both monomers share a common C_5 symmetry axis.

Rotation around this axis has a relevant cost of about 5 kcal mol^{-1}. Oppositely, rotation around the axis of $C_{60}(6)$ is virtually free. However, the corresponding minimum (III) is about 2 kcal mol^{-1} less stable than I.

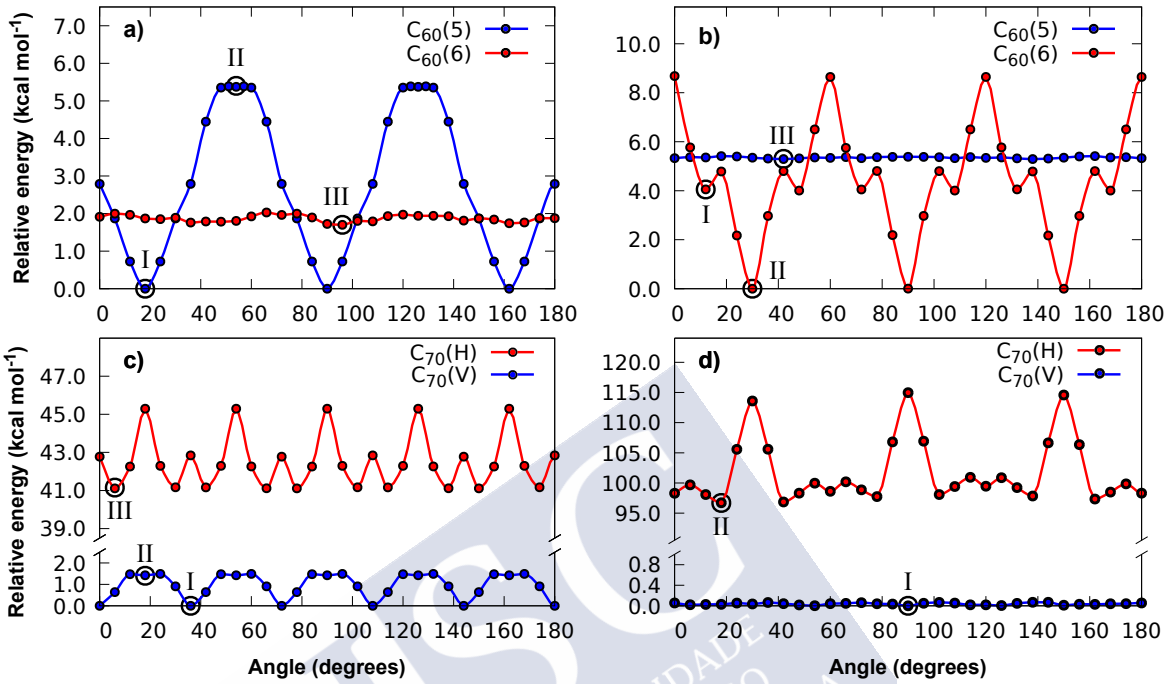

Figure 4.2: Energetic profile for the rotation of fullerene C_{60}/C_{70} inside the carbon-nanoring, obtained at the B97-D2/def2-TZVP level. (a) C_{60}@[10]CPP. (b) C_{60}@[6]CPPA.(c) C_{70}@[10]CPP. (d) C_{70}@[6]CPPA. $C_{60}(5)$ corresponds to a spatial disposition of fullerene with 5-membered rings at the top/bottom of the ball. $C_{60}(6)$ corresponds to a spatial disposition of fullerene with 6-membered rings at the top/bottom of the ball. $C_{70}(V)$ corresponds to a spatial disposition of fullerene where C_{70} is placed vertically, *i.e.*, the major diameter is perpendicular to the plane of the CNR. Oppositely, for $C_{70}(H)$, the fullerene is placed horizontally, lying on the plane of the nanoring.

Figure 4.3 shows that a good qualitative correlation takes place between the stability of minima I–III and the interaction surface resulting from the NCI analysis. So, for the most stable minimum I, a large green surface (corresponding to vdW interactions) arises, resulting from the $\pi\cdots\pi$ interaction between the ten phenyl rings of [10]CPP directly facing the ten hexagonal rings of C_{60}. For minimum III, the isosurface is smaller, and for minimum II, it is almost irrelevant.

Once the most favourable orientation (minimum I) is found, the vertical departure of C_{60} from the CNR is analysed. Figure 4.4a clearly shows that this departure quickly becomes adverse, and a very fast destabilsation taking place: more than 5 kcal mol^{-1} in less than 1 Å. This single-potential well was also obtained by Yuan *et al.* at the M06-2X/6-31G* level.[25] The NCIPLOT analysis allows observing in a very visual way that the stability is directly related to the formation of a larger isosurface of vdW interaction between C_{60} and [10]CPP which reaches the maximum when the fullerene is fully hosted within the CNR (see Figure a.2, Appendix A). Thus, according to the results, it seems clear that C_{60} fits perfectly well inside [10]CPP.

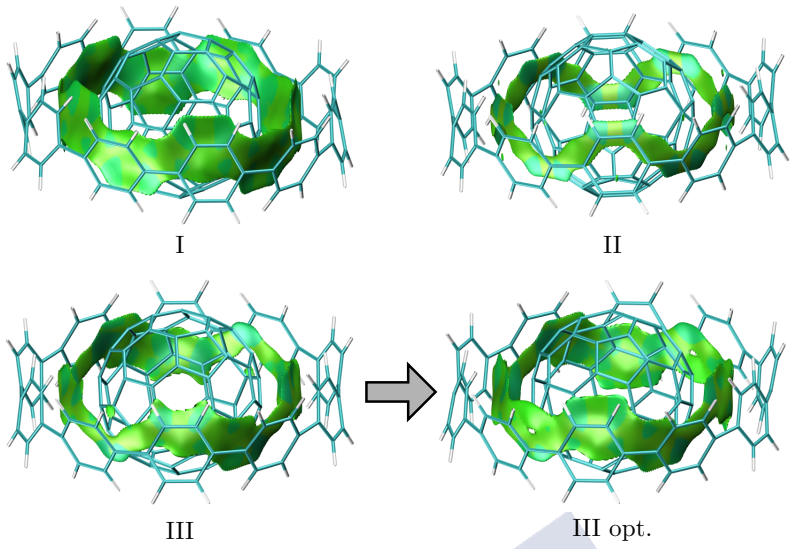

Figure 4.3: NCIPLOT gradient isosurface (0.3 a.u.) corresponding to the minima of Figure 4.2a, for the interaction between C_{60} and [10]CPP. Blue-green-red scale over the range −0.04 to 0.04 a.u.

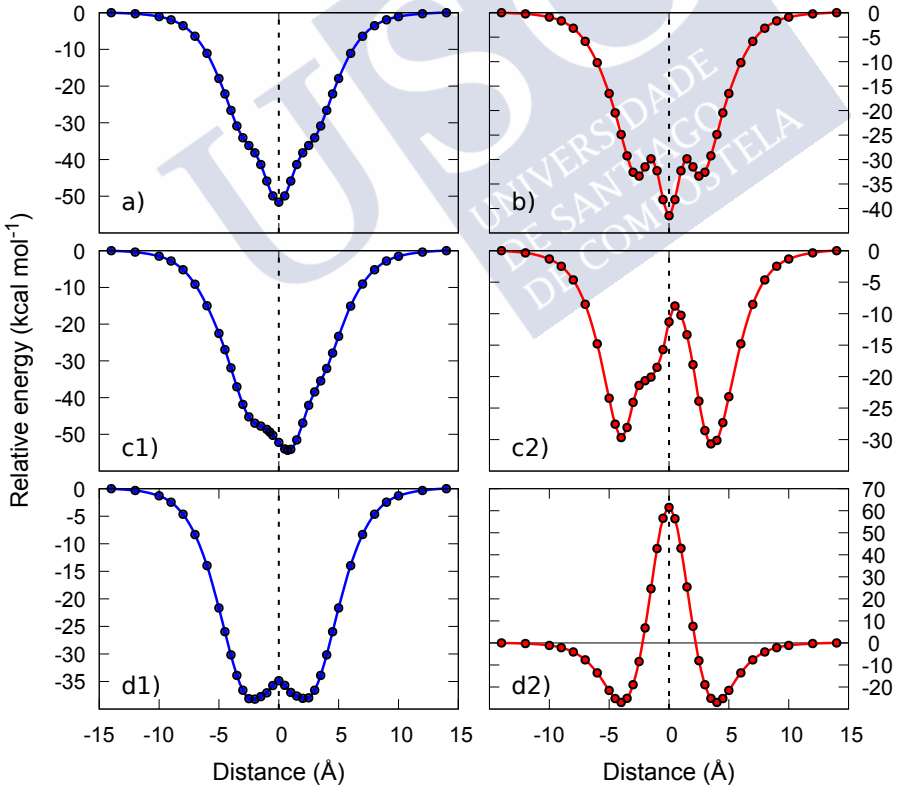

Figure 4.4: Energetic profile for the vertical departure of fullerene C_{60}/C_{70} from the carbon-nanoring, obtained at the B97-D2/def2-TZVP level. (a) C_{60}@[10]CPP; minimum I of Figure 4.2a. (b) C_{60}@[6]CPPA; minimum II of Figure 4.2b. (c) C_{70}@[10]CPP; (c1) minimum I, C_{70}(V), of Figure 4.2c; (c2) minimum III, C_{70}(H), of Figure 4.2c. (d) C_{70}@[6]CPPA; (d1) minimum I, C_{70}(V), of Figure 4.2d; and (d2) minimum II, C_{70}(H), of Figure 4.2d.

The next step is optimising minima I and III, without any geometrical restrictions. Whereas minimum I does not undergo any significant geometrical change (which is imperceptible in the NCIPLOT), minimum III suffers mainly two changes: the top/bottom hexagonal ring of C_{60} rotates inwards a few degrees and the CNR is slightly compressed, so that the strength of the interaction increases, as shown in Figure 4.3, getting close to the one obtained for minimum I. For that reason, the calculated complexation energies for these two minima are very similar: −49.78 and −49.27 kcal mol^{-1}, for I and III respectively (see Table 4.1).

Table 4.1: Energy results of the optimised main minima found (kcal mol^{-1}). $\Delta E_{\text{complex}}$ = complexation energy. ΔE_{def} = deformation energy. Dispersion = contribution of dispersion to the total complexation energy. The best complex of each case is highlighted in bold.

		$\Delta E_{\text{complex}}$	ΔE_{def}		Dispersion
			Fullerene	CNR	
C_{60}@[10]CPP	I	**−49.78**	0.11	0.23	−83.61
	III	−49.27	0.08	0.42	−83.55
C_{60}@[6]CPPA	I	−36.95	0.55	0.44	−89.76
	II	**−40.63**	0.47	0.25	−89.78
	III	−37.12	0.57	0.40	−89.12
C_{70}@[10]CPP	I	**−53.32**	0.09	0.55	−93.73
	IIIa	−43.88	0.34	4.29	−101.59
	IIIb	−45.24	0.68	4.26	−113.96
C_{70}@[6]CPPA	I	−40.92	0.23	0.75	−81.45
	II	−36.31	0.20	2.86	−77.09
	I'	**−41.53**	0.46	0.79	−93.29

As discussed in the Computational details section, another procedure for finding the minima of the complex (based on the systematic scanning of all orientations of C_{60} inside [10]CPP) is carried out. However, no new minima are found (see section A.3 in Appendix A).

4.3.2 C_{60}@[6]CPPA complex

As in the previous case, two different spatial dispositions of the fullerene are chosen ($C_{60}(5)$ and $C_{60}(6)$) and the energetic profiles arising from the rotation of both dispositions are obtained (Figure 4.2b). However, in this case the most favourable energy corresponds to $C_{60}(6)$ (minimum II), with an advantage larger than 5 kcal mol^{-1} relative to $C_{60}(5)$. Rotation around the axis of $C_{60}(6)$ shows an important barrier of about 9 kcal mol^{-1}, and the energy repeats every 60 degrees because both monomers share a common C_6 symmetry axis. Oppositely, rotation around the axis of $C_{60}(5)$ is virtually free.

Taking minimum II as starting point, Figure 4.4b shows the vertical departure of C_{60} from the CNR. This figure shows that although there is a local minimum at about 3 Å from the centre of the ring, the global minimum corresponds clearly to 0 Å, *i.e.*, C_{60} also fits perfectly well inside [6]CPPA.

The subsequent optimisation of the minima shows that I and II almost do not suffer any geometric change. For minimum III, however, C_{60} undergoes certain readjustment inside the [6]CPPA, trying to increase the interaction. The calculated complexation energies are −36.95, −40.63, and −37.12 kcal mol^{-1} for I, II, and III, respectively (see Table 4.1), that is to say, about ten kcal mol^{-1} smaller than those for the C_{60}@[10]CPP complex. This difference is in agreement with the difference between the interaction isosurfaces corresponding to both complexes: for the C_{60}@[6]CPPA complex, the NCIPLOT shows an important area for each of the six phenyl rings of the CNR, but a rather small one for each of the six acetylene bonds (see Figure 4.5).

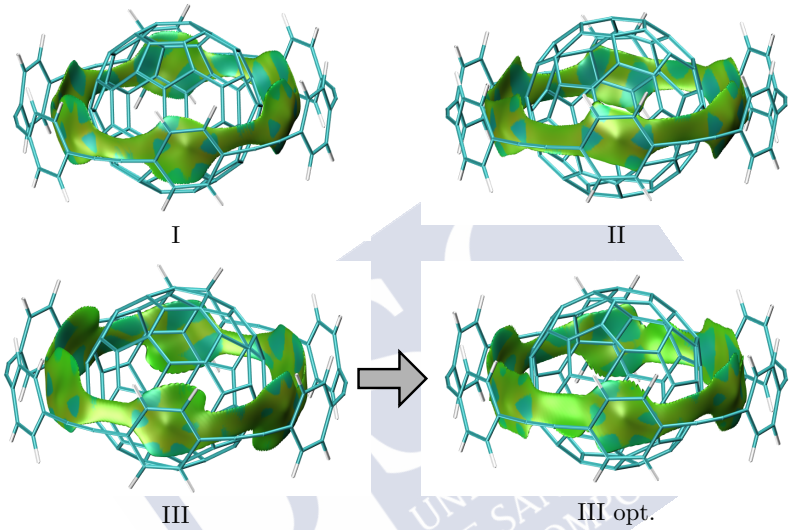

Figure 4.5: NCIPLOT gradient isosurface (0.3 a.u.) corresponding to the minima of Figure 4.2b, for the interaction between C_{60} and [6]CPPA. Blue-green-red scale over the range −0.04 to 0.04 a.u.

Finally, as in the case of the C_{60}@[10]CPP complex, the systematic searching of other minima does not give any result (see section A.4 in Appendix A).

4.3.3 C_{70}@[10]CPP complex

As in the case of C_{60}, two different spatial dispositions of C_{70} are chosen. Moreover, in this case the difference between both dispositions is more visible. In the first one (C_{70}(V)), C_{70} is placed vertically, *i.e.*, the major diameter is perpendicular to the plane of the CNR. In the second one, (C_{70}(H)), C_{70} is placed horizontally, lying on the plane of the nanoring. Figure 4.2c shows the energetic profile that arises from the rotation of both dispositions around an axis perpendicular to the plane of [10]CPP. According to this figure, it is clear that the C_{70}(H) spatial disposition is much more disadvantageous than the C_{70}(V) one (more than 40 kcal mol^{-1} worse). The explanation is obvious: the major diameter of C_{70} is too large and prevents the fullerene form properly fitting inside the CNR. Both profiles of the Figure 4.2c show repeated values, each 36 degrees. The profile for the rotation of C_{70}(V) shows a certain similarity with that of C_{60}(5) inside [10]CPP, with an absolute minimum (I) and an irrelevant minimum (II) located on the plateau of the maximum.

The main difference is that the energetic cost of rotation is rather smaller: less than 2 kcal mol^{-1}.

Figure 4.6 (left column) shows the NCIPLOT for minima I and III. First, the similarity between the isosurface corresponding to minimum I of C_{70}(V) and minimum I of C_{60}(5) is noneworthy (see Figure 4.3). Second, the isosurface corresponding to III shows areas of strong interactions, attractive (blue) as well as repulsive (red).

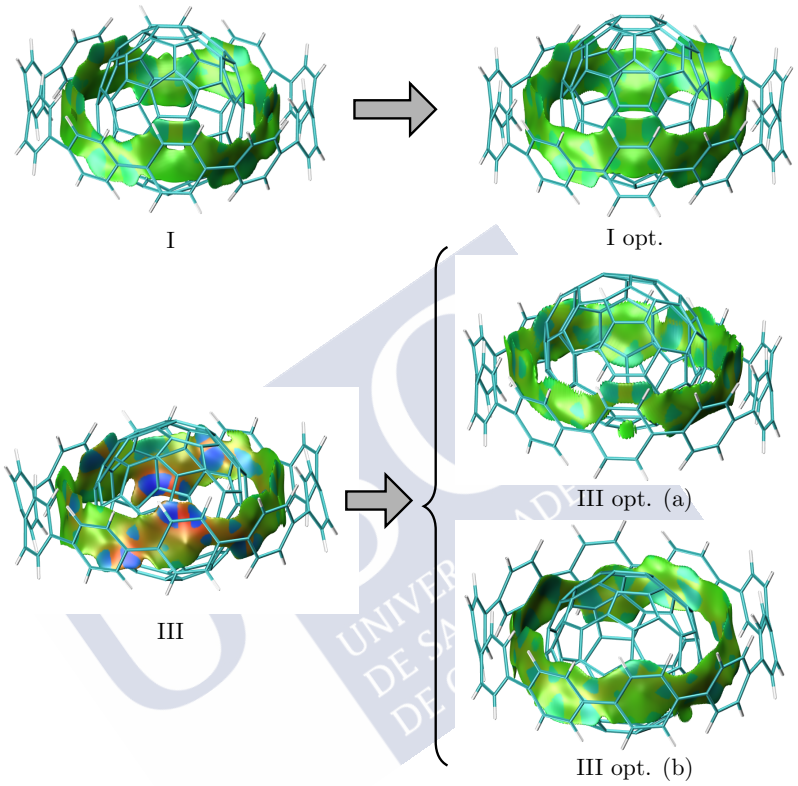

Figure 4.6: NCIPLOT gradient isosurface (0.3 a.u.) corresponding to the minima of Figure 4.2c, for the interaction between C_{70} and [10]CPP. (a) optimisation from the minimum of Figure 4.4c2. (b) optimisation from d = 0.0 Å of Figure 4.4c2. Blue-green-red scale over the range −0.04 to 0.04 a.u.

Taking minima I and III as starting points, Figure 4.4c shows the vertical departure of C_{70} from the CNR. According to this figure, neither minimum I nor minimum III show the maximum stability when the fullerene is fully hosted in the CNR (d = 0.0 Å). As expected, the most noticeable case is that of minimum III (C_{70}(H)), where the departure is almost 5 Å, with an increase of stability larger than 20 kcal mol^{-1}.

The vertical departure of C_{70} is fully confirmed after optimisation without any geometrical restrictions starting from the previous minima. For minimum I (C_{70}(V)), this departure is small (0.769 Å between the centres of monomers), and for C_{70}(H) is somewhat larger (1.506 Å, IIIa). Although the latter distance is smaller than predicted from Figure 4.4c2, this is easily explained: optimisation involves an important deformation of [10]CPP, which adopts an oval shape, suitable for fitting C_{70} in a horizontal disposition. Moreover, if the optimisation is not performed starting from the minimum of the Figure 4.4c2, but from d = 0.0 Å, a more stable structure (IIIb) is achieved (with only 0.951

Å between the centres of monomers). In this case, there is a large rearrangement of C_{70} inside the CNR, so that C_{70}(H) ends up in an intermediate disposition between C_{70}(V) and the "real" C_{70}(H) (minimum IIIa). Figure 4.6 (right column) shows the NCIPLOT for the optimised minima. For minimum I, only very slight differences relative to the starting point are observed: in the minimized structure the isosurface is something larger, covering all the small "cracks" of the interaction surface. However, for minimum III, both optimisations lead to striking changes of the NCI isosurface, which are consequence of the large rearrangement of the structure. Thus, the strongly repulsive and attractive regions disappear to give way to soft vdW interactions. This leads, in the case of IIIa, to a rather small isosurface, due to the significant vertical departure of C_{70} (1.506 Å).

The calculated complexation energies for the three optimised minima are −53.31, −43.88 and −45.24 kcal mol^{-1}, for C_{70}(V) and the two horizontal dispositions (IIIa and IIIb in Figure 4.6), respectively. As expected, the smaller complexation energy corresponds to IIIa, where C_{70} keeps a fully horizontal disposition, and therefore, it is forced to move away from the CNR. As also expected, after relaxation, the disadvantage of the horizontal disposition of C_{70} (see Figure 4.2c), although important, is drastically reduced (from 40 to 10 kcal mol^{-1}).

As for the two previous complexes, the systematic search of other minima does not give any new result (see section A.5 in Appendix A).

4.3.4 C_{70}@[6]CPPA complex

Figure 4.2d shows the energetic profile that arises from the rotation of C_{70} in the above-mentioned dispositions: C_{70}(V) and C_{70}(H). In this case the energetic difference between these two dispositions is much more noticeable than for the complex C_{70}@[10]CPP: of about 100 kcal mol^{-1} (although after geometric relaxation, this difference will decrease significantly). This fact, is certainly due to the somewhat smaller size of the [6]CPPA ring (13.22 Å *vs.* 13.86 Å for [10]CPP, regarding the diameter of the ring). The most favourable disposition (C_{70}(V)) shows, in addition, a virtually free rotation.

Figure 4.7 (left column) shows the NCIPLOT for minima I and II. The isosurface corresponding to II shows areas of strong interactions, attractive (blue) and, especially, repulsive (red). This huge repulsion corresponds to the area where the ends of the lying C_{70} "collide" with the CNR.

Taking minima I and II as starting points, Figure 4.4d shows the vertical departure of C_{70} from the CNR. According to this figure, neither minimum I nor minimum II show the maximum stability when the fullerene is fully hosted in the CNR (d = 0.0 Å). Both curves are fully symmetric with respect to the distance; this fact is due to [6]CPPA being a symmetrical ring with respect to the vertical axis and this axis is fully perpendicular to the symmetry plane bisecting each of the benzene rings of the nanoring. For C_{70}(H) (minimum II. Figure 4.4d2), the curve shows for d = 0.0 Å a larger energy than that for $d = \infty$, *i.e.*, the complex is not stable at all when C_{70} is fully hosted in the CNR. Also for that reason, the distance corresponding to the minimum is quite large (almost 5 Å), and the increase of stability larger than 90 kcal mol^{-1} relative to d = 0.0 Å.

Optimization of minima I and II (starting from the minima of Figure 4.4d) leads to significant geometrical changes. In both cases, C_{70} places outside of the nanoring, although with distances smaller than predicted by Figure 4.4d, due to the rearrangement

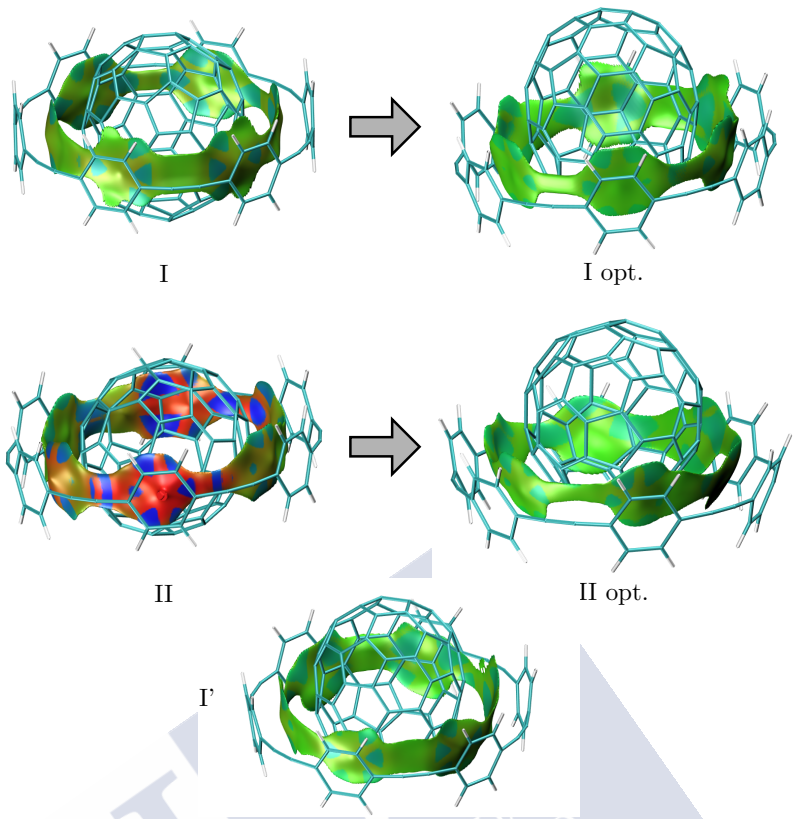

Figure 4.7: NCIPLOT gradient isosurface (0.3 a.u.) corresponding to the minima of Figure 4.2d, for the interaction between C_{70} and [6]CPPA. I' corresponds to the minimum found by the systematic search. Blue-green-red scale over the range −0.04 to 0.04 a.u.

caused by the geometrical relaxation of the nanoring. Thus, distances of 1.959 and 2.665 Å are obtained for minimum I and II, respectively; the first corresponding to a vertical disposition C_{70}(V), and the second to an intermediate disposition between the "real" C_{70}(H) and C_{70}(V). The complexation energy for these two minima is −40.92 and −36.31 kcal mol^{-1}, respectively.

In this case, the systematic searching of other minima does give a new minimum (I', see section A.6 in Appendix A), slightly better than I, with complexation energy of −41.53 kcal mol^{-1}. The main difference between I and I' is that in the latter C_{70} is not laid absolutely "vertical": the major axis of C_{70} is rotated 1.6 degrees relative to the axis perpendicular to the plane of the CNR. Although this departure is subtle, it is enough for C_{70} not needing to leave from the CNR as much as with the case of minimum I: 1.285 Å, *i.e.*, about 0.7 Å apart. This fact shows that sometimes a very small readjustment of the fullerene inside the CNR is able to lead to an important modification of the distance between the centres of monomers, favouring the guest to remain more inside the host leading to higher complexation energy.

4.3.5 Comparison between complexes

Table 4.1 shows clearly the two main trends as regards the complexation energy. First, [10]CPP is a much better fullerene receptor than [6]CPPA, with an advantage of about

10 kcal mol^{-1} (9.15 and 11.98 kcal mol^{-1} for C_{60} and C_{70}, respectively). Second, C_{70} is better than C_{60} as a guest, with an advantage of 3.54 and 0.90 kcal mol^{-1} depending on the CNR.

The good performance of [10]CPP for catching fullerenes C_{60} and C_{70} is easily explained from the visualization of the structure of its complexes: as commented above, the best minimum (both for C_{60} and C_{70}) corresponds to a structure where each of the ten rings of [10]CPP is directly faced to a six-membered ring of the fullerene (see Figure a.3, Appendix A). This spatial arrangement explain why C_{60} remains fully hosted in the CNR whereas C_{70} moves vertically from the centre of the CNR (0.769 Å): the interaction zone of C_{60} lies exactly at the middle of the fullerene, whereas it is slightly displaced in C_{70}. The important advantage of C_{70} *vs.* C_{60} (3.53 kcal mol^{-1}) comes from dispersion (see Table 4.1), since the short axis of C_{70} is slightly larger than the axis of C_{60}. So, the monomers are slightly closer for C_{70}, as shown in Figure a.4 (Appendix A). For that reason, dispersion with C_{70} is slightly larger, especially with the central region of the fullerene (see Figure a.5, Appendix A).

The much better behaviour of [10]CPP as a fullerene receptor regarding that of [6]CPPA (with an advantage of about 10 kcal mol^{-1}), can be explained by means of three main factors:

1. [6]CPPA holds only six π clouds ([10]CPP, ten) and, as it can be seen in the NCI pictures (Figures 4.3 and 4.5–4.7), the alkyne bonds give rise to a much smaller interaction.

2. From an electrostatic point of view, [10]CPP is slightly better than [6]CPPA. In order to analyse that question, Figure 4.8 shows maps of the molecular electrostatic potential, MEP, of the four monomers involved in the complex formation. C_{60} and C_{70} show an almost neutral MEP, but slightly positive on the top of the rings. For that reason, a negative MEP region inside de CNR will favour the complex formation. As can easily be seen in Figure 4.8, the negative region of [10]CPP is larger and stronger than that of [6]CPPA.

3. [10]CPP has a slightly larger size than [6]CPPA, which seems better suited for the size of fullerene. Although the size difference is small (13.86 *vs.* 13.22 Å regarding the diameter of the ring), it is significant enough to generate noticeable structural and energetic differences. For instance, C_{70}(V) goes out of [6]CPPA rather more than [10]CPP: 1.285 *vs.* 0.769 Å. On the other hand, C_{70}(H) hardly fits into both CNRs, but the situation is much worse for [6]CPPA: Figure 4.4c2 and 4.4d2 show a maximum at the $d = 0.0$ Å region, but for [6]CPPA this maximum is so great that as result the complex is much less stable than the separated monomers.

Probably these three effects are not very strong individually (especially the second and third ones), but their joint action is able to get an important advantage for [10]CPP *vs.* [6]CPPA. This advantage was experimentally established for the interaction with C_{60}.[22]

As regard fullerenes, there is a small advantage of C_{70} *vs.* C_{60}. A qualitative explanation can be supported by the electrostatics: the first nonvanishing multipole moment is the 64-pole for C_{60} and the quadrupole for C_{70}. However, this effect (if any) is unable to explain the difference of 3.53 kcal mol^{-1} for the interaction with [10]CPP. In this case, as

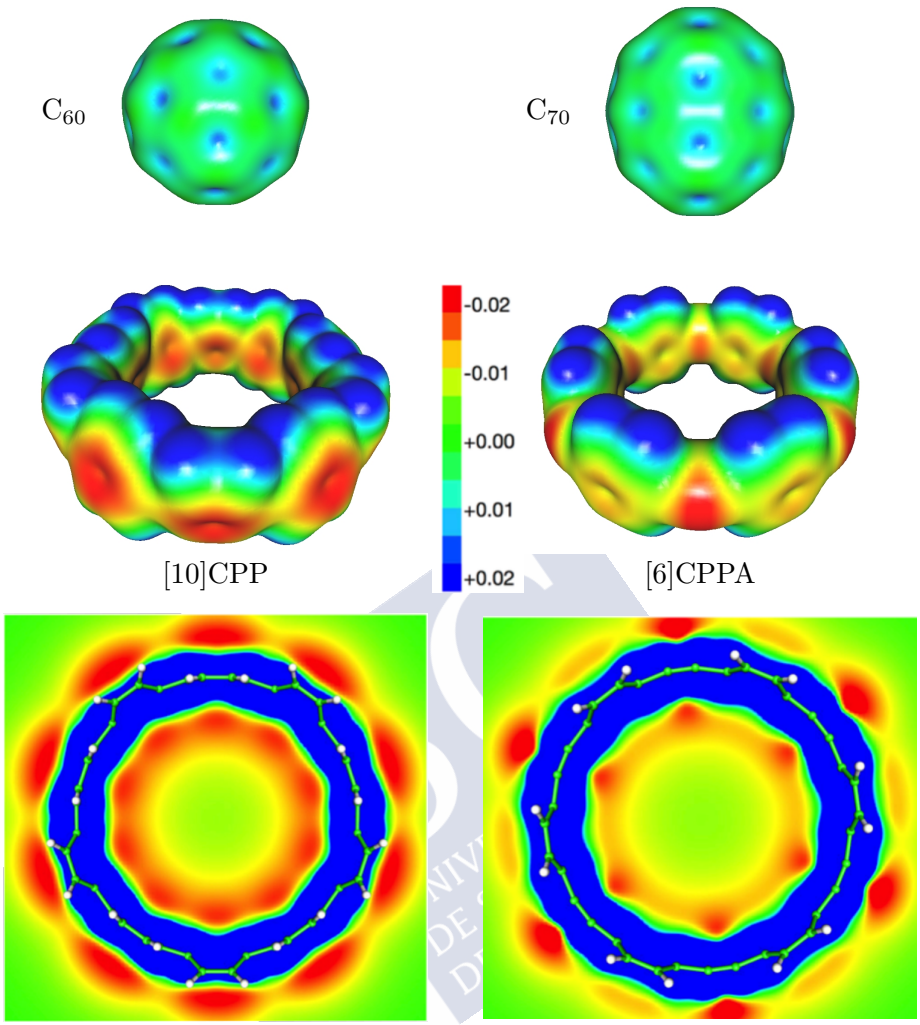

Figure 4.8: Up: Molecular electrostatic potential, MEP, on an electron density isosurface of 0.001 a.u. for the fullerenes and the CNRs. Down: MEP on the plane of the two CNRs (the symmetry plane bisecting each of the bezene rings of the nanoring).

commented above, the C_{70} advantage comes from the increased dispersion generated by its slightly larger size. For that reason, it seems clear that the behaviour of the two fullerenes as guests (regarding complexation energies) is very similar, and the important advantage of C_{70} is a particular fact rather than a general one. Anyway, in this particular case, one would think that [10]CPP would allow the selective separation of C_{60} and C_{70}, given the important difference of complexation energy between them. This statement should be very cautiously considered taking into account that we are only discussing complexation energies (not Gibbs free energies) in the gas phase.

The results in Table 4.1 show that dispersion plays a crucial role in the complexation energy. So, the contribution from the pure B97 functional is clearly repulsive, ranging from +33.83 to +68.71 kcal mol^{-1} (+40.41 kcal mol^{-1} for the strongest complex, C_{70}@[10]CPP-I). However, unlike what happened in the complexes of our latest works,[13,14] there is not any correlation between the dispersion contributions and the complexation energies. This

is due to the large structural differences between the complexes studied in this work: *i.e.*, two very different CNRs and very different arrangements of the fullerenes (C_{70}(V) *vs.* C_{70}(H), C_{60}(5) *vs.* C_{60}(6)). So, the balance between the different contributions to the interaction energy (electrostatic, exchange/repulsion, induction and dispersion) must be quite complicated and very different for the different complexes.

Regarding the energy of deformation that encompasses the formation of the complexes studied, Table 4.1 clearly shows that the CNRs, and especially the fullerenes, are quite rigid, non-deformable structures. There are few exceptions to this rule, and they are limited to the cases where C_{70} is tried to be placed horizontally (C_{70}(H)) lying on the plane of the nanoring, as expected. Except in such cases, the deformation is very small, and therefore, the deformation energy is well below 1 kcal mol^{-1}.

Finally, in order to get information about the basis set performance, the B97-D2/def2-TZVP results are compared with those obtained using the def2-SVP and def2-QZVP basis sets (only single-point calculations are performed for the latter). Figure a.6 (Appendix A) shows that the def2-TZVP complexation energies are already very close to the quadruple-zeta ones (actually, this already happened even with the def2-SVP complexation energies, for complexes with [6]CPPA). Thus, the results (see Figure a.6 and Table a.1, Appendix A) show that using a larger basis set than def2-TZVP does not change the results to any significant extent. So, as can be seen in Table a.2 (Appendix A), the conclusions commented on above remain the same, both qualitatively and quantitatively: [10]CPP is a considerably better fullerene receptor than [6]CPPA, and, C_{70} is a slightly better guest than C_{60}. On the other hand, the small basis set def2-SVP performs reasonably well, thus demonstrating the ability of this basis set to lead to satisfactory pre-screening.

4.3.6 Comparison between DFT functionals

As justified above (Computational details), the B97-D2/def2-TZVP level is used throughout the main calculations. However, it might be of interest performing some calculations with other methods to check their performance. Figure 4.9 (and Table a.3, Appendix A) shows good correlation of the B97-D2 results with those of B3LYP-D3(BJ) (the latter ones supposed as the best reference available, see Computational details). The same happens with BLYP-D2 complexation energies, something unsurprising in the light of our previous calculations.[17] Likewise, the TPSS-D3(BJ) results are virtually the same as those of the BLYP-D2 ones. The PBE0-D3(BJ) complexation energies are somewhat smaller than the others. However, although the results of the five DFT-D methods are slightly different, they are absolutely coherent, being perfectly correlated between them (Figure a.7, Appendix A), so the five functionals would virtually lead to the same analysis of the results (already stated in the previous section) regarding the comparison between the two CNRS and the two fullerenes, *i.e.*, [10]CPP is rather better than [6]CPPA as a host, and C_{70} is something better than C_{60} as a guest. The behaviour of M06-2X is mainly similar to that of the five DFT-D methods, but with a couple of perceptible differences. The main one is the small complexation energies: about 6–13 kcal mol^{-1} smaller than those of DFT-D methods. This underestimation is not new, according to previous calculations.[6,12,17,18] The second difference refers to the ability of C_{60} and C_{70} as guests. In all cases C_{70} behaves better than C_{60}, but for DFT-D methods the difference between them is significant when complexed with [10]CPP and slight when complexed with [6]CPPA; just the

opposite takes place with M06-2X. Regarding M06-2X results, it is worth analysing the result obtained by Yuan et al.[25] for the C_{60}@[10]CPP complex: complexation energy of 48.63 kcal mol^{-1}. Respectfully, we believe that this value might be a mistake that seems clear when Figure 4.9 and Figure a.7 (in Appendix A) are observed: their value deviates completely from the trend observed for all other M06-2X calculations (our estimation of about -40 kcal mol^{-1} seems reasonable).

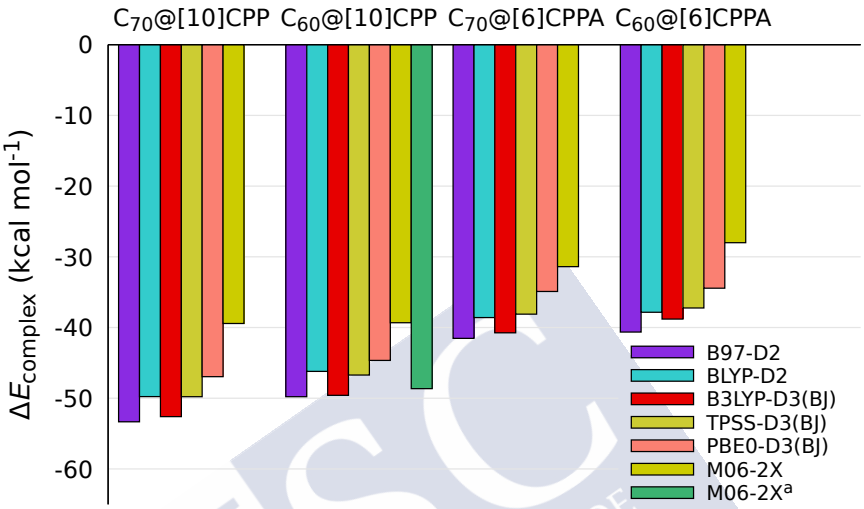

Figure 4.9: Complexation energy obtained with different DFT methods. Complexes are sorted by decreasing energy. M06-2X calculations have been performed by us or taken from literature when available (see Table a.3, in Appendix A). M06-2X^{a}–Yuan *et al.*[25]

4.4 Conclusions

The comprehensive analysis of all the possible complexes between the carbon-nanorings [10]CPP and [6]CPPA with the fullerenes C_{60} and C_{70}, shows that [10]CPP is an excellent "catcher" of fullerenes. Thus, the ten phenyl rings of this CNR interact optimally with the ten six-membered rings of the central region of the fullerene (exactly central for C_{60} and slightly displaced for C_{70}). For that reason, C_{60} remains fully hosted in the CNR whereas C_{70} moves vertically from the centre of the CNR (0.769 Å).

The results show that with the two CNRs, C_{70} gives rise to larger complexation energy than C_{60}. This fact is especially relevant for the interaction with [10]CPP, where the advantage of C_{70} reaches 3.53 kcal mol^{-1}, which might suggest that a selective separation of the two fullerenes might be viable.

As commented in the Computational details section, two different methods were applied for searching for all the possible minima of the complexes. One of them, "cheaper" computationally speaking, but with a certain amount of arbitrariness: it is rather fast, but it is possible for some minima to go unnoticed. The second one is systematic, more robust, with an almost complete full-scan of all the arrangements of the fullerene inside the CNR. For that reason is extremely "expensive". After comparing the results obtained by both methods, it seems clear that the most economical method would be valid in most

cases. According to our results, this could be absolutely true for the complexes where the fullerene remains perfectly inside the CNR. When the fullerene moves away vertically from the centre of the CNR, the use of the cheapest method is a little more problematic. That it is what happened for the C_{70}@[6]CPPA complex, where the systematic search found a new minimum, slightly better than the one obtained by the simplest method. This new minimum showed a spatial arrangement that is somewhat different, with the fullerene closer to the CNR. However, the effect on the complexation energy was rather small: just 0.61 kcal mol^{-1}. For that reason, the convenience of using the systematic search is more than questionable, and in most cases a limited search using certain criteria, should be more than enough to localize the most relevant minima.

The comparison of the results produced by the functional used along the exhaustive study (B97-D2) with other functionals (BLYP-D2, B3LYP-D3(BJ), TPSS-D3(BJ), PBE0-D3(BJ) and M06-2X), shows that the conclusions are basically the same, especially regarding the DFT-D methods. The behaviour of M06-2X is mostly similar to that of the five DFT-D methods, though it importantly underestimates complexation energies.

References

(1) F. D'Souza and O. Ito, *Chemical Communications*, 2009, 4913–4928.

(2) H. Imahori and S. Fukuzumi, *Advanced Functional Materials*, 2004, **14**, 525–536.

(3) P. Hudhomme and J. Cousseau, in *Fullerenes: Principles and Applications (2)*, The Royal Society of Chemistry, Cambridge, UK, 2012, pp. 416–461.

(4) E. M. Pérez and N. Martín, *Chemical Society Reviews*, 2008, **37**, 1512–1519.

(5) L. Kobryn, W. P. Henry, F. R. Fronczek, R. Sygula and A. Sygula, *Tetrahedron Letters*, 2009, **50**, 7124–7127.

(6) M. R. Kennedy, L. A. Burns and C. D. Sherrill, *The Journal of Physical Chemistry A*, 2012, **116**, 11920–11926.

(7) P. A. Denis, *RSC Advances*, 2013, **3**, 25296–25305.

(8) M. Yanney and A. Sygula, *Tetrahedron Letters*, 2013, **54**, 2604–2607.

(9) I. Welsh and M. Lein, *Journal of Computational Chemistry*, 2014, **35**, 181–191.

(10) C. Mück-Lichtenfeld, S. Grimme, L. Kobryn and A. Sygula, *Physical Chemistry Chemical Physics*, 2010, **12**, 7091–7097.

(11) Y. Zhao and D. G. Truhlar, *Physical Chemistry Chemical Physics*, 2008, **10**, 2813–2818.

(12) T. Janowski, P. Pulay, A. S. Karunarathna, A. Sygula and S. Saebø, *Chemical Physics Letters*, 2011, **512**, 155–160.

(13) D. Josa, J. Rodríguez-Otero and E. M. Cabaleiro-Lago, *Physical Chemistry Chemical Physics*, 2015, **17**, 13206–13214.

(14) D. Josa, I. González-Veloso, J. Rodríguez-Otero and E. M. Cabaleiro-Lago, *Physical Chemistry Chemical Physics*, 2015, **17**, 6233–6241.

(15) D. Josa, L. Azevedo dos Santos, I. González-Veloso, J. Rodríguez-Otero, E. M. Cabaleiro-Lago and T. de Castro Ramalho, *RSC Advances*, 2014, **4**, 29826–29833.

(16) D. Josa, J. Rodríguez-Otero, E. M. Cabaleiro-Lago, L. A. Santos and T. C. Ramalho, *The Journal of Physical Chemistry A*, 2014, **118**, 9521–9528.

(17) D. Josa, J. Rodríguez-Otero, E. M. Cabaleiro-Lago and M. Rellán-Piñeiro, *Chemical Physics Letters*, 2013, **557**, 170–175.

(18) D. Josa, J. Rodríguez-Otero and E. M. Cabaleiro-Lago, *Physical Chemistry Chemical Physics*, 2011, **13**, 21139–21145.

(19) T. Kawase and H. Kurata, *Chemical Reviews*, 2006, **106**, 5250–5273.

(20) J. Xia, J. W. Bacon and R. Jasti, *Chemical Science*, 2012, **3**, 3018–3021.

(21) T. Iwamoto, Y. Watanabe, H. Takaya, T. Haino, N. Yasuda and S. Yamago, *Chemistry - A European Journal*, 2013, **19**, 14061–14068.

(22) T. Iwamoto, Y. Watanabe, T. Sadahiro, T. Haino and S. Yamago, *Angewandte Chemie - International Edition*, 2011, **50**, 8342–8344.

(23) K. Yuan, Y.-J. Guo and X. Zhao, *The Journal of Physical Chemistry C*, 2015, **119**, 5168–5179.

(24) Y. Zhao and D. G. Truhlar, *Journal of the American Chemical Society*, 2007, **129**, 8440–8442.

(25) K. Yuan, C.-H. Zhou, Y.-C. Zhu and X. Zhao, *Physical Chemistry Chemical Physics*, 2015, **17**, 18802–18812.

(26) K. Yuan, J.-S. Dang, Y.-J. Guo and X. Zhao, *Journal of Computational Chemistry*, 2015, **36**, 518–528.

(27) K. Yuan, Y.-J. Guo, T. Yang, J.-S. Dang, P. Zhao, Q.-Z. Li and X. Zhao, *Journal of Physical Organic Chemistry*, 2014, **27**, 772–782.

(28) R. Jasti, J. Bhattacharjee, J. B. Neaton and C. R. Bertozzi, *Journal of the American Chemical Society*, 2008, **130**, 17646–17647.

(29) T. Kawase, H. R. Darabi and M. Oda, *Angewandte Chemie - International Edition*, 1996, **35**, 2664–2666.

(30) T. Kawase, K. Tanaka, N. Fujiwara, H. R. Darabi and M. Oda, *Angewandte Chemie - International Edition*, 2003, **42**, 1624–1628.

(31) S. Grimme, *Journal of Computational Chemistry*, 2004, **25**, 1463–1473.

(32) S. Grimme, *Journal of Computational Chemistry*, 2006, **27**, 1787–1799.

(33) S. Grimme, J. Antony, S. Ehrlich and H. Krieg, *The Journal of Chemical Physics*, 2010, **132**, 154104.

(34) S. Grimme, S. Ehrlich and L. Goerigk, *Journal of Computational Chemistry*, 2011, **32**, 1456–1465.

(35) R. Ahlrichs, M. Bär, M. Häser, H. Horn and C. Kölmel, *Chemical Physics Letters*, 1989, **162**, 165–169.

(36) S. Grimme, C. Mück-Lichtenfeld and J. Antony, *The Journal of Physical Chemistry C*, 2007, **111**, 11199–11207.

(37) M. J. Frisch, G. W. Trucks, H. B. Schlegel, G. E. Scuseria, M. A. Robb, J. R. Cheeseman, G. Scalmani, V. Barone, B. Mennucci, G. A. Petersson, H. Nakatsuji, M. Caricato, X. Li, H. P. Hratchian, A. F. Izmaylov, J. Bloino, G. Zheng, J. L. Sonnenberg, M. Hada, M. Ehara, K. Toyota, R. Fukuda, J. Hasegawa, M. Ishida, T. Nakajima, Y. Honda, O. Kitao, H. Nakai, T. Vreven, J. A. Montgomery, Jr., J. E. Peralta, F. Ogliaro, M. Bearpark, J. J. Heyd, E. Brothers, K. N. Kudin, V. N. Staroverov, R. Kobayashi, J. Normand, K. Raghavachari, A. Rendell, J. C. Burant, S. S. Iyengar, J. Tomasi, M. Cossi, N. Rega, J. M. Millam, M. Klene, J. E. Knox, J. B. Cross, V. Bakken, C. Adamo, J. Jaramillo, R. Gomperts, R. E. Stratmann, O. Yazyev, A. J. Austin, R. Cammi, C. Pomelli, J. W. Ochterski, R. L. Martin, K. Morokuma, V. G. Zakrzewski, G. A. Voth, P. Salvador, J. J. Dannenberg, S. Dapprich, A. D. Daniels, Ö. Farkas, J. B. Foresman, J. V. Ortiz, J. Cioslowski and D. J. Fox, *Gaussian 09 Revision E.01*, Gaussian Inc. Wallingford CT 2009.

(38) S. Boys and F. Bernardi, *Molecular Physics*, 1970, **19**, 553–566.

(39) E. R. Johnson, S. Keinan, P. Mori-Sánchez, J. Contreras-García, A. J. Cohen and W. Yang, *Journal of the American Chemical Society*, 2010, **132**, 6498–6506.

(40) J. Contreras-García, E. R. Johnson, S. Keinan, R. Chaudret, J.-P. Piquemal, D. N. Beratan and W. Yang, *Journal of Chemical Theory and Computation*, 2011, **7**, 625–632.

(41) W. Humphrey, A. Dalke and K. Schulten, *Journal of Molecular Graphics*, 1996, **14**, 33–38.

USC UNIVERSIDAD DE SANTIAGO DE COMPOSTELA

Chapter 5

Size and shape effects on complexes of fullerenes with carbon nanorings: C_{50} and C_{76} as [10]CPP and [6]CPPA guest

5.1 Introduction

Nowadays, one of the most active fields in fullerene chemistry is the design of fullerene receptors. This has allowed the development of applications in different fields, such as solar energy conversion, optoelectronics, catalysis and switching.[1–3] Dispersion forces are essential for the stabilisation of fullerene complexes by means of non-covalent interactions.[4,5] Therefore the use of concave–convex complementarity can be an excellent strategy to maximize these forces in order to design new molecular receptors. In this way, the use of concave[6] receptors capable of adapting to the convex surface of fullerenes allows maximizing the stabilisation by dispersion. However, the challenge is to find appropriate concave fullerene receptors, since they are relatively rare given that curved molecules are not always an easy synthetic target due to their tensioned structures.[7] Nonetheless, the recent interest in concave–convex $\pi\cdots\pi$ interactions has lead to an important number of works has published in this field.[8–21] Buckybowls[10,16,18,19,22–24] and subphthalocyanines[5,23,25–28] stand out among the best kind of fullerene receptors. Another type of receptors that have recently drawn attention are the so-called carbon-nanorings, CNRs. These hoop-shaped π-conjugated hydrocarbon molecules possess nanosized concave cavities that can act as host for π-conjugated molecules with convex surfaces such as fullerenes. Cycloparaphenylenes ([n]CPP) and cycloparaphenyleneacetylenes ([n]CPPA) stand out among CNRs. [n]CPPs contain a series of 1,4-phenylene units, and they represent the simplest structural unit of armchair carbon nanotubes, CNTs,[29–32] whereas [n]CPPAs are formed by alternating 1,4-phenylene and ethynylene units. Both species adopt rigid and belt-shaped structures with well-defined cavities.

The first synthesis and characterization of [9]-, [12]-, and [18]cycloparaphenylene was performed in 2008.[33] A cost-effective gram-scale synthesis of [8]- and [10]cycloparaphenylenes (CPPs) was developed in 2012 for the first time, and the highly efficient concave–convex $\pi\cdots\pi$ interaction between [10]CPP and C_{60} was validated by X-ray diffraction analysis

in the solid-state.[34] On the other hand, [6]CPPA had already been synthesized in 1996 by Kawase *et al.*[35] The same authors proved the formation of stable complexes between this CNR and fullerenes C_{60} and C_{70}, attributing the driving force in forming [n]CPPA supramolecular complexes to concave–convex $\pi\cdots\pi$ interactions.[29,36]

In our previous work, a comprehensive analysis of all possible complexes between the carbon-nanorings [10]CPP and [6]CPPA with the fullerenes C_{60} and C_{70}, was carried out.[37] According to our results, both CNRs are excellent "catchers" of both fullerenes, especially [10]CPP, which is in agreement with the experimental findings of Iwamoto *et al.*[38,39] C_{70} performs very slightly better than C_{60}, which also matches with the experimental results.[39] Therefore, the largest complexation energy corresponds to C_{70}@[10]CPP complex, amounting to -53.32 kcal mol^{-1}. According to our results, the better behaviour of [10]CPP is explained by means of three factors (none of them are very strong, but the accumulation of them lead to an important difference of about 10 kcal mol^{-1}): 1) [6]CPPA holds only six π rings ([10]CPP, ten) and the alkyne bonds give rise to a much smaller interaction. 2) From an electrostatic point of view, the more negative MEP region inside [10]CPP matches better than that of [6]CPPA, with the slightly positive surface of both fullerenes. 3) Taking into account that both fullerenes (C_{70} fully vertically placed and C_{60}) show a similar diameter, the slightly larger size of [10]CPP "hole" regarding that of [6]CPPA (something more than half an Å) seems better suited for the size of these fullerenes.

After C_{60} and C_{70} (although at a great distance), some of the most common fullerenes are C_{50} and C_{76}. In addition, it happens that these two fullerenes have a relatively similar size to that of C_{60} and C_{70}. Therefore, it could be of great interest to study the behaviour of a fullerene slightly smaller than C_{60} and another fullerene slightly larger than C_{70}. It seems that one of the most important factors for a stronger interaction between CNR and fullerene is the complementarity of size between the host and the guest, and therefore, the study of fullerenes C_{50} and C_{76} (and their comparison with the results previously obtained for C_{60} and C_{70}) can provide valuable information on this issue. Therefore, we believe it is desirable to perform a systematic study of all the complexes that can be established between the CNRs [10]CPP and [6]CPPA, and the fullerenes C_{50} and C_{76}. In the present manuscript, a systematic and exhaustive search of all spatial arrangements of the complexes is carried out; the interaction energy corresponding to all minima is evaluated, and the ability of these CNRs as hosts for these fullerenes is analysed and interpreted (Figure 5.1).

C_{50} has 271 isomers consisting of only hexagons and pentagons. Among them, it seems clear that two isomers (with D_{5h} and D_3 symmetry) are the most favourable ones.[40–44] Note that these most stable D_3 and D_{5h} isomers are the only C_{50} fullerene isomers without three pentagons directly or sequentially fused; they only have isolated and double pentagon configurations (it is generally believed that pentagon adjacencies would decrease the stability of fullerenes). Precisely, there are six and five pentagon-pentagon fusions within the D_3 and D_{5h} isomers, respectively.

Likewise, C_{76} only appears to present two isomers (symmetry D_2 and T_d, respectively) and both have isolated pentagons. Both experimental and theoretical studies predicted a clear preference for the isomer with D_2 symmetry (besides, there is only this isomer with an electronic closed shell structure).[45–49]

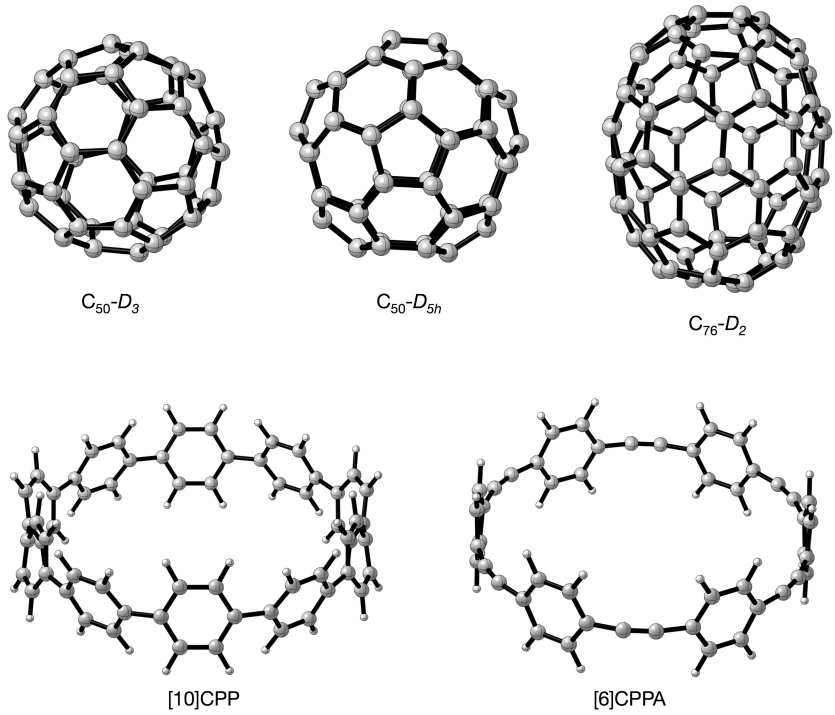

Figure 5.1: Monomers studied in this work.

5.2 Computational details

Since dispersion effects are crucial to study $\pi\cdots\pi$ interactions, dispersion-corrected DFT methods seem mandatory. Among them, Grimme's empirical dispersion correction is one of the most popular procedures. The original version (DFT-D),[50] was modified in 2006 (DFT-D2),[51] and further corrected in 2010 (DFT-D3),[52] and 2011 (DFT-D3(BJ)).[53]

As already explained in several previous works of our group,[16–21] the B97-D2 method appears to be a reasonable balance between the computational cost and the accuracy of the results. Therefore, the B97-D2/def2-TZVP level of calculation and the resolution of identity approximation (RI) implemented in Turbomole program suite,[54] with the def2-TZVPP auxiliary basis set, was used along the whole manuscript.

Counterpoise corrections, CP, are applied to all reported interaction energies to avoid basis set superposition error, BSSE.[55] According to this method, the interaction energy of a system A$\cdots$B is calculated according to the following:

$$\Delta E_{\text{int}} = E_{\text{AB}}^{\text{AB}}(\text{AB}) - \left(E_{\text{A}}^{\text{AB}}(\text{AB}) + E_{\text{B}}^{\text{AB}}(\text{AB})\right)$$

where superscript refers to the geometry (that of the system AB) and the parenthesis indicates the basis set used (the full basis set of the system A$\cdots$B). If, in addition, the energy cost involved in the deformation of each monomer to adopt the geometry of the dimer is considered:

$$\Delta E_{\text{def}} = \left(E_{\text{A}}^{\text{AB}}(\text{A}) - E_{\text{A}}^{\text{A}}(\text{A})\right) + \left(E_{\text{B}}^{\text{AB}}(\text{B}) - E_{\text{B}}^{\text{B}}(\text{B})\right)$$

then, the full complexation energy is obtained as follows:

$$\Delta E_{\text{complex}} = \Delta E_{\text{int}} + \Delta E_{\text{def}}$$

The visualization of non-covalent interactions regions is conducted using the NCIPLOT-3.0 program.[56,57] Then, graphic displays of concave–convex $\pi\cdots\pi$ interactions are obtained using the VMD 1.9.1 software.[58] NCI enables identification of non-covalent interactions based on the peaks that appear in the reduced density gradient (RDG) at low densities. Plotting a RDG isosurface for a low value of RDG, the non-covalent regions clearly appear in the supramolecular complex. These interactions correspond to both favourable and unfavourable interactions. In order to differentiate between them, the sign of the second eigenvalue of the density Hessian times the density is colour-mapped onto the isosurface: blue, green an red indicate strongly attractive interactions, weak vdW interactions, and strongly repulsive interactions, respectively. To save computation time, promolecular densities have been used, as previously done with good results in similar systems.[19,37]

When the CNR$\cdots$fullerene complex is formed, the spatial orientation of the fullerene inside the belt may lead to a large number of different energy minima. Thus, the search for the absolute minimum is not a very easy task. In our previous work,[37] in order to explore the potential energy surface (PES), two different procedures were carried out. The first method is to place the fullerene inside the CNR and then studying the energetic profile that emerges from the fullerene rotation around an axis perpendicular to the belt. To make this rotation, a couple of different spatial dispositions of the fullerene are chosen. Obviously, the choice of these orientations, although it is made with certain criteria, is somewhat arbitrary. Once found the most favourable minima of those profiles, the energetic change that arises from the vertical departure of the fullerene is also studied. By "vertical departure", we mean the displacement of the fullerene along the vertical Z-axis, *i.e.*, the distance between the centroid of the fullerene and that of the CNR, being 0.0 Å when the fullerene is fully hosted in the CNR. Finally, the minima found are optimised without any geometrical restrictions, and for the minimized complexes the complexation energy is calculated.

Another safer and more costly procedure (although even it does not provide total certainty) was also followed: the fullerene is placed at the centre of the CNR and then it is allowed to rotate in all the directions through a scanning of the three Euler angles (α, β, γ), using steps of 12 degrees (see Figure b.1). This procedure leads to the computation of a huge number of single point calculations for searching all the space. For that reason, these single point calculations are performed with the same functional (B97-D2) but with a smaller basis set, namely the def2-SVP (with the corresponding def2-SVP auxiliary basis set for the RI approximation). Once the more stable minima are found, they are optimised without any geometrical restrictions using the chosen level (B97-D2/def2-TZVP), and subsequently the complexation energies are calculated at this level. After comparing the results obtained by both methods, it seemed clear that the most economical method would be valid in most cases. According to our results, this could be absolutely true for the complexes where the fullerene remains perfectly inside the CNR. When the fullerene moves away from the centre of the CNR, the use of the cheapest method is a little more problematic.[37] Following these guidelines, along the present manuscript the first method was used by default, restricting the use of the second one just to the cases in which the fullerene is significantly got away from the centre of the CNR.

5.3 Results and discussion

5.3.1 Calculation of complexation energies

As already mentioned in the introduction, it seems clear that two isomers of the C_{50} fullerene (with D_3 and D_{5h} symmetry) are clearly the most favourable ones.[40–44] Therefore we focus our study exclusively on these two isomers: C_{50}-D_3 and C_{50}-D_{5h}. After searching the best orientation (see Appendix B, section B.2, for the details) the complexation energy of the dimer (Table 5.1) amounts to -39.40 kcal mol^{-1}, a quantity significantly smaller than that obtained for fullerenes C_{60} and C_{70} in our previous work (around -50 kcal mol^{-1}).[37] Figure 5.2 shows the NCIPLOT picture corresponding to this C_{50}-D_3@[10]CPP complex. For the C_{50}-D_{5h}@[10]CPP dimer, the complexation energy (Table 5.1) is somewhat larger than that for the D_3 isomer: -42.01 kcal mol^{-1}. Figure 5.2 shows that a good qualitative correlation takes place between the complexation energies of C_{50}-D_3@[10]CPP and C_{50}-D_{5h}@[10]CPP and the interaction surface resulting from the NCI analysis. So, for the most favourable complex, a large green surface (corresponding to vdW interactions) arises, resulting from the $\pi\cdots\pi$ interaction between the ten phenyl rings of [10]CPP directly faced to ten rings (five hexagonal, five pentagonal) of C_{50}-D_{5h}. This favourable orientation is very similar to that found in complexes C_{60}@[10]CPP and C_{70}@[10]CPP,[37] although in those cases the ten rings were all hexagonal. For C_{50}-D_3@[10]CPP complex, the isosurface is clearly smaller, which is in agreement with an appreciably smaller complexation energy.

Table 5.1: Energy results of the optimised minima found (kcal mol^{-1}). $\Delta E_{complex}$ = complexation energy. ΔE_{def} = deformation energy. Dispersion = contribution of dispersion to the total complexation energy

		$\Delta E_{complex}$	ΔE_{def}		Dispersion
			Fullerene	CNR	
C_{50}@[10]CPP	D_3	−39.40	0.04	0.36	−57.88
	D_{5h}	−42.01	0.05	0.46	−62.14
C_{50}@[6]CPPA	D_3	−36.54	0.06	0.13	−63.78
	D_{5h}	−36.37	0.03	0.13	−68.68
C_{76}@[10]CPP		−54.10	0.30	1.99	−109.57
C_{76}@[6]CPPA		−42.12	0.21	1.33	−85.16
C_{60}@[10]CPP[a]		−49.78	0.11	0.23	−83.61
C_{60}@[6]CPPA[a]		−40.63	0.47	0.25	−89.78
C_{70}@[10]CPP[a]		−53.32	0.09	0.55	−93.73
C_{70}@[6]CPPA[a]		−41.53	0.46	0.79	−93.29

[a] Data from our previous work (ref. 37).

For the best orientation of the C_{50}-D_3@[6]CPPA dimer, the complexation energy (Table 5.1) amounts to -36.54 kcal mol^{-1}, a quantity slightly smaller than that obtained for fullerenes C_{60} and C_{70} in our previous work (around -41 kcal mol^{-1}) and for the complex with [10]CPP.[37] Figure 5.2 shows the NCIPLOT picture corresponding to this C_{50}-D_3@[6]CPPA complex. The case of the C_{50}-D_{5h}@[6]CPPA complex is very similar

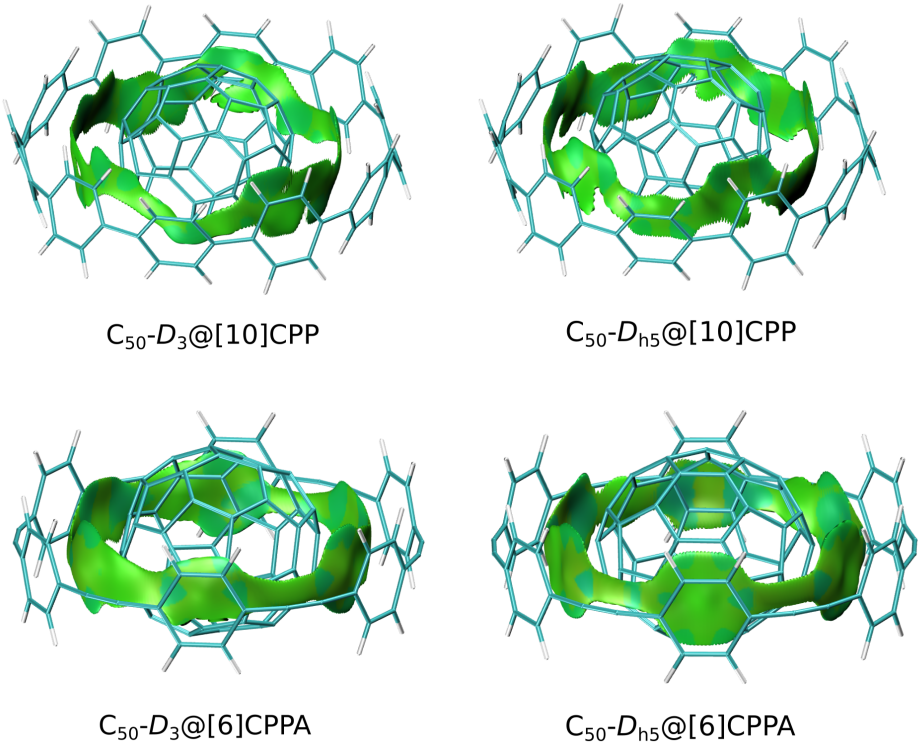

Figure 5.2: NCIPLOT gradient isosurface (0.3 a.u.) for the interaction between C_{50} and both CNRs. Blue-green-red scale over the range −0.04 to 0.04 a.u.

and the complexation energy for the final structure amounts to −36.37 kcal mol^{-1}. This similarity is fairly well reflected in the corresponding NCIPLOT pictures of Figure 5.2, where it can be seen that the green surface of the C_{50}-D_{5h}@[6]CPPA complex is of a very similar size (and shape) to that of C_{50}-D_3@[6]CPPA. Thus, NCI surface could give a rough indication of the favourable contact surface between host and guest and therefore of the stability of the complex.

The complexation energy of the C_{76}@[10]CPP dimer (Table 5.1) is −54.10 kcal mol^{-1}, an amount substantially higher than that obtained with fullerene C_{50} (by almost 15 kcal mol^{-1}). Moreover, this value is somewhat larger than that obtained for fullerenes C_{60} and C_{70} in our previous work (around −50 kcal mol^{-1}).[37] Figure 5.3a shows the NCIPLOT picture corresponding to this C_{76}@[10]CPP complex. This figure shows an isosurface significantly larger than those obtained with the C_{50} fullerene (Figure 5.2), a fact that reveals, from a purely qualitative point of view, NCI surfaces exhibit a good correlation with the complexation energies obtained for the different complexes. Moreover, the isosurface of Figure 5.3a exhibits several bluish areas, which correspond to strongly attractive interactions

In our previous work, we showed that C_{70} clearly departs vertically (1.29 Å) from the plane of [6]CPPA.[37] Therefore, this is almost certainly the case with C_{76}. For that reason, to find all the possible minima of the C_{76}@[6]CPPA complex, a scanning of the three Euler angles is systematically performed (see Appendix B, section B.3). In our previous work, we showed that this procedure is safer to locate the most favourable structures in cases in which the fullerene comes out appreciably from the ring,[37] all of this

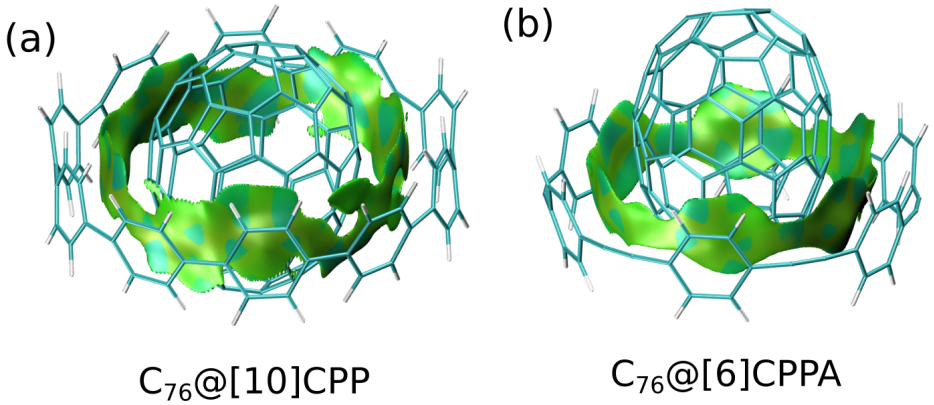

Figure 5.3: NCIPLOT gradient isosurface (0.3 a.u.) for the interaction between C_{76} and both CNRs. Blue-green-red scale over the range −0.04 to 0.04 a.u.

nevertheless penalized by a large computational cost. The results show that in the best orientation C_{76} remains virtually perpendicular to the plane of the CNR, with a substantial vertical departure: 2.43 Å. The calculated complexation energy (Table 5.1) is −42.12 kcal mol^{-1}, a somewhat more negative value (about −6 kcal mol^{-1}) than that which occurs with C_{50}@[6]CPPA complex, but much worse than in the case of C_{76}@[10]CPP complex. Figure 5.3b corresponds to the NCIPLOT picture of this C_{76}@[6]CPPA complex and shows an isosurface with a shape and size rather similar to that obtained for the C_{50}@[6]CPPA complex (Figure 5.2, bottom). However, the main difference is the appearance of several areas of more attractive interactions (blue), which correlates qualitatively well with the complexation energies (almost −6 kcal mol^{-1} more stable with C_{76} than with C_{50}).

5.3.2 Comparation between complexes

In order to carry out a more complete analysis and have a global picture of the interaction between fullerenes and CNRs, in the present discussion we will include the results obtained in our previous work.[37] In this way, we compare the energetic and geometric characteristics of all the complexes formed by a CNR ([10]CPP and [6]CPPA) with the four fullerenes, listed from smallest to largest: C_{50}, C_{60}, C_{70} and C_{76}.

The results of Table 5.1 confirm one of the previous conclusions:[37] [10]CPP is a much better fullerene receptor than [6]CPPA. The advantage of [10]CPP versus [6]CPPA (two CNRs of comparable size) is due to the loss of the interaction of four phenyl rings with the fullerene, not adequately counterbalanced by the weaker interaction with the alkyne bonds. However, the advantage is not constant and it is directly related to the fullerene size, decreasing from almost 12 for C_{76} to just over 5 kcal mol^{-1} for C_{50} (C_{70} and C_{60} just occupy an intermediate position). In view of the differential characteristics that exist between both CNRs, this fact is not surprising, and if the fullerene becomes too small, it is reasonable that the difference disappears completely.

Figure 5.4 summarizes the evolution of the complexation energy as the fullerene size increases. It shows, for complexes with both CNRs, a continued increase of this energy (purple curve). However, when the complexes of [10]CPP are analysed, it can be seen that the upper limit is already practically reached with C_{70}, so that with C_{76} the increase

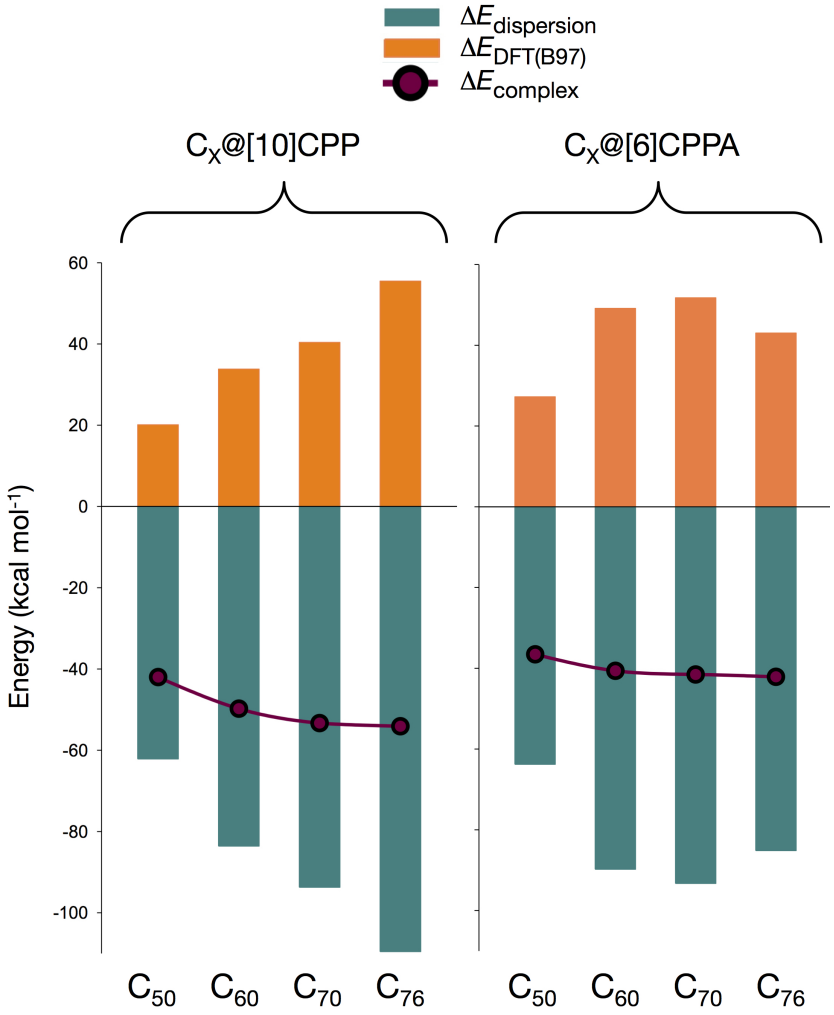

Figure 5.4: Complexation energy, $\Delta E_{\text{complex}}$, and its two main contributions (empirical dispersion contribution, $\Delta E_{\text{dispersion}}$, and pure B97 interaction, $\Delta E_{\text{DFT(B97)}}$) for all the complexes between a fullerene and a CNR.

of complexation energy is very small (less than -1 kcal mol^{-1}, according to Table 5.1). This fact is even more pronounced with the complexes of [6]CPPA, since in this case that limit is reached already with fullerene C_{60} (the change to C_{70} supposes a change of less than -1 kcal mol^{-1} and little more than -0.5 kcal mol^{-1} when the fullerene is changed to C_{76}). For all this, we can conclude that in the case of [10]CPP, the fullerene with the most efficient encapsulation is C_{70}, in the sense that an increase in the size of the fullerene does not represent a significant improvement. In the same way, in the case of [6]CPPA, the most efficient fullerene would be C_{60}. On the other hand, if we have a mixture of fullerenes of various sizes, [10]CPP would be adequate to separate C_{70} (and others larger than it) from the smaller fullerenes. In the same way, [6]CPPA would be adequate to separate C_{60} (and others larger than it) from the smaller fullerenes. If in the mixture we only had the two most common fullerenes (C_{60} and C_{70}), [10]CPP could be useful for the selective separation, but [6]CPPA is not. Obviously, these statements are rather qualitative and therefore quite limited since they focus exclusively on gas phase calculations. Obtaining more reliable results is a challenging task, and it is necessary to

take into account several contributions, being particularly relevant the calculation of the gas Gibbs free energy (including entropy and enthalpy contributions) and the solvation free energy.[59,60] However, as we have recently verified,[60] the energy differences in the gas phase correlate quite well with the differences in association Gibbs energies; so the really complicated challenge is to obtain absolute values of the latter, while the relative values of the calculations in gas phase could provide a more than acceptable information when comparing the interaction in different complexes.

In order to analyse in more detail the balance of energy contributions to the stability of the complexes, the interaction energy can be decomposed according to a simple method. So, the two contributions of the model employed are taken into account, that is, the pure B97 interaction energy and the empirical dispersion contribution to the interaction energy. As it can be seen from Figure 5.4 (and Table 5.1), dispersion plays a crucial role in the interaction energy of complexes because the contribution from the pure B97 functional is clearly repulsive; therefore, dispersion is responsible for the binding in complexes. If we take into account all the complexes, there is no good correlation between complexation energy and dispersion contribution (see Figure b.7), contrary to what happened in other cases recently studied by us.[16,17] This is easily explained given the important structural differences between both CNRs. Thus, if we look at the results separately, the correlation improves a lot. Even so, in the case of [6]CPPA it is still pretty bad. This is probably due to the fact that interaction with this CNR does not always take place in the same way: both C_{70}, and especially C_{76}, move away from the centre of the ring, unlike complexes with [10]CPP where all fullerenes remain completely inside the ring. This differential circumstance between the two CNRs is clearly shown in Figure 5.4: while for [10]CPP the complexation energy grows continuously with the increase in the size of the fullerene, and this is accompanied by a continuous increase of repulsion energy and of dispersion contribution (increasingly negative), in the case of [6]CPPA, the continuous growth of complexation energy is related to the balance between repulsion and dispersion contributions, since both energies show a maximum for C_{70} and then decrease. All this is clearly related to the fact mentioned above: C_{76} departs significantly from the centre of the ring plane (which reduces dispersion), which is accompanied by a significant decrease in repulsion, giving as a total result a continuously growing complexation energy (although the increase is very small from C_{60} onwards).

An alternative way to analyse the dispersion energy is to count the number of carbon-carbon contacts below 4 Å in each complex (see Table 5.2). Therefore, a rather good correlation between this number and the dispersion contribution can be observed, even taking into account jointly the complexes of both CNRs (see Figure b.8). Thus, as in the case with the dispersion energy itself, when the complexes of [10]CPP are considered, a continuous increase in the number of contacts is observed, while for the complexes of the [6]CPPA a maximum is reached for C_{70} (see Figure 5.4).

The discussion on stabilities above is deeply related with the structural and geometric issues of the formed dimer. Therefore, an important aspect for selective complexation of fullerenes is the size and shape complementarity between the CNR and the fullerene. While C_{60} is spherically shaped, the other fullerenes employed in the study are less symmetrical. A simple way to describe the shape and size of the fullerenes consist on fitting the position of the carbon atoms to the minimum-volume ellipsoid containing them (it has to be noticed that these diameters are usually larger than the atom-atom diameters,

Table 5.2: Characteristics of the most stable complexes formed: N_{contacts} is the number of C–C contacts below 4.0 Å and R_{average} (Å) is the average distance if all those contacts are taken into account.

	N_{contacts}	R_{average}		N_{contacts}	R_{average}
C_{50}@[10]CPP	115	3.76	C_{50}@[6]CPPA	141	3.68
C_{60}@[10]CPP	160	3.67	C_{76}@[6]CPPA	180	3.54
C_{70}@[10]CPP	185	3.68	C_{60}@[6]CPPA	203	3.59
C_{76}@[10]CPP	214	3.62	C_{70}@[6]CPPA	184	3.63

since the ellipsoid is a smooth surface while the fullerenes have truncated hexagonal and pentagonal faces). Thus, the value of the three diameters along the principal axis of the ellipsoid supplies that information (Table 5.3). C_{60}, as expected, is the only fully spherical fullerene, with three equivalent diameters of 7.1 Å. C_{70} is roughly like a stretched C_{60} (rugby-ball shape) with a long axis amounting to 8.4 Å and two equivalent short axis of 7.3 Å, *i.e.*, slightly wider than C_{60}. C_{76} is clearly the biggest and least spherical species among the fullerenes studied, something like a crushed rugby ball: a very long axis of 9.0 Å, and a ellipsoidal section (perpendicular to the major axis) with diameters of 8.1 and 7.3 Å, the latter very similar to that of C_{70}. Finally, both C_{50} isomers are like a smaller and somewhat crushed C_{60} species, with two diameters of the order of $6.6-6.8$ Å (instead of 7.1 Å) and a smaller diameter of about $6.0-6.2$ Å. As shown in Table 5.1, in the complexes the deformation energy associated to the fullerene is almost negligible, at most 0.5 kcal mol^{-1}, *i.e.*, all the fullerenes are very rigid and they deform very little upon complexation. In the case of the CNR, the deformation is not very large either, though there are some cases in which the deformation energy already reaches values amounting to almost 2 kcal mol^{-1}. In order to quantify the geometrical distortion of the CNRs, their ellipticity (also called flattening) is evaluated (see Figure b.9). Similarly to the case of ellipsoids, the obtained diameters are slightly oversized since the ellipse shows a curved shape whereas the real hexagon rings are planar. Table 5.4 shows the most important parameters of the ellipses corresponding to the CNRs, both isolated and forming part of complexes with all fullerenes. According to this table, [10]CPP is perfectly circular with a diameter of 13.8 Å, something bigger than that of [6]CPPA (diameter = 13.1 Å). If the values of all the complexes are observed, it can be stated that deformation of the CNR ring (regarding to the difference between the two axes and, consequently, to its *flattening*) is practically negligible, except in two cases: the complexes of C_{76} with both

Table 5.3: Diameters (Å) along the principal axis of the minimum-volume ellipsoid containing the carbon atoms of all the fullerenes.

	D1	D2	D3
C_{50}-D_3	6.764	6.660	6.214
C_{50}-D_{5h}	6.762	6.682	6.002
C_{60}	7.098	7.098	7.098
C_{70}	8.398	7.318	7.286
C_{76}	8.954	8.078	7.346

CNRs, where the ring loses its circular shape and elongates in order to be closer to the fullerene. This circumstance is not surprising, since precisely these complexes give rise to a significant deformation energy of the CNR (Table 5.1: 1.33 and 1.99 kcal mol^{-1}). The explanation of this fact seems quite evident and is based on the geometric characteristics of C_{76}: it is the only one of the studied fullerenes whose section perpendicular to the major axis is not circular but elliptical, as discussed above. Another feature that allows to quantify the deformation of the CNR is the analysis of its expansion or reduction, easily estimated by calculating the variation in the area of the ellipse to which we have fitted it. Again, the complexes formed with C_{76} are those in which the CNR shows (Table 5.4) a greater variation in size (specifically a reduction). In the remaining cases, this variation is smaller. However, two cases should be noted where the variation is not a contraction, but an expansion: C_{60}@[6]CPPA and C_{70}@[6]CPPA. The results show that the energy cost of expansion of the ring is important, since an almost negligible expansion (1.005) already leads to an appreciable deformation energy (close to 1 kcal mol^{-1}). In general, if an attractive interaction between the fullerene and the CNR takes place, it would be expected that the CNR would always contract (given the high nondeformability of the fullerenes). However, in these two complexes, this is not possible due to the small space that [6] CPPA has to accommodate these two large fullerenes. One could wonder why this expansion does not happen for C_{76}, which is even bigger. However, the answer looks easy: C_{76} is already too large and it moves away from the centre of [6]CPPA, so its section decreases considerably. Therefore, in this case is where a greater contraction of the CNR ring takes place (and where a greater *flattening* of the ellipse happens). Therefore, it can be observed that in those cases in which the CNR is a little small (such as [6] CPPA) to accommodate the fullerene, a very subtle balance of interactions takes place that can cause the CNR to expand slightly (what is happening with C_{60} and C_{70}), but when this

Table 5.4: Geometric parameters for the fitting of the CNR to an ellipse.

	Major axis (Å)	Minor axis (Å)	Flattening[a]	Relative variation of area[b]
[10]CPP	13.839	13.839	0.000	–
C_{50}-D_3@[10]CPP	13.813	13.775	0.003	0.994
C_{50}-D_{5h}@[10]CPP	13.786	13.782	0.000	0.992
C_{76}@[10]CPP	13.941	13.614	0.023	0.991
C_{60}@[10]CPP	13.806	13.806	0.000	0.995
C_{70}@[10]CPP	13.825	13.823	0.000	0.998
[6]CPPA	13.147	13.133	0.001	–
C_{50}-D_3@[6]CPPA	13.116	13.113	0.000	0.996
C_{50}-D_{5h}@[6]CPPA	13.144	13.122	0.002	0.999
C_{76}@[6]CPPA	13.319	12.757	0.042	0.984
C_{60}@[6]CPPA	13.178	13.171	0.001	1.005
C_{70}@[6]CPPA	13.174	13.170	0.000	1.005

[a] Flattening = (major axis − minor axis) / major axis.
[b] Relative variation of area = (major axis × minor axis)/(major axis × minor axis)$_{\text{isolated CNR}}$.

expansion is already too expensive the fullerene moves away from the CNR and then the latter undergoes an appreciable contraction (what is happening with C_{76}).

In summary, we can conclude that complexation of these systems is governed for the complementarity (of size and shape) between the CNR and the fullerene. While the fullerene is extremely rigid, the CNR has a certain ability to adapt (in shape and size) to the fullerene, with the aim of optimising the interaction between both monomers.

5.4 Conclusions

The comprehensive study of the complexes formed by a CNR ([10]CPP and [6]CPPA) with the fullerenes C_{50} and C_{76}, allow us to complete the picture (previously started[37] with the fullerenes C_{60} and C_{70}) and to analyse more broadly the trends that take place in complexes between a CNR and a fullerene of increasing size.

As in the case of C_{60}/C_{70}, both C_{50} and C_{76} are "caught" by both CNRs with considerable complexation energy, going from -36 to -54 kcal mol^{-1} for C_{50}@[6]CPPA and C_{76}@[10]CPP, respectively. Almost in all cases, the fullerene remains fully inside the nanoring, except in the case of C_{76}@[6]CPPA, where the fullerene undergoes a substantial vertical departure out of the ring: 2.43 Å (more than 1 Å higher than in the case of the C_{70}), which is undoubtedly due to C_{76} being too large for this smaller CNR.

The visualization of non-covalent interactions conducted by way of the NCI method gives rise to an illustrative picture of the interactions established between the host (CNR) and the guest molecule (fullerene). Moreover, from a purely qualitative point of view, the size and shape of the interaction regions exhibit a good correlation with the complexation energies obtained for all the complexes.

Taking into account the full set of fullerenes (C_{50}, C_{60}, C_{70} and C_{76}) the global results show (for both CNRs) that the complexation energy grows continuously as fullerene size grows. This fact is not surprising, since funtamentally by increasing the size of the ring, the dispersion contribution increases accordingly (as long as the fullerene fits inside the ring). However, if we look at the results more closely, we see that the increase in complexation energy is not uniform. This way, for the complexes with [10]CPP the upper limit of the energy is already reached for C_{70}. This fact is even more noticeable for the complexes with [6]CPPA, since in this case that limit is reached already with fullerene C_{60}. For that reason, we can state that C_{70} is the fullerene with the most efficient encapsulation for the [10]CPP nanoring, whereas C_{60} is that one for the [6]CPP nanoring. Although C_{50} and C_{76} are also very good guests for these rings, C_{50} is a little small and C_{76} a little large to get a perfect fit.

In summary, we can state that these systems are basically controlled for the complementarity (of size and shape) between the CNR and the fullerene. Although there may be certain degree of flexibility, it seems clear that for each fullerene there must be a specific CNR, whose size gives rise to the finest encapsulation.

References

(1) F. D'Souza and O. Ito, *Chemical Communications*, 2009, 4913–4928.

(2) H. Imahori and S. Fukuzumi, *Advanced Functional Materials*, **14**, 525–536.

(3) P. Hudhomme and J. Cousseau, in *Fullerenes: Principles and Applications (2)*, The Royal Society of Chemistry, Cambridge, 2012, pp. 416–461.

(4) E. M. Pérez and N. Martín, *Chemical Society Reviews*, 2015, **44**, 6425–6433.

(5) E. M. Cabaleiro-Lago, J. Rodríguez-Otero and J. A. Carrazana-García, *Physical Chemistry Chemical Physics*, 2017, **19**, 26787–26798.

(6) H. Isobe, S. Hitosugi, T. Yamasaki and R. Iizuka, *Chemical Science*, 2013, **4**, 1293–1287.

(7) E. M. Pérez and N. Martín, *Chemical Society Reviews*, 2008, **37**, 1512–1519.

(8) L. Kobryn, W. P. Henry, F. R. Fronczek, R. Sygula and A. Sygula, *Tetrahedron Letters*, 2009, **50**, 7124–7127.

(9) M. R. Kennedy, L. A. Burns and C. D. Sherrill, *The Journal of Physical Chemistry A*, 2012, **116**, 11920–11926.

(10) P. A. Denis, *RSC Advances*, 2013, **3**, 25296–25305.

(11) M. Yanney and A. Sygula, *Tetrahedron Letters*, 2013, **54**, 2604–2607.

(12) I. Welsh and M. Lein, *Journal of Computational Chemistry*, 2014, **35**, 181–191.

(13) C. Mück-Lichtenfeld, S. Grimme, L. Kobryn and A. Sygula, *Physical Chemistry Chemical Physics*, 2010, **12**, 7091–7097.

(14) Y. Zhao and D. G. Truhlar, *Physical Chemistry Chemical Physics*, 2008, **10**, 2813–2818.

(15) T. Janowski, P. Pulay, A. A. Sasith Karunarathna, A. Sygula and S. Saebø, *Chemical Physics Letters*, 2011, **512**, 155–160.

(16) D. Josa, J. Rodríguez-Otero and E. M. Cabaleiro-Lago, *Physical Chemistry Chemical Physics*, 2015, **17**, 13206–13214.

(17) D. Josa, I. González-Veloso, J. Rodríguez-Otero and E. M. Cabaleiro-Lago, *Physical Chemistry Chemical Physics*, 2015, **17**, 6233–6241.

(18) D. Josa, L. Azevedo dos Santos, I. González-Veloso, J. Rodríguez-Otero, E. M. Cabaleiro-Lago and T. de Castro Ramalho, *RSC Advances*, 2014, **4**, 29826–29833.

(19) D. Josa, J. Rodríguez-Otero, E. M. Cabaleiro-Lago, L. A. Santos and T. C. Ramalho, *Journal of Physical Chemistry A*, 2014, **118**, 9521–9528.

(20) D. Josa, J. Rodríguez-Otero, E. M. Cabaleiro-Lago and M. Rellán-Piñeiro, *Chemical Physics Letters*, 2013, **557**, 170–175.

(21) D. Josa, J. Rodríguez-Otero and E. M. Cabaleiro-Lago, *Physical Chemistry Chemical Physics*, 2011, **13**, 21139–21145.

(22) M. A. Petrukhina and L. T. Scott, *Fragments of Fullerenes and Carbon Nanotubes*, John Wiley & Sons, Hoboken, New Jersey, 2012.

(23) P. A. Denis, *New Journal of Chemistry*, 2014, **38**, 5608–5616.

(24) P. A. Denis, *Journal of Physical Organic Chemistry*, 2014, **27**, 918–925.

(25) C. G. Claessens and T. Torres, *Chemical Communications*, 2004, **0**, 1298–1299.

(26) P. A. Denis and M. Yanney, *Chemical Physics Letters*, 2015, **640**, 140–146.

(27) G. E. Morse and T. P. Bender, *ACS Applied Materials and Interfaces*, 2012, **4**, 5055–5068.

(28) I. Sánchez-Molina, B. Grimm, R. M. Krick Calderon, C. G. Claessens, D. M. Guldi and T. Torres, *Journal of the American Chemical Society*, 2013, **135**, 10503–10511.

(29) T. Kawase and H. Kurata, *Chemical Reviews*, 2006, **106**, 5250–5273.

(30) H. A. Wegner, *Angewandte Chemie - International Edition*, 2017, **56**, 10995–10996.

(31) S. E. Lewis, *Chemical Society Reviews*, 2015, **44**, 2221–2304.

(32) E. R. Darzi and R. Jasti, *Chemical Society Reviews*, 2015, **44**, 6401–6410.

(33) R. Jasti, J. Bhattacharjee, J. B. Neaton and C. R. Bertozzi, *Journal of the American Chemical Society*, 2008, **130**, 17646–17647.

(34) J. Xia, J. W. Bacon and R. Jasti, *Chemical Science*, 2012, **3**, 3018–3021.

(35) T. Kawase, H. R. Darabi and M. Oda, *Angewandte Chemie - International Edition*, 1996, **35**, 2664–2666.

(36) T. Kawase, K. Tanaka, N. Fujiwara, H. R. Darabi and M. Oda, *Angewandte Chemie - International Edition*, 2003, **42**, 1624–1628.

(37) I. González-Veloso, J. Rodríguez-Otero and E. M. Cabaleiro-Lago, *Physical Chemistry Chemical Physics*, 2016, **18**, 31670–31679.

(38) T. Iwamoto, Y. Watanabe, T. Sadahiro, T. Haino and S. Yamago, *Angewandte Chemie - International Edition*, 2011, **50**, 8342–8344.

(39) T. Iwamoto, Y. Watanabe, H. Takaya, T. Haino, N. Yasuda and S. Yamago, *Chemistry - A European Journal*, 2013, **19**, 14061–14068.

(40) W. G. Xu, Y. Wang and Q. S. Li, *Journal of Molecular Structure: THEOCHEM*, 2000, **531**, 119–125.

(41) N. Shao, Y. Gao and X. C. Zeng, *Journal of Physical Chemistry C*, 2007, **111**, 17671–17677.

(42) X. Zhao, *Journal of Physical Chemistry B*, 2005, **109**, 5267–5272.

(43) W. Q. Tian, J. K. Feng, Y. A. Wang and Y. Aoki, *Journal of Chemical Physics*, 2006, **125**, 094105.

(44) X. Lu, Z. Chen, W. Thiel, P. V. Rague, R. Huang and L. Zheng, *Journal of the American Chemical Society*, 2004, **126**, 14871–14878.

(45) D. E. Manolopoulos, *Journal of the Chemical Society, Faraday Transactions*, 1991, **87**, 2861–2862.

(46) F. Diederich and R. L. Whetten, *Accounts of Chemical Research*, 1992, **25**, 119–126.

(47) J. R. Colt and G. E. Scuseria, *The Journal of Physical Chemistry*, 1992, **96**, 10265–10268.

(48) B.-C. Wang, L. Chen and Y.-N. Chiu, *Fullerene Science and Technology*, 1995, **3**, 611–625.

(49) A. R. Khamatgalimov and V. I. Kovalenko, *Fullerenes, Nanotubes and Carbon Nanostructures*, 2015, **23**, 148–152.

(50) S. Grimme, *Journal of Computational Chemistry*, 2004, **25**, 1463–1473.

(51) S. Grimme, *Journal of Computational Chemistry*, 2006, **27**, 1787–1799.

(52) S. Grimme, J. Antony, S. Ehrlich and H. Krieg, *Journal of Chemical Physics*, 2010, **132**, 154104.

(53) S. Grimme, S. Ehrlich and L. Goerigk, *Journal of Computational Chemistry*, 2011, **32**, 1456–1465.

(54) R. Ahlrichs, M. Bär, M. Häser, H. Horn and C. Kölmel, *Chemical Physics Letters*, 1989, **162**, 165–169.

(55) S. F. Boys and F. Bernardi, *Molecular Physics*, 1970, **19**, 553–566.

(56) E. R. Johnson, S. Keinan, P. Mori-Sánchez, J. Contreras-García, A. J. Cohen and W. Yang, *Journal of the American Chemical Society*, 2010, **132**, 6498–6506.

(57) J. Contreras-García, E. R. Johnson, S. Keinan, R. Chaudret, J. P. Piquemal, D. N. Beratan and W. Yang, *Journal of Chemical Theory and Computation*, 2011, **7**, 625–632.

(58) W. Humphrey, A. Dalke and K. Schulten, *Journal of Molecular Graphics*, 1996, **14**, 33–38.

(59) C. Velez-Vega, D. J. J. McKay, T. Kurtzman, V. Aravamuthan, R. A. Pearlstein and J. S. Duca, *Journal of Chemical Theory and Computation*, 2015, **11**, 5090–5102.

(60) E. M. Cabaleiro-Lago, J. Rodríguez-Otero and A. Gil, *Chemical Science*, 2016, **7**, 2924–2928.

USC
UNIVERSIDADE
DE SANTIAGO
DE COMPOSTELA

Chapter 6

Assessment of electronic transitions involving intermolecular charge transfer in complexes formed by fullerenes and donor–acceptor nanohoops

6.1 Introduction

Organic photovoltaic devices, which could constitute a good alternative for replacing the traditional solar cells based on silicon, are characterized by an organic species acting as electron donor upon excitation by light absorption, and a second organic material that acts as electron acceptor.[1–3] The charge transfer process between donor and acceptor is determined by the characteristics of the active layer of the organic photovoltaic device. Besides a suitable choice of donor and acceptor species, a molecular architecture ensuring an intimate contact between them, facilitating the charge transfer process, is essential in building these devices.[4,5]

While different donor species have been employed in organic photovoltaic cells, most devices employ fullerenes as electron acceptors due to their unique structural and electronic properties.[3,6,7] Since their discovery,[8] and especially since the large-scale production of fullerenes started in 1990,[9,10] a great variety of functionalized fullerenes has been synthesized. These functionalized fullerenes can be designed to maintain the desirable properties of the original fullerenes while solving some of the most problematic aspects of these materials.[11–13] Thus, by adequately binding organic replacements to fullerenes, one can adjust their solubility, energy levels, intermolecular interactions, solid-state orientation, or surface energy.

One of the most active fields in fullerene chemistry is devoted to the development of suitable receptors leading to stable fullerene inclusion complexes.[14,15] Fullerene receptors can be of different types, but those that have been attracting more attention lately are concave receptors.[16–18] Interactions with fullerenes are mostly controlled by dispersion;[15] the electrostatic interaction is in most cases negligible considering the almost neutral characteristic of most fullerenes, and polarization is only relevant when fullerenes interact

with charged species.[19–21] Therefore, the design of efficient fullerene receptors mostly relies on favourable dispersion interactions, trying to maximize the contact surface between the fullerene and the host molecule. The use of concave receptors capable of adapting to the convex surface of fullerenes allows maximizing the number of atom contacts at short distances thus maximizing the stabilisation by dispersion.

Among the most obvious candidates for concave–convex complexes with fullerenes are the so-called buckybowls, *i.e.* polycyclic aromatic hydrocarbons exhibiting bowl-shaped geometries,[16,17] though other species as porphyrins[22–27] and subphthalocyanines[22,28–31] have also been employed. Corannulene $C_{20}H_{10}$ is the simplest of these buckybowls and it has been the subject of different studies to determine the characteristics of its interaction with fullerenes (mostly C_{60}).[22,32–35] In fact, Sygula *et al.* showed that C_{60} can be effectively encapsulated by a pincer formed by two corannulene moieties linked together by means of a cyclooctatetraene tether, just relying in concave–convex $\pi\cdots\pi$ interactions.[18,36–40]

Fullerenes and endohedral fullerenes can also be encapsulated inside carbon nanotubes, forming structures known as peapods.[41–44] Thus, another possibility for coordinating fullerenes, also based on concave–convex $\pi\cdots\pi$ interactions, would be the use of carbon nanohoops. These carbon nanohoops are hoop-shaped π conjugated hydrocarbons possessing a nanosized cavity that can act as host in an inclusion complex with fullerenes.[43,45]

Cycloparaphenylenes (CPPs) are carbon nanohoops where paraphenylene units are linked together in a cyclic arrangements, representing the simplest structural unit of armchair carbon nanotubes.[43,45–49] The ability of CPPs for encapsulating fullerenes has been theoretically predicted,[50–55] and CPPs have already been successfully employed for encapsulating different fullerenes. Yamago *et al.* presented the inclusion complex of C_{60} and [10]CPP, the shortest fullerene C_{60} peapod,[56] and its structure was later confirmed by Jasti *et al.*[57] Yamago *et al.* later reported the selective encapsulation of C_{70} by [10]CPP and [11]CPP.[58] Likewise, [4]cyclochrysenylene, which has a similar diameter to [10]CPP, encapsulates C_{60} with an extremely high binding energy.[59] Also, CPPs can be employed for the selective separation of fullerenes of a given size from a mixture of different fullerenes.[60] Therefore, the use of CPPs to encapsulate fullerenes seems a promising method in order to selectively complex a given fullerene but also to obtain new functional materials.

These nanohoops can be further modified in order to tune their characteristics, especially regarding to their donor/acceptor behaviour and complementarity towards fullerenes. Very recently, a series of studies have been done trying to modify nanohoops inserting donor/acceptor motifs as a means of controlling the HOMO/LUMO levels and therefore changing their charge transfer ability. In two of these cases, the nanohoops correspond to substituted CPPs. Thus, while Darzi *et al.* have modified CPPs by inserting alkylated pyridinium moieties that can act as acceptors,[61] the strategy followed by Kuwabara *et al.* introduces an anthraquinone (CPAq) or tetracyanoanthraquinone (CPTcaq) unit as part of the nanohoop (see Figure 6.1).[62] In this latter case, the phenylene units act as donors while the anthraquinone act as acceptor.

It can be observed in Figure 6.1 that the insertion of the anthraquinone unit in [10]CPAq induces important changes in the molecular electrostatic potential, so the centre of this unit emerge slightly positive, while markedly negative regions develop around the carbonyl oxygens. These changes are even more pronounced in [10]CPTcaq, where the central ring of the anthracene unit is clearly positive. For comparison purposes, an unsubstituted cycloparaphenylene of similar size as [12]CPP shows a typical behaviour

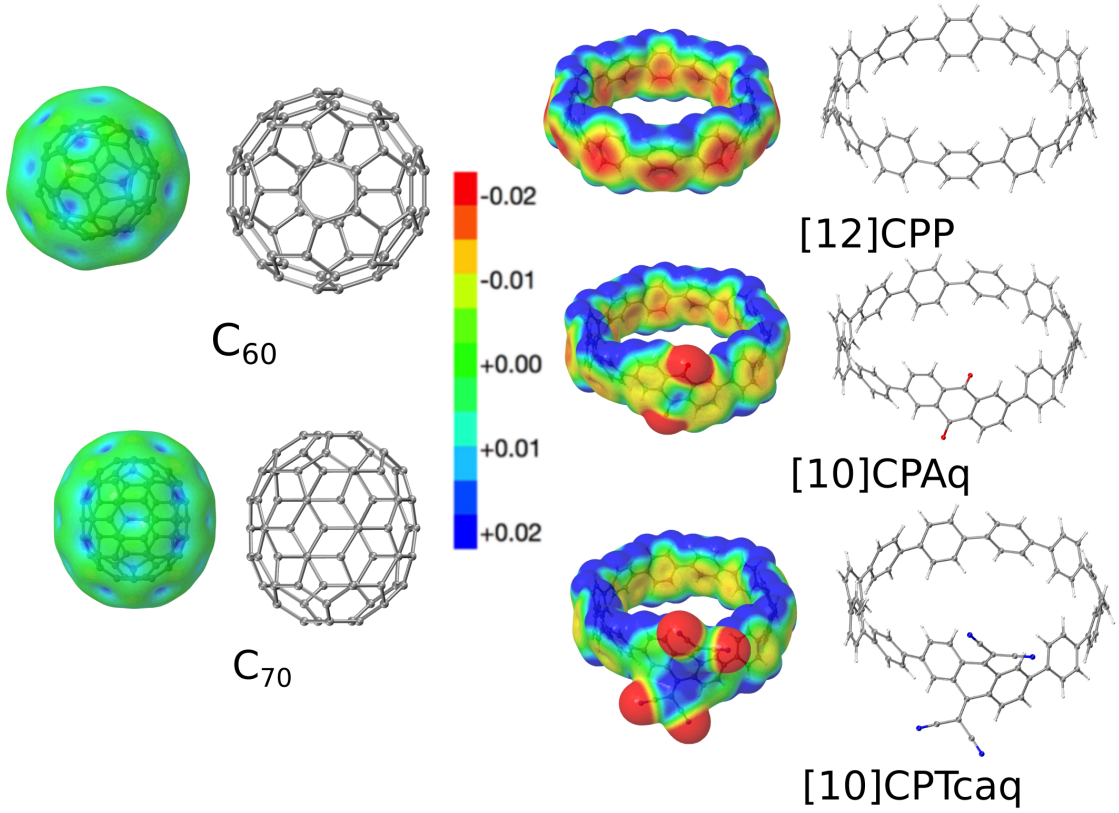

Figure 6.1: Fullerenes and nanohoops studied together with their molecular electrostaic potentials (MEPs) mapped on a 0.001 a.u. electron density isosurfaces at the B97-D2/def2-TZVP level.

already observed in other cycloparaphenylenes, with negative MEP regions corresponding to the phenyl rings. More interestingly, the insertion of the anthracene moieties promotes changes in molecular orbital energy levels. While [12]CPP has a HOMO/LUMO gap of 5.59 eV (see Figure c.1, in Appendix C), the gap in [10]CPAq decreases to 4.81 eV, mostly due to a decrease of LUMO energies. The gap is even narrower in [10]CPTcaq, again as a result of LUMO stabilisation. It is worth noting (see Figure c.2, in Appendix C) that the LUMOs in [10]CPAq and [10]CPTcaq are mainly localised onto the anthracene moiety while HOMOs are located onto the phenylenes, in agreement with Kuwabara's observation of donor/acceptor transitions.[62] Also, the HOMO levels of the rings are higher than the ones for fullerenes, while the opposite is true for LUMO levels (with the exception of [10]CPTcaq) suggesting that the lower energy transitions could correspond to charge transfer from the rings to the fullerenes.

Even though these modified nanohoops have been built as donor/acceptor moieties, it will be interesting to check their behaviour as fullerene hosts. Therefore, in the present work, a computational study is presented for complexes formed by Kuwabara's nanohoops ([10]CPAq and [10]CPTcaq) with fullerenes C_{60} and C_{70}, to determine their suitability to encapsulate fullerenes and also regarding their capability for acting as effective electron donors to the encapsulated fullerene. [12]CPP, a nanohoop of similar size of the ones obtained by Kuwabara *et al.*,[62] has been employed as model for the behaviour of complexes formed with unsubstituted cycloparaphenylenes.

6.2 Computational details

Non-covalent interactions involving fullerenes are mostly controlled by dispersion, so a proper description of dispersion energy is essential for the study of supramolecular complexes containing fullerenes. Considering the size of the systems studied, the only practical approach for obtaining reliable complexation energies is the use of density functional theory together with an empirical correction for describing dispersion.[63–66] However, there are not many reliable data in similar systems as to be employed as benchmark to select a proper functional. Kennedy *et al.* studied the interaction in corannulene dimer,[67] a system showing concave–convex $\pi\cdots\pi$ interactions, using a variety of DFT functionals including dispersion correction, and the results are compared to the values obtained by Janowsky and Pulay at the QCISD(T)/aug-cc-pVTZ level.[68] The best behaviour was obtained for B3LYP-D3, that is, B3LYP including the D3 empirical dispersion correction by Grimme with the Becke-Johnsson damping function.[65,66] However, B97-D2 (with an older empirical dispersion correction)[64] performs almost equally well at a reduced computational cost. Taking this into account, and in order to keep consistency with our previous studies, the B97-D2 functional was employed throughout this work. The def2-TZVP basis set[69] has been used together with the resolution of the identity approach in order to speed up calculations, with def2-TZVPP as auxiliary basis set.[70] Optimised structures and complexation energies have been obtained at the B97-D2/def2-TZVP level using the TURBOMOLE 6.3 program suite.[71]

The counterpoise correction has been applied in the calculation of the complexation energies to avoid the basis set superposition error (BSSE).[72,73] The complexation energy is the result of a pure interaction energy term obtained at the geometry of the dimer plus a term describing the energy cost associated with the changes in geometry undergone by the monomers when forming the dimer, the so-called deformation or preparation energy. Therefore, the complexation energy is obtained as

$$\Delta E_{\text{complex}} = \Delta E_{\text{int}} + \Delta E_{\text{def}} \tag{6.1}$$

with ΔE_{def} being the deformation energy obtained as:

$$\Delta E_{\text{def}} = \left(E_{\text{A}}^{\text{AB}}(\text{A}) - E_{\text{A}}^{\text{A}}(\text{A})\right) + \left(E_{\text{B}}^{\text{AB}}(\text{B}) - E_{\text{B}}^{\text{B}}(\text{B})\right) \tag{6.2}$$

while the interaction energy (ΔE_{int}) is:

$$\Delta E_{\text{int}} = E_{\text{AB}}^{\text{AB}}(\text{AB}) - E_{\text{A}}^{\text{AB}}(\text{AB}) - E_{\text{B}}^{\text{AB}}(\text{AB}) \tag{6.3}$$

Superscripts indicate the geometry (AB is the complex geometry, while A and B refer to the isolated monomers) and terms in parentheses specify the basis set used (AB is the whole basis set of the dimer).

Non-covalent interactions can be visualised with the so-called Non-Covalent interaction Index (NCI), based on a plot of the reduced density gradient at low densities.[74] The values of the density times the sign of the second eigenvalue of the density Hessian are colour-mapped onto a reduced density gradient isosurface. Promolecular densities have been used as previously done with good results in similar systems.[52,75] NCI analysis has been performed with the NCIPLOT-3.0 program[76] and graphic displays of concave–convex $\pi\cdots\pi$ interactions are obtained using VMD 1.9.2 software.[77]

In order to study the electronic transitions in these complexes and whether they correspond to charge transfer transitions between the nanohoop and the fullerene or intramolecular ones (intra-nanohoop or intra-fullerene), the absorption spectra were obtained by means of TD-DFT calculations including 24 excited states at the CAM-B3LYP/TZVP level.[78] This functional is known to provide reasonable results for charge transfer transitions.[79] These calculations have been performed with the ORCA 4.0 program,[80] using the RIJCOSX approach in order to reduce computational time.[81–83]

6.3 Results and discussion

6.3.1 Structure and stability

To deal with the problem of how the fullerene is optimally oriented inside the nanohoop, the centre of the fullerene was located initially in two positions: the centre of mass (CM) and the centre of the ring (CR) of [10]CPAq and [10]CPTcaq. The centres of mass of both nanohoops are slightly displaced towards the anthracene moiety (see Figure c.3 in Appendix C), so at that place the fullerene would be closer to the rings of the nanohoop. Once the fullerene is located at these two points (CM and CR), it is rotated in order to find the most favourable orientation. Finally, using this orientation, the fullerene is displaced out of the ring (perpendicular to the ring diameter), and the most favourable structure found in this process is then used as a starting point for fully unrestricted geometry optimisation. As in a previous study by our group (see chapter 4),[52] in the case of C_{60} complexes with nanohoops, the procedure described above is carried out using two different orientations of the fullerene inside the ring: rotating along a C_5 symmetry axis, with a 5-membered ring at the top and the bottom ($C_{60}(5)$), and rotating along a C_3 symmetry axis passing through the centre of two hexagonal rings ($C_{60}(6)$). In the case of [12]CPP, the centre of mass and the geometrical centre of [12]CPP are the same. For this reason, and for the sake of homogeneity, another additional initial location was chosen. Indeed, our results show that a location distanced from the centre (about 1.5 Å) is slightly more favourable (Figure c.4 in Appendix C). This is because the size of [12]CPP is too large to fit well with the size of the fullerene, and therefore a location where the fullerene is closer to one of the sides of the ring (keeping an appropriate distance for a better $\pi\cdots\pi$ interaction with the phenylenes of the nanoring) is clearly advantageous. According to our calculations (see also Figure c.5 in Appendix C), in the case of [10]CPAq and [10]CPTcaq locating the fullerene on the CM is also more favourable: around 5 kcal mol^{-1} for the C_{60}@[10]CPTcaq complex and less than 1 kcal mol^{-1} for the C_{60}@[10]CPAq complex.

All this is a consequence of the fact that the three nanohoops are larger than necessary to adequately encapsulate fullerene. C_{60} fits well into the ring of [10]CPP,[52,56] with a diameter around 15 Å. In the present case, [10]CPAq, [10]CPTcaq, and [12]CPP have a diameter larger than 16 Å, so the fullerene moves towards the ring in order to maximize the favourable interactions with its phenylene units. The effect of this change of position is larger in [10]CPTcaq than in [10]CPAq because the former ring is more elliptically shaped, as indicated by its CM being 1.5 Å apart from the CR, while the difference is only 0.5 Å in [10]CPAq (see also Table c.1 and Figure c.3, in Appendix C).

Figure 6.2 shows the energetic profile when C_{60} is rotated with its centre lying on the

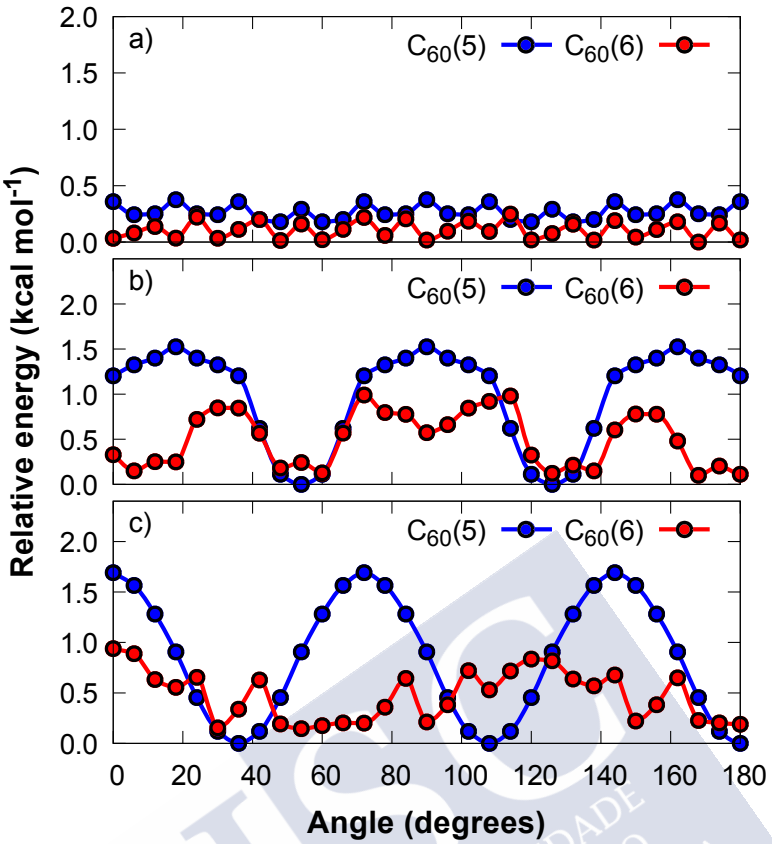

Figure 6.2: Energetic profile for the rotation of C_{60} on the centre of mass of different nanohoops. (a) C_{60}@[10]CPAq. (b) C_{60}@[10]CPTcaq. (c) C_{60}@[12]CPP. In the latter case, it does not refer to the centre of mass, but to an off-centre location, as commented in the text.

centre of mass (CM) of the nanohoops. The energy changes upon rotation in [10]CPTcaq and [12]CPP appear similar for both complexes because the fullerene is located at similar distances from the phenylene rings, leading to a similar dispersion energy in both cases. In contrast, in the case of C_{60}@[10]CPAq, although the fullerene is somewhat displaced from the centre of the ring, it remains practically at the middle (displaced by less than half an Å) and, therefore, the energy profile is very different. On the other hand, the orientation of C_{60} inside the ring ($C_{60}(5)$ or $C_{60}(6)$) has little impact on the energetics of the complexes, with energy differences of barely 0.2 kcal mol^{-1} favouring the $C_{60}(5)$ orientation for C_{60}@[10]CPTcaq and C_{60}@[12]CPP, and the $C_{60}(6)$ orientation for C_{60}@[10]CPAq. Also, as expected, the interaction quickly weakens when C_{60} is displaced along the z-axis to increase the distance between the centre of the fullerene and the plane of the nanohoop (see Figure c.6 in Appendix C). This happens because the diameter of the nanohoop is too large for C_{60} so the latter prefers to stay inside the ring to maximize the number of favourable interactions.

After this preliminary search, the complexes are fully optimised starting from the most favourable structure found in the procedure described above. The complexation energies for these structures are summarised in Table 6.1. Globally, all complexes with the fullerene close to the anthracene unit behave similarly, with complexation energies ranging from −31 kcal mol^{-1} in [10]CPAq to −32 kcal mol^{-1} in [10]CPTcaq, with the complexes with [12]CPP lying in between.

Table 6.1: Energies for the complexes with C_{60} (kcal mol^{-1}). $\Delta E_{\text{complex}}$ is the complexation energy, ΔE_{def} is the deformation energy of the monomers, ΔE_{disp} is the contribution of dispersion to the total complexation energy, and R_{centre} is the distance between the centres of the host and guest.

Complex[a]	$\Delta E_{\text{complex}}$	ΔE_{def}		ΔE_{disp}	R_{centre} (Å)
		Fullerene	Ring		
$(C_{60}(5)@[10]CPAq)_A$	−31.10	0.04	3.67	−56.05	2.309
$(C_{60}(6)@[10]CPAq)_A$	−31.23	0.08	3.02	−55.99	2.356
$(C_{60}(5)@[10]CPTcaq)_A$	−31.37	0.14	3.02	−55.93	2.247
$(C_{60}(6)@[10]CPTcaq)_A$	−32.20	0.10	2.84	−57.42	2.288
$C_{60}(5)@[12]CPP$	−31.45	0.13	3.27	−56.69	2.254
$C_{60}(6)@[12]CPP$	−31.28	0.01	3.49	−56.01	2.216
$C_{60}(5)@[10]CPAq$	−32.08	0.10	2.71	−57.17	2.280
$C_{60}(6)@[10]CPAq$	−31.90	0.07	3.15	−57.54	2.286
$C_{60}(5)@[10]CPTcaq$	−33.87	0.09	2.46	−59.73	2.307
$C_{60}(6)@[10]CPTcaq$	−33.80	0.04	2.93	−60.00	2.288

[a] Subscript A denotes when the fullerene is closer to the anthracene unit. These complexes (together with those of [12]CPP) were found starting from structures obtained from the preliminary search (Figure 6.2).

It can be observed that the initial orientation of the fullerene inside the ring has little impact on the stability of the complexes. In fact, in the complexes with [10]CPAq the complexation energies barely differ by 0.1 kcal mol^{-1} depending on the orientation of C_{60}. The difference is slightly larger with [10]CPTcaq, reaching 0.8 kcal mol^{-1} in favour of the $C_{60}(6)$ orientation. In the reference complex with [12]CPP the behaviour is similar, though in this case the $C_{60}(5)$ orientation is slightly favoured. This could be attributed to a more favourable overlap of the central hexagonal rings in C_{60} with the phenylene rings in [12]CPP (the same behaviour was found with [10]CPP);[52] in [10]CPAq and [10]CPTcaq complexes the anthracene unit forces the ring to be twisted somewhat hindering these favourable interactions. Though quite small, these differences can be roughly traced back to dispersion contributions, which are somewhat larger in the preferred complexes. In this way, the largest difference in complexation energy (0.8 kcal mol^{-1}) corresponds to the complexes with [10]CPTcaq, where the largest difference in dispersion energy is also obtained (1.5 kcal mol^{-1}).

Table 6.1 also shows that in the optimised complexes the distance between the centres of host and guest is quite large (2.2–2.4 Å), even larger than the initial displacement (0.5–1.5 Å). In this way, the rings are deformed (the oval is stretched) in order to better accommodate the fullerene at one end of them. This is clearly reflected by the significant deformation energies: around 3 kcal mol^{-1}. At this point, the following question arises: C_{60} moves closer to the anthracene unit because the interaction with this area is particularly good, or simply because moving closer to any side of the ring provides a better accommodation? Taking this into account, C_{60} was also located closer to the phenylene units opposite the anthracene substituent as additional starting points for geometrical optimisation. $C_{60}(5)$ is placed with the hexagonal rings directly facing those

of the nanohoop, while in the case of $C_{60}(6)$ the minimum structure obtained from rotation is employed. After optimisation of these structures the stability of the complexes increases by around 1 kcal mol^{-1} in [10]CPAq and around 2 kcal mol^{-1} in [10]CPTcaq, compared to minima with C_{60} closer to the anthracene substituent (see Table 6.1). These results are clearly related to an increase in dispersion energies when C_{60} is located opposite the anthracene unit. Figure 6.3 shows the most stable complexes of C_{60} with the three nanohoops.

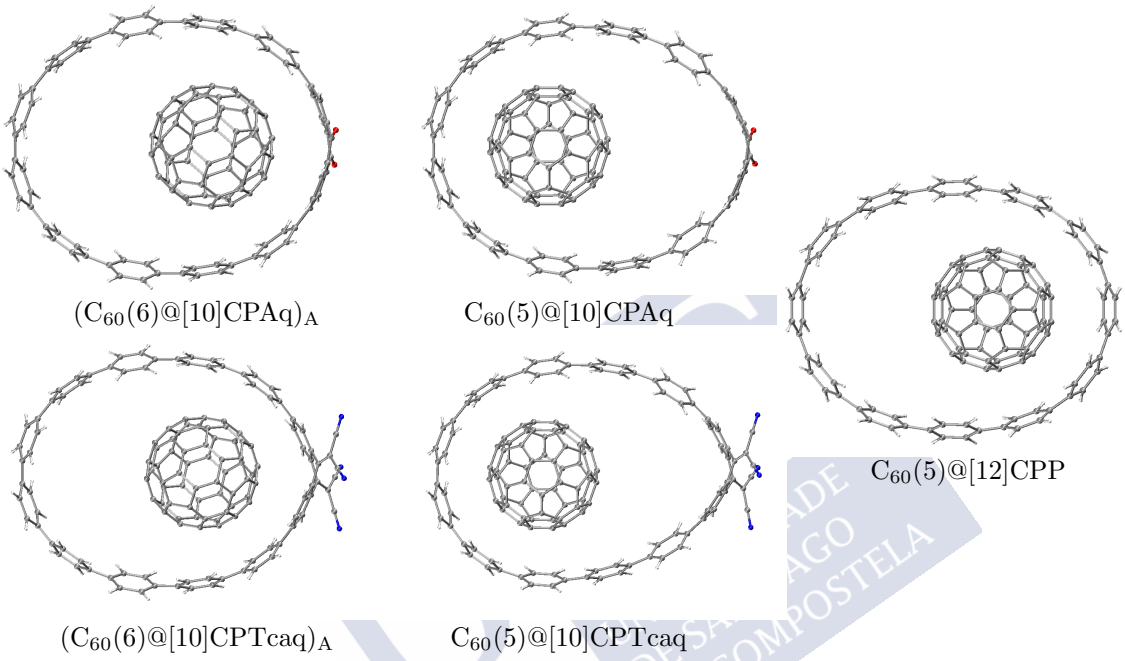

Figure 6.3: Most stable structures found for C_{60} complexes with the nanohoops.

Comparing complexes with the fullerene located close to the anthracene unit with similar complexes with the fullerene displaced to the opposite side of the nanohoop, it seems that the anthracene unit is too rigid to adapt to the shape of C_{60} as soundly as the more flexible phenylene chain, so C_{60} is more effectively surrounded by carbon atoms when located on the opposite side of the anthracene unit. The nanohoops all have similar diameters, so the position of the fullerene inside them is similar and independent of whether C_{60} is closer to the anthracene unit or not (distances between geometrical centres of fullerene and nanohoop are around 2.2–2.3 Å in all complexes). The results also display the flexibility of these nanohoops, which can adapt fairly well to the shape of the fullerene at a moderate energy cost of 3–4 kcal mol^{-1}. Even the almost circular [10]CPAq (see Table c.1, in Appendix C) deforms easily when hosting C_{60}, leading to structures similar to the ones obtained for [10]CPTcaq.

As in C_{60} complexes, two different orientations have been considered for putting C_{70} inside the nanohoops. In C_{70}(V) the fullerene has its larger axis perpendicular to the plane of the nanohoop, while in the other arrangement, C_{70}(H), the large axis lies within the nanohoop. These are similar to the orientations used by Yuan *et al.* in the study of complexes of C_{70} with [11]CPP.[50] These two orientations have been employed to carry out a preliminary exploration of the energetics of the complex as indicated above, by rotating and displacing the fullerene inside the nanohoops.

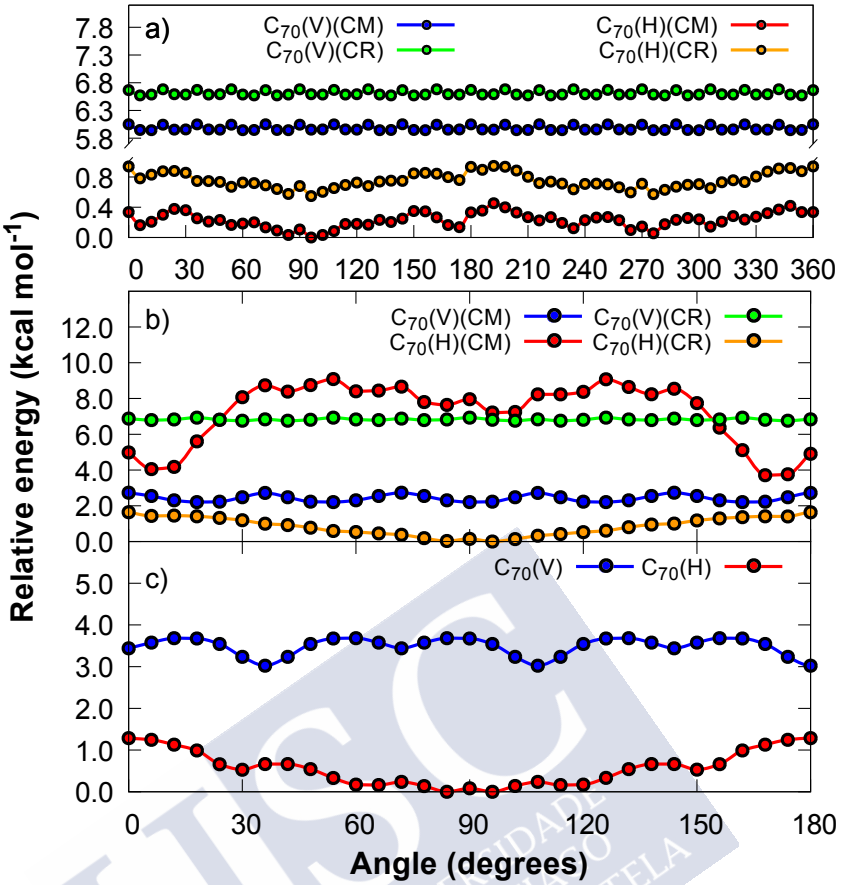

Figure 6.4: Energetic profile for the rotation of C_{70} inside different nanohoops. (a) C_{70}@[10]CPAq. (b) C_{70}@[10]CPTcaq. (c) C_{70}@[12]CPP.

Figure 6.4 shows that in most cases the C_{70}(H) orientation is energetically favoured, since with the larger axis inside the nanohoop the fullerene is able to fill the cavity to a larger extent. As in the complex with C_{60}, locating C_{70} in the centre of mass of [10]CPAq leads to a more favourable arrangement and a larger interaction energy than placing the fullerene at the geometrical centre, as it can be observed in Figure 6.4a. Recall that both centres are quite close in this ring, but the centre of mass allows for a closer contact of the fullerene with the phenylene units of the ring. However, in the complex with [10]CPTcaq, the behaviour is different, and when the fullerene is located on the centre of mass with orientation C_{70}(H), the fullerene is too close to the nanohoop, leading to a larger repulsion than when it is located on the geometrical centre of the ring. This is also the reason why C_{70}(V)(CM) has a lower energy than C_{70}(H)(CM) because in C_{70}(V) orientation, the fullerene is not so close to the nanohoop.

After the most favourable orientation upon rotation is found, the fullerene is vertically displaced outside the nanohoop. Contrary to what happens in C_{60} complexes, in some cases C_{70} prefers to be slightly displaced out of the ring (see Figure c.7, in Appendix C). While in [10]CPAq complexes the centre of the fullerene is preferred to be on the plane of the ring, there is a displacement of around 0.5 Å in [10]CPTcaq and [12]CPP complexes. When C_{70} is placed inside [10]CPAq in any of the two dispositions a small departure from the centre of the nanohoop produces a reduction in the number of contacts between the

Table 6.2: Energy for the complexes with C_{70} (kcal mol^{-1}). $\Delta E_{\text{complex}}$ is the complexation energy, ΔE_{def} is the deformation energy of the monomers, ΔE_{disp} is the contribution of dispersion to the total complexation energy, R_{centre} is the distance between the centres of the host and guest.

Complex[a]	$\Delta E_{\text{complex}}$	ΔE_{def}		ΔE_{disp}	R_{centre} (Å)
		Fullerene	Ring		
$(C_{70}(V)@[10]CPAq)_A$	−35.00	0.16	3.91	−63.41	2.335
$(C_{70}(H)@[10]CPAq)_A$	−37.13	0.07	2.66	−63.48	1.770
$(C_{70}(V)@[10]CPTcaq)_A$	−36.44	0.08	3.24	−65.26	2.237
$(C_{70}(H)@[10]CPTcaq)_A$	−37.34	0.16	2.71	−64.75	1.690
$C_{70}(V)@[12]CPP$	−35.25	0.04	3.13	−63.42	2.201
$C_{70}(H)@[12]CPP$	−36.41	0.90	1.44	−60.60	1.580
$C_{70}(V)@[10]CPAq$	−35.59	0.04	2.91	−63.44	2.193
$C_{70}(H)@[10]CPAq$	−36.74	0.16	2.14	−62.36	1.709
$C_{70}(V)@[10]CPTcaq$	−37.37	0.05	2.28	−65.05	2.207
$C_{70}(H)@[10]CPTcaq$	−38.61	0.10	1.59	−64.60	1.676

[a] Subscript A denotes when the fullerene is closer to the anthracene unit. These complexes (together with those of [12]CPP) were found starting from structures obtained from the preliminary search (Figure 6.4).

two monomers, and for this reason the C_{70} is found in the same plane as the nanohoop. On the other hand the departure from [10]CPTcaq produces a reduction in the repulsion energy because this small movement allows a better fit. Finally, for $C_{70}(V)@[12]CPP$ the displacement allows a better contact between the phenylene units of both monomers (see Figure c.8, in Appendix C).

The complexes are fully optimised at the B97-D2/def2-TZVP level, and the results are shown in Table 6.2 with the most stable structures displayed in Figure 6.5. Table 6.2 shows that the position of the fullerene inside the ring, near the anthracene unit or away from it, has a minor impact on the value of the dispersion contribution. In line with the results shown above, the most favourable complexes have C_{70} with the long axis within the cavity of the nanohoop, with complexation energies around 1–2 kcal mol^{-1} more favourable than in complexes with $C_{70}(V)$. In principle, it could be considered that these larger complexation energies are a consequence of the larger contact surface between fullerene and nanohoop in $C_{70}(H)$ resulting in larger dispersion interactions. However, dispersion energies are similar for $C_{70}(H)$ and $C_{70}(V)$ complexes, and even favour the latter (phenyl rings in C_{70} are directly facing the phenylene rings of the nanohoop). Therefore, the preference for $C_{70}(H)$ is not a direct consequence of favourable dispersion interactions but it is, at least in part, related to the smaller deformation energies of the nanohoop observed in $C_{70}(H)$ complexes. The same effect related to decreased deformation energies is behind the preference for C_{70} to be opposite the anthracene moiety. The stability of [12]CPP complexes is quite similar to that of the other nanohoops, though slightly smaller. Considering optimised structures with the fullerene located on the side of the ring opposite the anthracene unit, it can be observed that there is no increase in stability (or a marginal one) in [10]CPAq complexes relative to [12]CPP complexes, while in the

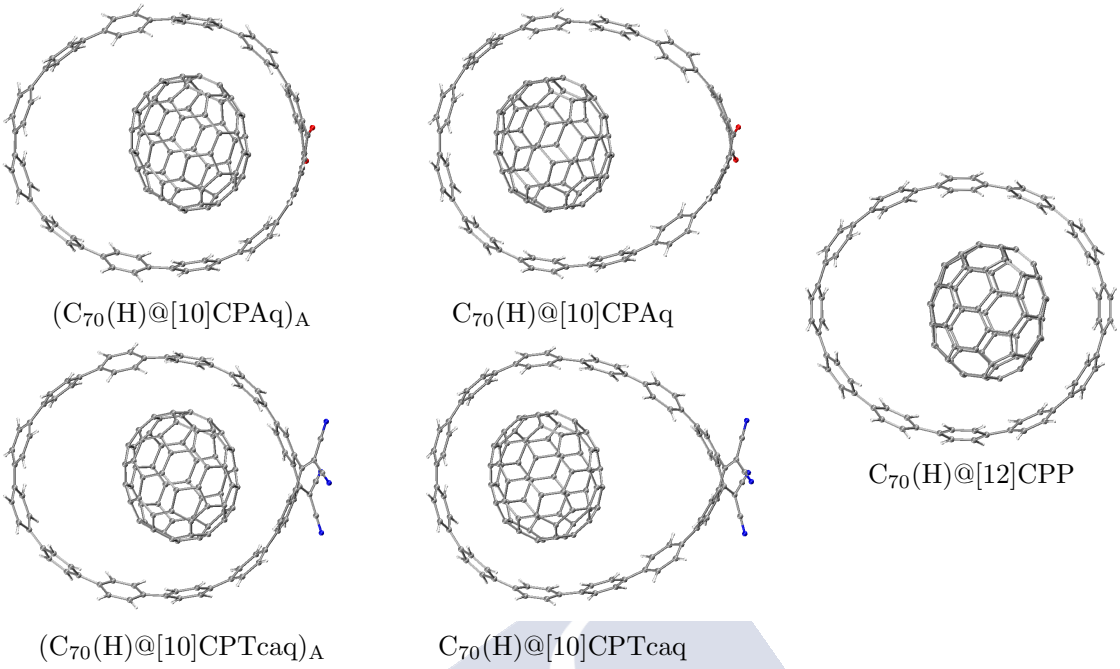

Figure 6.5: Most stable structures found for the C_{70} near the anthracene fragment and near the nanohoop.

case of [10]CPTcaq there is an increase in stability of -2.2 kcal mol^{-1}, partly related to a decrease in deformation energy of the ring, but mainly due to increased dispersion contribution.

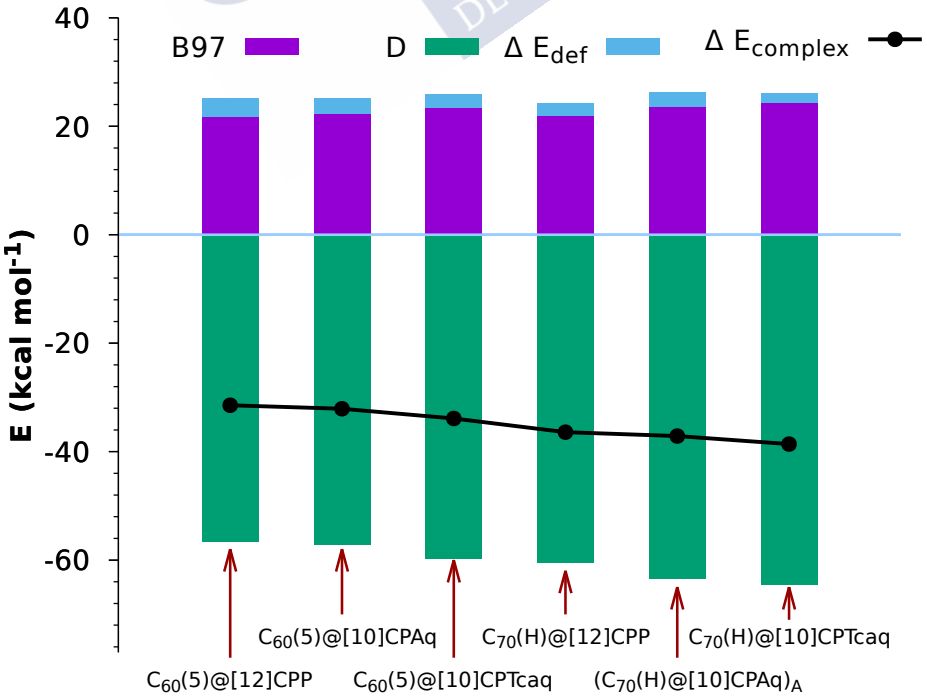

Figure 6.6: Different contributions of the complexation energy for the most stable complexes.

Figure 6.6 shows a comparison of the stabilities of the most stable complexes found with each of the nanohoops and fullerenes studied, together with the different contributions to the final complexation energy. As commented above, the stabilities of the complexes with a given fullerene do not show large differences. However, the presence of the larger C_{70} leads to larger complexation energies compared to those of complexes with C_{60}. Since complexes with C_{70} are favoured in C_{70}(H) orientation, the nanohoop is better filled up with this fullerene, resulting in complexation energies around -5 kcal mol^{-1} larger than those obtained for C_{60}. As observed in Figure 6.6, this gain in stability is mainly related to larger dispersion contribution in C_{70} complexes. Also, it can be observed that the presence of the anthracene substituent favours complexation relative to [12]CPP, even when in most structures the fullerene is opposite the anthracene moiety. It seems that the change in the shape of the ring induced by the anthracene unit favours the fact that the fullerene is more fully surrounded by the ring when the fullerene is located on the opposite side of the ring (also with smaller deformation energy costs).

6.3.2 Density analysis of the complexes

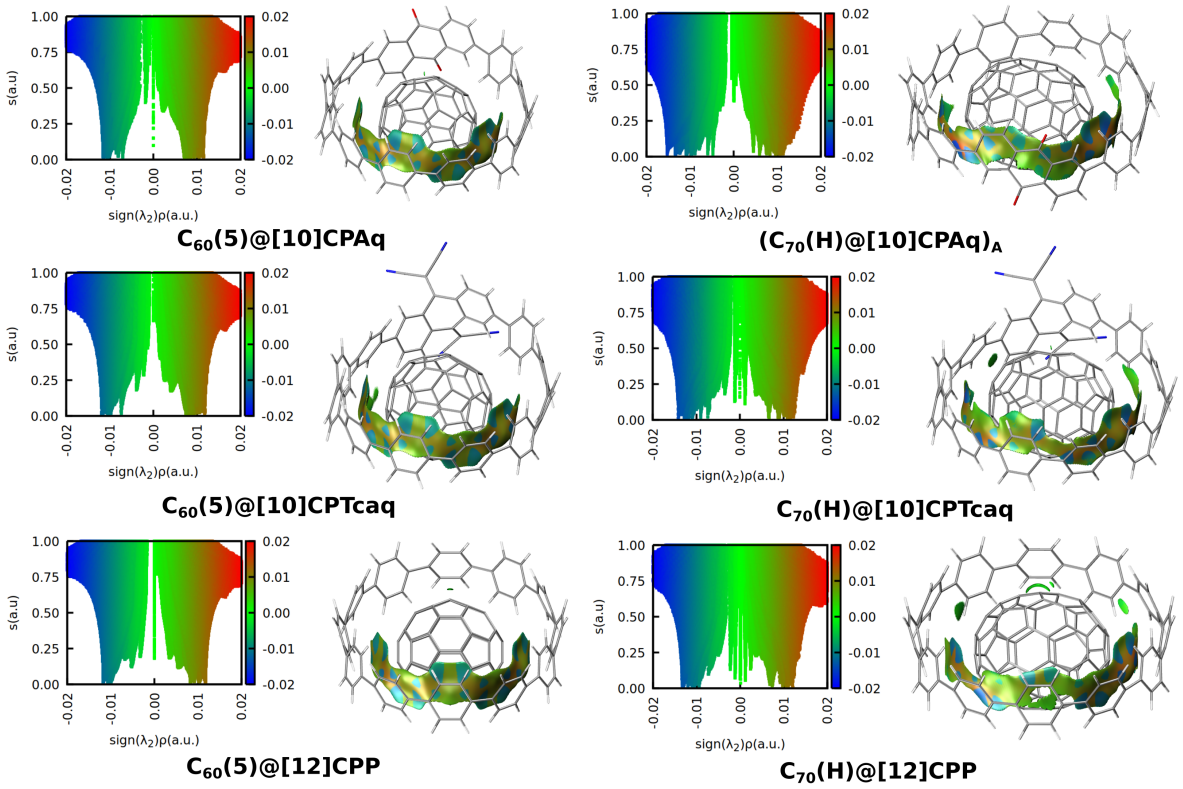

Figure 6.7: 2D and 3D NCI plots for the most stable structures found. The product of the density times the sign of the second eigenvalue of its Hessian is mapped onto an isosurface of reduced density gradient with value 0.3 a.u. The colour scale goes from -0.025 a.u. (blue) to $+0.025$ a.u. (red).

Figure 6.7 shows the NCI surfaces of the most stable complexes. In all these complexes the fullerene only establishes interactions with the nearest part of the nanohoop since the fullerene is too small to fill the cavity of the ring. In C_{60} complexes the hexagonal

rings of the fullerene interact with the phenylene units of the nanohoop as indicated by the NCI surface resembling a series of fused hexagons. The NCI surface is larger in C_{70} complexes due to the larger contact surface of C_{70} lying with its long axis into the nanohoop. This larger contact area is also reflected in the 2D NCI plots of C_{70} complexes, displaying a larger number of peaks than in their C_{60} counterparts. These peaks indicate a larger number of favourable C–C interactions, though they are somewhat counterbalanced by a larger number of destabilising contacts (a large number of peaks at positive values). Overall, the plots are pretty similar, in agreement with the results displayed above, indicating no significant differences among the systems studied. The values obtained for the densities at the intermolecular bond critical points from the atoms in molecules analysis carried out with Multiwfn corroborate this observation.[84] In all cases, the bond critical points (BCPs) that link the fullerene and the nearest part of the nanohoop have electron densities between 0.003 to 0.008 a.u. (see Table c.2, and Figure c.9, in Appendix C)

6.3.3 Electronic transitions

Other than their use as fullerene receptors, the substituted carbon nanohoops synthesized by Kuwabara *et al.* and studied in this work have gained interest because of their donor/acceptor structure. As already indicated by Kuwabara *et al.* in both [10]CPAq and [10]CPTcaq, the anthracene unit can act as an electron acceptor upon excitation, while the rest of the cycloparaphenylene units of the nanohoop acts as electron donor.[62] As a consequence, these nanohoops exhibit absorption bands around 330 and 440–450 nm. An analysis of the characteristics of the molecular orbitals at the B3LYP/6-31G* level suggested that the LUMO and the LUMO+1 are localised on the anthracene unit while the HOMOs are spread on the rest of the nanohoop.[62] Therefore, a HOMO-LUMO transition could correspond to a charge transfer transition from the phenylene units to the anthracene moiety. The results obtained at the CAM-B3LYP/TZVP level in this work are in line with these findings, with predicted absorption bands near the wavelengths observed by Kuwabara *et al.* and an orbital structure also suggesting a charge transfer HOMO-LUMO transition (see Figures c.2 and c.10, in Appendix C). In the case of [10]CPAq and [10]CPTcaq the HOMO mainly corresponds to the fragment of the CPP in the nanohoop while the LUMO is found in the anthracene fragment. [12]CPP, on the other hand, presents the HOMO and the LUMO all over the nanohoop. In order to understand better the charge transfer process that could occur in these systems, the electron densities of the ground and excited states are used to plot difference density maps of several excited states. Considering the difference density between the ground state and the excited states of the four most intense transitions (see Figure c.11, in Appendix C), only in the case of [10]CPTcaq charge transfer transitions are observed. Neither [10]CPAq nor [12]CPP show significant charge separation on transition for at least the four most intense transitions as predicted by CAM-B3LYP/TZVP calculations. When complexes are considered, the presence of the fullerene unit inside the rings promotes changes on the observed spectra, with the most intense absorption bands being shifted to larger wavelengths (Figure c.10, in Appendix C). The analysis of the frontier orbitals (Figure c.12 in Appendix C) shows the HOMOs spread along the phenylene units of the nanohoops, while the LUMOs are located on the fullerene in most cases, with the exception of [10]CPTcaq, where the LUMO

is localised on the anthracene unit as already observed in the isolated nanohoop.

Figure 6.8 shows the difference density maps for the most stable complexes found for the dimers studied. It can be observed in the top row of Figure 6.8 that in the case of $C_{60}(5)$@[10]CPAq complex the four most intense transitions clearly correspond to two different situations regarding charge separation. While for the transitions corresponding to the largest wavelengths around 400 nm, the charge rearrangement involves only the fullerene and therefore are intramonomer transitions, the transitions located at around 360 nm clearly show how charge is transferred from the paraphenylene units of the nanohoop to the fullerene. Therefore, in these latter cases the transitions lead to intermolecular charge transfer as indicated by this difference density maps.

Following a proposal by Jacquemin *et al.*, from the difference density maps one can obtain the barycentres of positive and negative charge accumulation (donating and accepting), the distance between them and the amount of charge transferred.[85,86] Table 6.3 compiles these properties for the transitions shown in Figure 6.8. It is worth noting that considering the size and shape of the molecules, the sole value of distance between centres is not conclusive about the intra or intermolecular nature of the transition. There could be a significant charge transfer from the ring to the fullerene, but due to the ring symmetry, the centres of positive charge (spread over the nanoring) and negative charge (spread over the fullerene) can be close by. Thus, the values of Table 6.3 need to be considered together with Figure 6.8 in order to properly assign intermolecular charge transfer transitions.

Table 6.3: Amount of charge transfer and distance for the four most important transitions. N_{tr} is the number of transition, q is the amount of charge transferred and R is the distance between the positive and negative barycentres following ref. 85 and 86.

	N_{tr}	q	R (Å)	N_{tr}	q	R (Å)
C_{60}@[10]CPAq	19	0.468	0.268	20	0.457	0.273
	22	0.926	3.255	24	0.871	3.378
C_{60}@[10]CPTcaq	16	0.363	0.166	18	0.456	0.331
	19	0.427	0.208	22	0.933	3.331
C_{60}@[12]CPP	14	0.316	0.065	17	0.442	0.082
	19	0.462	0.235	20	0.452	0.239
$(C_{70}$@[10]CPAq$)_{\mathrm{A}}$	2	0.237	0.013	3	0.558	2.005
	5	0.492	2.380	8	0.330	0.473
C_{70}@[10]CPTcaq	2	0.245	0.177	3	0.413	1.816
	6	0.480	2.351	18	0.800	2.874
C_{70}@[12]CPP	2	0.243	0.088	4	0.483	1.480
	5	0.537	0.893	6	0.554	0.889

Considering the four most intense transitions of $C_{60}(5)$@[10]CPAq, it can be clearly observed that for two of them (those at 360 nm) a large amount of charge is transferred, with a distance between the barycentres of charge amounting to 3.3–3.4 Å. These values indicate that charge is effectively transferred upon excitation from the nanohoop to the fullerene, in concordance with the density maps in Figure 6.8. On the other hand, the transitions around 400 nm display some charge transfer (to a lesser extent), but the distance

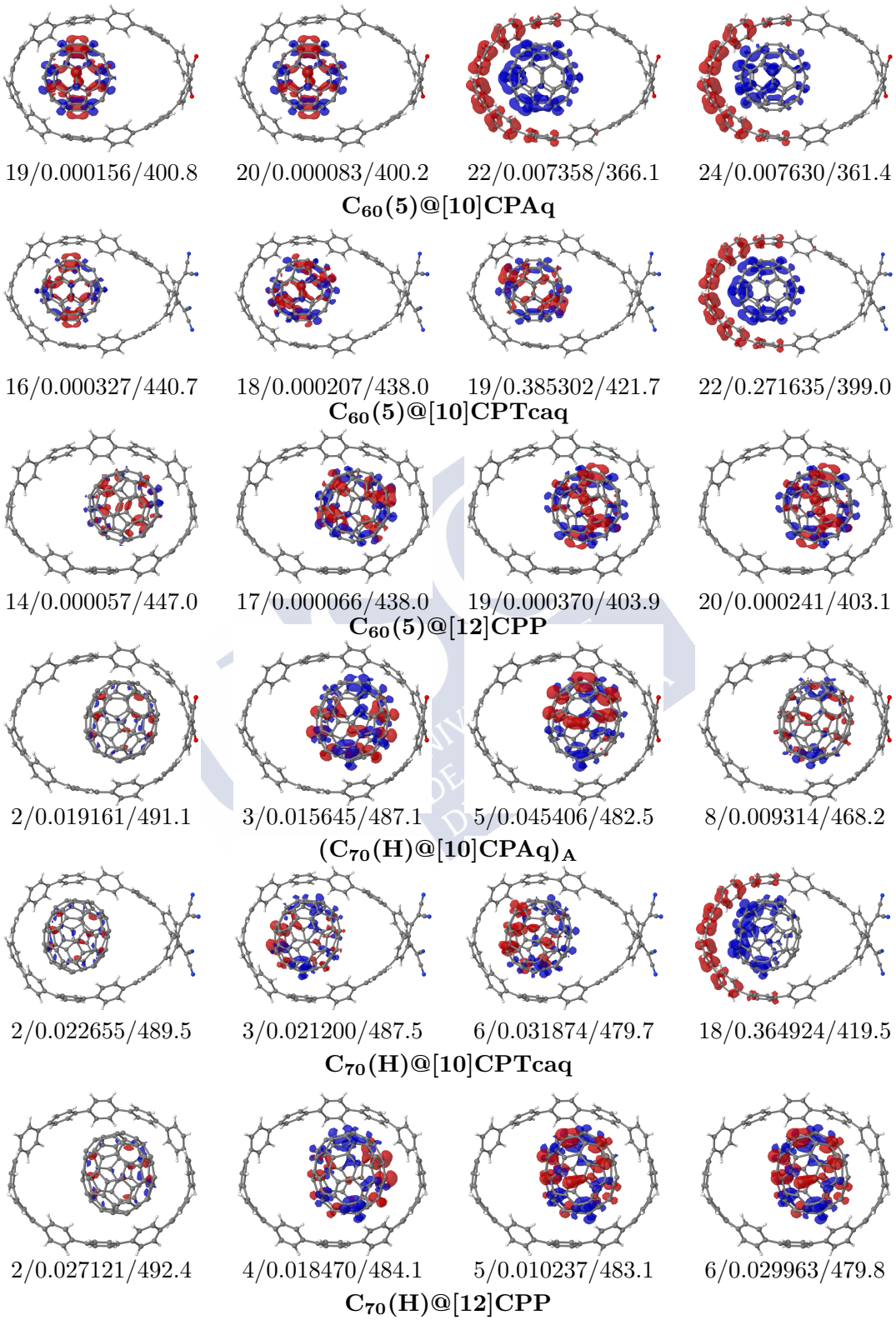

Figure 6.8: Difference density between the excited state and the ground state for the four most intense transitions in the most stable structures found. The numbers are the number of the transition/oscillator strength/wavelength (nm). Surface correspond to −0.001 a.u. (red) and 0.001 a.u. (blue).

between the barycentres is markedly shorter (0.3 Å), in agreement with an intramonomer (fullerene) charge transfer (see also Figure c.13, in Appendix C). It is worth noting that the most intense transitions observed correspond to charge transfer excitations.

In the case of C_{60}(5)@[10]CPTcaq, the behaviour is pretty similar. Again, the transitions at larger wavelengths display intramonomer charge transfer, but there is at least one transition, the second most intense one at 400 nm, that clearly shows intermolecular charge transfer, with a distance between centres of charge of 3.3 Å as in the previous case. On the other hand, the complex of C_{60} with [12]CPP has signals with much smaller intensities. At least the four most intense ones correspond to intrafullerene charge rearrangement, as confirmed by distances between charge centres below 0.3 Å. However, when more transitions are considered, there is at least one transition in which the intermolecular transfer occurs (see Table c.4 and Figure c.14, in Appendix C). The intensities of these intermolecular transitions are much smaller than the most intense intramolecular transitions in Figure 6.8, though their presence suggests that charge transfer between C_{60} and an unsubstituted nanohoop can be possible.

Regarding complexes with C_{70}, the overall picture is similar, though the results shows a lower tendency to intermolecular charge transfer. Thus, in complexes with [10]CPAq, all transitions are pretty weak, though stronger than with C_{60}, and the four transitions shown in Figure 6.8 correspond to intrafullerene transitions. This is confirmed by the values in Table 6.3 with distances between charge centres below 0.3 Å. In the complex with [10]CPTcaq one of the four most intense transitions, in fact the strongest one, corresponds to charge separation between molecules, as revealed by a distance of almost 3 Å between charge centres. (In isolated nanohoops, the transfer from phenylenes to the anthracene can result in large distances between charge centres associated with intramolecular transitions (see Table c.3, in Appendix C)). Finally, [12]CPP complexes with C_{70} do not show intermolecular charge transfer for the most intense transitions. Nevertheless, if more transitions are considered the behaviour is similar to that obtained in C_{60} complex (Table c.4 and Figure c.14, in Appendix C).

To sum up, all complexes exhibit intramolecular charge transfer transitions, though in most cases this process is associated with small intensities, while the transfer between the nanohoop and the fullerene, when possible, displays larger intensities. Overall, charge separations smaller than 2.5 Å are associated with intramonomer charge transfer, while intermolecular processes are associated with larger distances. Also, among the most intense transitions observed there is no direct participation of the anthracene unit in the charge transfer process, contrary to what is observed in the isolated nanohoops. Nevertheless, the presence of the anthracene moiety seems to promote intermolecular charge transfer with stronger intensities ([12]CPP complexes do not show charge transfer transitions among the most intense ones) despite the charge transfer process taking place on the opposite side of the nanohoop. In fact, the spectra obtained for complexes with the fullerene close to the anthracene unit (Figure c.15 and Table c.5, in Appendix C) show no transition corresponding to intermolecular charge transfer. Only in the case of $(C_{70}$@[10]CPTcaq$)_A$ a transition is observed with the cycloparaphenylenes units acting as donors while both the fullerene and the tetracyanoantraquinone moiety act as acceptors.

It could be considered that the differences in the behaviour of substituted nanorings relative to [12]CPP are related to the presence of the anthracene moiety. In order to check this possibility, complexes formed by the fullerenes and [10]CPA (similar to [10]CPAq

substituting the quinone oxygens by hydrogen atoms) have been studied. Considering the optimised structures and complexation energies the results are pretty similar to those obtained for the complexes discussed in previous sections (see Figure c.16 and Table c.8). The most relevant effect is that in the case of [10]CPA the most stable structures locate the fullerene closer to the anthracene moiety, leading to a moderate stabilisation relative to [10]CPAq or [10]CPTcaq complexes. This preference could be related to the smaller steric hindrance of the unsubstituted anthracene, as well as to the change in MEPs. While the MEP of the region closer to the anthracene moiety is negative in [10]CPA (see Figure c.17), it becomes clearly positive in [10]CPAq and patircularly in [10]CPTcaq. Considering electronic transitions, it can be observed in Figure c.18 and Table c.9 that the behaviour obtained for [10]CPA complexes is pretty similar to that observed in substituted anthracene rings. Intermolecular charge transfer is observed in several transitions, as in [10]CPAq and [10]CPTcaq, though the intensities are somewhat smaller for [10]CPA complexes, specially compared to [10]CPTcaq ones.

6.3.4 Optimising nanohoop size

Table 6.4: Energies for the complexes with anthracene-substituted [8]CPPs at the B97-D2/def2-TZVP level. $\Delta E_{\text{complex}}$ is the complexation energy, ΔE_{def} is the deformation energy of monomers, ΔE_{disp} is the contribution of dispersion to the total complexation energy.

Complex	$\Delta E_{\text{complex}}$	ΔE_{def}		ΔE_{disp}
		Fullerene	Ring	
C_{60}(5)@[8]CPAq	−48.98	0.11	0.45	−82.04
C_{60}(6)@[8]CPAq	−48.75	0.00	0.75	−81.87
C_{60}(5)@[8]CPTcaq	−48.97	0.11	1.06	−85.13
C_{60}(6)@[8]CPTcaq	−48.14	0.21	1.60	−84.22
C_{70}(V)@[8]CPAq	−53.85	0.12	1.08	−95.52
C_{70}(V)@[8]CPTcaq	−53.23	0.16	2.03	−97.45

The results in previous sections indicate that anthracene-substituted CPPs can be prone to intermolecular charge transfer transitions, at least to a larger extent than unsubstituted CPPs. However, the nanohoop size is too large for fullerenes C_{60} and C_{70} (the most abundant ones) and therefore the complexation is not as good as it would be expected with a smaller nanohoop. For this reason, complexes formed with anthracene-substituted [8]CPPs (with a proper diameter for the fullerenes, similar to [10]CPP) have been studied to check whether they keep the charge transfer transitions observed in larger nanohoops while coordinating more effectively the fullerenes. Since the [8]CPPs are smaller, the fullerenes fit into their cavity, being located at the ring centre. (see Figure c.19, in Appendix C). Table 6.4 shows the values obtained for the complexation energies of these complexes. A significant increase is observed compared to complexes with anthracene-substituted [10]CPPs, reaching around −49 kcal mol^{-1} in complexes with C_{60} and around −53 kcal mol^{-1} in complexes with C_{70}. Therefore, the stability of the complexes is increased by 15–17 kcal mol^{-1} because in these complexes the contact surface between molecules is much larger and the fullerene interacts with the whole ring (see Figure c.19,

in Appendix C). The values obtained are in fact similar to those observed for the optimal [10]CPP complexes (-49.8 kcal mol^{-1} and -53.3 kcal mol^{-1} for C_{60} and C_{70}, respectively).[52] Another possibility for improving the match between host and guest would be to increase the size of the fullerene, though these larger fullerenes are much less common than C_{60} or C_{70}. As the fullerene size increases there are a larger number of possible isomers of similar energy; also, the structures can be less spherically-shaped and therefore less suitable to fit inside the nanohoop. In any case, we have tested the behaviour of complexes with C_{100} (larger spherical fullerenes are too large and do not fit within the cavity of the nanohoops), using the most stable isomer of D_2 symmetry.[87] After optimising the complexes using the smaller def2-SVP basis set (see Figure c.21), the complexation energies are obtained at the B97-D2/def2-TZVP level, with values of -58.9 kcal mol^{-1}, -58.6 kcal mol^{-1} and -59.5 kcal mol^{-1} for complexes with [10]CPAq, [10]CPTcaq and [12]CPP, respectively. As expected, the larger contact surface between fullerene and nanohoop increases the stability of the complexes, as already observed in previous work.[55] Regarding electronic transitions, the values listed in Table 6.5 together with the results shown in Figure c.20 indicate that the behaviour observed in anthracene-substituted [10]CPPs is kept when reducing the nanohoop size. Thus, different transitions corresponding to intermolecular charge transfer are observed among the most intense ones for the different complexes with anthracene-substituted [8]CPPs. In fact, the results seem to indicate that these smaller rings are even more prone to intermolecular charge transfer from the nanohoop to the fullerene. Therefore, it seems that anthracene-substituted [8]CPPs can provide remarkably stable complexes with fullerenes C_{60} and C_{70} simultaneously favouring intermolecular charge transfer.

Table 6.5: Amount of charge transfer and distance for the four most important transitions in complexes with anthracene-substituted [8]CPPs. N_{tr} is the number of transition, q is the amount of charge that is transferred and R is the distance between positive and negative barycentres following ref. 85 and 86.

	N_{tr}	q	R (Å)	N_{tr}	q	R (Å)
C_{60}(5)@[8]CPAq	19	0.454	0.214	22	0.951	2.776
	23	0.888	3.149	24	0.889	3.148
C_{60}(5)@[8]CPTcaq	19	0.420	0.222	20	0.419	0.225
	22	0.933	2.977	23	0.924	3.371
C_{70}(V)@[8]CPAq	2	0.244	0.038	4	0.431	0.676
	6	0.307	0.255	24	0.549	1.081
C_{70}(V)@[8]CPTcaq	3	0.881	2.553	13	0.468	1.917
	16	0.468	1.917	19	0.656	2.783

6.4 Conclusions

The complexes formed by fullerenes C_{60} and C_{70} with substituted cycloparaphenylenes that behave as donor/acceptor blocks have been computationally studied employing DFT-D methods. Cycloparaphenylenes including anthraquinone and tetracyanoantraquinone

units were considered, while the unsubstituted [12]CPP was employed as a reference system of similar size.

In all systems studied, the fullerenes are effectively encapsulated inside the nanohoops, though the cavity is too large to provide a proper match with the size of fullerenes C_{60} and C_{70}. As a consequence, even though the complexes show significant stability, it is smaller than that obtained by employing smaller rings as for example [10]CPP.[52] In order to maximize the contact area between the ring and the fullerene, the nanohoops undergo some distortion though, due to their flexibility, the stability is only slightly penalised. However, the relative stability of the structures depends heavily on deformation energies of the ring. The most stable minimum found for each complex is the one with the smallest deformation cost associated to changes on the shape of the ring.

Most stable complexes have C_{60} oriented along a C_5 symmetry axis perpendicular to the nanohoop plane, while in C_{70} complexes, the fullerene is oriented with its long axis inside the ring cavity. All complexes with a given fullerene have similar stability, amounting to around -32 kcal mol^{-1} for C_{60}, while C_{70} complexes reach stabilities between -36 and -39 kcal mol^{-1}. In most cases, the fullerene is located on the side furthest from the anthracene moiety, though energy differences between structures are rather small. Even though dispersion is the main stabilising factor in these complexes, the preference for a given structure is directly related not only to larger dispersion contributions, but also to the smaller deformation cost of the ring.

The analysis of the electronic spectra of the complexes studied reveals that in most complexes charge transfer transitions are possible, with the nanohoop acting as a donor and the fullerene as an acceptor. These transitions involving intermolecular charge transfer are usually among the most intense ones observed for these systems. Even though the anthracene unit of the nanohoop has no direct participation in the intermolecular charge transfer transitions observed, its presence facilitates the appearance of these transitions. In the unsubstituted systems with [12]CPP no intermolecular charge transfer transitions are observed among the most intense ones.

The only drawback of these nanohoops is the already mentioned excess size that prevents an accurate fit with the fullerene. The results indicate that decreasing the size of the nanohoop (using anthracene-substituted [8]CPPs) would fulfill the requirements of a proper size and shape match between guest and host, also favouring intermolecular charge transfer. In summary, these substituted nanohoops with donor/acceptor blocks could be an interesting option for promoting charge transfer to fullerenes upon light absorption, with a larger tendency to do so that the parent cycloparaphenylenes.

References

(1) C. Brabec, V. Dyakonov and U. Scherf, *Organic Photovoltaics: Materials, Device Physics, and Manufacturing Technologies*, ed. C. Brabec, V. Dyakonov and U. Scherf, Wiley-VCH Verlag GmbH & Co. KGaA, Weinheim, Germany, 2008.

(2) S. Günes, H. Neugebauer and N. S. Sariciftci, *Chemical Reviews*, 2007, **107**, 1324–1338.

(3) J. L. Delgado, P.-A. Bouit, S. Filippone, M. A. Herranz and N. Martín, *Chemical Communications*, 2010, **46**, 4853–4865.

(4) T. M. Clarke and J. R. Durrant, *Chemical Reviews*, 2010, **110**, 6736–6767.

(5) K. M. Pelzer and S. B. Darling, *Molecular Systems Design & Engineering*, 2016, **1**, 10–24.

(6) G. Dennler, M. C. Scharber and C. J. Brabec, *Advanced Materials*, 2009, **21**, 1323–1338.

(7) B. C. Thompson and J. M. J. Fréchet, *Angewandte Chemie - International Edition*, 2008, **47**, 58–77.

(8) H. W. Kroto, J. R. Heath, S. C. O'Brien, R. F. Curl and R. E. Smalley, *Nature*, 1985, **318**, 162–163.

(9) R. E. Haufler, J. Conceicao, L. P. F. Chibante, Y. Chai, N. E. Byrne, S. Flanagan, M. M. Haley, S. C. O'Brien, C. Pan, Z. Xiao, W. E. Billups, M. A. Ciufolini, R. H. Hauge, J. L. Margrave, L. J. Wilson, R. F. Curl and R. E. Smalley, *Journal of Physical Chemistry*, 1990, **94**, 8634–8636.

(10) W. Krätschmer, L. D. Lamb, K. Fostiropoulos and D. R. Huffman, *Nature*, 1990, **347**, 354–358.

(11) A. Hirsch and M. Brettreich, *Fullerenes: Chemistry and Reactions*, Wiley-VCH, Weiheim, Germany, 2005.

(12) F. Langa and J.-F. Nierengarten, *Fullerenes: Principles and Applications*, Royal Society of Chemistry Publishing, Cambridge CB4 0WF, UK, 2012.

(13) T. Akasaka, A. Osuka, S. Fukuzumi, H. Kandori and Y. Aso, *Chemical Science of π-Electron Systems*, Springer Japan, Tokyo, 2015.

(14) N. Martín and J.-F. Nierengarten, *Supramolecular Chemistry of Fullerenes and Carbon Nanotubes*, Wiley-VCH Verlag GmbH & Co. KGaA, Weinheim, Germany, 2012.

(15) E. M. Pérez and N. Martín, *Chemical Society Reviews*, 2015, **44**, 6425–6433.

(16) M. A. Petrukhina and L. T. Scott, *Fragments of Fullerenes and Carbon Nanotubes*, John Wiley & Sons, Hoboken, New Jersey, 2012.

(17) L. T. Scott, H. E. Bronstein, D. V. Preda, R. B. M. Ansems, M. S. Bratcher and S. Hagen, *Pure and Applied Chemistry*, 1999, **71**, 209–219.

(18) A. Sygula, F. R. Fronczek, R. Sygula, P. W. Rabideau and M. M. Olmstead, *Journal of the American Chemical Society*, 2007, **129**, 3842–3843.

(19) J. A. Carrazana-García, J. Rodríguez-Otero and E. M. Cabaleiro-Lago, *Journal of Physical Chemistry B*, 2011, **115**, 2774–2782.

(20) P. García-Novo, A. Campo-Cacharrón, E. M. Cabaleiro-Lago and J. Rodríguez-Otero, *Physical Chemistry Chemical Physics*, 2012, **14**, 104–112.

(21) A. Campo-Cacharrón, E. M. Cabaleiro-Lago and J. Rodríguez-Otero, *Journal of Computational Chemistry*, 2014, **35**, 1533–1544.

(22) E. M. Cabaleiro-Lago, J. Rodríguez-Otero and J. A. Carrazana-García, *Physical Chemistry Chemical Physics*, 2017, **19**, 26787–26798.

(23) P. A. Denis, *New Journal of Chemistry*, 2018, **42**, 9956–9964.

(24) P. A. Denis and M. Yanney, *RSC Advances*, 2016, **6**, 50978–50984.

(25) C. L. Wang, W. B. Zhang, R. M. Van Horn, Y. Tu, X. Gong, S. Z. D. Cheng, Y. Sun, M. Tong, J. Seo, B. B. Y. Hsu and A. J. Heeger, *Advanced Materials*, 2011, **23**, 2951–2956.

(26) C. B. KC, K. Ohkubo, P. A. Karr, S. Fukuzumi and F. D'Souza, *Chemical Communications*, 2013, **49**, 7614–7616.

(27) K. Tashiro and T. Aida, *Chemical Society Reviews*, 2007, **36**, 189–197.

(28) P. A. Denis and M. Yanney, *Chemical Physics Letters*, 2015, **640**, 140–146.

(29) C. G. Claessens and T. Torres, *Chemical Communications*, 2004, **0**, 1298–1299.

(30) D. V. Konarev, S. I. Troyanov and R. N. Lyubovskaya, *CrystEngComm*, 2015, **17**, 3923–3926.

(31) I. Sanchez Molina, M. Ince, G. Bottari, C. G. Claessens, M. V. Martinez-Diaz and T. Torres, *Turkish Journal of Chemistry*, 2014, **38**, 1006–1012.

(32) D. Josa, L. Azevedo dos Santos, I. González-Veloso, J. Rodríguez-Otero, E. M. Cabaleiro-Lago and T. de Castro Ramalho, *RSC Advances*, 2014, **4**, 29826–29833.

(33) D. Josa, J. Rodríguez-Otero and E. M. Cabaleiro-Lago, *Physical Chemistry Chemical Physics*, 2015, **17**, 13206–13214.

(34) P. A. Denis, *Journal of Physical Organic Chemistry*, 2014, **27**, 918–925.

(35) P. A. Denis, *RSC Advances*, 2013, **3**, 25296–25305.

(36) L. Kobryn, W. P. Henry, F. R. Fronczek, R. Sygula and A. Sygula, *Tetrahedron Letters*, 2009, **50**, 7124–7127.

(37) C. Mück-Lichtenfeld, S. Grimme, L. Kobryn and A. Sygula, *Physical Chemistry Chemical Physics*, 2010, **12**, 7091–7097.

(38) M. Yanney and A. Sygula, *Tetrahedron Letters*, 2013, **54**, 2604–2607.

(39) V. H. Le, M. Yanney, M. McGuire, A. Sygula and E. A. Lewis, *Journal of Physical Chemistry B*, 2014, **118**, 11956–11964.

(40) M. Yanney, F. R. Fronczek and A. Sygula, *Angewandte Chemie - International Edition*, 2015, **54**, 11153–11156.

(41) B. W. Smith, M. Monthioux and D. E. Luzzi, *Nature*, 1998, **396**, 323–324.

(42) F. Simon and M. Monthioux, *Carbon Meta-Nanotubes: Synthesis, Properties and Applications*, ed. M. Monthioux, John Wiley & Sons, Ltd, Chichester, UK, 1st Edition, 2012.

(43) T. Kawase and H. Kurata, *Chemical Reviews*, 2006, **106**, 5250–5273.

(44) J. Hao, L. Guan, X. Guo, Y. Lian, S. Zhao, J. Dong, S. Yang, H. Zhang and B. Sun, *Journal of Nanoscience and Nanotechnology*, 2011, **11**, 7857–7862.

(45) S. E. Lewis, *Chemical Society Reviews*, 2015, **44**, 2221–2304.

(46) H. Omachi, Y. Segawa and K. Itami, *Accounts of Chemical Research*, 2012, **45**, 1378–1389.

(47) K. Miki, T. Matsushita, Y. Inoue, Y. Senda, T. Kowada and K. Ohe, *Chemical Communications*, 2013, **49**, 9092–9094.

(48) E. R. Darzi and R. Jasti, *Chemical Society Reviews*, 2015, **44**, 6401–6410.

(49) Y. Segawa, H. Omachi and K. Itami, *Organic Letters*, 2010, **12**, 2262–2265.

(50) K. Yuan, Y.-J. Guo and X. Zhao, *The Journal of Physical Chemistry C*, 2015, **119**, 5168–5179.

(51) K. Yuan, C.-H. Zhou, Y.-C. Zhu and X. Zhao, *Physical Chemistry Chemical Physics*, 2015, **17**, 18802–18812.

(52) I. González-Veloso, J. Rodríguez-Otero and E. M. Cabaleiro-Lago, *Physical Chemistry Chemical Physics*, 2016, **18**, 31670–31679.

(53) H. U. Rehman, N. A. McKee and M. L. McKee, *Journal of Computational Chemistry*, 2016, **37**, 194–209.

(54) K. Yuan, Y.-J. Guo, T. Yang, J.-S. Dang, P. Zhao, Q.-Z. Li and X. Zhao, *Journal of Physical Organic Chemistry*, 2014, **27**, 772–782.

(55) I. González-Veloso, E. M. Cabaleiro-Lago and J. Rodríguez-Otero, *Physical Chemistry Chemical Physics*, 2018, **20**, 11347–11358.

(56) T. Iwamoto, Y. Watanabe, T. Sadahiro, T. Haino and S. Yamago, *Angewandte Chemie - International Edition*, 2011, **50**, 8342–8344.

(57) J. Xia, J. W. Bacon and R. Jasti, *Chemical Science*, 2012, **3**, 3018–3021.

(58) T. Iwamoto, Y. Watanabe, H. Takaya, T. Haino, N. Yasuda and S. Yamago, *Chemistry - A European Journal*, 2013, **19**, 14061–14068.

(59) H. Isobe, S. Hitosugi, T. Yamasaki and R. Iizuka, *Chemical Science*, 2013, **4**, 1293–1287.

(60) Y. Nakanishi, H. Omachi, S. Matsuura, Y. Miyata, R. Kitaura, Y. Segawa, K. Itami and H. Shinohara, *Angewandte Chemie - International Edition*, 2014, **53**, 3102–3106.

(61) E. R. Darzi, E. S. Hirst, C. D. Weber, L. N. Zakharov, M. C. Lonergan and R. Jasti, *ACS Central Science*, 2015, **1**, 335–342.

(62) T. Kuwabara, J. Orii, Y. Segawa and K. Itami, *Angewandte Chemie - International Edition*, 2015, **54**, 9646–9649.

(63) S. Grimme, *Wiley Interdisciplinary Reviews: Computational Molecular Science*, 2011, **1**, 211–228.

(64) S. Grimme, *Journal of Computational Chemistry*, 2006, **27**, 1787–1799.

(65) S. Grimme, J. Antony, S. Ehrlich and H. Krieg, *Journal of Chemical Physics*, 2010, **132**, 154104.

(66) S. Grimme, S. Ehrlich and L. Goerigk, *Journal of Computational Chemistry*, 2011, **32**, 1456–1465.

(67) M. R. Kennedy, L. A. Burns and C. D. Sherrill, *The Journal of Physical Chemistry A*, 2012, **116**, 11920–11926.

(68) T. Janowski, P. Pulay, A. A. Sasith Karunarathna, A. Sygula and S. Saebø, *Chemical Physics Letters*, 2011, **512**, 155–160.

(69) F. Weigend and R. Ahlrichs, *Physical Chemistry Chemical Physics*, 2005, **7**, 3297–3305.

(70) F. Weigend, *Physical Chemistry Chemical Physics*, 2006, **8**, 1057–1065.

(71) TURBOMOLE V6.3 2011, a development of University of Karlsruhe and Forschungszentrum Karlsruhe GmbH, 1989-2007, TURBOMOLE GmbH, since 2007; available from, http://www.turbomole.com.

(72) S. F. Boys and F. Bernardi, *Molecular Physics*, 1970, **19**, 553–566.

(73) G. Chałasiński and M. M. Szczęśniak, *Chemical Reviews*, 2000, **100**, 4227–4252.

(74) E. R. Johnson, S. Keinan, P. Mori-Sánchez, J. Contreras-García, A. J. Cohen and W. Yang, *Journal of the American Chemical Society*, 2010, **132**, 6498–6506.

(75) D. Josa, J. Rodríguez-Otero, E. M. Cabaleiro-Lago, L. A. Santos and T. C. Ramalho, *Journal of Physical Chemistry A*, 2014, **118**, 9521–9528.

(76) J. Contreras-García, E. R. Johnson, S. Keinan, R. Chaudret, J.-P. Piquemal, D. N. Beratan and W. Yang, *Journal of Chemical Theory and Computation*, 2011, **7**, 625–632.

(77) W. Humphrey, A. Dalke and K. Schulten, *Journal of Molecular Graphics*, 1996, **14**, 33–38.

(78) T. Yanai, D. P. Tew and N. C. Handy, *Chemical Physics Letters*, 2004, **393**, 51–57.

(79) M. J. G. Peach, P. Benfield, T. Helgaker and D. J. Tozer, *The Journal of Chemical Physics*, 2008, **128**, 044118.

(80) F. Neese, *Wiley Interdisciplinary Reviews: Computational Molecular Science*, 2012, **2**, 73–78.

(81) F. Neese, F. Wennmohs, A. Hansen and U. Becker, *Chemical Physics*, 2009, **356**, 98–109.

(82) R. Izsák and F. Neese, *Journal of Chemical Physics*, 2011, **135**, 144105.

(83) T. Petrenko, S. Kossmann and F. Neese, *Journal of Chemical Physics*, 2011, **134**, 054116.

(84) T. Lu and F. Chen, *Journal of Computational Chemistry*, 2012, **33**, 580–592.

(85) D. Jacquemin, T. L. Bahers, C. Adamo and I. Ciofini, *Physical Chemistry Chemical Physics*, 2012, **14**, 5383–5388.

(86) T. Le Bahers, C. Adamo and I. Ciofini, *Journal of Chemical Theory and Computation*, 2011, **7**, 2498–2506.

(87) N. Shao, Y. Gao, S. Yoo, W. An and X. C. Zeng, *Journal of Physical Chemistry A*, 2006, **110**, 7672–7676.

USC
UNIVERSIDADE
DE SANTIAGO
DE COMPOSTELA

Chapter 7

Fullerene Size Controls the Selective Complexation of [11]CPP with Pristine and Endohedral Fullerenes

7.1 Introduction

Since their discovery, fullerenes have found a wide variety of applications in different fields such as optoelectronics, solar energy conversion or catalysis.[1–4] One of the most active fields in fullerene chemistry is devoted to developing suitable fullerene receptors, leading to stable fullerene inclusion complexes.[4–6] Non-covalent interactions involving fullerenes are mostly controlled by dispersion;[6,7] the electrostatic interaction is in most cases negligible considering the almost neutral character of most fullerenes, and polarization is only relevant when fullerenes interact with charged species.[6,8–11] Therefore, the design of efficient fullerene receptors mostly relies on favourable dispersion interactions, trying to maximize the contact surface between the fullerene and the host molecule.

An interesting approach to this problem is the use of receptors based on the so-called concave–convex $\pi\cdots\pi$ interactions.[12] The use of concave receptors capable of adapting to the convex surface of fullerenes allows maximizing the number of atom contacts at short distances thus maximizing the stabilisation by dispersion. Some of the most obvious candidates for these concave–convex complexes are buckybowls.[13,14] These species are polycyclic aromatic hydrocarbons exhibiting bowl-shaped geometries as a consequence of the impossibility of placing pentagonal and hexagonal rings in a planar sheet. The simplest of these buckybowls, corannulene $C_{20}H_{10}$, has been the subject of different studies regarding its ability for interacting with fullerenes (mostly C_{60}).[15–20] In fact, Sygula demonstrated the possibility of exclusively using concave–convex $\pi\cdots\pi$ interactions in order to encapsulate C_{60} by employing a pincer formed by two corannulene units linked together by means of a cyclooctatetraene tether.[21–27]

Even though corannulene is the most widely used buckybowl, other similar species have been employed as fullerene receptors.[15,16,19,27] In our research group we have shown that enlarging the bowl by annelating rings to its rim while keeping some flexibility leads to more stable complexes with fullerenes C_{60} and C_{70}.[15–17] Other species have been also employed as fullerene receptors, such as subphthalocyanines (another bowl-shaped family of species);[7,18,28–31] even planar porphyrins have been commonly employed for coordinating to fullerenes, specially considering their suitability for organic photovoltaic devices.[7,32–36]

Fullerenes can also be encapsulated inside carbon nanotubes, forming structures known as peapods.[12,37,38] Thus, another possibility for coordinating fullerenes, also based on concave–convex $\pi\cdots\pi$ interactions, would be the use of carbon nanorings.[12,39–44] These carbon nanorings are hoop-shaped π conjugated hydrocarbons possessing a nanosized cavity that can act as host in an inclusion complex with fullerenes. Cycloparaphenylenes (CPPs) are carbon nanorings where paraphenylene units are linked together in a cyclic way, representing the simplest structural unit of armchair carbon nanotubes.[12,40,41,45] CPPs are available with different number of paraphenylene units, so the diameter of their cavity can be tuned, spanning a range suitable for encapsulating species of the size of fullerene C_{60} or similar.[12,46–56] For instance, the diameter of the cavity changes from around 11 Å in [8]CPP to around 17 Å in [13]CPP. Yamago *et al.* reported the inclusion complex of C_{60} and [10]CPP, the shortest fullerene C_{60} peapod,[46] and its structure was later confirmed by X-ray analysis by Jasti *et al.*[52] Yamago *et al.* later reported the selective encapsulation of C_{70} by [10]CPP and [11]CPP.[47] In this case, due to the elongated shape of C_{70}, complexation with CPPs was also orientation-selective: in the [10]CPP complex, C_{70} lies with its long axis along the symmetry axis of the CPP, while in the [11]CPP complex it lies with its long axis inside the CPP. These results have been also confirmed by computational approaches.[48,53] Recently, Isobe *et al.* reported that [4]cyclochrysenylene, which is the simplest structural unit of a chiral carbon nanotube and has a diameter similar to [10]CPP, could encapsulate C_{60} with extremely high binding energy.[57,58]

Most studies and applications have been carried out with C_{60} and C_{70}, the most abundant fullerenes. However, shortly after the discovery of C_{60} the formation of a new fullerene moiety encapsulating a La atom ($La@C_{82}$) was reported,[59] opening the door for the field of endohedral metallofullerenes (EMFs).[60–63] Since then, a great number of different mono-, di- and tri- metallofullerenes of different size has been reported and characterized. Fullerene cages can also contain small clusters. One interesting aspect of these endofullerenes is that the carbon cage often displays a different isomer to that observed for the empty cage,[61,64] as a consequence of the presence of the endohedral unit and its strong interactions with the cage. CPP complexes with EMFs can show some special characteristics, as in $La@C_{82}$, showing partial charge transfer from the CPP to the fullerene.[65] Strong charge transfer has also been observed in the complex between [10]CPP and $Li^+@C_{60}$.[66] However, the studies on the complexation of these EMFs are much more scarce and in fact their application is severely hindered by difficulties related to extraction and purification of a given EMF. Itami *et al.* have shown that [11]CPP can be employed to selectively complex and extract $M@C_{82}$ and $M_2@C_{82}$ fullerenes from a soot containing a fullerene mixture, thus opening a possible path for EMF extraction and purification.[67]

Thus, there seems that the use of CPPs in order to encapsulate fullerenes constitutes a promising path in order to selectively complex and extract a given fullerene from a mixture, but also to obtain new functional materials. In order to get more insight into the characteristics of the process of complex formation and selectivity, in the present work a series of complexes formed by [11]CPP and different fullerenes are computational studied. The fullerenes considered include pristine fullerenes of different size but also endohedral metallofullerenes, as listed in Figure 7.1. The results obtained would help to understand the characteristics of the interaction in these complexes and provide with hints on the selectivity [11]CPP towards fullerenes.

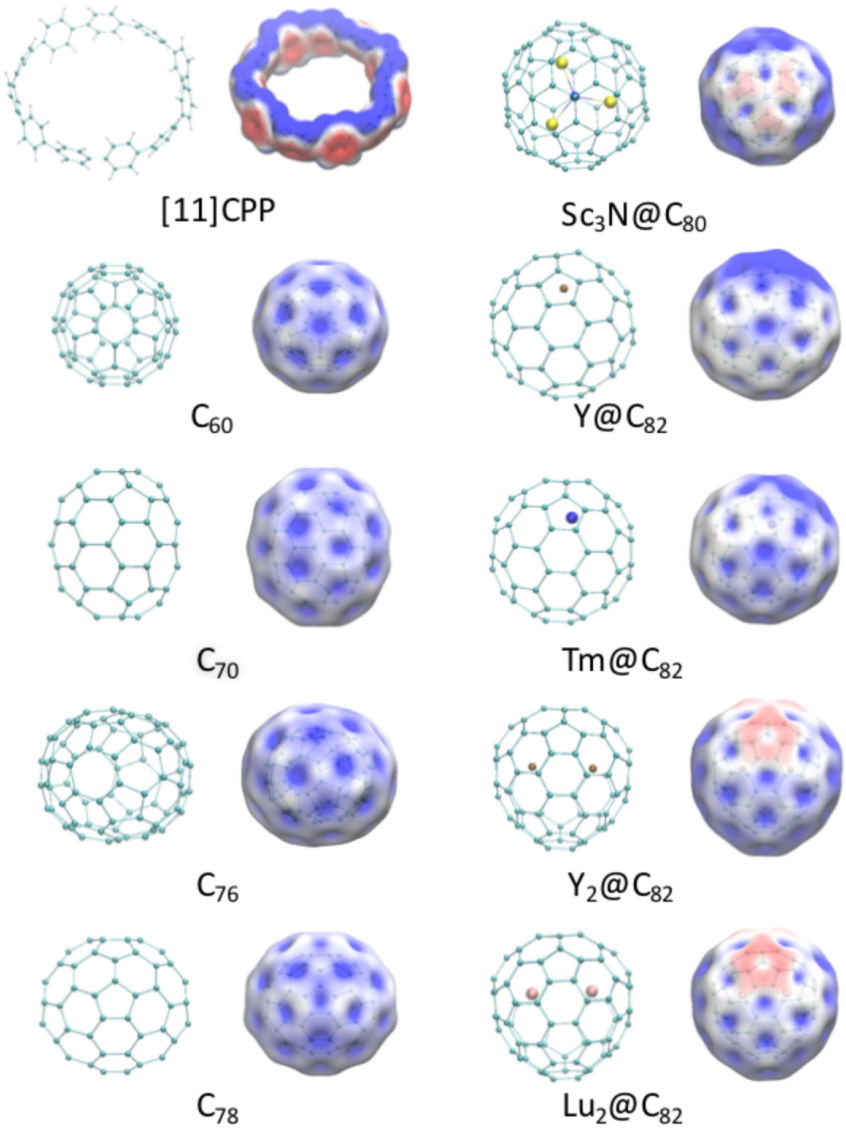

Figure 7.1: Fullerenes and [11]CPP considered in this work. Molecular electrostatic potential mapped onto an isosurface of isodensity 0.002 a.u. The colour scale runs from −0.015 a.u. (red) to 0.015 a.u. (blue).

7.2 Computational details

When the complex is formed, the spatial disposition of the fullerene inside the belt may lead to a large number of different energy minima. In order to locate the most stable structure for each of the dimers, a detailed potential energy search should be necessary, but it would be rather cumbersome and computationally demanding. Recently, it has been shown that a partial search using typical structures can be successful in finding the most stable structures at a lower computational cost than the full search (see chapter 4).[53] Besides, the stability of the different minima is usually pretty similar. Encouraged by these results, in this work, a partial search for minimum energy structures has been performed for each of the dimers studied. Thus, for each dimer, the fullerene is placed inside [11]CPP

and rotated according to the Euler angles in 90° steps. The most stable structure obtained is then optimised and selected for further analysis.

C_{60} has a small diameter and fits quite loosely inside the nanoring, so another approach was employed. The fullerene, adopting selected orientations, is placed inside [11]CPP and moved closer to the ring; when the minimum energy position is located, C_{60} is rotated along an axis perpendicular to the belt. Once the most favourable rotated structure is found, a vertical departure of the fullerene is considered, displacing the fullerene out of the nanoring (a displacement of 0.0 Å means that both molecular centres are at the same point). Finally, the most favourable structures found are optimised without any geometrical restrictions, and for the minimized complexes the complexation energy is calculated (see Figures d.1-d.3 in Appendix D).

Considering the size of the systems studied, the only practical approach for obtaining reliable complexation energies is the use of density functional theory together with an empirical correction for describing dispersion.[68–70] Among the different functionals available, TPSS has been chosen, supplemented with the empirical dispersion correction proposed by Grimme (D3) together with the Becke-Johnson damping function (TPSS-D3BJ, on the following TPSS-D). This functional has been selected because it closely reproduces the values for the interaction in corannulene dimer obtained by Janowsky and Pulay at the QCISD(T) level (see Figure d.4 in Appendix D).[71,72] Also, TPSS-D has been recently suggested as the method of choice for studying concave–convex complexes.[73] The basis set employed is the def2-TZVP basis set,[74] and the resolution of the identity approach has been employed in order to speed up calculations, with def2-TZVPP as auxiliary basis sets.[75] Def2-ecp effective core potentials have been employed for endohedral fullerenes containing Y,[76] Tm[77] and Lu.[78]

The geometries of the complexes are optimised at the TPSS-D/def2-TZVP level and then the complexation energies are obtained at the same level of calculation. The counterpoise method is applied in order to correct from the Basis Set Superposition Error (BSSE).[79,80] Therefore, the complexation energy for a given dimer is obtained as:

$$\begin{aligned}\Delta E_{\mathrm{AB}}^{\mathrm{comp}}(\mathrm{AB}) = &\left(E_{\mathrm{AB}}^{\mathrm{dimer}}(\mathrm{AB}) - E_{\mathrm{A}}^{\mathrm{isolated}}(\mathrm{A}) - E_{\mathrm{B}}^{\mathrm{isolated}}(\mathrm{B})\right) + \\ &\left(E_{\mathrm{A}}^{\mathrm{dimer}}(\mathrm{A}) + E_{\mathrm{B}}^{\mathrm{dimer}}(\mathrm{B}) - E_{\mathrm{A}}^{\mathrm{dimer}}(\mathrm{AB}) - E_{\mathrm{B}}^{\mathrm{dimer}}(\mathrm{AB})\right)\end{aligned} \tag{7.1}$$

where superscripts refer to the geometry employed and terms within parentheses to the basis set used. The first term corresponds to the change in energy when forming the complex, while the second one is the BSSE. This expression can be rearranged as:

$$\begin{aligned}\Delta E_{\mathrm{AB}}^{\mathrm{comp}}(\mathrm{AB}) = &\left(E_{\mathrm{AB}}^{\mathrm{dimer}}(\mathrm{AB}) - E_{\mathrm{A}}^{\mathrm{dimer}}(\mathrm{AB}) - E_{\mathrm{B}}^{\mathrm{dimer}}(\mathrm{AB})\right) + \\ &\left(E_{\mathrm{A}}^{\mathrm{dimer}}(\mathrm{A}) + E_{\mathrm{A}}^{\mathrm{isolated}}(\mathrm{A}) - E_{\mathrm{B}}^{\mathrm{dimer}}(\mathrm{B}) - E_{\mathrm{B}}^{\mathrm{isolated}}(\mathrm{B})\right)\end{aligned} \tag{7.2}$$

or

$$\Delta E_{\mathrm{comp}} = \Delta E_{\mathrm{inter}} + E_{\mathrm{def}} \tag{7.3}$$

The complexation is then the result of a pure interaction energy term obtained at the geometry of the dimer plus a term describing the energy cost associated to the changes in geometry undergone by the monomers when forming the dimer, the so-called deformation or preparation energy.[80,81] All calculations have been carried out using Turbomole 6.3.[82]

Non-covalent interactions can be visualized with the help of the non-covalent interaction index (NCI).[83,84] NCI enables identification of non-covalent interactions based on

the peaks that appear in the reduced density gradient (RDG) at low densities. Plotting a RDG isosurface for a low value of RDG, the non-covalent regions clearly appear in the supramolecular complex. These interactions correspond to both favourable and unfavourable interactions. In order to differentiate between them, the sign of the second eigenvalue of the density Hessian times the density is colour-mapped onto the isosurface: blue, green and red indicate strongly attractive interactions, weak vdW interactions, and strongly repulsive interactions, respectively. To save computation time, promolecular densities have been used, as previously done with good results in similar systems.[53] NCI analysis has been performed with the NCIPLOT-3.0 program[83] and graphic displays of concave–convex $\pi\cdots\pi$ interactions are obtained using VMD 1.9.1 software.[85]

7.3 Results and discussion

7.3.1 Fullerenes

The fullerenes considered in this work were selected based on the work of Itami *et al.*[67] and comprise pristine fullerenes, containing only carbon atoms, and endohedral fullerenes, where the carbon cage of the fullerene contains metal atoms or a small cluster. As shown in Figure 7.1, the pristine fullerenes studied are C_{60} and C_{70}, the most abundant fullerenes, together with the larger-sized C_{76} and C_{78}.[86] C_{60} has the well-know football ball structure with I_h symmetry while C_{70} exhibits an elongated shape as a rugby ball, with D_{5h} symmetry. C_{76}, on the other hand, has two stable isomers with D_2 and T_d symmetry; after optimisation at the TPSS-D/def2-TZVP level the D_2 structure is more stable by 11.6 kcal mol^{-1}, in agreement with the results in literature.[87] C_{78} has five different stable isomers whose stability has been studied in different previous work.[88–96] Most studies indicate that the most stable isomer corresponds to a structure of C_{2v} symmetry; after optimisation of the two possible C_{2v} isomers, the most stable one has been selected. The endohedral fullerenes considered are the scandium nitride endofullerene $Sc_3N@C_{80}$ (the third most abundant fullerene) and a series of derivatives of C_{82}. Among the latter the metallofullerenes including one Y or Tm atom are considered, together with the dimetallofullerenes including two Y or Lu atoms. As indicated above, the presence of the endohedral moiety usually leads to endofullerenes displaying a different isomer for the carbon cage as that observed for pristine fullerenes. The structures of the endofullerenes have been collected from literature, mostly from Popov and Dunsch.[97] The most stable isomer of $Sc_3N@C_{80}$ has a carbon cage of I_h symmetry; $Y@C_{82}$[97,98] and $Tm@C_{82}$[99] have the same carbon cage of C_{2v} symmetry, while $Y_2@C_{82}$ carbon cage corresponds to an isomer of C_{3v} symmetry.[97] The structure of $Lu_2@C_{82}$ has been considered to be similar to that of $Y_2@C_{82}$, and therefore has been constructed starting from it. It is worth noting that the symmetries above correspond to the carbon cage and they are often decreased due to the presence of the endohedral units.

An important aspect for the selective complexation of these fullerenes is the size and shape complementarity between the CPP and the fullerene. As indicated in previous work, C_{60} is effectively encapsulated by [10]CPP because it nicely fits within its cavity, leading to many intermolecular C–C contacts contributing to a large dispersion energy that it is the main stabilising contribution in the complex.[46,49,53] [10]CPP has a cavity with a diameter around 14 Å; considering that C–C intermolecular contacts usually display

distances around 3.5 Å, [10]CPP could encapsulate guest molecules of around 7 Å, which is precisely the size of C_{60}. [11]CPP shows a diameter of around 15 Å and therefore is capable of effectively encapsulate guests of somewhat larger size.

While C_{60} is spherically shaped, the other fullerenes employed in this study are less symmetrical, showing different diameters. As a simple way of describing the shape of the fullerenes studied, the position of the carbon atoms has been fitted to the minimum-volume ellipsoid containing them. Thus, the fullerenes can be easily described by the values of three diameters along the principal axis of the ellipsoid. It has to be noticed that these diameters are usually slightly larger than the atom-to-atom diameters since the ellipsoid is a smooth surface while the fullerenes have truncated hexagonal and pentagonal faces. The values obtained for the fullerenes studied are summarised in Table 7.1.

Table 7.1: Diameters (Å) along the principal axis of the minimum-volume ellipsoid containing the carbon atoms for the different fullerenes studied.

	D1	**D2**	**D3**		**D1**	**D2**	**D3**
$\mathbf{C_{60}}$	7.1	7.1	7.1	$\mathbf{Sc_3N@C_{80}}$	8.1	8.3	8.4
$\mathbf{C_{70}}$	7.3	7.3	8.4	$\mathbf{Y@C_{82}}$	8.0	8.5	8.6
$\mathbf{C_{76}}$	7.3	8.1	9.0	$\mathbf{Tm@C_{82}}$	8.0	8.5	8.6
$\mathbf{C_{78}}$	7.7	8.0	9.0	$\mathbf{Y_2@C_{82}}$	8.2	8.4	8.7
–	–	–	–	$\mathbf{Lu_2@C_{82}}$	8.1	8.4	8.7

C_{60}, as expected, has three equivalent diameters amounting to 7.1 Å, while C_{70} shows the well-known rugby-ball shape with a long axis amounting to 8.4 Å and a shorter one of 7.3 Å. These dimensions are the reason why the most stable complex of C_{70} with [10]CPP shows the fullerene standing up along the long axis;[47,48,53] C_{70} short axis is similar in size to C_{60} and so it can fit inside [10]CPP, while its long axis is around 1 Å longer and cannot accommodate into the cavity. C_{76} is the less spherical species among the fullerenes studied, with three clearly differentiated diameters: a long one reaching 9.0 Å, a shorter one similar to C_{70} and an intermediate diameter of 8.1 Å. A similar behaviour is observed in C_{78}, though the asymmetry is slightly smaller: the two shorter diameters are pretty similar so C_{78} is close to a prolate shape. Regarding endofullerenes, $Sc_3N@C_{80}$ is nearly spherical, while all C_{82} fullerenes show similar characteristics, close to an oblate shape, with the short axis around 8.1 Å and the longer ones around 8.6−8.7 Å. Therefore, the fullerenes considered show a variety of sizes and shapes that will affect their complexation with [11]CPP (the cavity is optimal for species around 8 Å). It has to be taken into account, though, that fullerenes can adopt different orientations other than those along the principal axis in order to fit into the cavity. More importantly, [11]CPP is quite flexible and can also adapt to the shape of these fullerenes. However, it can be expected that given a proper size that can fit into the cavity, more spherical molecules would allow a larger number of stabilising interactions.

Another aspect that can affect complexation is the electrostatic complementarity of host and guest. Figure 7.1 also shows the Molecular Electrostatic Potentials (MEPs) of the molecules studied. The nanoring displays negative regions associated to the phenyl rings and positive ones on the rim of the ring due to the hydrogen atoms. Therefore, the cavity is mostly negative and will favour inclusion of electron-deficient species. As

already shown in previous work, C_{60} and C_{70} show almost zero MEP, with just very slight positive regions,[7,15] and the same behaviour is observed in C_{76} and C_{78} (see Figure 7.1). On the other hand, the presence of the endohedral unit in endofullerenes introduces larger asymmetries on the charge distribution leading to MEPs showing quite noticeable positive and negative regions. $Sc_3N@C_{80}$ exhibits slightly negative regions on the carbon cage above and below the regions occupied by the endohedral cluster. $Y@C_{82}$ shows a markedly positive region where the Y atom contacts the carbon cage, and a similar though weaker region is observed in $Tm@C_{82}$. A similar behaviour is observed in dimetallofullerenes; the regions near the endohedral atoms are clearly positive, though in this case regions with negative MEP can also be clearly observed. Therefore, from an electrostatic point of view the C_{82} fullerenes would be oriented with the endohedral atoms on the plane of [11]CPP, thus allowing complementary MEP regions to be in close contact.

7.3.2 [11]CPP complexes with pristine Fullerenes. C_{60}, C_{70}, C_{76}, C_{78}

The results obtained for the complexes of [11]CPP with pristine fullerenes are summarized in Table 7.2 and Figure 7.2. As already observed in previous work,[46,49,53] C_{60} fits on the cavity of [10]CPP, so it can be expected that the cavity provided by [11]CPP is somewhat too large so the fullerene can be displaced within the nanoring. Therefore, a preliminary exploration of the energetics of the complex has been performed by placing C_{60} inside the nanoring and checking the effects of displacing and rotating C_{60} (see Figure d.3, Appendix D). While the stability of the complex decreases when the fullerene is displaced out of the cavity of the nanoring, it slightly increases when displaced towards the phenyl groups of the ring. In order to find the most stable structure of the complex, C_{60} was located inside the nanoring with two different orientations (one orientation along the axis passing through the pentagonal rings and another one through the hexagonal rings). The fullerene was then rotated along these axes and the most favourable orientations were employed for subsequent optimisation at the TPSS-D/def2-TZVP level of calculation. The most stable structure found for the complex with C_{60} is the one displayed in Figure 7.2. C_{60} is oriented along the axis passing through two pentagonal rings, and laterally displaced towards the phenylene units, the distance between the molecular centres of [11]CPP and C_{60} amounting to 0.9 Å (Table 7.2). This indicates that the cavity is too large for C_{60}, so the fullerene moves towards one side trying to establish a closer contact with the phenylene units.

This can be observed in the NCI plots in Figure 7.2; there is a surface indicating weak intermolecular contacts between the fullerene and the nanoring, but due to the displacement of fullerene, these are only partially established, with no contacts with the phenylene units farther apart. The results also indicate that [11]CPP is rather flexible so the cavity can be deformed in order to adapt to the shape of the fullerene inside without a great energetic cost. As shown in Table 7.2, the deformation energy associated to the more rigid fullerene is negligible, while it amounts to 1.2 kcal mol^{-1} for the nanoring. Thus, the ring loses its circular shape and elongates in order to be closer to the fullerene (see Table d.1 in Appendix D). If the fullerene is more centred on the nanoring, there are contacts with all phenylene units, though weaker, so the stability decreases by around 1 kcal mol^{-1} (see Figure d.7 in Appendix D).

Table 7.2: Characteristics of the complexes formed by [11]CPP and pristine fullerenes. ΔE_{comp} is the complexation energy, $E_{\text{def,ful}}$ is the deformation energy of the fullerene, $E_{\text{def,CPP}}$ is the deformation energy of the nanoring, ΔE_{disp} is the contribution of dispersion to the total complexation energy, all in kcal mol^{-1}. R_{centre} is the distance between the centres of host and guest; N_{contacts} is the number of C–C contacts below 4.0 Å and R_{average} is the average distance of these contacts.

	ΔE_{comp}	$E_{\text{def,ful}}$	$E_{\text{def,CPP}}$	ΔE_{disp}	R_{centre} (Å)	N_{contacts}	R_{average} (Å)
[11]CPP-C_{60}	−35.72	0.04	1.19	−45.58	0.85	86	3.76
[11]CPP-C_{70}	−45.39	0.03	0.75	−58.17	0.16	112	3.78
[11]CPP-C_{76}	−48.33	0.22	1.06	−73.15	0.01	179	3.68
[11]CPP-C_{78}	−51.33	0.19	0.54	−72.38	0.04	182	3.70

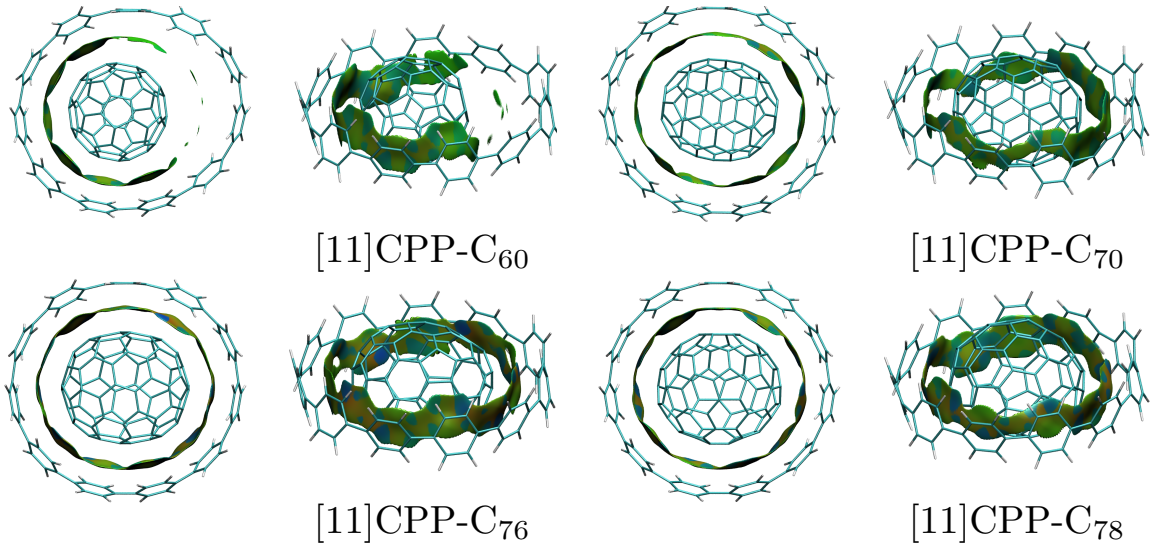

Figure 7.2: Most stable structures found for the complexes of [11]CPP with pristine fullerenes. The views on the right side are rotated by 60 degrees. The surfaces are the NCI plots. The product of the density times the sign of the second eigenvalue of its Hessian is mapped onto an isosurface of reduced density gradient with value 0.3 a.u. The colour scale goes from −0.02 a.u. (blue) to +0.02 a.u. (red).

C_{70} can be considered as a prolate ellipsoid, and a previous study by Yuan already showed that it can adopt different orientations within the [11]CPP cavity, though a structure with the C_{70} lying along its long axis within the cavity of the nanoring is preferred.[47,48] In agreement with these results, the most stable structure shown in Figure 7.2 has C_{70} lying along its long axis so it can establish stabilising interactions with all the phenylene units, as indicated by the NCI plot. The fullerene is almost centred within the CPP cavity, as indicated by the intercentre distance of 0.2 Å (Table 7.2). Rotations within the ring are not specially penalised and the energy changes by small quantities upon rotation of the fullerene (see Figure d.5 in Appendix D). Even though the cavity should be large enough for C_{70} to fit in, there is a slight deformation of CPP as revealed by the deformation energy of 0.8 kcal mol^{-1}. This is a result of CPP adapting to the elongated shape of C_{70} in

order to bring carbon atoms closer favouring the stability of the complex (the carbon ring of [11]CPP can be fitted to an ellipse with axis amounting to 15.5 Å and 14.6 Å, Table d.1 in Appendix D). C_{76} is the less symmetric of the fullerenes considered, but it presents a quite elongated shape by one of its principal axes, with a diameter of around 9.0 Å. Considering different orientations of the fullerene inside the carbon nanoring, two almost isoenergetic complexes have been obtained. The complex with C_{76} lying along its longest axis is slightly less stable (by 0.2 kcal mol^{-1}) than the structure shown in Figure 7.2. C_{76} is located in the centre of the nanoring and establishes favourable interactions with all phenylene units. In fact, the NCI plots suggest that the interactions of C_{76} with the nanoring are stronger than in other fullerenes as indicated by the blue regions in the NCI plot. C_{78}, despite its larger number of carbon atoms, is more spherically shaped than C_{76} and no axis is as large as the largest in C_{76}. The most stable structure shown in Figure 7.2 displays C_{78} filling the cavity of [11]CPP and interacting with all phenylene units.

Comparing the evolution of the complexation energies as the size of the pristine fullerene grows, it becomes clear (Table 7.2) that there is a size effect, so the complexation energies increase as the size of the fullerene grows. So, while C_{60} fits too loosely into the cavity of the ring leading to the smallest complexation energies, as the size of the fullerene grows the cavity is better filled so favourable interactions can be established with the whole nanoring. The results roughly follow the observations of Itami *et al.*[67] As already observed in similar complexes,[53] the main contribution to the stability of the complexes is dispersion. Considering dispersion contributions in Table 7.2, there is an increase with fullerene size but dispersion reaches a maximum contribution for C_{76} and decreases for C_{78}. This could be a consequence of the asymmetric shape of C_{76} allowing closer contacts than expected by its size.

Table 7.2 also list the number of carbon–carbon contacts below 4 Å in each complex, a quantity that should roughly correlate with the dispersion contribution. Though 3.4−3.5 Å could be a more reasonable distance for optimal van der Waals contact, carbon atoms are not at their optimal positions in the complexes so very few C–C contacts correspond to distances below 3.5 Å (just 1 such contact in [11]CPP-C_{60}). Considering that other contacts at slightly larger distance still contribute significantly to dispersion, we chose the cutoff at 4 Å as a simple way of measuring host-guest complementarity as in previous work.[7] In all complexes the average distance for these contacts is around 3.7−3.8 Å. In C_{60} complex the number of close contacts amounts to 86, because the nanoring is deformed so it can surround more effectively the fullerene. In the structure with the fullerene lying on the centre of the ring, the number of close contacts decreases to 34, leading to a much smaller dispersion contribution (−39 kcal mol^{-1}, see Figure d.7 in Appendix D). In C_{70} complex, though, the number of close contacts increases significantly reaching 112, because C_{70} is lying with its long axis inside the carbon nanoring, favouring close contacts with the phenylene units of the ring. With the C_{70} standing up, the number of contacts and therefore the contribution of dispersion are significantly smaller.

The number of contacts at short intermolecular distances favours dispersion, but it is also accompanied by an increase of repulsion due to a larger steric hindrance. In the case of C_{76} complex dispersion contributes the most, as also revealed by a large number of C–C contacts. Also, in C_{76} complex the average distance of these close contacts is the shortest. Recall that dispersion is favoured by a large number of contacts at short distances. The combination of a large number of contacts with the shortest average

distance makes dispersion contribution in C_{76} to be the largest among the complexes studied. In C_{78} complex, the number of C–C contacts is slightly larger but due to the larger average distances the contribution of dispersion is slightly smaller than in C_{76}. As commented above, repulsion also increases for C_{76}, so the final balance makes C_{78} complex more stable than the C_{76} one. This can be observed on the values obtained with the TPSS functional; the complexation energy without dispersion shows values of 9.9 kcal mol^{-1}, 12.8 kcal mol^{-1}, 24.8 kcal mol^{-1} and 21.1 kcal mol^{-1} for C_{60}, C_{70}, C_{76} and C_{78}. Therefore, the repulsion is larger in C_{76} counterbalancing its larger dispersion contribution.

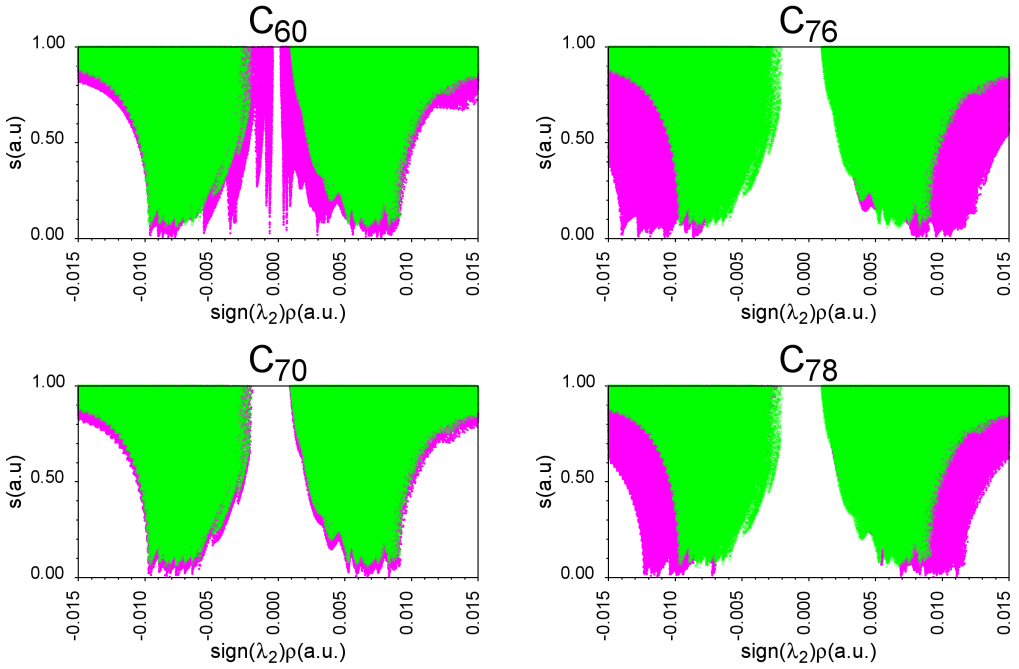

Figure 7.3: NCI two-dimensional plots for the complexes with pristine fullerenes. In green the results obtained for C_{70} are shown as reference, displaced by 0.05 a.u. in s for clarity.

These effects are also revealed by the 2D NCI plots in Figure 7.3, where the characteristics of the complexes are compared. It can be observed that the complex with C_{60} shows interaction regions at lower values of the density as compared with C_{70}. This is a consequence of the position of the fullerene, displaced from the centre of [11]CPP, and with [11]CPP deforming in order to achieve more favourable contacts. Therefore, there are contacts in similar regions as those observed for C_{70}, but some of them are weaker due to the smaller size of C_{60}. Considering the complex with C_{60} in the centre of the [11]CPP, it becomes clear that the intermolecular contacts are weaker due to the longer intermolecular distances, so they appear at smaller values of the density (Figure d.7 in Appendix D). The plot for C_{76} is quite different compared to C_{70}. Favourable interactions are observed at larger densities, so it would seem that the interaction should be stronger. However, these favourable interactions are matched with steric clashes also at larger densities. The NCI plot for C_{76} reflects, as commented above, that the fullerene fits tightly into the CPP cavity leading to large repulsion and dispersion terms. This agrees with the values obtained above for the number of close contacts and dispersion contribution.

7.3.3 [11]CPP complexes with $Sc_3N@C_{80}$, $Y@C_{82}$, $Tm@C_{82}$, $Y_2@C_{82}$, $Lu_2@C_{82}$

Figure 7.4 shows the most stable structures found for the complexes of [11]CPP with the endohedral fullerenes considered in this work, while Table 7.3 summarizes some of their characteristics. It can be observed in Figure 7.4 that the general aspect of all complexes is similar, with the fullerene fitting quite nicely within the cavity of [11]CPP and establishing favourable interactions with all the phenylene units. In all cases, the fullerene is oriented inside the cavity in such a way that the endohedral atoms are in the plane of the nanoring; that is, the carbon atoms that interact with the endohedral unit are always oriented towards the phenylene rings. Structures with other orientations relative to [11]CPP are less stable. This behaviour is probably related to the asymmetry of the electron charge already shown in Figure 7.1. The MEP of endofullerenes is more positive in the regions where the endohedral unit contacts the carbon cage. Considering that the MEP of the phenylene rings is clearly negative, fullerenes are oriented with their positive regions towards the phenylenes to facilitate stabilising electrostatic interactions.

In the complex with $Sc_3N@C_{80}$ the fullerene is located at the centre of the carbon nanoring; since the fullerene is more spherically shaped than C_{76} or C_{78} it seems to fit

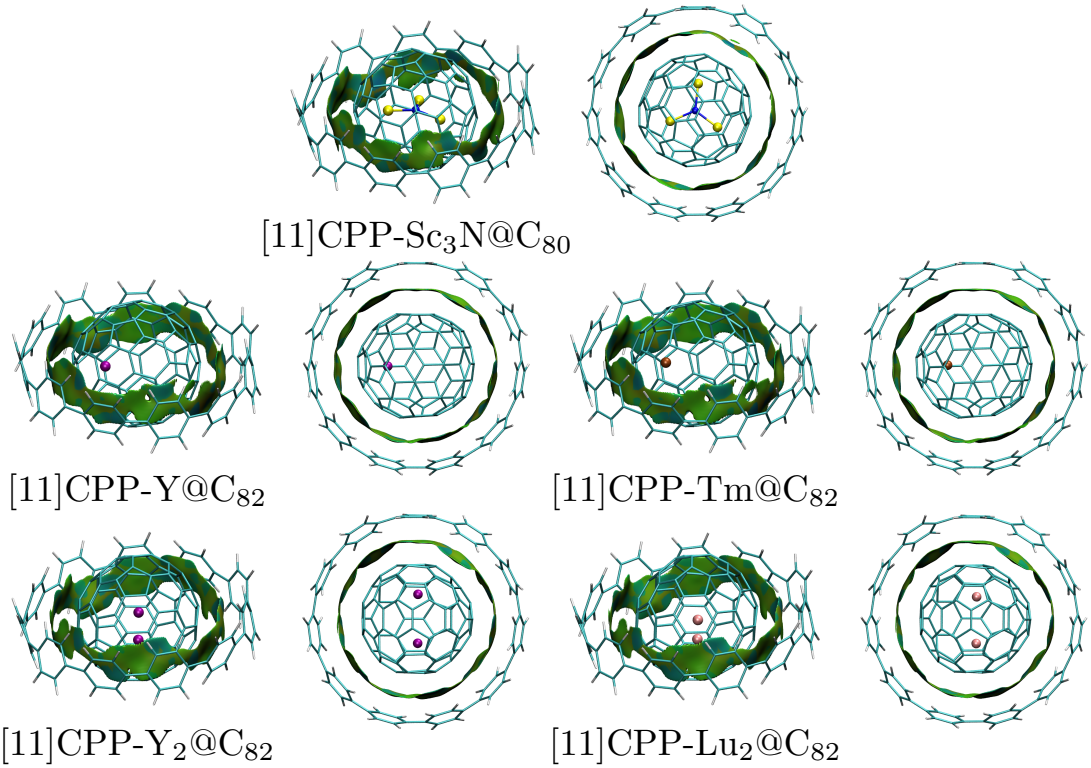

Figure 7.4: Most stable structures found for the complexes of [11]CPP with endohedral fullerenes. The views on the left side are rotated by 60 degrees. The surfaces are the NCI plots. The product of the density times the sign of the second eigenvalue of its Hessian is mapped onto an isosurface of reduced density gradient with value 0.3 a.u. The colour scale goes from −0.02 a.u. (blue) to +0.02 a.u. (red).

Table 7.3: Characteristics of the complexes formed by [11]CPP and endohedral fullerenes. ΔE_{comp} is the complexation energy, $E_{def,ful}$ is the deformation energy of the fullerene, $E_{def,CPP}$ is the deformation energy of the nanoring, ΔE_{disp} is the contribution of dispersion to the total complexation energy, all in kcal mol^{-1}. R_{centre} is the distance between the centres of host and guest; $N_{contacts}$ is the number of C–C contacts below 4.0 Å and $R_{average}$ is the average distance of these contacts.

	ΔE_{comp}	$E_{def,ful}$	$E_{def,CPP}$	ΔE_{disp}	R_{centre} (Å)	$N_{contacts}$	$R_{average}$ (Å)
[11]CPP-Sc_3N@C_{80}	−51.92	0.25	0.48	−69.74	0.08	159	3.72
[11]CPP-Y@C_{82}	−52.49	0.13	0.46	−71.62	0.09	174	3.73
[11]CPP-Tm@C_{82}	−53.12	0.34	0.44	−71.27	0.12	172	3.73
[11]CPP-Y_2@C_{82}	−51.62	0.07	0.57	−70.25	0.14	163	3.73
[11]CPP-Lu_2@C_{82}	−51.59	0.09	0.49	−70.07	0.17	160	3.73

more loosely inside the cavity, leading to a smaller number of C–C close contacts and therefore to a smaller contribution from dispersion energy. However, the complexation energy is larger than in any of the pristine fullerenes. A possible reason for this behaviour could be the same already indicated for C_{76} and C_{78}; the TPSS contribution to the complexation energy without the dispersion correction amounts to 17.8 kcal mol^{-1} in the Sc_3N@C_{80} complex, significantly smaller than the values obtained in C_{76} and C_{78} complexes. Therefore, there seems that the less symmetrical C_{76} and C_{78} are more constrained inside the nanoring cavity, leading to a larger number of contacts at closer interatomic distances and therefore to larger dispersion contributions, but also to increased repulsion as indicated by the TPSS values. In the case of the complex with Sc_3N@C_{80} the number of contacts is smaller and occur at larger average distances, but the complex is more stable due to a decreased repulsion (a more favourable electrostatic term associated to the more polar endofullerene cannot be ruled out in this case).

The rest of the endofullerenes employed in this work correspond to different derivatives of C_{82} including one or two metal atoms inside the cage. The monometallic endofullerenes Y@C_{82} and Tm@C_{82} have an unpaired electron and are doublets, while the dimetallic Y_2@C_{82} and Lu_2@C_{82} fullerenes are closed-shell species. Despite the different carbon cages and multiplicity the characteristics of the complexes with these C_{82} fullerenes are pretty similar as indicated in Table 7.3. Y@C_{82} and Tm@C_{82} are very similar, with complexation energies just differing by 0.5 kcal mol^{-1}. In any case, the complexes with the monometallic fullerenes show the largest complexation energies among the complexes studied, in agreement with the results of Itami *et al.*[67] The number of C–C contacts is high, reaching more than 170 contacts at an average distance of 3.73 Å. However, as commented in the case of the complex with Sc_3N@C_{80}, the larger interatomic distances compared to those observed in C_{76} and C_{78} also reflect on a decreased repulsive contribution. The TPSS contribution to the complexation energy in C_{82} fullerenes is around 18−19 kcal mol^{-1} in all cases, significantly smaller than the 25 kcal mol^{-1} of C_{76} complex. As a consequence, even though dispersion dominates the interaction in these systems and one could expect that the larger the dispersion the larger the stability of the complex, other factors can alter this trend, so complexes with smaller dispersion contributions are more stable due to comparatively smaller contributions from repulsion. In the case of the dimetallic derivatives the number of close contacts is slightly smaller, so the dispersion

contribution decreases as well as the complexation energies. Nevertheless, the stability of these complexes is among the largest for the complexes studied. In the case of the C_{82} derivatives there seems that an optimal balance is achieved between the need for close contacts favouring dispersion, but not too close as to trigger repulsion. The same could be said of the complex with $Sc_3N@C_{80}$.

7.3.4 Global trends in stability and charge transfer between fullerene and nanoring

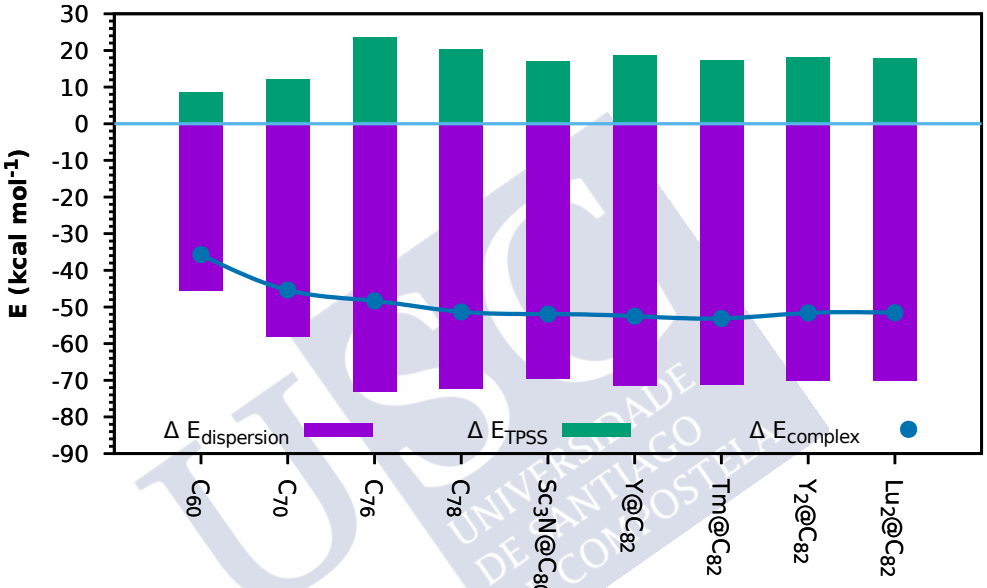

Figure 7.5: Complexation energies for the complexes studied with the full set of fullerenes. The decomposition of the total complexation energy into its TPSS and dispersion contributions is shown.

Figure 7.5 summarizes the results obtained for the different complexes studied. It can be observed that the complexation energy increases with the size of the fullerene but it already reaches a plateau with C_{78}. This indicates that in complexes with C_{78}, $Sc_3N@C_{80}$ and C_{82} fullerenes, the cavity is filled by the fullerene to a similar extent, so [11]CPP would complex these species with similar strength. This occurs because the dispersion contribution is fairly the same in all these cases, as well as the pure TPSS contribution. On the other hand, C_{60} and C_{70} are too small for the cavity so the repulsive contribution obtained with TPSS is significantly smaller than in larger fullerenes. However, since these smaller fullerenes are not capable of filling the cavity of the nanoring, the dispersion contribution also decreases leading to less stable complexes. C_{76} complexes behave somewhat differently; as indicated above and shown in Figure 7.5, the most stable structure found has a too large dispersion contribution as expected from its size, but this enhanced dispersion is counterbalanced by a larger TPSS repulsion, so the stability falls in line with the fullerene size (for other isomers of C_{76} complex the behaviour is similar to the rest of the series, see Figure d.7 in Appendix D). Complexes are most favoured with fullerenes capable of totally filling the cavity of the nanoring and therefore establishing a large number

of stabilising atom-atom contacts. This tendency to fill up the cavity is counterbalanced by the repulsion, so in some cases an oversized dispersion does not reflect on the final stability of the complex. These results are roughly in line with those obtained by Itami *et al.*,[67] showing that [11]CPP can selectively coordinate C_{82} endohedral fullerenes and extract them from a mixture containing smaller pristine fullerenes. The results indicate a negligible effect of the endohedral unit upon complexation energies. As a way to check this behaviour, complexation energies have been obtained for complexes with C_{82} and C_{80} deleting the endohedral species. The values obtained amount to -51.6 kcal mol^{-1} for C_{80} (I_h), -52.5 kcal mol^{-1} for C_{82} (C_{2v}), and -52.1 kcal mol^{-1} for C_{82} (C_{3v}), barely 0.5$-$0.6 kcal mol^{-1} from the results obtained with the endohedral species.

Finally, it could be also of interest to check whether there is a significant amount of charge transfer between host and guest. Yamago *et al.* have reported that for the complex of [11]CPP with La@C_{82} a significant amount of charge transfer is observed.[65] Mulliken analysis showed a charge transfer of 0.07 a.u. from the CPP to the fullerene. On the other hand, Itami *et al.* indicated that no significant charge transfer is observed in [11]CPP-Gd@C_{82} complex.[67] Table 7.4 shows the amount of charge transferred obtained from a Mulliken and Natural Bond Orbital (NBO) analysis for the complexes considered in this study, as obtained at the TPSS/def2-TZVP level with g09.[100] Mulliken analysis suggests smaller charge transfers than the one obtained in La@C_{82},[65] with values amounting to around 0.03$-$0.04 a.u. in most fullerene complexes. However, partial charges can be largely variable depending on the method employed, so these values should be considered with caution. As listed in Table 7.4, NBO charges show a somewhat different picture, with larger amounts of charge transferred in complexes with bigger fullerenes. However, a NBO second order perturbation analysis of the orbital interactions does not reveal important donor/acceptor contributions from the CPP to the fullerene (see Table d.2 in Appendix D). The contribution of charge transfer can be estimated following a procedure proposed by Stone and Misquitta,[101] where induction contributions from Symmetry Adapted Perturbation Theory (SAPT) are obtained employing dimer- and monomer-centred basis sets. The difference between both quantities gives an estimation of the charge transfer stabilisation. The results obtained at the SAPT0[102,103] level with the def2-SVP basis set employing PSI4[104] amount to barely -1 kcal mol^{-1} (-0.87 kcal mol^{-1} and -0.76 kcal mol^{-1} for [11]CPP-C_{78} and [11]CPP-Sc_3N@C_{80}), so it can be stated that charge transfer plays no significant role in the stability of these complexes, which are mostly controlled by dispersion.

Table 7.4: Total charge of fullerenes (a.u.) in the complexes with [11]CPP obtained at the TPSS-D/def2-TZVP level.

	Mulliken	NBO		Mulliken	NBO
[11]CPP-C_{60}	0.007	-0.025	[11]CPP-Sc_3N@C_{80}	-0.050	-0.096
[11]CPP-C_{70}	0.013	-0.052	[11]CPP-Y@C_{82}	-0.037	-0.079
[11]CPP-C_{76}	-0.028	-0.095	[11]CPP-Tm@C_{82}	-0.030	-0.080
[11]CPP-C_{78}	-0.028	-0.092	[11]CPP-Y_2@C_{82}	-0.025	-0.077
–	–	–	[11]CPP-Lu_2@C_{82}	-0.031	-0.069

7.4 Conclusions

A computational study has been carried out in dimers formed by the nanoring [11]cycloparaphenylene and a set of fullerenes of varying size. The fullerenes employed include pristine fullerenes C_{60}, C_{70}, C_{76} and C_{78}, as well as endofullerenes, comprising the clusterfullerene $Sc_3N@C_{80}$, monometallic endofullerenes $Y@C_{82}$ and $Tm@C_{82}$, and dimetallic endofullerenes $Y_2@C_{82}$ and $Lu_2@C_{82}$.

Complexation energies span a range between -36 kcal mol^{-1} to -53 kcal mol^{-1} depending on the fullerene considered. These large differences in stability suggest that [11]CPP could selectively encapsulate some of these fullerenes. In all cases, dispersion is the main stabilising factor, so the complexes arrange in order to maximize the number of favourable interatomic contacts and therefore maximize the dispersion contribution to the stability. As a consequence, in the complex formed with C_{60}, the fullerene is displaced almost 1 Å towards one side of the ring so it only interacts with some of the phenylene units on [11]CPP, being the least stable of the complexes studied. For the rest of the fullerenes studied the interaction is established with all the phenylene units. All endohedral fullerenes are oriented inside the cavity of the nanoring so the carbon atoms contacting with the endohedral unit are also interacting with the phenylene units of the nanoring. This could be a consequence of the greater polarity of these endofullerenes, which show positive regions in their MEPs around the carbon atoms contacting with the endohedral units.

The complexation energies for the complexes with fullerenes larger than C_{76} are within barely 2 kcal mol^{-1}. All complexes with C_{82} derivatives show similar stabilities despite differences in carbon cage, multiplicity and endohedral species, indicating that the nature of the endohedral species does not significantly affect to the interaction. Therefore, there seems that once the fullerene is large enough as to fill the cavity, it can adopt an orientation allowing to maximize dispersion interactions with the carbon ring and thus leading to similar stabilities. In consequence, [11]CPP could be capable of separating the fullerenes larger than C_{76} from a mixture also containing C_{70} and C_{60}, though the ring cannot possibly discriminate among the larger fullerenes.

References

(1) H. W. Kroto, J. R. Heath, S. C. O'Brien, R. F. Curl and R. E. Smalley, *Nature*, 1985, **318**, 162–163.

(2) A. Hirsch and M. Brettreich, *Fullerenes: Chemistry and Reactions*, Wiley-VCH, Weiheim, Germany, 2005.

(3) F. Langa and J.-F. Nierengarten, *Fullerenes: Principles and Applications*, Royal Society of Chemistry Publishing, Cambridge CB4 0WF, UK, 2012.

(4) T. Akasaka, A. Osuka, S. Fukuzumi, H. Kandori and Y. Aso, *Chemical Science of π-Electron Systems*, Springer Japan, Tokyo, 2015.

(5) N. Martín and J.-F. Nierengarten, *Supramolecular Chemistry of Fullerenes and Carbon Nanotubes*, Wiley-VCH Verlag GmbH & Co. KGaA, Weinheim, Germany, 2012.

(6) E. M. Pérez and N. Martín, *Chemical Society Reviews*, 2015, **44**, 6425–6433.

(7) E. M. Cabaleiro-Lago, J. Rodríguez-Otero and J. A. Carrazana-García, *Physical Chemistry Chemical Physics*, 2017, **19**, 26787–26798.

(8) J. A. Carrazana-García, J. Rodríguez-Otero and E. M. Cabaleiro-Lago, *Journal of Physical Chemistry B*, 2011, **115**, 2774–2782.

(9) P. García-Novo, A. Campo-Cacharrón, E. M. Cabaleiro-Lago and J. Rodríguez-Otero, *Physical Chemistry Chemical Physics*, 2012, **14**, 104–112.

(10) A. Campo-Cacharrón, E. M. Cabaleiro-Lago and J. Rodríguez-Otero, *Journal of Computational Chemistry*, 2014, **35**, 1533–1544.

(11) D. Vijay, H. Sakurai, V. Subramanian and G. N. Sastry, *Physical Chemistry Chemical Physics*, 2012, **14**, 3057–3065.

(12) T. Kawase and H. Kurata, *Chemical Reviews*, 2006, **106**, 5250–5273.

(13) M. A. Petrukhina and L. T. Scott, *Fragments of Fullerenes and Carbon Nanotubes*, John Wiley & Sons, Hoboken, New Jersey, 2012.

(14) L. T. Scott, H. E. Bronstein, D. V. Preda, R. B. M. Ansems, M. S. Bratcher and S. Hagen, *Pure and Applied Chemistry*, 1999, **71**, 209–219.

(15) D. Josa, L. Azevedo dos Santos, I. González-Veloso, J. Rodríguez-Otero, E. M. Cabaleiro-Lago and T. de Castro Ramalho, *RSC Advances*, 2014, **4**, 29826–29833.

(16) D. Josa, J. Rodríguez-Otero and E. M. Cabaleiro-Lago, *Physical Chemistry Chemical Physics*, 2015, **17**, 13206–13214.

(17) D. Josa, J. Rodríguez-Otero, E. M. Cabaleiro-Lago, L. A. Santos and T. C. Ramalho, *Journal of Physical Chemistry A*, 2014, **118**, 9521–9528.

(18) P. A. Denis, *New Journal of Chemistry*, 2014, **38**, 5608–5616.

(19) P. A. Denis, *Journal of Physical Organic Chemistry*, 2014, **27**, 918–925.

(20) P. A. Denis, *RSC Advances*, 2013, **3**, 25296–25305.

(21) A. Sygula, F. R. Fronczek, R. Sygula, P. W. Rabideau and M. M. Olmstead, *Journal of the American Chemical Society*, 2007, **129**, 3842–3843.

(22) Y. Zhao and D. G. Truhlar, *Physical Chemistry Chemical Physics*, 2008, **10**, 2813–2818.

(23) C. Mück-Lichtenfeld, S. Grimme, L. Kobryn and A. Sygula, *Physical Chemistry Chemical Physics*, 2010, **12**, 7091–7097.

(24) M. Yanney and A. Sygula, *Tetrahedron Letters*, 2013, **54**, 2604–2607.

(25) V. H. Le, M. Yanney, M. McGuire, A. Sygula and E. A. Lewis, *Journal of Physical Chemistry B*, 2014, **118**, 11956–11964.

(26) M. Yanney, F. R. Fronczek and A. Sygula, *Angewandte Chemie - International Edition*, 2015, **54**, 11153–11156.

(27) P. A. Denis, *Chemical Physics Letters*, 2014, **591**, 323–327.

(28) C. G. Claessens and T. Torres, *Chemical Communications*, 2004, **0**, 1298–1299.

(29) P. A. Denis and M. Yanney, *Chemical Physics Letters*, 2015, **640**, 140–146.

(30) G. E. Morse and T. P. Bender, *ACS Applied Materials and Interfaces*, 2012, **4**, 5055–5068.

(31) I. Sánchez-Molina, B. Grimm, R. M. Krick Calderon, C. G. Claessens, D. M. Guldi and T. Torres, *Journal of the American Chemical Society*, 2013, **135**, 10503–10511.

(32) P. A. Denis and M. Yanney, *RSC Advances*, 2016, **6**, 50978–50984.

(33) K. Tashiro and T. Aida, *Chemical Society Reviews*, 2007, **36**, 189–197.

(34) C. L. Wang, W. B. Zhang, R. M. Van Horn, Y. Tu, X. Gong, S. Z. D. Cheng, Y. Sun, M. Tong, J. Seo, B. B. Y. Hsu and A. J. Heeger, *Advanced Materials*, 2011, **23**, 2951–2956.

(35) A. Mateo-Alonso, C. Sooambar and M. Prato, *Comptes Rendus Chimie*, 2006, **9**, 944–951.

(36) C. B. KC, K. Ohkubo, P. A. Karr, S. Fukuzumi and F. D'Souza, *Chemical Communications*, 2013, **49**, 7614–7616.

(37) B. W. Smith, M. Monthioux and D. E. Luzzi, *Nature*, 1998, **396**, 323–324.

(38) F. Simon and M. Monthioux, *Carbon Meta-Nanotubes: Synthesis, Properties and Applications*, ed. M. Monthioux, John Wiley & Sons, Ltd, Chichester, UK, 1st Edition, 2012.

(39) M. Iyoda and H. Shimizu, *Chemical Society Reviews*, 2015, **44**, 6411–6424.

(40) H. A. Wegner, *Angewandte Chemie - International Edition*, 2017, **56**, 10995–10996.

(41) S. E. Lewis, *Chemical Society Reviews*, 2015, **44**, 2221–2304.

(42) H. Omachi, Y. Segawa and K. Itami, *Accounts of Chemical Research*, 2012, **45**, 1378–1389.

(43) K. Miki, T. Matsushita, Y. Inoue, Y. Senda, T. Kowada and K. Ohe, *Chemical Communications*, 2013, **49**, 9092–9094.

(44) M. Hasegawa, K. Kobayakawa, H. Matsuzawa, T. Nishinaga, T. Hirose, K. Sako and Y. Mazaki, *Chemistry - A European Journal*, 2017, **23**, 3267–3271.

(45) E. R. Darzi and R. Jasti, *Chemical Society Reviews*, 2015, **44**, 6401–6410.

(46) T. Iwamoto, Y. Watanabe, T. Sadahiro, T. Haino and S. Yamago, *Angewandte Chemie - International Edition*, 2011, **50**, 8342–8344.

(47) T. Iwamoto, Y. Watanabe, H. Takaya, T. Haino, N. Yasuda and S. Yamago, *Chemistry - A European Journal*, 2013, **19**, 14061–14068.

(48) K. Yuan, Y.-J. Guo and X. Zhao, *The Journal of Physical Chemistry C*, 2015, **119**, 5168–5179.

(49) K. Yuan, C.-H. Zhou, Y.-C. Zhu and X. Zhao, *Physical Chemistry Chemical Physics*, 2015, **17**, 18802–18812.

(50) Y. Segawa, H. Omachi and K. Itami, *Organic Letters*, 2010, **12**, 2262–2265.

(51) R. Jasti, J. Bhattacharjee, J. B. Neaton and C. R. Bertozzi, *Journal of the American Chemical Society*, 2008, **130**, 17646–17647.

(52) J. Xia, J. W. Bacon and R. Jasti, *Chemical Science*, 2012, **3**, 3018–3021.

(53) I. González-Veloso, J. Rodríguez-Otero and E. M. Cabaleiro-Lago, *Physical Chemistry Chemical Physics*, 2016, **18**, 31670–31679.

(54) E. S. Hirst and R. Jasti, *Journal of Organic Chemistry*, 2012, **77**, 10473–10478.

(55) H. U. Rehman, N. A. McKee and M. L. McKee, *Journal of Computational Chemistry*, 2016, **37**, 194–209.

(56) K. Yuan, Y.-J. Guo, T. Yang, J.-S. Dang, P. Zhao, Q.-Z. Li and X. Zhao, *Journal of Physical Organic Chemistry*, 2014, **27**, 772–782.

(57) H. Isobe, S. Hitosugi, T. Yamasaki and R. Iizuka, *Chemical Science*, 2013, **4**, 1293–1297.

(58) S. Hitosugi, K. Ohkubo, R. Iizuka, Y. Kawashima, K. Nakamura, S. Sato, H. Kono, S. Fukuzumi and H. Isobe, *Organic Letters*, 2014, **16**, 3352–3355.

(59) Y. Chai, T. Guo, C. Jin, R. E. Haufler, L. P. F. Chibante, J. Fure, L. Wang, J. M. Alford and R. E. Smalley, *The Journal of Physical Chemistry*, 1991, **95**, 7564–7568.

(60) X. Lu, L. Echegoyen, A. L. Balch, S. Nagase and T. Akasaka, *Endohedral Metallofullerenes: Basics and Applications*, CRC Press Taylor & Francis Group, Boca Raton, FL, USA, 2015.

(61) A. A. Popov, S. Yang and L. Dunsch, *Chemical Reviews*, 2013, **113**, 5989–6113.

(62) M. Rudolf, S. Wolfrum, D. M. Guldi, L. Feng, T. Tsuchiya, T. Akasaka and L. Echegoyen, *Chemistry - A European Journal*, 2012, **18**, 5136–5148.

(63) A. A. Popov, *Endohedral Fullerenes: Electron Transfer and Spin*, Springer International Publishing, Gewerbestrasse, Switzerland, 2017.

(64) Y. Wang, S. Díaz-Tendero, F. Martín and M. Alcamí, *Journal of the American Chemical Society*, 2016, **138**, 1551–1560.

(65) T. Iwamoto, Z. Slanina, N. Mizorogi, J. Guo, T. Akasaka, S. Nagase, H. Takaya, N. Yasuda, T. Kato and S. Yamago, *Chemistry - A European Journal*, 2014, **20**, 14403–14409.

(66) H. Ueno, T. Nishihara, Y. Segawa and K. Itami, *Angewandte Chemie - International Edition*, 2015, **54**, 3707–3711.

(67) Y. Nakanishi, H. Omachi, S. Matsuura, Y. Miyata, R. Kitaura, Y. Segawa, K. Itami and H. Shinohara, *Angewandte Chemie - International Edition*, 2014, **53**, 3102–3106.

(68) S. Grimme, *Wiley Interdisciplinary Reviews: Computational Molecular Science*, 2011, **1**, 211–228.

(69) S. Grimme, J. Antony, S. Ehrlich and H. Krieg, *Journal of Chemical Physics*, 2010, **132**, 154104.

(70) S. Grimme, S. Ehrlich and L. Goerigk, *Journal of Computational Chemistry*, 2011, **32**, 1456–1465.

(71) T. Janowski, P. Pulay, A. A. Sasith Karunarathna, A. Sygula and S. Saebø, *Chemical Physics Letters*, 2011, **512**, 155–160.

(72) M. R. Kennedy, L. A. Burns and C. D. Sherrill, *The Journal of Physical Chemistry A*, 2012, **116**, 11920–11926.

(73) E. M. Cabaleiro-Lago, B. Fernández and J. Rodríguez-Otero, *Journal of Computational Chemistry*, 2018, **39**, 93–104.

(74) F. Weigend and R. Ahlrichs, *Physical Chemistry Chemical Physics*, 2005, **7**, 3297–3305.

(75) F. Weigend, *Physical Chemistry Chemical Physics*, 2006, **8**, 1057–1065.

(76) K. Eichkorn, F. Weigend, O. Treutler and R. Ahlrichs, *Theoretical Chemistry Accounts: Theory, Computation, and Modeling (Theoretica Chimica Acta)*, 1997, **97**, 119–124.

(77) M. Dolg, H. Stoll and H. Preuss, *The Journal of Chemical Physics*, 1989, **90**, 1730–1734.

(78) X. Cao and M. Dolg, *The Journal of Chemical Physics*, 2001, **115**, 7348–7355.

(79) S. F. Boys and F. Bernardi, *Molecular Physics*, 1970, **19**, 553–566.

(80) G. Chałasiński and M. M. Szczęśniak, *Chemical Reviews*, 2000, **100**, 4227–4252.

(81) M. von Hopffgarten and G. Frenking, *Wiley Interdisciplinary Reviews: Computational Molecular Science*, 2012, **2**, 43–62.

(82) TURBOMOLE V6.3 2011, a development of University of Karlsruhe and Forschungszentrum Karlsruhe GmbH, 1989-2007, TURBOMOLE GmbH, since 2007; available from, http://www.turbomole.com.

(83) J. Contreras-García, E. R. Johnson, S. Keinan, R. Chaudret, J.-P. Piquemal, D. N. Beratan and W. Yang, *Journal of Chemical Theory and Computation*, 2011, **7**, 625–632.

(84) E. R. Johnson, S. Keinan, P. Mori-Sánchez, J. Contreras-García, A. J. Cohen and W. Yang, *Journal of the American Chemical Society*, 2010, **132**, 6498–6506.

(85) W. Humphrey, A. Dalke and K. Schulten, *Journal of Molecular Graphics*, 1996, **14**, 33–38.

(86) Starting geometries taken from http://www.nanotube.msu.edu/fullerene/ last accesed in 3/12/2017.

(87) A. R. Khamatgalimov and V. I. Kovalenko, *Fullerenes, Nanotubes and Carbon Nanostructures*, 2015, **23**, 148–152.

(88) T. Wakabayashi, K. Kikuchi, S. Suzuki, H. Shiromaru and Y. Achiba, *Journal of Physical Chemistry*, 1994, **98**, 3090–3091.

(89) K. Kikuchi, N. Nakahara, T. Wakabayashi, S. Suzuki, H. Shiromaru, Y. Miyake, K. Saito, I. Ikemoto, M. Kainosho and Y. Achiba, *Nature*, 1992, **357**, 142–145.

(90) R. Taylor, G. J. Langley, T. J. S. Dennis, H. W. Kroto and D. R. M. Walton, *Journal of the Chemical Society, Chemical Communications*, 1992, **6**, 1043–1046.

(91) F. Diederich and R. L. Whetten, *Accounts of Chemical Research*, 1992, **25**, 119–126.

(92) P. W. Fowler, R. C. Batten and D. E. Manolopoulos, *Journal of the Chemical Society, Faraday Transactions*, 1991, **87**, 3103–3104.

(93) N. Shao, Y. Gao and X. C. Zeng, *Journal of Physical Chemistry C*, 2007, **111**, 17671–17677.

(94) Y. Lin, W. Cai and X. Shao, *Journal of Molecular Structure: THEOCHEM*, 2006, **760**, 153–158.

(95) R. D. Bendale and M. C. Zerner, *Journal of Physical Chemistry*, 1995, **99**, 13830–13833.

(96) J. C. Niles and X. Q. Wang, *The Journal of Chemical Physics*, 1995, **103**, 7040–7047.

(97) A. A. Popov and L. Dunsch, *Chemistry - A European Journal*, 2009, **15**, 9707–9729.

(98) E. Y. Misochko, A. V. Akimov, V. A. Belov, D. A. Tyurin, V. P. Bubnov, I. E. Kareev and E. B. Yagubskii, *Physical Chemistry Chemical Physics*, 2010, **12**, 8863–8869.

(99) L. Zheng, H. He, M. Yang, Q. Zeng and M. Yang, *Journal of Physics Condensed Matter*, 2010, **22**, 235301.

(100) M. J. Frisch, G. W. Trucks, H. B. Schlegel, G. E. Scuseria, M. A. Robb, J. R. Cheeseman, G. Scalmani, V. Barone, B. Mennucci, G. A. Petersson, H. Nakatsuji, M. Caricato, X. Li, H. P. Hratchian, A. F. Izmaylov, J. Bloino, G. Zheng, J. L. Sonnenberg, M. Hada, M. Ehara, K. Toyota, R. Fukuda, J. Hasegawa, M. Ishida, T. Nakajima, Y. Honda, O. Kitao, H. Nakai, T. Vreven, J. A. Montgomery, Jr., J. E. Peralta, F. Ogliaro, M. Bearpark, J. J. Heyd, E. Brothers, K. N. Kudin, V. N. Staroverov, R. Kobayashi, J. Normand, K. Raghavachari, A. Rendell, J. C. Burant, S. S. Iyengar, J. Tomasi, M. Cossi, N. Rega, J. M. Millam, M. Klene, J. E. Knox, J. B. Cross, V. Bakken, C. Adamo, J. Jaramillo, R. Gomperts, R. E. Stratmann, O. Yazyev, A. J. Austin, R. Cammi, C. Pomelli, J. W. Ochterski, R. L. Martin, K. Morokuma, V. G. Zakrzewski, G. A. Voth, P. Salvador, J. J. Dannenberg, S. Dapprich, A. D. Daniels, Ö. Farkas, J. B. Foresman, J. V. Ortiz, J. Cioslowski and D. J. Fox, *Gaussian 09 Revision E.01*, Gaussian Inc. Wallingford CT 2009.

(101) A. J. Stone and A. J. Misquitta, *Chemical Physics Letters*, 2009, **473**, 201–205.

(102) E. G. Hohenstein, R. M. Parrish, C. D. Sherrill, J. M. Turney and H. F. Schaefer III, *Journal of Chemical Physics*, 2011, **135**, 174107.

(103) E. G. Hohenstein and C. D. Sherrill, *Journal of Chemical Physics*, 2010, **132**, 184111.

(104) R. M. Parrish, L. A. Burns, D. G. Smith, A. C. Simmonett, A. E. DePrince, E. G. Hohenstein, U. Bozkaya, A. Y. Sokolov, R. Di Remigio, R. M. Richard, J. F. Gonthier, A. M. James, H. R. McAlexander, A. Kumar, M. Saitow, X. Wang, B. P. Pritchard, P. Verma, H. F. Schaefer, K. Patkowski, R. A. King, E. F. Valeev, F. A. Evangelista, J. M. Turney, T. D. Crawford and C. D. Sherrill, *Journal of Chemical Theory and Computation*, 2017, **13**, 3185–3197.

Chapter 8

Endohedral alkali cations promote charge transfer transitions in complexes of C_{60} with [10]cycloparaphenylenes

8.1 Introduction

Cycloparaphenylenes (CPPs) are hoop-shaped nanorings where paraphenylene units are linked together in a cyclic way, corresponding to the simplest structural unit of armchair carbon nanotubes.[1,2] The progress attained in the synthetic procedures has allowed the production of CPPs of different size, so currently CPPs containing from 5 to 21 cycloparaphenylene units,[3–6] as well as different derivatives,[7–11] are available.[1,2] Since the diameter of the cavity of the CPP can be controlled according to the number of cycloparaphenylene units, these species are specially well suited for encapsulating different molecules just choosing the CPP giving the best size match with the guest.[2,12]

The possibility of having a size-adjustable concave π cavity makes CPPs an obvious candidate for encapsulating spherically-shaped π species as fullerenes.[2,12,13] The discovery of buckminsterfullerene C_{60} marked the starting point for the characterization of a variety of similarly cage-shaped molecules with specific properties and chemistry that make them amenable for a wide range of possible applications in solar energy conversion, optoelectronics, catalysis, and others.[14–16] The most abundant of these species are the fullerenes C_{60} and C_{70}, and therefore these are the species that have been mostly used for different applications. However, shortly after the discovery of C_{60}, a new fullerene encapsulating a Lanthanum atom was reported, the first example of a large family of so-called endohedral fullerenes, *i.e.* carbon cages bearing different species inside, ranging from metallic atoms to small clusters.[17,18] An interesting characteristic of these endohedral fullerenes is that quite often the interactions between the endohedral unit and the carbon cage lead to a structure for the carbon cage that would not be obtained for the pristine fullerene. In most cases, these endofullerenes require larger carbon cages than that of the C_{60} fullerene.[17,18]

A special case to be mentioned is $Li^+@C_{60}$ endofullerene, which can be produced and isolated by bombardment of Li^+ plasma with C_{60} vapour.[19–22] This is the only case of isolable metallofullerene produced by metal insertion into the existing pristine fullerene.

While the presence of the Li^+ cation hardly changes the size and shape of the carbon cage, $Li^+@C_{60}$ is a stronger electron-acceptor than pristine C_{60}. Considering that fullerenes are used as acceptors in most organic photovoltaic devices,[23,24] the enhanced electron-accepting characteristics of $Li^+@C_{60}$ make it a suitable choice for this kind of applications.[25–29] On the other hand the presence of the cation inside the fullerene cage has a significant impact on the reactivity of the C_{60} unit. $Li^+@C_{60}$ shows enhanced reactivity in electron transfer reactions with electron donors,[30] and Diels-Alder reactions have been reported to proceed faster than the analogous process with pristine C_{60}.[31,32] This enhanced reactivity has been explained as a consequence of the lowering of the LUMO energy leading to a higher electron-acceptor behaviour.

As commented above, different fullerenes can be effectively encapsulated by using CPP of appropriate cavity size.[2,12] Yamago *et al.* reported the inclusion complex between C_{60} and [10]CPP, the shortest fullerene C_{60} peapod,[33] and its structure was later confirmed by X-ray analysis by Jasti *et al.*[34] Yamago *et al.* later reported the selective encapsulation of C_{70} by [10]CPP and [11]CPP: in [10]CPP complex, C_{70} lies with its long axis along the symmetry axis of the CPP, while in the [11]CPP complex it lies with its long axis inside the CPP.[35] These results have been also confirmed by computational approaches.[36–39] C_{60} is also encapsulated by [4]cyclochrysenylene, the simplest structural unit of a chiral carbon nanotube.[40] Also, CPPs have been employed for the selective separation of mixtures of fullerenes.[36,41]

These CPPs are also capable of forming stable complexes with $Li^+@C_{60}$, as reported by Ueno *et al.*[42] The results obtained for the complex between $Li^+@C_{60}$ and [10]CPP suggest that the positive charge of Li^+ is not only delocalised throughout the C_{60} cage as already observed in isolated $Li^+@C_{60}$, but also delocalised to the CPP unit.[42,43] Also, the results obtained for the absorption spectra of the complex suggest that significant charge transfer takes place from the CPP to the fullerene unit, leading to broadened bands in the near IR region and around 350 nm.

To the best of our knowledge, the only computational study on such a system corresponds to a study on different Saturn systems including the [10]CPP complex with $Li^+@C_{60}$. The results suggest that a stable complex is formed, exhibiting significant charge transfer from the CPP to the fullerene.[43] In order to get a deeper insight into the characteristics of this interesting species, in this work a computational study is carried out in complexes formed by [10]CPP and a series of alkali cation-including C_{60} (see Figure 8.1). Even though the Li^+-containing species is the only one isolated thus far, a comparison with the analogous complexes containing Na^+ and K^+ cations will help to reveal their specific features, and to what extent the characteristics of the complexes are modified by the presence of the endohedral cation compared to complexes with pristine C_{60}.

8.2 Computational details

The inclusion complexes of fullerenes inside CPPs can be considered to be controlled by concave–convex $\pi\cdots\pi$ interactions.[12,13,44] This kind of interaction is typical of complexes formed between fullerenes and curved π surfaces, and it is considered the driving force of fullerene receptors as the one proposed by Sygula,[45] based on two corannulene pincers. Though corannulene and other buckybowls have been employed as receptors relying on

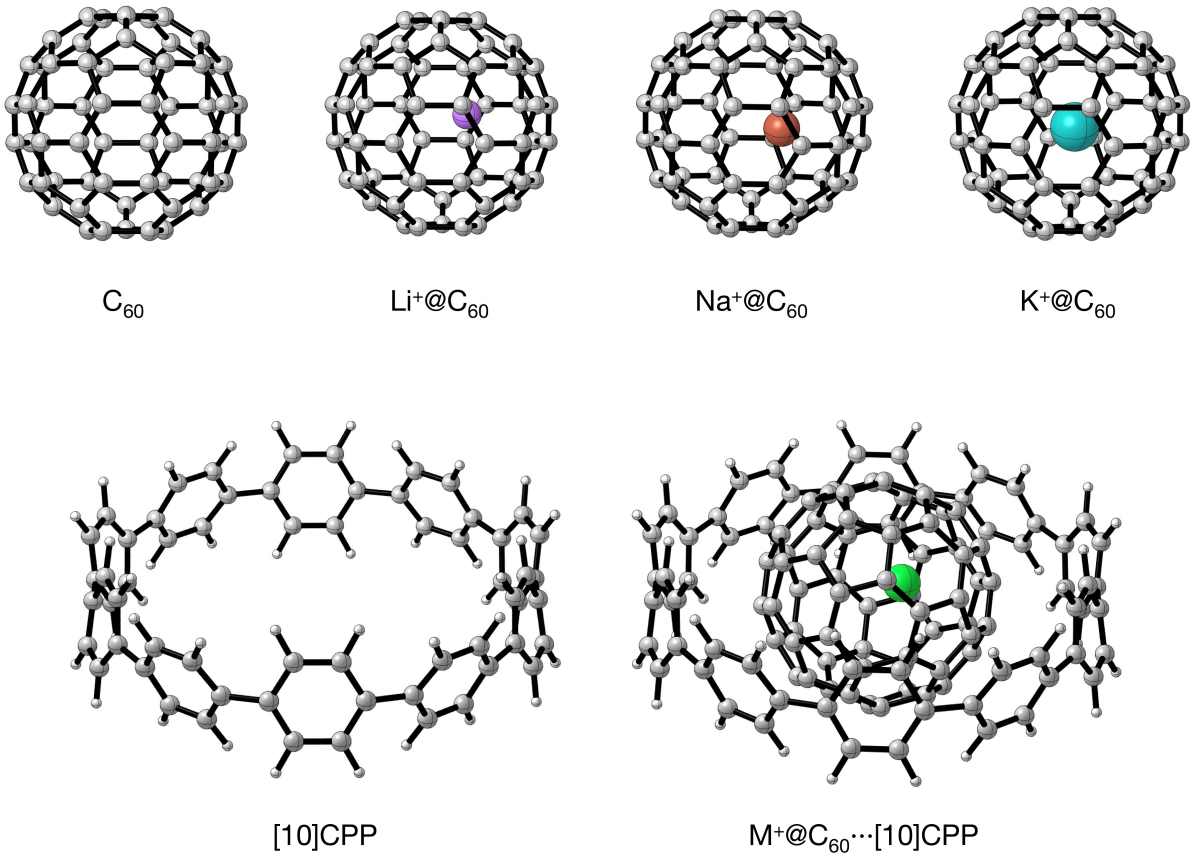

Figure 8.1: Species studied in this work

concave–convex $\pi\cdots\pi$ interactions,[46–53] CPPs have emerged as another possibility of exploiting these interactions, with the advantage of having available receptors of adjustable cavity size. Concave–convex $\pi\cdots\pi$ interactions are mostly governed by dispersion, so the design of receptors often relies on extending the contact surface between the host and the guest.[44] Therefore, the inclusion of dispersion effects is essential to study concave–convex $\pi\cdots\pi$ interactions, and it is expected to be so even in the case of the charged $M^+@C_{60}$ complexes. Thus, the use of dispersion-corrected DFT methods is almost compulsory. Among them, Grimme's empirical dispersion correction is one of the most popular and efficient procedures.[54] The original version (DFT-D),[55] was modified in 2006 (DFT-D2),[56] and further corrected in 2010 (DFT-D3),[57] and 2011 (DFT-D3(BJ)).[58]

Several previous works of our group have shown that the B97-D2 method displays a reasonable balance between the computational cost and the accuracy of the results.[59,60] In addition, we have also shown that the TPSS-D3(BJ) method can be an accurate option for studying $\pi\cdots\pi$ interactions.[36,61] The main difference between these two models is that the D3 flavour includes coordination number dependent dispersion coefficients. Therefore, B97-D2 and TPSS-D3(BJ) methods (using the def2-TZVP basis set) plus the resolution of identity approximation (RI) implemented in Turbomole program suite[62,63] (with the def2-TZVPP auxiliary basis set) have been employed for studying the systems considered in the present work.

When the $M^+@C_{60}\cdots$[10]CPP complex is formed, the spatial arrangement of the fullerene inside the belt may lead to a large number of different energy minima. Thus,

the search for the global minimum is not an easy task. In order to explore the Potential Energy Surface (PES) of the complexes, the following scanning procedure (already used in a previous work)[36] was carried out: the fullerene is placed at the centre of the [10]CPP and then it is allowed to rotate through a scanning of the three Euler angles (α, β, γ), using steps of 6 degrees. This procedure leads to the computation of a huge number of single point calculations for searching all the space. For that reason, these single point calculations are performed with the DFTB+ method (with the "3ob" parameters) to save computation time.[64–66] After this preliminary search, the most stable structures are fully optimised with the TPSS-D3(BJ) and B97-D2 methods and the def2-TZVP basis set using Turbomole 6.3, and subsequently the complexation energies are calculated as described below.

The counterpoise correction is applied to all reported interaction energies to avoid the basis set superposition error, BSSE.[67,68] According to this procedure, the interaction energy of a system A$\cdots$B is obtained as:

$$\Delta E_{\text{int}} = E_{\text{AB}}^{\text{AB}}(AB) - \left(E_{\text{A}}^{\text{AB}}(AB) + E_{\text{B}}^{\text{AB}}(AB)\right) \tag{8.1}$$

where superscripts refer to the geometry (that of the system AB) and the terms in parenthesis indicate the basis set used (the full basis set of the system A$\cdots$B). If, in addition, the energy cost involved in the deformation of each monomer to adopt the geometry of the dimer is considered:

$$\Delta E_{\text{def}} = \left(E_{\text{A}}^{\text{AB}}(A) - E_{\text{A}}^{\text{A}}(A)\right) + \left(E_{\text{B}}^{\text{AB}}(B) - E_{\text{B}}^{\text{B}}(B)\right) \tag{8.2}$$

the complexation energy is obtained as follows:

$$\Delta E_{\text{complex}} = \Delta E_{\text{int}} + \Delta E\text{def} \tag{8.3}$$

In order to study the electronic transitions and charge transfer between the host and the guest, TD-DFT calculations including 24 excited states at the CAM-B3LYP/TZVP level[69] with the RIJCOSX approach[70,71] were performed using ORCA 4.0 program package.[72] This functional has been shown to give reasonable results for charge transfer transitions[73] and it was already used in similar complexes.[74,75]

8.3 Results and discussion

8.3.1 $M^+@C_{60}$ endofullerenes

The structure of the endohedral $Li^+@C_{60}$ fullerene has been the subject of different studies trying to elucidate the position of the Li^+ cation inside the C_{60} cage and its dynamics. It has been found that the most favourable locations are close to the hexagonal rings of C_{60}, and that Li^+ moves by hopping and tunnelling among these equivalent minima. At temperatures below 100 K, Li^+ occupies two equivalent locations displaced towards a hexagonal ring and about 1.34 Å from the fullerene C_{60} centre,[19–22] in line with different theoretical estimations.[76–78] Thus, before studying how the $M^+@C_{60}\cdots$[10]CPP complex is formed, a study has been carried out to determine the location of the cation (Li^+, Na^+, K^+) inside the carbon cage of C_{60} and how this cation modifies the fullerene properties.

The cation has been located in three different places as starting points for unrestricted geometrical optimisations with the B97-D2 and TPSS-D3(BJ) methods. These three locations are: over the centre of a five-membered ring (R5), over the centre of a six-membered ring (R6), and in the centre of the fullerene (C). The main geometric and energetic results are shown in Table 8.1 for the B97-D2 method (results with TPSS-D3(BJ) are listed in Table e.1 in Appendix E).

Table 8.1: Energetic and geometric results of the optimised minima found for the $M^+@C_{60}$ complexes as obtained at the B97-D2/def2-TZVP level. Energies (kcal mol^{-1}) relative to the most stable minimum of each case. The optimisation is performed starting with the cation in three different locations inside C_{60}: R5 (with the cation close to a five-membered ring); R6 (with the cation close to a six-membered ring); C (with the cation at the centre of the fullerene).

	R5	R6	C
	Relative Energy (kcal mol^{-1})		
$Li^+@C_{60}$	0.36	0.00	22.24
$Na^+@C_{60}$	0.14	0.00	7.22
$K^+@C_{60}$	0.25	0.31	0.00
	Distance to C_{60} centre (Å)		
$Li^+@C_{60}$	1.424	1.408	0.000
$Na^+@C_{60}$	0.894	0.900	0.000
$K^+@C_{60}$	0.218	0.228	0.000

It can be observed in Table 8.1 that the most favourable position of Li^+ cation inside the C_{60} carbon cage is close to a six-membered ring, though the stability is pretty similar for the structure with the cation close to a five-membered ring. Locating Li^+ on the fullerene centre leads to an energy penalty of 22 kcal mol^{-1}, because in this position the Li^+ is too far away from the aromatic rings. In its most favourable position, the cation is located at about 1.4 Å from the centre of C_{60}, and therefore at around 1.8 Å above a six-membered face and about 2.3 Å from the nearest carbon atom. Thus, the carbon cage gives room enough for the small Li^+ cation to be located in an optimal position for the interaction with the aromatic inner surface of fullerene (1.8−1.9 Å for the interaction of Li^+ with benzene or phenol);[79,80] as a consequence, the cation occupies an off-centre position inside the carbon cage. This result agrees with the X-ray structure and with the B3LYP calculations previously performed.[76] In this type of complex (in which a small cation participates) it is not surprising that the results obtained with a functional that does not take dispersion into account (as B3LYP) are very similar to those obtained by a functional that it does (B97-D2). This is undoubtedly because these complexes are dominated by the combination of electrostatic and induction interactions, as already indicated in previous work in similar systems (in fact, the main contribution comes from the polarization of the carbon cage by the cation).[76,81]

In the case of the Na^+ cation, the results are similar to those for Li^+, and the most stable location for the cation is again close to a hexagonal ring. However, due to the larger size of Na^+, the cation is displaced 0.9 Å from the fullerene centre in order to interact with the fullerene inner surface at a favourable distance around 2.4 Å. While the small

Li^+ cation can be considered to be interacting with a single aromatic ring, as the cation becomes larger it can be expected that it can effectively interact with several aromatic rings, thus leading to a decrease in energy differences among the different locations. This is already observed in Na^+ (the cation located on the centre of the carbon cage penalises only by 7 kcal mol^{-1} instead of 22 kcal mol^{-1} for Li^+), and it is even clearer for K^+. Thus, in $K^+@C_{60}$ the three starting structures considered lead to almost isoenergetic structures, barely separated in energy by 0.3 kcal mol^{-1} though slightly favouring in this case the position of the cation located at the centre of the carbon cage. Due to the larger size of K^+, with the cation at the centre of C_{60}, the distance to the inner surface is around 3.3 Å, somewhat larger to that observed in other complexes of K^+ with aromatic species,[79,80] but allowing stabilising contacts with the whole inner surface of C_{60}.[82] In summary, the cations are located within the carbon cage according to their size to adopt a proper distance for the interaction with the inner surface of fullerene; so, the cation becomes closer to the centre of the fullerene as its size increases, already reaching with K^+ the central position.

As indicated in previous work, the interaction of cations with curved π systems is dominated by induction and electrostatics.[76,81] Considering the increasing polarizing power of the cations when going from K^+ to Li^+, it can be expected that the fullerene will be more intensely perturbed by Li^+ than by the other cations. There are hints of charge transfer between the cations and the fullerene so the positive charge of the complex is effectively distributed on the fullerene surface. It could be expected though, that at least in $Li^+@C_{60}$ the region near Li^+ would exhibit more positive charge. The Molecular Electrostatic Potentials (MEPs) of the $M^+@C_{60}$ complexes suggest (Figure e.1 in Appendix E) that the positively charged region is extended virtually uniformly over the entire external surface of the complex. The region close to the cation is slightly more positive than the opposite face of the fullerene (Figure e.2 in Appendix E), though the differences are small and it is quite likely that they have little or no effect on the location of the endofullerene inside the nanoring (though in other cases the effect of the cation can be relevant as already shown for the reactivity of Diels-Alder reactions).[31,32] Also, the MEPs obtained for the different $M^+@C_{60}$ species are very similar, indicating that the carbon cage can effectively shield the cation inside, hence the characteristics of the outer surfaces of $M^+@C_{60}$ are almost the same. This similarity between the different cation-containing $M^+@C_{60}$ complexes is also observed on the characteristics of frontier orbitals. The presence of the cation inside the C_{60} cage produces a shift on the values of the frontier orbitals relative to pristine C_{60}. However, both HOMO and LUMO are stabilised by a similar amount, so the HOMO-LUMO gap is basically the same in all fullerenes considered in this work (see Figure e.3 in Appendix E).

It has to be indicated that the results obtained with the TPSS-D3(BJ) method are similar (see Table e.1 in Appendix E) though there are some differences, especially in Na^+ complexes with all optimisations leading to a complex with the cation occupying the centre of the carbon cage. The differences surely are related with the dispersion model employed, but do not seem too relevant nor do they substantially modify the conclusions obtained, and they are not expected to affect the characteristics of the interaction between $M^+@C_{60}$ and [10]CPP. In any case, in the following the discussion will be centred on B97-D2 results (see TPSS-D3(BJ) ones in Appendix E).

8.3.2 $M^+@C_{60}\cdots$[10]CPP complexes

8.3.2.1 Structure and stability

As commented in the Computational Details section, to explore the potential energy surface of the complexes and find the most stable minima, a preliminary scanning procedure was applied where the endofullerene is rotated inside the [10]CPP ring (see the details in section E.4 in Appendix E). After this preliminary search, the most stable structures are fully optimised with the B97-D2 and the TPSS-D3(BJ) functionals, and subsequently the complexation energies are obtained. Table 8.2 shows results for the best structures found for the $M^+@C_{60}\cdots$[10]CPP complexes using the B97-D2 (see Figure 8.2) method considering two main orientations of the fullerene inside the ring (the trends obtained by TPSS-D3(BJ) are quite similar, though complexation energies are systematically about 3−5 kcal mol^{-1} less negative, see Table e.2). In structures labelled as $C_{60}(5)$ the axis that goes through the centre of a 5-membered top and bottom rings of C_{60} is placed perpendicularly to the nanoring; in those labelled as $C_{60}(6)$ the axis goes through the centre of a 6-membered top and bottom rings of C_{60} (see Figure 8.2 and e.18).

Table 8.2: Energetic results (kcal mol^{-1}) and point charges of the best structure found for the $M^+@C_{60}\cdots$[10]CPP complexes. $\Delta E_{\text{complex}}$ = complexation energy; E_{def} = deformation energy; ΔE_{disp} = contribution of dispersion to the total complexation energy; Q = charge of the fullerene according to Mulliken (Mull) and NBO analysis.

$M^+@C_{60}$[a]	$\Delta E_{\text{complex}}$	$\Delta E_{\text{def,fuller}}$	$\Delta E_{\text{def,[10]CPP}}$	ΔE_{disp}	$Q_{\text{fuller,Mull}}$	$Q_{\text{fuller,NBO}}$
$C_{60}(5)$	−49.78	0.11	0.23	−83.61	−0.058	−0.046
$C_{60}(6)$	−49.27	0.08	0.42	−83.55	−0.048	−0.090
$Li^+@C_{60}(5)$	−60.36	0.09	0.40	−84.81	0.783	0.895
$Li^+@C_{60}(6)$	−61.25	0.09	0.54	−85.39	0.746	0.817
$Na^+@C_{60}(5)$	−60.35	0.18	0.40	−85.09	0.776	0.890
$Na^+@C_{60}(6)$	−61.29	0.11	0.54	−85.76	0.739	0.814
$K^+@C_{60}(5)$	−60.10	0.43	0.40	−85.51	0.773	0.893
$K^+@C_{60}(6)$	−61.08	0.30	0.60	−85.99	0.742	0.819

[a] For each case the result of the best structure exhibiting a fullerene arrangement of $C_{60}(5)$ and $C_{60}(6)$ types is shown. $C_{60}(5)$: the axis that goes through the centre of a 5-membered top and bottom rings of C_{60} is placed perpendicularly to the nanoring; $C_{60}(6)$: the axis goes through the centre of a 6-membered top and bottom rings of C_{60}.

The most noteworthy result of Table 8.2 is that the presence of a cation (Li^+, Na^+, K^+) within the C_{60} cage produces a considerable improvement (of the order of −10 kcal mol^{-1}) on the complexation energy. On the other hand, there are no significant differences in the contribution of dispersion to the stability of the different complexes, indicating that the structures are pretty similar in all cases. Therefore, the differences must undoubtedly come from changes in the electrostatic and induction contributions to the stability. The cationic nature of $M^+@C_{60}$ produces stronger electrostatic interactions with the inner negative regions of [10]CPP. Another interesting conclusion that can be drawn from the results is that the complexation energy is very similar regardless of the cation involved. This result is not so strange either, since the cation inside the fullerene is effectively

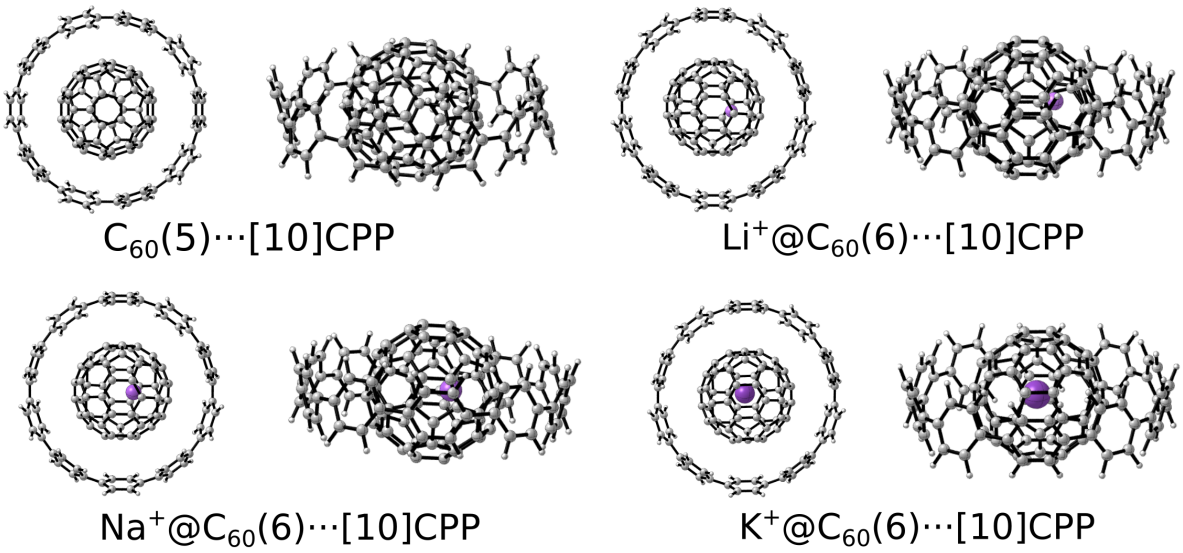

Figure 8.2: Most stable complexes found for the complexes of [10]CPP with C_{60} and $M^+@C_{60}$ at the B97-D2/def2-TZVP level.

shielded by the carbon cage and, as commented above, the positive charge is evenly spread among the sixty carbon atoms, irrespective of the nature of the cation inside the cage.

Regarding the two different spatial arrangements of the endofullerene relative to [10]CPP, the results are the same in all cases: the $C_{60}(6)$ is the preferred one, *i.e.*, the axis that goes through the centre of a 6-membered top and bottom rings of C_{60} is placed perpendicularly to the nanoring plane (or in other words, the fullerene is arranged with a six-membered ring at the top and bottom). Although the preference for this arrangement is not too large (never exceeding 1 kcal mol^{-1}), it is striking that it is precisely the opposite to the one observed with the pristine fullerene, since in that case (as already discussed in our previous work)[36] the favoured rearrangement is $C_{60}(5)$. Using the M05-2X functional, Rehman *et al.* came to the same conclusion, though the energy difference in favour of $C_{60}(6)$ arrangement is much smaller: only of 0.2 kcal mol^{-1}.[43] Therefore, it seems that in the cationic endofullerenes there must be some effect that makes the natural preference towards the $C_{60}(5)$ arrangement reversed. Dispersion is responsible of part of this change, since it becomes slightly more favourable for $C_{60}(6)$ structures in $M^+@C_{60}$. Also, a plausible hypothesis (in the light of the results of the point charges in Table 8.2) is based on the higher charge transfer that takes place when the fullerene adopts a $C_{60}(6)$ arrangement. Thus, for example, in the case of Li^+ cation, NBO results indicate that the charge transfer from [10]CPP to the fullerene is 0.183 a.u. for structure $C_{60}(6)$, but only 0.115 a.u. for structure $C_{60}(5)$. Similar results are obtained for the three cations, such that the $C_{60}(6)$ rearrangement always displaces more charge than the other arrangement (about 0.08 and 0.04 using NBO and Mulliken charges, respectively).

Despite being a complex formed by a cationic species, the interaction is clearly controlled by the contribution of dispersion, that roughly depends on the contact surface between host and guest (the same could be said of the repulsive term). Since the geometry of the C_{60} cage hardly changes when the cations are included, the match between [10]CPP and the different fullerenes is similar in all cases, leading to similarly stable

complexes. The final stabilities are tuned with significant but smaller contributions from electrostatics and induction. The presence of a cationic guest leads to more stable complexes, but without differentiating among cations due to the shielding and delocalization of charge accomplished by the carbon cage.

To improve the understanding of the interaction energy of the complexes, the contributions to the interaction energy have been estimated using two different approaches. The large size of the systems studied forces us to use a smaller basis set as def2-SVP, but at least a qualitative picture of the nature of the interaction can be obtained. Table 8.3 shows the values of contributions to the interaction energy obtained with SAPT0[83] (dispersion values from B97-D2) using PSI4.[84] As commented above, dispersion contributions are very similar in all complexes, so the energy differences must come from other contributions. As observed from the SAPT0 data in Table 8.3, it is clear that the extra stability of complexes containing $M^+@C_{60}$ comes from increased stabilising contributions from electrostatics (around -6 kcal mol^{-1}) and induction (around -8 kcal mol^{-1}). Therefore, as commented above, the presence of the cation enhances the electrostatic interaction but also the contribution from induction (in SAPT0 the induction term also includes the contributions from charge transfer).

Table 8.3: Contributions to the interaction energy obtained from two different procedures for the most stable complexes using the B97-D2 geometry. Local energy decomposition (LED) based on DLPNO-CCSD(T), and SAPT0, both with the def2-SVP basis set.

	SAPT0				LED			
	$E_{\text{disp,B97-D2}}$	E_{elec}	E_{rep}	E_{ind}	E_{disp}	E_{prep}	$E_{\text{Elec+Exch}}$	E_{CT}
C_{60}	−83.61	−32.13	71.00	−6.02	−84.20	186.72	−141.65	−6.71
$Li^+@C_{60}$	−85.39	−38.25	73.63	−14.08	−86.91	226.71	−187.12	−8.78
$Na^+@C_{60}$	−85.76	−38.20	73.89	−14.05	−87.03	226.93	−186.88	−8.74
$K^+@C_{60}$	−85.99	−37.78	72.92	−13.81	−86.75	223.67	−184.28	−8.52

E_{disp}: includes contributions from weak pairs and triple excitations; E_{CT}: charge transfer contribution; $E_{\text{Elec+Exch}}$: electrostatic plus inter-fragment exchange interaction; E_{prep}: preparation energy.

A totally different partitioning of the interaction energy can be accomplished by means of the Local Energy Decomposition (LED)[85] based on DLPNO-CCSD(T)[86,87] as implemented in ORCA 4.0.[72] LED allows obtaining insights into the nature of intermolecular interactions by defining two fragments and decomposing the DLPNO-CCSD(T) energy into physically meaningful contributions, which have been grouped for the sake of simplicity in Table 8.3 (see all individual contributions in Table e.6 in Appendix E). As indicated in Table 8.3, the largest contribution comes from the preparation energy, which represents how much energy is needed to bring the fragments into the electronic structure optimal for the interaction. This preparation energy is much larger in cation-containing complexes than in the complex with pristine C_{60}, but this effect is compensated by large electrostatic interactions. The sum of these two terms favours complexes with $M^+@C_{60}$ by around 5 kcal mol^{-1}. Besides, the charge transfer term also favours complexes with $M^+@C_{60}$, while dispersion contributions are pretty similar and quite close to the values obtained from the empirical model. Despite total complexation energies being less negative than the results

obtained with B97-D2 (the def2-SVP basis set is not flexible enough; see Figure e.19 for an estimation of the performance of DLPNO-CCSD(T) in concave–convex systems), the overall picture indicates that the stability gain observed in $M^+@C_{60}$ relative to pristine C_{60} ones is mainly related with changes in the electrostatic and (to a lesser extent) charge transfer contributions. This is consistent with the description of the interaction obtained from SAPT0.

8.3.2.2 Electronic transitions and charge transfer

An interesting feature of the complexes studied in this work is their use in photovoltaic devices or electronic switches, based on charge transfer from the CPP to the fullerene upon light absorption. In their isolation and characterization of [10]CPP$\cdots Li^+@C_{60}$ complex, Ueno *et al.* indicated that changes are registered on the absorption spectrum related to possible charge transfer transitions from the nanoring to the fullerene guest.[42] These charge transfer transitions seem to appear as broadened bands in the near infrared region and around 350 nm.

In order to study the electronic transitions in these complexes and whether they correspond to charge transfer transitions between the nanoring and the fullerene or intramolecular ones (intra-nanoring or intra-fullerene), the absorption spectra were obtained by means of TD-DFT calculations including 24 excited states at the CAM-B3LYP/TZVP level. Figure e.20 shows the absorption spectra of [10]CPP and the fullerenes considered in this work. [10]CPP shows an intense absorption band located around 325 nm at this level of calculation, in agreement with previous observations.[3] Pristine C_{60} exhibits a very weak absorption band around 350 nm, though there are other extremely weak transitions in the region between 400 and 500 nm. The presence of the cation changes significantly the characteristics of the spectra, and more intense signals appear around 350 nm and, especially, between 400 and 550 nm. These bands show similar positions to those observed in pristine C_{60}, though the intensity is larger due to the asymmetry introduced by the metal ion. In the case of $K^+@C_{60}$ the behaviour is very similar to that found in pristine C_{60}. This could be a consequence of K^+ being located almost at the centre of the carbon cage and thus introducing less asymmetry in the electronic structure of the fullerene than in the more off-centred $Li^+@C_{60}$ and $Na^+@C_{60}$ complexes. The analysis of these transitions shows that they mostly correspond to charge transfer from one region of the endofullerene to the region near the cation. In summary, any of the monomers show absorption bands in the near infrared region and therefore any new band observed must be a consequence of interactions in the complex (though not necessarily a charge transfer one).

Figure 8.3 shows the spectra obtained for the most stable complexes of [10]CPP with the fullerenes considered in this work in the region above 300 nm. It can be observed that two sets of bands appear in most complexes. There is one band in the region between 400 and 550 nm, that is compatible with the signal produced by the isolated fullerenes as indicated above. The most striking feature of the spectra of the cation-containing complexes is the appearance of a new band in the near infrared region, centred around 700 nm, and that cannot be originated from intramonomer transitions (the largest wavelength for an intrafullerene transition is around 500 nm).

Therefore, this new band must come from interactions in the complex absent in the isolated monomers, in agreement with the observations of Ueno *et al.*[42] The absorption

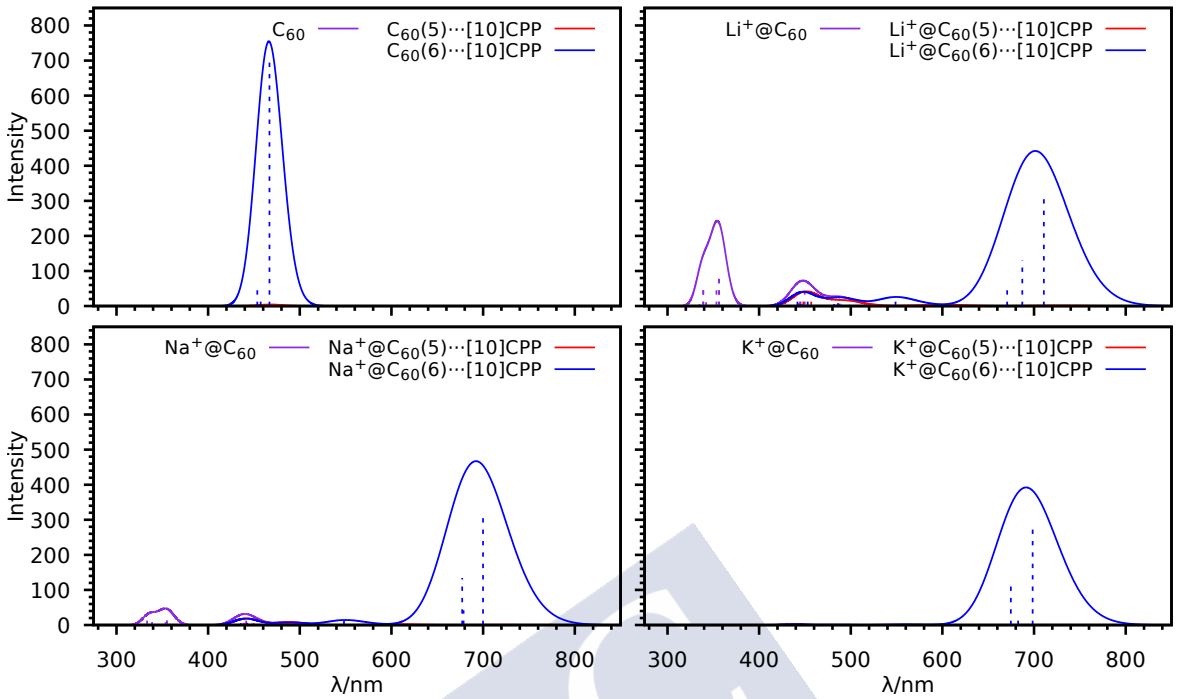

Figure 8.3: Absorption spectra for the $M^+@C_{60}\cdots$[10]CPP complexes obtained at the CAM-B3LYP/TZVP level, using B97-D2 geometries.

band at 700 nm appears in all complexes except in the one with pristine fullerene. Therefore, it is a clear indication of a differential behaviour associated to the presence of the endohedral cation, also in agreement with the observations of Ueno *et al.*[42] An interesting aspect of the spectra in Figure 8.3 is the different behaviour observed depending on the orientation of the fullerene inside the nanoring. As observed in Figure 8.3, while the complexes with $C_{60}(6)$ orientations give raise to an absorption band at 700 nm, this is not the case for the complexes with orientation $C_{60}(5)$. This could be a consequence of a smaller intensity in the case of $C_{60}(5)$ orientation, but even if the spectra are normalised (see Figure e.20 in Appendix E), complexes with orientation $C_{60}(5)$ do not show significant absorption in the region of 700 nm, or at least a very weak one compared to complexes with orientation $C_{60}(6)$. In the normalised spectra it can be clearly seen how the complexes with $C_{60}(5)$ orientation show absorption bands in the region between 400−550 nm that can be associated to transitions within the fullerenes. In complexes with $M^+@C_{60}$ the band is broadened compared to the complex with pristine fullerene, but this effect is also observed for isolated $M^+@C_{60}$.

However, it remains to be determined if the transitions giving rise to this new band are associated to charge transfer from [10]CPP to the fullerenes. Figure 8.4 shows the difference density between the excited state and the ground state for the four most intense transitions in the most stable structures. It can be observed that in the case of the complexes with pristine C_{60}, most transitions depicted in Figure 8.4 correspond to intra-fullerene charge rearrangements. Therefore, no charge transfer from the [10]CPP donor to the C_{60} acceptor is observed with the exception of one of the transitions in [10]CPP$\cdots C_{60}$ at around 380 nm. The behaviour is totally different in the case of $M^+@C_{60}$ complexes, with many of the transitions corresponding to an effective charge transfer from the nanor-

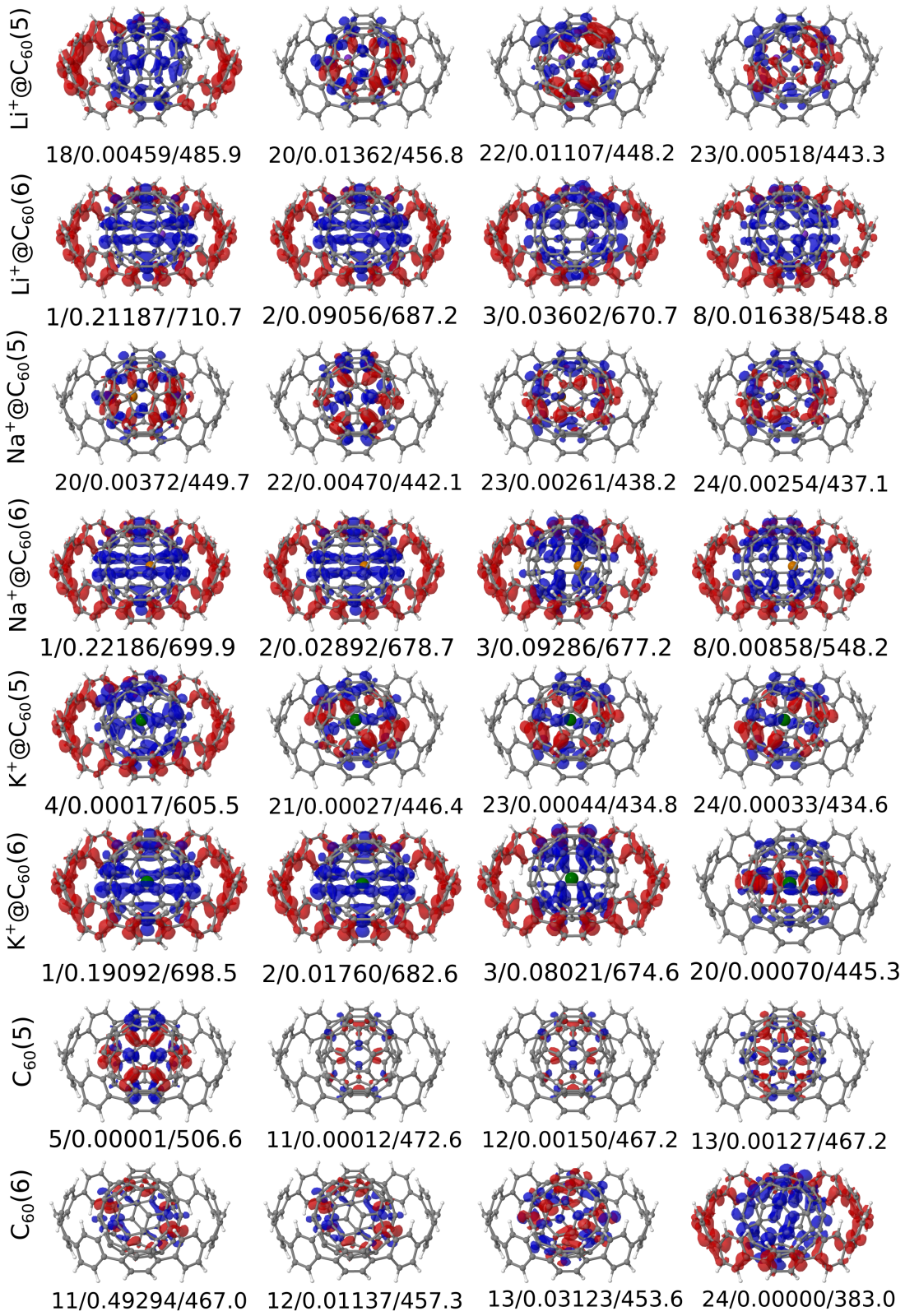

Figure 8.4: Difference density between the excited state and the ground state for the four most intense transitions in the most stable complexes found with B97-D2 (Table 8.2). Each of the rows corresponds to one of the fullerenes. The numbers are the number of the transition/oscillator strength*100/wavelength (nm). Surface corresponds to −0.001 a.u. (red) and 0.001 a.u. (blue).

ing to the fullerene, and located at around 700 nm as commented above. It can be observed that, overall, the $C_{60}(6)$ rearrangement of fullerene inside the nanoring facilitates intermolecular charge transfer in all complexes, while $C_{60}(5)$ mostly exhibits intrafullerene transitions, in agreement with the spectra in Figure 8.3.

In the case of $Li^+@C_{60}$ complexes, the four transitions depicted in Figure 8.4 correspond to intermolecular charge transfer if the fullerene is in $C_{60}(6)$ orientation, leading to absorption bands at around 700 nm. A similar pattern is obtained for the other $M^+@C_{60}$ complexes: if the fullerene is in $C_{60}(6)$ orientation, the most intense transitions correspond to intermolecular charge transfer from the nanoring to the endofullerene. While the behaviour of Na^+ and Li^+ containing complexes is very similar, the oscillator strengths of these transitions become weaker for K^+-containing complexes, in accordance with the spectra in Figure 8.3. It is also worth noting that in the case of complexes with $M^+@C_{60}$, the most intense transitions correspond to the lowest energy levels leading to absorption in the region around 700 nm. This is clearly different from the behaviour obtained for complexes with pristine fullerene or with $C_{60}(5)$ orientation, where the most intense transitions are much higher in energy, corresponding to the region around 450−500 nm. In $M^+@C_{60}$ complexes with $C_{60}(5)$ orientation, though, transitions are obtained for wavelengths in the 700 nm region, but due to the orientation of the fullerene, the intensity of these transitions is much smaller than those observed for the $C_{60}(6)$ orientation ($C_{60}(6)$ has intense transitions around 700 nm and weak ones around 450 nm, while the opposite happens for $C_{60}(5)$). Since the stability of these two orientations is pretty similar, it can be expected that both structures would be populated in a real sample, so the spectra should reveal mixed features.

In order to quantify the amount of charge transfer for a given transition, Jacquemin *et al.* proposed an index based on electron density, which allows computing both the amount of charge transferred and the distance between the barycentres of the negative and positive regions.[88,89] Table 8.4 summarizes these indexes for the transitions shown in Figure 8.4. It can be observed in Table 8.4 that for the cationic endofullerenes the charge transferred is larger in the cases in which the $C_{60}(6)$ rearrangement is involved. In all the cases where intermolecular charge transfer is observed, the amount of charge transferred from the host to the guest is large, and it is associated to lower energy transitions. Regarding the distances in Table 8.4, these have little relation to the character (inter or intra-monomer) of the transitions. In fact, it would even seem that for intermolecular charge transfer transitions the separation between barycentres of charge is smaller than for intramonomer transitions. This is a consequence of transitions from [10]CPP to the fullerenes spreading the charge symmetrically along the fullerene surface. For the intrafullerene transitions, charge is displaced from a region far from the cation, to a closer region leading to slightly larger distances between charge barycentres, while for intermolecular transitions charge is displaced from the whole ring of [10]CPP and distributed on the surface of the fullerene. Therefore, even though there is a significant displacement of charge, it is distributed quite symmetrically, leading to charge barycentres close to the centre of the C_{60} cage (see Figure e.22 and Table e.7 in Appendix E).

In any case, even though the distances between barycentres of charge are not determinant, the combination of the results in Figure 8.4 together with the amount of charge transferred clearly states that the new band that appears around 700 nm in the spectra of the complexes is directly related to intermolecular charge transfer from the [10]CPP host

Table 8.4: Amount of charge transferred and distance for the four most intense transitions as shown in Figure 8.3. N_{tr} is the transition to the N^{th} excited state, q is the amount of charge transferred and R is the distance between barycentres of positive and negative charges following ref. 88 and 89.

	N_{tr}	q	R (Å)		N_{tr}	q	R (Å)
$Li^+@C_{60}(6)$	1	0.978	0.440	$Li^+@C_{60}(5)$	18	0.918	0.706
	2	0.980	0.440		20	0.505	1.163
	3	0.975	0.470		22	0.527	0.779
	8	0.958	0.553		23	0.458	0.858
$Na^+@C_{60}(6)$	1	0.978	0.324	$Na^+@C_{60}(5)$	20	0.485	0.762
	2	0.980	0.323		22	0.544	0.402
	3	0.979	0.671		23	0.449	0.600
	8	0.959	0.454		24	0.459	0.598
$K^+@C_{60}(6)$	1	0.979	0.099	$K^+@C_{60}(5)$	4	0.985	0.076
	2	0.980	0.099		21	0.539	0.171
	3	0.979	0.130		23	0.523	0.140
	20	0.465	0.178		24	0.532	0.141
$C_{60}(6)$	11	0.361	0.000	$C_{60}(5)$	5	0.512	0.000
	12	0.376	0.000		11	0.265	0.000
	13	0.484	0.000		12	0.294	0.000
	24	0.981	0.001		13	0.370	0.000

to the $M^+@C_{60}$ guest. In fact, analysing all computed transitions it can be concluded that all transitions above 490 nm are associated to charge transfer from [10]CPP to the $M^+@C_{60}$ guest.

8.4 Conclusions

The complexes formed by [10]CPP and $M^+@C_{60}$ endofullerenes have been studied using DFT methods and their behaviour has been analysed taking the complex formed with pristine C_{60} as reference.

The results indicate that in these cationic endofullerenes, the cation is located at a proper distance for interacting with the aromatic inner surface of the carbon cage, and therefore it is displaced towards the centre of the fullerene as its size increases; while Li^+ occupies a clear off-centre position, K^+ is almost located on the centre of the carbon cage. Despite these different locations, the positive charge is effectively shielded by the fullerene, so it is shared among the sixty carbon atoms and evenly spread over the surface of C_{60}. As a consequence, the nature of the cation has little influence on the results obtained for the complexes.

Compared to the complex formed by [10]CPP and C_{60}, the complexes containing $M^+@C_{60}$ endofullerenes are very similar in terms of structure and stability. However, the presence of the cationic moiety has a clear impact on the stability of the complexes, which is reinforced by around -10 kcal mol^{-1}, regardless of the cation, compared to the complex

with pristine C_{60}. Though the interaction is dominated by dispersion contributions of similar magnitude in all complexes, the presence of the cation leads to an increase on electrostatic and induction interactions responsible of the enhancement on stability.

The inclusion of the cations has a clear impact on the absorption spectra of the complexes. In all complexes containing $M^+@C_{60}$ an absorption band appears around 700 nm, which is absent in the complex with pristine C_{60}. The analysis of the transitions clearly indicates that these new bands are associated to intermolecular charge transfer from the [10]CPP host to the $M^+@C_{60}$ guest, and therefore render these species as a promising option in the field of organic photovoltaic devices.

References

(1) S. E. Lewis, *Chemical Society Reviews*, 2015, **44**, 2221–2304.

(2) D. Wu, W. Cheng, X. Ban and J. Xia, *Asian Journal of Organic Chemistry*, 2018, **7**, 2161–2181.

(3) T. Iwamoto, Y. Watanabe, Y. Sakamoto, T. Suzuki and S. Yamago, *Journal of the American Chemical Society*, 2011, **133**, 8354–8361.

(4) H. Omachi, Y. Segawa and K. Itami, *Accounts of Chemical Research*, 2012, **45**, 1378–1389.

(5) E. Kayahara, V. K. Patel and S. Yamago, *Journal of the American Chemical Society*, 2014, **136**, 2284–2287.

(6) Y. Segawa, A. Yagi, K. Matsui and K. Itami, *Angewandte Chemie - International Edition*, 2016, **55**, 5136–5158.

(7) S. Hashimoto, E. Kayahara, Y. Mizuhata, N. Tokitoh, K. Takeuchi, F. Ozawa and S. Yamago, *Organic Letters*, 2018, **20**, 5973–5976.

(8) T. A. Schaub, J. T. Margraf, L. Zakharov, K. Reuter and R. Jasti, *Angewandte Chemie - International Edition*, 2018, **57**, 16348.

(9) S. Nishigaki, M. Fukui, H. Sugiyama, H. Uekusa, S. Kawauchi, Y. Shibata and K. Tanaka, *Chemistry - A European Journal*, 2017, **23**, 7227–7231.

(10) T. Kuwabara, J. Orii, Y. Segawa and K. Itami, *Angewandte Chemie - International Edition*, 2015, **54**, 9646–9649.

(11) E. R. Darzi and R. Jasti, *Chemical Society Reviews*, 2015, **44**, 6401–6410.

(12) T. Kawase and H. Kurata, *Chemical Reviews*, 2006, **106**, 5250–5273.

(13) N. Martín and J.-F. Nierengarten, *Supramolecular Chemistry of Fullerenes and Carbon Nanotubes*, Wiley-VCH Verlag GmbH & Co. KGaA, Weinheim, Germany, 2012.

(14) H. W. Kroto, J. R. Heath, S. C. O'Brien, R. F. Curl and R. E. Smalley, *Nature*, 1985, **318**, 162–163.

(15) A. Hirsch and M. Brettreich, *Fullerenes: Chemistry and Reactions*, Wiley-VCH, Weiheim, Germany, 2005.

(16) F. Langa and J.-F. Nierengarten, *Fullerenes: Principles and Applications*, Royal Society of Chemistry Publishing, Cambridge CB4 0WF, UK, 2012.

(17) X. Lu, L. Echegoyen, A. L. Balch, S. Nagase and T. Akasaka, *Endohedral Metallofullerenes: Basics and Applications*, CRC Press Taylor & Francis Group, Boca Raton, FL, USA, 2015.

(18) A. A. Popov, S. Yang and L. Dunsch, *Chemical Reviews*, 2013, **113**, 5989–6113.

(19) S. Aoyagi, E. Nishibori, H. Sawa, K. Sugimoto, M. Takata, Y. Miyata, R. Kitaura, H. Shinohara, H. Okada, T. Sakai, Y. Ono, K. Kawachi, K. Yokoo, S. Ono, K. Omote, Y. Kasama, S. Ishikawa, T. Komuro and H. Tobita, *Nature Chemistry*, 2010, **2**, 678–683.

(20) S. Aoyagi, Y. Sado, E. Nishibori, H. Sawa, H. Okada, H. Tobita, Y. Kasama, R. Kitaura and H. Shinohara, *Angewandte Chemie - International Edition*, 2012, **51**, 3377–3381.

(21) S. Aoyagi, A. Tokumitu, K. Sugimoto, H. Okada, N. Hoshino and T. Akutagawa, *Journal of the Physical Society of Japan*, 2016, **85**, 094605.

(22) S. Aoyagi, K. Miwa, H. Ueno, H. Okada, Y. Matsuo and K. Kokubo, *Royal Society open science*, 2018, **5**, 180337.

(23) C. Brabec, V. Dyakonov and U. Scherf, *Organic Photovoltaics: Materials, Device Physics, and Manufacturing Technologies*, ed. C. Brabec, V. Dyakonov and U. Scherf, Wiley-VCH Verlag GmbH & Co. KGaA, Weinheim, Germany, 2008.

(24) G. Dennler, M. C. Scharber and C. J. Brabec, *Advanced Materials*, 2009, **21**, 1323–1338.

(25) S. Fukuzumi and K. Ohkubo, *Dalton Transactions*, 2013, **42**, 15846–15858.

(26) K. Ohkubo, Y. Kawashima, H. Sakai, T. Hasobe and S. Fukuzumi, *Chemical Communications*, 2013, **49**, 4474–4476.

(27) H. Sakai, T. Kamimura, F. Tani and T. Hasobe, *Journal of Porphyrins and Phthalocyanines*, 2015, **19**, 242–250.

(28) C. M. Tran, H. Sakai, Y. Kawashima, K. Ohkubo, S. Fukuzumi and H. Murata, *Organic Electronics: physics, materials, applications*, 2017, **45**, 234–239.

(29) M. Supur, Y. Kawashima, K. Ohkubo, H. Sakai, T. Hasobe and S. Fukuzumi, *Physical Chemistry Chemical Physics*, 2015, **17**, 15732–15738.

(30) H. Ueno, S. Aoyagi, Y. Yamazaki, K. Ohkubo, N. Ikuma, H. Okada, T. Kato, Y. Matsuo, S. Fukuzumi and K. Kokubo, *Chemical Science*, 2016, **7**, 5770–5774.

(31) Y. García-Rodeja, M. Solà, F. M. Bickelhaupt and I. Fernández, *Chemistry - A European Journal*, 2017, **23**, 11030–11036.

(32) H. Ueno, H. Kawakami, K. Nakagawa, H. Okada, N. Ikuma, S. Aoyagi, K. Kokubo, Y. Matsuo and T. Oshima, *Journal of the American Chemical Society*, 2014, **136**, 11162–11167.

(33) T. Iwamoto, Y. Watanabe, T. Sadahiro, T. Haino and S. Yamago, *Angewandte Chemie - International Edition*, 2011, **50**, 8342–8344.

(34) J. Xia, J. W. Bacon and R. Jasti, *Chemical Science*, 2012, **3**, 3018–3021.

(35) T. Iwamoto, Y. Watanabe, H. Takaya, T. Haino, N. Yasuda and S. Yamago, *Chemistry - A European Journal*, 2013, **19**, 14061–14068.

(36) I. González-Veloso, J. Rodríguez-Otero and E. M. Cabaleiro-Lago, *Physical Chemistry Chemical Physics*, 2016, **18**, 31670–31679.

(37) I. González-Veloso, E. M. Cabaleiro-Lago and J. Rodríguez-Otero, *Physical Chemistry Chemical Physics*, 2018, **20**, 11347–11358.

(38) K. Yuan, Y.-J. Guo and X. Zhao, *The Journal of Physical Chemistry C*, 2015, **119**, 5168–5179.

(39) K. Yuan, C.-H. Zhou, Y.-C. Zhu and X. Zhao, *Physical Chemistry Chemical Physics*, 2015, **17**, 18802–18812.

(40) H. Isobe, S. Hitosugi, T. Yamasaki and R. Iizuka, *Chemical Science*, 2013, **4**, 1293–1287.

(41) Y. Nakanishi, H. Omachi, S. Matsuura, Y. Miyata, R. Kitaura, Y. Segawa, K. Itami and H. Shinohara, *Angewandte Chemie - International Edition*, 2014, **53**, 3102–3106.

(42) H. Ueno, T. Nishihara, Y. Segawa and K. Itami, *Angewandte Chemie - International Edition*, 2015, **54**, 3707–3711.

(43) H. U. Rehman, N. A. McKee and M. L. McKee, *Journal of Computational Chemistry*, 2016, **37**, 194–209.

(44) E. M. Pérez and N. Martín, *Chemical Society Reviews*, 2015, **44**, 6425–6433.

(45) A. Sygula, F. R. Fronczek, R. Sygula, P. W. Rabideau and M. M. Olmstead, *Journal of the American Chemical Society*, 2007, **129**, 3842–3843.

(46) M. A. Petrukhina and L. T. Scott, *Fragments of Fullerenes and Carbon Nanotubes*, John Wiley & Sons, Hoboken, New Jersey, 2012.

(47) D. Josa, J. Rodríguez-Otero, E. M. Cabaleiro-Lago, L. A. Santos and T. C. Ramalho, *Journal of Physical Chemistry A*, 2014, **118**, 9521–9528.

(48) D. Josa, L. Azevedo dos Santos, I. González-Veloso, J. Rodríguez-Otero, E. M. Cabaleiro-Lago and T. de Castro Ramalho, *RSC Advances*, 2014, **4**, 29826–29833.

(49) D. Josa, I. González-Veloso, J. Rodríguez-Otero and E. M. Cabaleiro-Lago, *Physical Chemistry Chemical Physics*, 2015, **17**, 6233–6241.

(50) D. Josa, J. Rodríguez-Otero and E. M. Cabaleiro-Lago, *Physical Chemistry Chemical Physics*, 2015, **17**, 13206–13214.

(51) P. A. Denis, *Journal of Physical Organic Chemistry*, 2014, **27**, 918–925.

(52) P. A. Denis, *RSC Advances*, 2013, **3**, 25296–25305.

(53) P. A. Denis, *Chemical Physics Letters*, 2014, **591**, 323–327.

(54) S. Grimme, *Wiley Interdisciplinary Reviews: Computational Molecular Science*, 2011, **1**, 211–228.

(55) S. Grimme, *Journal of Computational Chemistry*, 2004, **25**, 1463–1473.

(56) S. Grimme, *Journal of Computational Chemistry*, 2006, **27**, 1787–1799.

(57) S. Grimme, J. Antony, S. Ehrlich and H. Krieg, *Journal of Chemical Physics*, 2010, **132**, 154104.

(58) S. Grimme, S. Ehrlich and L. Goerigk, *Journal of Computational Chemistry*, 2011, **32**, 1456–1465.

(59) D. Josa, J. Rodríguez-Otero and E. M. Cabaleiro-Lago, *Physical Chemistry Chemical Physics*, 2011, **13**, 21139–21145.

(60) D. Josa, J. Rodríguez-Otero, E. M. Cabaleiro-Lago and M. Rellán-Piñeiro, *Chemical Physics Letters*, 2013, **557**, 170–175.

(61) E. M. Cabaleiro-Lago, B. Fernández and J. Rodríguez-Otero, *Journal of Computational Chemistry*, 2018, **39**, 93–104.

(62) TURBOMOLE V6.3 2011, a development of University of Karlsruhe and Forschungszentrum Karlsruhe GmbH, 1989-2007, TURBOMOLE GmbH, since 2007; available from, http://www.turbomole.com.

(63) R. Ahlrichs, M. Bär, M. Häser, H. Horn and C. Kölmel, *Chemical Physics Letters*, 1989, **162**, 165–169.

(64) B. Aradi, B. Hourahine and T. Frauenheim, *Journal of Physical Chemistry A*, 2007, **111**, 5678–5684.

(65) M. Gaus, A. Goez and M. Elstner, *Journal of Chemical Theory and Computation*, 2013, **9**, 338–354.

(66) M. Kubillus, T. Kubař, M. Gaus, J. Řezáč and M. Elstner, *Journal of Chemical Theory and Computation*, 2015, **11**, 332–342.

(67) S. F. Boys and F. Bernardi, *Molecular Physics*, 1970, **19**, 553–566.

(68) G. Chałasiński and M. M. Szczęśniak, *Chemical Reviews*, 2000, **100**, 4227–4252.

(69) T. Yanai, D. P. Tew and N. C. Handy, *Chemical Physics Letters*, 2004, **393**, 51–57.

(70) F. Neese, F. Wennmohs, A. Hansen and U. Becker, *Chemical Physics*, 2009, **356**, 98–109.

(71) R. Izsák and F. Neese, *Journal of Chemical Physics*, 2011, **135**, 144105.

(72) F. Neese, *Wiley Interdisciplinary Reviews: Computational Molecular Science*, 2012, **2**, 73–78.

(73) M. J. G. Peach, P. Benfield, T. Helgaker and D. J. Tozer, *The Journal of Chemical Physics*, 2008, **128**, 044118.

(74) E. M. Cabaleiro-Lago, J. Rodríguez-Otero and J. A. Carrazana-García, *Physical Chemistry Chemical Physics*, 2017, **19**, 26787–26798.

(75) I. González-Veloso, J. Rodríguez-Otero and E. M. Cabaleiro-Lago, *Physical Chemistry Chemical Physics*, 2018, **20**, 27791–27803.

(76) J. A. Carrazana-García, J. Rodríguez-Otero and E. M. Cabaleiro-Lago, *Journal of Physical Chemistry B*, 2011, **115**, 2774–2782.

(77) O. Vital de Oliveira, A. d. S. Gonçalves, O. V. D. Oliveira and A. d. S. Gonçalves, *Computational Chemistry*, 2004, **2**, 51–58.

(78) D. Vijay, H. Sakurai, V. Subramanian and G. N. Sastry, *Physical Chemistry Chemical Physics*, 2012, **14**, 3057–3065.

(79) C. Coletti and N. Re, *Journal of Physical Chemistry A*, 2006, **110**, 6563–6570.

(80) A. Campo-Cacharrón, E. M. Cabaleiro-Lago and J. Rodríguez-Otero, *Theoretical Chemistry Accounts*, 2012, **131**, 1–13.

(81) A. Campo-Cacharrón, E. M. Cabaleiro-Lago and J. Rodríguez-Otero, *Journal of Computational Chemistry*, 2014, **35**, 1533–1544.

(82) I. González-Veloso, J. A. Carrazana-García, D. Josa, J. Rodríguez-Otero and E. M. Cabaleiro-Lago, *Computational and Theoretical Chemistry*, 2015, **1053**, 123–129.

(83) T. M. Parker, L. A. Burns, R. M. Parrish, A. G. Ryno and C. D. Sherrill, *Journal of Chemical Physics*, 2014, **140**, 094106.

(84) J. M. Turney, A. C. Simmonett, R. M. Parrish, E. G. Hohenstein, F. A. Evangelista, J. T. Fermann, B. J. Mintz, L. A. Burns, J. J. Wilke, M. L. Abrams, N. J. Russ, M. L. Leininger, C. L. Janssen, E. T. Seidl, W. D. Allen, H. F. Schaefer, R. A. King, E. F. Valeev, C. D. Sherrill and T. D. Crawford, *Wiley Interdisciplinary Reviews: Computational Molecular Science*, 2012, **2**, 556–565.

(85) W. B. Schneider, G. Bistoni, M. Sparta, M. Saitow, C. Riplinger, A. A. Auer and F. Neese, *Journal of Chemical Theory and Computation*, 2016, **12**, 4778–4792.

(86) C. Riplinger and F. Neese, *Journal of Chemical Physics*, 2013, **138**, 034106.

(87) C. Riplinger, B. Sandhoefer, A. Hansen and F. Neese, *Journal of Chemical Physics*, 2013, **139**, 134101.

(88) D. Jacquemin, T. L. Bahers, C. Adamo and I. Ciofini, *Physical Chemistry Chemical Physics*, 2012, **14**, 5383–5388.

(89) T. Le Bahers, C. Adamo and I. Ciofini, *Journal of Chemical Theory and Computation*, 2011, **7**, 2498–2506.

USC
UNIVERSIDADE
DE SANTIAGO
DE COMPOSTELA

Chapter 9

Conclusions

A theoretical study of the complexes formed by fullerenes and carbon nanorings has been carried out to provide a deeper knowledge of the characteristics of these systems and their potential for selective encapsulation forming donor/acceptor pairs for photovoltaic devices. The systems studied were dimers formed by different fullerenes, comprising pristine fullerenes of different size and shape as well as fullerenes bearing endohedral species, with a series of carbon nanorings, mostly cycloparaphenylenes, of different size.

The main conclusions of this study are:

- The potential energy surface of these complexes is quite flat, showing a variety of minima with similar complexation energies. The DFT-D methods tested, as well as the M06-2X, supply similar trends for the complexation energies and structures of the complexes. However, M06-2X greatly underestimates complexation energies and therefore is not recommended for studying the interaction in these systems.

- Despite the flatness of the potential energy surface, in most cases a restricted exploration based on choosing some orientations of the fullerene and rotating and displacing them inside the nanoring is fair enough for exploring the potential surface of the complexes. Also, an even more strict exploration based on rotations of the fullerene inside the ring following Euler angles has proven effective, but with a very high computational cost.

- [10]CPP is a better "catcher" than [6]CPPA for pristine fullerenes because its structure with more phenyl units allows to establish more favourable interactions between the fullerene and the nanoring. The main component of these interactions is dispersion, so an increased interacting surface produces more stable complexes.

- When the size of the fullerene increases, the strength of the interaction increases until reaching a certain size, after which, the complexation energy remains almost constant because the cavity of the nanoring is roughly filled. In the case of the [10]CPP this limit is already reached with C_{70} while in [6]CPPA it is reached even before, with C_{60}, due to the smaller size of the nanoring.

- Anthracene-substituted [10]CPPs are too big for fullerenes C_{60} and C_{70}, so the complexes are not as stable as those showing a proper size match (as [10]CPP-C_{60}). Thus, fullerenes move away from the centre. This displacement of the fullerene away

from the anthracene moiety but still in the plane of the nanohoop is accompanied by a deformation of the host with the purpose to increase the interaction surface. Despite the large contribution from dispersion to the stability of these complexes, the amount of energy spent in this deformation will determine the relative stabilities of the complexes.

- Intermolecular charge transfer is possible in complexes formed by anthracene-substituted nanohoops and fullerenes, as revealed by different very intense transitions. In these complexes the fullerene acts as an acceptor due to its electron-deficient behaviour whereas the cycloparaphenylene units in the nanohoop act as donors. Even though the anthracene moiety has not direct participation in the charge transfer process, its presence seems to promote intermolecular charge transfer.

- The use of anthracene-substituted nanohoops ([8]CPP derivatives) ensuring a proper size match with the encapsulated fullerene provides a system showing both a remarkable stability while keeping the charge transfer properties observed with larger nanorings.

- Carbon nanorings could be employed for the selective separation of fullerenes of different size. Thus, [11]CPP can discriminate between fullerenes larger than C_{76} from a mixture containing smaller fullerenes. However, the interaction is mainly controlled by dispersion and by a proper size match between the fullerene and the carbon nanoring and, therefore, [11]CPP could not possibly be employed for separation among different C_{80} and C_{82} derivatives.

- Despite all the complexes with endohedral fullerenes being controlled by dispersion, the fullerene is oriented with the carbon atoms contacting with the endohedral unit and simultaneously interacting with the phenylene units of the nanoring. Probably, this is a consequence of the greater polarity of these endofullerenes, which show electrostatic positive regions (that interact favourably with the negative regions of the phenylene units in the nanoring) around the carbon atoms contacting with the endohedral units.

- Complexes formed by [11]CPP and different endohedral fullerenes show very similar stabilities, unregarding of the metallic species inside, their number or even whether it is a closed- or open-shell structure. This indicates that the fullerene carbon cage is capable of fully shielding the endohedral unit, so that the inner surface of the nanoring only "feels" this carbon cage.

- Even when the endohedral unit is an alkali cation, the fullerene carbon cage does not display a clearly positive region, indicating that the positive charge is distributed over all the carbon atoms and is effectively shielded from the nanoring.

- The presence of the endohedral cation hardly affects to the structure of the complex with [10]CPP when compared with the pristine fullerene, though the most favourable orientation of C_{60} inside the ring changes. However, the cation produces an enhancement of around 20% on the stability of the complex as a consequence of larger electrostatic and inductive contributions.

- The endohedral cation also promotes intermolecular charge transfer transitions, with a new intense band appearing on the absorption spectra around 700 nm, related to electron transfer from the carbon nanoring to the fullerene.

- Overall, the interaction between fullerenes and carbon nanorings is mostly controlled by dispersion, so the stability roughly increases with the increase of the contact surface between guest and host. This is the principal factor controlling stability and the main design parameter for obtaining efficient receptors. Besides, other smaller factors can alter the stability, such as the energy cost for ring deformation or the presence of more polar regions in both fullerene and carbon nanoring.

- Modification of the electronic characteristics of the fullerene (including endohedral species) or of the nanoring (by proper functionalization as reported for the anthracene-substituted derivatives) can promote intermolecular charge transfer from the nanoring to the hosted fullerene.

In summary, the proper combination of size and shape matching, and the electronic complementarity opens a promising way to obtain systems for organic photovoltaic devices, selective encapsulation of fullerenes or for building up microscopically ordered donor/acceptor structures.

USC UNIVERSIDADE DE SANTIAGO DE COMPOSTELA

USC
UNIVERSIDADE
DE SANTIAGO
DE COMPOSTELA

Appendix A

Supplementary information Chapter 4

A.1 Rotation throught Euler angles

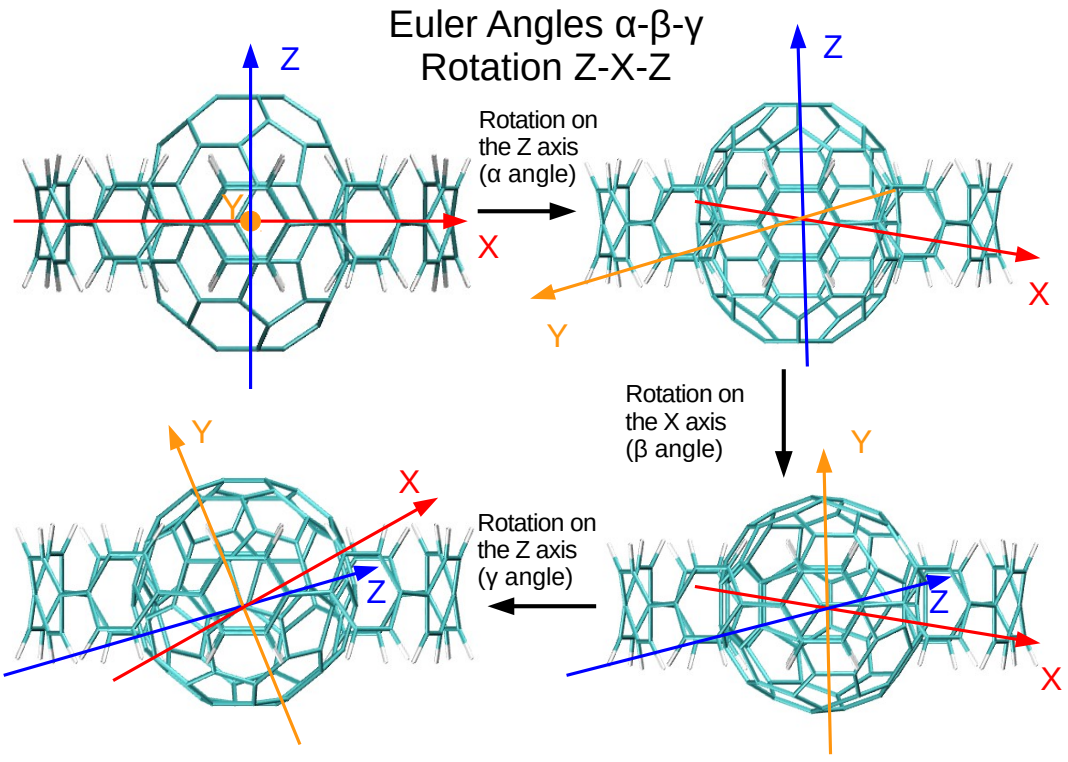

Figure a.1: Description of the rotation through the three Euler angles.

A.2 Vertical departure of the C_{60}

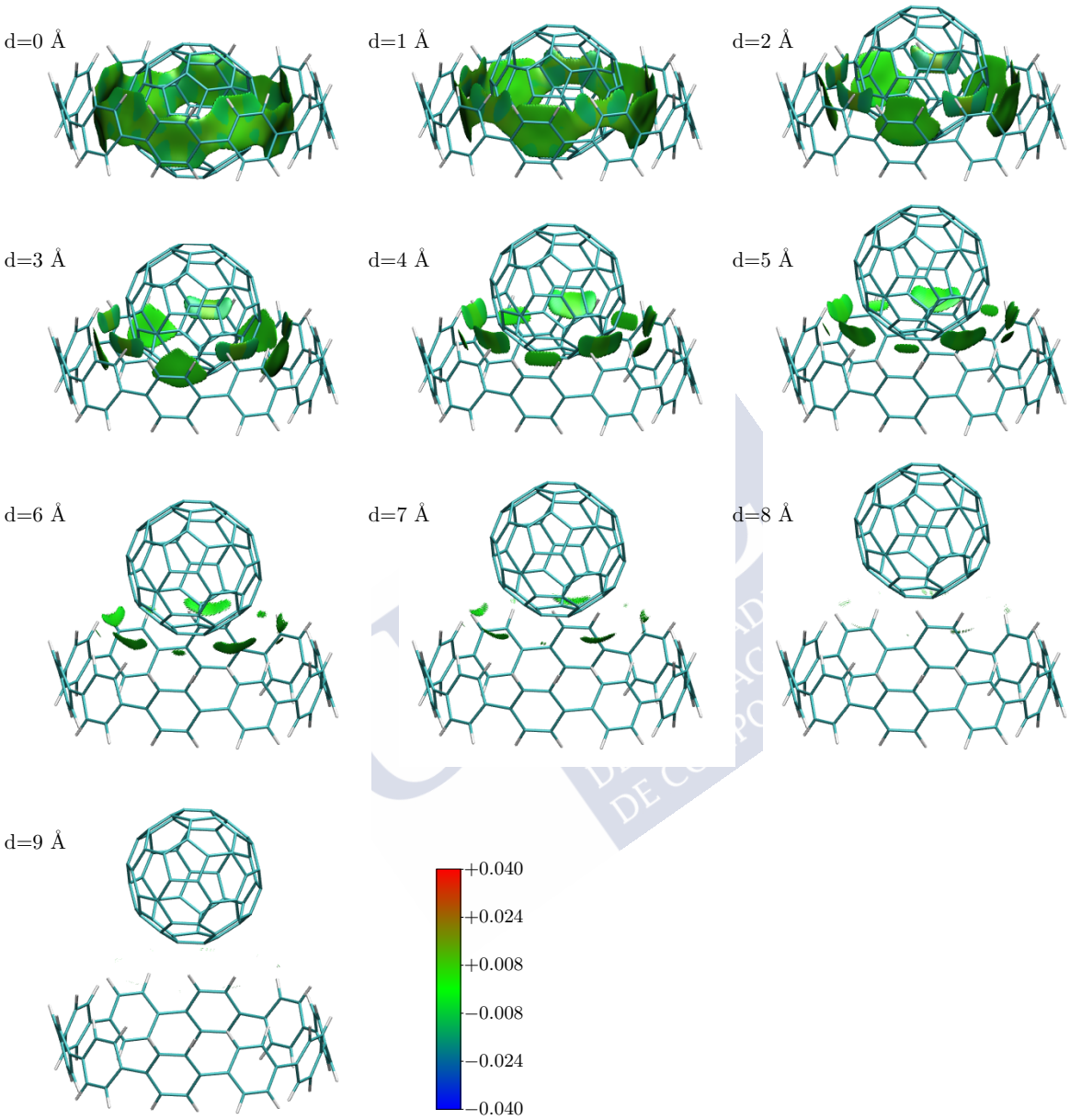

Figure a.2: NCIPLOT gradient isosurface (0.3 a.u.) corresponding to the vertical departure of C_{60} from [10]CPP (Figure 4.4a shows the energetic profile). Shortly after 8 Å, the isosurface vanishes.

A.3 Searching minima of complex C_{60}@[10]CPP with a systematic scanning procedure.

1) Scanning the three Euler angles:

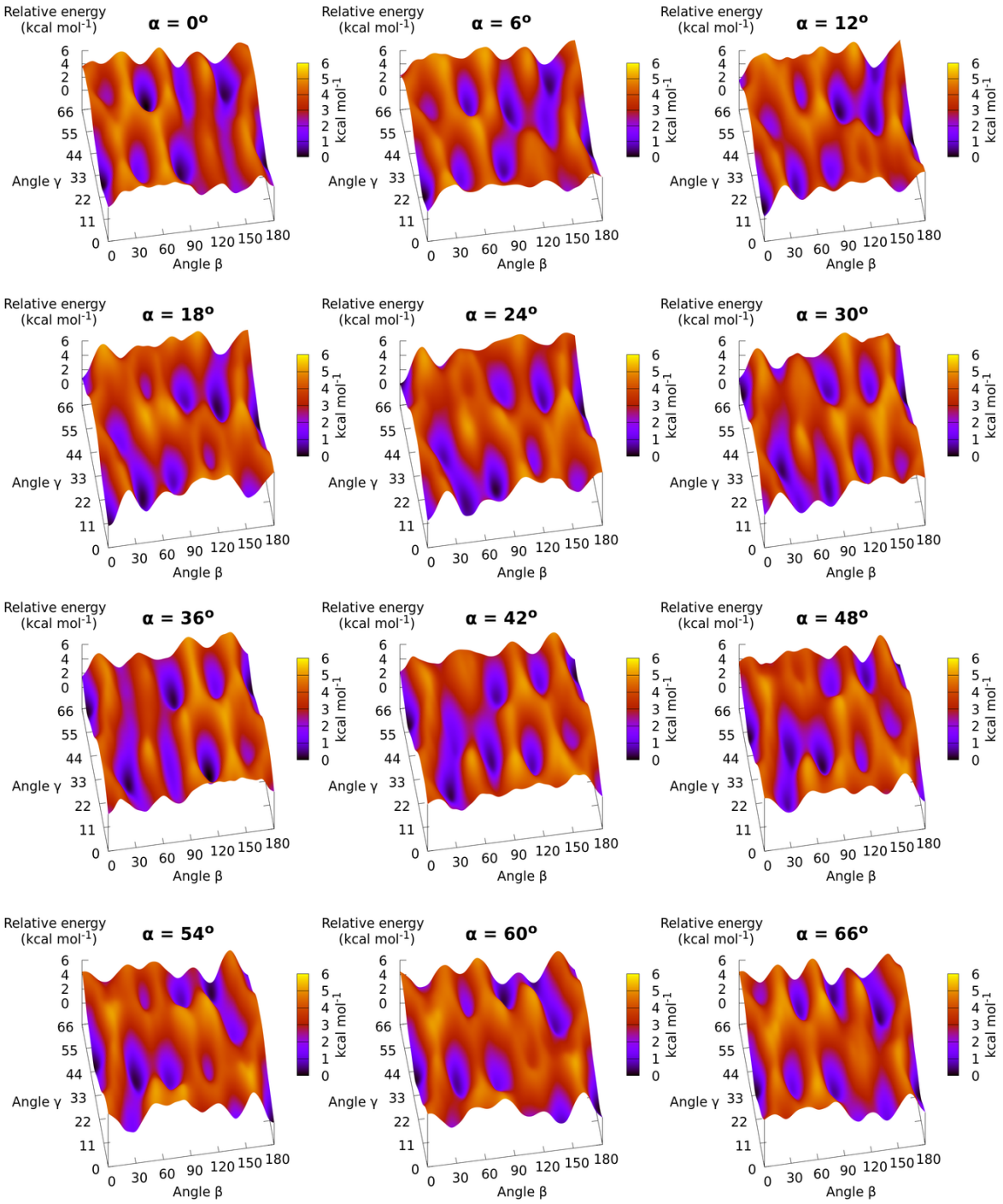

2) Looking for the minima:

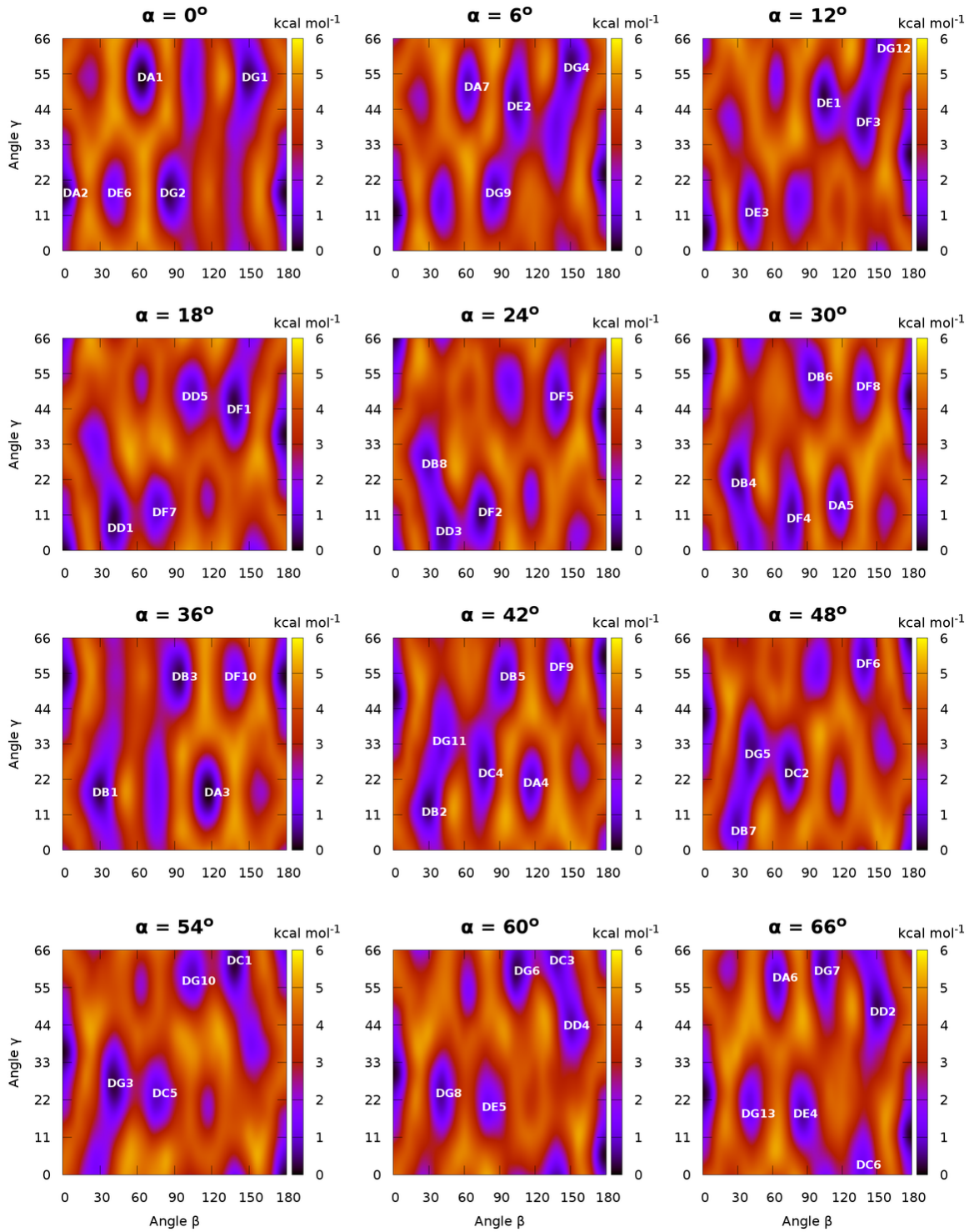

3) Classifying the minima in "families":

4) Optimization of the best structure of each family at the B97-D2/def2-TZVP level. Complexation energy calculation ($\Delta E_{\text{complex}}$). All energies are in kcal mol^{-1}.

	$\Delta E_{\text{complex}}$	ΔE_{def}		Dispersion
		C_{60}	[10]CPP	
DA1	−49.78	0.11	0.23	−83.61
DB1	−49.27	0.08	0.39	−83.52
DC1	−49.24	0.08	0.42	−83.64
DD1	−49.23	0.10	0.42	−83.65
DE1	−49.23	0.11	0.43	−83.62
DF1	−49.26	0.07	0.40	−83.60
DG1	−49.23	0.13	0.40	−83.56

DA1 corresponds to minimum I of Figure 4.3.
DB1–DG1 are virtually the same structure and correspond to minimum III of Figure 4.3.

USC UNIVERSIDADE DE SANTIAGO DE COMPOSTELA

A.4 Searching minima of complex C_{60}@[6]CPPA with a systematic scanning procedure.

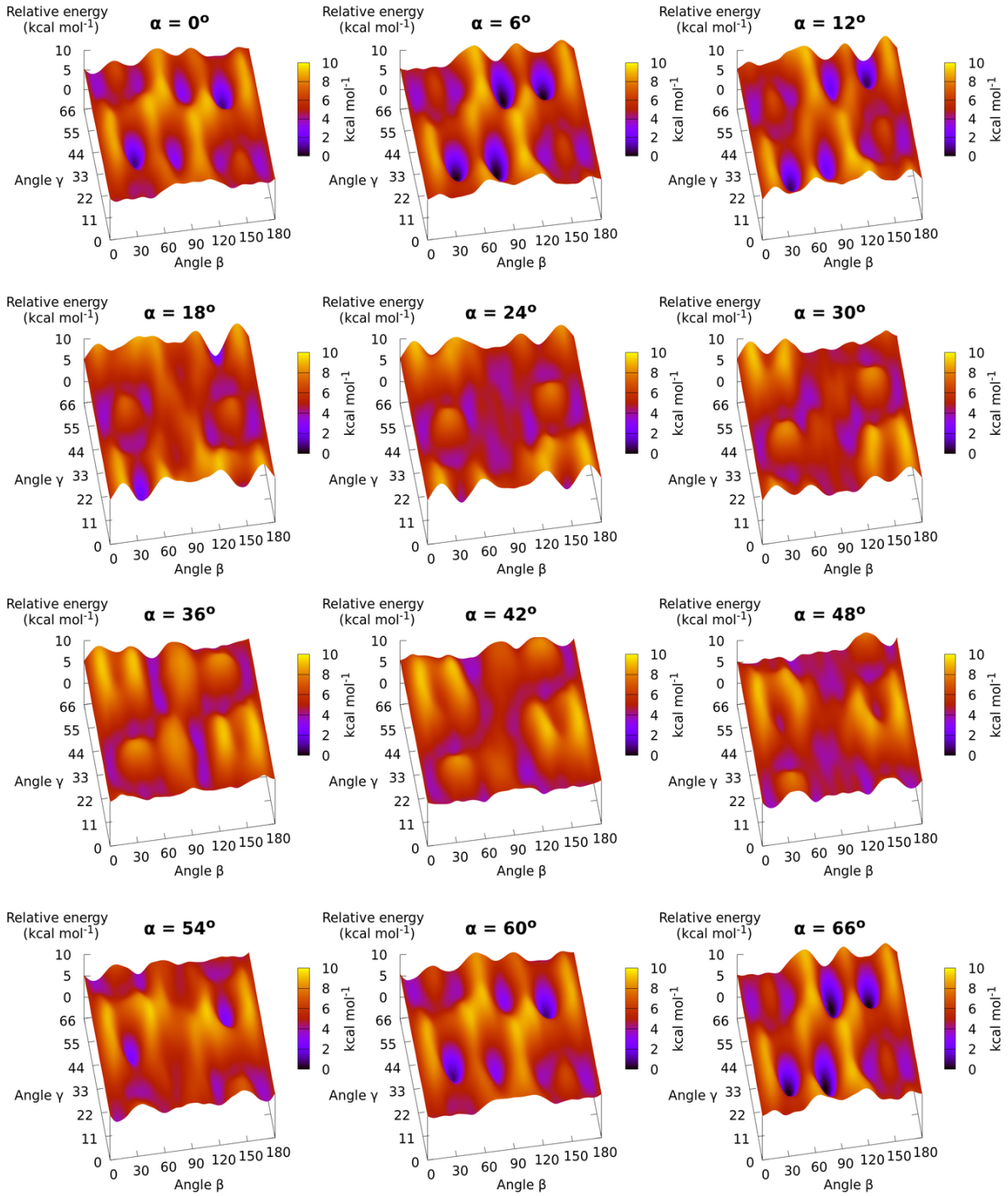

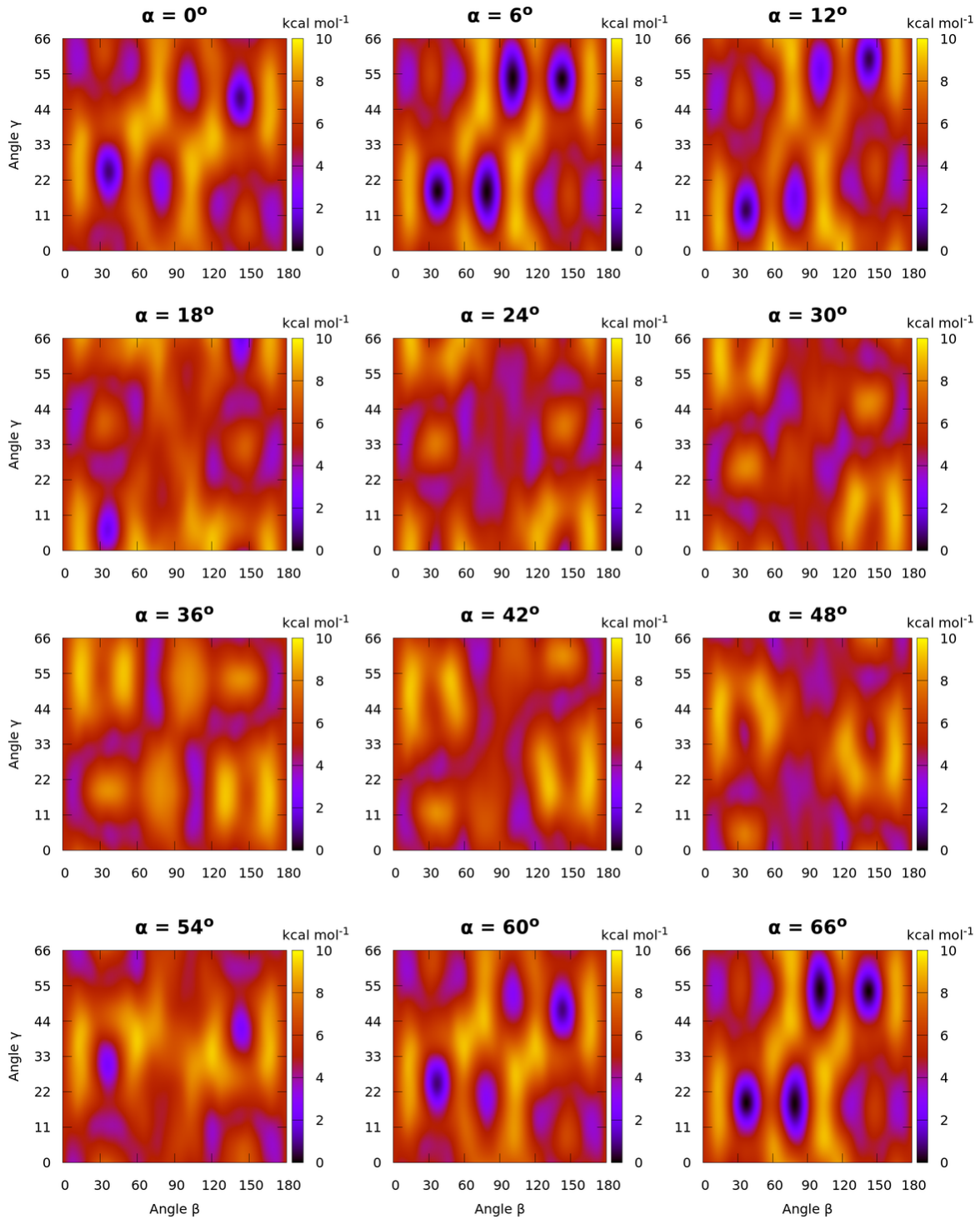

All the B97-D2/def2-TZVP optimisations from the minima led to minima II or III of Figure 4.5.

A.5 Searching minima of complex C_{70}@[10]CPP with a systematic scanning procedure.

In this case (and in the next one), the search has been performed with a slightly more complicated procedure. This is because in these cases, our previous results indicate that it is likely the fullerene is not fully hosted in the CNR. For that reason, several different distances between the centre of the fullerene and that of the CNR have been tested. Thus, for each combination of the three Euler angles, four different "heights" have been tested: 0.5, 2.0, 3.5 and 5.0 Å, and the most favourable energy is chosen. Therefore, the number of calculations quadruples, reaching almost 18000 single points.

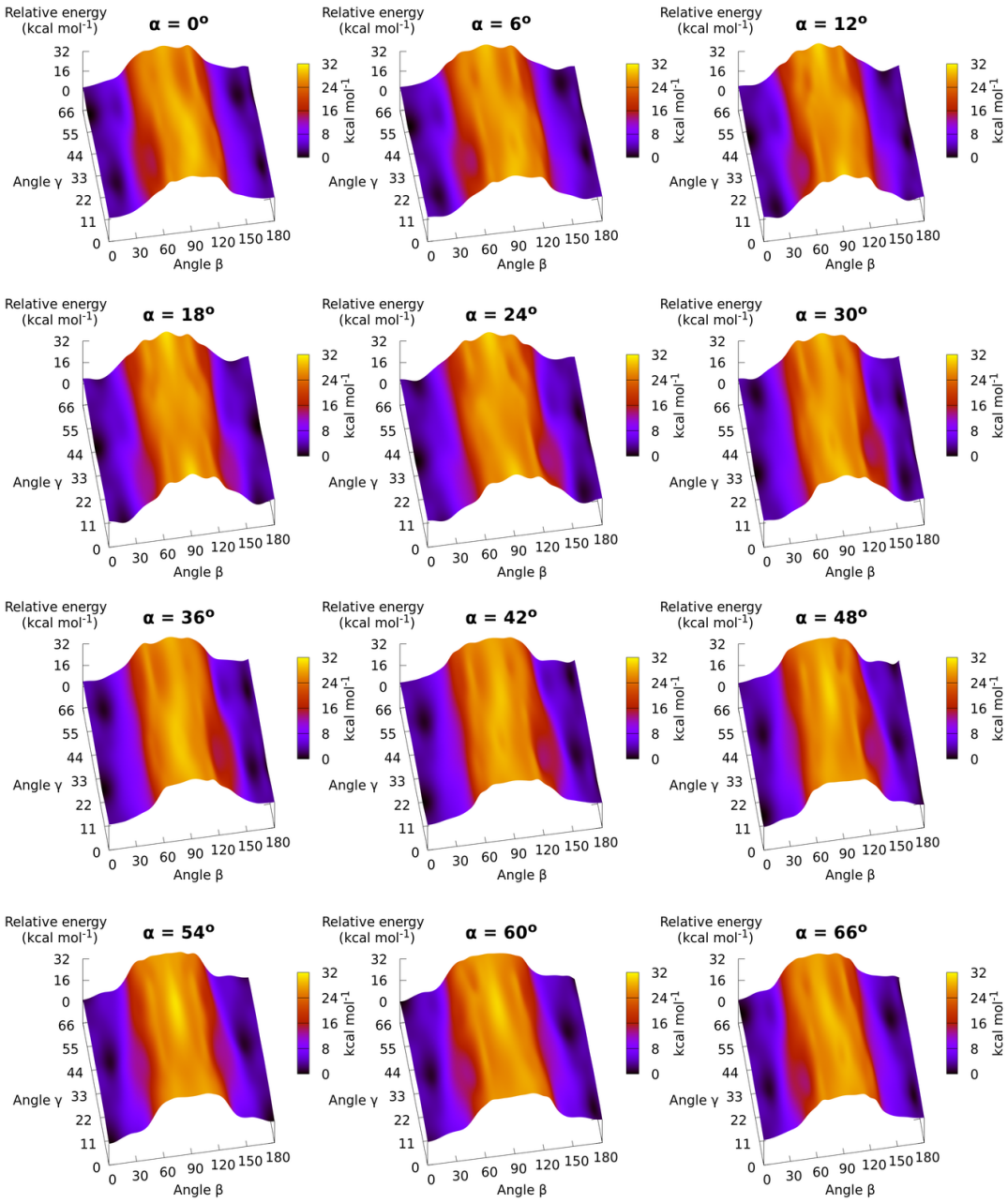

This Figure shows the preferred "height" for each combination of the three Euler angles:

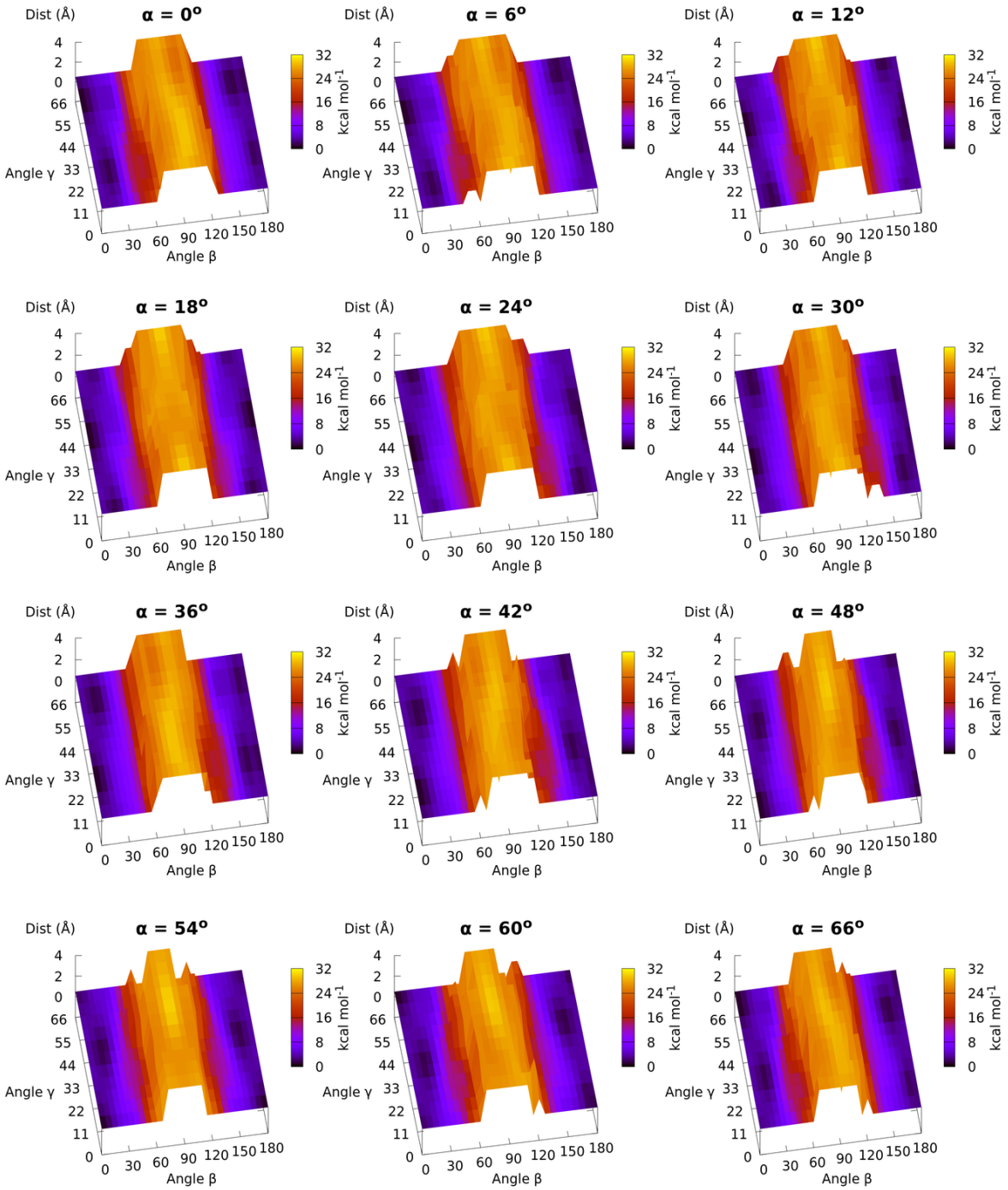

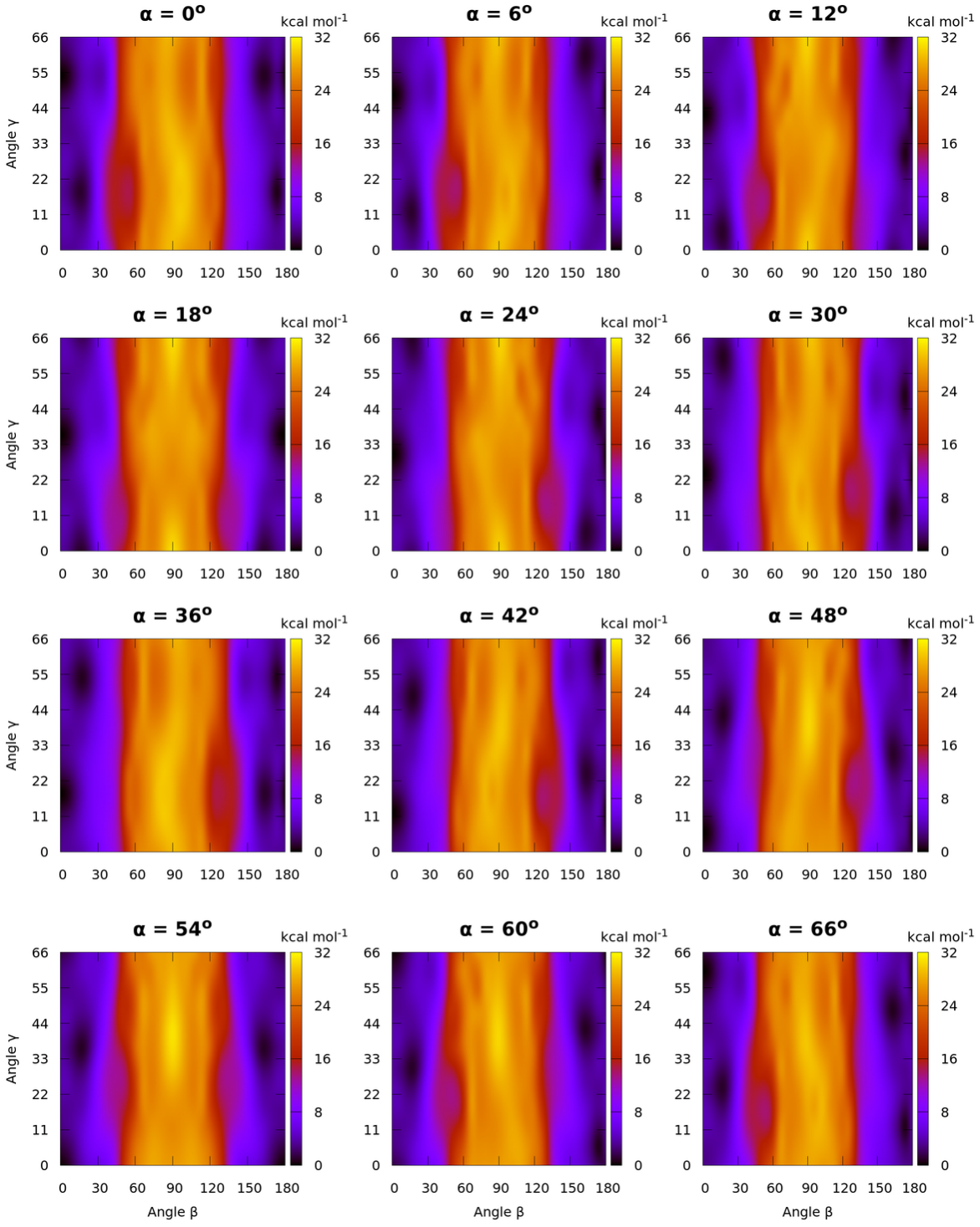

All the B97-D2/def2-TZVP optimisations from the minima led to minima I or III of Figure 4.6.

A.6 Searching minima of complex C_{70}@[6]CPPA with a systematic scanning procedure.

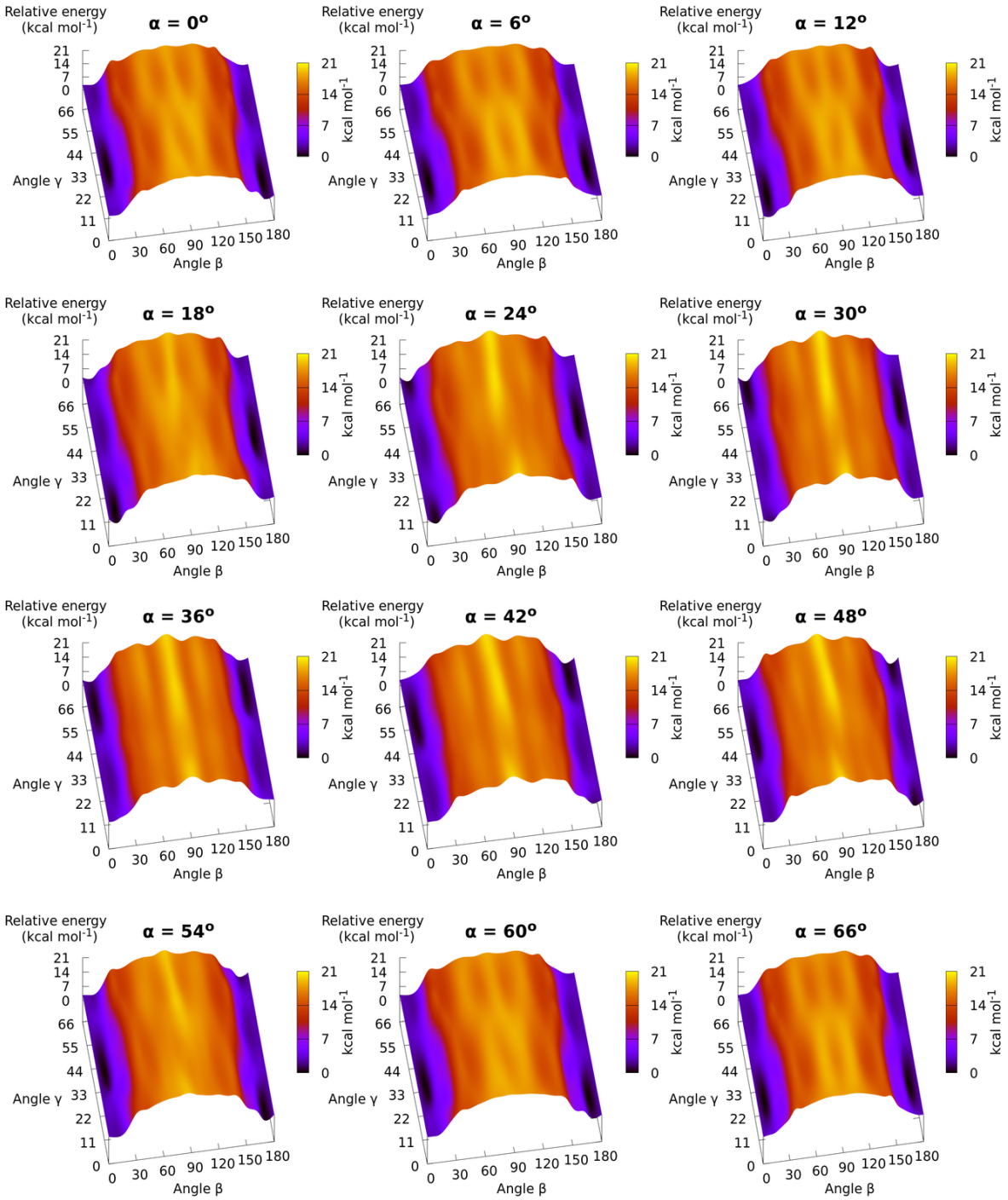

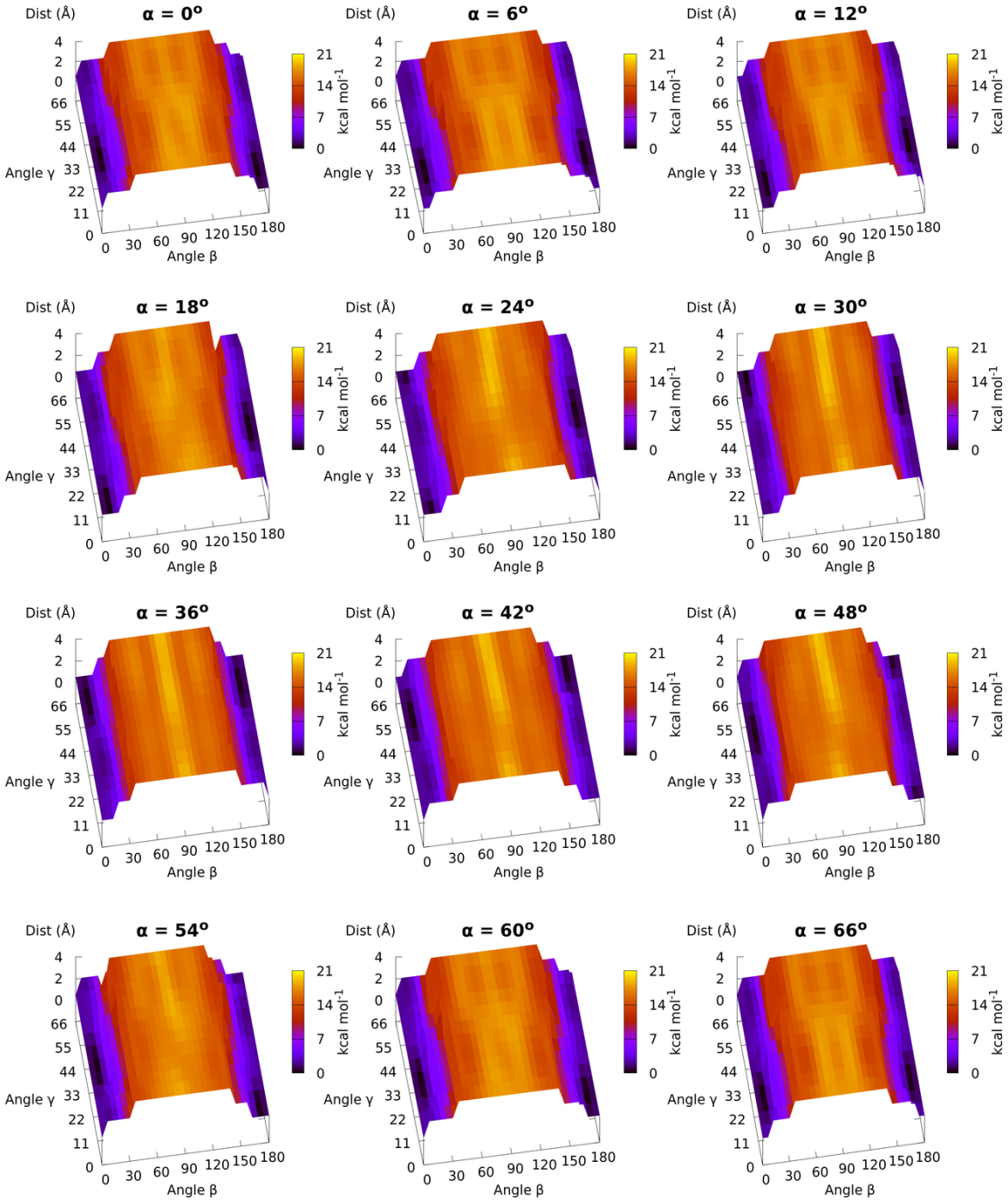
α = 0°
α = 6°
α = 12°
α = 18°
α = 24°
α = 30°
α = 36°
α = 42°
α = 48°
α = 54°
α = 60°
α = 66°
Dist (Å)
Angle γ
Angle β
kcal mol-1

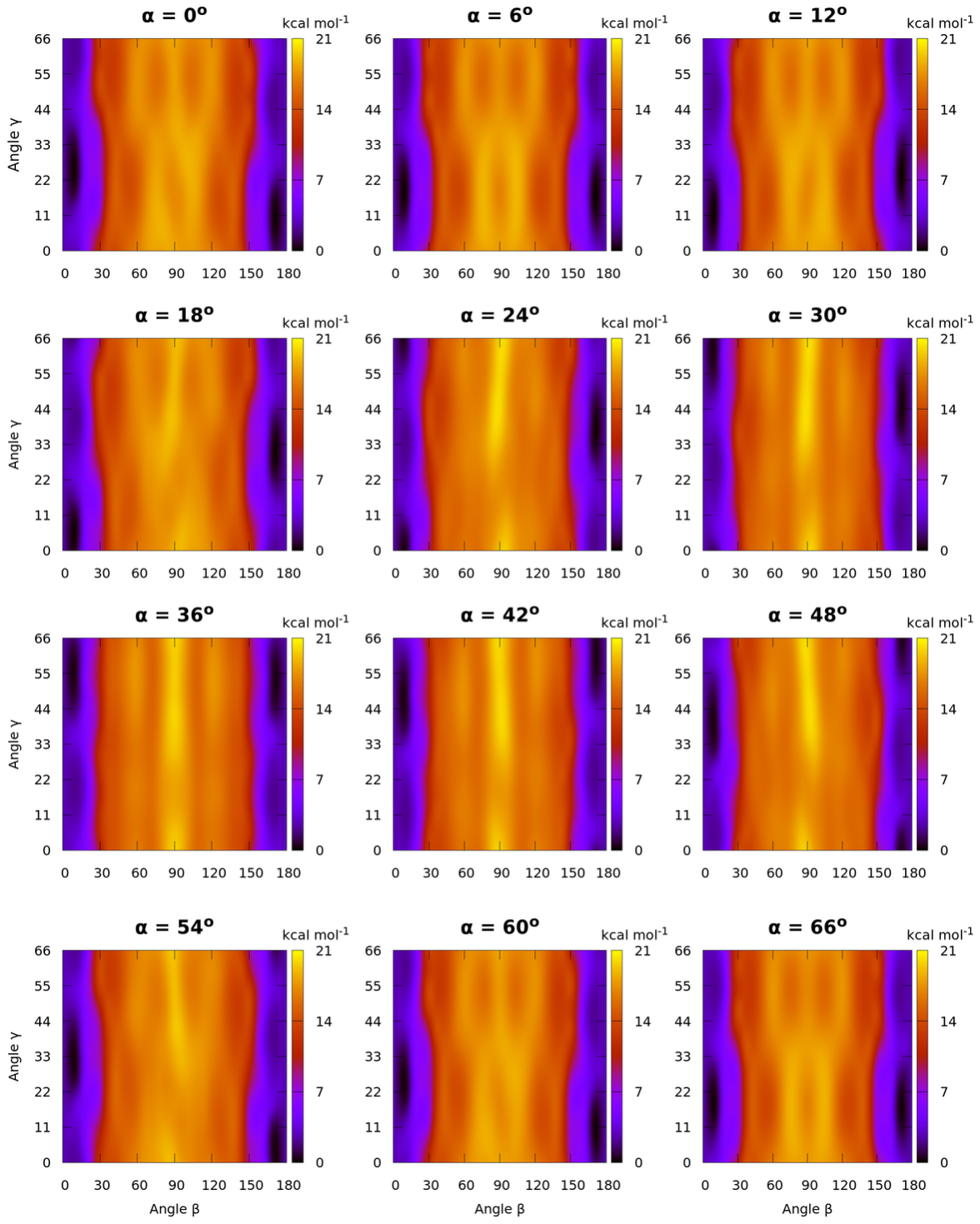

Optimization from the minimum $\alpha = 0°,\ \beta = 6°,\ \gamma = 24°$, leads to a minimum, **I'** , more favourable than that obtained previously.

A.7 Interaction between [10]CPP and fullerenes

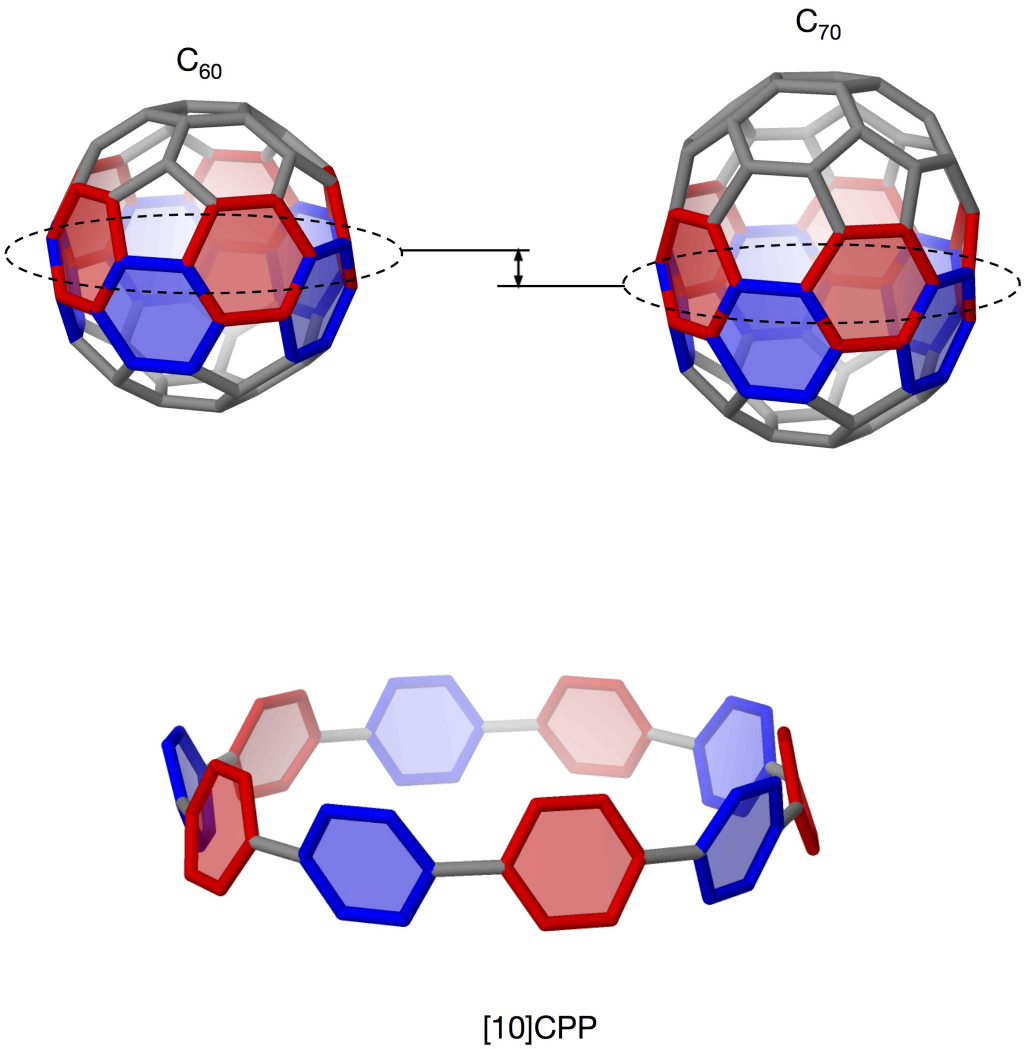

Figure a.3: The best minimum (both for C_{60} and C_{70}) corresponds to a structure where each of the ten rings of [10]CPP is directly faced to a six-membered ring of the fullerene. Every six-membered ring of [10]CPP inclined outward (blue) is directly facing a six-membered ring of fullerene having the same disposition. The same happens with the rings inclined inward (red). So, the strong interaction that takes place, explains why C_{60} remains fully hosted in the CNR whereas C_{70} moves vertically from the centre of the CNR (0.769 Å): the interaction zone of C_{60} lies exactly at the middle of the fullerene, whereas it is slightly displaced in C_{70}.

A.8 Distance between centres of the six-membered ring

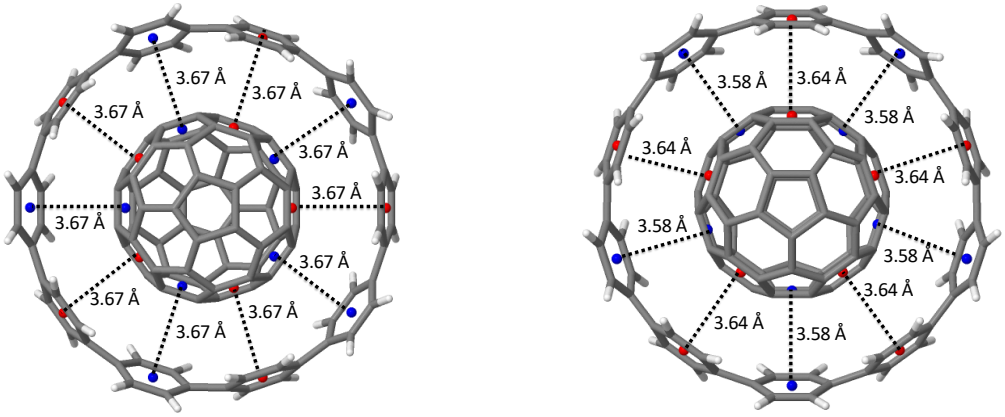

C_{60}@[10]CPP C_{70}@[10]CPP

Figure a.4: Distance between the centre of the six-membered ring of the CNR and the six-membered ring of the fullerene directly faced to it.

A.9 Dispersion breakdown

Computed dispersion between [10]CPP and the three "pieces" of C_{60} and C_{70} (kcal mol^{-1})

1) With the central ring of the fullerene:

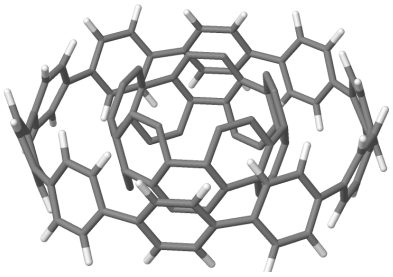

with C_{60}:−75.69

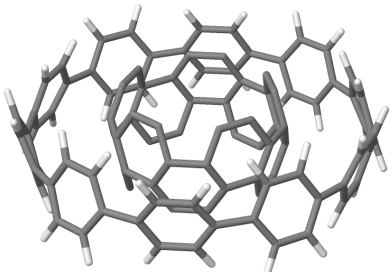

with C_{70}:−81.15 Δ=5.46

2) With the common "cap" of the fullerene:

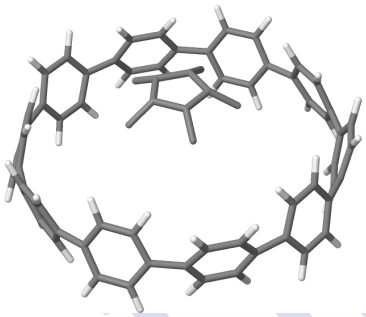

with C_{60}:−3.96

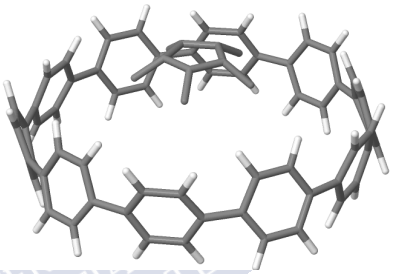

with C_{70}:−4.18 Δ=0.22

3) With the different "cap" of the fullerene:

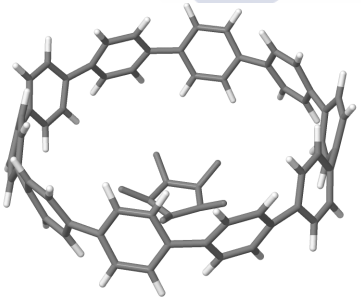

with C_{60}:−3.96

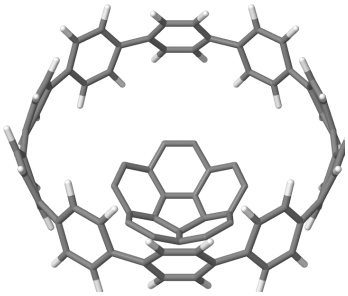

with C_{70}:−8.40 Δ=4.44

TOTAL:

with C_{60}:−83.61 with C_{70}:−93.73 Δ=10.12

dispersion values of Table 4.1: $-83.61 - (-93.73) = 10.12$

Figure a.5: The largest contribution to the difference of dispersion generated by C_{60} and C_{70} comes from the central region of the fullerene (5.46 kcal mol^{-1}, 54%). This is due to the fact that monomers are slightly closer for C_{70}, as shown in Figure a.4. Although the dispersion is much more favourable for C_{70} (10.12 kcal mol^{-1}), this is partially offset with a worse exchange+repulsion, so the final balance is only 3.53 kcal mol^{-1} with regard to the interaction of C_{60}.

A.10 Complexation energy

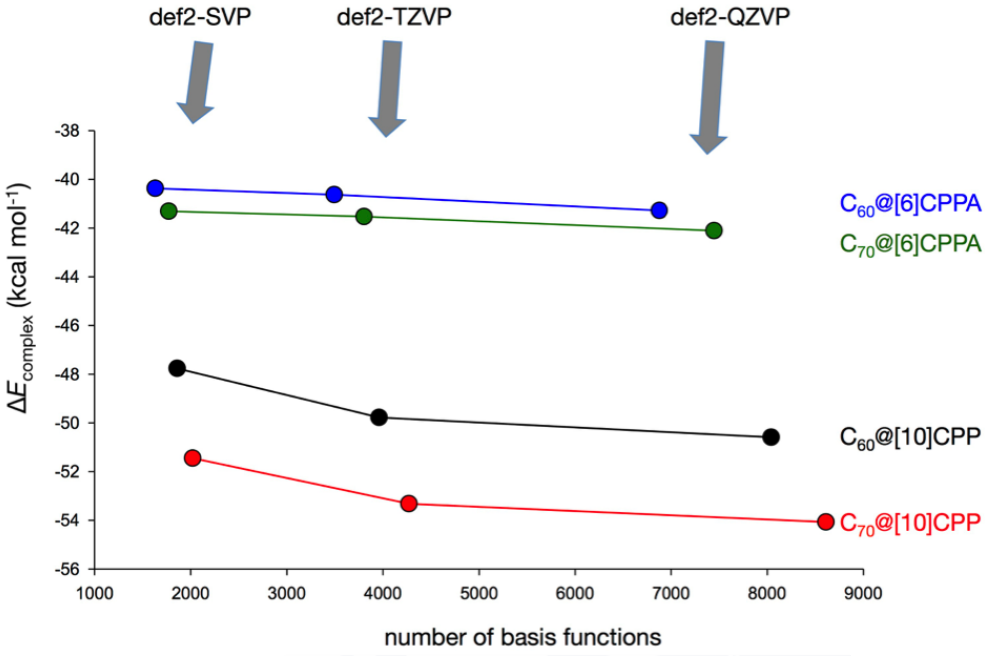

Figure a.6: B97-D2 complexation energy (kcal mol^{-1}) obtained with different basis sets. Only the best complex of each case is shown.

Table a.1: B97-D2 complexation energy (kcal mol^{-1}) obtained with different basis sets.

	def2-SVP	def2-TZVP	def2-QZVP[a]
C_{60}@[10]CPP	−47.76	−49.78	−50.59
C_{60}@[6]CPPA	−40.37	−40.63	−41.28
C_{70}@[10]CPP	−51.45	−53.32	−54.07
C_{70}@[6]CPPA	−41.31	−41.53	−42.11

[a] Using def2-TZVP geometries. Auxiliary basis set for RI: def2-QZVPP.

Table a.2: Differences between B97-D2 complexation energies (kcal mol^{-1}).

	def2-SVP	def2-TZVP	def2-QZVP	
C_{60}@[10]CPP-C_{60}@[6]CPPA	−7.39	−9.15	−9.31	difference between [10]CPP and [6]CPPA
C_{70}@[10]CPP-C_{70}@[6]CPPA	−10.14	−11.79	−11.96	
C_{70}@[10]CPP-C_{60}@[6]CPPA	−3.69	−3.54	−3.48	difference between C_{60} and C_{70}
C_{70}@[6]CPPA-C_{70}@[6]CPPA	−0.94	−0.90	−0.83	

Table a.3: Complexation energy (kcal mol^{-1}) obtained with different methods. For hybrid functionals (B3LYP and PBE0) only single point calculations are performed, using the B97-D2 geometries. All the DFT-D calculations are performed with the def2-TZVP basis set. M06-2X with 6-31G/6-311G Pople basis set, plus diffuse functions (+) and polarization functions (d,p).

	B97-D2	BLYP-D2	B3LYP-D3(BJ)	TPSS-D3(BJ)	PBE0-D3(BJ)	M06-2X
C_{60}@[10]CPP	−49.78	−46.19	−49.58	−46.71	−44.65	−48.63 (−39.31)
C_{60}@[6]CPPA	−40.63	−37.84	−38.80	−37.24	−34.43	−28.00
C_{70}@[10]CPP	−53.32	−49.76	−52.59	−49.78	−46.94	−39.74
C_{70}@[6]CPPA	−41.53	−38.58	−40.75	−38.10	−34.90	−31.38

[a] K. Yuan, C.-H. Zhou, Y.-C. Zhu and X. Zhao, *Physical Chemistry Chemical Physics*, 2015, **17**, 18802–18812.

[b] Value obtained by us at the M06-2X/6-311+G(d,p)//B97-D2/def2-TZVP level.

[c] Y. Zhao and D. G. Truhlar, *Journal of the American Chemical Society*, 2007, **129**, 8440–8442.

[d] Value obtained by us at the M06-2X/6-311+G(d,p) level using the geometry of T. Iwamoto, Y. Watanabe, T. Sadahiro, T. Haino and S. Yamago, *Angewandte Chemie - International Edition*, 2011, **50**, 8342–8344.

[e] Average value between −31.1 (Y. Zhao and D. G. Truhlar, *Journal of the American Chemical Society*, 2007, **129**, 8440–8442) and −31.66 (K. Yuan, Y.-J. Guo and X. Zhao, *The Journal of Physical Chemistry C*, 2015, **119**, 5168–5179).

USC UNIVERSIDADE DE SANTIAGO DE COMPOSTELA

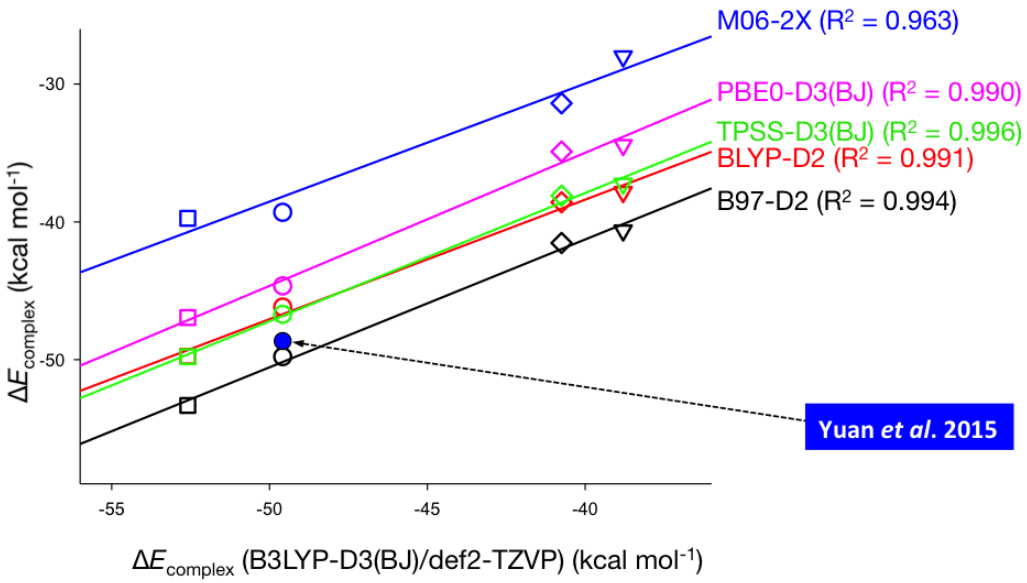

Figure a.7: DFT *vs.* B3LYP-D3(BJ) complexation energy (kcal mol^{-1}). The numeric data are included in Table a.3.

B97-D2: $y = 0.9276x - 4.174$.
BLYP-D2: $y = 0.8674x - 3.685$.
TPSS-D3(BJ): $y = 0.9309x - 0.6674$.
PBE0-D3(BJ): $y = 0.9660x + 3.657$.
M06-2X: $y = 0.8396x + 3.608$.

Circles: C_{60}@[10]CPP Triangles down: C_{60}@[10]CPP
Squares: C_{70}@[10]CPP Diamonds: C_{70}@[6]CPPA
Filled circle: C_{60}@[10]CPP M06-2X, obtained by Yuan *et al.*[1], and very far from all the other M06-2X results.

[1]K. Yuan, C.-H. Zhou, Y.-C. Zhu and X. Zhao, *Physical Chemistry Chemical Physics*, 2015, **17**, 18802–18812

Appendix B

Supplementary information Chapter 5

B.1 Rotation throught Euler angles

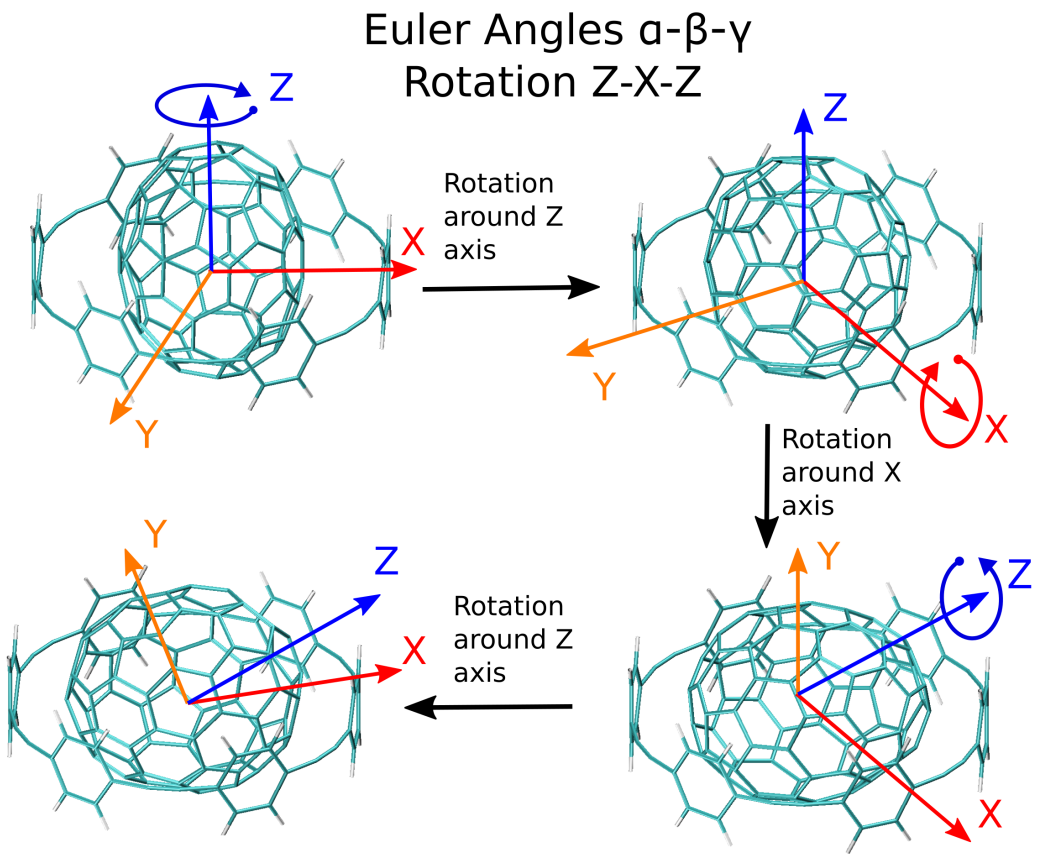

Figure b.1: Description of the rotation through the three Euler angles. In the case of C_{76}, the Z-axis corresponds to the principal C_2 axis.

B.2 Details of the search for the best orientation of C_{50}@[10]CPP, C_{50}@[6]CPPA and C_{76}@[10]CPP complexes

C_{50}@[10]CPP complex

To study the interaction between fullerene C_{50}-D_3 and [10]CPP, two different spatial dispositions of the fullerene are chosen. In the first one, C_{50}-$D_3(C_3)$, the principal rotation axis (C_3) of the fullerene is placed perpendicularly to the CNR plane and in the centre of the ring (see Figure b.2). In the second one, C_{50}-$D_3(C_2)$, one of the three perpendicular C_2 axes is that placed perpendicularly to the CNR. Figure b.3a shows the energetic profile that arises from the rotation around those two axes: it shows that the rotation around both axes is virtually free, with less than one-tenth kcal mol^{-1} of energy variation. On the other hand, the disposition of the fullerene with the C_3 axis perpendicular to the CNR is slightly favourable (by about 1.5 kcal mol^{-1}). The vertical departure from the CNR of the fullerene with this disposition is showed in Figure b.4a. This departure rather quickly becomes adverse, significant destabilisation taking place: more than 1.5 kcal mol^{-1} in less than 1 Å. Thus, according to the results, it seems clear that C_{50}-D_3 fits perfectly well inside [10]CPP. The next step is running the optimisation without any geometrical restrictions starting from minimum of Figure b.4a: none significant geometrical changes take place.

To study the interaction between fullerene C_{50}-D_{5h} and [10]CPP, two different spatial dispositions of the fullerene are chosen. In the first one, C_{50}-$D_{5h}(C_5)$, the principal rotation axis (C_5) of the fullerene is placed perpendicularly to the CNR and in the centre of the ring (see Figure b.2). In the second one, C_{50}-$D_{5h}(C_2)$, one of the five C_2 axes is that placed perpendicularly to the CNR. Figure b.3b shows the energetic profile that arises from the rotation around those two axes. This figure shows that C_{50}-$D_{5h}(C_5)$ disposition is clearly favourable (about 4 kcal mol^{-1} better than C_{50}-$D_{5h}(C_2)$). It also shows that rotation around C_2 is virtually free, with less than two-tenth kcal mol^{-1} of energy variation. However, rotation around the principal rotation axis involves a small but perceptible variation of about half a kcal mol^{-1}, with several minima. Starting from one of these equivalent minima, the vertical departure of the fullerene is analysed (Figure b.4b). Unlike the D_3 isomer, in this case the most advantageous location of the fullerene is slightly outside the CNR: about 0.5 Å. After geometrical optimisation of this minimum, this fact is confirmed at least to some extent, in such a way that the separation between the geometric centres of both monomers amounts to 0.50 Å (almost all of this separation, 0.48 Å, corresponds to the vertical displacement of the fullerene, the rest being an almost negligible horizontal displacement outside the geometric centre of the CNR).

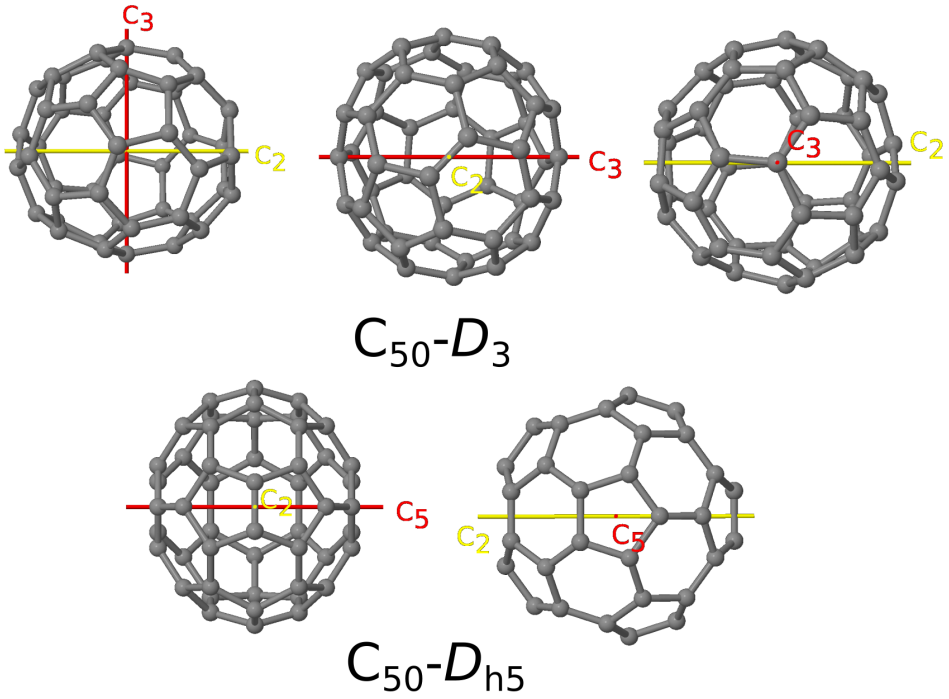

Figure b.2: Main axes for the two isomers of C_{50}.

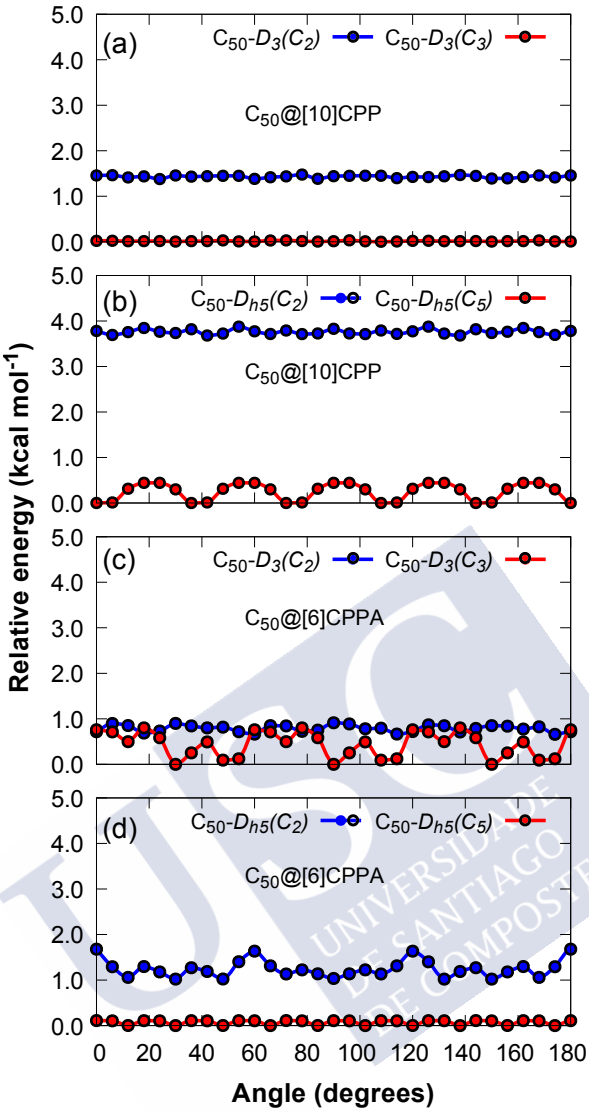

Figure b.3: Energetic profile for the rotation of fullerene C_{50} (D_{5h} and D_3 symmetry) inside the carbon nanorings [10]CPP and [6]CPPA.

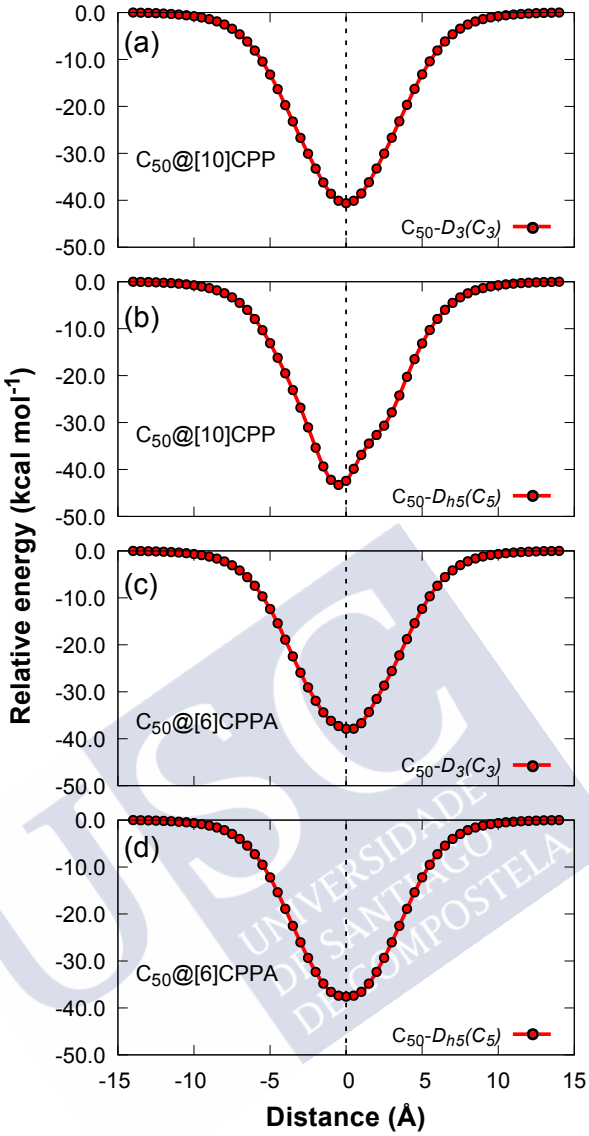

Figure b.4: Energetic profile for the vertical departure of fullerene C_{50} (D_{5h} and D_3 symmetry) inside the carbon nanorings [10]CPP and [6]CPPA.

C_{50}@[6]CPPA complex

Figure b.3c shows the energetic profile that arises from the rotation around the C_2 and C_3 axes of the D_3 isomer of C_{50}, commented above. This figure shows that C_{50}-$D_3(C_3)$ orientation is slightly favourable (about 1 kcal mol^{-1} better than C_{50}-$D_3(C_2)$). It also shows that rotation around C_2 is virtually free, with less than two-tenth kcal mol^{-1} of energy change. However, rotation around the principal rotation axis involves a small but perceptible variation of about one kcal mol^{-1}, with several minima. Starting from one of these equivalent minima the vertical departure of the fullerene is analysed (Figure b.4c). This departure fairly quickly becomes adverse; thus, according to the results, it seems clear that C_{50}-D_3 fits nicely inside [6]CPPA. Starting from the minimum, the geometrical optimisation produces scarce geometrical changes and the complexation energy of the final structure (Table 5.1) amounts to -36.54 kcal mol^{-1}, a quantity slightly smaller than that obtained for fullerenes C_{60} and C_{70} in our previous work (around -41 kcal mol^{-1}) and for the complex with [10]CPP.[1] Figure 5.2 shows the NCIPLOT picture corresponding to this C_{50}-D_3@[6]CPPA complex.

Figure b.3d shows the energetic profile that arises from the rotation around the C_2 and C_5 axes of the D_{5h} isomer of C_{50}. This figure shows that C_{50}-$D_{5h}(C_5)$ disposition is slightly favourable (about 1 kcal mol^{-1} better than C_{50}-$D_{5h}(C_2)$). It also shows that rotation around C_5 is virtually free, with less than two-tenth kcal mol^{-1} of energy variation. As in most of the previous cases, the study of the vertical departure of the fullerene shows that C_{50}-D_{5h} fits perfectly well inside the CNR (Figure b.4d).

C_{76}@[10]CPP complex

To study the interaction between fullerene C_{76}-D_2 and [10]CPP, two different spatial orientations of the fullerene are chosen (see Figure b.5). In the first one, $C_{76}(C_2)$, the principal rotation axis (C_2) of the fullerene is placed perpendicularly to the CNR plane and in the centre of the ring. In the second one, $C_{76}(6)$, the chosen axis goes through the centre of the 6-membered top and bottom rings of C_{76}. In both cases the fullerene is placed vertically, *i.e.*, the major diameter of the ball is perpendicular to the plane of the CNR (according to our previous work with the also ovoid C_{70}, the laying arrangements are strongly penalized[1]). Figure b.6a shows the energetic profile that arises from the rotation around those two axes: it shows that the rotation around both axes has a small energy cost (of a few kcal mol^{-1}) and that the orientation of the fullerene with the C_2 axis fully perpendicular to the CNR is significantly favourable (by about 10 kcal mol^{-1}). The vertical departure of the fullerene with this orientation from the CNR is showed in Figure b.6b: even though two minima appear at a distance of about 3 Å, the clearly more stable location (by almost 10 kcal mol^{-1}) is, as in the previous cases, the one in which C_{76} fits perfectly well inside [10]CPP, *i.e.*, $d = 0.0$ Å.

[1] I. González-Veloso, J. Rodríguez-Otero and E. M. Cabaleiro-Lago, *Physical Chemistry Chemical Physics*, 2016, **18**, 31670–31679

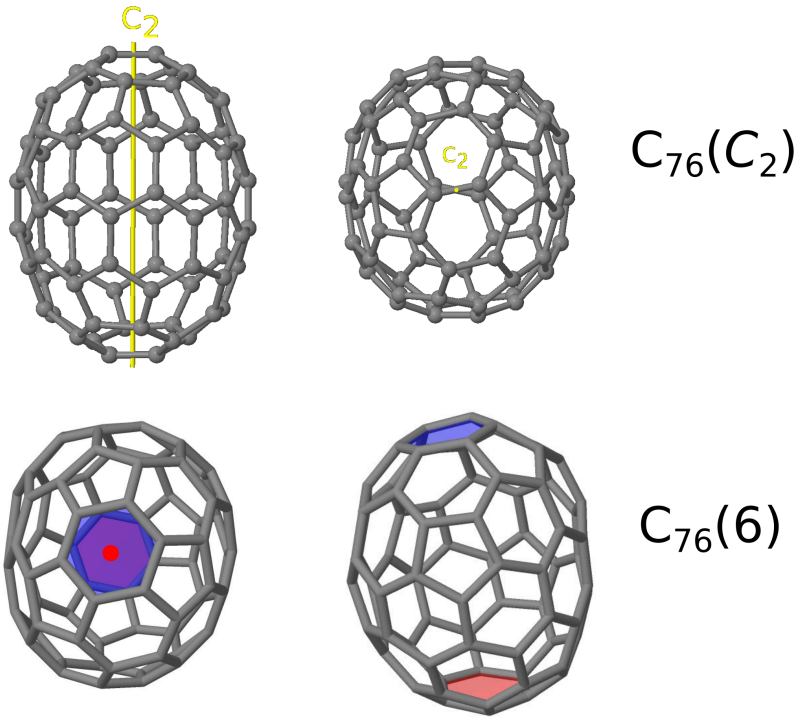

Figure b.5: C_{76}: main axis, $C_{76}(C_2)$, and axis through the centre of the 6-membered top and bottom rings, $C_{76}(6)$.

USC UNIVERSIDADE DE SANTIAGO DE COMPOSTELA

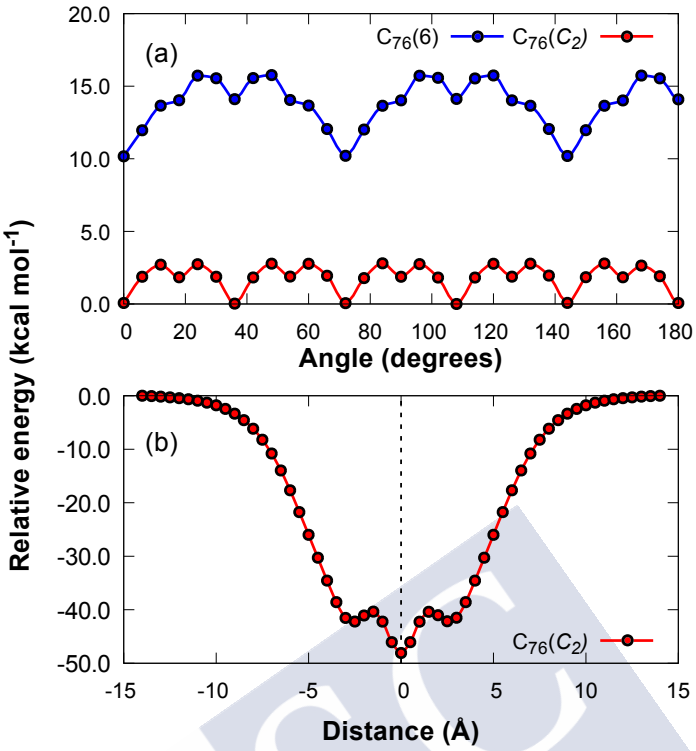

Figure b.6: Energetic profile for the rotation (a) and for the vertical departure (b) of fullerene C_{76} inside the carbon nanorings [10]CPP and [6]CPPA.

B.3 Searching minima of complex C_{76}@[6]CPPA with a systematic scanning procedure

Several different distances between the centre of the fullerene and that of the CNR have been tested. Thus, for each combination of the three Euler angles, four different "heights" have been tested: 0.5, 2.0, 3.5 and 5.0 Å, and the most favourable energy is chosen.

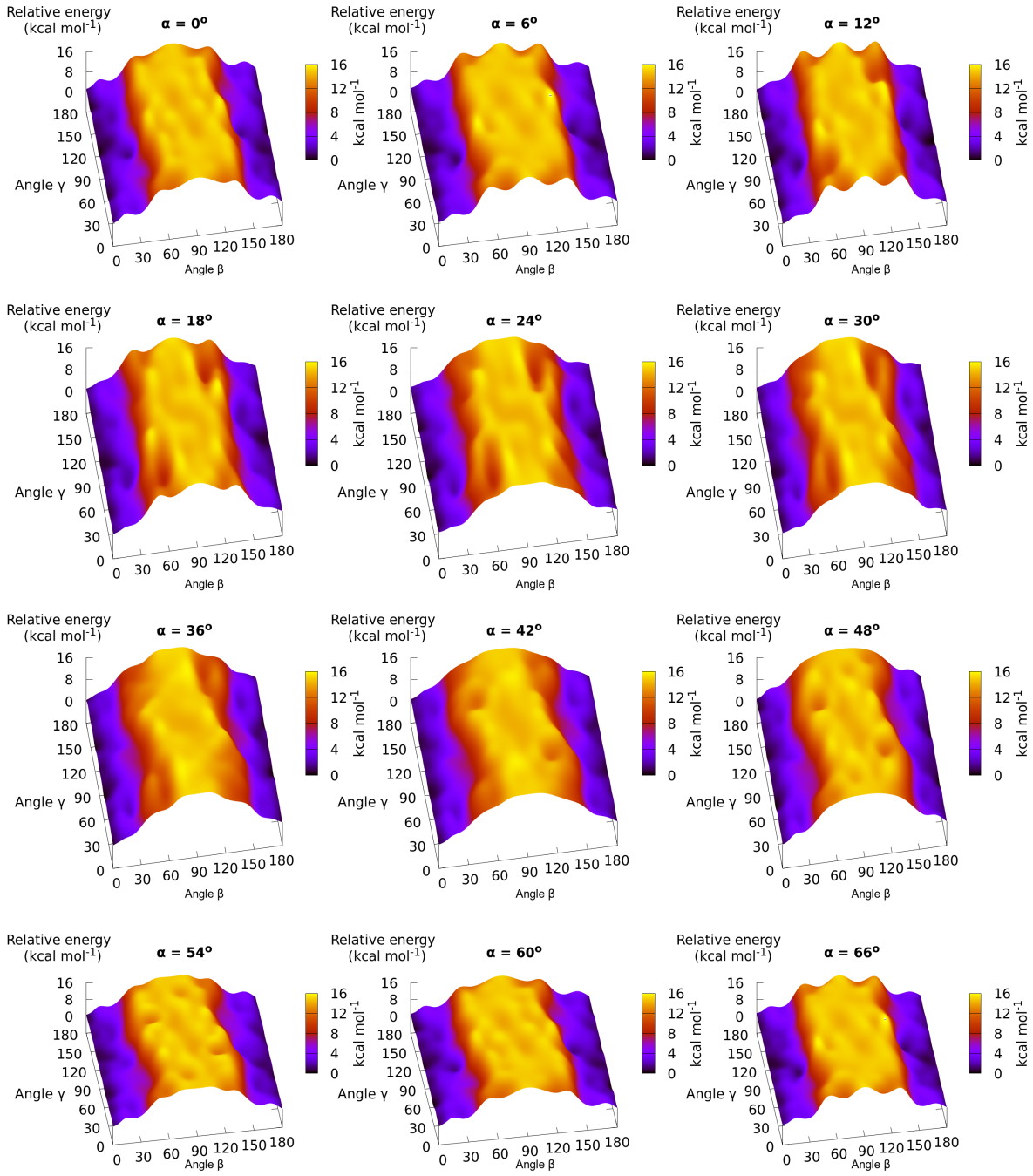

This figure shows the preferred "height" for each combination of the three Euler angles:

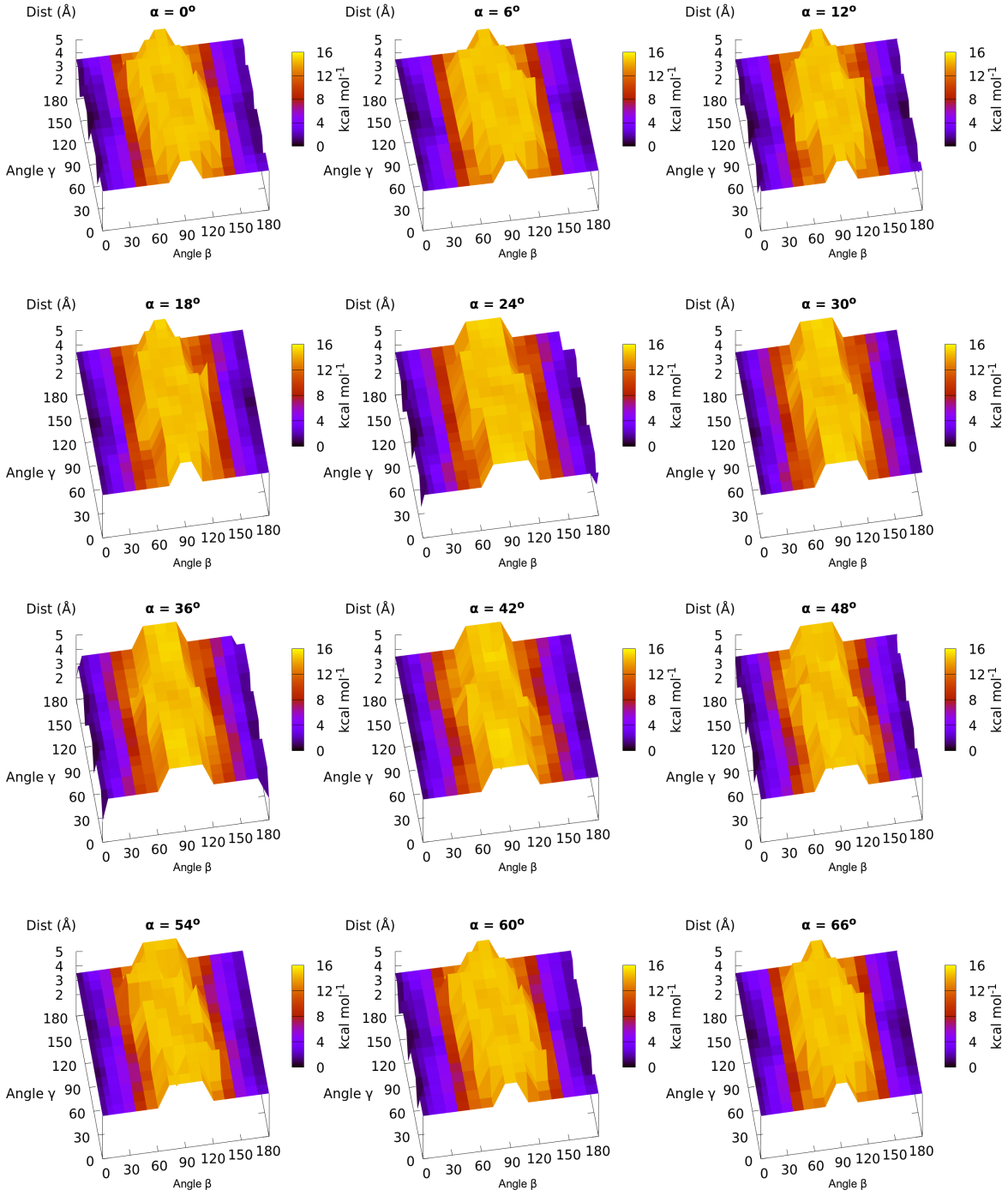

Looking for the minima:

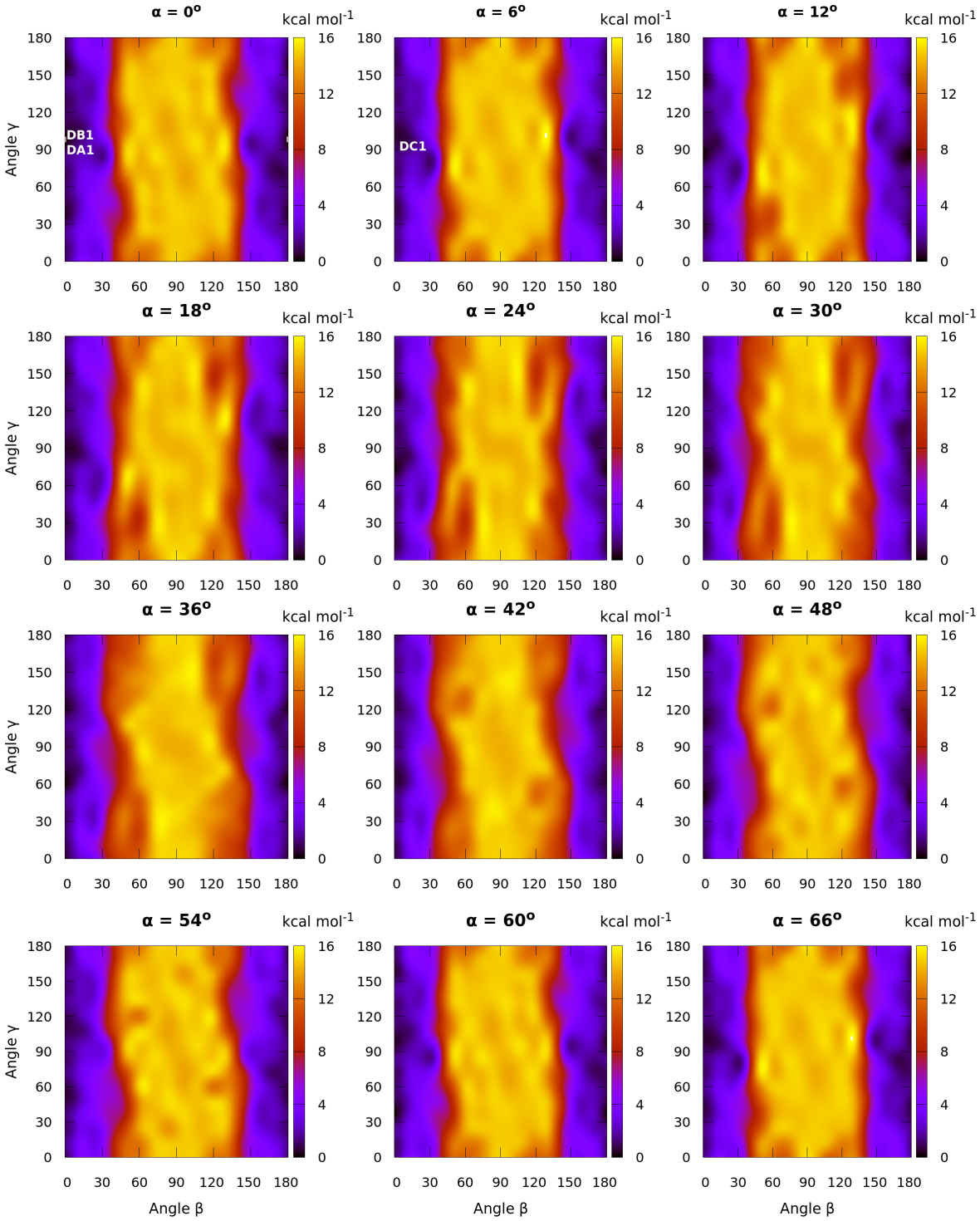

B.4 Vertical departure of the C_{60}

The three best minima obtained from the scanning corresponds to:
DA1: $\alpha = 0°$, $\beta = 0°$, $\gamma = 96°$ $d = 2.0$ Å
DB1: $\alpha = 0°$, $\beta = 0°$, $\gamma = 108°$ $d = 3.5$ Å
DC1: $\alpha = 6°$, $\beta = 12°$, $\gamma = 96°$ $d = 3.5$ Å

After geometrical optimisation at the B97-D2/def2-TZVP level, the computed values are:

	Dist (Å)	Angle (degrees)	$\boldsymbol{\Delta E_{\text{complex}}}$	ΔE_{def}		Dispersion
				Fullerene	CNR	
DA1	2.43	0.2°	**−42.12**	0.21	1.33	−85.16
DB1	2.54	0.1°	**−41.06**	0.18	1.48	−82.42
DC1	2.62	3.1°	**−41.62**	0.14	1.31	−82.18

The differences between them are quite scarce: in all three cases a vertical or almost vertical disposition of the C_{76} (at most, there is a departure of 3 degrees) takes place and the fullerene is separated from the centre of the CNR by a considerable distance (2.43–2.62 Å).

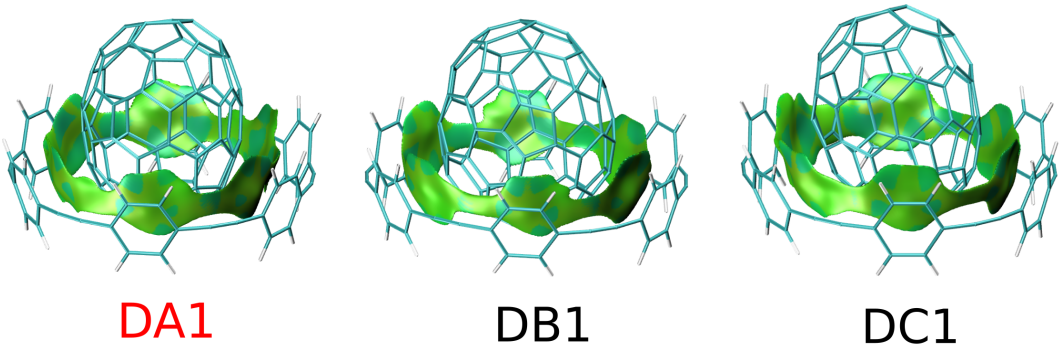

NCIPLOT gradient isosurface (0.3 a.u.) corresponding to the three minima. Scale over the range −0.04 to 0.04 a.u. The three plots are also very similar.

B.5 Complexation energy versus dispersion and N_{contacts}

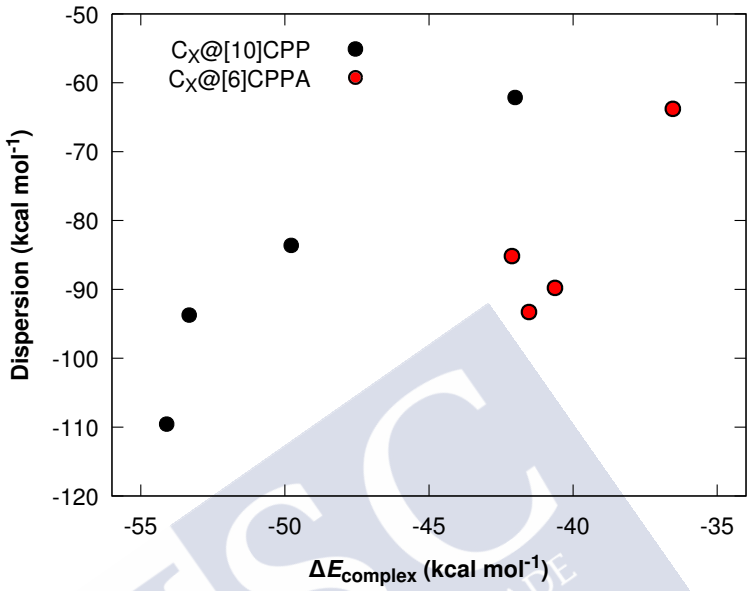

Figure b.7: Dispersion versus complexation for complexes between a fullerene (C_{50}-C_{60}-C_{70}-C_{76}) and a CNR.

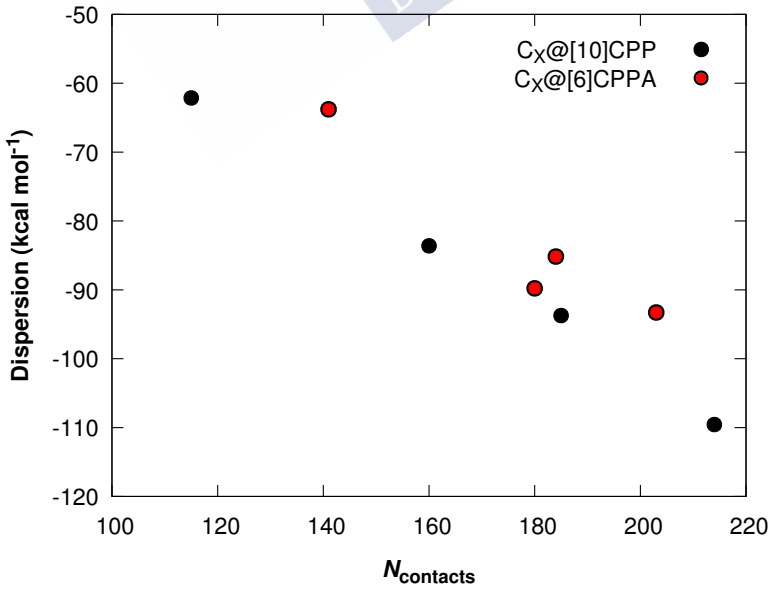

Figure b.8: Dispersion versus number of contacts for complexes between a fullerene (C_{50}-C_{60}-C_{70}-C_{76}) and a CNR.

B.6 Fitting into an ellipse

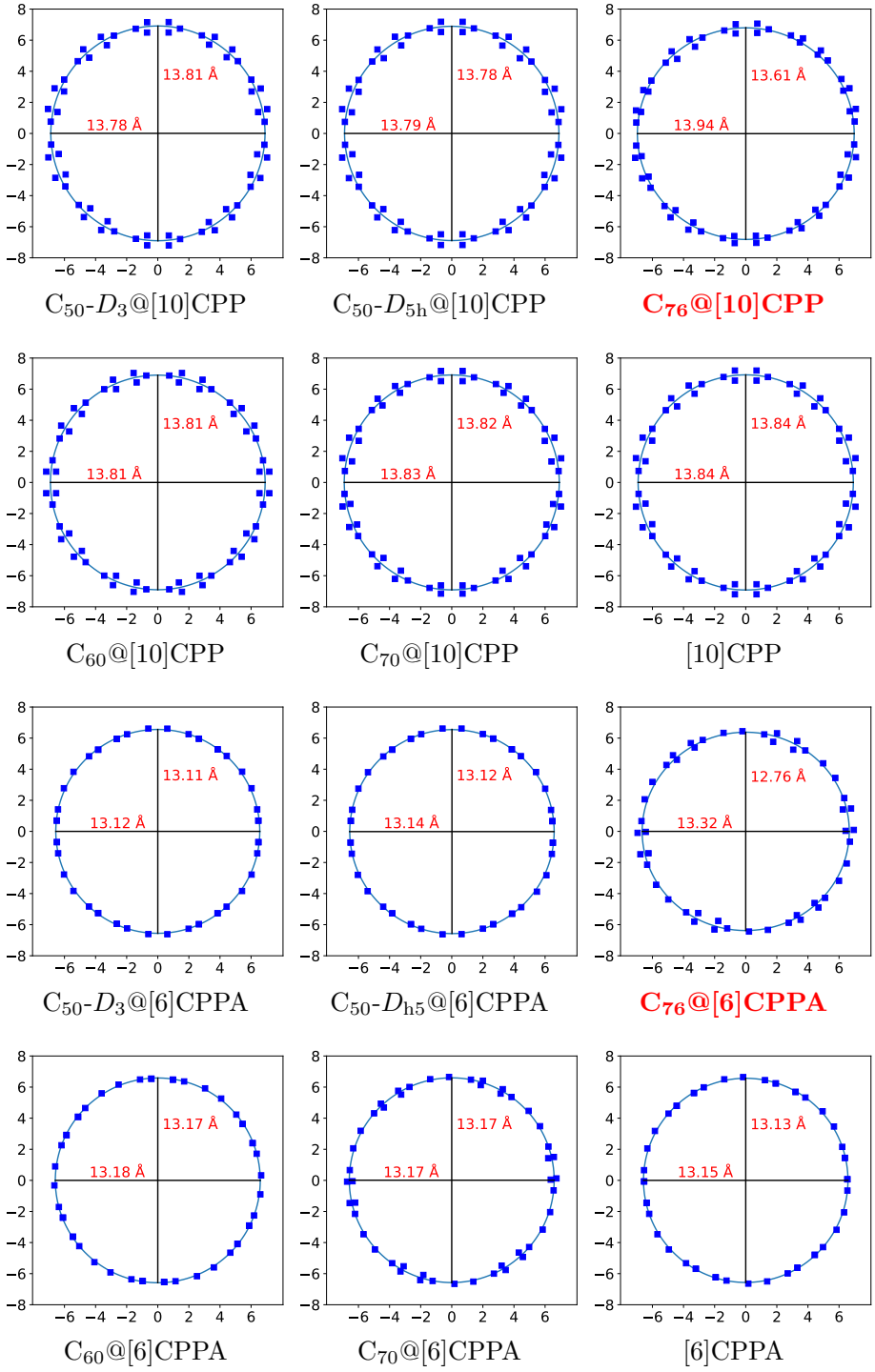

Figure b.9: Fitting the CNR to an ellipse, both isolated and forming part of complexes with all the fullerenes. For fitting the data, hydrogen coordinates are removed and carbon coordinates are projected on the horizontal plane, *i.e.*, vertical Z coordinates are removed. The only two cases with significant deformation are highlighted in red.

Appendix C

Supplementary information Chapter 6

C.1 Fitting nanohoops and most stable complexes

Table c.1: Fitting the nanohoop into an ellipse, for the isolated nanohoops and in different complexes. Radii in Å; f is the flattening $f = (R_1 - R_2)/R_1$

	R_1	R_2	f	$1/f$
[12]CPP	8.29	8.29	0.000	16587.00
[10]CPAq	8.42	8.24	0.021	48.09
[10]CPTcaq	9.04	7.69	0.149	6.70
$(C_{60}(5)@[10]CPAq)_A$	**9.22**	**7.21**	**0.218**	**4.59**
$(C_{60}(6)@[10]CPAq)_A$	**9.07**	**7.39**	**0.185**	**5.42**
$(C_{60}(5)@[10]CPTcaq)_A$	**9.47**	**7.16**	**0.244**	**4.10**
$(C_{60}(6)@[10]CPTcaq)_A$	**9.46**	**7.19**	**0.240**	**4.17**
$C_{60}(5)@[12]CPP$	**9.15**	**7.24**	**0.209**	**4.80**
$C_{60}(6)@[12]CPP$	**9.17**	**7.23**	**0.211**	**4.73**
$C_{60}(5)@[10]CPAq$	9.24	7.21	0.220	4.54
$C_{60}(6)@[10]CPAq$	9.27	7.17	0.227	4.40
$C_{60}(5)@[10]CPTcaq$	9.77	6.87	0.297	3.37
$C_{60}(6)@[10]CPTcaq$	9.83	6.81	0.308	3.25
$(C_{70}(V)@[10]CPAq)_A$	**9.18**	**7.26**	**0.209**	**4.78**
$(C_{70}(H)@[10]CPAq)_A$	**8.78**	**7.68**	**0.125**	**7.97**
$(C_{70}(V)@[10]CPTcaq)_A$	**9.56**	**7.06**	**0.261**	**3.83**
$(C_{70}(H)@[10]CPTcaq)_A$	**9.13**	**7.51**	**0.177**	**5.66**
$C_{70}(V)@[12]CPP$	**9.14**	**7.27**	**0.204**	**4.89**
$C_{70}(H)@[12]CPP$	**8.74**	**7.70**	**0.119**	**8.41**
$C_{70}(V)@[10]CPAq$	9.25	7.20	0.222	4.51
$C_{70}(H)@[10]CPAq$	8.89	7.58	0.148	6.77
$C_{70}(V)@[10]CPTcaq$	9.74	6.91	0.290	3.45
$C_{70}(H)@[10]CPTcaq$	9.33	7.35	0.213	4.70

C.2 HOMO-LUMO Orbitals

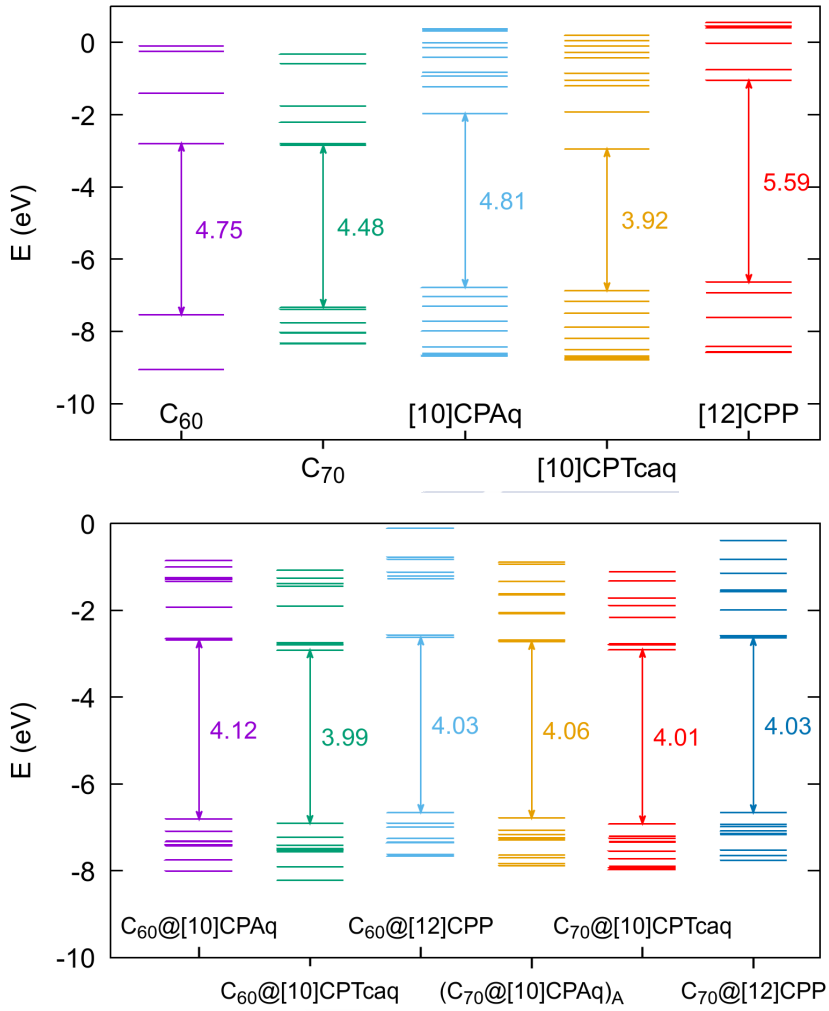

Figure c.1: Schematic energy levels of the highest and lowest occupied molecular orbitals in monomers and complexes. CAM-B3LYP/def2-TZVP//B97-D/def2-TZVP.

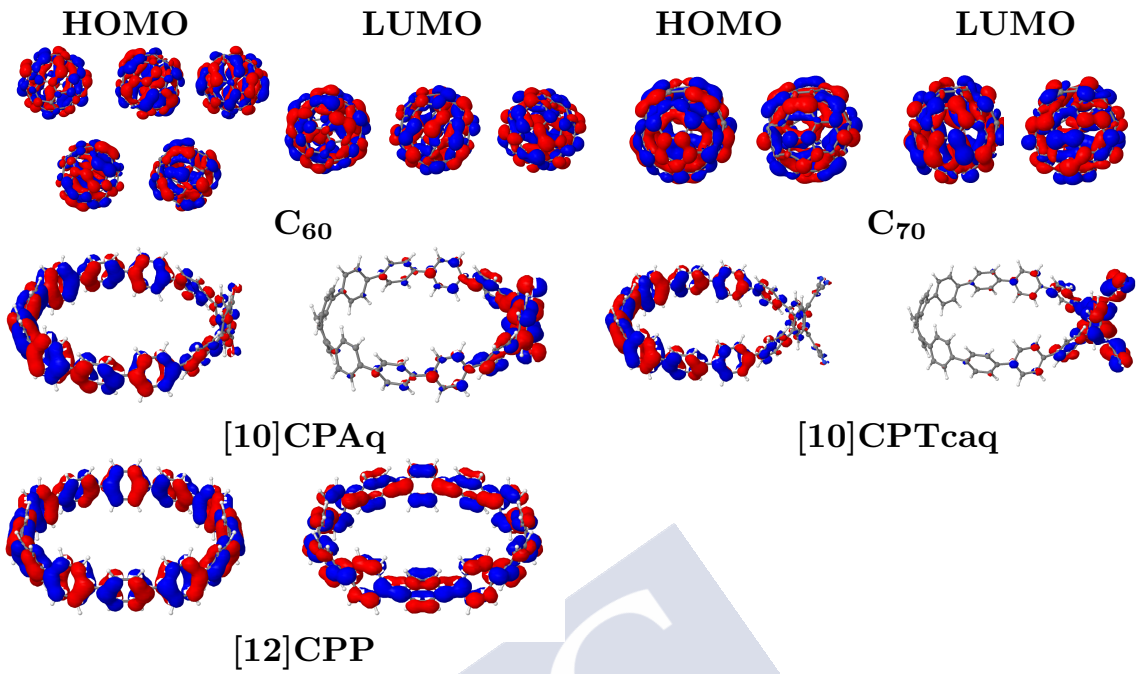

Figure c.2: HOMO and LUMO orbitals in monomers at the CAM-B3LYP/def2-TZVP//B97-D2/def2-TZVP level.

USC UNIVERSIDADE DE SANTIAGO DE COMPOSTELA

C.3 Centre of mass and centre of the ring in the nanohoops

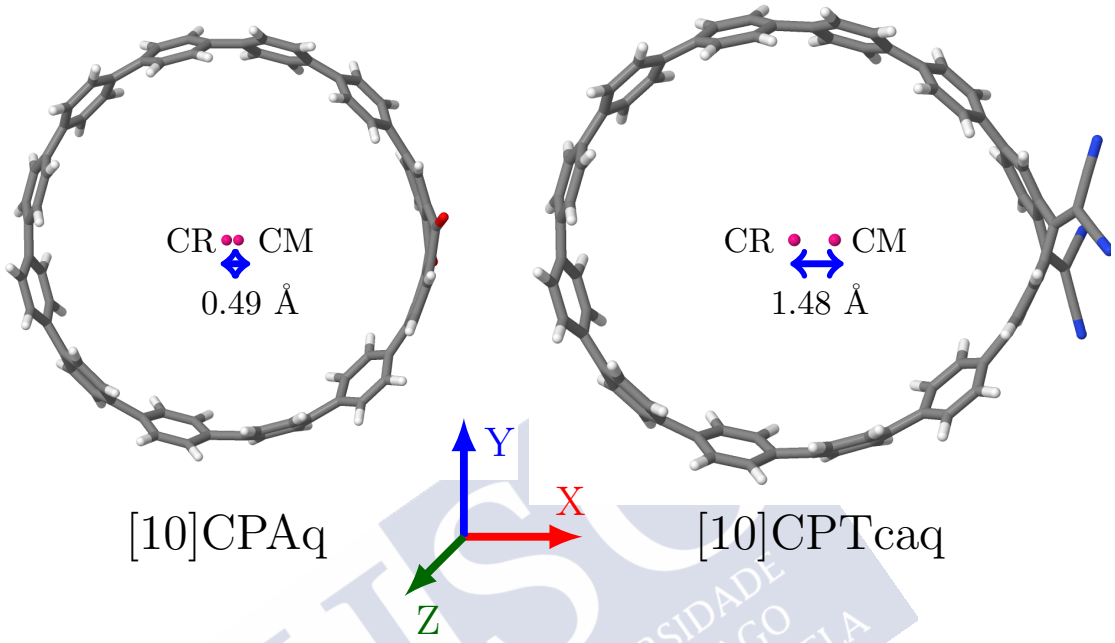

Figure c.3: Distance between the centre of mass (CM) and the centre of the ring (CR) in [10]CPAq and [10]CPTcaq.

C.4 Energetic profile for X axis displacement

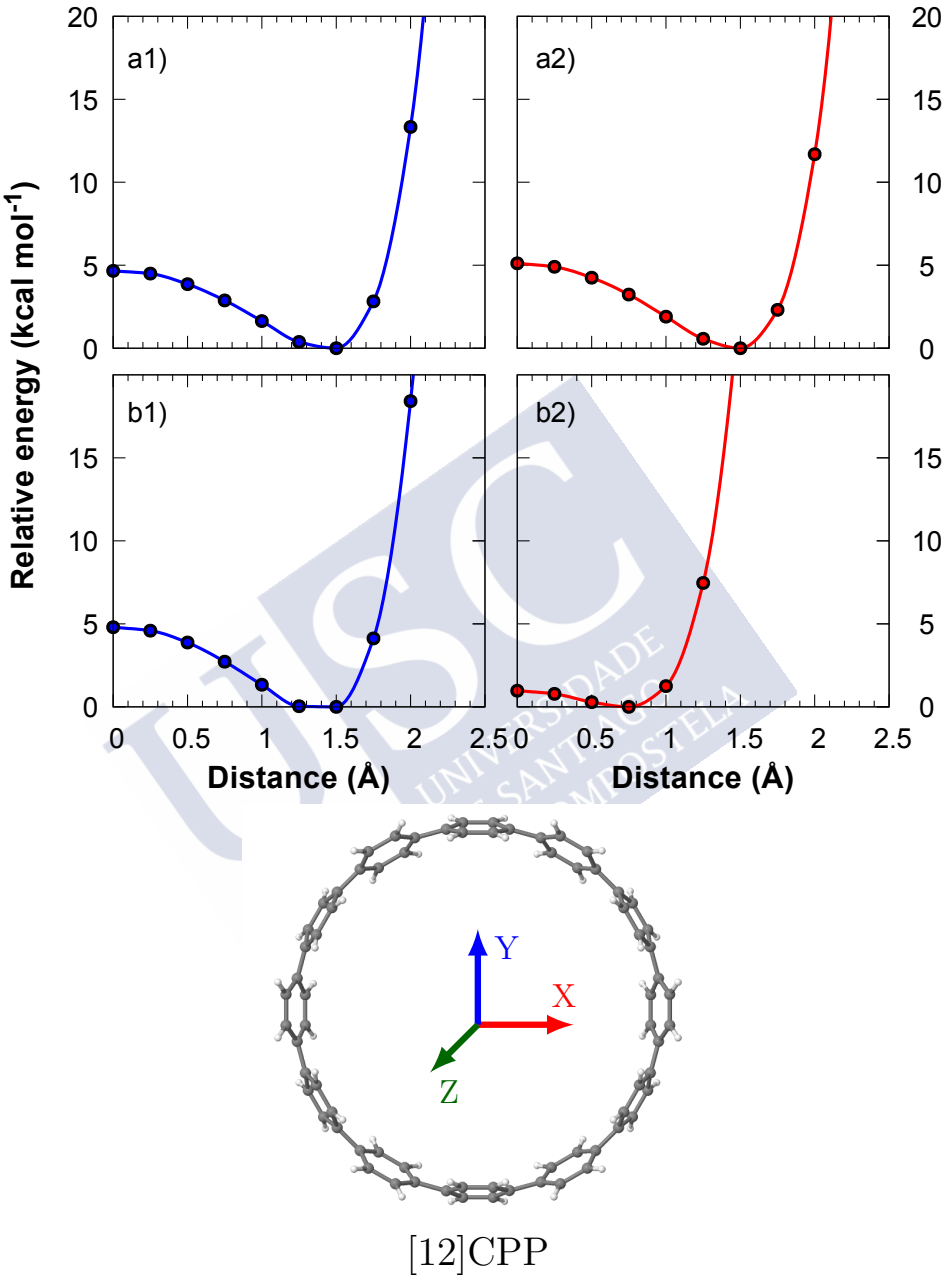

Figure c.4: Energetic profile for the displacement inside the ring of the fullerene along the X axis in the [12]CPP. a1) C_{60}(5)@[12]CPP. a2) C_{60}(6)@[12]CPP. b1) C_{70}(V)@[12]CPP. b2) C_{70}(H)@[12]CPP.

C.5 Energetic profile at the centre of the nanohoops

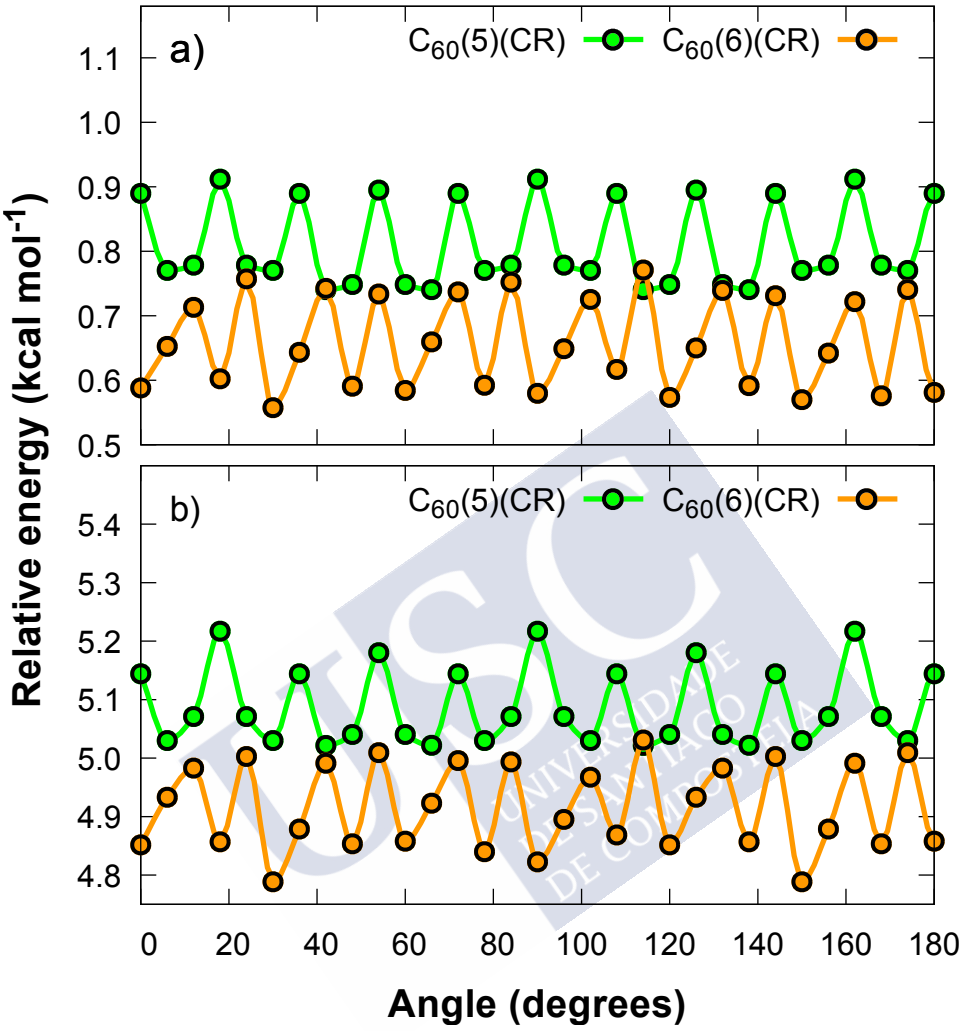

Figure c.5: Energetic profile for C_{60} at the centre of different nanorings. The minimum energy is the one that was found in the centre of mass. a) C_{60}@[10]CPAq. b) C_{60}@[10]CPTcaq.

C.6 Energetic profile for the departure of the fullerene

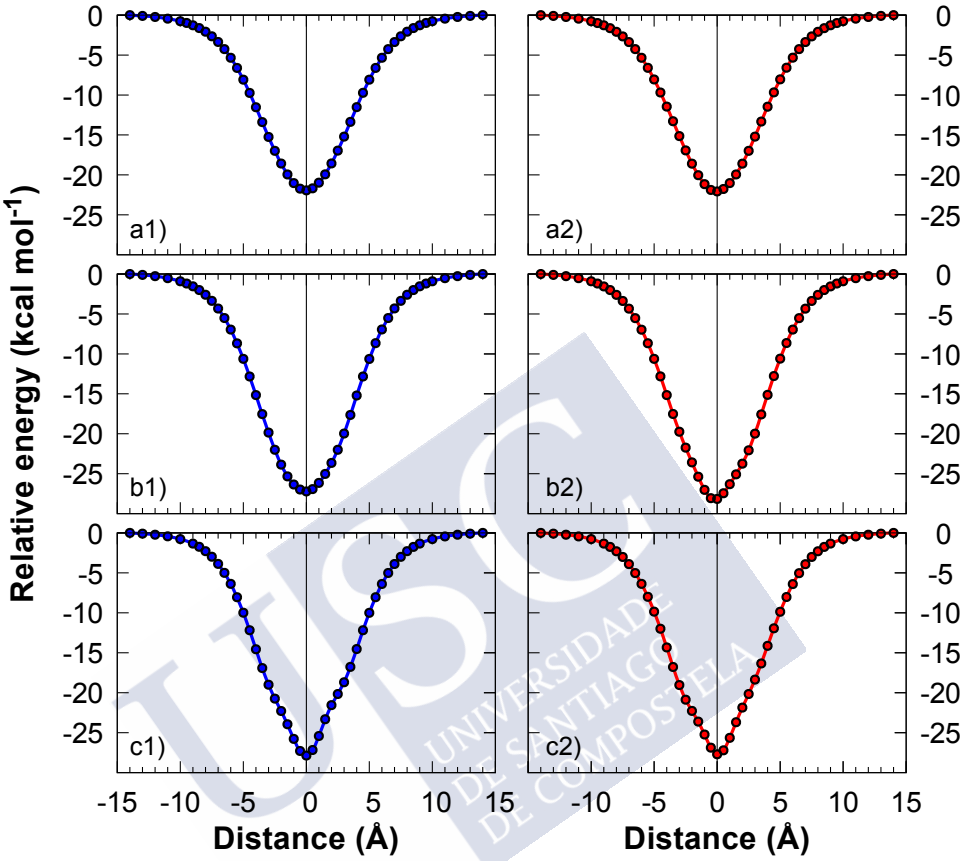

Figure c.6: Energetic profile for the departure in Z axis of C_{60} inside different nanorings. a1) C_{60}(5)@[10]CPAq(CM). a2) C_{60}(6)@[10]CPAq(CM). b1) C_{60}(5)@[10]CPTcaq(CM). b2) C_{60}(6)@[10]CPTcaq(CM) c1) C_{60}(5)@[12]CPP c2) C_{60}(6)@[12]CPP. In all cases the zero position corresponds to the fullerene placed on the centre of mass, except for [12]CPP where it refers to an analogous off-centre location as commented in the text.

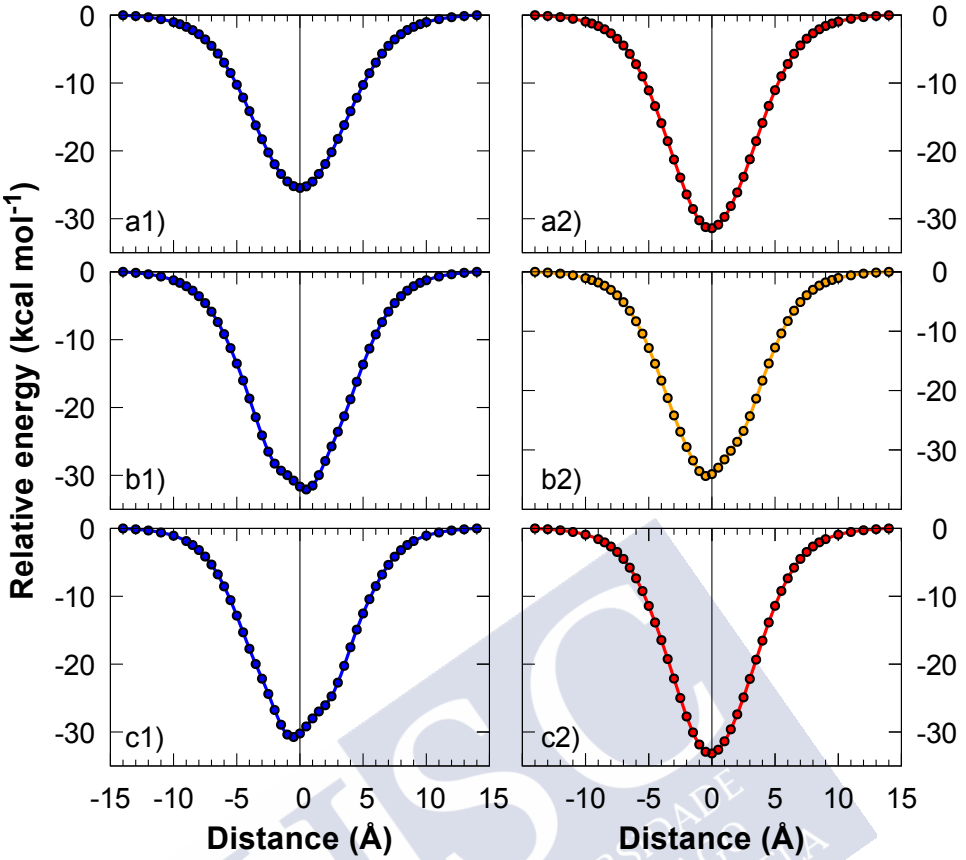

Figure c.7: Energetic profile for the departure along the Z axis of C_{70} inside different nanorings. a1) C_{70}(V)@[10]CPAq. a2) C_{70}(H)@[10]CPAq. b1) C_{70}(V)@[10]CPTcaq. b2) C_{70}(H)@[10]CPTcaq. c1) C_{70}(V)@[12]CPP. c2) C_{70}(H)@[12]CPP. For the C_{70} location and orientation, see the colour code of Figure 6.4.

C.7 NCIPLOT images for the departure of C_{70}

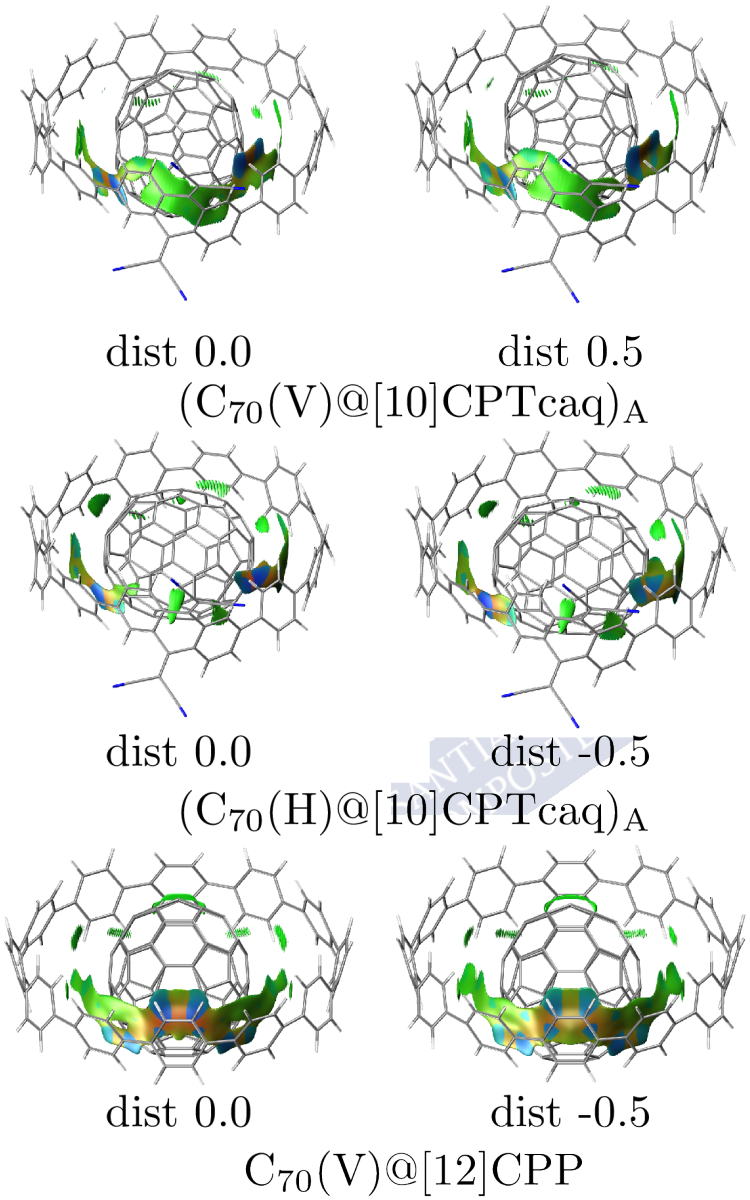

Figure c.8: 3D NCI plot for some departures in Z axis. The gradient isosurface (0.3 a.u.) and the blue-green-red scale over the range −0.020 and 0.020 are according to the sign of the second eigenvalue of the Hessian times the density.

C.8 Bond critical points in complexes

Table c.2: Electron density for the bond critical points between the fullerene and the nanohoop for the most stable complexes. N_{BCP} is the number identifying the critical point.

	N_{BCP}	density	N_{BCP}	density	N_{BCP}	density
C_{60}(5)@[10]CPAq	46	3.5488×10^{-3}	52	4.0001×10^{-3}	41	6.2832×10^{-3}
	58	6.0449×10^{-3}	71	5.9740×10^{-3}	126	5.3069×10^{-3}
	147	5.5101×10^{-3}	227	6.0365×10^{-3}	256	6.1260×10^{-3}
	260	5.7289×10^{-3}	262	4.1004×10^{-3}		
C_{60}(5)@[12]CPP	447	5.3130×10^{-3}	435	6.1156×10^{-3}	429	6.2170×10^{-3}
	396	5.6096×10^{-3}	378	5.2550×10^{-3}	316	5.2561×10^{-3}
	293	5.6104×10^{-3}	241	6.2164×10^{-3}	236	6.1170×10^{-3}
	225	5.3152×10^{-3}	317	1.4187×10^{-6}		
C_{60}(5)@[10]CPTcaq	234	5.6126×10^{-3}	229	6.1239×10^{-3}	231	6.3227×10^{-3}
	247	5.6299×10^{-3}	263	5.4047×10^{-3}	320	5.0822×10^{-3}
	340	5.3137×10^{-3}	429	6.1519×10^{-3}	460	6.1674×10^{-3}
	463	3.7299×10^{-3}				
$(C_{70}(H)$@[10]CPAq$)_A$	479	2.8962×10^{-3}	486	3.6466×10^{-3}	498	7.2906×10^{-3}
	475	8.9597×10^{-3}	471	5.0610×10^{-3}	440	5.6311×10^{-3}
	400	4.6650×10^{-3}	317	5.7298×10^{-3}	269	6.6851×10^{-3}
	245	7.2984×10^{-3}	229	5.3144×10^{-3}	240	2.3307×10^{-3}
	312	1.4615×10^{-5}				
$C_{70}(H)$@[12]CPP	509	5.1486×10^{-4}	456	5.2036×10^{-3}	463	3.0516×10^{-3}
	469	6.9759×10^{-3}	440	7.6802×10^{-3}	382	5.7325×10^{-3}
	294	6.3607×10^{-3}	242	6.9929×10^{-3}	232	7.1830×10^{-3}
	222	5.4532×10^{-3}	506	1.0358×10^{-3}	507	1.4853×10^{-5}
$C_{70}(H)$@[10]CPTcaq	536	4.9145×10^{-4}	242	3.9005×10^{-3}	241	8.3776×10^{-3}
	243	7.4993×10^{-3}	279	4.3445×10^{-3}	324	6.6088×10^{-3}
	369	7.0420×10^{-3}	416	6.1472×10^{-3}	451	5.5305×10^{-3}
	486	7.0265×10^{-3}	490	7.7682×10^{-3}		

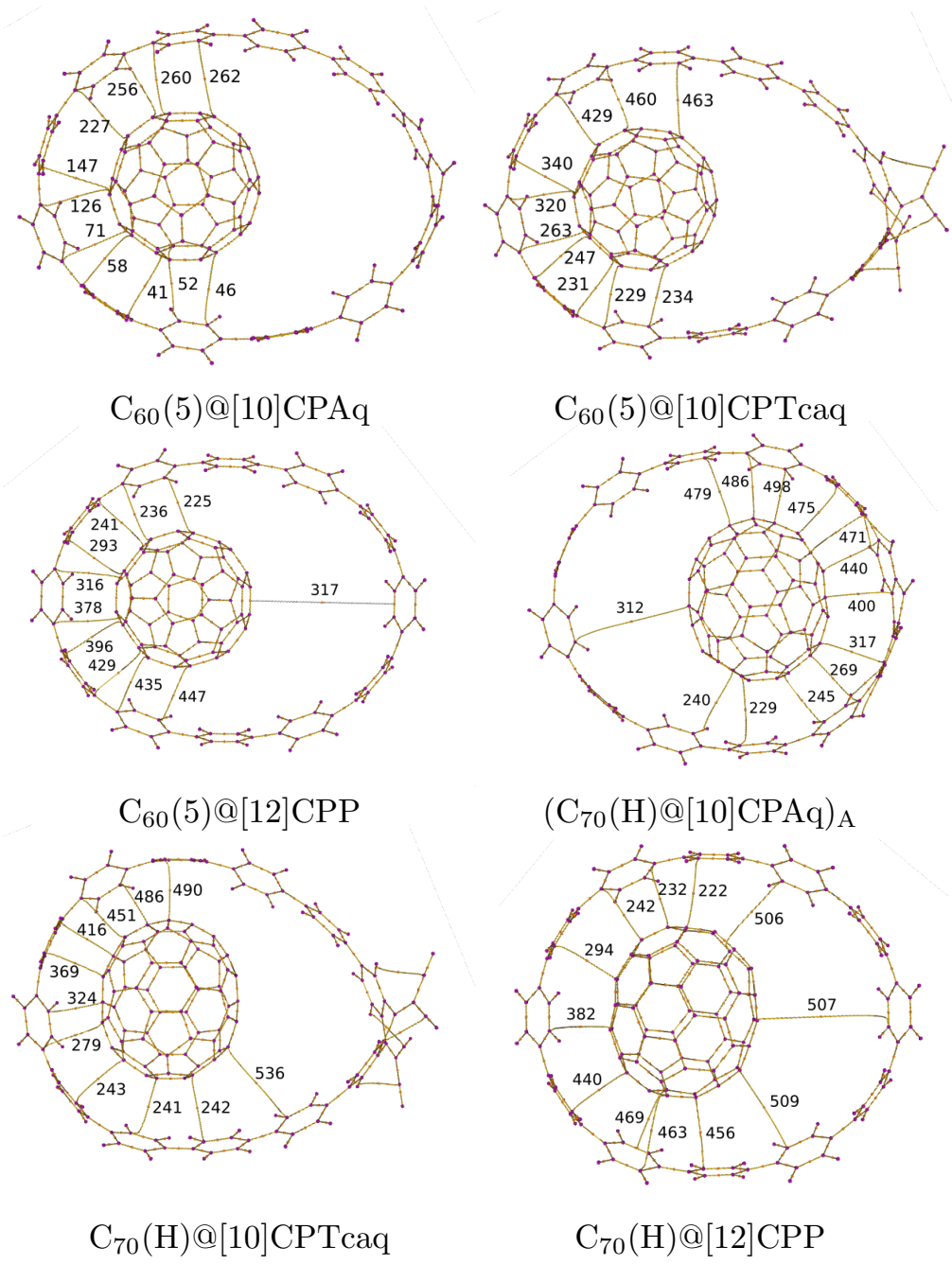

Figure c.9: Bond critical points for the most stable complexes. The numbers refer to the values listed in Table c.2.

C.9 Absorption spectra

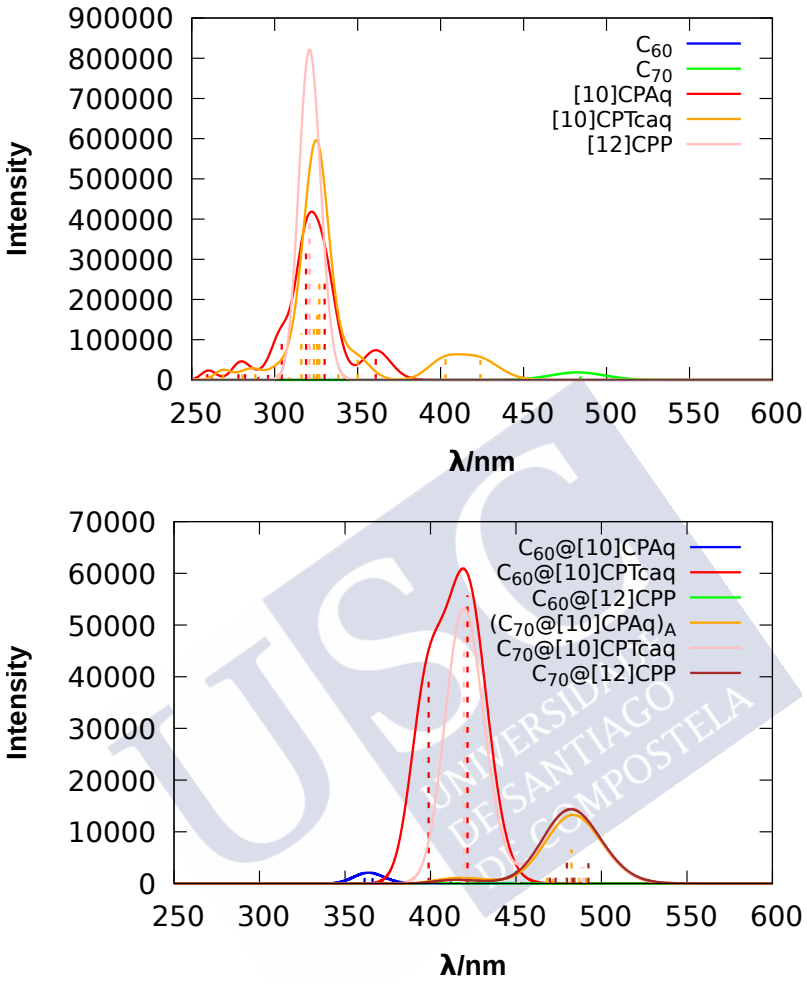

Figure c.10: Absorption spectra for the monomers and complexes studied at CAM-B3LYP/TZVP level.

C.10 Charge transfer in monomers

Table c.3: Amount of the charge transfer and the distance for the four most important transitions in monomers. N_{tr} is the number of the transition, q is the amount of charge that it transferred and R is the distance between positive and negative barycentre following the works of Jacquemin *et al.*[1] and LeBahers *et al.*[2]

	N_{tr}	q	R (Å)	N_{tr}	q	R (Å)
C_{60}	20	0.368	0.000	21	0.354	0.000
	22	0.375	0.000	24	0.405	0.000
C_{70}	5	0.325	0.584	6	0.348	0.633
	7	0.335	0.532	8	0.358	0.582
[10]CPAq	2	0.658	0.052	5	0.450	1.606
	6	0.465	1.517	7	0.665	0.317
[10]CPTcaq	6	0.869	**15.001**	7	0.423	2.036
	8	0.435	1.979	9	0.569	**10.116**
[12]CPP	2	0.401	0.000	3	0.362	0.001
	7	0.327	0.000	17	0.298	0.001

[1]D. Jacquemin, T. L. Bahers, C. Adamo and I. Ciofini, *Physical Chemistry Chemical Physics*, 2012, **14**, 5383–5388

[2]T. Le Bahers, C. Adamo and I. Ciofini, *Journal of Chemical Theory and Computation*, 2011, **7**, 2498–2506

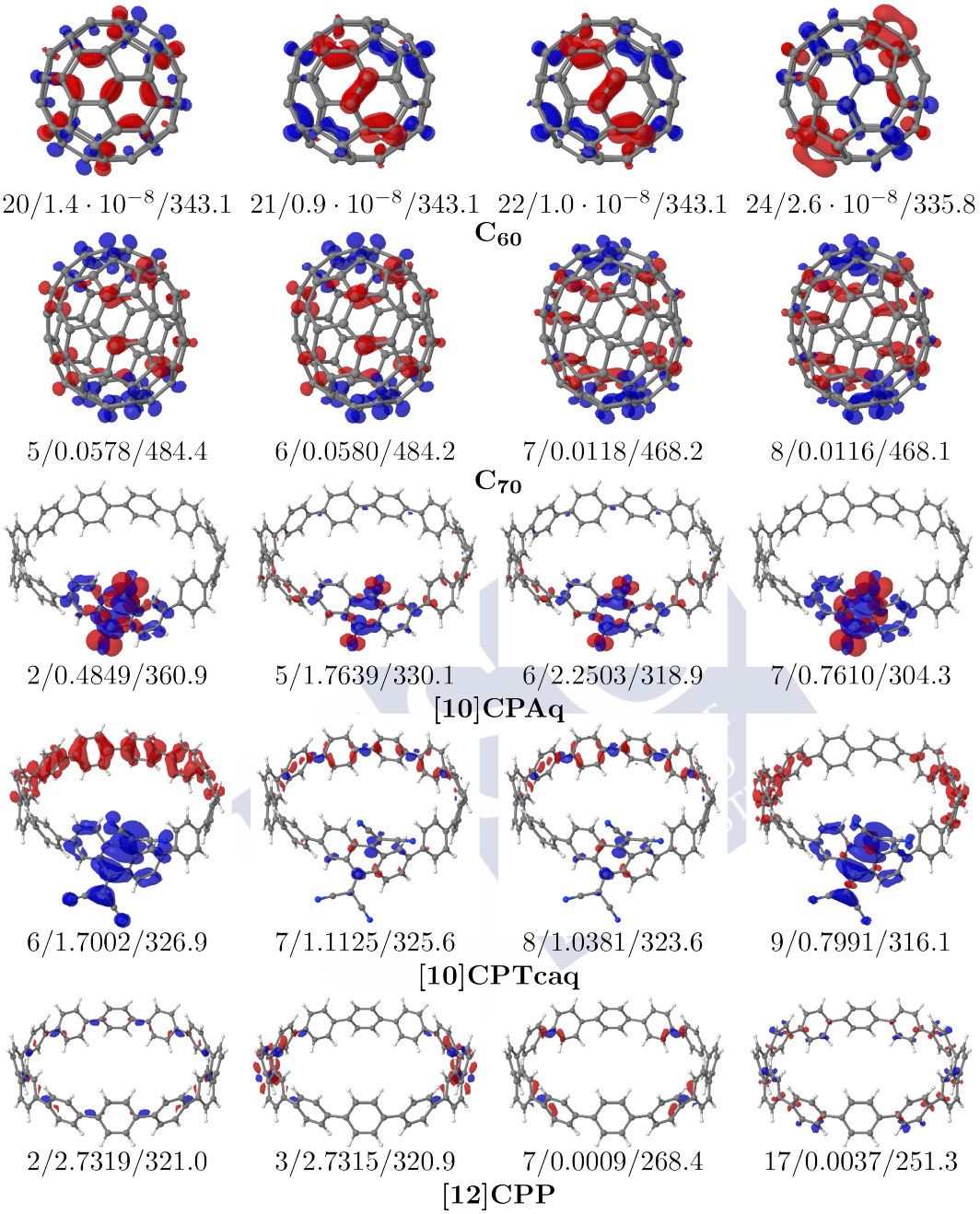

Figure c.11: Difference density between the excited state and the ground state for the four most intense transitions in monomers. The numbers are the number of the transition/oscillator strength/wavelenght (nm). Surfaces correspond to −0.001 a.u. (red) and 0.001 a.u. (blue).

C.11 HOMO-LUMO orbitals for complexes

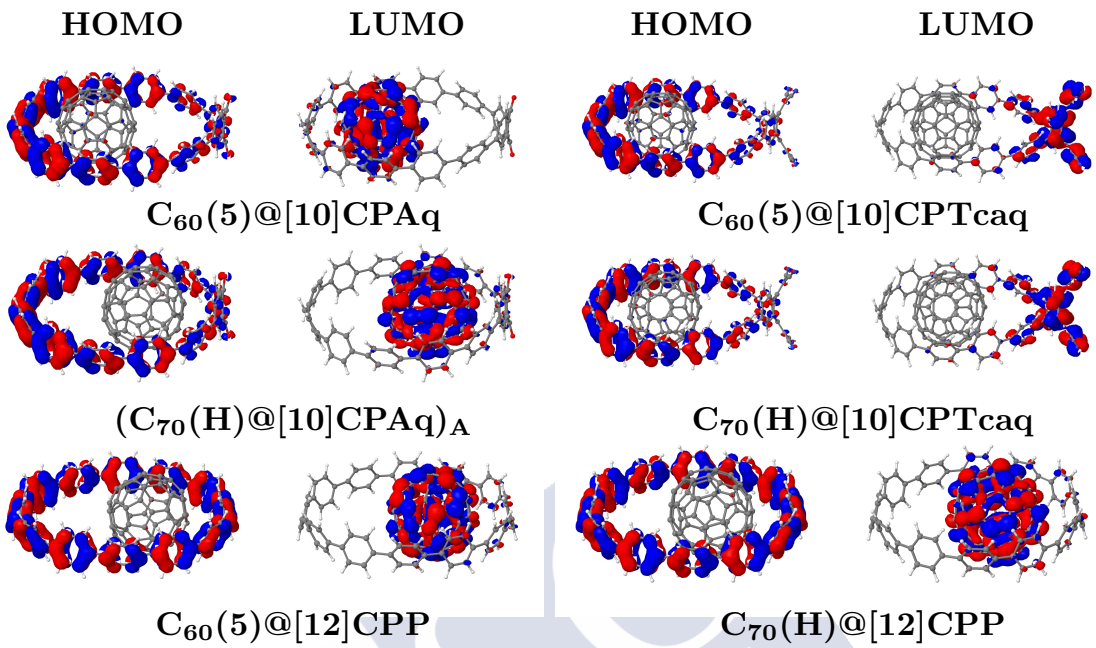

Figure c.12: HOMO and LUMO orbitals in complexes at the CAM-B3LYP/def2-TVZVP//B97-D2/def2-TZVP level.

C.12 Position of the barycentres

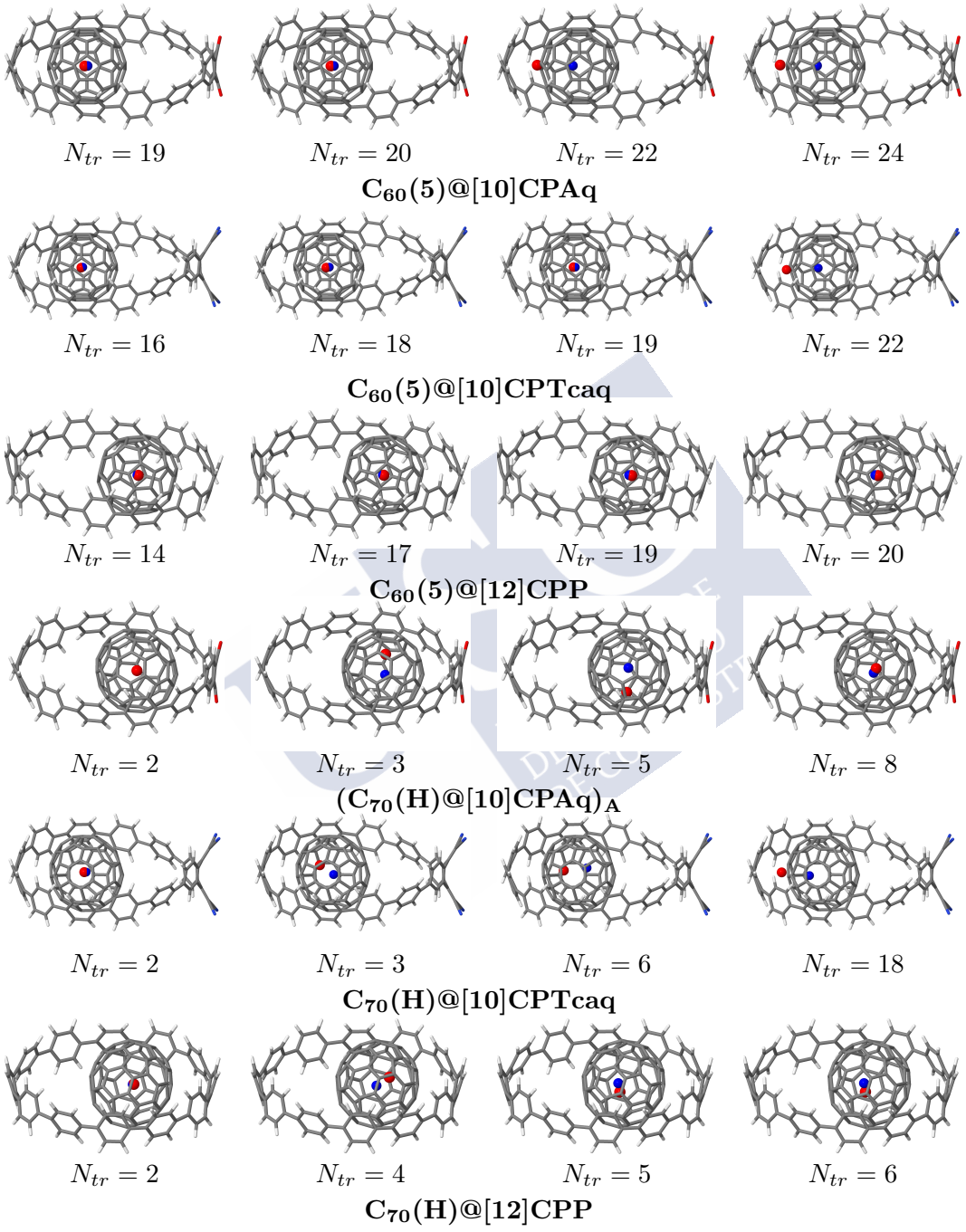

Figure c.13: Position of the barycentres of charge in the most stable complexes. The blue sphere corresponds to the positive barycentre and the red sphere is the negative barycentre.

C.13 Charge transfer in different nanohoops

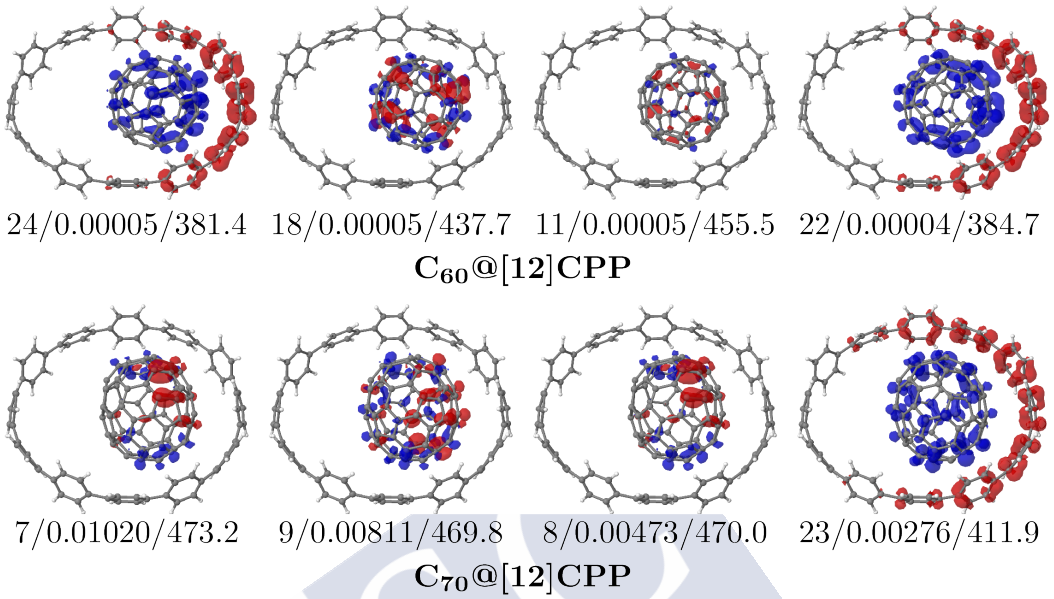

Figure c.14: Difference density between the excited state and the ground state for the five to eight most intense transition in C_{60}@[12]CPP and C_{70}@[12]CPP. The numbers are the number of the transition/oscillator strength/wavelength (nm). Surfaces correspond to −0.001 a.u. (red) and 0.001 a.u. (blue).

Table c.4: Amount of the charge transfer and the distance for the five to eight most important transitions in the most stable complexes between fullerenes and [12]CPP. N_{tr} is the number of the transition, q is the amount of charge transferred and R is the distance between positive and negative barycentre following the works of Jacquemin *et al.*[1] and LeBahers *et al.*[2]

	N_{tr}	q	R (Å)	N_{tr}	q	R (Å)
C_{60}@[12]CPP	11	0.257	0.145	18	0.431	0.083
	22	0.931	2.709	24	0.841	2.856
C_{70}@[12]CPP	07	0.329	1.401	08	0.357	1.371
	09	0.454	1.137	23	0.970	2.161

[1]D. Jacquemin, T. L. Bahers, C. Adamo and I. Ciofini, *Physical Chemistry Chemical Physics*, 2012, **14**, 5383–5388

[2]T. Le Bahers, C. Adamo and I. Ciofini, *Journal of Chemical Theory and Computation*, 2011, **7**, 2498–2506

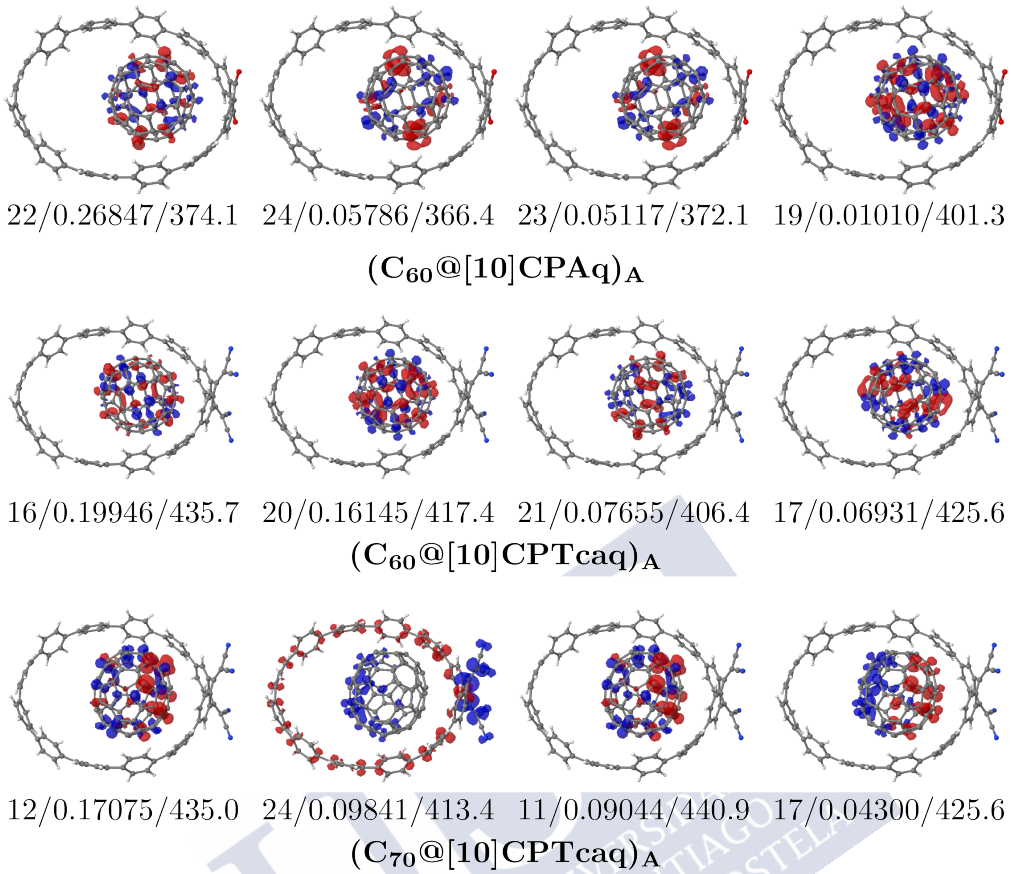

Figure c.15: Difference density between the excited state and the ground state for the four most intense transitions with the fullerene near the anthracene unit. The numbers are the number of the transition/oscillator strength/wavelength (nm). Surfaces correspond to −0.001 a.u. (red) and 0.001 a.u. (blue).

Table c.5: Amount of the charge transfer and the distance for the four most important transitions in complexes with the fullerene near the anthracene. N_{tr} is the number of the transition, q is the amount of charge transferred and R is the distance between positive and negative barycentre following the works of Jacquemin *et al.*[1] and LeBahers *et al.*[2]

	N_{tr}	q	R (Å)	N_{tr}	q	R (Å)
$(C_{60}@[10]CPAq)_A$	19	0.476	0.038	22	0.375	0.122
	23	0.359	0.102	24	0.378	0.100
$(C_{60}@[10]CPTcaq)_A$	16	0.403	0.137	17	0.454	0.110
	20	0.471	0.116	21	0.381	0.234
$(C_{70}@[10]CPTcaq)_A$	11	0.511	1.463	12	0.526	1.459
	17	0.424	3.120	24	0.798	4.507

[1]D. Jacquemin, T. L. Bahers, C. Adamo and I. Ciofini, *Physical Chemistry Chemical Physics*, 2012, **14**, 5383–5388, p. 1

[2]T. Le Bahers, C. Adamo and I. Ciofini, *Journal of Chemical Theory and Computation*, 2011, **7**, 2498–2506

C.14 Complexation energies at B3LYP-D3(BJ)/-def2-TZVP level

Table c.6: Energies for the complexes with C_{60} (kcal mol^{-1}) obtained at the B3LYP-D3(BJ)/def2-TZVP level using the B97-D2/def2-TZVP geometries. $\Delta E_{\text{complex}}$ is the complexation energy, ΔE_{def} is the deformation energy of the monomers, ΔE_{disp} is the contribution of dispersion to the total complexation energy.

Complex[a]	$\Delta E_{\text{complex}}$	ΔE_{def}		ΔE_{disp}
		Fullerene	Ring	
$(C_{60}(5)@[10]CPAq)_A$	−29.96	−0.10	3.31	−49.54
$(C_{60}(6)@[10]CPAq)_A$	−29.42	−0.09	2.77	−48.91
$(C_{60}(5)@[10]CPTcaq)_A$	−29.77	−0.02	2.78	−49.26
$(C_{60}(6)@[10]CPTcaq)_A$	−30.28	−0.09	2.65	−50.05
$C_{60}(5)@[12]CPP$	−30.67	−0.01	2.89	−49.91
$C_{60}(6)@[12]CPP$	−29.89	−0.12	3.26	−49.04
$C_{60}(5)@[10]CPAq$	−31.15	−0.04	2.37	−50.19
$C_{60}(6)@[10]CPAq$	−30.51	−0.09	2.99	−50.24
$C_{60}(5)@[10]CPTcaq$	−33.06	−0.06	2.04	−52.43
$C_{60}(6)@[10]CPTcaq$	−32.51	−0.12	2.67	−52.40

[a] Subscript A denotes when the fullerene is closer to the anthracene unit.

Table c.7: Energies for the complexes with C_{70} (kcal mol^{-1}) obtained at the B3LYP-D3(BJ)/def2-TZVP level using the B97-D2/def2-TZVP geometries. $\Delta E_{\text{complex}}$ is the complexation energy, ΔE_{def} is the deformation energy of the monomers, ΔE_{disp} is the contribution of dispersion to the total complexation energy.

Complex[a]	$\Delta E_{\text{complex}}$	ΔE_{def}		ΔE_{disp}
		Fullerene	Ring	
$(C_{70}(V)@[10]CPAq)_A$	−33.73	0.04	3.58	−56.07
$(C_{70}(H)@[10]CPAq)_A$	−35.69	0.01	2.12	−55.76
$(C_{70}(V)@[10]CPTcaq)_A$	−34.91	−0.06	2.95	−57.24
$(C_{70}(H)@[10]CPTcaq)_A$	−35.42	0.10	2.35	−56.51
$C_{70}(V)@[12]CPP$	−34.12	−0.08	2.88	−55.51
$C_{70}(H)@[12]CPP$	−34.83	0.04	1.02	−53.17
$C_{70}(V)@[10]CPAq$	−34.40	−0.09	2.63	−55.62
$C_{70}(H)@[10]CPAq$	−35.18	0.13	1.77	−54.86
$C_{70}(V)@[10]CPTcaq$	−36.30	−0.06	1.94	−57.09
$C_{70}(H)@[10]CPTcaq$	−37.11	0.06	1.15	−56.74

[a] Subscript A denotes when the fullerene is closer to the anthracene unit.

C.15 [10]CPA molecules

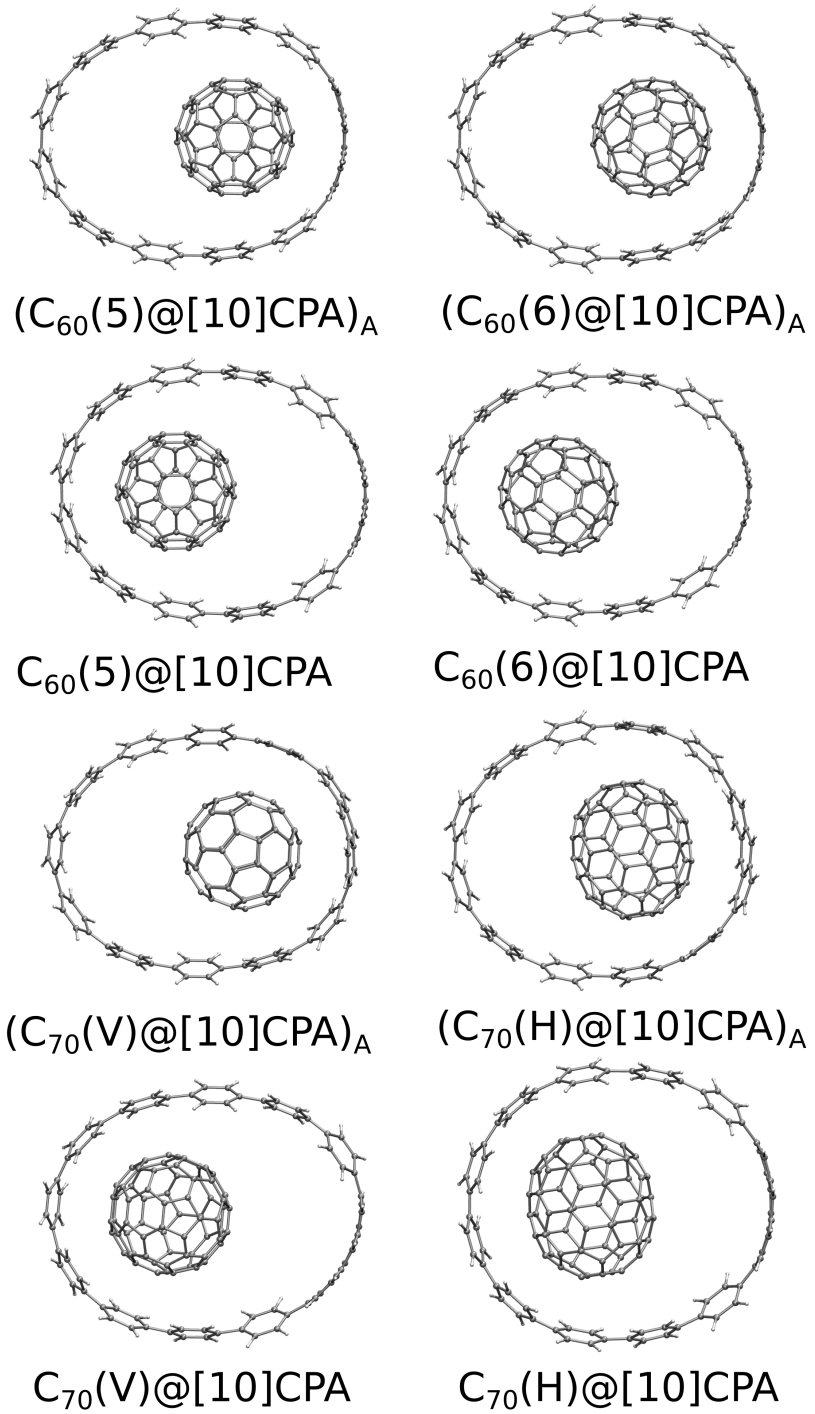

Figure c.16: Most stable structures found for [10]CPA complexes.

C.16 [10]CPA complexation energy

Table c.8: Energy for the complexes with [10]CPA (kcal mol^{-1}). $\Delta E_{\text{complex}}$ is the complexation energy, ΔE_{def} is the deformation energies of monomers, ΔE_{disp} the contribution of dispersion to the total complexation energy, R_{centre} is the distance between the centres of the host and guest.

Complex[a]	$\Delta E_{\text{complex}}$	ΔE_{def}		ΔE_{disp}	R_{centre} (Å)
		Fullerene	Ring		
$(C_{60}(5)@[10]CPA)_A$	−31.45	0.08	4.94	−59.01	2.288
$(C_{60}(6)@[10]CPA)_A$	−31.02	0.09	4.59	−57.68	2.270
$C_{60}(5)@[10]CPA$	−30.77	0.10	3.27	−55.74	2.389
$C_{60}(6)@[10]CPA$	−30.38	0.07	4.24	−56.90	2.422
$(C_{70}(V)@[10]CPA)_A$	−35.70	0.17	4.43	−65.24	2.206
$(C_{70}(H)@[10]CPA)_A$	−38.01	0.13	2.51	−64.66	1.670
$C_{70}(V)@[10]CPA$	−34.61	0.12	3.90	−63.15	2.290
$C_{70}(H)@[10]CPA$	−36.15	0.11	1.58	−60.11	1.779

[a] Subscript A denotes when the fullerene is closer to the anthracene unit.

USC UNIVERSIDADE DE SANTIAGO DE COMPOSTELA

C.17 [10]CPA MEP

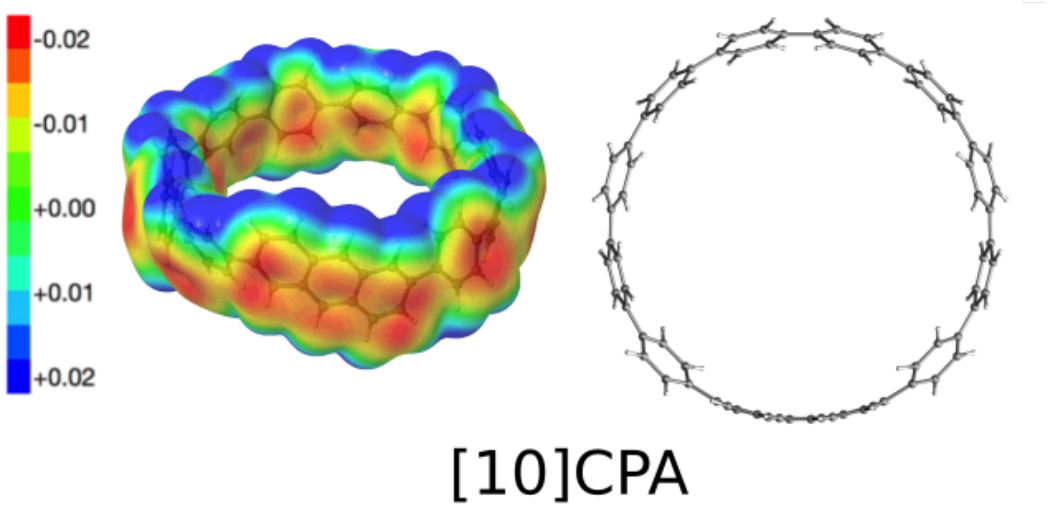

Figure c.17: [10]CPA nanohoop studied together with its molecular electrostatic potential (MEPs) mapped on a 0.001 a.u. electron density isosurfaces at the B97-D2/def2-TZVP level.

USC UNIVERSIDADE DE SANTIAGO DE COMPOSTELA

C.18 [10]CPA charge transfer

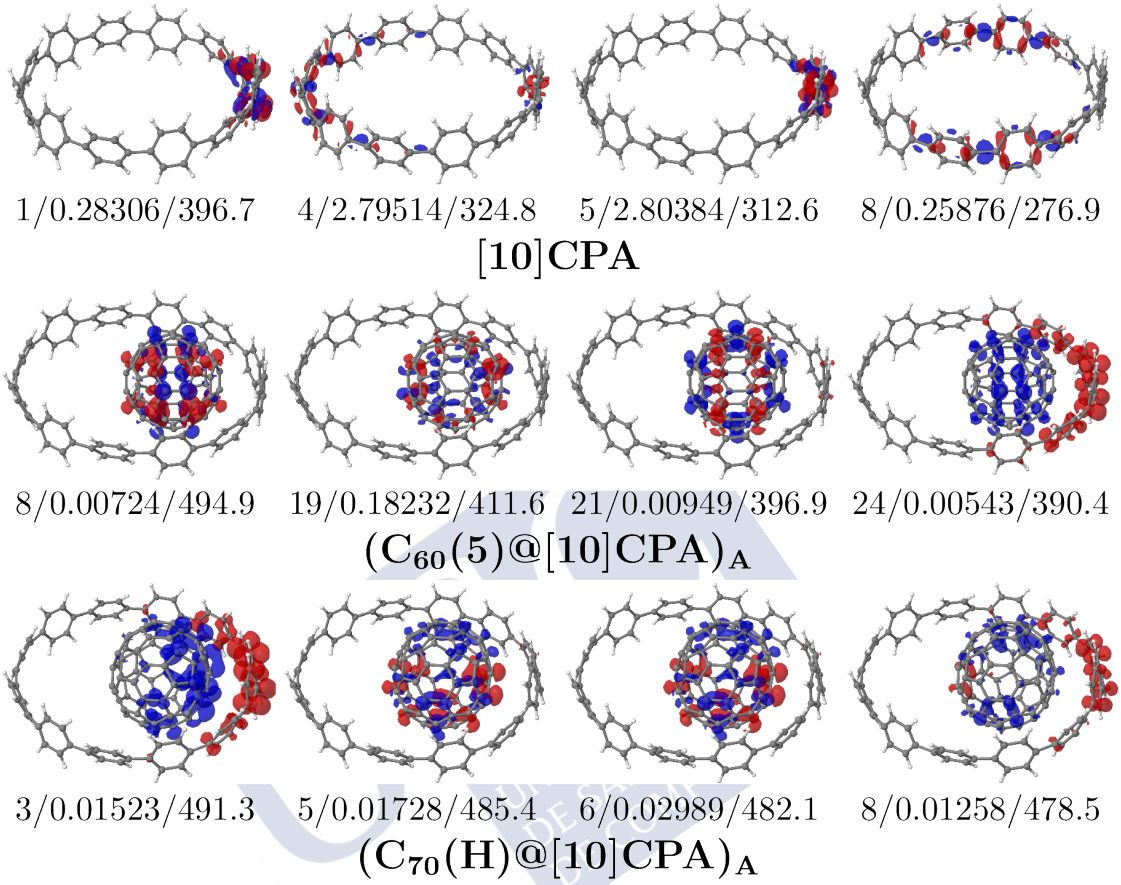

Figure c.18: Difference density between the excited state and the ground state for the four most intense transitions in the most stable structures found in [10]CPA and their complexes. The numbers are the number of the transition/oscillator strength/wavelength (nm). Surfaces correspond to −0.001 a.u. (red) and 0.001 a.u. (blue).

Table c.9: Amount of the charge transfer and the distance for the four most important transitions found in [10]CPA and the most stable [10]CPA complexes. N_{tr} is the number of the transition, q is the amount of charge transferred and R is the distance between positive and negative barycentre following the works of Jacquemin *et al.*[1] and LeBahers *et al.*[2]

	N_{tr}	q	R (Å)	N_{tr}	q	R (Å)
[10]CPA	1	0.282	0.012	4	0.392	0.094
	5	0.216	0.132	8	0.414	0.219
$(C_{60}(5)@[10]CPA)_A$	8	0.570	0.433	19	0.387	0.388
	21	0.502	0.958	24	0.852	4.382
$(C_{70}(H)@[10]CPA)_A$	3	0.945	3.895	5	0.526	2.055
	6	0.548	2.006	8	0.555	3.599

USC UNIVERSIDADE DE SANTIAGO DE COMPOSTELA

[1] D. Jacquemin, T. L. Bahers, C. Adamo and I. Ciofini, *Physical Chemistry Chemical Physics*, 2012, **14**, 5383–5388

[2] T. Le Bahers, C. Adamo and I. Ciofini, *Journal of Chemical Theory and Computation*, 2011, **7**, 2498–2506

C.19 Anthracene-substituted [8]CPP complexes

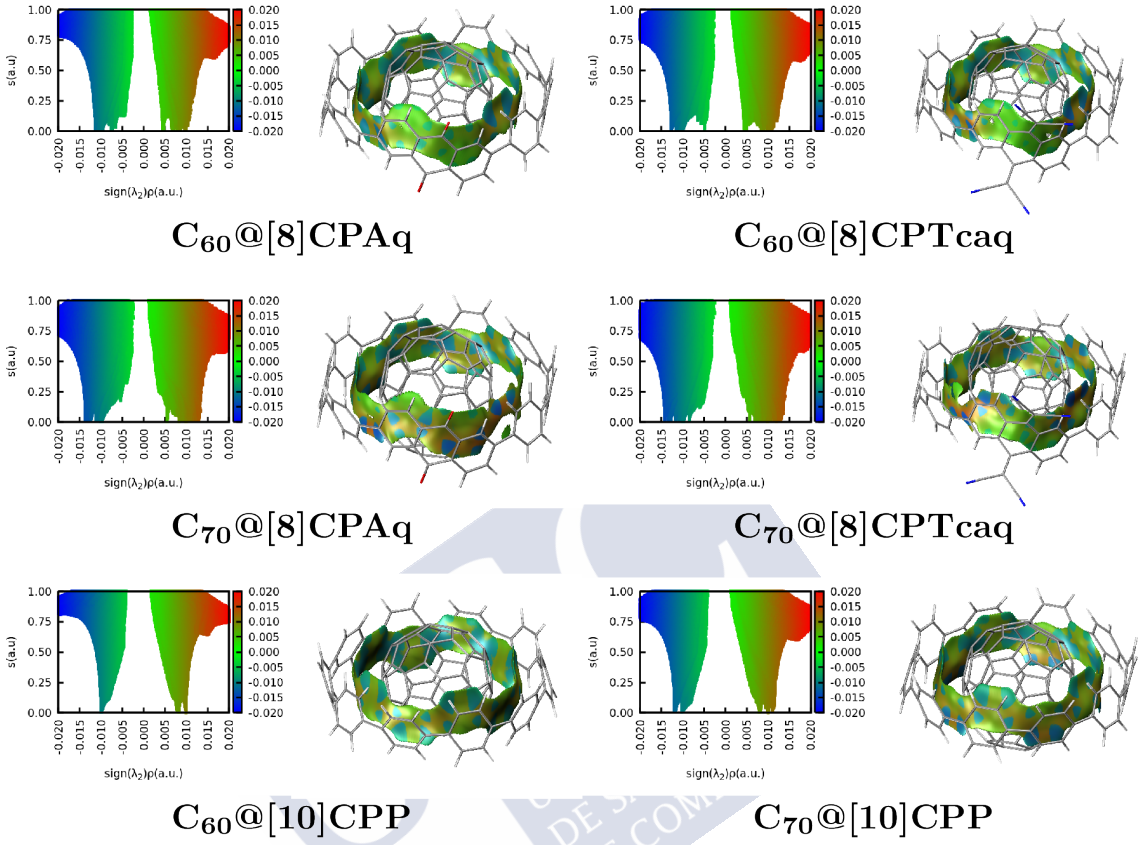

Figure c.19: 2D and 3D NCI plots for the most stable structures found for anthracene-substituted [8]CPP complexes. The product of the density times the sign of the second eigenvalue of its Hessian is mapped onto an isosurface of reduced density gradient with value 0.3 a.u. The colour scale goes from −0.020 a.u. (blue) to +0.020 a.u. (red).

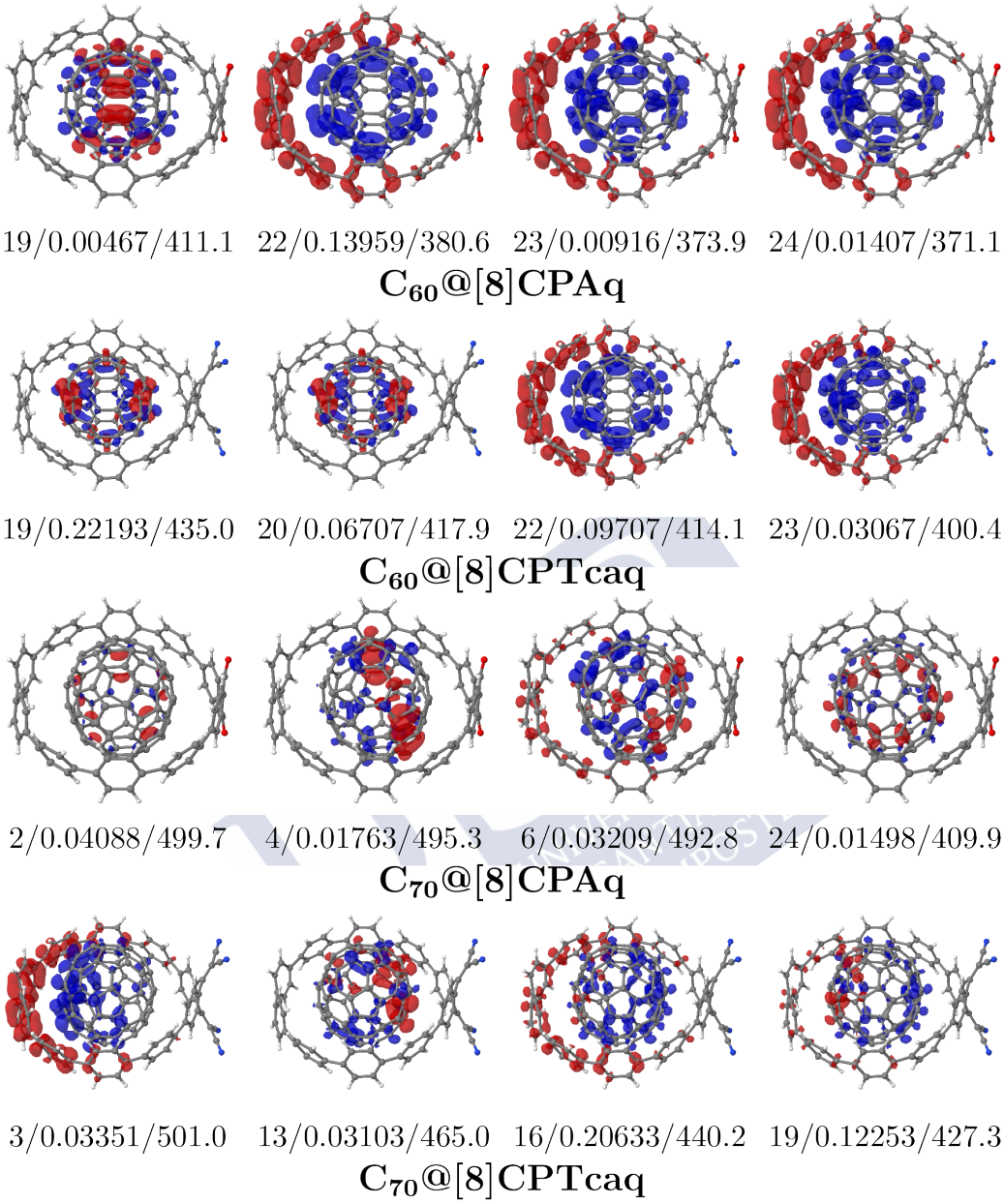

Figure c.20: Difference density between the excited state and the ground state for the four most intense transitions in anthracene-substituted [8]CPX complexes. The numbers are the number of the transition/oscillator strength/wavelength (nm). Surfaces correspond to −0.001 a.u. (red) and 0.001 a.u. (blue).

C.20 Structures for C_{100} with the nanohoops

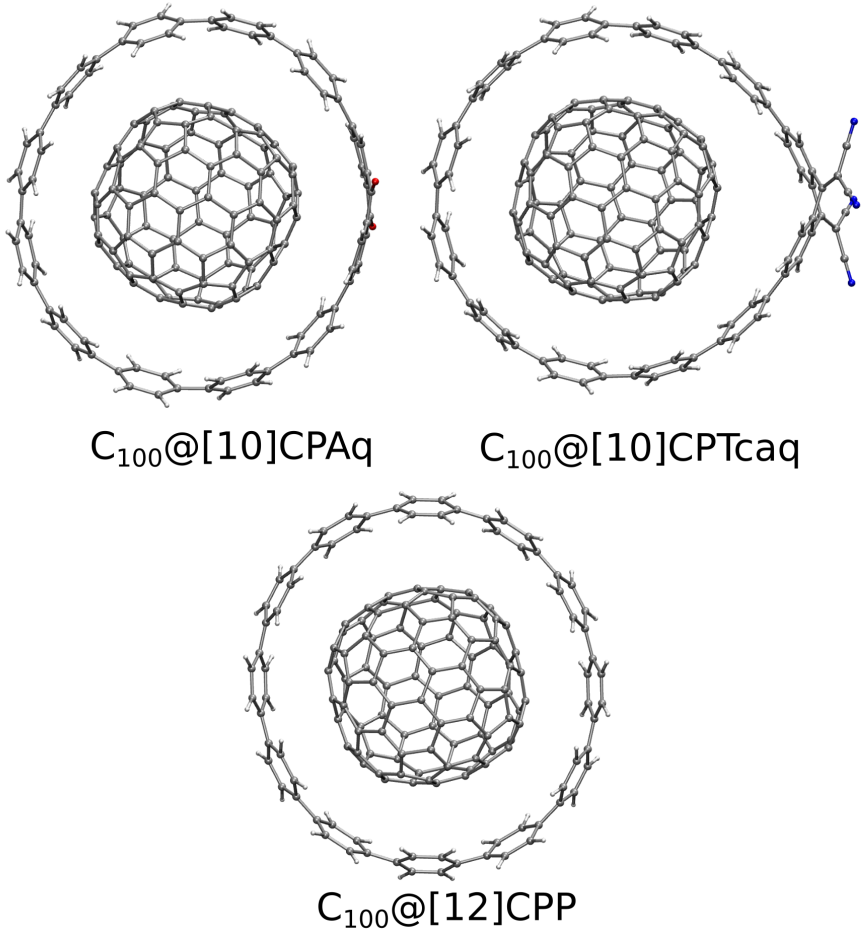

Figure c.21: Most stable structures found for C_{100} complexes with the nanohoops.

USC
UNIVERSIDADE
DE SANTIAGO
DE COMPOSTELA

Appendix D

Supplementary information Chapter 7

D.1 Fitting to an ellipse

Table d.1: Results of fitting the carbon atoms in the nanoring to an ellipse for the different complexes studied. Radii in Å; f is the flattening $f = (R_1 - R_2)/R_1$.

	R_1	R_2	f	$1/f$
[11]CPP-C_{60}	15.8	14.2	0.101	10
[11]CPP-C_{70}	15.5	14.6	0.057	18
[11]CPP-C_{76}	15.5	14.7	0.055	18
[11]CPP-C_{78}	15.3	14.7	0.039	26
[11]CPP-$Sc_3N@C_{80}$	15.1	15.1	0.001	1514
[11]CPP-$Y@C_{82}$	15.4	14.9	0.028	36
[11]CPP-$Tm@C_{82}$	15.3	15.0	0.024	41
[11]CPP-$Y_2@C_{82}$	15.2	15.1	0.004	253
[11]CPP-$Lu_2@C_{82}$	15.2	15.1	0.008	127

D.2 NBO second order perturbation analysis

Table d.2: Second order perturbation analysis obatined as the energies of delocalization of electrons from filled NBOs into empty NBOs (E_2). Values greater than 0.5 kcal mol^{-1} for the π donation from [11]-CPP to the fullerenes are shown.

Donor	**Acceptor**	**E_2(kcal mol^{-1})**
	[11]CPP-C_{70}	
BD(2)C85-C86	BD*(2)C45-C46	0.54
	[11]CPP-C_{76}	
BD(2)C91-C92	BD*(2)C3-C48	0.89
BD(2)C100-C101	BD*(2)C35-C40	0.87
CR(1)C185	RY*(7)C75	0.53
	[11]CPP-C_{78}	
BD(2)C81-C82	BD*(2)C13-C15	0.80
BD(2)C83-C188	BD*(2)C1-C3	0.82
BD(2)C114-C115	BD*(2)C63-C64	0.81
BD(2)C116-C117	BD*(2)C58-C61	0.81
BD(2)C123-C124	BD*(2)C59-C60	0.62
BD(2)C126-C127	BD*(2)C46-C49	0.60
BD(2)C135-C136	BD*(2)C8-C10	0.57
BD(2)C138-C139	BD*(2)C2-C4	0.57
	[11]CPP-$Sc_3N@C_{80}$	
BD(2)C96-C101	BD*(2)C45-C64	0.52
BD(2)C102-C107	BD*(2)C43-C63	0.67
BD(2)C108-C109	BD*(2)C58-C59	0.73
	[11]CPP-$Y_2@C_{82}$	
BD(2)C87-C88	BD*(2)C75-C76	0.62
BD(2)C89-C150	LP(1)C77	1.37
BD(2)C90-C91	LP(1)C21	1.64
BD(2)C114-C119	LP*(1)C47	0.60
BD(2)C122-C123	BD*(2)C41-C59	0.54
BD(2)C129-C130	BD*(2)C39-C40	0.51
BD(2)C132-C133	LP(1)C45	1.22
BD(2)C141-C142	BD*(2)C42-C69	0.55
	[11]CPP-$Lu_2@C_{82}$	
BD(2)C87-C88	BD*(2)C75-C76	0.61
BD(2)C89-C194	LP(1)C77	1.26
BD(2)C90-C91	LP(1)C21	1.62
BD(2)C99-C100	BD*(2)C4-C5	0.51
BD(2)C114-C119	LP*(1)C47	0.66
BD(2)C122-C123	BD*(2)C41-C59	0.52

D.3 HOMO-LUMO

Table d.3: Highest occupied and lowest unoccupied orbitals for the molecules considered in this work.

	HOMO (eV)	LUMO (eV)
[11]CPP	−4.848	−2.554
C_{60}	−5.757	−4.039
C_{70}	−5.753	−3.980
C_{76}	−5.293	−4.184
C_{78}	−5.209	−4.408
$Sc_3N@C_{80}$	−5.208	−3.691
$Y_2@C_{82}$	−4.355	−3.923
$Lu_2@C_{82}$	−5.000	−3.863
$Y@C_{82}$-α	−4.767	−4.011
$Y@C_{82}$-β	−5.333	−4.643
$Tm@C_{82}$-α	−5.302	−4.620
$Tm@C_{82}$-β	−4.895	−4.594

USC UNIVERSIDADE DE SANTIAGO DE COMPOSTELA

D.4 Euler angle

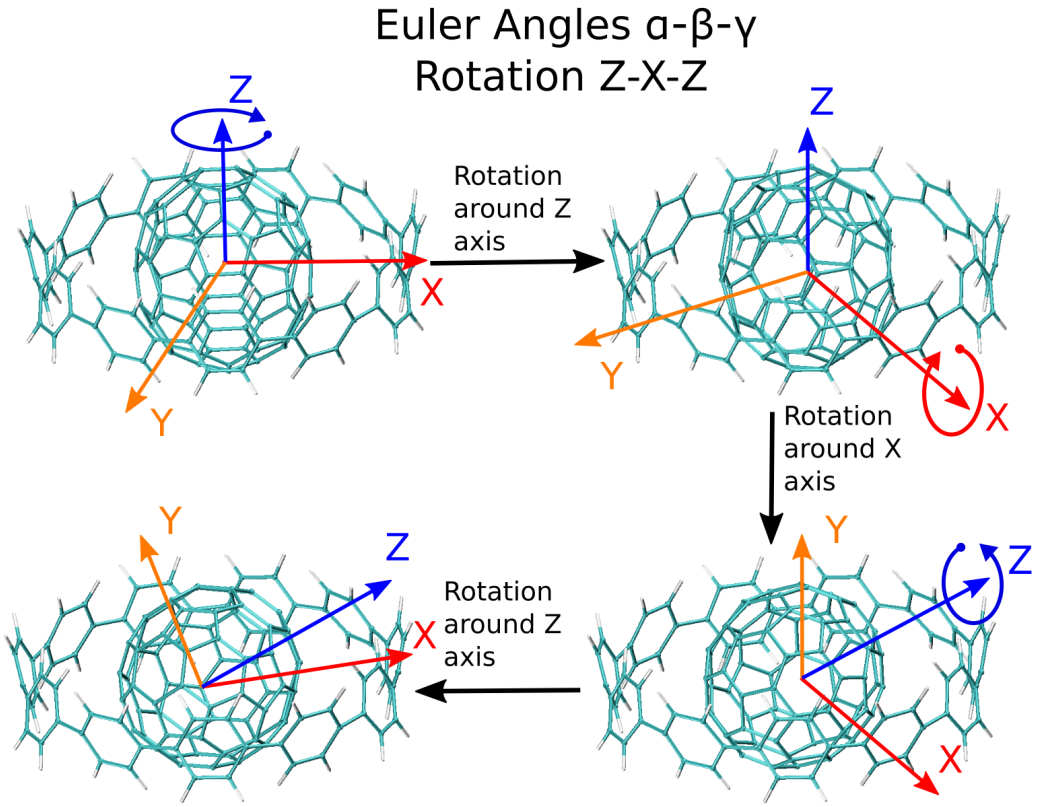

Figure d.1: Diagram showing how the rotation along the Euler angles was performed.

D.5 Energy profile in Euler rotations

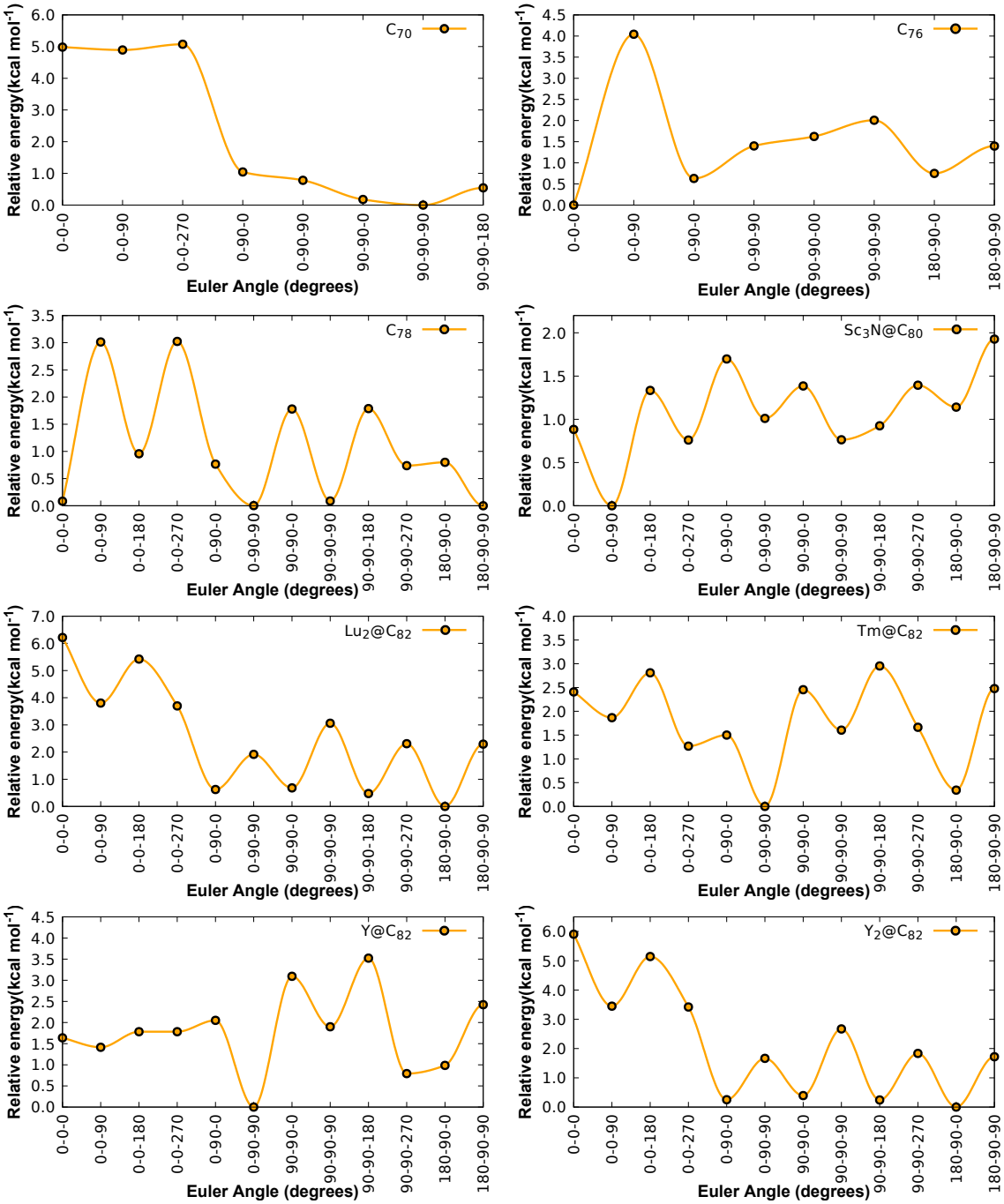

Figure d.2: Energy profiles obtained upon rotation of the different fullerenes along the Euler angles. The values in the X-axis correspond to Euler angles $\alpha - \beta - \gamma$.

D.6 Energy profile C_{60}

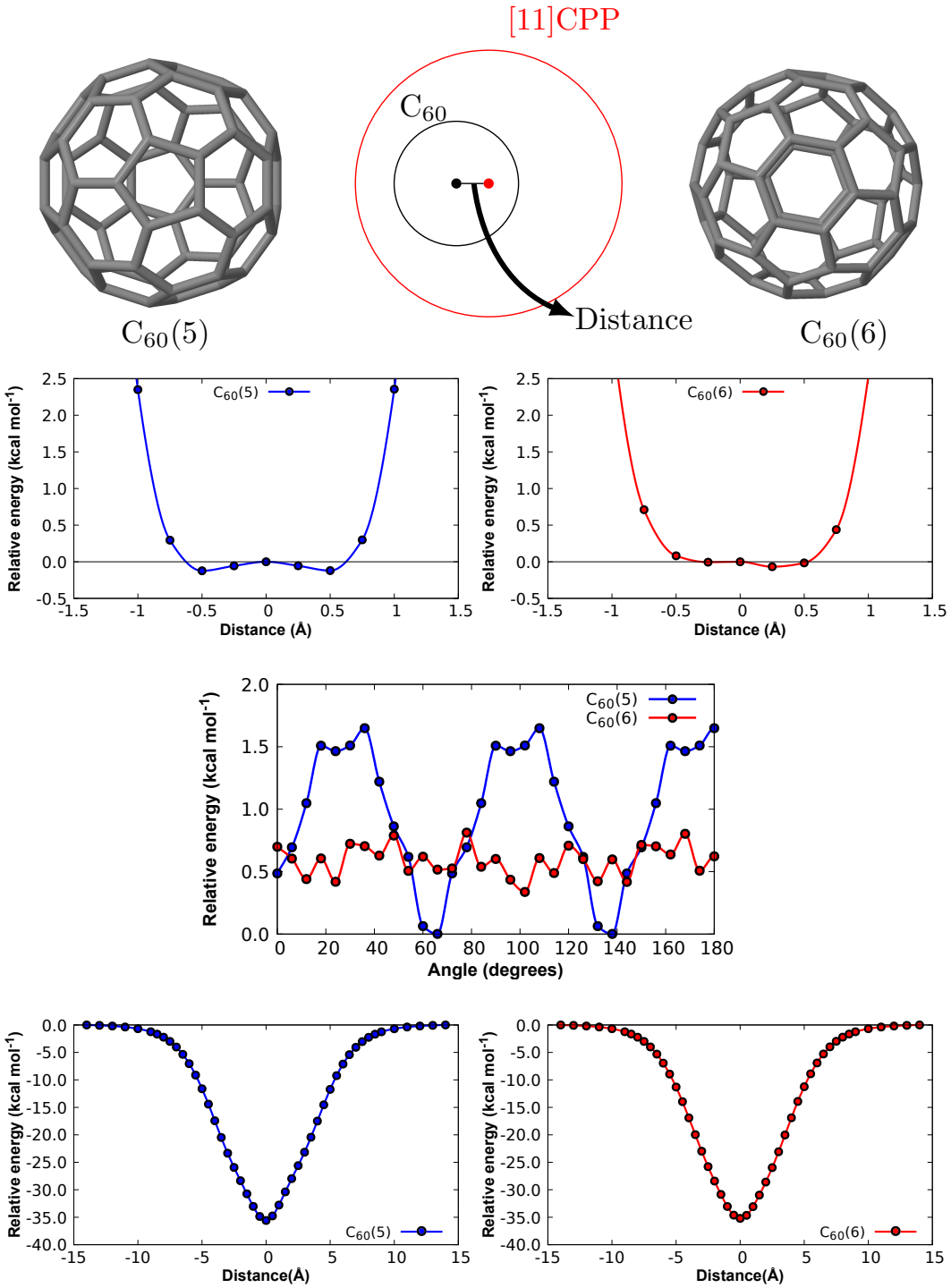

Figure d.3: Energy profiles obtained upon rotation of the C_{60}. Upper plots correspond to displacements inside the nanoring using two different orientations for C_{60} as explained in the top figures. Bottom plots show how energy changes as the fullerene is moved outside the nanoring. The plot in the centre shows energy changes when C_{60} is rotated along an axis perpendicular to the nanoring.

D.7 Interaction energy in corannulene dimer

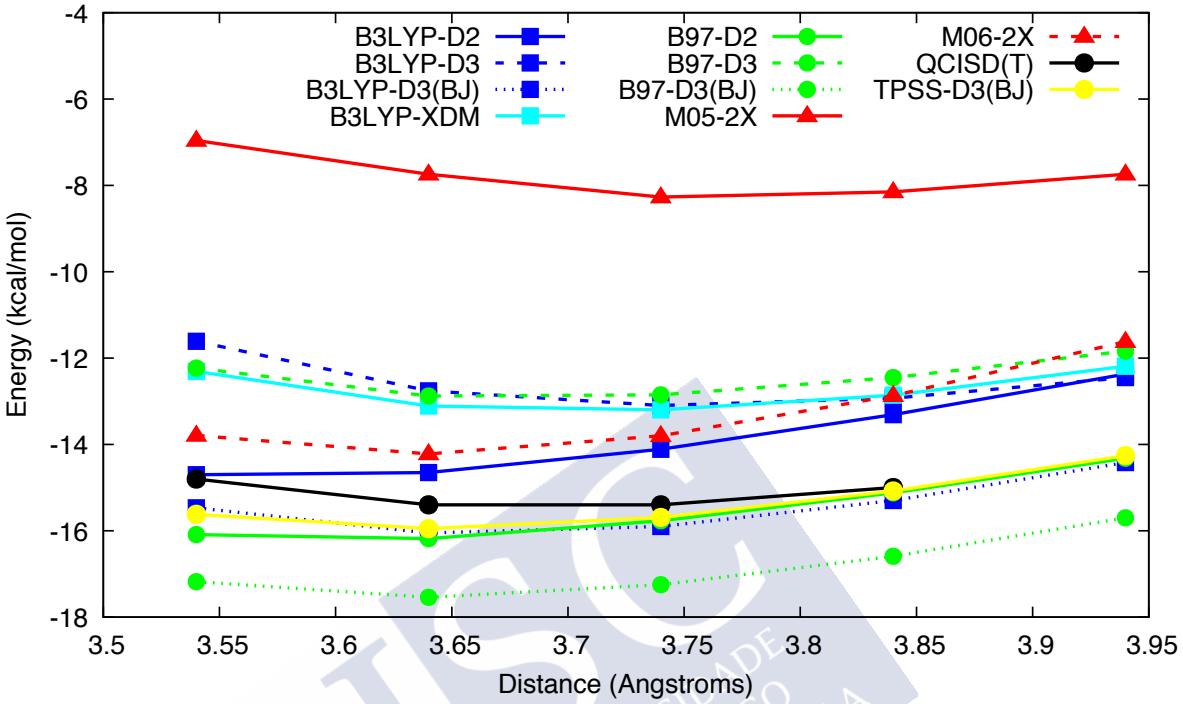

Figure d.4: Performance of different DFT methods to reproduce the interaction energy in corannulene dimer. Adapted from Kennedy *et al.*[1], adding values obtained at the TPSS-D/def2-TZVP level.

[1]M. R. Kennedy, L. A. Burns and C. D. Sherrill, *The Journal of Physical Chemistry A*, 2012, **116**, 11920–11926

D.8 Energy profile C_{70}

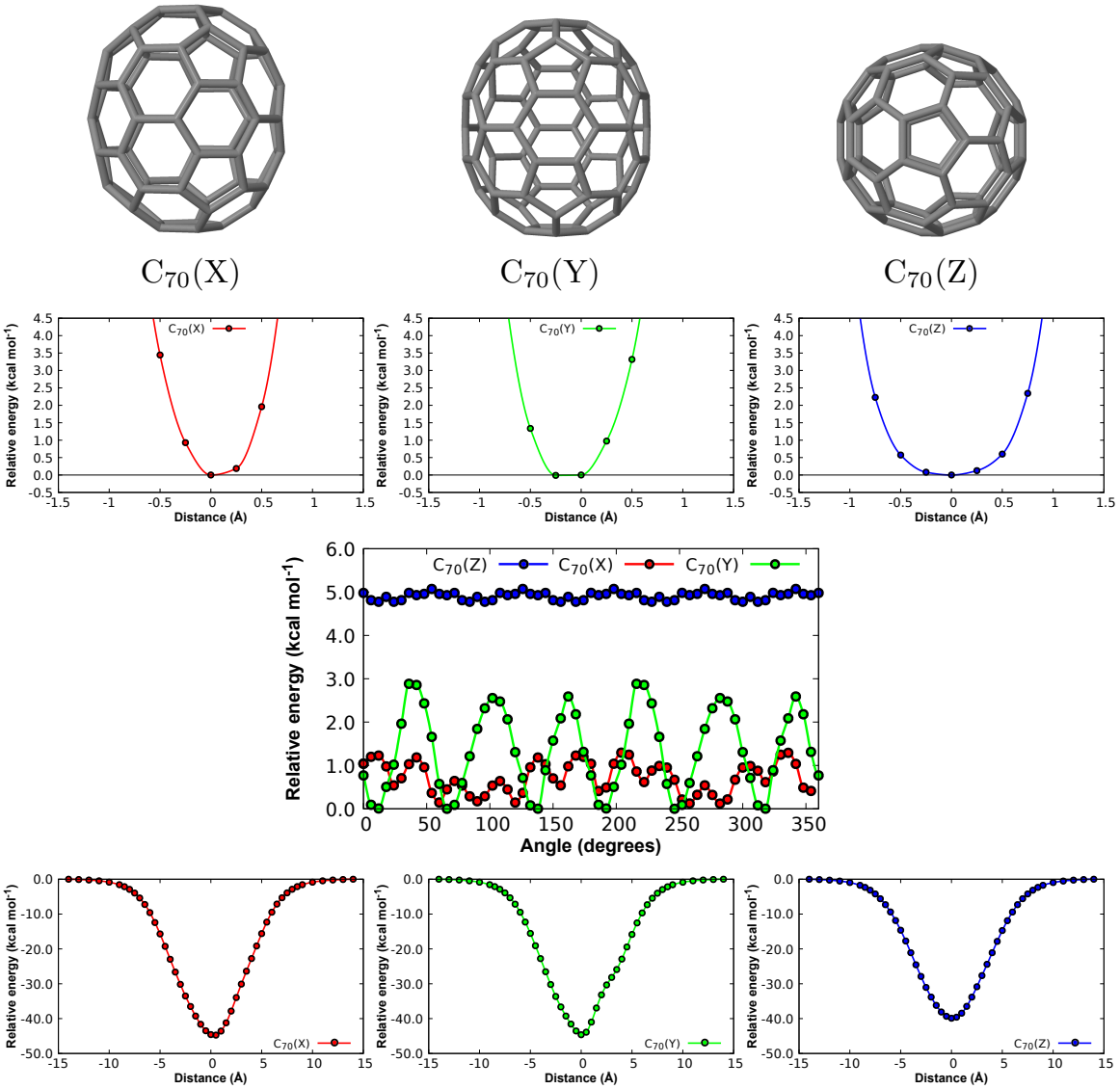

Figure d.5: Energy profiles obtained upon rotation of the C_{70}. Top figures correspond to displacements inside the nanoring using three different orientations for C_{70}. Bottom ones show how energy changes as the fullerene is moved outside the nanoring. The plot in the centre shows energy changes when C_{70} is rotated along an axis perpendicular to the nanoring.

D.9 Energy profile C_{80}@Sc_3N

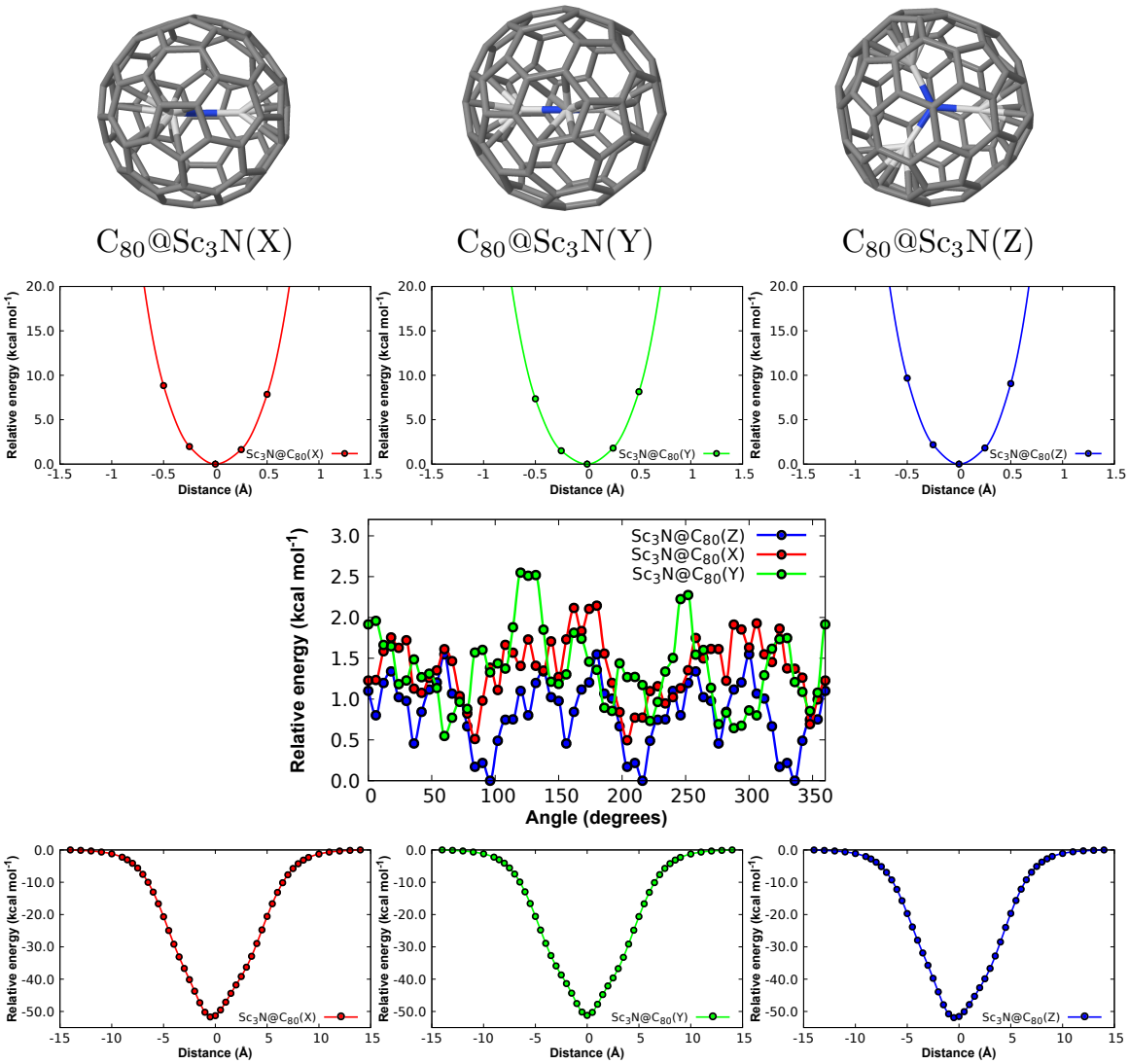

Figure d.6: Energy profiles obtained upon rotation of the Sc_3N@C_{80}. Top figures correspond to displacements inside the nanoring using three different orientations for Sc_3N@C_{80}. Bottom ones show how energy changes as the fullerene is moved outside the nanoring. The plot in the centre shows energy changes when Sc_3N@C_{80} is rotated along an axis perpendicular to the nanoring.

D.10 Additional structures for C_{60} and C_{76}

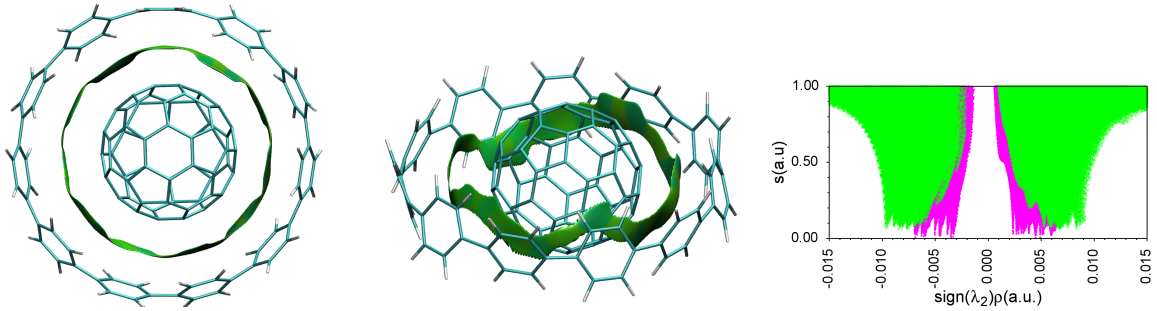

[11]CPP-C_{60}

Another structure for C_{60} complex (radii of [11]CPP are 15.2 Å, 15.0 Å)

	ΔE_{comp}	ΔE_{disp}	N_{contacts}	R_{average} (Å)
C_{60}-6	−34.74	−39.01	34	130.8

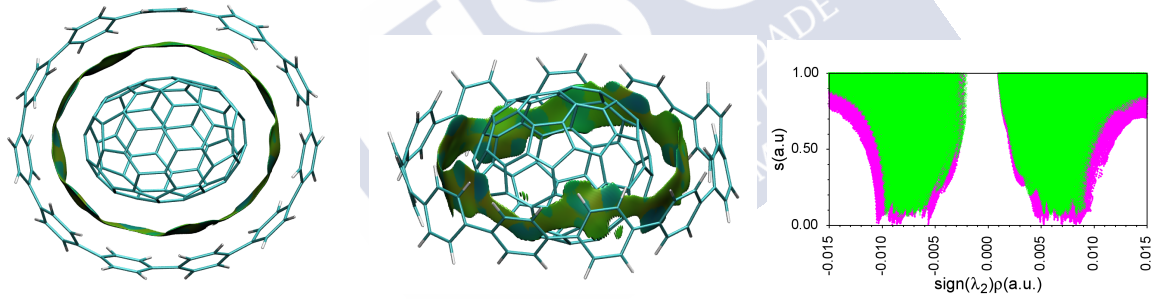

[11]CPP-C_{76}

Another structure for C_{76} complex (radii of [11]CPP are 15.2 Å, 15.0 Å)

	ΔE_{comp}	ΔE_{disp}	N_{contacts}	R_{average} (Å)
C_{76}-b	−48.15	−63.50	124	3.98

Figure d.7: Other structures obtained for C_{60} ([11]CPP-C_{60}-6) and C_{76} ([11]CPP-C_{76}-b) mentioned in the text. The energies are in kcal mol^{-1}.

D.11 2D-NCIPLOT for endohedral fullerene

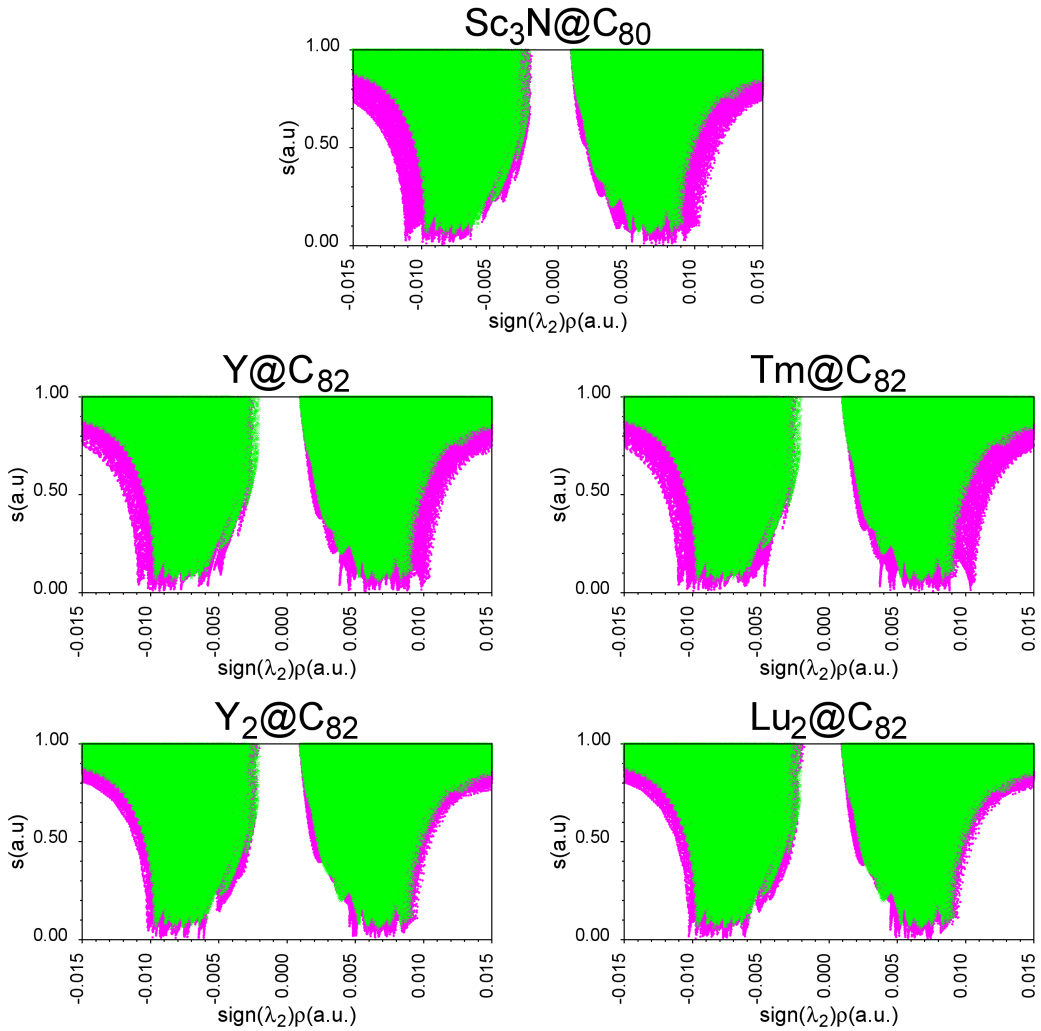

Figure d.8: NCI two-dimensional plots for the complexes with endohedral fullerenes. In green the results obtained for C_{70} are shown as reference, displaced by 0.05 a.u. for clarity.

D.12 Correlation between dispersion energy and complexation energy

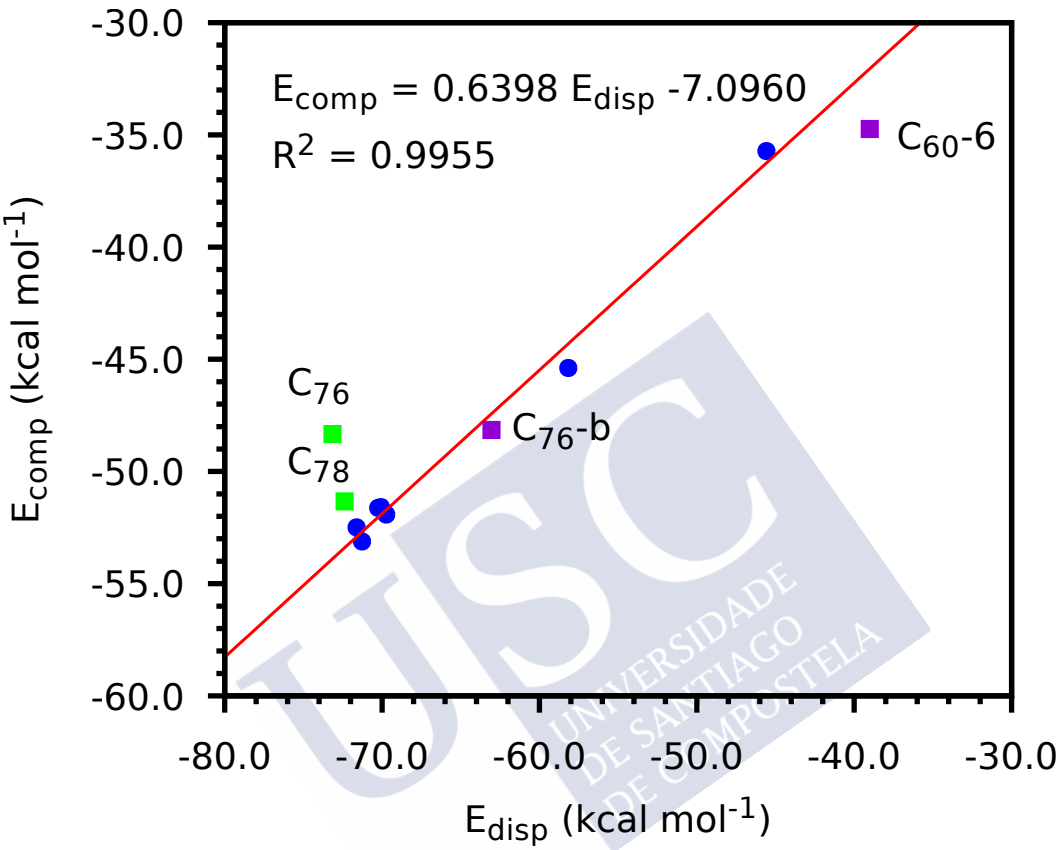

Figure d.9: Correlation between dispersion and total complexation energy. It can be observed that the main outlier is C_{76}. The almost isoenergetic C_{76}-b follows the global trend.

Appendix E

Supplementary information Chapter 8

E.1 Energetic and geometric results for $M^+@C_{60}$ complexes

Table e.1: Energetic and geometric results of the optimised minima found for the $M^+@C_{60}$ complexes. Energies (kcal mol^{-1}) relative to the most stable minimum of each case as obtained at the TPSS-D3(BJ)/def2-TZVP level. The optimisation is performed starting with the cation in three different locations inside C_{60}: R5 (with the cation close to a five-membered ring); R6 (with the cation close to a six-membered ring); C (with the cation at the centre of the fullerene).

	R5	**R6**	**C**
	Relative energy (kcal mol^{-1})		
$\mathbf{Li^+@C_{60}}$	0.32	**0.00**	3.55
$\mathbf{Na^+@C_{60}}$	–[a]	–[a]	**0.00**
$\mathbf{K^+@C_{60}}$	**0.00**	0.18	1.77
	Distance to C_{60} centre (Å)		
$\mathbf{Li^+@C_{60}}$	1.402	1.426	0.000
$\mathbf{Na^+@C_{60}}$	–[a]	–[a]	0.000
$\mathbf{K^+@C_{60}}$	0.528	0.533	0.000

[a] The three optimisations led to the same final structure (with the Na^+ cation at the centre of C_{60}) at the TPSS-D3(BJ) level.

E.2 Molecular electrostatic potential

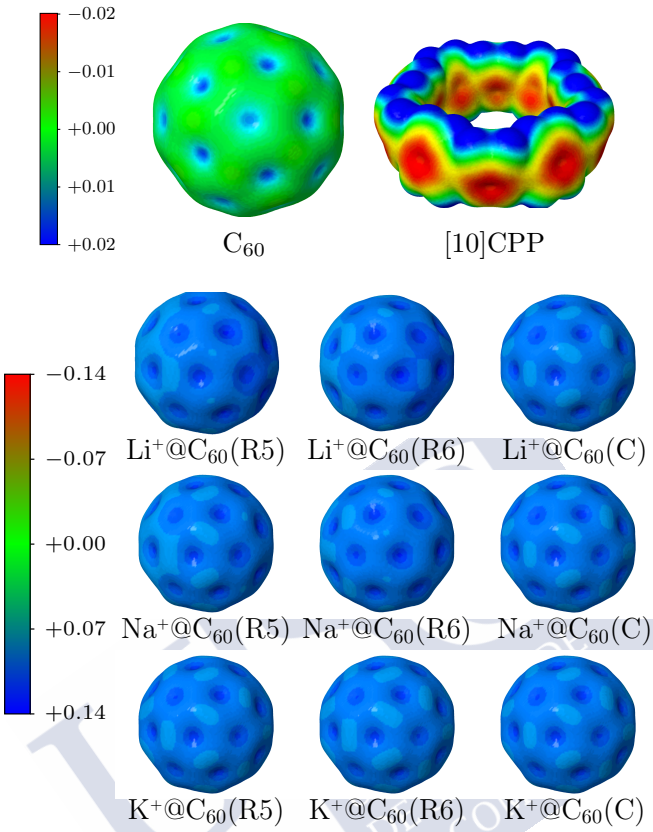

Figure e.1: Molecular electrostatic potential mapped onto an isosurface of isodensity 0.001 a.u. Top: pristine C_{60} and [10]CPP CNR; bottom: $M^+@C_{60}$ calculated at the B97-D2/def2-TZVP level.

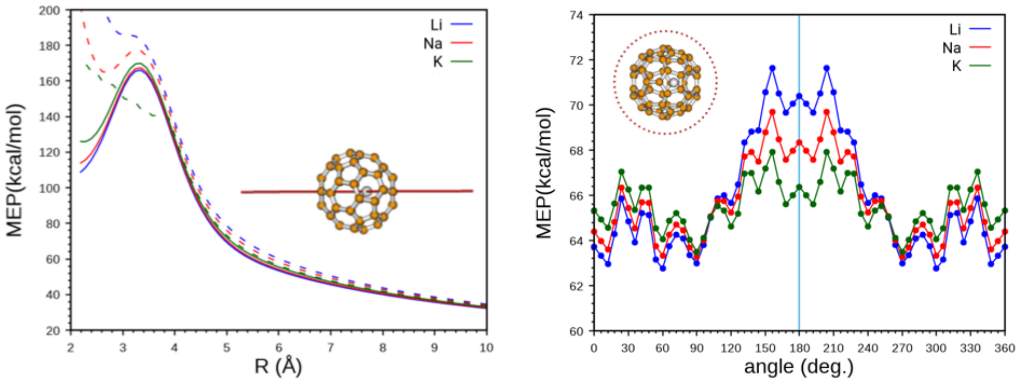

Figure e.2: Molecular electrostatic potential at the B97-D2/def2-TZVP level in selected points. Left: along a line passing through the cation and hexagonal rings. Solid line: the opposite side of the cation; dotted line: the same side. Right: on a circumference at 10 a.u. from the centre of the carbon cage. The cation is at 180°.

E.3 HOMO-LUMO monomers

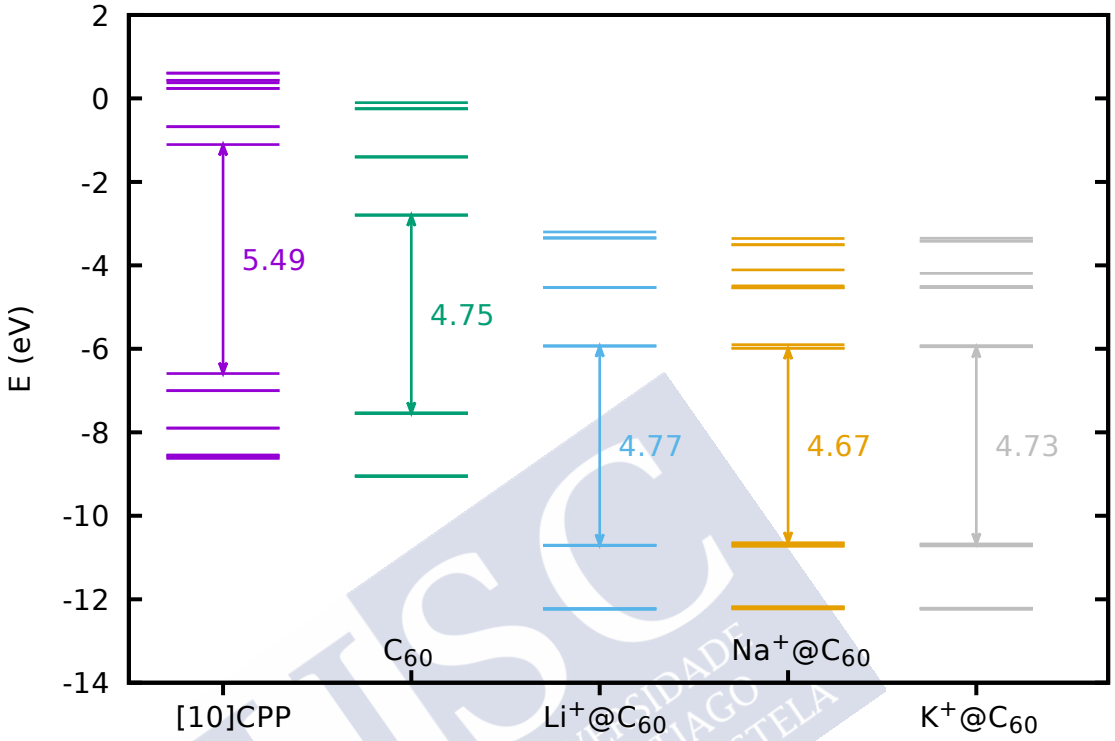

Figure e.3: Schematic energy levels of the highest and lowest occupied molecular orbitals in monomers. CAM-B3LYP/TZVP//B97-D2/def2-TZVP.

E.4 Searching of the most stable structure of $M^+@C_{60}\cdots$[10]CPP complexes

As commented in the Computational Details section, to explore the potential energy surface (PES) of the complexes and find their most stable minima, a preliminary scanning procedure was applied where the endofullerene (with fixed geometry) is rotated inside the [10]CPP ring (with fixed geometry) in all the directions changing the three Euler angles (α, β, γ) using steps of 6 degrees. Single point energy calculations were performed for each geometry at the DFTB level to save computation time. For the [10]CPP the chosen geometry was that obtained with B3LYP (nearly equal to that obtained by B97-D2 and TPSS-D3(BJ)). For the $Na^+@C_{60}$ endofullerene, two different geometries were taken into account, specifically the most stable structure obtained by each of the two functionals. That is, the R6 found with B97-D2 (cation close to a six-membered ring), and C (cation at the centre of the cage), the only one found with TPSS-D3(BJ). For the $K^+@C_{60}$ endofullerene, a similar strategy was followed, employing C and R5 structures (cation close to a five-membered ring).

In the case of $Na^+@C_{60}\cdots$[10]CPP complex, once the lower energy structures are found, those with the same geometry are eliminated by a comparison of structure and dispersion energy. The data of the scans are found in Figures e.4–e.7. The minimum energy structures from these scans are fully optimised with both functionals (B97-D2 and TPSS-D3(BJ)) and the complexation energies are obtained (Figure e.8). For the $K^+@C_{60}\cdots$[10]CPP complex the same strategy is followed (scans in Figures e.9–e.12). However, there is a large number of structures of similar energy, so in this case it was necessary to classify structures by families (see Figures e.13–e.14), to then carry out the full optimisation of only the best structures of each family (with both functionals, B97-D2 and TPSS-D3(BJ)). The most favourable structures at both levels and their complexation energies are shown in Figure e.15.

There are not DFTB+ parameters for the Li^+ cation. For this reason we can not perform the scan of the Euler angles and then choose a simple procedure for searching the best energy minima of the $Li^+@C_{60}\cdots$[10]CPP complex. Thus, we opted for selecting the best structures of $Na^+@C_{60}\cdots$[10]CPP complex, replace Na^+ with Li^+ and perform a reoptimisation (without restrictions) with the two levels of calculation considered (the optimised structures and their complexation energies are shown in Figure e.16). With this procedure, there is no certainty that we will find the absolute minimum energy structure. However, in light of the results obtained with the complexes including Na^+ and K^+, it does not seem that this is too relevant, since there are many minima in the PES with small energy differences (indicating a very flat PES), so finding just the best of them is not going to be very relevant when it comes to reproducing the properties of these complexes.

For the $Li^+@C_{60}\cdots$[10]CPP complex the experimental geometry is available.[1] Therefore, another option to computationally study this complex could be to use that geometry. However, if we use it as a starting point, the results lead to more unstable structures than those obtained from the previous calculations (see Table e.3). This is not surprising since the experimental geometry is the one corresponding to the crystalline structure, in which,

[1] H. Ueno, T. Nishihara, Y. Segawa and K. Itami, *Angewandte Chemie - International Edition*, 2015, **54**, 3707–3711

for example, the structure of the nanoring [10]CPP is very different from the one it has in the gas phase (with non-parallel phenyl rings). This results in a large deformation energy of [10]CPP (which becomes close to 3 kcal mol^{-1}), as can be seen in Table e.3.

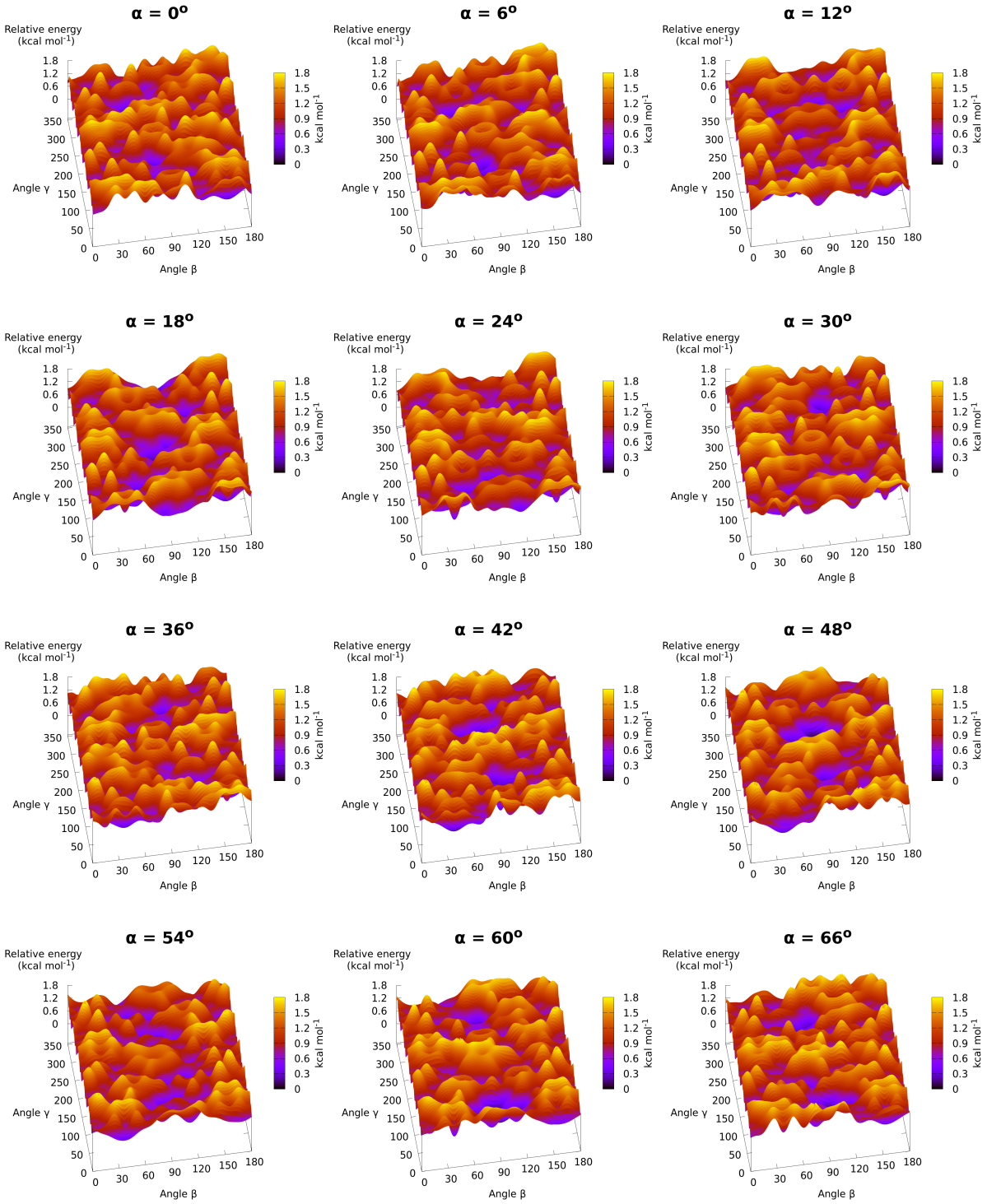

Figure e.4: Potential energy surface of $Na^+@C_{60}\cdots$[10]CPP complex obtained with DFTB+ by changing the orientation of the fullerene inside [10]CPP. Geometry of the endofullerene: cation near a hexagonal ring as found with B97-D2.

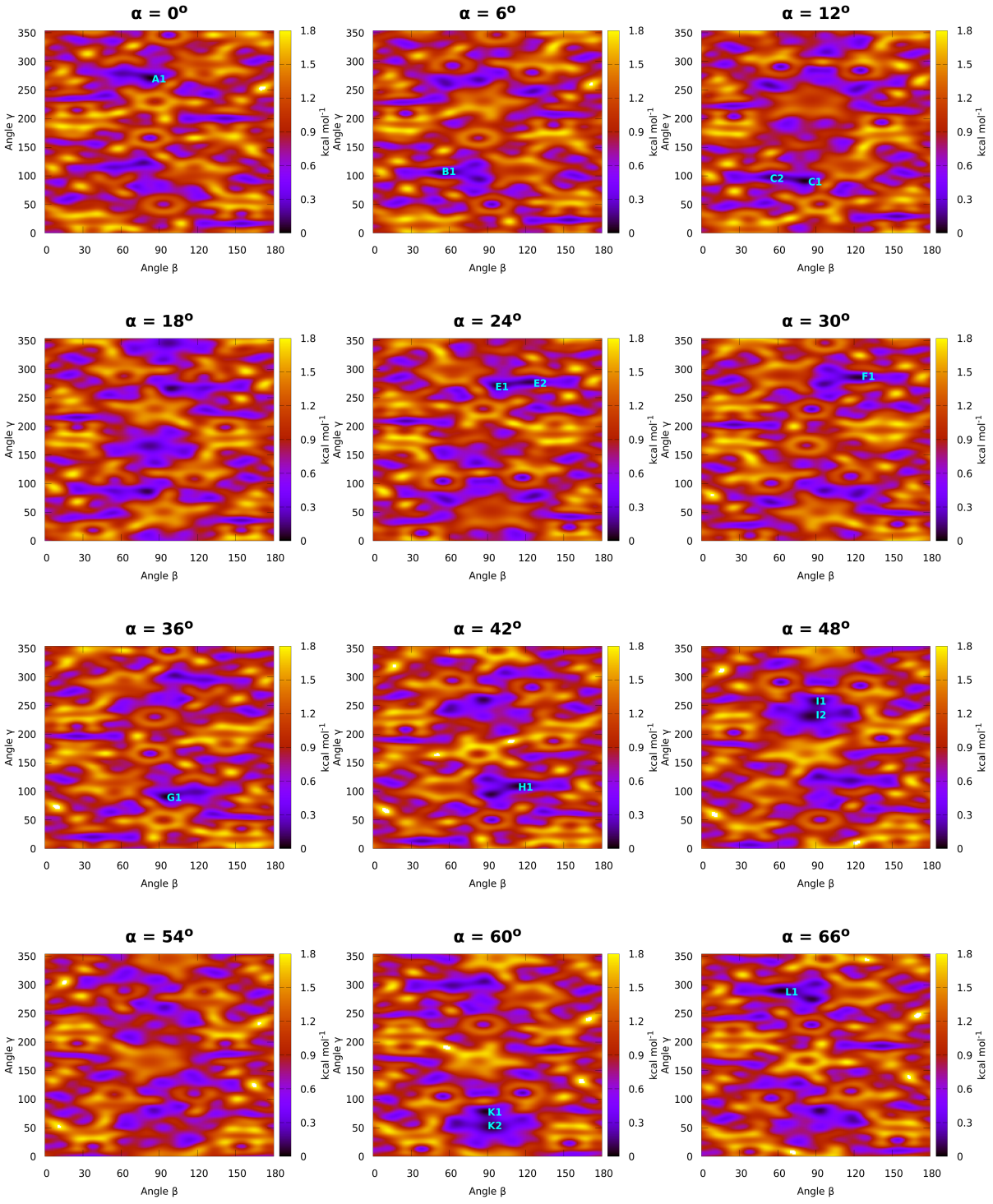

Figure e.5: 2D potential energy surface of $Na^+@C_{60}\cdots$[10]CPP complex obtained with DFTB+ by changing the orientation of the fullerene inside [10]CPP. Geometry of the endo-fullerene: cation near a hexagonal ring as found with B97-D2. Labels correspond to the most stable structures.

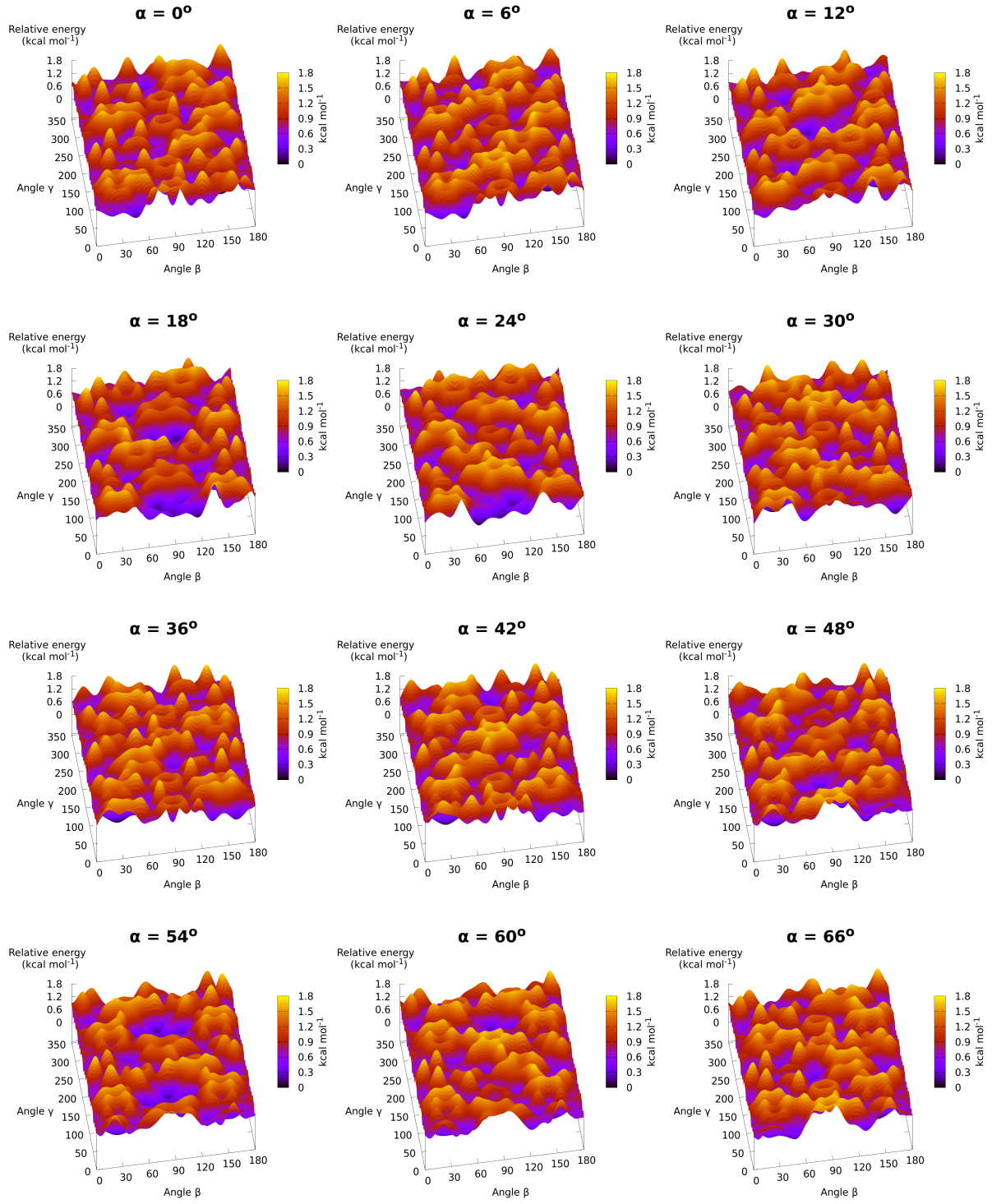

Figure e.6: Potential energy surface of $Na^{+}@C_{60}\cdots$[10]CPP complex obtained with DFTB+ by changing the orientation of the fullerene inside [10]CPP. Geometry of the endofullerene: cation at the centre of the carbon cage as found with TPSS-D3(BJ).

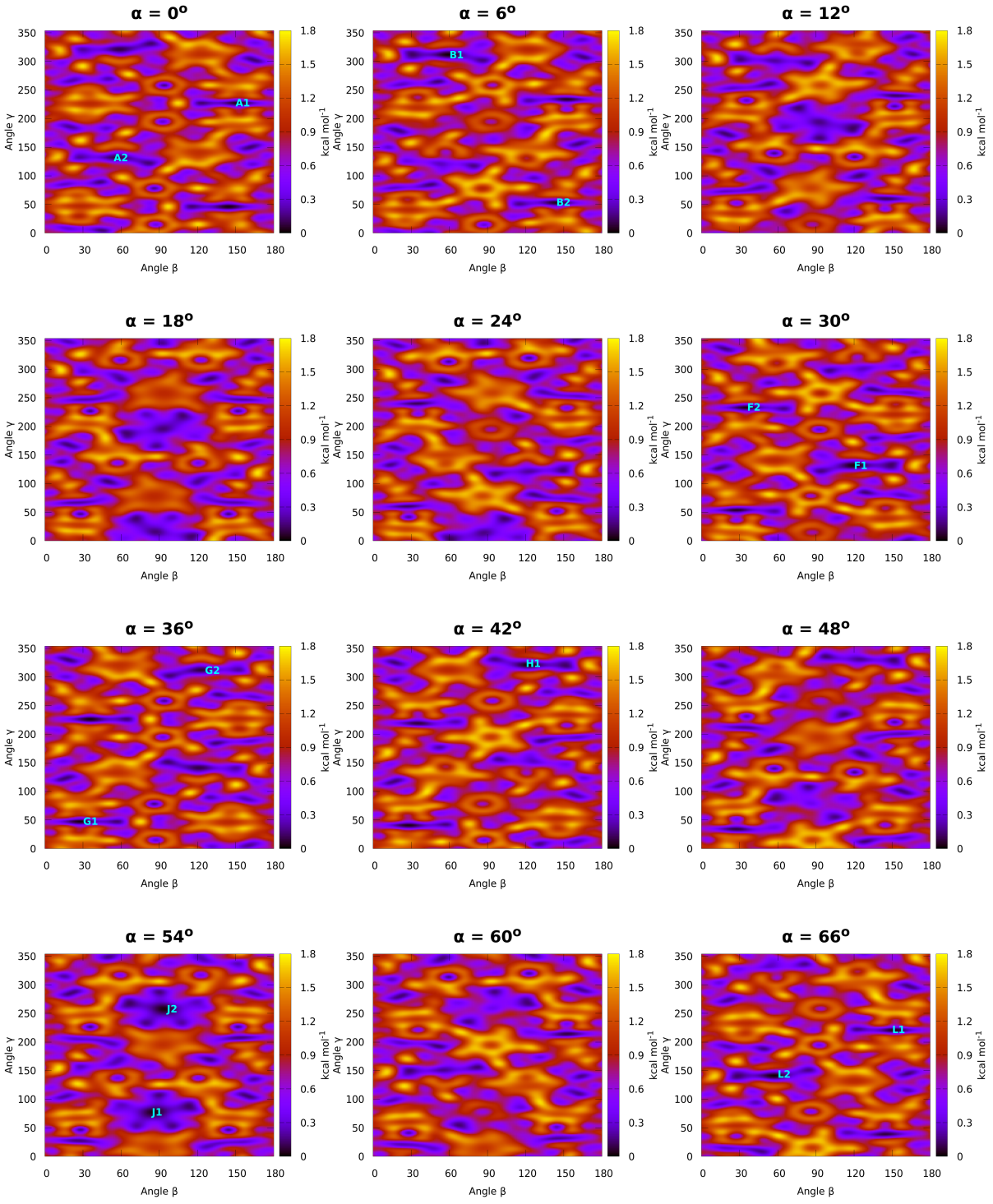

Figure e.7: Potential energy surface of $Na^{+}@C_{60}\cdots$[10]CPP complex obtained with DFTB+ by changing the orientation of the fullerene inside [10]CPP. Geometry of the endofullerene: cation at the centre of the carbon cage as found with TPSS-D3(BJ). Labels correspond to the most stable structures.

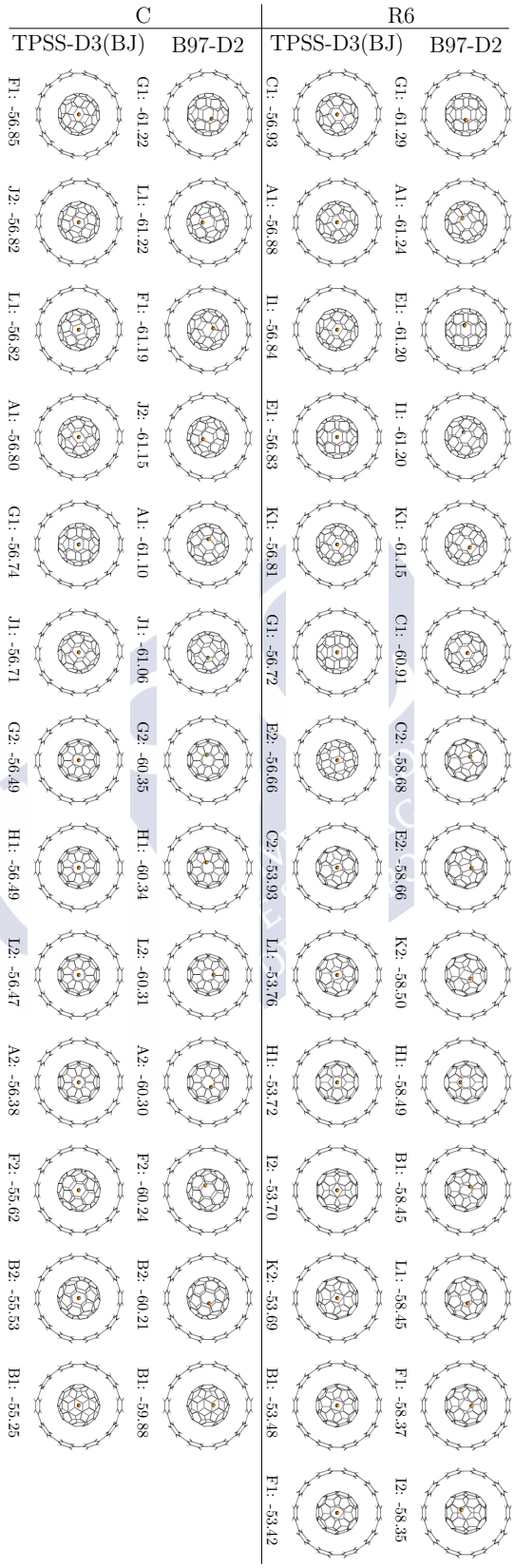

Figure e.8: Most stable structures optimised after scan of $Na^+@C_{60}\cdots$[10]CPP complex. The complexation energy for each complex is included (kcal mol^{-1}). C and R6 refer to the starting location of Na^+ cation inside C_{60}, not to the final optimised structures of the complexes.

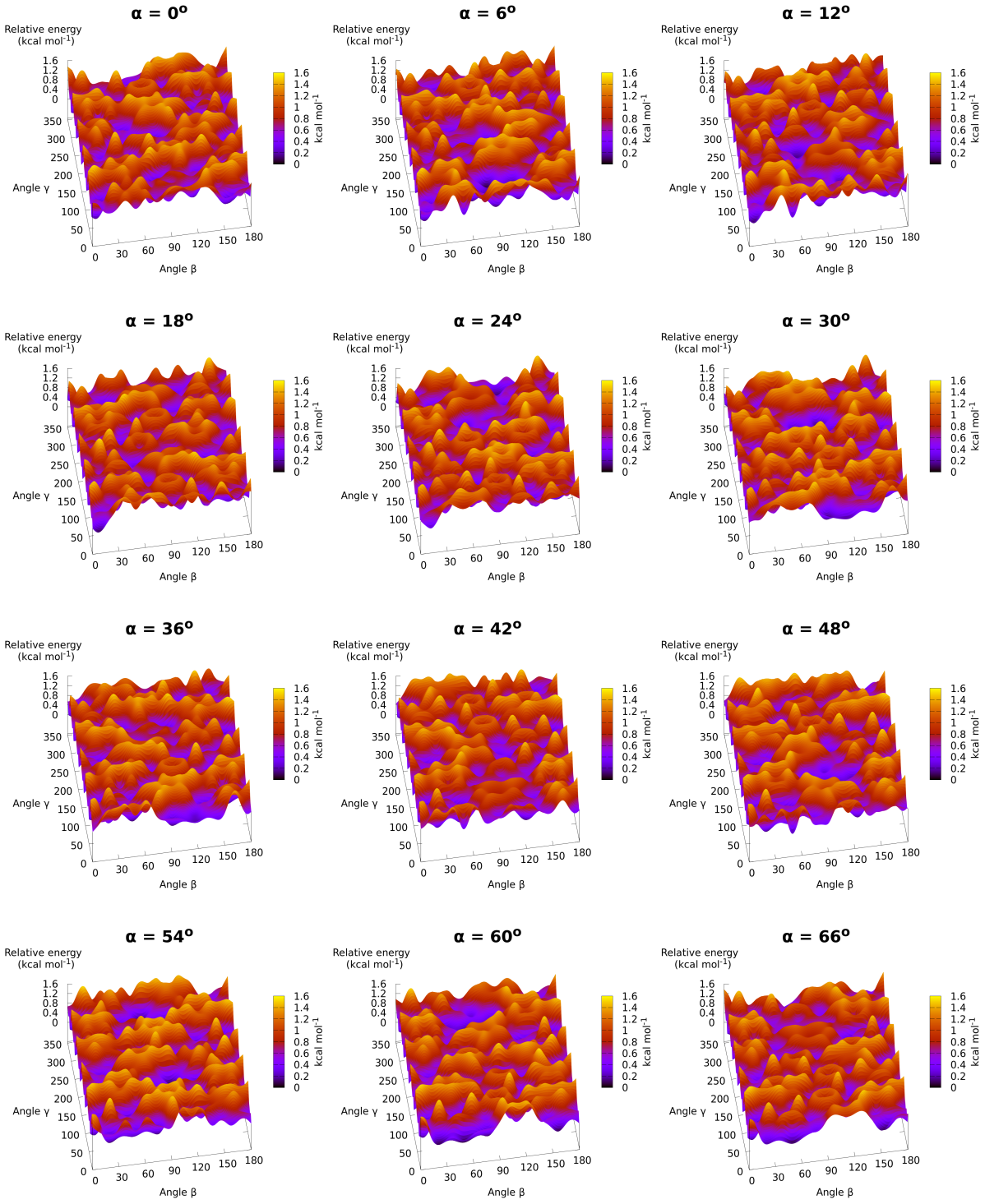

Figure e.9: Potential energy surface of $K^+@C_{60}\cdots$[10]CPP complex obtained with DFTB+ by changing the orientation of the fullerene inside [10]CPP. Geometry of the endofullerene: cation at the centre of the carbon cage as found with B97-D2.

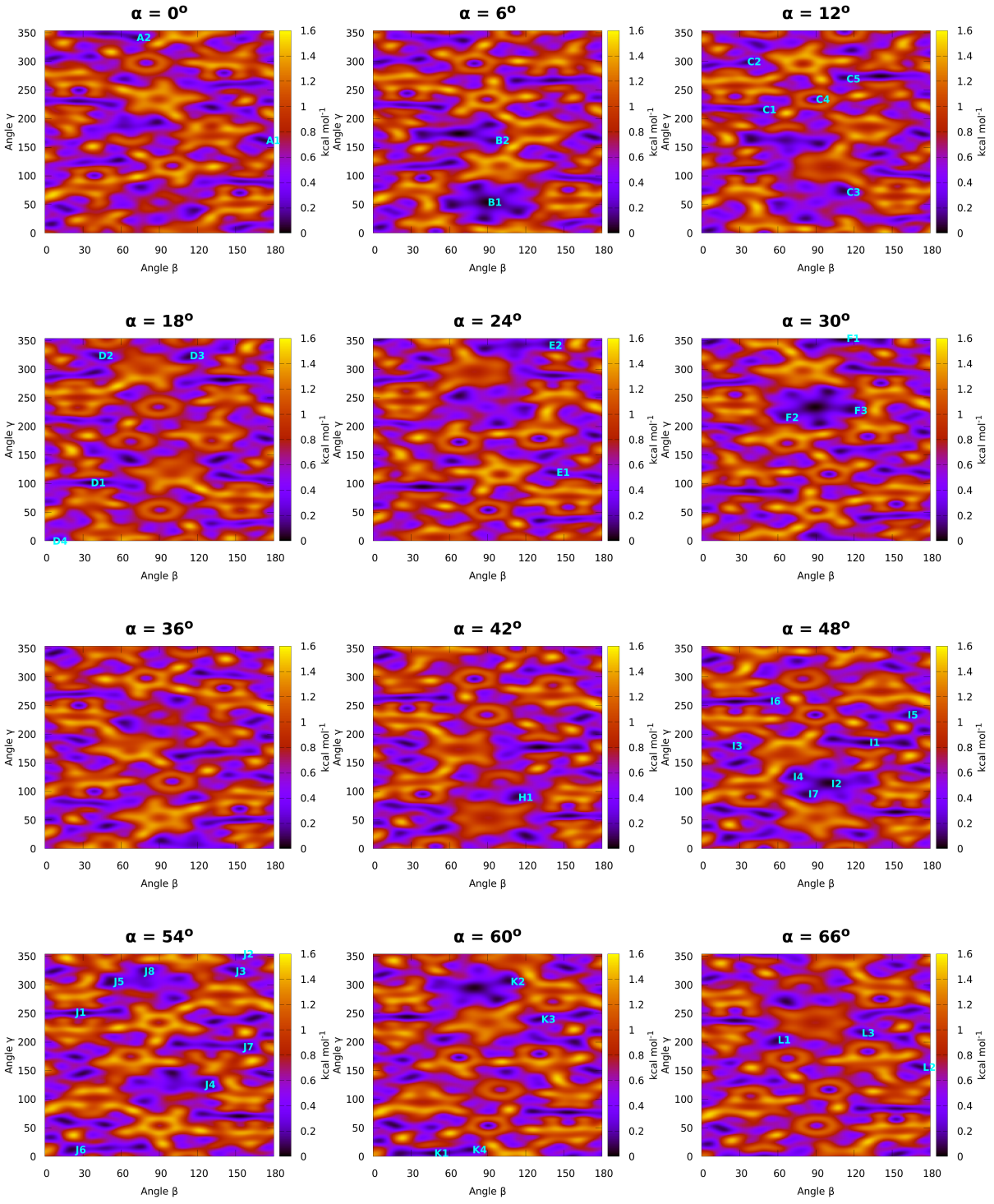

Figure e.10: 2D energy surface of $K^+@C_{60}\cdots$[10]CPP complex obtained with DFTB+ by changing the orientation of the fullerene inside [10]CPP. Geometry of the endofullerene: cation at the centre of the carbon cage as found with B97-D2. Labels correspond to the most stable structures.

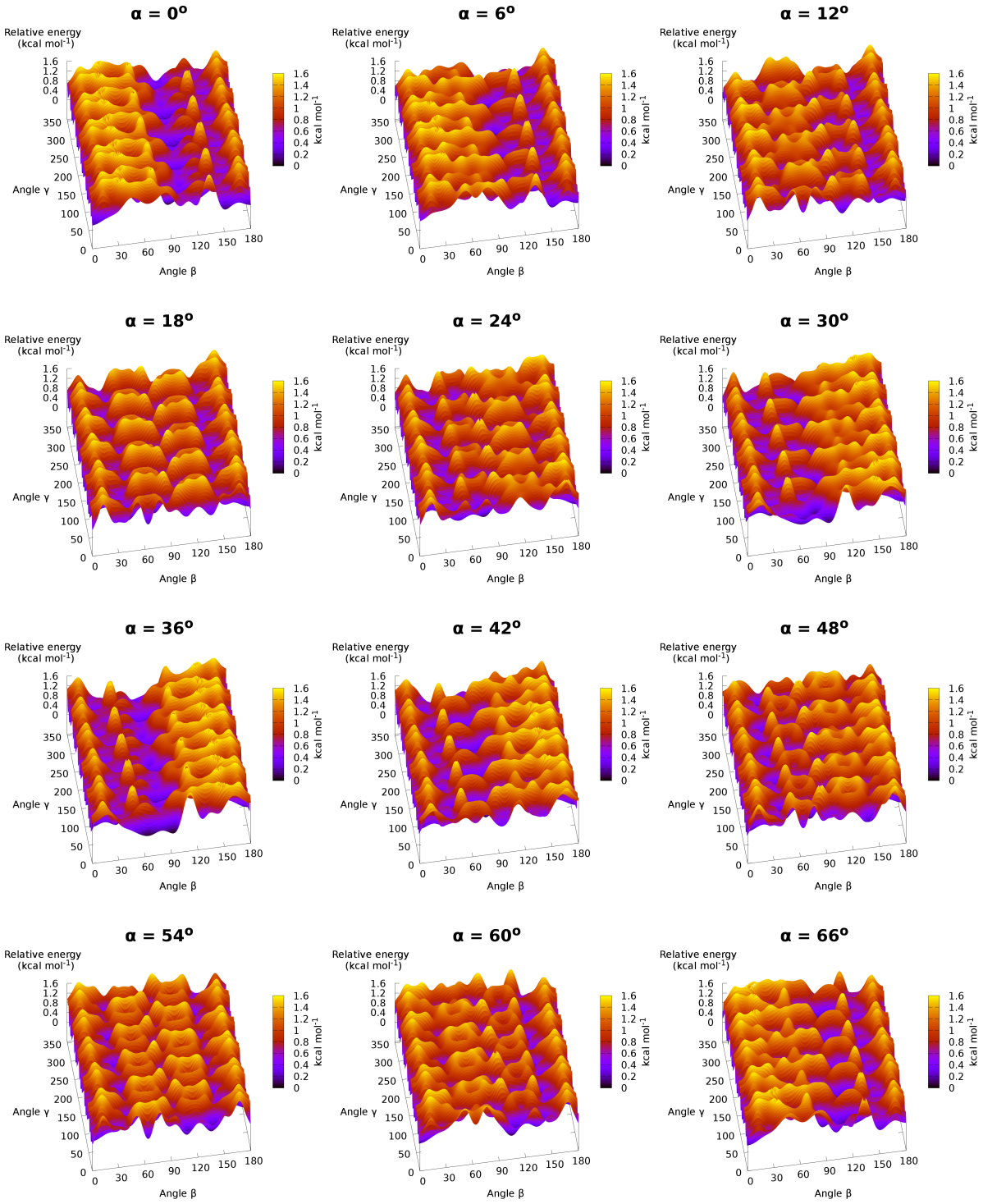

Figure e.11: Potential energy surface of $K^+@C_{60}\cdots$[10]CPP complex obtained with DFTB+ by changing the orientation of the fullerene inside [10]CPP. Geometry of the endofullerene: cation near a pentagonal ring as found with TPSS-D3(BJ).

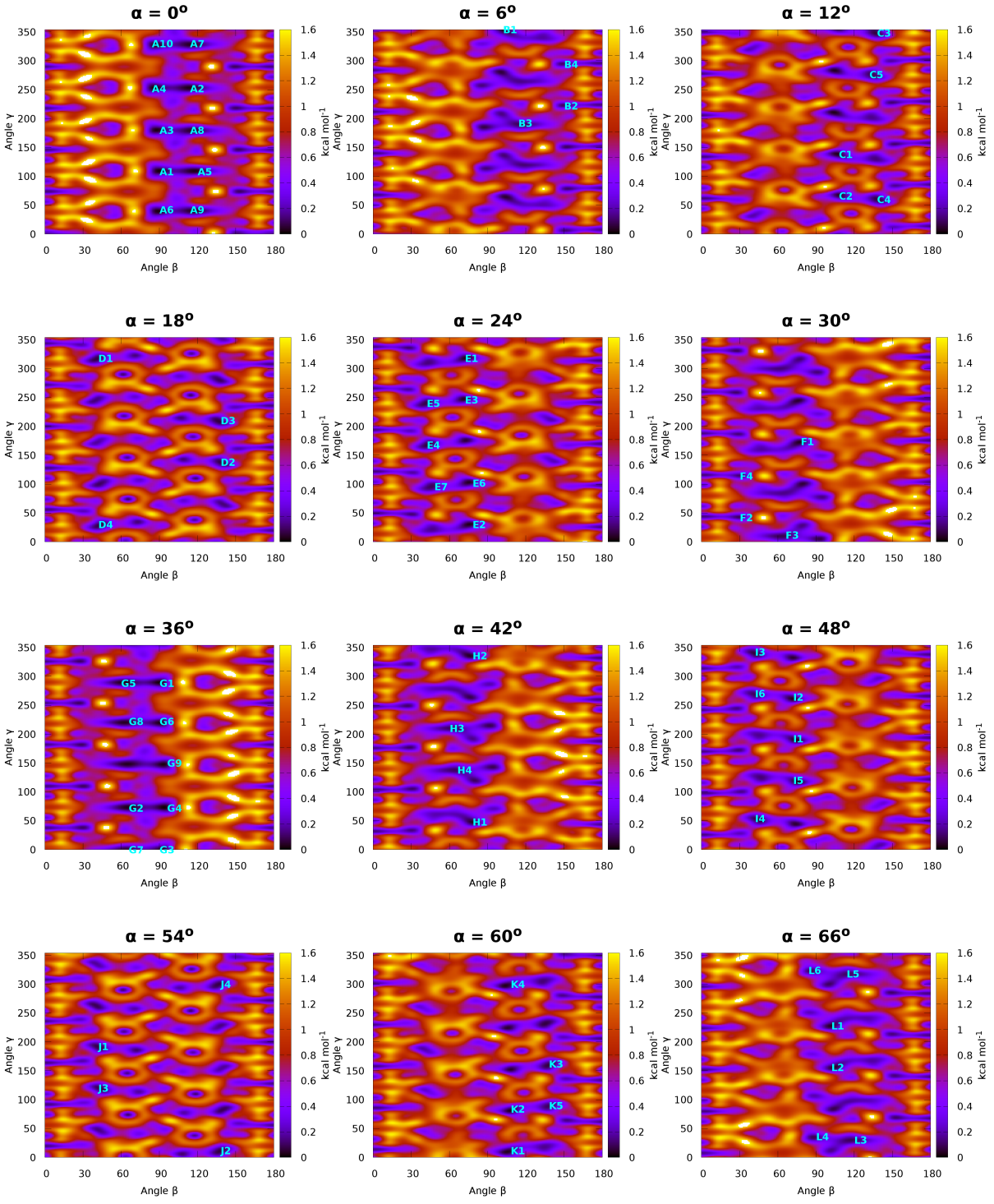

Figure e.12: Potential energy surface of $K^+@C_{60}\cdots$[10]CPP complex obtained with DFTB+ by changing the orientation of the fullerene inside [10]CPP. Geometry of the endofullerene: cation near a pentagonal ring as found with TPSS-D3(BJ). Labels correspond to the most stable structures.

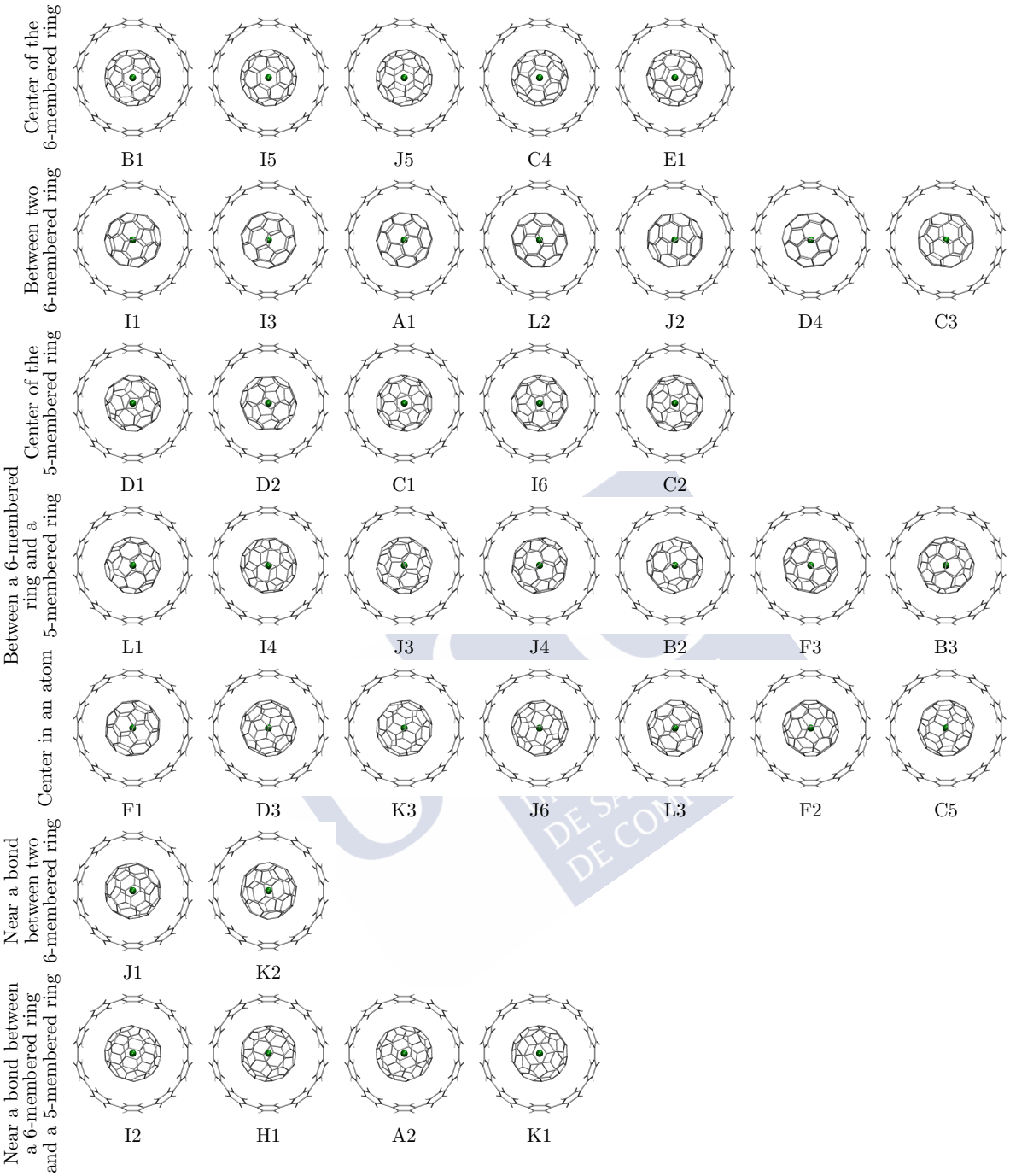

Figure e.13: Classification in families of the minima found of $K^+@C_{60}\cdots$[10]CPP complex. Geometry of the endofullerene: cation at the centre of the carbon cage as found with B97-D2.

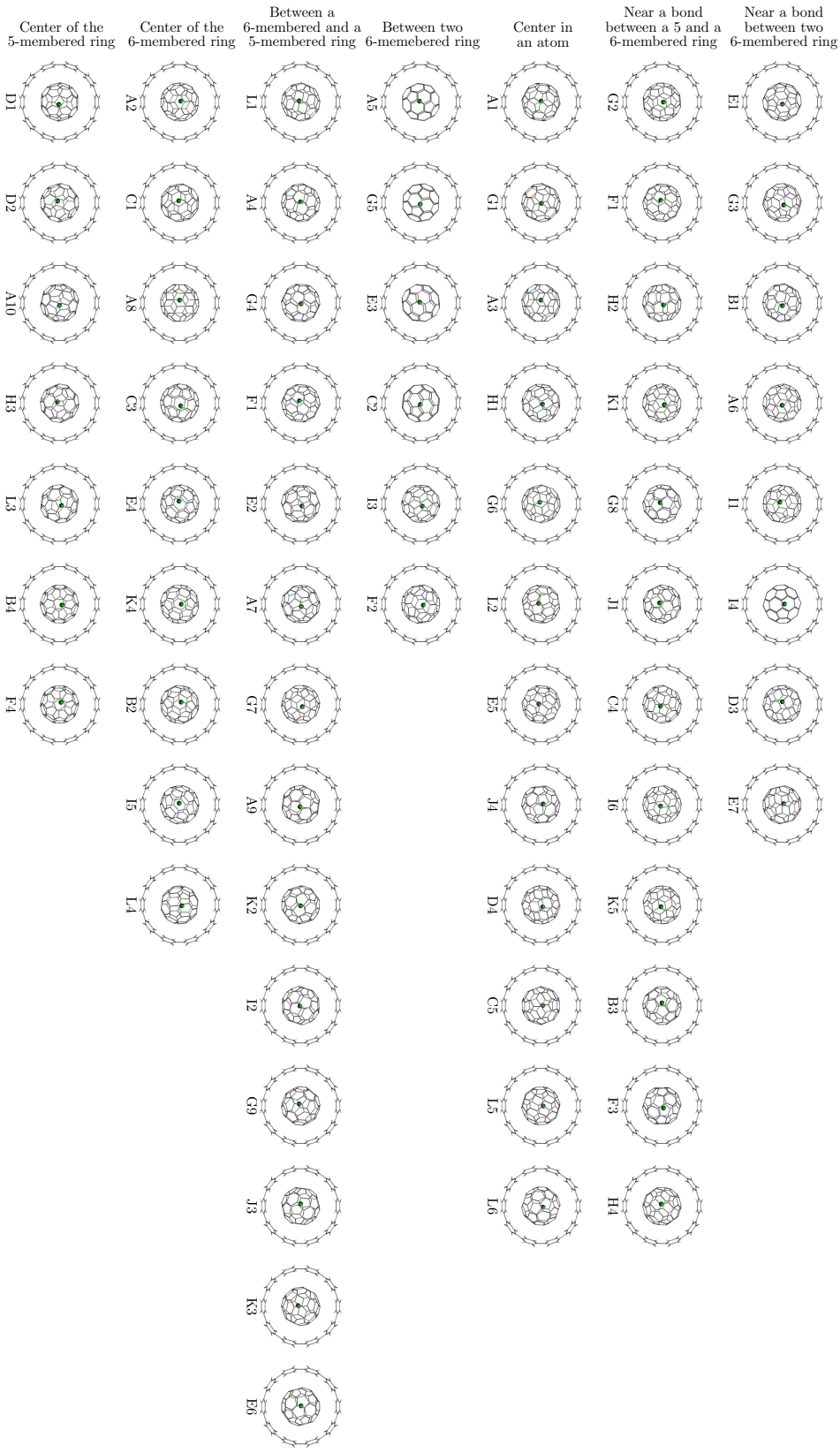

Figure e.14: Classification in families of the minima found of $K^+@C_{60}\cdots$[10]CPP complex. Geometry of the endofullerene: cation near a pentagonal ring as found with TPSS-D3(BJ).

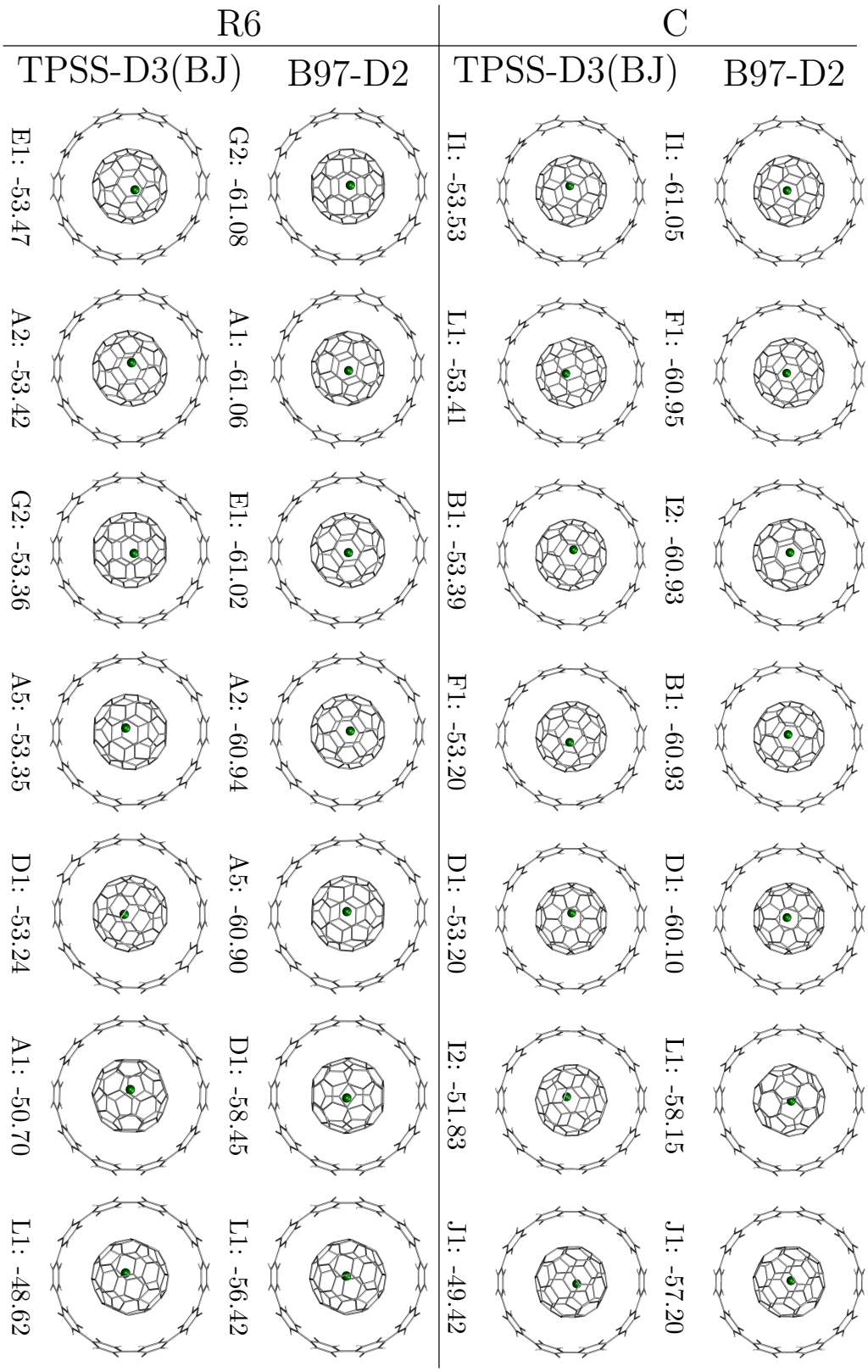

Figure e.15: Most stable structures optimised after scan of $K^+@C_{60}\cdots$[10]CPP complex. The complexation energy for each complex is included (kcal mol^{-1}). R5 and C refer to the starting location of K^+ cation inside C_{60}, not to the final optimised structures of the complexes.

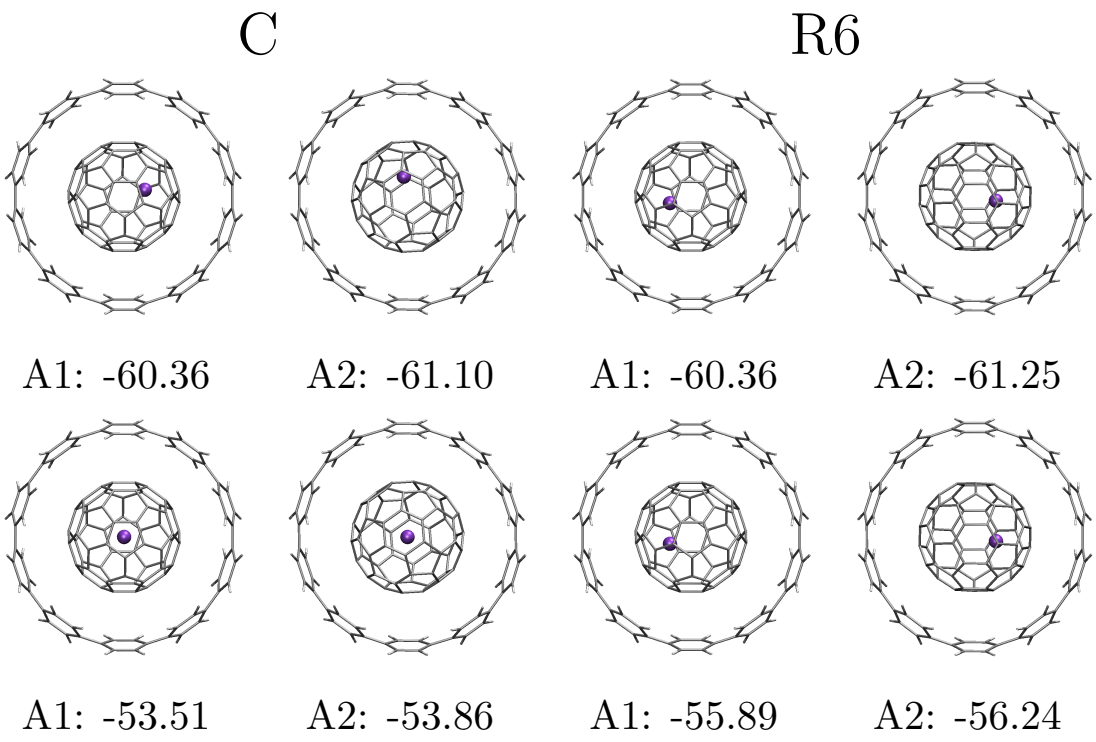

Figure e.16: Optimised most stable structures of $Li^+@C_{60}\cdots$[10]CPP complex. The complexation energy for each complex is included (kcal mol^{-1}). Top line: B97-D2. Bottom line: TPSS-D3(BJ). C and R6 refer to the starting location of Li^+ cation inside C_{60}, not to the final optimised structures of the complexes.

Table e.2: Energetic results (kcal mol^{-1}) and point charges of the best structure found for the M$^+$@C$_{60}\cdots$[10]CPP complexes with TPSS-D3(BJ). $\Delta E_{\text{complex}}$ = complexation energy; E_{def} = deformation energy; ΔE_{disp} = contribution of dispersion to the total complexation energy; Q = charge of the fullerene according to Mulliken (Mull) and NBO analysis.

M$^+$@C$_{60}$	$\Delta E_{\text{complex}}$	$\Delta E_{\text{def,fuller}}$	$\Delta E_{\text{def,[10]CPP}}$	ΔE_{disp}	$Q_{\text{fuller,Mull}}$	$Q_{\text{fuller,NBO}}$
C$_{60}$(5)	−46.71	0.21	0.19	−66.88	−0.047	−0.051
C$_{60}$(6)	−45.56	0.16	0.46	−66.52	−0.053	−0.092
Li$^+$@C$_{60}$(5)	−55.89	0.10	0.37	−65.70	0.805	0.899
Li$^+$@C$_{60}$(6)	−56.24	0.12	0.56	−65.58	0.758	0.824
Na$^+$@C$_{60}$(5)	−56.49	0.42	0.39	−66.98	0.802	0.895
Na$^+$@C$_{60}$(6)	−56.93	0.27	0.68	−66.75	0.756	0.821
K$^+$@C$_{60}$(5)	−53.20	0.22	0.41	−63.29	0.799	0.896
K$^+$@C$_{60}$(6)	−53.53	0.16	0.65	−63.18	0.751	0.825

Table e.3: Energetic results (kcal mol^{-1}) and point charges of the best structure found for the M$^+$@C$_{60}\cdots$[10]CPP complexes optimised starting from the experimental geometries of Ueno *et al.*[1] $\Delta E_{\text{complex}}$ = complexation energy; E_{def} = deformation energy; ΔE_{disp} = contribution of dispersion to the total complexation energy; Q = charge of the fullerene according to Mulliken (Mull) and NBO analysis.

B97-D2						
M$^+$@C$_{60}$	$\Delta E_{\text{complex}}$	$\Delta E_{\text{def,fuller}}$	$\Delta E_{\text{def,[10]CPP}}$	ΔE_{disp}	$Q_{\text{fuller,Mull}}$	$Q_{\text{fuller,NBO}}$
C$_{60}$(5)	−58.57	0.06	2.87	−84.35	0.762	0.823
C$_{60}$(6)	−58.70	0.11	2.81	−83.58	0.746	0.814
TPSS-D3(BJ)						
M$^+$@C$_{60}$	$\Delta E_{\text{complex}}$	$\Delta E_{\text{def,fuller}}$	$\Delta E_{\text{def,[10]CPP}}$	ΔE_{disp}	$Q_{\text{fuller,Mull}}$	$Q_{\text{fuller,NBO}}$
C$_{60}$(5)	−53.63	0.33	2.97	−64.90	0.772	0.827
C$_{60}$(6)	−55.87	0.36	0.72	−65.70	0.760	0.824

[1] H. Ueno, T. Nishihara, Y. Segawa and K. Itami, *Angewandte Chemie - International Edition*, 2015, **54**, 3707–3711

E.5 Structures of the most favourable complexes

Figures e.8, e.15, and e.16 show the best minima for the three complexes $M^+@C_{60}\cdots$[10]CPP (M=Na^+, K^+, Li^+) obtained with the B97-D2 and TPSS-D3(BJ) functionals. To analyse and discuss the geometry of the most favourable structures, different aspects have been taken into account.

First, the final location of the cation within C_{60} is observed. Figure e.17 details the place of the cation within the complex for the most stable structures of each case, and reflects the fact that the structures found for each cation are very similar, since the distances shown are very similar for all the structures of the same cation. The only exception is the TPSS-D3(BJ) structures with the Li^+ cation, because this is the only case where two types of structures can be found (C and R6). In an approximate way, all the information of Figure e.17 is summarized in Tables e.4 and e.5. Using the B97-D2 method the final structure of the endofullerene is always R6 for the complexes that include Li^+ or Na^+, in such a way that although even if we start from a centred position of the cation it moves towards one of the six-membered ring of C_{60}. When the TPSS-D3(BJ) functional is used, the results are slightly different, and Li^+ remains at the centre when starting from a central position (although this structure is worse than the R6). Using this functional, the final position of the Na^+ cation is always at the centre. As for the complexes that include K^+ cation, using both functionals the final structure of the endofullerene is always R6, in such a way that although even if we start from a C or R5 location it moves towards one of the six-membered ring of C_{60}. If the results of Table e.5 are compared with those of the endofullerenes ($M^+@C_{60}$) discussed in the manuscript (Table 8.1), it can be observed that the complexation process with [10]CPP does not cause a perceptible displacement of Li^+ and Na^+ cations; the K^+ cation does undergo a small displacement (0.3 Å away from the centre). In summary, only the location of the K^+ cation undergoes a significant change when the endofullerene joins the CNR: it moves a little towards the inner surface of the fullerene and points to a six-membered ring.

Table e.4: Most favourable location of the cation inside C_{60} in the endofullerene ($M^+@C_{60}$) and in the final complex with [10]CPP ($M^+@C_{60}\cdots$[10]CPP). R5: cation on a five-membered ring of C_{60}. R6: cation on a six-membered ring of C_{60}. C: cation at the centre of the fullerene.

	B97-D2		TPSS-D3(BJ)	
	$M^+@C_{60}$	$M^+@C_{60}\cdots$[10]CPP	$M^+@C_{60}$	$M^+@C_{60}\cdots$[10]CPP
Li^+	R6	R6	R6	R6
Na^+	R6	R6	C	C
K^+	C	R6	R5	R6

Table e.5: Distance (Å) between the cation and the centre of C_{60} and between the cation and the nearest six-membered ring of C_{60} in the final $M^+@C_{60}\cdots$[10]CPP complex.

	B97-D2		TPSS-D3(BJ)	
	centre	6 ring	centre	6 ring
Li^+	1.4	1.9	1.3 [0.0][a]	1.8 [3.3][a]
Na^+	0.9	2.4	0.0	3.3
K^+	0.3	3.0	0.6	2.7

[a] In square brackets the values of the C type structures (A1, A2 of Figure e.16).

USC UNIVERSIDADE DE SANTIAGO DE COMPOSTELA

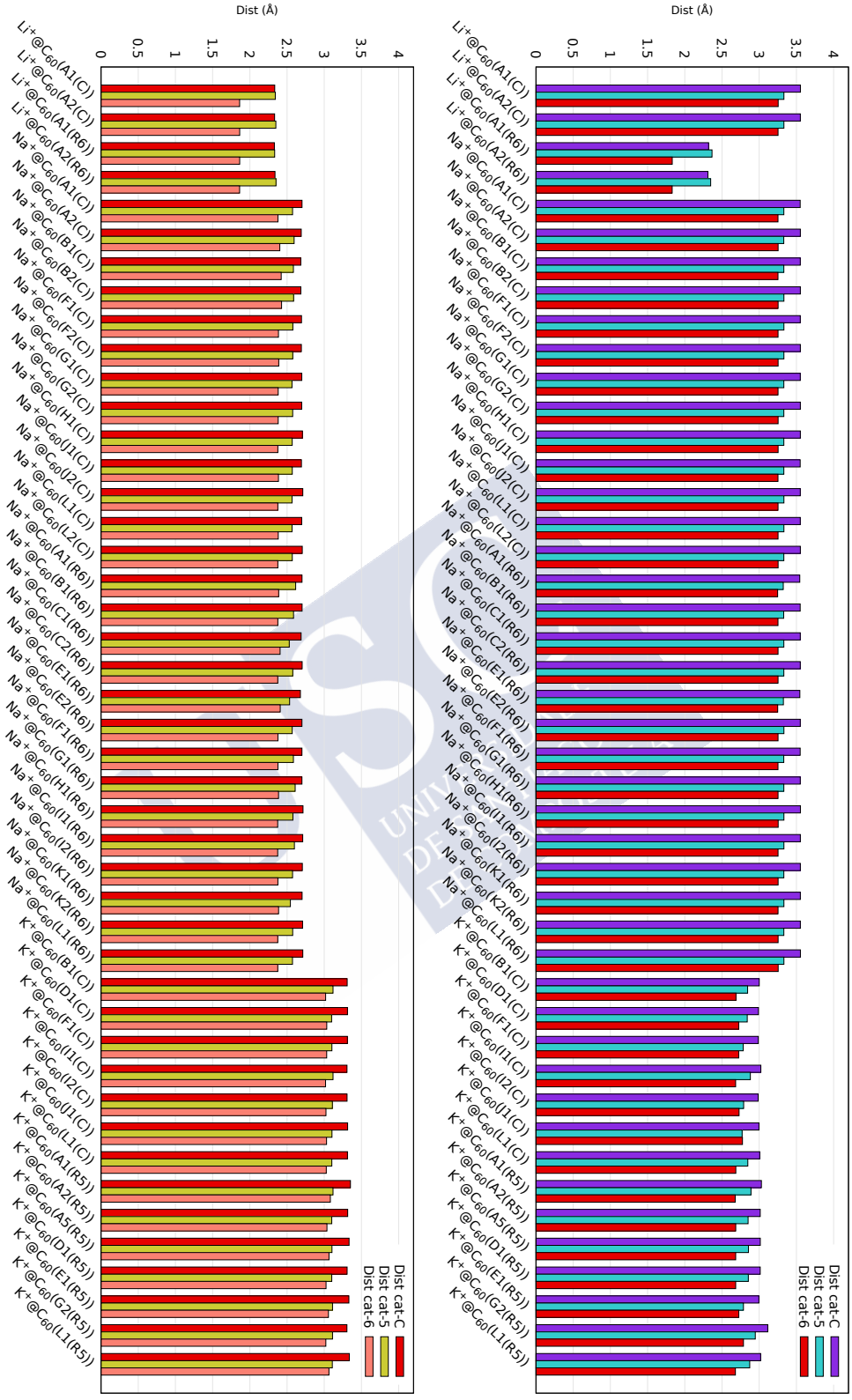

Figure e.17: Distance from the cation to the nearest carbon of the fullerene (Dist cat-C), to the nearest centre of the 5 membered ring (Dist cat-5) and to the nearest centre of the 6 membered ring (Dist cat-6). Left: B97-D2. Right: TPSS-D3(BJ).

Secondly two main different spatial arrangements of the fullerene are obtained (Figure e.18). In the first one ($C_{60}(5)$), the axis that goes through the centre of a 5-membered top and bottom rings of C_{60} is placed perpendicularly to the CNR, and in the second one ($C_{60}(6)$), the axis goes through the centre of a 6-membered top and bottom rings of C_{60}.

For the three cations the most favourable arrangement is which we call $C_{60}(6)$. This does not mean that the $C_{60}(5)$ arrangement is not found; in all cases (Figures e.8, e.15 and e.16) both types of structures are obtained (although always the best one corresponds to a $C_{60}(6)$ kind, though by a narrow energy margin). It is striking that for the endofullerenes studied in the present work the most favourable arrangement is the $C_{60}(6)$ in all cases, while for pristine C_{60} the contrary occurs; that is, the most favourable arrangement is the $C_{60}(5)$. In our previous work we demonstrated that the preference for the $C_{60}(5)$ arrangement is based on the good match between the fullerene and the carbon nanoring, the structure allowing the ten rings of [10]CPP to be directly faced to the six-membered rings of the fullerene.[2] Therefore, it seems evident that in $M^+@C_{60}\cdots$[10]CPP complexes the cation causes the natural preference towards the $C_{60}(5)$ arrangement to be overcome

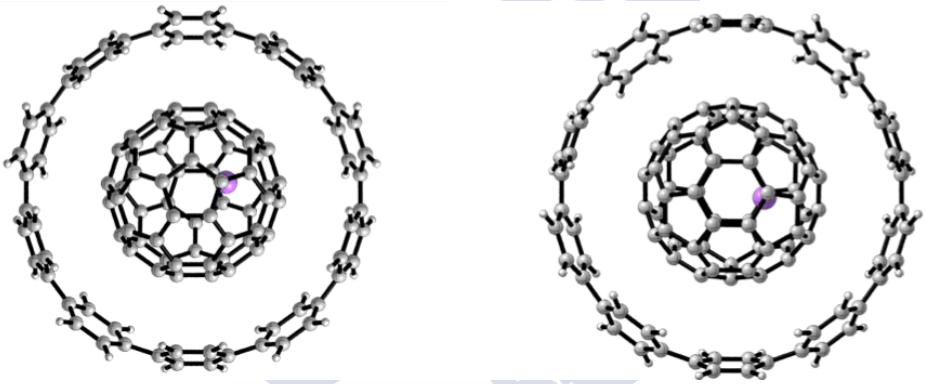

Figure e.18: Main orientations of the fullerene inside the nanoring. Left: $C_{60}(5)$. Right: $C_{60}(6)$.

Finally, and with the aim of completely describing the geometry of the complexes, it is necessary to know how the cation is located with respect to the CNR that "catches" the endofullerene. In all cases, the cation is placed inside the fullerene pointing towards the external nanoring, as expected from an electrostatic point of view: the cation is oriented towards the inner side of the [10]CPP which presents a significantly negative MEP (see Figure e.1).

[2] I. González-Veloso, J. Rodríguez-Otero and E. M. Cabaleiro-Lago, *Physical Chemistry Chemical Physics*, 2016, **18**, 31670–31679

E.6 Comparison of interaction energy in corannulene dimer for different methodologies

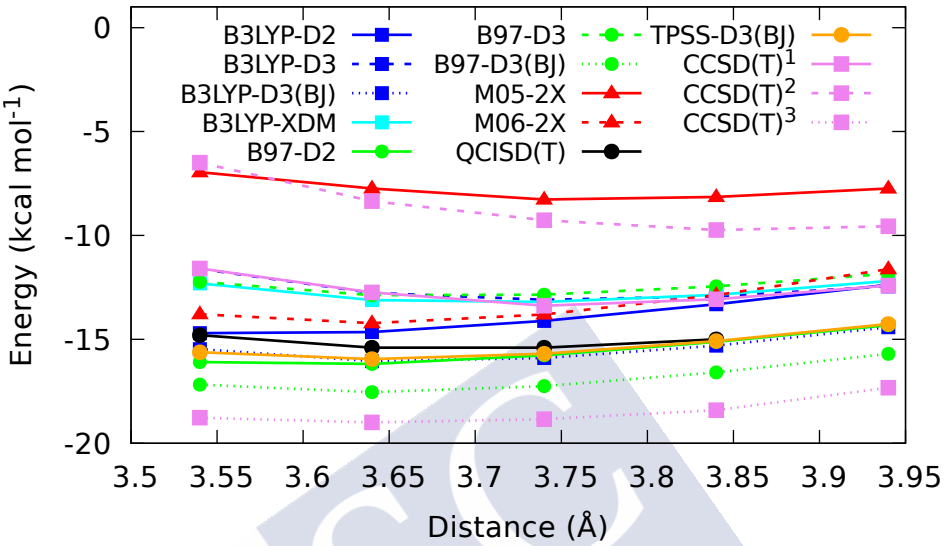

Figure e.19: Interaction energy for the corannulene dimer as a function of the intermolecular distance. QCISD(T) benchmark values obtained by T. Janowski and P. Pulay.[3] Data for B3LYP, B97, M05-2X and M06-2X are taken from M. R. Kennedy *et al.*[4]

[1] DLPNO-CCSD(T)/def2-SVP and default cutoffs.
[2] DLPNO-CCSD(T)/def2-SVP and tight cutoffs.
[3] DLPNO-CCSD(T)/def2-TZVP and default cutoffs.

Using QCISD(T) values as a reference, B97-D2 and TPSS-D3(BJ) produce a very slight overestimation of the interaction energy. DLPNO-CCSD(T)/def2-SVP produces reasonable results (although with a significant underestimation) probably due to the cancellation of errors for using a small basis and using the default cutoffs. The use of def2-TZVP basis and tight PNOs would be prohibitive for systems of the size of those studied in the present work.

[3] T. Janowski, P. Pulay, A. A. Sasith Karunarathna, A. Sygula and S. Saebø, *Chemical Physics Letters*, 2011, **512**, 155–160

[4] M. R. Kennedy, L. A. Burns and C. D. Sherrill, *The Journal of Physical Chemistry A*, 2012, **116**, 11920–11926

E.7 Local Energy Decomposition based on DLPNO-CCSD(T)

Table e.6: Contributions to the interaction energy obtained by Local Energy Decomposition (LED) analysis based on DLPNO-CCSD(T) with the def2-SVP basis set for the most stable compounds using the B97-D2 geometry.

	C_{60}	$Li^+@C_{60}$	$Na^+@C_{60}$	$K^+@C_{60}$
$\boldsymbol{E_{disp}}$	−22.18	−18.89	−19.05	−18.64
$\boldsymbol{E_{CT}}$	−6.71	−8.78	−8.74	−8.52
$\boldsymbol{E_{Elec}}$	−97.46	−134.11	−133.87	−131.94
$\boldsymbol{E_{Exch}}$	−44.19	−53.01	−53.01	−52.34
$\boldsymbol{E_{IWP}}$	−57.12	−63.67	−63.61	−63.84
$\boldsymbol{E_{IT}}$	−4.90	−4.35	−4.37	−4.27
$\boldsymbol{E_{prep,\ HF}}$	174.51	208.42	208.52	205.61
$\boldsymbol{E_{prep,\ corr}}$	12.21	18.29	18.41	18.06
$\boldsymbol{\Delta E_{def,fuller}}$	0.30	0.29	0.25	0.26
$\boldsymbol{\Delta E_{def,[10]CPP}}$	1.34	2.59	2.57	2.62
$\boldsymbol{\Delta E_{complex}}$	−44.21	−53.22	−52.9	−52.98

$\boldsymbol{E_{disp}}$: genuine dispersion; $\boldsymbol{E_{CT}}$: charge transfer contribution; $\boldsymbol{E_{Elec}}$: electrostatic interaction; $\boldsymbol{E_{Exch}}$: inter-fragment exchange; $\boldsymbol{E_{IWP}}$: contribution from weak pairs; $\boldsymbol{E_{IT}}$: contribution of triple excitations; $\boldsymbol{E_{prep,HF}}$: HF contribution to preparation energy at the HF level; $\boldsymbol{E_{prep,corr}}$: correlation contribution to preparation energy.

E.8 Absorption spectra for the monomers

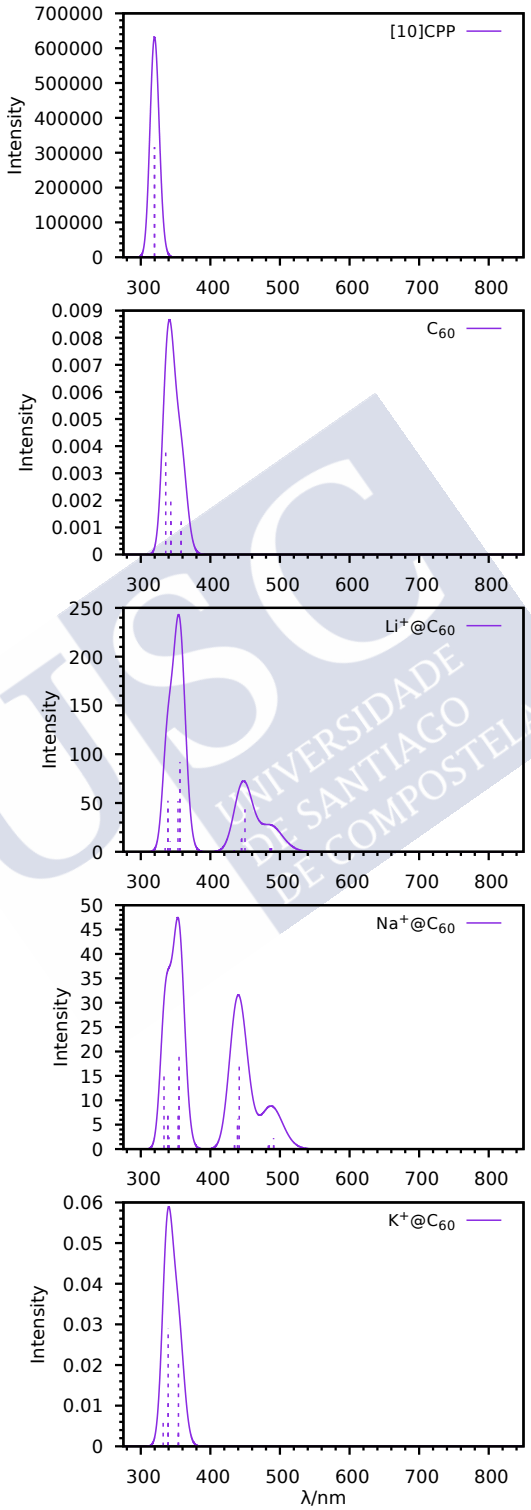

Figure e.20: Absorption spectra for the monomers obtained at the CAM-B3LYP/TZVP level, using B97-D2 geometries.

E.9 Absorption spectra for the complexes

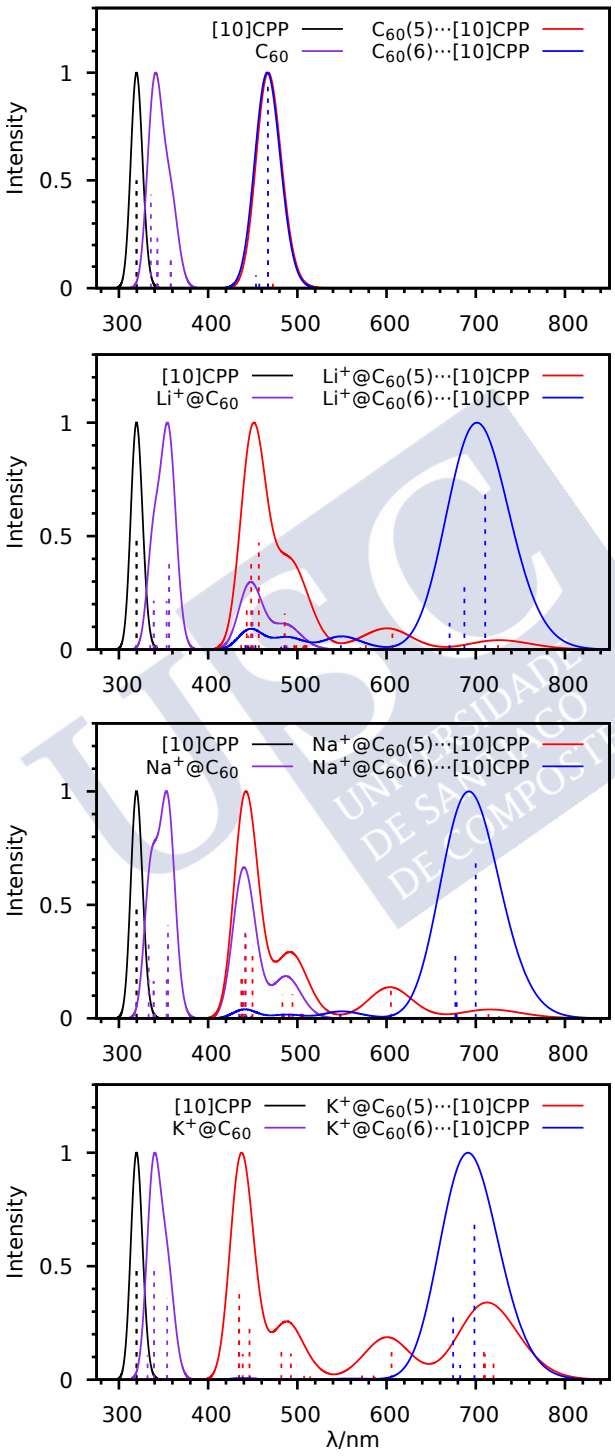

Figure e.21: Normalised absorption spectra for the $M^{+}@C_{60}\cdots$[10]CPP complexes obtained at the CAM-B3LYP/TZVP level, using B97-D2 geometries.

E.10 Position of the barycentres

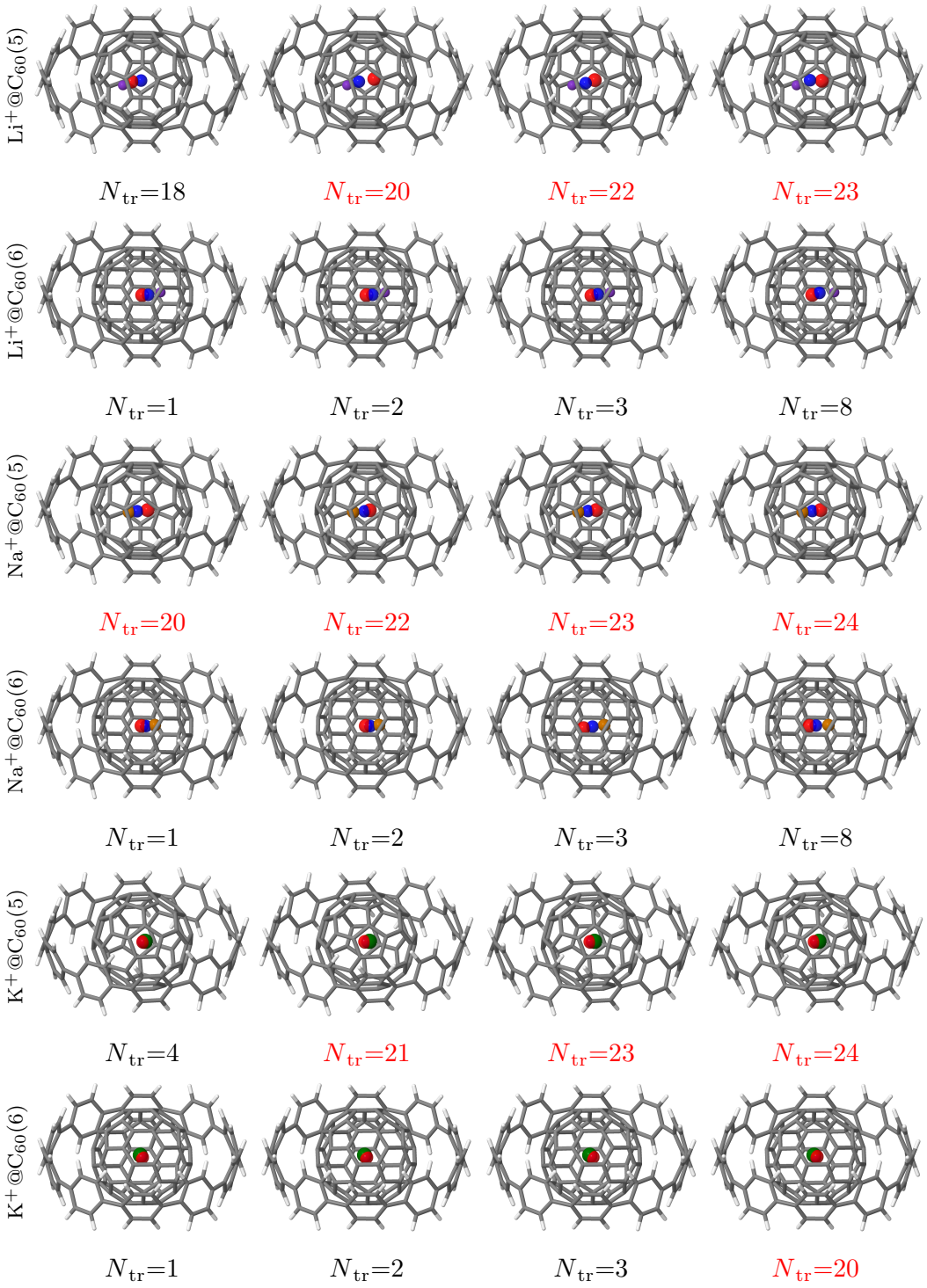

Figure e.22: Position of the barycentres (blue and red dots) of charge for the transitions of $M^+@C_{60}\cdots$[10]CPP complexes shown in Figure 8.4. N_{tr} is the number of the transition and the red colour corresponds to intrafullerene transitions.

Table e.7: Distance (Å) between the cation and the barycentres of charge for the most stable $M^+@C_{60}\cdots$[10]CPP complexes. N_{tr} is the number of the transition, $R_{cat\text{-}neg}$ is the distance between the cation and the negative barycentre and $R_{cat\text{-}pos}$ is the distance between the cation and the positive barycentre. Intrafullerene transitions in bold.

	N_{tr}	$R_{cat\text{-}neg}$ (Å)	$R_{cat\text{-}pos}$ (Å)	N_{tr}	$R_{cat\text{-}neg}$ (Å)	$R_{cat\text{-}pos}$ (Å)
$Li^+@C_{60}(5)$	18	1.365	0.681	**20**	**0.890**	**2.045**
	22	**0.965**	**1.712**	**23**	**1.063**	**1.879**
$Li^+@C_{60}(6)$	1	0.969	1.405	2	0.969	1.404
	3	0.932	1.401	8	1.107	1.651
$Na^+@C_{60}(5)$	**20**	**0.602**	**1.363**	**22**	**0.822**	**1.210**
	23	**0.706**	**1.304**	**24**	**0.706**	**1.302**
$Na^+@C_{60}(6)$	1	0.642	0.962	2	0.642	0.962
	3	0.845	1.510	8	0.907	1.360
$K^+@C_{60}(5)$	**4**	**0.160**	**0.228**	**21**	**0.183**	**0.352**
	23	**0.211**	**0.349**	**24**	**0.209**	**0.349**
$K^+@C_{60}(6)$	1	0.176	0.274	2	0.176	0.274
	3	0.183	0.309	**20**	**0.180**	**0.339**

USC UNIVERSIDADE DE SANTIAGO DE COMPOSTELA

E.11 Charge transfer in different complexes with TPSS-D3(BJ) geometry

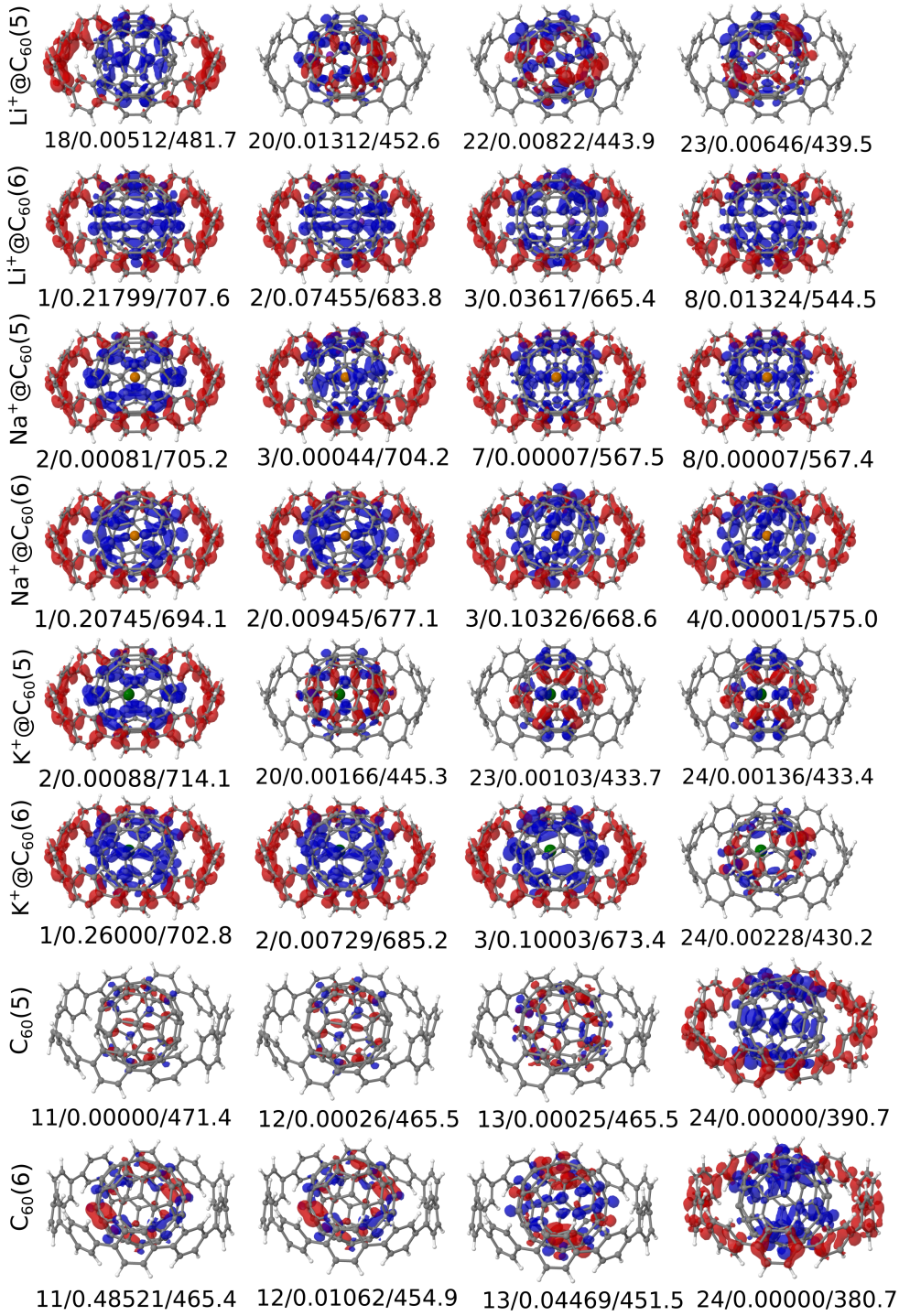

Figure e.23: Difference density between the excited state and the ground state for the four most intense transitions in the most stable complexes (with TPSS-D3(BJ)) obtained at the CAM-B3LYP/TZVP level. Each of the rows corresponds to one of the fullerenes. The numbers are the number of the transition/oscillator strength*100/wavelength (nm). Surface corresponds to −0.001 a.u. (red) and 0.001 a.u. (blue).

E.12 Absorption spectra with TPSS-D3(BJ) geometry

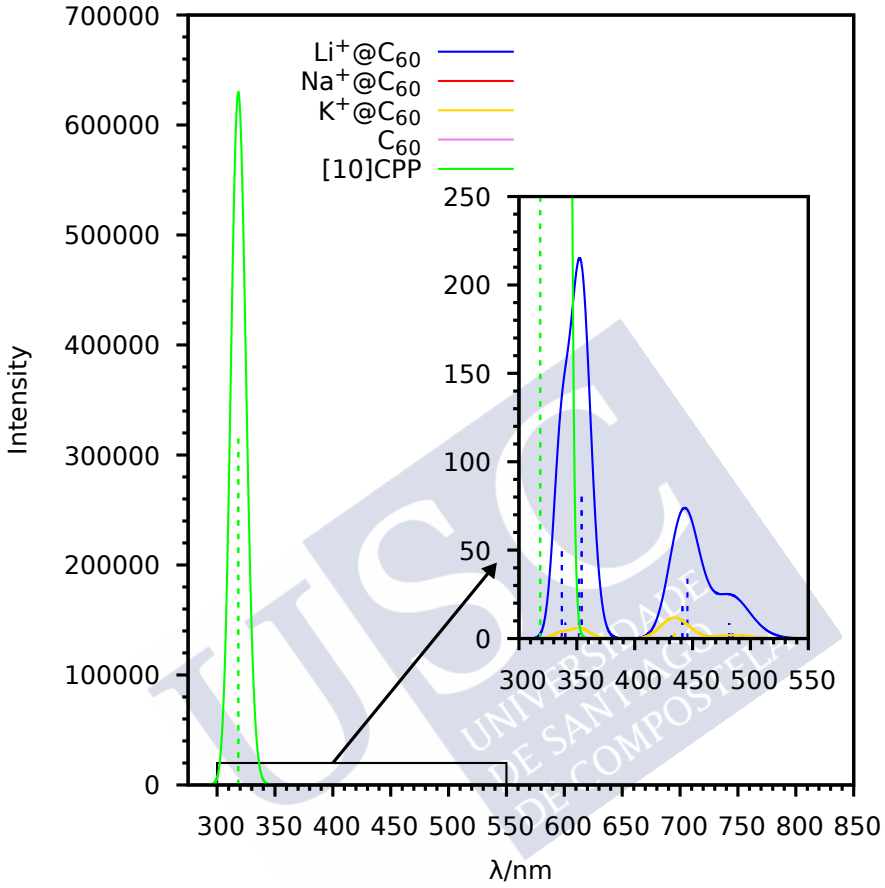

Figure e.24: Absorption spectra for the monomers (fullerene, cationic endofullerenes, [10]CPP) obtained at the CAM-B3LYP/TZVP level, with TPSS-D3(BJ) geometries.

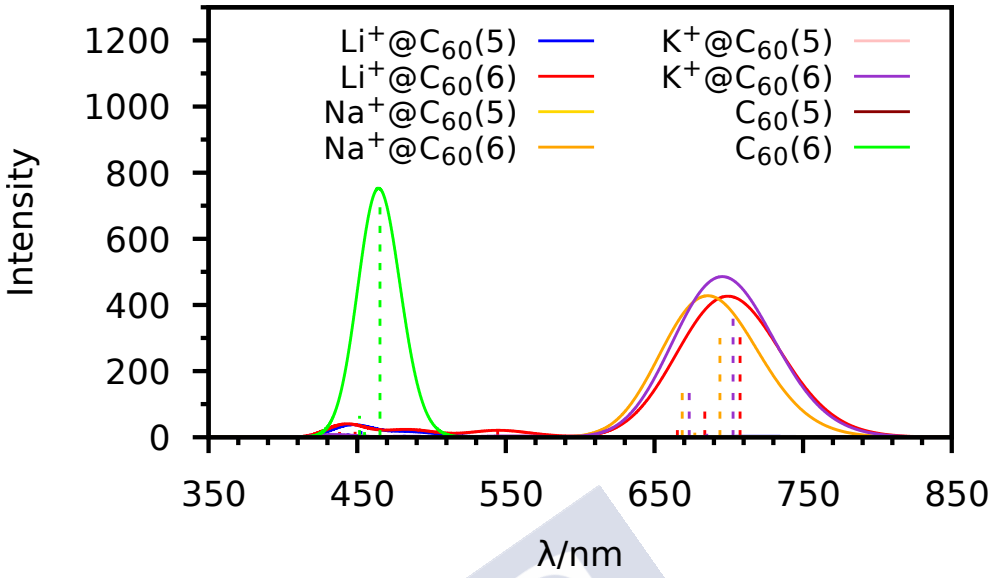

Figure e.25: Absorption spectra for the $M^+@C_{60}\cdots$[10]CPP complexes obtained at the CAM-B3LYP/TZVP level, using TPSS-D3(BJ) geometries.